Ancillary Ligand Effects on Fundamental Transformations in Metallocene Catalyzed Olefin Polymerization

Thesis by

Paul James Chirik

In Partial Fulfillment of the Requirements for the
Degree of Doctor of Philosophy

Division of Chemistry and Chemical Engineering
California Institute of Technology
Pasadena, California

2000
(Submitted April 3, 2000)

For Mom and Dad

Acknowledgments

It is difficult for me to fully express my gratitude and appreciation for all those who have offered their support during my education at Caltech but I will do my best in the next couple of pages.

First, I would like to thank my research advisor, John Bercaw, for his guidance, thoughtfulness and friendship during my tenure in his group. Working with John has been an exceptional experience and I am indebted to him for the education he has provided. Additionally, Jay Labinger has served as an excellent "second advisor" and I am grateful for his suggestions and input. I would also like to thank my committee: Bob Grubbs, Harry Gray, Doug Rees and Andy Myers for their time and helpful suggestions throughout my graduate career. Special thanks go to Harry for warming up the crowd before every talk I have given at Caltech. I would also like to acknowledge my undergraduate advisor, Joe Merola, for inspiring me to go to graduate school and sharing his passion for organometallic chemistry and science in general.

The Bercaw group is a unique cast of characters and I would like to mention some of them here. I would like to thank Tim Herzog and Jim Gilchrist for showing me all there is to know about vacuum lines and air-sensitive chemistry, Shannon Stahl for teaching me how to think about mechanisms and how to get away with a cheap elbow on the basketball court, and Mike Abrams for keeping me away from chemical physics seminars.

I have been fortunate to share a lab with some truly wonderful people. Steve Miller has been an excellent line mate and friend and was very understanding when I made him split his pants in a softball game. In addition to being a fine tennis partner and authority on fashion, Susan Schofer has been offered a tremendous amount of support and friendship for which I never express in words and am truly grateful. Chris Jones has been a great addition to the lab and will be the first person I call when the Flyers win the Stanley Cup and Virginia Tech wins a national championship. Deanna Zubris has been an amazing friend, confidant and colleague since I started at Caltech and I certainly would not have made it this far without her. Best of luck to my new line mate Sara Klamo.

I would like to thank Chris Brandow for all of his help and suggestions with both theory and experiments and for all of those body checks he threw at

me walking down the hall. Lily Ackerman has been a great addition to the group V project and I appreciate her help with proofreading and EPR experiments. Thanks to John Scollard for all of his computer wizardry and Chris Levy for keeping me honest in the Hogs homerun race. Ola Wendt and Matt Holtcamp were excellent postdocs who were always there to answer a tough question. Dario Veghini provided me with lots of inspirational pep talks about science and kept me from getting lost when running in San Marino. I would also like to thank some other "Hogs": Jeff Yoder, Antek Wong-Foy, Andy Kiely, Endy Min, Cory Nelson and Shigenobu Miyake.

Several people outside of the Bercaw group have been very helpful throughout my time at Caltech. I would like to acknowledge the efforts of Nathan Dalleska and Peter Green with the GC/MS experiments described in Chapter 5. I would also like to thank "Slick" Rick Gerhart, Dian Buchness, Steve Gould, Chris Smith and Pat Anderson for attempting to keep the place sane and running smoothly.

I am also indebted to the Caltech X-ray crystallographic facility for all of my structural data. In addition to being a fine outfielder and having a nose for a free lunch, Larry Henling mounted all of my crystals, no matter how poor in quality, and managed to get data from them. Mike Day, Dick Marsh and Bill Schaefer were also helpful in solving structures and providing a quiet place for me to work on my thesis.

I also would like to thank a very special group of people who made an enormous contribution to my Caltech experience. "Michigan" Jim Brauher has been a great training partner and an even better friend; "Big" Don Thomas and Frank "The Chief" Camacho for keeping me in my place but at the same time being great role models. Kathy Miller has been my San Marino Mom for the past four years and I will never forget cruisin' on the freeway in Porsche. "Chicago" Paul Kulesa, Richard Maya, Carlo Cossu and Gerard O'Rielly were always quick to make me laugh, even though it was usually at my expense. Carl Foote has been a great basketball teammate and source of 70's music trivia. I would also like to thank Jim Anderson and Miguel Francis for always keepin' it real. I will never forget the "Friday Night Feasts" and the great times we all had together.

Finally, I would like to thank my parents, Joseph and Carol Chirik, and my brother, Joseph Chirik, for being so supportive throughout the years. You guys are the best!

Abstract

The preparation of a series of unlinked and *ansa*-zirconocene dihydride complexes from hydrogenation of the corresponding dimethyl complexes is described. In general, sterically demanding ligands promote formation of monomeric dihydride complexes. The *ansa*-zirconocene dihydride, *meso*-$[Me_2Si(\eta^5\text{-}C_5H_3\text{-}3\text{-}CMe_3)_2ZrH_2]_2$, has been characterized by X-ray diffraction. The monomeric, *ansa*-zirconocene, *rac*-$Me_2Si(\eta^5\text{-}C_5H_2\text{-}2\text{-}SiMe_3\text{-}4\text{-}CMe_3)_2ZrH_2$ ($BpZrH_2$) undergoes thermal reductive elimination of dihydrogen forming, $BpZr(\mu_2\text{-}N_2)ZrBp$ which displays a side-on coordination of the dinitrogen fragment.

Rates of olefin insertion and β-hydrogen elimination have been measured for a series of zirconocene and hafnocene dihydride and alkyl hydride complexes. In both cases, increased cyclopentadienyl substitution slows the rate of insertion or elimination, although the former is more sensitive to steric perturbations. From these studies, the transition state for olefin insertion/β-hydrogen elimination has been established. Equilibration of zirconocene isobutyl hydride complexes with the corresponding normal butyl hydrides has allowed for determination of the relative ground state energies of the two alkyl hydride metallocenes. These data in combination with the activation barriers for β-hydrogen elimination have allowed for delineation of ground and transition state effects in these processes. Likewise, ancillary ligand effects on the rate of alkyl isomerization have also been examined with a series of isotopically labeled zirconocene alkyl complexes. In general, increasing the substitution on the cyclopentadienyl rings has little effect on the rates of isomerization.

The preparation of *ansa*-tantalocene olefin-hydride complexes is described. These complexes serve as models for the transition state for olefin insertion in the corresponding group IV metallocene olefin polymerization catalysts. Preparation of the C_1-symmetric ethylene hydride complex, $Me_2Si(\eta^5\text{-}C_5H_4)(\eta^5\text{-}C_5H_3\text{-}3\text{-}CHMe_2)Ta(\eta^2\text{-}C_2H_2)(H)$ affords predominantly (~95 %) of one isomer, where the ethylene ligand is coordinated on the side of the wedge away from the isopropyl substituent. Similar results have been obtained with related tantalocene propylene-hydride and styrene-hydride complexes, the latter being characterized by X-ray diffraction. Additionally, several singly and doubly

bridged tantalocene trimethyl complexes have been prepared and characterized by X-ray diffraction.

Ancillary Ligand Effects on Fundamental Transformations in Metallocene Catalyzed Olefin Polymerization

TABLE OF CONTENTS

List of Figures

Chapter 1:

Chapter 2:

Chapter 3:

Chapter 4:

Chapter 5:

Chapter 6:

List of Tables

Chapter 1:

Chapter 3:

Chapter 5:

Chapter 6:

Chapter 1

Preparation and Characterization of Monomeric and Dimeric Group IV Metallocene Dihydrides Having Alkyl-Substituted Cyclopentadienyl Ligands.*

Abstract

A series of zirconocene dihydride complexes of the general form, $[(R_nCp)_2ZrH_2]_n$ having substituted cyclopentadienyl ligands has been prepared by hydrogenation of the corresponding dimethyl complexes. The most sterically crowded members ($Cp^*(\eta^5\text{-}C_5HMe_4)ZrH_2$, ($Cp^* = \eta^5\text{-}C_5H_5$)), $Cp^*\{\eta^5\text{-}C_5H_3\text{-}1,3\text{-}(CMe_3)_2\}ZrH_2$ and $\{\eta^5\text{-}C_5H_3\text{-}1,3\text{-}(CMe_3)_2\}_2ZrH_2$) are monomeric; those less crowded members ($[Cp^*\{\eta^5\text{-}C_5H_4(CMe_3)\}ZrH_2]_2$, $[Cp^*(THI)ZrH_2]_2$ (THI = η^5-tetrahydroindenyl) and $[\{\eta^5\text{-}C_5H_3\text{-}1,3\text{-}(CHMe_2)_2\}_2ZrH_2]_2$) are predominantly dimeric in benzene solution. $Cp^*\{\eta^5\text{-}C_5H_3\text{-}1,3\text{-}(CHMe_2)_2\}ZrH_2$ and $(\eta^5\text{-}C_5HMe_4)_2ZrH_2$ exist as equilibrium mixtures of monomer and dimer in benzene solution. The hydride ligands rapidly exchange with D_2, affording the dideuteride complexes. Deuterium incorporation into some of the substituents on the cyclopentadienyl rings of the monomeric dihydride complexes is also observed. The X-ray structures of $Cp^*_2HfH_2$, $Cp^*\{\eta^5\text{-}C_5H_4(CMe_3)\}ZrCl_2$, $Cp^*\{\eta^5\text{-}C_5H_3\text{-}1,3\text{-}(CHMe_2)_2\}ZrCl_2$ and $\{\eta^5\text{-}C_5H_3\text{-}1,3\text{-}(CMe_3)_2\}_2ZrCl_2$ are reported.

Introduction

Transition metal hydrides constitute an important class of compounds due to their prevalence in both catalytic and stoichiometric processes.[1] Hydride complexes of group 4 metallocenes have been implicated as catalysts and as important intermediates in olefin hydrogenation[2] and polymerization reactions.[3] Despite their widespread utility, the molecularity and structures of zirconocene and hafnocene dihydrides have not been systematically investigated.

Early reports of zirconocene dihydride complexes concern the preparation of simple alkyl substituted *bis*(cyclopentadienyl) complexes of the general form, $\{(\eta^5\text{-}C_5H_4R)_2ZrH_2\}_n$ (R = H, Me, $CHMe_2$, CMe_3; $n \geq 2$), obtained via hydrogenation of the corresponding dimethyl complexes at elevated temperature (80 °C) and pressure (60 atm).[4] *Bis*(tetrahydroindenyl)zirconium dihydride dimer has also been prepared via hydrogenation of the corresponding *bis*(indenyl)zirconium dimethyl complex as a result of hydrogenation of both the zirconium methyl bonds as well as the benzo groups of the indenyl ligands.[5] Zirconocene dihydrides, $[(\eta^5\text{-}C_5H_4CMe_3)_2ZrH_2]_2$ and $[(\eta^5\text{-}C_5H_4SiMe_3)_2ZrH_2]_2$ have been prepared via an alternate route, reduction of metallocene dichloride complexes with borohydride or aluminohydride reagents.[6,7]

More recently, *ansa*-zirconocene dihydride complexes have been synthesized. Buchwald[8] has reported the synthesis of [*rac*-(EBTHI)$MH_2]_2$ (EBTHI = ethylene-1,2-*bis*-(η^5-tetrahydroindenyl); M = Zr, Hf) via reduction of the corresponding dichloride complexes with $NaBEt_3H$. Royo[9] has used similar methodology to prepare dimeric, doubly [$SiMe_2$]-bridged $[(Me_2Si)_2(\eta^5\text{-}C_5H_3)_2MH_2]_2$ (M = Zr, Hf). Parkin has prepared $[OpZrH_2]_2$ (Op = $Me_2Si(\eta^5\text{-}C_5Me_4)_2$) via hydrogenation of the dimethyl complex at elevated temperatures in cyclohexane solution.[10] In all cases, stable dimeric zirconocene dihydrides resulted, with no reports of detectable amounts of the monomer in solution, although facile interconversion of $[OpZrH_2]_2$ with monomer was implicated by its variable temperature ^1H NMR behavior.[10]

Very few monomeric zirconocene and hafnocene dihydride complexes have been prepared and isolated. Like their group 3 counterparts,[11] most group

4 metallocene hydride complexes are subject to dimerization through formation of relatively robust 3 center, 2 electron hydride bridges. In fact, to our knowledge, the only monomeric zirconocene and hafnocene dihydride complexes prepared to date are those employing two bulky pentamethylcyclopentadienyl (Cp*) ligands, $Cp^*_2MH_2$.[12] Elucidation of the effects of ligand array on the position of the monomer-dimer equilibrium has not been established. In this report we describe the preparation and solution behavior of a variety of new zirconocene dihydride complexes, and through this study explore some of the factors that govern the monomer-dimer equilibrium. The H/D exchange reactions of these hydride complexes with deuterium are described. We also present the results of X-ray crystal structure determinations for monomeric $Cp^*_2HfH_2$, together with some representative precursors, $Cp^*\{\eta^5\text{-}C_5H_4(CMe_3)\}ZrCl_2$, $Cp^*\{\eta^5\text{-}C_5H_3\text{-}1,3\text{-}(CHMe_2)_2\}ZrCl_2$ and $\{\eta^5\text{-}C_5H_3\text{-}1,3\text{-}(CMe_3)_2\}_2ZrCl_2$.

Results and Discussion

Synthesis and Solution Behavior of Zirconocene Dihydrides.

Preparations of "mixed ring" zirconocene dichloride complexes have been carried out in a straightforward manner by addition of the corresponding lithiocyclopentadienide to readily available Cp^*ZrCl_3.[13] Thus, $Cp^*\{\eta^5\text{-}C_5H_4(CMe_3)\}ZrCl_2$[14] (**1**), $Cp^*\{\eta^5\text{-}C_5H_3\text{-}1,3\text{-}(CMe_3)_2\}ZrCl_2$ (**2**), $Cp^*\{\eta^5\text{-}C_5H_3\text{-}1,3\text{-}(CHMe_2)_2\}ZrCl_2$ (**3**), $Cp^*(Ind)ZrCl_2$ (**4**) (Ind = $(\eta^5\text{-}C_9H_7)$), and $Cp^*(\eta^5\text{-}C_5HMe_4)ZrCl_2$ (**5**) have been prepared in yields ranging from 60 - 83%. Additionally, $\{\eta^5\text{-}C_5H_3\text{-}1,3\text{-}(CMe_3)_2\}_2ZrCl_2$ (**6**) and $\{\eta^5\text{-}C_5H_3\text{-}1,3\text{-}(CHMe_2)_2\}_2ZrCl_2$ (**7**) have been obtained in moderate yield from the reaction of two equivalents of the lithiocyclopentadienide with $ZrCl_4$ in refluxing toluene. All of the dichloride complexes are air stable and can be purified either by recrystallization or sublimation at 140 °C (10^{-4} Torr).

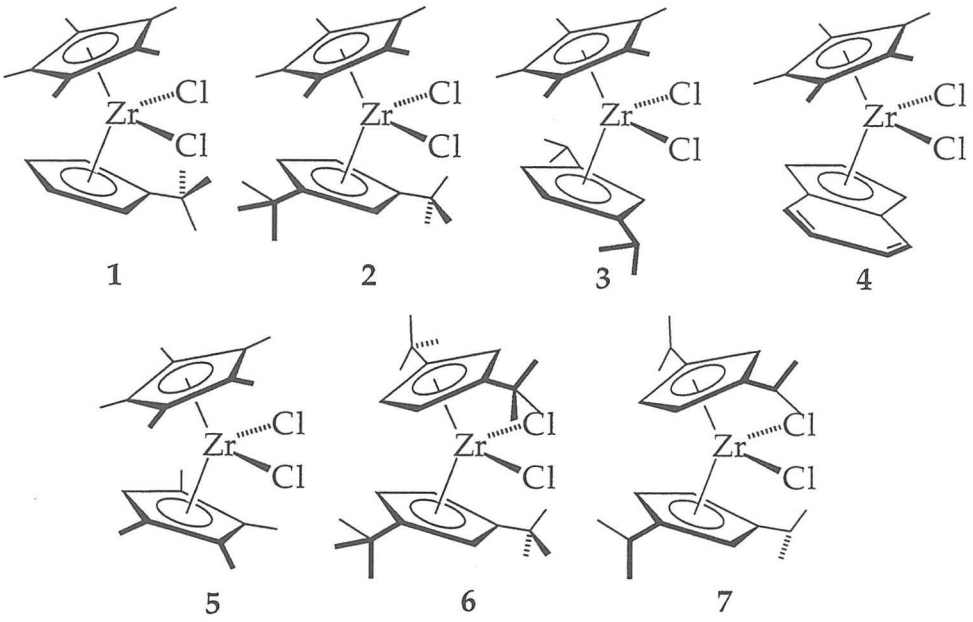

Figure 1. A series of zirconocene dichloride complexes.

Single crystals of **1**, **3** and **6** were obtained from toluene solution and their structures were established by X-ray diffraction. As shown in Figures 2 - 4 the cyclopentadienyl substituents arrange themselves to avoid both the narrow ("back") portion of the zirconocene wedge and the large chloride ligands. Thus, the *tert*-butyl substituent of **1** is situated slightly off the center of the wedge with [CMe_3] methyl groups arranged to minimize interactions with the cyclopentadienyl [CH]'s and the chloride ligands; the isopropyl groups for **3** are lateral, related by a mirror plane that bisects the Cl-Zr-Cl plane, with one [C-CH_3] bond oriented perpendicular to the cyclopentadienyl plane and the other directed into the wedge away from the chlorine atom; the four *tert*-butyl groups for **6** are pairwise related by a crystallographic two-fold symmetry axis that bisects the Cl-Zr-Cl angle.

During the course of our investigations, we have obtained X-ray quality crystals of $Cp^*_2HfH_2$, which has been prepared via reduction of the dichloride complex with two equivalents of *n*-BuLi under an atmosphere of dihydrogen.[12b] To our knowledge, this is the first monomeric group IV metallocene dihydride to be characterized crystallographically. The crystals obtained for the diffraction experiment were twinned, and as a result location of the hydride ligands was not possible. Despite the complications of crystal twinning, we are confident that the structure is indeed the monomeric dihydride as shown in Figure 5. It is

noteworthy that, presumably due to the small size of the hydride ligands, the two (η^5-C_5Me_5) ligands assume a very "closed" metallocene structure. As can be seen from the data in Table 1, the centroid-Hf-centroid (θ = 144.1(2) and 145.0(2)°) and cyclopentadienyl normal-cyclopentadienyl normal (α = 145.2(2) and 145.9(2)°) angles for the two independent molecules in the unit cell are much larger than those for **1**, **3**, **6** or other hafnocene dichloride complexes that have been structurally characterized (θ = 129 to 131°; α = *ca.* 121 to 128°). Chloride ligands thus exert an unfavorable steric repulsion on those ring carbons most out of the metallocene wedge, resulting in smaller values for θ and α, and larger differences between these two angles.

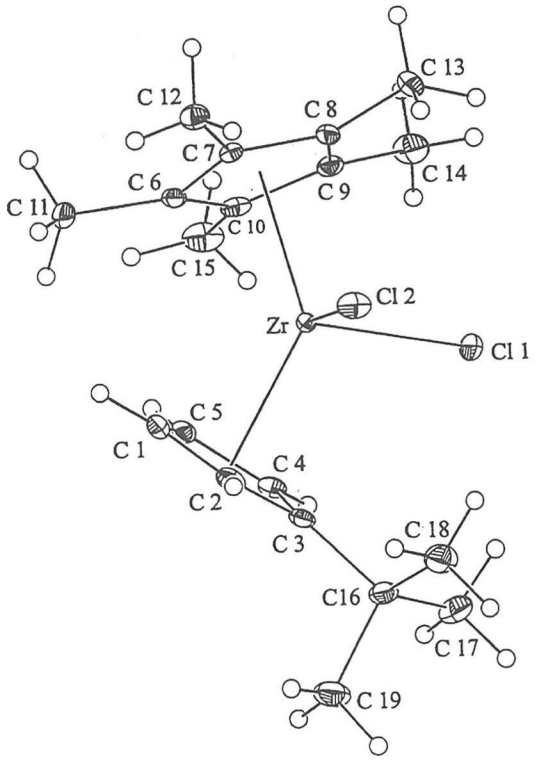

Figure 2. Molecular structure of **1** with selected atoms labeled (50% probability ellipsoids).

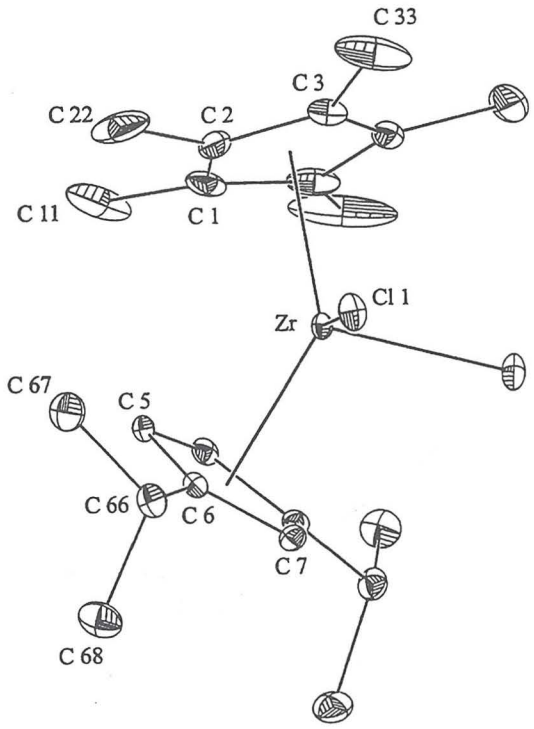

Figure 3. Molecular structure of **3** with selected atoms labeled (50% probability ellipsoids; hydrogen atoms omitted for clarity).

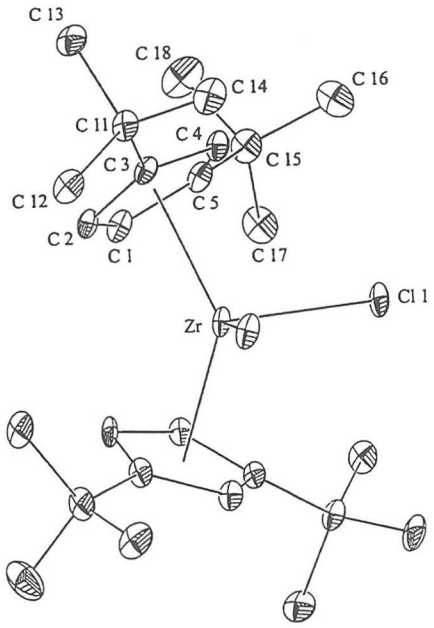

Figure 4. Molecular structure of **6** with selected atoms labeled (50% probability ellipsoids; hydrogen atoms omitted for clarity).

Compound[a]	θ (°)	α (°)
$Cp^*_2HfH_2$	144.1(2)	145.2(2)
	145.0(2)	145.9(2)
$Cp^*\{\eta^5\text{-}C_5H_4(CMe_3)\}ZrCl_2$ (**1**)	130.68(1)	124.73(1)
$Cp^*\{\eta^5\text{-}C_5H_3\text{-}1,3\text{-}(CHMe_2)_2\}ZrCl_2$ (**3**)	131.49(2)	126.87(8)
$\{\eta^5\text{-}C_5H_3\text{-}1,3\text{-}(CMe_3)_2\}_2ZrCl_2$ (**6**)	129.7(1)	121.1(1)
Cp_2HfCl_2[30]	129.23	126.54
	129.14	127.60
$Cp^*CpHfCl_2$[31]	130.59	126.70
$(C_5H_4\text{-}CH_2CH_3)_2HfCl_2$[32]	129.96	125.71

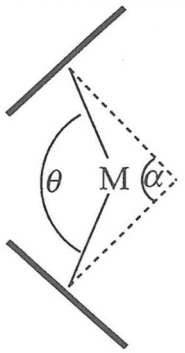

[a]A search of the Cambridge Structural Database produced 3 hafnocene dichloride complexes. Allen, F.H.; Davies, J.E.; Galloy, J.J.; Johnson, O.; Kennard, O.; Macrae, C.F.; Mitchell, E.M.; Smith, J.M.; Watson, D.G. *J. Chem. Info. Comp. Sci.* **1991**, *31*, 187.

Table 1. Centroid-M-Centroid (Θ) and Cyclopentadienyl Normal-Cyclopentadienyl Normal (α) Angles for $Cp^*_2HfH_2$, **1**, **3**, **6** and related hafnocene dichlorides.

Treatment of the metallocene dichloride complexes with two equivalents of methyllithium in diethyl ether affords the zirconocene dimethyl complexes in good yields (eq. 1).

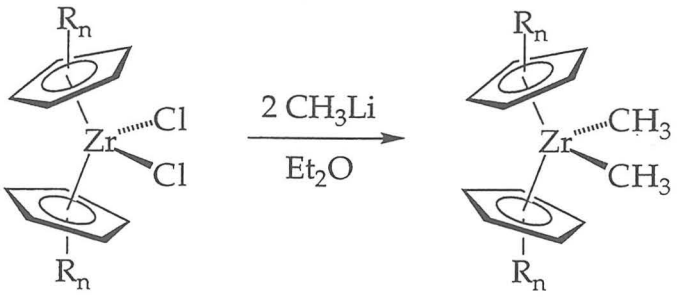

(1)

The dimethyl complexes are air sensitive and are readily soluble in aromatic, hydrocarbon and ethereal solvents. For each compound, a diagnostic Zr-CH_3 resonance in the ^{1}H NMR spectrum is observed slightly upfield of $SiMe_4$ (see Experimental Section). Purification of these compounds can be achieved either by recrystallization from cold petroleum ether or by sublimation at 80 °C (10^{-4} Torr).

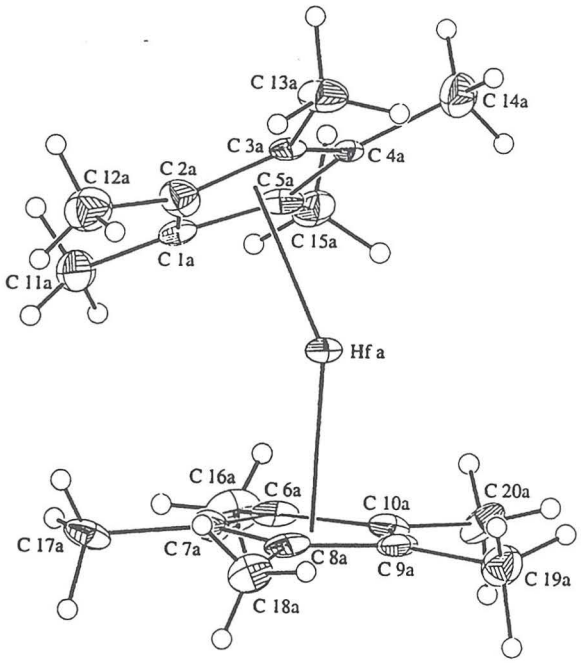

Figure 5. Molecular structure of $(\eta^5\text{-}C_5Me_5)_2HfH_2$ (50% probability ellipsoids).

Hydrogenation of the entire series of dimethylzirconcenes proceeds readily and quantitatively (^{1}H NMR), even at room temperature and 1 atm H_2, unlike the more forcing conditions previously reported for the preparation of zirconocene dihydrides from the dimethyl derivatives (eq. 2).

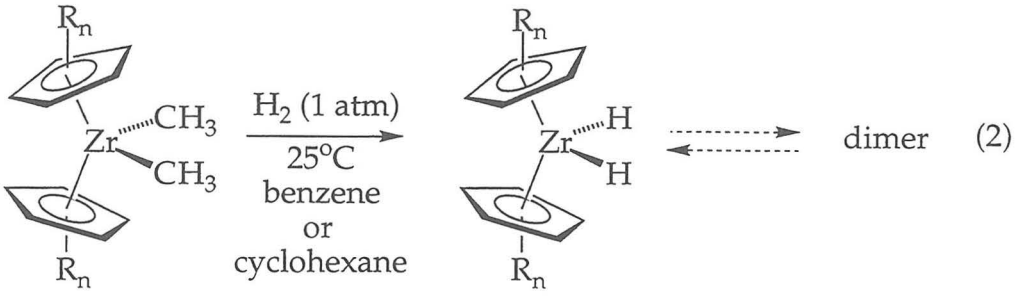

(2)

The resulting highly air sensitive dihydride complexes are soluble in aromatic solvents. In general, the dimeric dihydrides are less soluble than the monomeric dihydrides. This procedure provides an attractive alternate route to previously reported $[Cp^*CpZrH_2]_2$ (Cp = (η^5-C_5H_5)).[13]

Hydrogenation of $Cp^*(Ind)ZrMe_2$ results in quantitative formation of $[Cp^*(THI)ZrH_2]_2$ (**11**), as a result of σ bond metathesis reactions of the Zr-CH_3 with H_2 and subsequent hydrogenation of the indenyl ring. This finding is similar to that reported for the hydrogenation of *bis*(indenyl)zirconium dimethyl.[5] Monitoring the reaction of $Cp^*(Ind)ZrMe_2$ with H_2 by ^1H NMR reveals the intermediacy of $Cp^*(THI)ZrMe_2$, suggesting that the zirconocene dihydride that is generated in the early stages of the reaction serves as a catalyst for hydrogenation of the benzo groups of both starting $Cp^*(Ind)ZrMe_2$ and initially formed $Cp^*(Ind)ZrH_2$. This suggestion is further supported by the qualitative rate enhancement for final conversion to **11** that is observed when $Cp^*(Ind)ZrMe_2$ is hydrogenated in the presence of **11**. Moreover, **11** also catalyzes the hydrogenation of dibenzoferrocene[15] to *bis*(tetrahydroindenyl)iron.[16]

Proton NMR spectroscopy has proven particularly useful for the characterization of the new zirconocene dihydride complexes.[5] The number of zirconium hydride resonances observed and their chemical shifts are useful in determining the molecularity of the dihydride species in solution. Monomeric zirconium dihydrides exhibit a single downfield resonance ($\delta \sim 7$ to 8), whereas dimeric dihydrides display separate resonances for terminal ($\delta \sim 4$ to 5) and bridging hydrides ($\delta \sim 1$ to -1). Solution molecular weights for the new dihydrides and ^1H NMR determined molecularities, along with those for

previously reported $Cp^*_2ZrH_2$,[12a] $[Cp^*(\eta^5\text{-}C_5H_5)ZrH_2]_2$,[13] and $[Cp^*(\eta^5\text{-}C_5H_2\text{-}1,2,4\text{-}Me_3)ZrH_2]_2$[13] are given in Table 2.

Compound	MW[a]	[Zr] (M)	molecularity in solution[b]
$[Cp^*CpZrH_2]_2$	606 (294)	ref. 13	dimeric
8	675 (348)	0.013	dimeric
11	670 (344)	0.040	dimeric
14	773 (392)	0.014	dimeric
10	740 (369)	0.049	monomer and dimer observed
15	564 (335)	0.041	monomer and dimer observed
9	446 (406)	0.044	monomeric
$Cp^*(\eta^5\text{-}C_5H_2\text{-}1,2,4\text{-}Me_3)ZrH_2$	342 (336)	ref. 13	monomeric
13	480 (448)	0.033	monomeric
12	346 (349)	0.029	monomeric
$Cp^*_2ZrH_2$	402 (394)	ref. 12a	monomeric

[a] Solution molecular weights determined by ebulliometry at indicated concentration in benzene-d_6 (calculated MW for monomer) at 296K. Errors in molecular weights are estimated as +/-20 %.

[b] Molecularity at 296K as established by ^{1}H NMR in benzene-d_6 or toluene-d_8 (see text).

Table 2. Molecular weights for zirconocene dihydrides and molecularity indicated by ^{1}H NMR spectroscopy.

In all cases the measured molecular weights and ^{1}H NMR data are in agreement. Thus, for example, the molecular weight indicates that $Cp^*_2ZrH_2$ is monomeric and accordingly a single resonance at δ 7.46 is observed at room temperature in benzene-d_6 for the equivalent [ZrH_2]. Similarly, monomeric $Cp^*(\eta^5\text{-}C_5HMe_4)ZrH_2$ (**12**), $Cp^*\{\eta^5\text{-}C_5H_3\text{-}1,3\text{-}(CMe_3)_2\}ZrH_2$ (**9**) and $\{\eta^5\text{-}C_5H_3\text{-}1,3\text{-}(CMe_3)_2\}_2ZrH_2$ (**13**) exhibit singlets at δ 7.45, δ 7.09 and δ 7.36, respectively, for their [ZrH_2] resonances.

The other dihydride complexes exhibit ^{1}H NMR spectra that are quite temperature dependent, suggesting equilibria between at least two forms. Thus, the 500 MHz spectrum for $[Cp^*CpZrH_2]_2$ at room temperature displays no resonances attributable to $[ZrH_2]$. Cooling a sample to 250K in toluene-d_8 solution allows for observation of signals for terminal (δ 4.26 (br, multiplet)) and bridging (δ -2.65 (br, multiplet) hydrides and one set of cyclopentadienyl resonances (δ 5.72 (η^5-C_5H_5) and δ 1.93 {η^5-$C_5(CH_3)_5$}). Somewhat unexpectedly, further cooling to 225K reveals two sets of hydride signals (δ 4.31 multiplet) and δ 4.14 (multiplet); δ -0.10 (multiplet) and δ -2.68 (br, multiplet)) and two sets of cyclopentadienyl resonances (δ 5.77 (major) and δ 5.65 (minor); δ 2.00 (minor) and δ 1.95 (major); [major]:[minor] ≈ 3:1). These data suggest that above 225K *two* dimeric hydride isomers are in rapid equilibrium, presumably the cis and trans isomers via monomeric $[Cp^*CpZrH_2]$ as shown in Figure 6.

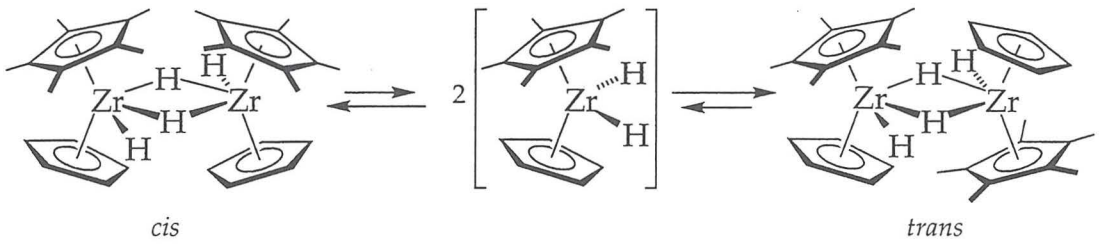

Figure 6. Isomers of $[Cp^*CpZrH_2]_2$.

Considering the unfavorable steric interactions between cyclopentadienyl ligands across the $[HZr(\mu_2\text{-}H)_2ZrH]$ units, we tentatively assign the major isomer as *trans* (Figure 6).

The related complex $[Cp^*(\eta^5\text{-}C_5H_4\text{-}CMe_3)ZrH_2]_2$ (8) exhibits very similar behavior, although the two isomeric dihydride dimers are observable at room temperature in approximately equal amounts. Signals for the terminal hydrides are observed at δ 4.08 (br, multiplet) and δ 3.90 (br, multiplet) whereas the bridging hydrides appear at δ -0.76 and δ -2.56. Heating the sample in cyclohexane-d_{12} to 340 K results in coalescense of the peaks attributable to protons of the Cp* (δ 1.97) and CMe_3 (δ 1.38) groups. Curiously, the more sterically congested (8) undergoes slower isomer interconversion in comparison to $[Cp^*CpZrH_2]_2$.

Variable temperature NMR studies on $[Cp^*(\eta^5\text{-}C_5H_3\text{-}1,3\text{-}CHMe_2)ZrH_2]_2$ (**10**) reveal yet another dynamic equilibrium for this complex. At room temperature the 500 MHz NMR spectrum displays a single set of ligand resonances in addition to a broad signal centered at δ 4.06 for the zirconium hydride resonance, intermediate between those found for the monomeric and dimeric chemical shift values. We interpret a shift in this range as a weighted average between monomeric and dimeric dihydrides that are in rapid equilibrium. Cooling a sample of **10** ([Zr] = 0.049 M) to 200 K in toluene-d_8 allows for observation of roughly equal amounts of two isomeric dihydride dimers. Terminal hydride resonances are observed at δ 4.20 and δ 3.92 whereas bridging hydrides appear at δ -1.14 and δ -1.25. Warming the sample to 240 K results in coalescence of the $CHMe_2$ peaks (δ = 1.39) as well as the terminal hydrides (δ = 4.02). At 250 K, the signals attributable to the protons of the Cp* ligands for the two isomers coalesce at δ 2.05. Continued heating of a sample of **10** above room temperature results in a gradual shift of the zirconium hydride resonance downfield, implicating increased concentration of the monomeric dihydride at higher temperatures. At 310 K, the zirconium hydride appears as a broad singlet centered at δ = 5.45 and at 340 K the resonance shifts to δ = 6.70. At 360 K, the hydride resonance approaches its maximum value of δ = 6.90, and the value of the chemical shift of this peak does not change with further heating of the sample (T = 380 K). At these temperatures, we propose that monomeric **10** is the predominant species in solution (Figure 7).

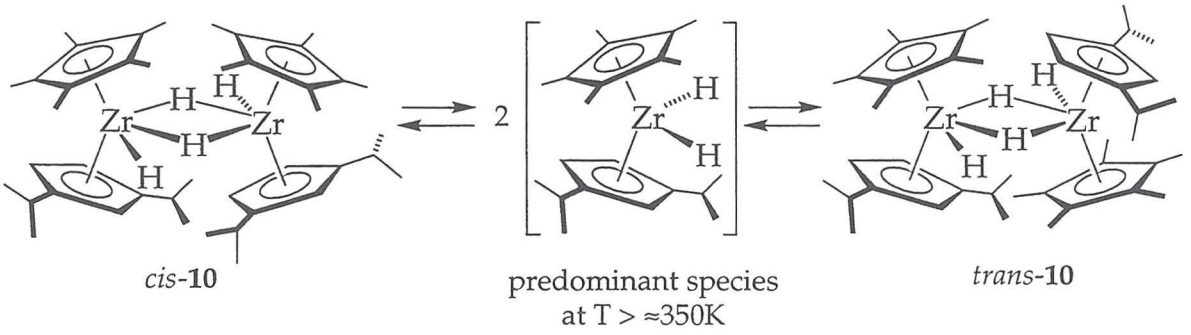

cis-**10** predominant species at T > ≈350K *trans*-**10**

Figure 7. Monomer-dimer equilibria for **10**.

Variable temperature NMR data for $(\eta^5\text{-}C_5Me_4H)_2ZrH_2$ (**15**) also reveal significant amounts of both monomer and dimer in rapid equilibrium. Thus, the 500 MHz NMR spectrum at 296 K ([Zr] = 0.041 M) displays a very broad singlet for the zirconium hydride resonance centered at δ = 2.80. Warming of the

sample results in both a sharpening of the zirconium hydride resonance as well as a shift downfield. As with **10**, the spectrum of **15** at 380 K in benzene-d_6 solution displays a zirconium hydride resonance at $\delta = 7.11$, implicating the presence of a monomeric zirconocene hydride. At temperatures between 296 K and 380 K, the chemical shift gradually shifts downfield from $\delta = 2.80$ to $\delta = 7.11$. Perhaps the most intriguing feature of **15** is its ability to form hydride bridges and hence a dimer, albeit only at low temperatures. Considering that $Cp^*_2ZrH_2$ and **12** are monomeric, it is quite remarkable that removal of one methyl group from the other (η^5-C_5Me_5) ligand of **12** is sufficient to permit formation of a dimeric **15**. Clearly, there is just enough steric protection to dimer formation for both $Cp^*_2ZrH_2$ and **12**.

H/D exchange reactions for zirconocene dihydrides with D_2. When each member of the series of zirconocene dihydrides is exposed to one atmosphere of dideuterium in benzene solution, rapid exchange of hydride ligands is observed (*e. g.*, equation 3).

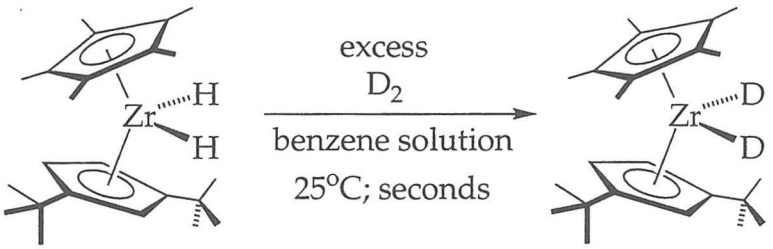

9 **9-d_2** (3)

The rate of exchange is sufficiently rapid to be observed by ^{1}H NMR. Exposure of a benzene-d_6 solution of **9** to one atmosphere of H_2 results in broadening and upfield shifting of the [ZrH_2] resonance (toward that for dissolved H_2); no resonance for H_2 is observed, indicative of exchange on the ^{1}H NMR time scale.

Treatment of dimeric **8** and **11** with dideuterium results in rapid exchange of deuterium into both bridging and terminal hydride positions at room temperature (*e. g.*, equation 4).

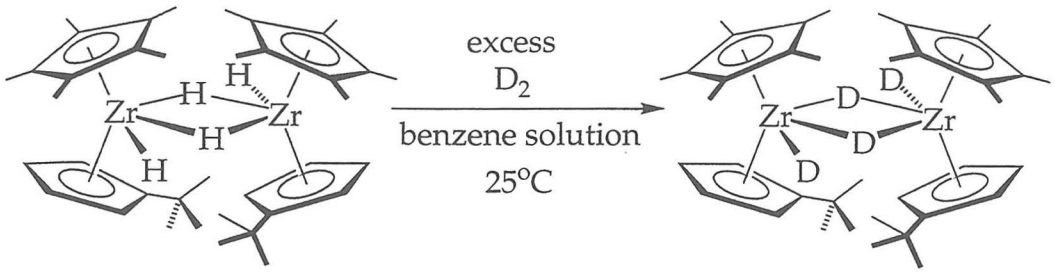

(4)

Although we are unable to rule out direct reaction of D_2 with the terminal and/or bridging hydride ligands of the dimers, rapid exchange of both bridging and terminal hydride positions of the dimeric complexes suggests a facile monomer-dimer equilibrium (consistent with the variable temperature ^1H NMR studies above), allowing for rapid incorporation of deuterium into both hydride positions.

Deuterium incorporation into the C-H positions of the cyclopentadienyl ligands is much slower than for the hydride positions, and H/D exchange occurs preferentially only with certain of the C-H bonds of the monomeric dihydride complexes. Thus, reaction of monomeric $Cp^*_2ZrH_2$ with D_2 at 23 °C results in gradual incorporation of deuterium into the C-H positions of the two (η^5-C_5Me_5) ligands over a period of 12 hours. Benzene-d_6 solutions of $Cp^*(\eta^5\text{-}C_5HMe_4)ZrH_2$ (**12**) under D_2 result in rapid exchange of the two hydride positions at room temperature, and over the course of several hours at 25 °C, selective deuteration of the Cp* ligands and two of the methyl groups of the tetramethylcyclopentadienyl ligand occurs, the ones that appear at δ 1.81 in the ^1H NMR spectrum; the latter is approximately five times faster than the former. NOE difference spectroscopy reveals that these are the 1,4 methyl groups of the (η^5-C_5Me_4H) ligand. Thus, irradiation of the methyl groups at δ = 1.81 results in an NOE enhancement of the (η^5-$C_5Me_4\mathit{H}$) resonance, while irradiation of the downfield methyl groups (δ = 2.45) does not produce a detectable NOE enhancement. Deuteration of the two other methyl groups of the (η^5-C_5Me_4H) ligand is eventually observed (^2H NMR), although this exchange occurs at a much slower rate, requiring several days at room temperature or several hours at 80 °C. Similar observations have been made by Parkin, *et al.*: exposure of $[\{Me_2Si(\eta^5\text{-}C_5Me_4)_2\}ZrH_2]_2$ to D_2 results in rapid exchange of the hydride positions and slower deuterium incorporation preferentially into the methyl

groups α to the [$SiMe_2$] linker.[17] As might be expected, the X-ray structure of $(\eta^5\text{-}C_5HMe_4)_2ZrCl_2$ reveals that the less sterically demanding [C-H] groups are in the narrow portion of the zirconocene wedge.[18] Taken together these observations suggest that the methyl groups that are most accessible for formation of "tuck-in" intermediates are those directed toward the side of the metallocene wedge in the ligand array (eq. 5).

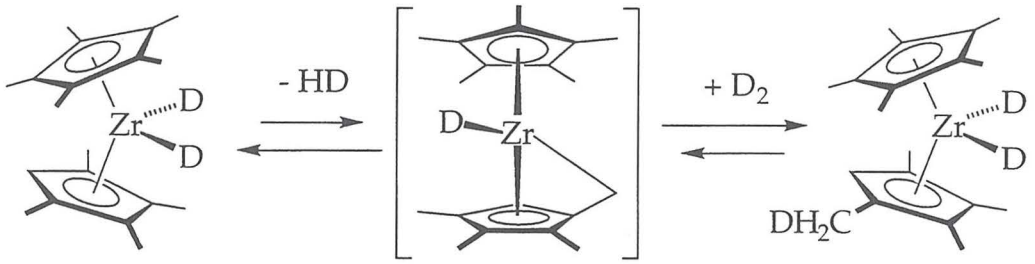

12-d_2 **12**-d_3 (5)

The remarkably exacting orientations for metallation of a methyl-substituted cyclopentadienyl ligand is perhaps most evident in the H/D exchange reactions for $Cp^*\{\eta^5\text{-}C_5H_3\text{-}1,3\text{-}(CMe_3)_2\}ZrH_2$ (**9**). Treatment of **9** with D_2 at 23 °C results in slow exchange with the C-H positions of the [CMe_3] groups over a period of several hours. Interestingly, no deuterium incorporation into the Cp* ligand (or remaining three C-H bonds of the $\{\eta^5\text{-}C_5H_3\text{-}1,3\text{-}(CMe_3)_2\}$ ligand) is observed under these conditions (eq. 6).

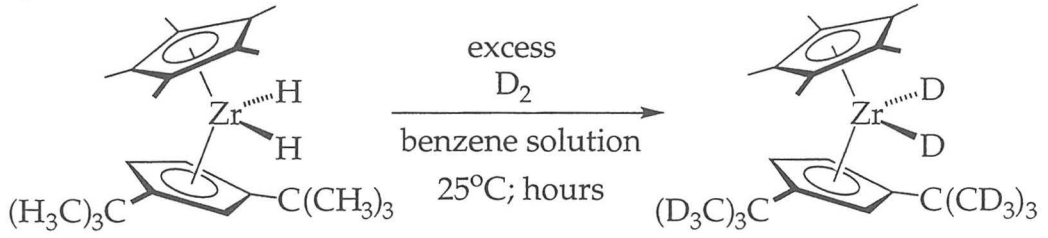

9 **9**-d_{20} (6)

Since no "tuck-in" derivative resulting from metallation of a [CMe_3] builds up to ^1H NMR detectable concentrations under these conditions, we conclude that the two *tert*-butyl substituents of the other cyclopentadienyl ligand must constrain the Cp* ligand in orientations unsuited to metallation of a methyl group.

Treatment of dimeric [Cp*{η^5-C_5H_3-1,3-$(CHMe_2)_2$}ZrH_2]$_2$ (**10**) or [(η^5-C_5HMe_4)$_2ZrH_2$]$_2$ (**15**) with dideuterium in benzene-d_6 rapidly leads to exchange of the hydride positions, but not the methyl groups of the Cp*, isopropyl substituents or (η^5-C_5HMe_4) ligands, even after several days at room temperature.[19] This large reduction in rate likely reflects the requirement that formation of the "tuck-in" intermediates occurs from the monomer, which is present in only very low concentrations for the (predominantly) dimeric complexes.

Conclusions

A series of zirconocene dihydride complexes of the general form, [(R_nCp)$_2ZrH_2$]$_x$, having substituted cyclopentadienyl ligands has been prepared by hydrogenation of the corresponding dimethyl complexes. The molecularity of these compounds in solution varies with the size and/or number of alkyl substituents on the cyclopentadienyl rings. The most sterically crowded members of the series: Cp*{η^5-C_5H_3-1,3-$(CMe_3)_2$}ZrH_2 (**9**), Cp*(η^5-C_5HMe_4)ZrH_2 (**12**) and {η^5-C_5H_3-1,3-$(CMe_3)_2$}$_2ZrH_2$ (**13**) are monomeric; the less crowded members: [Cp*(η^5-C_5H_4-CMe_3)ZrH_2]$_2$ (**8**), [Cp*(THI)ZrH_2]$_2$ (**11**) and [{η^5-C_5H_3-1,3-$(CHMe_2)_2$}$_2ZrH_2$]$_2$ (**14**) are predominantly dimeric in solution, whereas [Cp*{η^5-C_5H_3-1,3-$(CHMe_2)_2$}ZrH_2]$_2$ (**10**) and [(η^5-C_5HMe_4)$_2ZrH_2$]$_2$ (**15**) form equilibrium mixtures of both monomers and dimers, the predominant form depending on temperature and concentration. Variable temperature NMR studies on the dimeric dihydride complexes having mixed cyclopentadienyl ligands, *e. g.*, **9** and even [Cp*CpZrH_2]$_2$, reveal comparable amounts of two different dimeric hydrides, presumably cis and trans isomers. It is likely that unfavorable steric interactions in the cis isomers are relieved by twisting of the two zirconocene units such that their "equatorial planes" are not coincident. Such twisting has been established for an *ansa* titanocene monohydride[20] and for *ansa* yttrocene hydrides.[21]

Whether monomeric or dimeric the hydride ligands of these dihydride complexes undergo rapid exchange with D_2. For the monomeric members of the series, further H/D exchange leads to incorporation of deuterium into some of the alkyl substituents of the cyclopentadienyl ligands. The likely mechanism involves the monomeric dihydride undergoing intramolecular σ bond

metathesis between an alkyl C-H bond and a Zr-H bond, leading to "tuck-in" intermediates. The relative rates for H/D exchange of methyl substituents indicate this process has a strong orientational preference for the back of the zirconcene wedge. *Tert*-butyl groups undergo H/D exchange at a similar rate. Metallation of these C-H bonds also likely involves a reversible, intramolecular σ bond metathesis process analogous to that reported earlier for $(\eta^5\text{-}C_5Me_4R)_2ZrH_2$ (R = CH_3, CH_2CH_3, CH_2CMe_3).[17]

Experimental

General Considerations. All air and moisture sensitive compounds were manipulated using standard vacuum line, Schlenk or cannula techniques, or in a drybox under a nitrogen atmosphere as described previously.[22] Molecular weights were determined by ebulliometry as described previously.[23] Argon, dinitrogen, dihydrogen and dideuterium were purified by passage over columns of MnO on vermiculite and activated molecular sieves. Solvents for air and moisture sensitive reactions were stored under vacuum over titanocene[23] or sodium benzophenone ketyl. Toluene-d_8 and cyclohexane-d_{12} were distilled from sodium benzophenone ketyl and stored over titanocene. Preparations of $C_5H_5\text{-}CMe_3$[24], $C_5H_4\text{-}1,3\text{-}CMe_3$[25], $C_5H_4\text{-}1,3\text{-}CHMe_2$[26], Cp^*ZrCl_3[13], $(\eta^5\text{-}C_5HMe_4)_2ZrCl_2$[19] and lithium indenide[27] were carried out as described previously. Tetramethylcyclopentadiene was purchased from Quantum Chemical Company and used as received. Preparation of the lithiocyclopentadienides was accomplished via addition of 1.6 M *n*-BuLi to a petroleum ether solution of the cyclopentadiene followed by filtration.

NMR spectra were recorded on a Bruker AM500 (500.13 MHz for ^1H, 125.77 MHz for ^{13}C) spectrometer. All ^1H and ^{13}C NMR chemical shifts are relative to TMS using ^1H (residual) or ^{13}C chemical shifts of the solvent as a secondary standard. Elemental Analyses were carried out at the Caltech Elemental Analysis Facility by Fenton Harvey. Complete combustion of the zirconocene dihydrides has proven difficult and many times V_2O_5 or Thermolite oxidant was added in order to gain satisfactory analyses.

$Cp^*(\eta^5\text{-}C_5H_4\text{-}CMe_3)ZrCl_2$ (1). A 250 mL round bottom flask equipped with stir bar was charged with Cp^*ZrCl_3 (5.16 g, 15.60 mmol) and Me_3CCpLi (2.00 g, 15.60 mmol) and a 180° needle valve was attached. On the vacuum line, 100 mL

of toluene was added by vacuum transfer, and the reaction mixture was warmed to room temperature and stirred for 5 days. Toluene was removed *in vacuo* , leaving a yellow solid. In air, about 50 mL of CH_2Cl_2 was added along with 20 mL of 4 M HCl. The CH_2Cl_2 layer was separated and combined with the 15 mL extracts of the aqueous layer. The CH_2Cl_2 solution was dried over $MgSO_4$ and filtered. Crystallization from CH_2Cl_2/hexanes afforded (**1**) in 60.5% yield (3.94 g). Anal. for $C_{19}H_{28}Zr_1Cl_2$: C: 54.52% H: 6.74%. Found C: 54.63% H: 6.82%. ^1H NMR (benzene-d_6): δ = 1.80 (s, 15H, Cp*), 1.45 (s, 9H, C*Me*$_3$), 6.15 (m, 2H, C_5H_4); 5.55 (m, 2H, C_5H_4). ^{13}C NMR (benzene-d_6): δ = 12.60 (C_5Me_5), 112.6 (C_5Me_5); 32.45 (C*Me*$_3$), 146.6 (*C*Me$_3$); 118.4, 122.5 ($C_5H_4CMe_3$).

Cp*(η^5-C_5H_4-CMe_3)$ZrMe_2$. A medium frit assembly was charged with Cp*(η^5-C_5H_4-CMe_3)$ZrCl_2$ (2.20 g; 5.28 mmol) and evacuated. Et_2O was added by vacuum transfer at -78 °C forming a slurry. At -78 °C, against an Ar counterflow, 1.4 M MeLi (8.30 mL, 11.60 mmol) solution was added via syringe. The reaction mixture was stirred and warmed to room temperature. With stirring a clear solution and white precipitate forms. The reaction mixture was stirred for 16 hours after which time the Et_2O was removed *in vacuo* and replaced with toluene. The yellow toluene solution was filtered, and the remaining white precipitate was washed with toluene. The toluene was removed leaving a yellow powder. Recrystallization from cold petroleum ether affords Cp*(η^5-C_5H_4-CMe_3)$ZrMe_2$ in 60.4% yield (1.20 g). Anal. for $C_{21}H_{34}Zr_1$ C: 66.78% H: 9.07% Found: C: 65.96 % H: 9.11 %. ^1H NMR (benzene-d_6): δ = 1.74 (s, 15H, Cp*), 1.26 (s, 9H, C*Me*$_3$), -0.30 (s, 6H, Zr-C*H*$_3$), 5.80 (m, 2H, C_5H_4); 5.44 (m, 2H, C_5H_4). ^{13}C NMR (benzene-d_6): δ = 12.11 (C_5Me_5), 110.15 (C_5Me_5); 32.25 (C*Me*$_3$), 142.97 (*C*Me$_3$), 33.17 (Zr-*C*H$_3$) 117.82, 108.67 ($C_5H_4CMe_3$).

[Cp*(η^5-C_5H_4-CMe_3)ZrH_2]$_2$ (8). In the dry box, a thick-walled glass reaction vessel equipped with stir bar was charged with Cp*(η^5-C_5H_4-CMe_3)$ZrMe_2$ (0.754 g, 2.01 mmol). On the vacuum line, the thick-walled reaction vessel was evacuated, and about 25 mL of petroleum ether was added by vacuum transfer. The reaction vessel was warmed to room temperature and 1 atmosphere of H_2 was admitted. The reaction vessel was sealed, and the mixture was stirred for one week, depositing a white solid over time. The reaction vessel was taken into the dry box, the contents transferred into a frit assembly, and the solid was collected on the frit and was washed with cold petroleum ether. Drying the solid

in vacuo for five hours affords $[Cp^*(\eta^5\text{-}C_5H_4\text{-}CMe_3)ZrH_2]_2$ in 65% yield (0.452 g). Anal. for $C_{19}H_{30}Zr$: C: 65.26% H: 8.65%. Found (V_2O_5 oxidant) C: 63.37 % H: 8.61%; Found (Added Thermolite oxidant) C: 60.50%; H: 8.34%. ^1H NMR (benzene-d_6): δ = 1.95, 1.97 (s, 15H, Cp*), 1.36, 1.39 (s, 9H, C*Me*$_3$), 4.08, 3.09 (m, 2H, Zr-*H*$_t$), -0.76, -2.56 (m, 2H, Zr-*H*$_b$), 4.55, 4.83, 4.96, 5.85, 6.07, 6.62 (m, C_5H_4). ^{13}C NMR (benzene-d_6): δ = 13.77, 13.89 (C_5Me_5), 115.85, 116.01 (C_5Me_5); 33.26, 33.36 (C*Me*$_3$), 141.40, 141.62 (*C*Me$_3$); 105.50, 104.85, 104.50, 103.49, 103.07, 100.70, 98.65 ($C_5H_4CMe_3$).

Cp*(Indenyl)ZrCl$_2$ (4). This compound was prepared in the same manner as **1** with 4.10 g (12.34 mmol) of Cp^*ZrCl_3 and 1.52 g of lithium indenide (12.34 mmol). Crystallization from CH_2Cl_2/hexanes afforded Cp*(Indenyl)$ZrCl_2$ in 82.4 % yield (4.20 g). Anal. Calcd for $C_{19}H_{22}Zr_1Cl_2$: C: 55.32% H: 5.38%. Found C: 55.22% H: 5.10%. ^1H NMR (benzene-d_6): δ = 1.81 (s, 15H, Cp*), 5.89 (m, 2H, Cp); 5.80 (m, 2H, Cp), 7.08 (m, 2H, benzo), 7.51 (m, 2H, benzo). ^{13}C NMR (benzene-d_6): δ = 12.69 (C_5Me_5), 104.27 (C_5Me_5), 118.30, 121.87, 123.50, 125.72, 127.04 (Ind).

Cp*(Indenyl)ZrMe$_2$. This compound was prepared in the same manner as $Cp^*(\eta^5\text{-}C_5H_4\text{-}CMe_3)ZrMe_2$ with 2.35 g of Cp*(Indenyl)$ZrCl_2$ (5.69 mmol) and 8.90 mL of 1.4 M MeLi. Recrystallization from cold petroleum ether affords Cp*(Indenyl)$ZrMe_2$ in 70.8% yield (1.50 g). Anal. for $C_{21}H_{28}Zr_1$ C: 67.86% H: 7.56% Found: C: 67.88% H: 8.06%. ^1H NMR (benzene-d_6): δ = 1.71 (s, 15H, Cp*), -0.84 (s, 3H, Zr-C*H*$_3$), 5.81 (m, 2H, Cp); 5.37 (m, 2H, Cp), 7.39 (m, 2H, benzo), 7.09 (m, 2H, benzo). ^{13}C NMR (benzene-d_6): δ = 11.79 (C_5Me_5), 100.70 (C_5Me_5), 36.06 (Zr-CH_3), 117.45, 118.34, 122.78, 124.61, one peak not located (Ind).

[Cp*(THI)ZrH$_2$]$_2$ (11). This compound was prepared in the same manner as **8** with 1.35 g of Cp*(Indenyl)$ZrMe_2$ (3.63 mmol) yielding $[Cp^*(THI)ZrH_2]_2$ in 68.0% yield (0.850 g). Anal. for $C_{19}H_{28}Zr_1$ Calculated C: 65.64% H: 8.12%. Found (with V_2O_5 oxidant) C: 65.46% H: 8.36%. ^1H NMR (benzene-d_6): δ = 2.01 (s, 15H, Cp*), 5.18 (s, 2H, Zr-*H*$_t$), -1.86 (s, 2H, Zr-*H*$_b$), 5.78 (m, 1H, Cp); 5.01 (m, 1H, Cp), 4.65 (m, 1H, Cp), 0.85, 1.92, 2.12, 2.65 (m, THI). ^{13}C NMR (benzene-d_6): δ = 13.61 (C_5Me_5), 116.47 (C_5Me_5), 98.78, 103.45, 108.93 (Cp), 22.38, 24.36, 25.17, 28.03 (THI).

Cp*{η^5-C_5H_3-1,3-$(CHMe_2)_2$}$ZrCl_2$ (3). This compound was prepared in the same manner as **1** with 2.73 g Cp^*ZrCl_3 (8.22 mmol) and 1.22 g {C_5H_3-1,3-$(CHMe_2)_2$}Li (8.22 mmol). Crystallization from CH_2Cl_2/hexanes afforded Cp*(η^5-C_5H_3-1,3-$(CHMe_2)_2$)$ZrCl_2$ in 83.3% yield (3.00 g). Anal. for $C_{21}H_{32}Zr_1Cl_2$: C: 56.48% H: 7.22%. Found C: 56.53% H: 7.32%. ^{1}H NMR (benzene-d_6): δ = 1.83 (s, 15H, Cp*), 3.19 (sept., 2H, C*H*Me_2), 0.96 (d, 6H, CH*Me*$_2$), 1.16 (d, 6H, CH*Me*$_2$), 5.30 (d, 2H,C_5H_3) 6.05 (t, 1H, C_5H_3). ^{13}C NMR (benzene-d_6): 11.34 (C_5Me_5), 106.47 (C_5Me_5); 36.06 (CHMe_2), 22.00, 23.85 (CH*Me*$_2$), 112.5, 114.73, 122.84 (C_5H_3).

Cp*{η^5-C_5H_3-1,3-$(CHMe_2)_2$}$ZrMe_2$. This compound was prepared in the same manner as Cp*(η^5-C_5H_4-CMe_3)$ZrMe_2$ with 2.00 g of Cp*{η^5-C_5H_3-1,3-$(CHMe_2)_2$}$ZrCl_2$ (4.56 mmol) and 6.80 mL of 1.4 M MeLi (9.56 mmol). Recrystallization from cold petroleum ether affords Cp*{η^5-C_5H_3-1,3-$(CHMe_2)_2$}$ZrMe_2$ in 91.2% yield (1.65 g). Anal. for $C_{23}H_{38}Zr_1$ C: 68.08 H: 9.44 Found: C: 68.06 H: 9.22. ^{1}H NMR (benzene-d_6): δ = 1.78 (s, 15H, Cp*), -0.39 (s, 3H, Zr-CH_3), 2.83 (sept., 2H, C*H*Me_2), 0.94 (d, 6H, CH*Me*$_2$), 1.22 (d, 6H, CH*Me*$_2$), 4.93 (d, 2H,C_5H_3) 6.05 (t, 1H, C_5H_3). ^{13}C NMR (benzene-d_6): 12.08 (C_5Me_5), 103.30 (C_5Me_5); 28.84 (Zr-CH_3), 35.79 (CHMe_2), 22.70, 25.90 (CH*Me*$_2$), 111.42, 117.68, 137.78 (C_5H_3).

[Cp*(η^5-C_5H_3-1,3-$(CHMe_2)_2$)ZrH_2]$_2$ (10). This compound was prepared in the same manner as **8** with 0.680 g of Cp*{η^5-C_5H_3-1,3-$(CHMe_2)_2$}$ZrMe_2$ (1.71 mmol). Recrystallization from cold petroleum ether affords [Cp*({η^5-C_5H_3-1,3-$(CHMe_2)_2$}ZrH_2]$_2$ in 72.2% yield (0.456 g). Anal. for $C_{21}H_{34}Zr_1$ C: 66.78% H: 9.07% Found: C: 67.13% H: 9.04%. ^{1}H NMR (benzene-d_6): δ = 2.05 (s, 15H, Cp*), 4.06 (br s, 2H, Zr-H_2), 3.21 (sept., 2H, C*H*Me_2), 1.27 (d, 6H, CH*Me*$_2$), 1.30 (d, 6H, CH*Me*$_2$), 5.03 (d, 2H,C_5H_3) 6.15 (t, 1H, C_5H_3). ^{13}C NMR (benzene-d_6): 13.44 (C_5Me_5), 107.55 (C_5Me_5), 30.01 (CHMe_2), 25.58, 23.77 (CH*Me*$_2$), 95.51, 103.16, 118.48(C_5H_3).

Cp*{η^5-C_5H_3-1,3-$(CMe_3)_2$}$ZrCl_2$ (2). This compound was prepared in the same manner as **1** with 3.00 g of Cp^*ZrCl_3 (10.09 mmol) and 3.62 g of {C_5H_3-1,3-$(CMe_3)_2$}Li$(DME)_{1.5}$ (10.09 mmol). Recrystallization from CH_2Cl_2/hexanes afforded Cp*{η^5-C_5H_3-1,3-$(CMe_3)_2$}$ZrCl_2$ in 71.0% yield (3.56 g). Anal. for $C_{23}H_{36}Zr_1Cl_2$: C: 58.20% H: 7.62%. Found C: 57.75% H: 7.89%.

^{1}H NMR (benzene-d_6): δ = 1.82 (s, 15 H, Cp*), 1.28 (s, 18 H, CMe_3), 5.46 (d, 2H, C_5H_3), 6.38 (d, 1H, C_5H_3). ^{13}C NMR (benzene-d_6): 12.05 (C_5Me_5), 113.45 (C_5Me_5), 31.60 (CMe_3), 142.50 (CMe$_3$), 109.75, 114.63, 123.50 (C_5H_3).

Cp*{η^5-C$_5$H$_3$-1,3-(CMe$_3$)$_2$}ZrMe$_2$. This compound was prepared in the same manner as Cp*{η^5-C$_5$H$_4$-CMe$_3$]ZrMe$_2$ with 1.25 g of Cp*{η^5-C$_5$H$_3$-1,3-(CMe$_3$)$_2$}ZrCl$_2$ (2.64 mmol) and 4.10 mL of 1.4 M MeLi (5.79 mmol). Recrystallization from cold petroleum ether affords Cp*{η^5-C$_5$H$_3$-1,3-(CMe$_3$)$_2$}ZrMe$_2$ in 84.1% yield (0.96 g). Anal. for $C_{23}H_{36}Zr_1$ C: 68.42% H: 8.99% Found: C: 68.26% H: 9.30%. ^{1}H NMR (benzene-d_6): δ = 1.78 (s, 15 H, Cp*), -0.20 (s, 6H, Zr-CH_3), 1.25 (s, 18 H, CMe_3), 5.00 (d, 2H, C_5H_3), 6.41 (d, 1H, C_5H_3). ^{13}C NMR (benzene-d_6): 12.28 (C_5Me_5), 117.86 (C_5Me$_5$), 33.95 (Zr-*Me*), 31.93 (CMe_3), 143.18 (CMe$_3$), 103.82, 106.87, 130.54 (C_5H_3).

Cp*{η^5-C$_5$H$_3$-1,3-(CMe$_3$)$_2$}ZrH$_2$ (13). This compound was prepared in the same manner as **8** with 0.950g of Cp*(η^5-C$_5$H$_3$-1,3-(CMe$_3$)$_2$)ZrMe$_2$ (2.19 mmol). Drying the solid *in vacuo* for several hours affords Cp*{η^5-C$_5$H$_3$-1,3-(CMe$_3$)$_2$}ZrH$_2$ in 78.8% yield (0.700 g). Anal for $C_{21}H_{32}Zr$ C: 60.08% H: 9.44% Found C: 66.60% H: 8.60%; (Added Thermolite oxidant) C: 66.85% H: 9.14%. ^{1}H NMR (benzene-d_6): δ = 2.05 (s, 15 H, Cp*), 7.09 (s, 2H, Zr-H_2), 1.30 (s, 18 H, CMe_3), 4.92 (d, 2H, C_5H_3), 6.70 (d, 1H, C_5H_3). ^{13}C NMR (benzene-d_6): 13.06 (C_5Me_5), 101.08 (C_5Me$_5$), 32.22 (CMe_3), 135.45 (CMe$_3$), 105.60, 109.08, 120.04 (C_5H_3).

Cp*(η^5-C$_5$HMe$_4$)ZrCl$_2$ (5). A 100 mL round bottom flask equipped with stir bar was charged with Cp*ZrCl$_3$ (3.00 g, 9.03 mmol), (C$_5$HMe$_4$)Li (1.15 g, 9.03 mmol), and a 180° needle valve and reflux condenser were attached. On the vacuum line 50 mL of toluene was added by vacuum transfer, and reaction mixture was heated to reflux for 2 days. The toluene removed *in vacuo* leaving a yellow solid. In air, about 50 mL of CH_2Cl_2 was added along with 20 mL of 4 M HCl. The CH_2Cl_2 layer was separated and combined with the 15 mL extracts of the aqueous layer. The CH_2Cl_2 solution was dried over $MgSO_4$ and filtered. Crystallization from CH_2Cl_2/hexanes afforded Cp*(η^5-C$_5$HMe$_4$)ZrCl$_2$ in 82.1% yield (3.10 g). Anal. for $C_{19}H_{28}Zr_1Cl_2$: C: 54.52% H: 6.74%. Found C: 54.68% H: 6.76%. ^{1}H NMR (benzene-d_6): δ = 1.85 (s, 15 H, Cp*), 1.65 (s, 6H, C$_5$*Me*$_4$H),

2.03 (s, 6H, C_5Me_4H), 5.14 (s, 1H, C_5Me_4H). ^{13}C NMR (benzene-d_6): δ = 12.83 (C_5Me_5), 110.45 (C_5Me_5), 12.98, 12.39 (C_5Me_4H), 119.32, 123.42, 132.40 (C_5Me_4H).

Cp*(C_5HMe_4)$ZrMe_2$. This compound was prepared in the same manner as Cp*(η^5-C_5H_4- CMe_3)$ZrMe_2$ with 2.00 g of Cp*(η^5-C_5HMe_4)$ZrCl_2$ (4.78 mmol) and 7.50 mL of 1.4 M MeLi (10.5 mmol). Drying the solid *in vacuo* affords Cp*(η^5-C_5HMe_4)$ZrMe_2$ in 79.3% yield (1.43 g). Anal. for $C_{21}H_{34}Zr_1$ C: 66.78% H: 9.07% Found: C: 66.68% H: 9.36%. ^1H NMR (benzene-d_6): δ = 1.78 (s, 15 H, Cp*), -0.56 (s, 6H, Zr-CH_3) 1.57 (s, 1H, C_5Me_4H), 1.96 (s, 6H, C_5Me_4H), 4.45 (s, 6H, C_5Me_4H). ^{13}C NMR (benzene-d_6): δ = 12.10 (C_5Me_5), 104.96 (C_5Me_5), 12.71, 12.08 (C_5Me_4H), 35.74 (Zr-CH_3), 117.13, 116.42, 123.39(C_5Me_4H).

Cp*(η^5-C_5HMe_4)ZrH_2 (15). This compound was prepared in the same manner as **8** with 1.40 g of Cp*(η^5-C_5HMe_4)$ZrMe_2$ (3.71 mmol). Recrystallization from cold petroleum ether affords Cp*(η^5-C_5HMe_4)ZrH_2 in 76.9% yield (1.00 g). Anal. for $C_{19}H_{30}Zr$ Calculated C: 65.26% H: 8.65%. Found C: 65.44% H: 9.09%. ^1H NMR (benzene-d_6): δ = 1.99 (s, 15 H, Cp*), 1.81 (s, 6H, C_5Me_4H), 2.45 (s, 6H, C_5Me_4H), 7.45 (s, 2H, Zr-*H*), 4.49 (s, 1H, C_5Me_4H). ^{13}C NMR (benzene-d_6): δ = 13.02 (C_5Me_5), 106.15 (C_5Me_5), 13.38, 14.37 (C_5Me_4H), 118.75, 119.18, 125.47 (C_5Me_4H).

{η^5-C_5H_3-1,3-(CMe_3)$_2$}$_2ZrCl_2$ (6). In a dry box, a 100 mL round bottom flask was charged with [Li(DME)][C_5H_3-1,3-(CMe_3)$_2$] (5.00 g, 18.13 mmol) and $ZrCl_4$ (2.11 g, 9.07 mmol). A reflux condenser and a 180° needle valve were attached. Via cannula, 50 mL of toluene was added to the reaction flask. The reaction mixture was heated to reflux forming a yellow solution. After three days, the toluene was removed *in vacuo* leaving a yellow/orange solid. In air, CH_2Cl_2 (~50 mL) was added along with 25 mL of 4 M HCl. The organic layer was collected, and the aqueous layer was washed with 10 mL portions of CH_2Cl_2. The combined organic layers were dried over $MgSO_4$ and filtered. The solvent was removed, leaving a yellow solid. The material was further purified by sublimation at 160 °C and 10^{-4} Torr yielding 3.10 g (66.70%) of a white solid. Anal for $C_{26}H_{42}Zr_1Cl_2$. Calcd C: 60.43% H: 8.19%. Found C: 60.74% H: 8.41%. ^1H NMR (benzene-d_6): δ = 1.30 (s, 18H, C_5H_3-(CMe_3)$_2$), 5.83 (m, 2H, C_5H_3-(CMe_3)$_2$), 6.62 (m, 1H, C_5H_3-(CMe_3)$_2$). ^{13}C NMR (benzene-d_6): δ =31.61 (C_5H_3-(CMe_3)$_2$), 145.09 (C_5H_3-(CMe_3)$_2$), 105.88, 118.79, 123.31 (C_5H_3-(CMe_3)$_2$).

{η^5-C_5H_3-1,3-$(CMe_3)_2$}$_2$$ZrMe_2$. A medium frit assembly was charged with {η^5-C_5H_3-1,3-$(CMe_3)_2$}$_2$$ZrCl_2$ and evacuated. Diethyl ether (15 mL) was added by vacuum transfer. Against an Ar counterflow at -80 °C, 1.4 M MeLi in Et_2O was added via syringe. The reaction mixture was slowly warmed to room temperature with stirring. After stirring for 36 hours, Et_2O removed in vacuo and replaced with toluene. The toluene solution was filtered away from white precipitate. The precipitate was washed three times with toluene on the frit. The toluene was removed in vacuo, and the product was recrystallized from cold petroleum ether affording 1.20 g (65.1 %) of {η^5-C_5H_3-1,3-$(CMe_3)_2$}$_2$$ZrMe_2$. Anal for $C_{28}H_{48}Zr_1$. C: 70.67% H: 10.17%. Found C: 70.75% H: 10.57%. ^{1}H NMR (benzene-d_6): δ = 1.28 (s, 18H, C_5H_3-(CMe_3)$_2$), 5.41 (m, 2H, C_5H_3-(CMe_3)$_2$), 6.55 (m, 1H, C_5H_3-(CMe_3)$_2$), 0.17 (s, 3H, Zr-CH_3). ^{13}C NMR(benzene-d_6): δ = 32.02 (C_5H_3-(CMe_3)$_2$), 139.14 (C_5H_3-(CMe_3)$_2$), 34.08 (Zr-CH_3) 101.32, 106.50, 116.12 (C_5H_3-(CMe_3)$_2$).

{η^5-C_5H_3-1,3-$(CMe_3)_2$}$_2$$ZrH_2$ (13). This compound was prepared in the same manner as **8** with 1.06 g of {η^5-C_5H_3-1,3-$(CMe_3)_2$}$_2$$ZrMe_2$ (2.44 mmol). After 5 days the material was transferred into a frit assembly, and the resulting white solid was filtered and dried in vacuo yielding 0.650 g (65.0%) of {η^5-C_5H_3-1,3-$(CMe_3)_2$}$_2$$ZrH_2$. Anal for $C_{26}H_{42}Zr$ C: 69.73% H: 9.90% Found C: 69.58% H: 10.06%. ^{1}H NMR (benzene-d_6): δ = 1.26 (s, 18H, C_5H_3-(CMe_3)$_2$), 5.34 (m, 2H, C_5H_3-(CMe_3)$_2$), 6.94 (m, 1H, C_5H_3-(CMe_3)$_2$), 7.36 (s, 2H, Zr-H). ^{13}C NMR(benzene-d_6): δ = 32.11 (C_5H_3-(CMe_3)$_2$), 142.19 (C_5H_3-(CMe_3)$_2$), 100.40, 105.75, not located (C_5H_3-(CMe_3)$_2$).

{η^5-C_5H_3-1,3(CHMe_2)$_2$}$_2$$ZrCl_2$ (7). In the dry box, a 250 mL round bottom flask was charged with Li_2[C_5H_3-1,3(CHMe_2)$_2$] (5.10 g, 34.29 mmol) and $ZrCl_4$ (3.99 g, 17.14 mmol). A reflux condenser and a 180° needle valve were attached. Via cannula, 100 mL of toluene was added to the reaction flask. The reaction mixture was heated to reflux, forming a yellow solution. After three days, the toluene was removed in vacuo leaving a tan powder. In air the solid was transferred into a sublimator, and the material sublimed at 160 °C and 10^{-4} Torr, yielding 5.30 g (69.4%). Anal for $C_{22}H_{34}Zr_1Cl_2$ C: 57.36% H: 7.44%. Found C: 57.20% H: 7.31%. ^{1}H NMR(benzene-d_6): δ = 1.04 (d, 12H, CHMe_2), 1.17 (d, 12H, CHMe_2), 3.11 (sept, 4H, C$H$$Me_2$), 5.62 (d, 2H, C_5H_3-(CHMe_2)$_2$), 6.26 (t, 1H,

C_5H_3-(1,3-$CHMe_2$)$_2$. ^{13}C NMR(benzene-d_6): 23.61 (CHMe_2), 23.81 (CHMe_2), 29.74 ($CHMe_2$), 107.53, 116.49, 142.29 (C_5H_3-(1,3-$CHMe_2$)$_2$).

{η^5-C_5H_3-1,3($CHMe_2$)$_2$}$_2$$ZrMe_2$. A medium frit assembly was charged with {η^5-C_5H_3-1,3($CHMe_2$)$_2$}$_2$$ZrCl_2$ (2.00 g, 4.49 mmol) and evacuated. Diethyl ether (25 mL) was added by vacuum transfer. Against an Ar counterflow at -80 °C, 1.4 M MeLi (7.1 mL, 9.9 mmol) in Et_2O added via syringe. The reaction mixture was slowly warmed to room temperature with stirring. After stirring for 16 hours Et_2O was removed in vacuo and replaced with toluene. The toluene solution was filtered away from white precipitate. The precipitate was washed three times with toluene on the frit. The toluene was removed in vacuo, and the product was recrystallized from cold petroleum ether, affording 1.60 g (88.1%) of {η^5-C_5H_3-1,3($CHMe_2$)$_2$}$_2$$ZrMe_2$. Anal for $C_{24}H_{40}Zr_1$. Calcd C: 68.67% H: 9.60%. Found C: 68.49% H: 9.46%. ^{1}H NMR (benzene-d_6): δ = 1.10 (d, 12H, CHMe_2), 1.20 (d, 12H, CHMe_2), -0.11 (s, 6H, Zr-CH_3), 2.74 (sept, 4H, $CHMe_2$), 5.38 (d, 2H, C_5H_3-($CHMe_2$)$_2$), 6.08 (t, 1H, C_5H_3-(1,3-$CHMe_2$)$_2$. ^{13}C NMR (benzene-d_6): 24.12 (CHMe_2), 24.44 (CHMe_2), 33.09 (Zr-CH_3), 29.04 ($CHMe_2$), 104.8, 110.40, 134.92(C_5H_3-(1,3-$CHMe_2$)$_2$).

[{(η^5-C_5H_3-1,3($CHMe_2$)$_2$}$_2$$ZrH_2$]$_2$ (14). In the dry box, a thick-walled glass reaction vessel was charged with {η^5-C_5H_3-1,3($CHMe_2$)$_2$}$_2$$ZrMe_2$ (0.700 g, 1.73 mmol). On the vacuum line the reaction vessel was degassed, and approximately 10 mL of petroleum ether was added by vacuum transfer. One atmosphere of H_2 was admitted to the reaction vessel, and the reaction mixture was stirred at room temperature depositing a white solid. After 3 days, the material was transferred into a frit assembly, and the resulting white solid was filtered and dried in vacuo yielding 0.550 g (85.0%) of [{(η^5-C_5H_3-1,3-($CHMe_2$)$_2$}$_2$$ZrH_2$]$_2$. Anal for $C_{22}H_{36}Zr_1$. Calcd C: 67.45% H: 9.26%. Found C: 67.17% H: 9.58%. ^{1}H NMR (benzene-d_6): δ = 1.35 (br s, 24H, CHMe_2), 3.15 (sept, 4H, $CHMe_2$), 3.85 (br s, 2H, Zr-H_t), -2.10 (br s, 2H, Zr-H_b), 5.05 (d, 2H, C_5H_3-($CHMe_2$)$_2$), 5.85 (t, 1H, C_5H_3-(1,3-$CHMe_2$)$_2$. ^{13}C NMR (benzene-d_6): 22.71 (CHMe_2), 26.98 (CHMe_2), 30.14 ($CHMe_2$), 98.23, 99.57, 104.56 (C_5H_3-(1,3-$CHMe_2$)$_2$).

(η^5-C_5HMe_4)$_2$$ZrMe_2$. A medium frit assembly was charged with (η^5-C_5HMe_4)$_2$$ZrCl_2$ (2.15 g, 5.32 mmol) and evacuated. Diethyl ether (25 mL)

was added by vacuum transfer. Against an Ar counterflow at -80 °C, 1.4 M MeLi (8.4 mL, 11.7 mmol) in Et_2O added via syringe. The reaction mixture was slowly warmed to room temperature with stirring. After stirring for 12 hours, the solution filtered away from white precipitate. The precipitate was washed three times with Et_2O on the frit. The Et_2O was removed in vacuo, affording 1.93 g (94.3 %) of $(\eta^5\text{-}C_5HMe_4)_2ZrMe_2$. Anal for $C_{20}H_{32}Zr_1$. Calcd C: 66.05% H: 8.87%. Found C: 65.88% H: 9.09%. ^1H NMR (benzene-d_6) δ = 1.68 (s, 12H, $C_5\mathit{Me}_4H$), 1.95 (s, 12H, $C_5\mathit{Me}_4H$), -0.55 (s, 6H, Zr-CH_3), 4.72 ($C_5Me_4\mathit{H}$). ^{13}C NMR (benzene-d_6) δ = 12.01, 13.50 ($C_5\mathit{Me}_4H$), 35.30 (Zr-CH_3), 105.56, 111.45, 122.29 (C_5Me_4H).

$[(\eta^5\text{-}C_5HMe_4)_2ZrH_2]_2$ (15). In the dry box, a thick-walled glass reaction vessel was charged with $(\eta^5\text{-}C_5HMe_4)_2ZrMe_2$ (1.00 g, 2.75 mmol). On the vacuum line the reaction vessel was degassed, and approximately 25 mL of petroleum ether was added by vacuum transfer. One atmosphere of H_2 was admitted to the reaction vessel, and the reaction was stirred at room temperature. After 5 days the material was transferred into a frit assembly, and the resulting yellow solid was washed with petroleum ether and dried in vacuo, yielding 0.800 g (86.8%) of $[(\eta^5\text{-}C_5HMe_4)_2ZrH_2]_2$. Anal for $C_{18}H_{28}Zr_1$. Calcd C: 64.41% H: 8.40%. Found C: 64.35% H: 8.77%. ^1H NMR (benzene-d_6) δ = 2.02 (s, 12H, $C_5\mathit{Me}_4H$), 2.14 (s, 12H, $C_5\mathit{Me}_4H$), 2.08 (br s, 2H, Zr-H_2), 45.56 ($C_5Me_4\mathit{H}$). ^{13}C NMR (benzene-d_6) δ = 13.36, 15.13 ($C_5\mathit{Me}_4H$), 108.39, 111.86, 115.41 (C_5Me_4H).

Deuteration Experiments. In a typical experiment, a J. Young NMR tube is charged with 5 mg of the a dihydride complex and dissolved in 0.5 mL of benzene-d_6 in the dry box. On the vacuum line the tube was frozen in liquid nitrogen and degassed using three freeze-pump-thaw cycles. While immersed in liquid nitrogen, one atmosphere of deuterium gas was admitted to the tube. The solution was then thawed rapidly in a water bath, and the tube rotated at room temperature to insure thorough mixing.

Structure Determination for 1, 3, 6. For all samples: 1) Suitable fragments were cut from single crystals, attached to a glass fiber and centered on an Enraf-Nonius CAD-4 diffractometer under an 85K stream of N_2 gas. 2) Unit cell parameters were obtained from the setting angles of 25 high angle reflections. 3) Two equivalent data sets were collected and merged in the appropriate point

group. 4) Three reference reflections were measured every hour during data collection to monitor crystal decay. 5) Lorentz and polarization corrections were applied. The data for **1** and **6** were corrected for decay of 0.32% and 0.19% respectively. An absorption correction was made for **6**. The structures of **1** and **6** were solved by Direct Methods, **3** was solved by the Patterson method. For 1, 3 and 6 difference Fourier maps were used to locate all missing atoms, including hydrogens. All hydrogen atoms were refined without restraints. For **1**, 2439 data were refined to R=0.015 (GOF=1.66); for **3**, 2546 data were refined to R=0.029 (GOF=1.83) and for **6**, 2330 data were refined to R=0.044 (GOF=2.04).

Acknowledgments: This work has been supported by the USDOE Office of Basic Energy Sciences (Grant No. DE-FG03-85ER13431) and Exxon Chemicals America.

Supplemental Information Available: ORTEP drawings showing the complete atom labeling schemes, cell and crystal packing diagrams, tables of atomic coordinates, complete bond distances and angles and anistropic displacement parameters for complexes **1**, **3**, **6** and $Cp^*_2HfH_2$ (36 pages).[28] Ordering and Internet access information is given on any current masthead page.

References.

The work in this chapter has been published previously. See Chirik, P.J.; Day, M.W.; Bercaw, J.E. *Organometallics* **1999**, *18*, 1873.

1. Collman, J.P.; Hegedus, L.S.; Norton, J.R.; Finke, R.G. in *Principles and Applications of Organotransition Metal Chemistry*: University Science Books, Mill Valley, California (1987) p. 80, 669.

2. Hoveyda, A.H.; Morken, J.P.; *Agnew. Chem. Int. Engl.* **1996**, *35*, 1262.

3. (a) Brintzinger, H.H.; Fischer, D.; Mülhaupt, R.; Rieger, B.; Waymouth, R.M. *Agnew. Chem. Int. Ed. Engl.* **1995**, *34*, 1143. (b) Piers, W.E. *Chem. Eur. J.* **1998**, *4*, 13. (c) Jordan, R.F. *Adv. Organomet. Chem.* **1991**, *32*, 325.

4. Couturier, S.; Gautheron, B. *J. Organomet. Chem.* **1978**, *157*, C61.

5. Weigold, H.; Bell, A.P.; Willing, R.I.; *J. Organomet. Chem.* **1974**, *73*, C23.

6. (a) Jones, S.B.; Peterson, J.L. *Inorg. Chem.* **1981**, *20*, 2289. (b) Larsonneur, A.; Choukroun, R.; Jaud, J. *Organometallics* **1993**, *12*, 3216.

7. Jones, S.B.; Peterson, J.L. *Organometallics* **1985**, *4*, 966.

8. Grossman, R.B.; Doyle, R.A.; Buchwald, S.L. *Organometallics* **1991**, *10*, 1501.

9. Cuenca, T.; Galakhov, M.; Royo, E.; Royo, P. *J. Organomet. Chem.* **1996**, *515*, 33.

10. Lee, H.; Desrosiers, P.J.; Guzei, I.; Rheingold, A.L.; Parkin, G. *J. Am. Chem. Soc.* **1998**, *120*, 3255.

11. Piers, W.E.; Shapiro, P.J.; Bunel, E.E.; Bercaw, J. E. *Synlett* **1990**, 74.

12. (a) Manriquez, J.; McAlister, D.R.; Sanner, R.D.; Bercaw, J.E. *J. Am. Chem. Soc.* **1978**, *100* , 2716. (b) Roddick, D.M.; Fryzuk, M.D.; Seidler, P.F.; Hillhouse, G.L.; Bercaw, J.E. *Organometallics* **1985**, *4*, 97.

13. Wolczanski, P.T.; Bercaw, J.E. *Organometallics* **1982**, *1*, 793.

14. This compound has been reported previously: Vanderheijen, H.; Hessen, B.; Orpen, A.G. *J. Am. Chem. Soc.* **1998**, *120*, 1112.

15. Wilkinson, G.; Pauson, P.L. *J. Am. Chem. Soc.* **1954**, *70*, 2024.

16. Hydrogenation of *rac*-(EBI)$ZrMe_2$ in benzene solution affords the previously reported {*rac*-(EBTHI)ZrH_2}$_2$ in 57% yield. See reference 8.

17. Parkin, G., personal communication.

18. Janiak, C.; Versteeg, U.; Lange, K.C.H.; Weiman, R.; Hahn, E. *J. Organomet. Chem.* **1995**, 501, 219.

19. Under more forcing conditions (*ca.* 2 atm D_2, 80 °C, 12 hr, benzene-d_6) H/D exchange for the methyl groups of the (η5-C_5HMe_4) ligands is accompanied by formation of (η^5-C_5HMe_5)$_2$Zr(H)($C_6D_xH_{5-x}$) and cyclohexane-d_n. Chirik, P. J.; Bercaw J. E., *unpublished results*.

20. Xin, S.; Harrod, J. F.; Samuel, E. *J. Am. Chem. Soc.* **1994**, *116*, 11562.

21. Mitchell, J. P.; Hajela, S.; Brookhart, S. K.; Hardcastle, K. I.; Henling, L. M.; Bercaw, J. E. *J. Am. Chem. Soc.* **1996**, *118*, 1045.

22. Burger, B.J.; Bercaw, J.E. In *Experimental Organometallic Chemistry*; ACS Symposium Series No. 357; Wayda, A.L.; Darensbourg, M.Y. Eds.; American Chemical Society: Washington, DC 1987; Chapter 4.

23. Marvich, R.H.; Brintzinger, H.H.; *J. Am. Chem. Soc.* **1971**, *93*, 2046.

24. Sullivan, M.F.; Little, W.F. *J. Organomet. Chem.* **1967**, *8*, 277.

25. Venier, C.G.; Casserly, E.W. *J. Am. Chem. Soc.* **1990**, *112*, 2808.

26. Herzog, T.A. *Ph.D. Thesis* California Institute of Technology, Pasadena, CA 1997.

27. Christopher, J.N.; Diamond, G.M.; Jordan, R.F.; Peterson, J.L. *Organometallics* **1996**, 15, 4038.

28. Crystallographic data have been deposited at CCDC, 12 Union Road, Cambridge CB2 1EZ, UK, and copies can be obtained on request, free of charge, by quoting the publication citation and the deposition number 102518.

30. Soloveichik, G.L.; Arkihireeva, T.M.; Bel'skii, V.K.; Bulychev, B.M. *Metalloorg. Khim.* **1988**, *1*, 226.

31. Rogers, R.D.; Benning, M.M.; Kurihara, L.K.; Moriarity, K.J.; Rausch, M.D. *J. Organomet. Chem.* **1985**, *293*, 51.

32. Yicheng, D.; Shen, W.; Rongguang, Z.; Shousan, C. *Kexue Tongbao (Chin.)* **1982**, *1436*, 27.

Chapter 2

Synthesis of Singly and Doubly Bridged *Ansa*-Zirconocene Dihydrides and Activation of Dinitrogen by a Monomeric Zirconocene Dihydride Complex.

Abstract

A series of singly and doubly bridged *ansa*-zirconocene dihydride complexes has been prepared from hydrogenation of the corresponding dimethyl complexes. For the singly [$SiMe_2$]-bridged species, the hydrogenation reaction is facile at 25 °C whereas for the doubly [$SiMe_2$]-bridged complexes hydrogenation occurs over the course of days at 87 °C. Hydrogenation of *meso*-$Me_2Si(\eta^5\text{-}C_5H_3\text{-}3\text{-}CMe_3)_2ZrMe_2$ affords the dimeric dihydride, $[Me_2Si(\eta^5\text{-}C_5H_3\text{-}3\text{-}CMe_3)_2ZrH_2]_2$, which has been characterized by X-ray diffraction. The *racemo* isomer of $Me_2Si(\eta^5\text{-}C_5H_2\text{-}2\text{-}SiMe_3\text{-}4\text{-}CMe_3)_2ZrMe_2$ ($BpZrMe_2$) reacts with dihydrogen affording the first example of a monomeric, *ansa*-zirconocene dihydride, *rac*-$Me_2Si(\eta^5\text{-}C_5H_2\text{-}2\text{-}SiMe_3\text{-}4\text{-}CMe_3)_2ZrH_2$ ($BpZrH_2$). In the presence of dinitrogen, *rac*-$BpZrH_2$ undergoes thermal reductive elimination of H_2 yielding the dinitrogen complex, $BpZr(\mu_2\text{-}N_2)ZrBp$, in which the dinitrogen ligand is coordinated in a side-on fashion with an N-N bond distance of 1.2450(38) Å. The doubly [$SiMe_2$]-bridged zirconium dimethyl complex, $[(Me_2Si)_2(\eta^5\text{-}C_5H_3)_2]ZrMe_2$ ($RpZrMe_2$), undergoes hydrogenation affording the hydride trimer, $[RpZr]_3$ $(\mu_3\text{-}H)_2(\mu_2\text{-}H)_3$, which has been characterized by X-ray diffraction. More substituted doubly [$SiMe_2$]-bridged zirconocene dihydrides such as $[(Me_2Si)_2(\eta^5\text{-}C_5H\text{-}3,5\text{-}(CHMe_2)_2)(\eta^5\text{-}C_5H_2\text{-}4\text{-}CH(CH_3)(CH_2CH_3))ZrH_2]_2$ ($[sec\text{-}BuThpZrH_2]_2$) and $[(Me_2Si)_2(\eta^5\text{-}C_5H\text{-}2,4\text{-}(CHMe_2)_2)(\eta^5\text{-}C_5H_2\text{-}4\text{-}CHMe_2)ZrH_2]_2$ ($[iPrThpZrH_2]_2$) have been prepared and shown to be robust dimers in solution.

Introduction

Group 4 *ansa*-metallocene complexes have received considerable attention due to their utility in olefin polymerization[1] and applicability as catalysts for a host of other enantioselective bond-forming processes.[2] For many of these transformations, a metallocene hydride or dihydride is believed to be the active species during the catalytic cycle. In the asymmetric hydrogenation of 1,1-disubstituted and trisubstituted alkenes with chiral *ansa*-zirconocene[3] and titanocene catalysts,[4] olefin insertion into metallocene hydride bonds is believed to be essential for stereoselectivity and catalyst turnover. Although group 4 *ansa*-metallocene hydrides are often implicated in a variety of catalytic cycles, the synthesis and characterization of these complexes has not been fully explored.

The synthesis of *rac*-$[(EBTHI)ZrH_2]_2$ (EBTHI = ethylene-1,2-bis(η^5-tetrahydroindenyl) from reduction of the dichloride complex has been reported by Buchwald and coworkers.[5] The dimeric structure of the dihydride has been proposed based on the observation of distinct terminal and bridging zirconium hydride resonances in ^1H NMR spectrum. Royo[6] has used similar synthetic methodology to prepare the doubly [$SiMe_2$]-bridged, $[(Me_2Si)_2(\eta^5\text{-}C_5H_3)_2ZrH_2]_2$, which has also been reported to be dimeric in solution on the basis of its ^1H NMR spectrum. Parkin has prepared $[Me_2Si(\eta^5\text{-}C_5Me_4)_2ZrH_2]_2$ ($[OpZrH_2]_2$) from hydrogenation of the dimethyl complex at elevated temperatures in cyclohexane solution.[7] Characterization of the hydride dimer has been accomplished by NMR spectroscopy and X-ray crystallography.

As part of our systematic investigation of ancillary ligand effects in group 4 metallocene chemistry, we sought to extend the scope of our studies to include *ansa*-zirconocene dihydride complexes. In this report, we describe the preparation and characterization of both singly and doubly [$SiMe_2$]-bridged zirconocene dihydrides from the hydrogenation of the corresponding dimethyl complexes. During the course of our investigations, we have been able to prepare the first example of a monomeric, *ansa*-zirconocene dihydride which undergoes reductive elimination of dihydrogen, resulting in the coordination and activation of dinitrogen. The zirconocene dinitrogen complex has been

characterized by X-ray diffraction and displays side-on coordination of the dinitrogen fragment.

Results and Discussion

Preparation of Singly Silylene-Bridged Zirconocene Dihydride Complexes.

The first synthetic target in our study was $[Me_2Si(C_5H_4\text{-}3\text{-}CMe_3)_2ZrH_2]_n$ ($DpZrH_2$) since the preparation of the zirconocene dichloride as the pure *meso* isomer has been reported.[8] Methylation of *meso*-$DpZrCl_2$ in diethyl ether affords a 2:1 mixture of *meso:rac* $DpZrMe_2$, arising from epimerization of the ligand at the zirconium center. Similar *racemo-meso* interconversions promoted by various salts and Grignard reagents have been observed previously with both group 3 and 4 metallocenes.[9] Preparation of pure *meso*-$DpZrMe_2$ (**1**) may be accomplished by addition of $AlMe_3$ to $DpZr(NMe_2)_2$ (eq. 1).[10] Slow cooling of a petroleum ether solution of **1** affords large yellow crystals suitable for X-ray diffraction. The solid state structure of **1** is shown in Figure 1 and confirms the identity of the *meso* isomer.

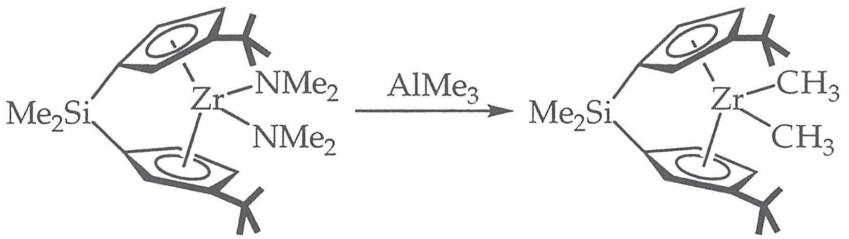

(1)

1

Compound **1** crystallizes in space group $P2_1/c$ and contains two molecules in the asymmetric unit. There are no differences in the geometry of these two molecules. The molecule displays a normal coordination environment for an *ansa*-metallocene with the two zirconium methyl groups contained in the metallocene wedge, displaying typical zirconium methyl bond lengths of 2.275(4) Å and 2.273(4) Å, respectively.

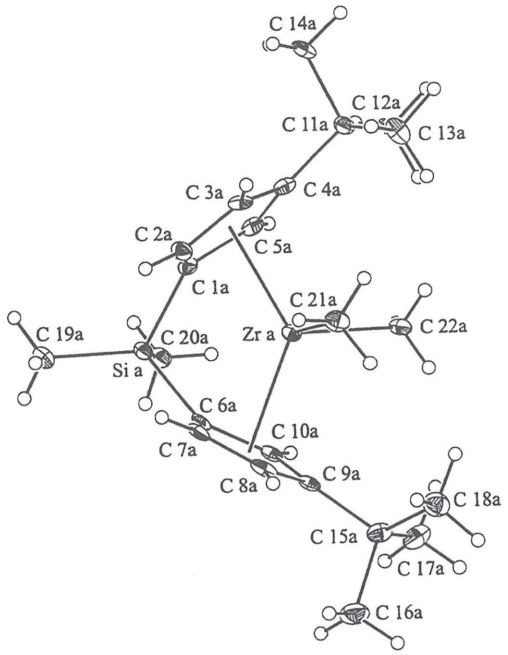

Figure 1. Molecular Structure of **1** with 50% probability ellipsoids.

Hydrogenation of **1** in benzene-d_6 proceeds over the course of hours at 25 °C, affording the dihydride dimer, *meso*-[DpZrH$_2$]$_2$ (**2**) (eq. 2). The ^{1}H NMR spectrum in benzene-d_6 indicates a C_1 symmetric structure, displaying inequivalent *tert*-butyl, dimethylsilyl and cyclopentadienyl resonances. Terminal zirconium hydride resonances are observed at 3.94 and 4.03 ppm whereas the bridging hydride resonances are located at -2.35 and -5.29 ppm. Upon standing in benzene-d_6, clear, colorless crystals of **2** are deposited over the course of several days at 25 °C. Complex **2** crystallizes in space group P_{-1} and the two halves of the dimer are related by a crystallographic center of inversion which is not consistent with the solution NMR spectrum. As result, the dihedral angle between the planes formed by the two metallocene wedges is zero and places the terminal hydrides in a *trans* relationship (eq. 2). Unfortunately, neither the bridging nor terminal hydride ligands have been found in the difference map. However, the zirconium-zirconium distance of 3.492 Å in **2** is consistent with other crystallographically characterized zirconocene hydride dimers which display metal-metal distances between 3.4 to 3.5 Å.[11]

A dihedral angle of zero degrees between the two zirconocene equatorial planes contrasts previous results for *ansa*-metallocene hydride complexes. The *ansa*-zirconocene dihydride, $[OpZrH_2]_2$[7] and the *ansa*-titanocene *rac*-$[(EBTHI)TiH]_2$[12] display significant, 53 ° in the latter case, twisting of the metallocene equatorial planes in order to alleviate unfavorable steric interactions between cyclopentadienyl substituents. A similar dihedral angle of 40 ° has been measured for the *ansa*-yttrocene hydride, *rac*-$[(\eta^5\text{-}C_5H_2\text{-}2\text{-}SiMe_3\text{-}4\text{-}CMe_3)_2Si(OC_{10}H_6C_{10}H_6O)YH_2]$ $[(BnBpYH_2)_2]$.[13] For **2**, the unfavorable steric interactions between the *tert*-butyl groups is reduced by rotating the ligand about the metal-cyclopentadienyl centroid, thus placing these substituents in a *trans*-like arrangement in the dihydride dimer.

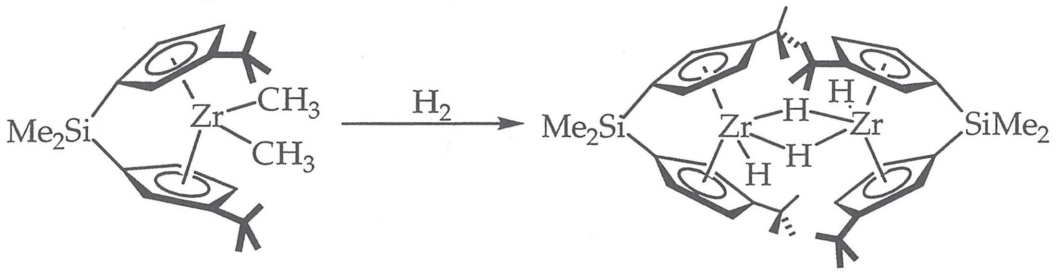

(2)

1 **2**

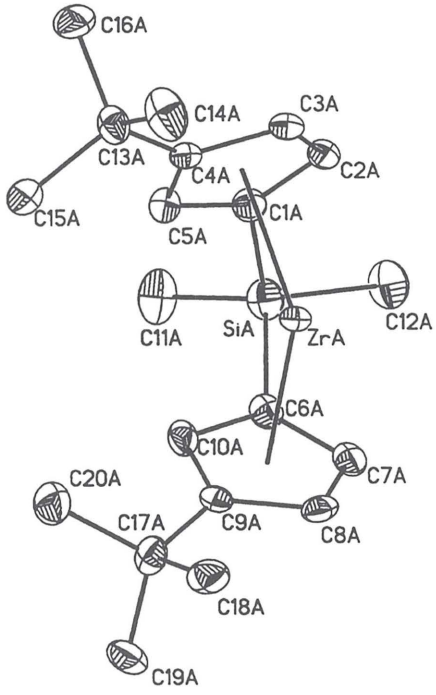

Figure 2. Molecular structure of one zirconium center of **2** with 30% probability ellipsoids and atom labeling scheme, as viewed in the equatorial plane. Hydrogen atoms omitted for clarity.

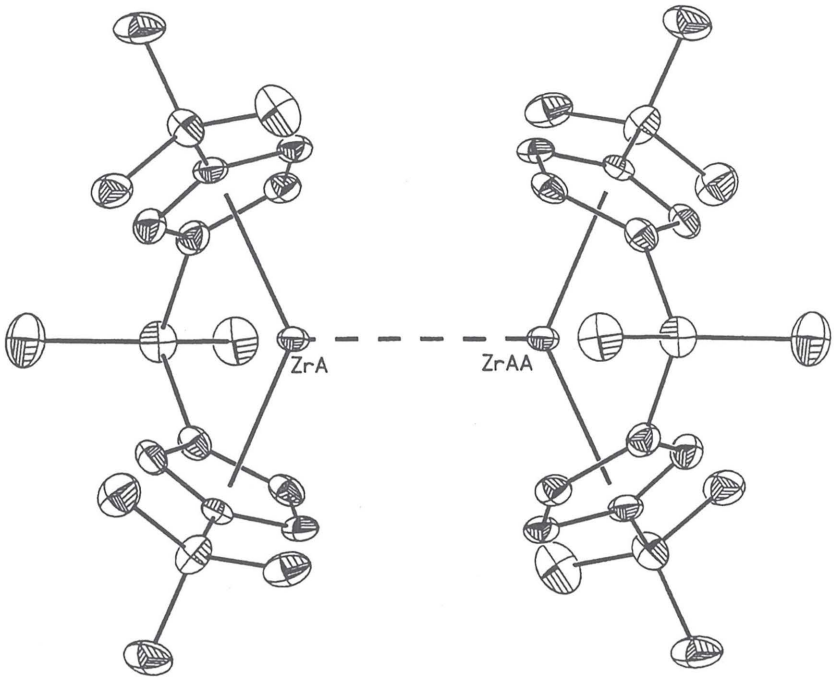

Figure 3. Molecular structure of **2** with 30% probability ellipsoids.

Since the solid state structure of **2** demonstrates the propensity of the *tert*-butyl substituents to adopt a *trans*-like arrangement allowing for the formation of hydride bridges, we sought to prepare the *racemo* isomer of **2** which would force the *tert*-butyl groups over the center of the metallocene wedge. Unfortunately, a synthetic method for the preparation of pure *rac*-$DpZrMe_2$ has not been devised. As a result, we turned our attention to $[Me_2Si(C_5H_2\text{-}2\text{-}SiMe_3\text{-}4\text{-}CMe_3)_2]ZrCl_2$ ($BpZrCl_2$) which yields solely the *racemo* isomer upon metallation.[14] One possible limitation of this approach is the synthetic difficulty associated with the preparation of *rac*-$BpZrCl_2$. The synthesis requires heating $ZrCl_4$ with the dipotassio salt of the ligand for one month and produces only a 15% yield of the desired zirconocene dichloride.[14] Once prepared, *rac*-$BpZrCl_2$ may be converted to *rac*-$BpZrMe_2$ by addition of methyllithium in diethyl ether (eq. 3). Unlike **1**, *rac*-$BpZrMe_2$ does not undergo epimerization in the presence of alkyllithium reagents or salts such as LiCl.

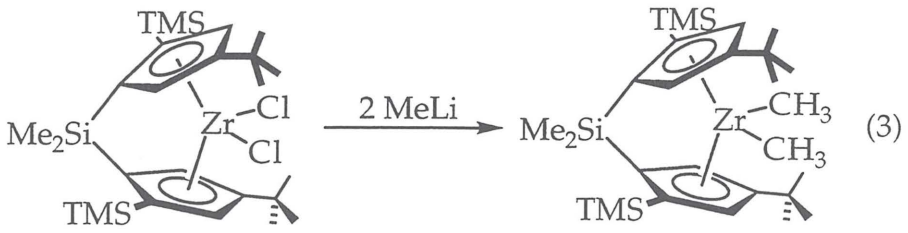

(3)

$BpZrCl_2$ 3

Hydrogenation of **3** in toluene affords *rac*-$BpZrH_2$ (**4**) (eq. 4). Following the hydrogenation reaction by NMR spectroscopy reveals that conversion of **3** to **4** takes place over the course of hours at 25 °C. This is considerably more rapid than the rates observed for the unlinked systems which hydrogenate over the course of days under the same conditions.[15] The ^1H NMR spectrum of **4** displays a singlet at 7.20 ppm for the Zr-H resonance indicative of a monomeric structure in solution.[15] This is in agreement with the experimentally determined solution molecular weight of 625 g/mol (568.6 g/mol calculated for monomer).

In the presence of dihydrogen, no Zr-H resonance is observed in the ^1H NMR spectrum of **4**, suggesting rapid exchange between free dihydrogen and the zirconium hydrides on the ^1H NMR timescale. Confirmation of this rapid exchange process has been obtained from addition of dideuterium gas to **4**. Exchange of the zirconium hydrides with deuterium is observed instantaneously at -78 °C. Interestingly, deuteration of the CMe_3 and $SiMe_3$ groups on the ligand array is observed over the course of 12 hours at 25 °C. Deuteration of the cyclopentadienyl substituents arises from formation of "tuck-in" intermediates, in which a C-H bond of an alkyl group adds to the zirconium center and is then deuterated via σ-bond metathesis with D_2.[15]

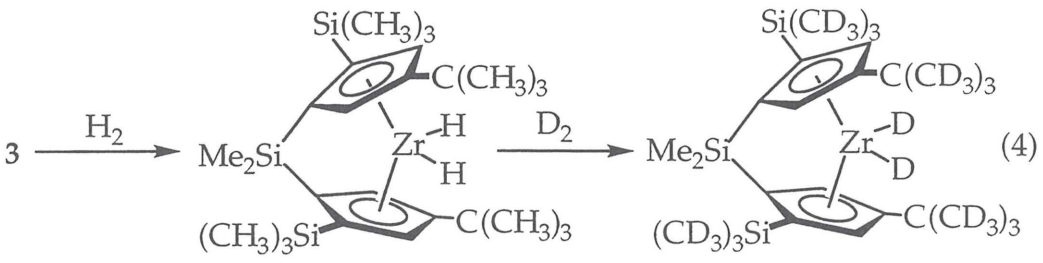

(4)

4

Allowing a yellow toluene solution of **4** to stand in the dry box under an atmosphere of dinitrogen results in rapid formation of a forest green solution. Cooling the solution to -30 °C precipitates rose colored crystals over the course of several days. X-ray diffraction reveals that the crystals are not the starting dihydride, **3**, but rather the dinitrogen complex, $BpZr(\mu_2\text{-}N_2)ZrBp$ (**5**). The solid state structure of **5**, shown in Figure 4, reveals a dimeric structure with a bridging, side-on dinitrogen fragment.

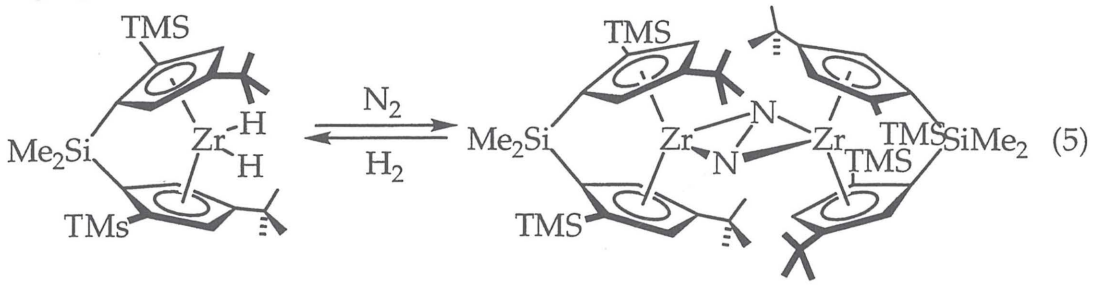

(5)

5

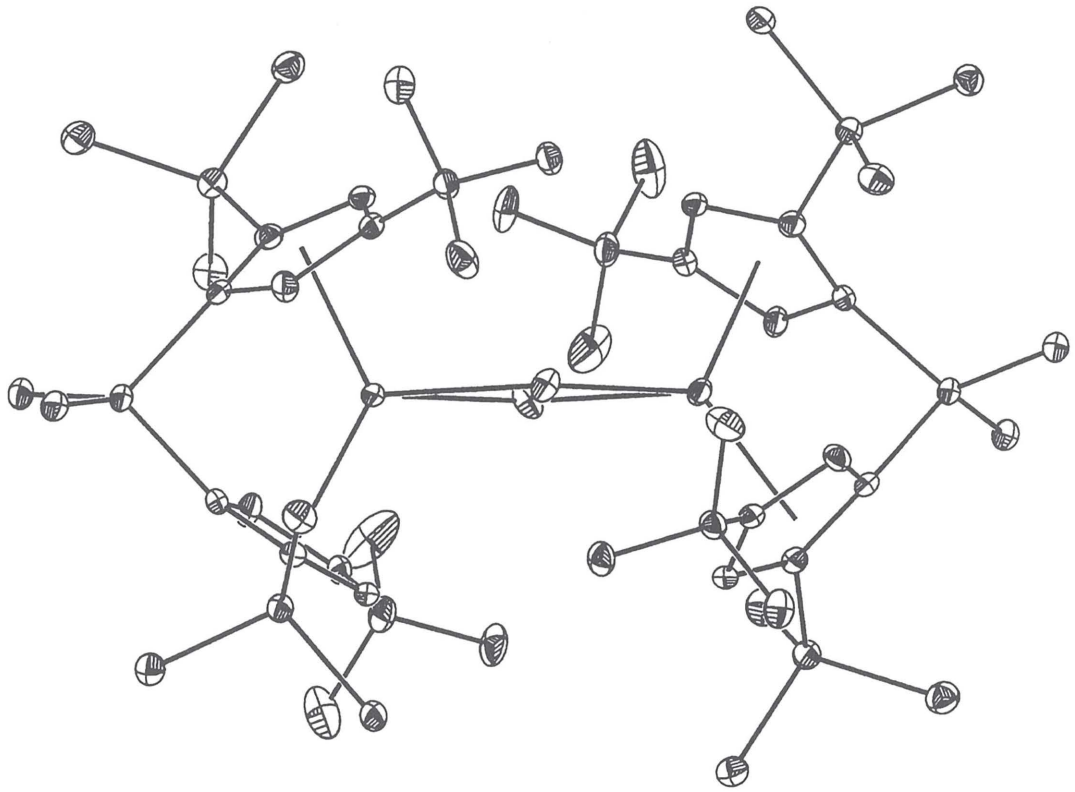

Figure 4. Molecular structure of **5** with 50% probability ellipsoids. Hydrogen atoms omitted for clarity.

Conversion of an early transition metal hydride to a dinitrogen complex is quite rare. Typically, coordinated dinitrogen undergoes rapid and irreversible displacement by dihydrogen forming a dihydride complex; competitive recoordination of N_2 is generally not observed. For example, treatment of $[(\eta^5\text{-}C_5Me_5)_2ZrN_2]_2N_2$ with dihydrogen at 0 °C affords $(\eta^5\text{-}C_5Me_5)_2ZrH_2$ in good yield.[16] Late transition metal (*e.g.*, Co, Ni) hydrides have been shown to eliminate dihydrogen and coordinate dinitrogen, although minimal perturbation of the N-N bond in the resulting dinitrogen complexes is observed.[17] To date, the only example of such a transformation with an early metal system is the conversion of $[PhP(CH_2SiMe_2NPh)_2]TaH_2$ ([NPN]TaH_2) to ([NPN]$TaH)_2N_2$ which displays both an end-on and side-on bound dinitrogen fragment.[18] Displacement of coordinated hydride ligands by dinitrogen may be essential in developing a transition metal based catalyst for N_2 fixation.

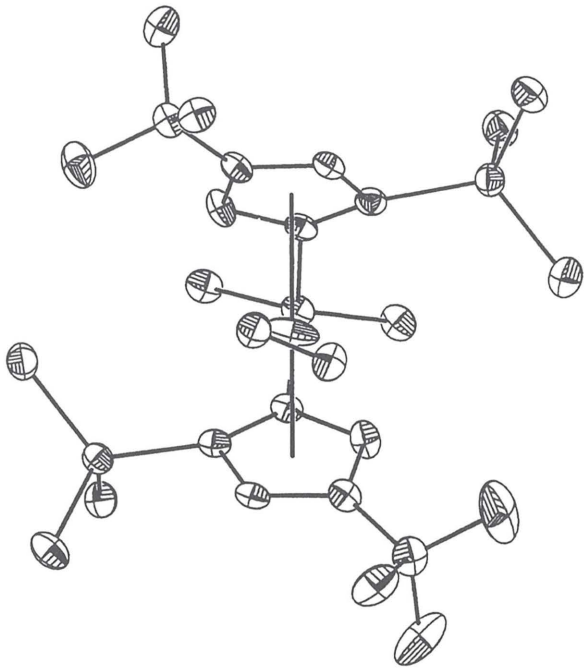

Figure 5. Molecular structure of one of the zirconium centers of **5** with 50% probability ellipsoids, as viewed in the equatorial plane. Hydrogen atoms omitted for clarity.

Side-on coordination of dinitrogen in a metallocene complex is also atypical. Classically, sodium reduction of metallocene dichloride complexes such

as $(\eta^5\text{-}C_5Me_5)_2MCl_2$ (M = Ti,[19] Zr,[20] Hf[21]) provides end-on bound dinitrogen ligands with relatively short (< 1.2 Å) N-N bond distances. More recently, Fryzuk has prepared a series of macrocyclic amido-phosphine zirconium complexes with side-on dinitrogen ligands.[22] In these molecules, long N-N bond distances (~1.4 -1.5 Å) are observed. To our knowledge, the only other example of a metallocene with a side-on dinitrogen fragment is $(\eta^5\text{-}C_5Me_5)_2SmN_2Sm(\eta^5\text{-}C_5Me_5)_2$ which has an unusually short N-N distance of 1.088 Å.[23] The N-N bond distance of 1.2450(38) Å of the dinitrogen ligand in **5** is intermediate between these structures. Comparison of this value to the established distance of 1.255 Å for $(C_6H_5)N{=}N(C_6H_5)$[24] suggests that the dinitrogen fragment in **5** posesses some double bond character. The two nitrogen atoms are approximately equidistant from the metal center with Zr-N(1) equal to 2.2680(8) Å and Zr-N(1) equal to 2.2712(8) Å. Bisection of the 147.8 ° Zr-N_1-Zr(A) bond angle yields a value of 73.9 ° which is contracted considerably from those typically observed with organic diazenes.[25]

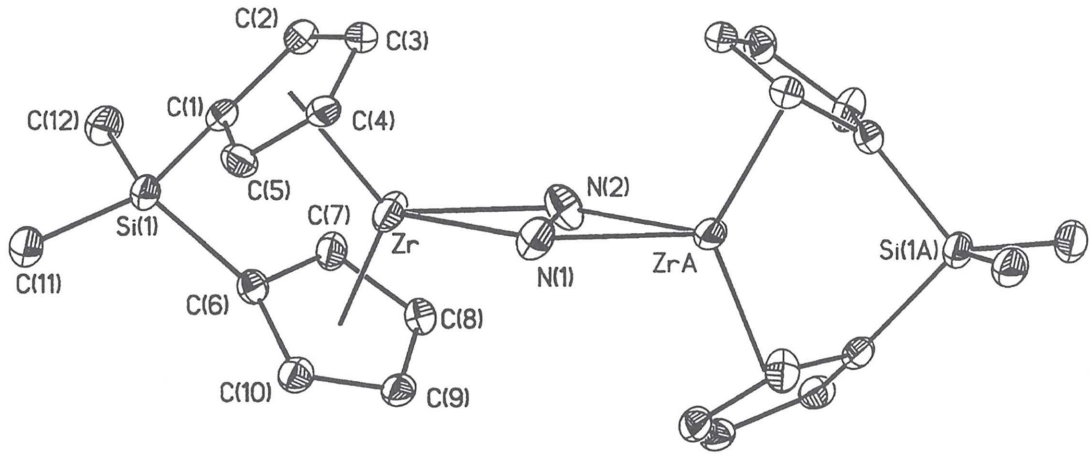

Figure 6. Partially labeled view of **5** with 50% probability ellipsoids. Hydrogen atoms and ligand substituents are omitted for clarity.

Unlike the solid state structure for **2**, **5** displays a dihedral angle of 46.4 ° between each metallocene wedge (Figure 6). The origin of this twist is believed

to be due to unfavorable steric interactions between the bulky *tert*-butyl substituents on each of the cyclopentadienyl rings (Figure 4). The twist angle observed in **5** is larger than the value of 32 ° observed with $[BnBpYH]_2$.[12] The distance between the two zirconium atoms in **5** is 4.366 Å which is significantly longer than the metal-metal distance observed in **2**. The increased distance between the metal centers is a consequence of the large bridging nitrogen atoms in **5** compared to the bridging hydrides in **2**.

Based on the solid state structure of **5**, the ^1H and ^{13}C NMR spectra would be expected to display equivalent *tert*-butyl, trimethylsilyl and $[Me_2Si]$ resonances based on the local C_2 symmetry of each zirconium center. However, twice the number of the expected peaks are observed in equal amounts. One possibility is that **5** coordinates additional dinitrogen in solution thus eliminating the C_2 symmetry of the molecule and results in additional NMR resonances. However, samples of **5** prepared under vacuum or under an atmosphere of argon both display the same NMR spectra as samples prepared under N_2, thus ruling out coordination of additional dinitrogen ligands. Another possibility is the presence of two sets of diastereomeric dimers, whereby one set of dimers is comprised of the (*R*, *R*) and (*S*, *S*) enantiomers (homochiral dimer) while the other set contains (*R*, *S*) and (*S*, *R*) chiralities at zirconium (heterochiral dimer). Similar behavior has been observed in the preparation of *rac*-$[BpYH_2]$ and *rac*-$[AbpYH_2]$ where both homochiral and heterochiral dimers are observed.[26] Although we have not confirmed this hypothesis by preparing enantiomerically pure **4** and consquently enantiopure **5**, we favor this explanation for the observed solution NMR behavior for **5**.

Toluene solutions of **5** are forest green and display two absorption bands at 392.0 nm and 612.0 nm. The solution FT-Raman spectrum has been collected in benzene solution and displays three resonances at 1182.6, 1001.5 and 984 cm^{-1} attributable to the Zr_2N_2 core. Assuming the Zr_2N_2 core is of D_{2h} symmetry, three bands, two of A_{1g} and one of B_{3g} symmetry, are predicted. Attempts to obtain resonance Raman spectra have been unsuccessful due to sample decomposition upon irradiation.

Exposure of **5** to one atmosphere of dihydrogen bleaches the green solution and regenerates the starting dihydride, **4** (eq. 5). Addition of a slight

excess of PMe_3 to **5** results in an immediate reaction, liberating dinitrogen and forming the *bis*-phosphine complex, *rac*-$BpZr(PMe_3)_2$ (eq. 6). Reactions of **4** with either carbon monoxide or ethylene result in decomposition.

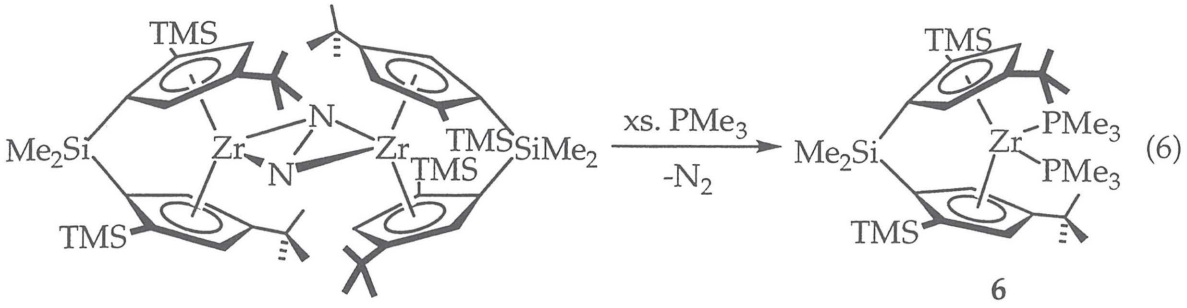

6 (6)

The mechanism of formation of **5** from **4**, whereby dihydrogen is displaced by dinitrogen, is of considerable interest due to its relevence in a potential catalytic cycle for the fixation of dinitrogen to ammonia. One mechanism is a photoinduced reductive elimination of H_2 from **5** followed by coordination of dinitrogen to the intermediate Zr(II) species (Figure 7, pathway *i*). However, parallel experiments have been conducted in the presence and absence of light and the rates (qualitatively) of conversion are identical thus ruling out a photochemical reaction. Another pathway is coordination of dinitrogen to **4** which induces reductive elimination of dihydrogen (Figure 7, pathway *ii*).[27] Stirring a toluene solution of **4** under argon open to a mercury bubbler results in decomposition of the dihydride at a comparable rate to conversion to **5** in presence of dinitrogen. In combination, these experiments suggest that formation of the dinitrogen complex, **5**, proceeds via thermal reductive elimination of dihydrogen followed by rapid trapping by dinitrogen (Figure 7, pathway *iii*).

The thermal reductive elimination of dihydrogen from **4** is quite unusual, considering unlinked, monomeric zirconocene dihydrides such as $Cp^*_2ZrH_2$ and $Cp^*(\eta^5\text{-}C_5H_3\text{-}1,3\text{-}(CMe_3)_2)ZrH_2$ display no propensity to eliminate H_2 even after months in solution.[15] From these observations, it would appear that the *ansa*-bridge in combination with the monomeric nature of **4** promotes reductive elimination and hence coordination of dinitrogen. This pathway contrasts those obtained in molybdocene dihydride complexes where an *ansa*-bridge inhibits reductive elimination. The origin of this effect is the apparent requirement for a

parallel ring structure in the intermediate Mo(II) complex which can not be readily achieved in the *ansa*-metallocene.[28] Reductive elimination promoted by an *ansa* bridge has been observed in a d^0, Ta(V) trihydride complex. The *ansa*-tantalocene, $Me_2Si(\eta^5\text{-}C_5Me_4)_2TaH_3$, undergoes reductive elimination over 100 times faster than $(\eta^5\text{-}C_5Me_5)_2TaH_3$.[29] The observed rate enhancement has been attributed to the reduced electron donating ability and hence destabilization of the Ta(V) complex in the *ansa* system. Similar electronic effects may be the reason for the increased rate of reductive elimination of **4** compared to unlinked zirconocene dihydrides.

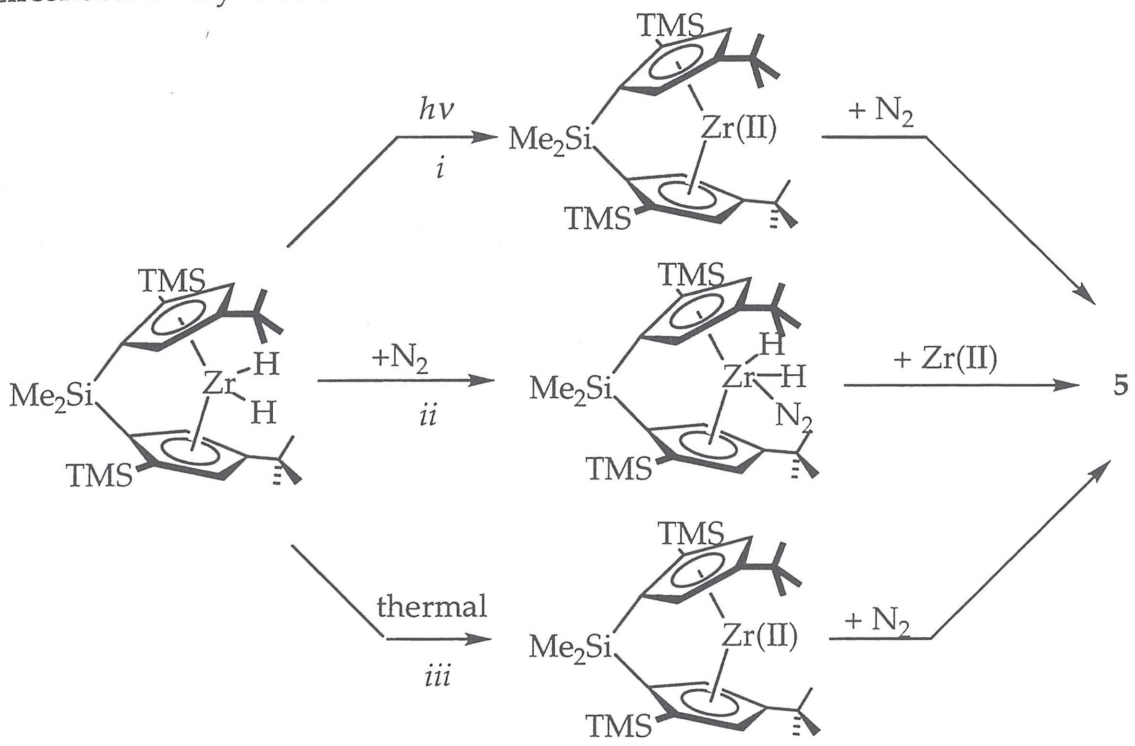

Figure 7. Possible mechanisms for the conversion of **4** to **5**.

Since the *ansa* bridge and the monomeric nature of **4** are believed to be responsible for the observed reactivity with dinitrogen, we sought to prepare other monomeric *ansa*-group 4 zirconocene dihydrides. These complexes would not only be useful in determining the generality of this unusual transformation but also may allow preparation of multigram quantities of a dinitrogen complex

which has not been possible with **5** due to the inability to prepare *rac*-$BpZrCl_2$ in reasonable yield.

Preparation of $Li_2[Me_2Si(C_5Me_4)(C_5H_2\text{-}2,4\text{-}(CHMe_2)_2]$ ($Li_2[iPr_2Tp]$) has been accomplished via standard procedures.[30] The design of this ligand was inspired by the observation that $[Me_2Si(\eta^5\text{-}C_5Me_4)_2ZrH_2]_2$ can be prepared in multigram quantities and is both monomeric and dimeric in solution.[7] We surmised that increasing the steric disposition of this ligand framework may afford zirconocenes that are monomeric in solution and hence would undergo facile thermal reductive elimination and coordinate dinitrogen. Reaction of $Li_2[iPr_2Tp]$ with $ZrCl_4$ in refluxing toluene for 24 hours affords $iPr_2TpZrCl_2$ in 50% yield. Methylation of the dichloride affords $iPr_2TpZrMe_2$ (**8**) which undergoes hydrogenation affording $[iPr_2TpZrH_2]_2$ (**9**) (Figure 8). The dihydride is completely insoluble in aromatic hydrocarbon solvents and as a result has been characterized in THF-d_8 as the solvento complex, iPr_2TpZrH_2(THF-d_8). Addition of five equivalents of PMe_3 to a benzene-d_6 solution of **9** provides no reaction, thus demonstrating the robust nature of the dihydride dimer. Accordingly, no reaction is observed with dinitrogen.

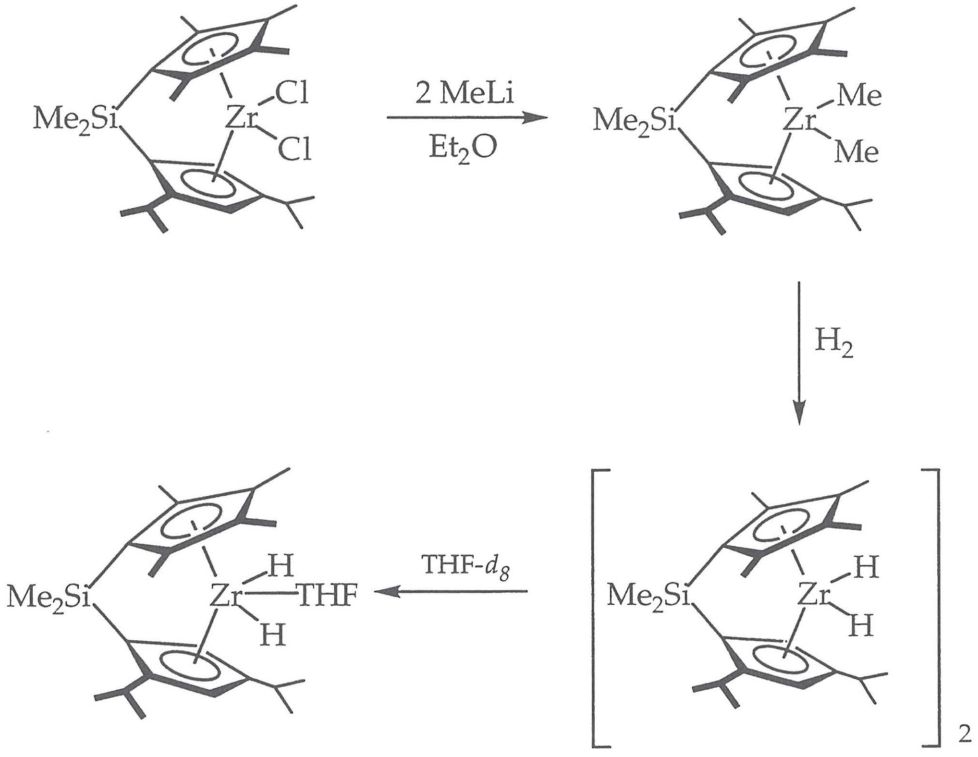

Figure 8. Preparation of $[iPr_2TpZrH_2]_2$ (**9**).

Attempts to increase the steric bulk of the ligand by replacement of the isopropyl substituents with *tert*-butyl groups have not been successful. The attempted synthesis of $Me_2Si(C_5Me_4H)(C_5H_3\text{-}2,4\text{-}(CMe_3)_2)$ via addition of LiC_5Me_4 to a THF solution of $C_5H_3\text{-}(CMe_3)_2SiMe_2Cl$ or via addition of $Li[C_5H_3\text{-}1,3\text{-}(CMe_3)_2]$ to $C_5Me_4SiMe_2Cl$ does not produce the desired product.

Preparation of Doubly Silylene-Bridged Zirconocene Dihydride Complexes.

In addition to singly [$SiMe_2$]-bridged metallocenes, we also targeted the preparation of doubly silylene bridged *ansa*-zirconocene dihydrides. Initially we focused on the preparation of complexes derived from the $[(Me_2Si)_2(\eta^5\text{-}C_5H_3)_2]$ ligand which has been previously reported by Royo.[31] Attempts to hydrogenate $[(Me_2Si)_2(\eta^5\text{-}C_5H_3)_2]ZrMe_2$ (**10**) at 25 °C produce no reaction, contrary to previous results with unlinked and singly [$SiMe_2$]-bridged zirconocenes. Heating the reaction mixture to 100 °C in benzene-d_6 results in formation of methane (by ^1H NMR) and precipitation of black crystals. The solid state structure of the black crystals has been determined by X-ray diffraction and reveals that the product of the reaction is not the expected dihydride, but rather the trimeric zirconocene cluster, $[(\eta^5\text{-}Me_2Si)_2(C_5H_3)_2)Zr]_3(\mu_3\text{-}H)_2(\mu\text{-}H)_3$ (**11**) (Figure 9). Preparation of $[(\eta^5\text{-}Me_2Si)_2(C_5H_3)_2]ZrH_2]_2$ has been achieved by reduction of the zirconocene dichloride with $NaBEt_3$.[32] Attempts to dissolve **11** in common organic solvents such as benzene, THF, toluene and methylene chloride have been unsuccessful and hence no spectroscopic data has been obtained.

The trimeric hydride, **11**, crystallizes in the tetragonal space group $P4_32_12$ as dichroic dark green/colorless crystals. The molecule lies on a two-fold axis through Zr(2) and H(2) and also contains a plane of symmetry that is defined by the three zirconium centers and the three μ_2-hydride ligands. All five hydride ligands have been found in the difference map and freely refined. The three zirconium centers and the three μ_2-hydride ligands are all coplanar and are capped above and below the plane with two μ_3-hydride ligands. As shown in Figure 10, the metallocene wedge defined by Zr(2) is tilted with respect to the plane formed by the three zirconium centers. The zirconium-μ_2-hydride

distances are shorter (1.93 Å and 1.96 Å) than the zirconium-μ_3-hydride ligand distances (2.04 Å, 2.17 Å).

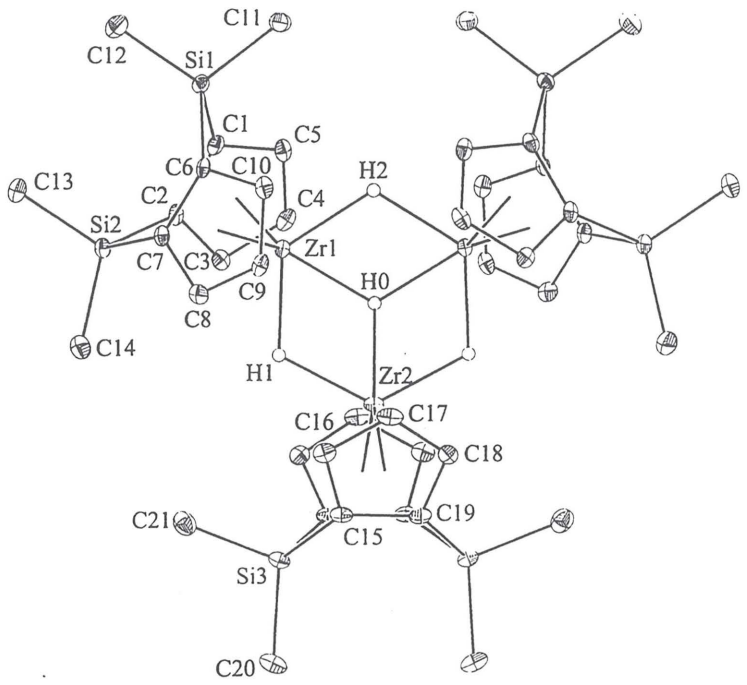

Figure 9. Molecular structure for **11** with 50% probability ellipsoids. Hydrogen atoms other than the five hydrides have been omitted for clarity.

The zirconium-zirconium distance in **11** is slightly shorter than the 3.492 Å observed for **2** and related dihydride dimers.[13] This distance is significantly longer than 3.124 Å observed in the triple hydride-bridged dimer, $[Zr_2H_3(BH_4)_5(PMe_3)_2]$,[33] and the tetrahydride-bridged dimer, $[Zr_2H_4(BH_4)_4(PMe_3)_4]$.[34] In these structures, only μ_2-hydride bridges are observed.

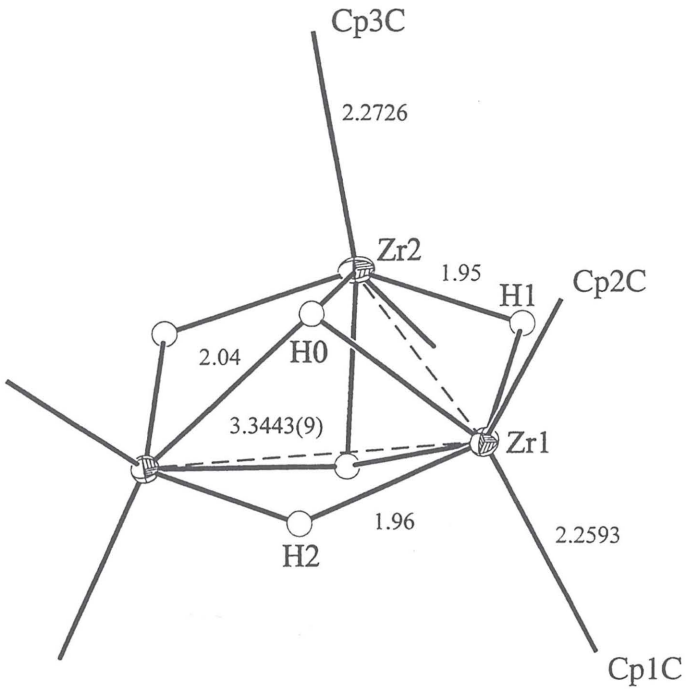

Figure 10. View of the zirconium hydride core of **11**. Distances are reported in Angstroms.

Increasing the substitution on the cyclopentadienyl ligand array has a dramatic impact on the hydrogenation reaction. Hydrogenation of *sec*-BuThpZrMe$_2$ (**12**) in benzene-d_6 solution at 87 °C results in clean and quantitative formation of [*sec*-BuThpZrH$_2$]$_2$ (**13**). The ^{1}H NMR spectrum displays two triplets, one at 4.25 ppm and the other at 0.13 ppm for the terminal and bridging hydrides, respectively. Although each zirconium is C_1 symmetric, the zirconium hydride resonances are accidently equivalent. The solution molecular weight for **13** has been determined and found to be 914 g/mol (monomer = 477 g/mol). Both the ^{1}H NMR and the solution molecular weight data are consistent with a dimeric structure in solution (eq. 7).

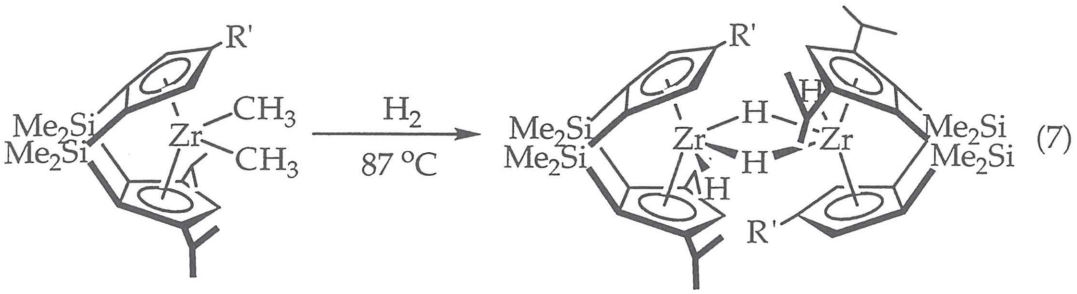

(7)

or isomer

R' = $CH(CH_3)(CH_2CH_3)$: **13**
R' = $CHMe_2$: **15**

Similar experiments have been conducted with iPrThpZrMe_2 (**14**). Hydrogenation of the dimethyl complex proceeds smoothly at 87 °C producing methane and one isomer of [iPrThpZrH_2]$_2$ (**15**). As with **13**, **15** displays a triplet at 4.25 ppm for the terminal zirconium hydrides and a triplet at 0.20 ppm for the bridging hydrides. Both **13** and **15** undergo exchange with D_2 gas over the course of several days at room temperature whereas the unlinked metallocene hydride dimers, [Cp*(CpR_n)ZrH_2}$_2$, undergo rapid exchange with deuterium at 25 °C.[15] These results suggest that **13** and **15** form more robust dimers than the corresponding unlinked zirconocene dihydride dimers.

In an attempt to prepare a monomeric, doubly silylene-bridged zirconocene dihydride, a tertiary center was incorporated into the 4-position of the monosubstituted cyclopentadienyl ring. Preparation of TMSThpZrMe_2 (**16**) has been accomplished via methylation of the dichloride complex. Unfortunately, hydrogenation of **16** at 87 °C results in liberation of methane and decomposition of the organozirconium complex.

Perturbation of the overall symmetry of the zirconocene was also attempted with the goal of preparing a monomeric, doubly silylene-bridged zirconocene dihydride. Methylation of the C_2 symmetric, $(Me_2Si)_2(\eta^5\text{-}C_5H\text{-}(CHMe_2)_2)_2ZrCl_2$[35] (TipZr$Cl_2$) (**17**) affords the dimethyl complex, TipZrMe_2 (**18**) in high yield. Hydrogenation at 87 °C over the course of 24 hours results in formation of [TipZrH_2]$_2$ (**19**) (Figure 11). At 22 °C, the ^{1}H NMR spectrum of **19** in benzene-d_6 displays resonances at -5.65 and 2.10 for the terminal and bridging hydride ligands. Warming the sample to 67 °C results in a gradual shift

of the hydride resonance downfield to 3.10 ppm. We interpret a chemical shift in this range to be a weighted average of both the monomer and dimer in solution (Figure 11). Continued heating of the sample produces no further change in the NMR spectrum.

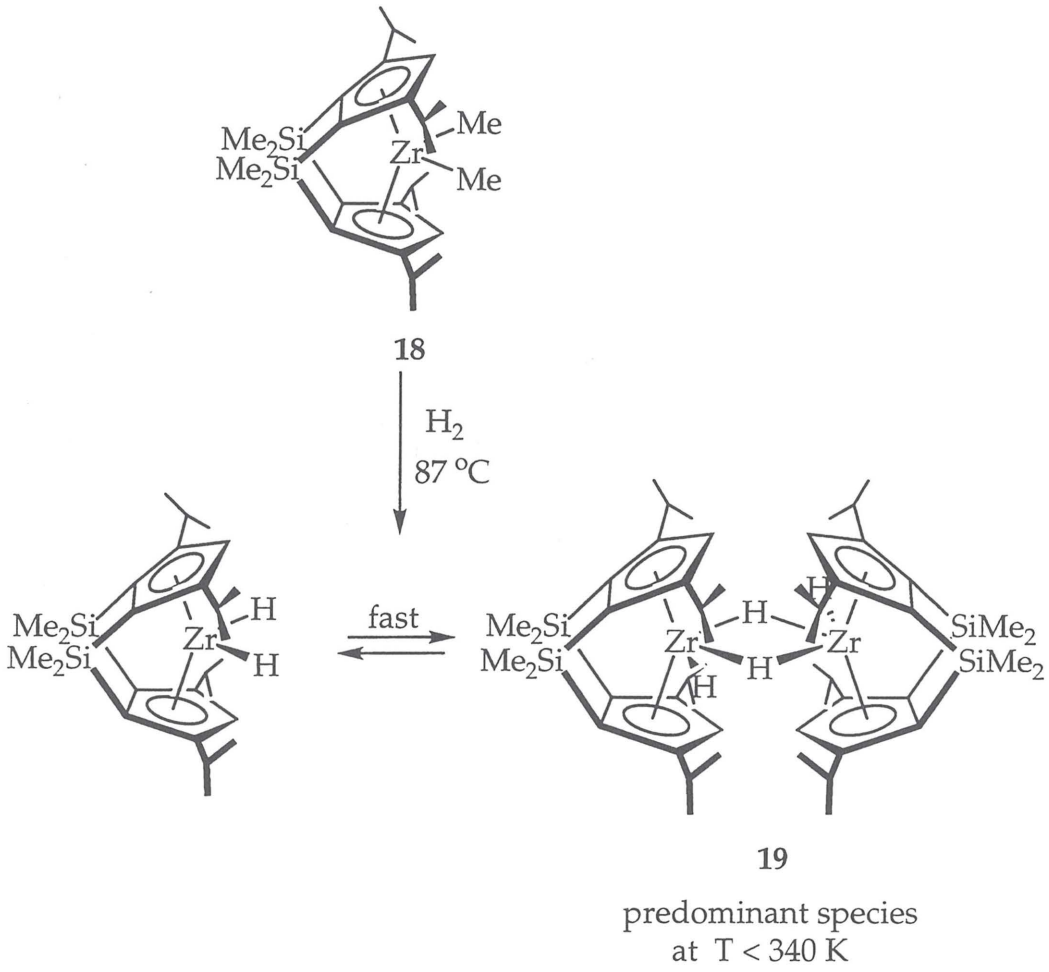

Figure 11. Hydrogenation of **18** to **19**.

Although the increased substitution of **19** compared to **13** and **15** resulted in some destabilization of dihydride dimer, a monomeric dihydride was still not obtained. Another approach is to prepare doubly silylene-bridged C_{2v} symmetric metallocenes with bulky substituents in front of the metallocene wedge. Reaction of $(Me_2Si)_2(\eta^5\text{-}C_5H_2\text{-}4\text{-}(CMe_3)_2)_2ZrCl_2$ ($BsZrCl_2$, **20**)[40] with two equivalents of methyl lithium results in formation of $BsZrMe_2$ (**21**). Addition of dihydrogen to a benzene-d_6 solution of **21** at 87 °C results in formation of methane, although no tractible zirconocene dihydride product has been identified. Monitoring the reaction by ^1H NMR spectroscopy reveals that the

benzene-d_6 is hydrogenated to isotopomers of cyclohexane, thus implicating the presence of a zirconocene dihydride.[15] Performing the reaction in cyclohexane-d_{12} produces methane and results in H/D exchange in the alkane solvent but no zirconocene dihydride could be observed. It appears that the zirconocene dihydride is formed in the above reactions, but may be too unstable for observation and as a result, readily decomposes upon formation.

In all of the doubly silylene-linked zirconocene dimethyl complexes studied, elevated temperatures are required for hydrogenation of the zirconium methyl groups. This contrasts previous results with unlinked and singly-bridged systems where hydrogenation occurs readily at room temperature. The higher barrier for σ-bond metathesis is believed to be due to steric blocking of the empty $1a_1$ orbital of the zirconocene dimethyl complex by the dimethylsilylene linker (Figure 12) thus increasing the energy for H_2 binding. A similar effect has been noted in the chlorination of these compounds with $PbCl_2$.[36]

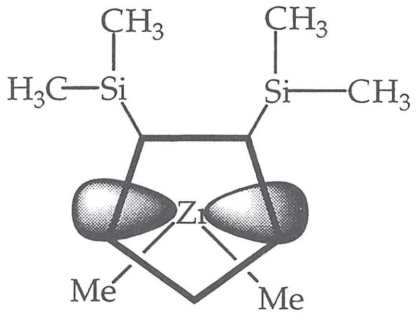

Figure 12. Sterically blocking of the $1a_1$ orbital by the dimethylsilylene linkers.

Conclusions

A series of *ansa*-zirconocene dihydride complexes has been prepared from hydrogenation of the corresponding dimethyl complexes. The *tert*-butyl substituted metallocene **2** is dimeric in the solid state and in solution, due to the ability of the *tert*-butyl groups to orient themselves in a *trans* disposition. The first example of a monomeric *ansa*-zirconocene dihydride has been prepared via hydrogenation of **3**, yielding **4**. Exposure of **4** to dinitrogen results in thermal reductive elimination of dihydrogen and coordination of dinitrogen, forming the side-on bound dinitrogen complex, **5**, which has an atypical N-N bond length of

1.2450(38) Å. Doubly silylene bridged zirconocene dihydrides have also been prepared via hydrogenation of the dimethyl complexes. In these complexes, elevated temperatures are required for hydrogenation due to steric blocking of the $1a_1$ orbital by the dimethylsilylene linking groups.

Experimental

General Considerations. All air and moisture sensitive compounds were manipulated using standard vacuum line, Schlenk or cannula techniques, or in a drybox under a nitrogen atmosphere as described previously.[37] Molecular weights were determined by ebulliometry as described previously.[37] Argon, dinitrogen, dihydrogen and dideuterium gases were purified by passage over columns of MnO on vermiculite and activated molecular sieves. Solvents for air- and moisture-sensitive reactions were dried over titanocene[38] or sodium benzophenone ketyl. Toluene-d_8 and cyclohexane-d_{12} were distilled from sodium benzophenone ketyl and stored over titanocene. Tetahydrofuran-d_8 was distilled from benzophenone ketyl and stored over 4Å molecular sieves. Preparations of *meso*-$Me_2Si(\eta^5\text{-}C_5H_3\text{-}3\text{-}CMe_3)_2Zr(NMe_2)_2$,[8] **12**, **14**,[39] **17**[35], **20**, **21**,[40] and **10**[31] were carried out as described previously.

***meso*-[$Me_2Si(C_5H_3\text{-}3\text{-}CMe_3)_2$]$ZrMe_2$ (1).** In the dry box, a 50 mL round bottom flask was charged with 0.500 g (1.04 mmol) of *meso*-$DpZr(NMe_2)_2$. Approximately 25 mL of toluene was added forming an orange solution. Via pipette, 0.500 g (6.94 mmol) of trimethylaluminum was added. With time, a darker orange solution forms. The reaction was stirred for 16 hours after which time a 180 º needle valve was attached to the flask and the toluene was removed *in vacuo* leaving a dark, oily solid. Petroleum ether was added forming an orange solid and recrystallization at -30 ºC over the course of 3 days afforded 0.257 g (58.3%) of **1**. ^{1}H (benzene-d_6): δ = 0.026 (s, 6H, Zr*Me*$_2$); 0.158 (s, 3H, Si*Me*$_2$); 0.258 (s, 3H, Si*Me*$_2$); 1.39 (s, 18H, C*Me*$_3$); 5.39 (s, 1H, Cp); 5.73 (s, 1H, Cp); 6.71 (s, 1H, Cp). ^{13}C (benzene-d_6): -5.682 (Si*Me*$_2$); -3.237 (Si*Me*$_2$); 31.39 (Zr*Me*$_2$); 33.81 (Zr*Me*$_2$); 31.99 (C*Me*$_3$) 144.76 (*C*Me$_3$); 98.08, 111.75, 112.15, 120.45, *1 not located* (Cp). Anal. Calcd. for $C_{22}H_{36}Zr_1Si_1$: C, 62.94; H, 8.64. Found C, 62.76; H, 8.42.

meso-**[[$Me_2Si(C_5H_3$-3-$CMe_3)_2$]$ZrH_2]_2$ (2).** In the dry box, a thick-walled glass bomb was charged with 0.150 g (0.354 mmol) of **1**. On the vacuum line, approximately 15 mL of toluene was added by vacuum transfer. At room temperature, 1 atmosphere of dihydrogen was added. The reaction mixture was stirred for 16 hours and the toluene was removed *in vacuo* and replaced with petroleum ether affording a white solid. The solid was collected by filtration and dried *in vacuo* yielding 0.087 g (62.1%) of **2**. ^{1}H (benzene-d_6): δ = 0.202 (s, 3H, SiMe_2); 0.239 (s, 3H, SiMe_2); 0.370 (s, 3H, SiMe_2); 0.386 (s, 3H, SiMe_2); 3.94 (m, 1H, ZrH_{term}); 4.03 (m, 1H, ZrH_{term}); -2.35 (t, 7.5 Hz, 1H, ZrH_{br}); -5.30 (m, 1H, ZrH_{br}); 1.34 (s, 18 H, CMe_3); 1.40 (s, 18 H, CMe_3); 4.99, 5.06, 5.90, 6.06, 6.16, 6.23 (m, 1H, Cp). ^{13}C (benzene-d_6): -6.60 (SiMe_2); -6.40 (SiMe_2); -1.93 (SiMe_2); -1.79 (SiMe_2); 33.30 (CMe_3); 33.40 (CMe_3); 152.49 (CMe_3); 152.88 (CMe_3); 91.25, 101.92, 102.66, 104.72, 106.90, 110.25, 110.51, 118.74, *2 not located* (Cp). Anal. Calcd. for $C_{20}H_{32}Zr_1Si_1$: C, 61.32; H, 8.23. Found C, 61.76; H, 8.56.

rac-**[$Me_2Si(C_5H_2$-2-$SiMe_3$-4-$CMe_3)_2$]$ZrMe_2$ (3).** In the dry box, a medium swivel frit assembly was charged with 1.10 g (1.82 mmol) of $BpZrCl_2$. On the vacuum line, approximately 30 mL of diethyl ether was added by vacuum transfer. At -80 °C against an argon counterflow, 2.90 mL (4.1 mmol) of 1.4 M MeLi solution in ether was added. The reaction was warmed to room temperature and stirred. Upon reaching room temperature, a yellow solution and white precipitate formed. After 24 hours, the ether was removed *in vacuo* and was replaced with toluene. The white precipitate was removed by filtration and was washed with recycled toluene. The toluene was removed *in vacuo* and the yellow solid was recrystallized from cold petroleum ether affording 0.980 g (91%) of **3**. ^{1}H (benzene-d_6): δ = 0.23 (s, 6H, ZrMe_2); 0.31 (s, 18 H, SiMe_3); 1.38 (s, 18 H, CMe_3); 6.05 (s, 2H, Cp); 7.21 (s, 2H, Cp). ^{13}C (benzene-d_6): δ = -0.810 (SiMe_2); 2.16 (SiMe_3); 30.94 (CMe_3); 34.09 (ZrMe_2); 106.65, 116.14, 125.60, 129.47, *1 not located* (Cp), 148.92 (CMe_3). Anal. Calcd. for $C_{20}H_{32}Zr_1Si_1$: C, 61.32; H, 8.23. Found C, 61.76; H, 8.56. Anal. Calcd. for $C_{28}H_{52}Zr_1Si_3$: C, 59.61; H, 9.29. Found C, 59.27; H, 9.01.

rac-**[$Me_2Si(C_5H_2$-2-$SiMe_3$-4-$CMe_3)_2$]ZrH_2 (4).** Prepared in an analogous manner to **2** with 0.940 g (1.58 mmol) of **3** yielding 0.750 g (84%) of a green solid identified as **4**. ^{1}H (benzene-d_6): δ = 0.35 (s, 18H, SiMe_3); 0.49 (s, 6H, SiMe_2); 1.49 (s, 18H, CMe_3); 5.96 (s, 2H, Cp); 7.83 (s, 2H, Cp); 7.25 (bs, 2H, ZrH); ^{13}C (benzene-

d$_6$): δ = 2.23 (Si*Me*$_3$); 2.82 (Si*Me*$_2$); 32.17 (C*Me*$_3$); 152.9 (CMe$_3$); 98.63, 11.34, 118.27, 119.49, 123.22 (Cp). Anal. Calcd. for $C_{26}H_{48}Zr_1Si_3$: C, 58.25; H, 9.02. Found C, 57.98; H, 8.67.

***rac*-[[Me$_2$Si(C$_5$H$_2$-2-SiMe$_3$-4-CMe$_3$)$_2$]Zr]$_2$(μ$_2$-N$_2$) (5).** In the dry box, a Teflon capped scintillation vial was charged with 57.0 mg (0.100 mmol) of **4** and approximately 2.0 mL of toluene. The solid was dissolved forming a green solution and allowed to stand at room temperature for 1 week after which time a red solid had deposited on the bottom of the vial. The solid was collected by filtration, washed with petroleum ether, transferred into a flask and dried *in vacuo* affording 21.0 mg (35.7%) of **5**. ^{1}H NMR (toluene-*d*$_8$): δ = 0.441 (s, 18H, Si*Me*$_3$); 0.454 (s, 18H, Si*Me*$_3$); 0.651 (s, 6H, Si*Me*$_2$); 0.923 (s, 6H, Si*Me*$_2$); 1.47 (s, 18 H, C*Me*$_3$); 1.67 (s, 18H, C*Me*$_3$); 4.77 (s, 2H, Cp); 5.11 (s, 2H, Cp); 6.14 (s, 2H, Cp); 6.66 (s, 2H, Cp). ^{13}C NMR (toluene-*d*$_8$): δ = -0.940 (Si*Me*$_2$); -0.108 (Si*Me*$_2$); 32.51 (C*Me*$_3$); 33.50 (C*Me*$_3$); 2 CMe$_3$ not located; 104.0, 104.20, 105.4, 107.91, 110.18, 112.24, 115.67, 117.21, 117.34 (Cp). UV-VIS (toluene): 392.0 nm; 612.0 nm. FT-RAMAN (benzene-*d*$_6$): 1182.6 cm^{-1}; 1001.5 cm^{-1}; 984 cm^{-1}. Anal. Calcd. for C-$_{52}$H$_{92}$Si$_6$Zr$_2$N$_2$: C, 56.97; H, 8.46; N, 2.56. Found C, 56.69; H, 8.76; N, 2.68

***rac*-[Me$_2$Si(C$_5$H$_2$-2-SiMe$_3$-4-CMe$_3$)$_2$]Zr(PMe$_3$)$_2$ (6).** In the dry box, a J. Young NMR tube was charged with 5.0 mg (4.30 x 10^{-3} mmol) of **5**. On the vacuum line, the tube was degassed with three freeze-pump-thaw cycles. Via calibrated gas volume, 3 equivalents of PMe$_3$ were added at -196 °C. The tube was thawed and shaken and the progress of the reaction monitored by NMR spectroscopy. ^{1}H (benzene-*d*$_6$): δ = -0.15 (s, 18H, Si*Me*$_3$); 0.19 (s, 6H, Si*Me*$_2$); 0.85 (d, 36 Hz, 18H, P*Me*$_3$); 1.22 (s, 18H, C*Me*$_3$); 6.44, 6.70 (m, 2H, Cp). ^{31}P (benzene-*d*$_6$): δ = 34.04.

Me$_2$ Si(η^5-C$_5$Me$_4$)(η^5-C$_5$H$_2$-2,4-(CHMe$_2$)$_2$)ZrCl$_2$ (7). In the dry box, a round bottom flask was charged with 3.66 g (11.23 mmol) of Li$_2$[iPr$_2$Tp] and 2.61 g (11.23 mmol) of ZrCl$_4$. A reflux condensor and 180° needle valve were attached. On the vacuum line, approximately 50 mL of toluene were added along with 5 mL of THF. The reaction mixture was heated to reflux for 3 days after which time the toluene was removed *in vacuo* leaving a yellow paste. Approximately 100 mL of CH_2Cl_2 and 25 mL of 4 M HCl were added. The organic layer was collected and the aqueous layer washed with 3 small portions of CH_2Cl_2. The organic layers were combined and dried over $MgSO_4$ for 1 hour. After filtration, the solvent was removed by rotovap, leaving a yellow tar. Pentane was added

and a white solid precipitated. The solid was washed with small portions of diethyl ether and pentane and dried *in vacuo*. Analytically pure material may be obtained via vacuum sublimation (10^{-4} torr) at 160 °C. ^{1}H (benzene-d_6): δ = 0.816 (s, 3H, Si*Me*$_2$); 0.945 (s, 3H, Si*Me*$_2$); 1.10 (d, 6.6 Hz, 3H); 1.21 (d, 6.5 Hz, 3H); 1.24 (d, 6.5 Hz, 3H); 1.26 (d, 6.5 Hz, 3H); 1.87 (s, 3H, C$_5$*Me*$_4$); 1.90 (s, 3H, C$_5$*Me*$_4$); 1.98 (s, 3H, C$_5$*Me*$_4$); 2.01 (s, 3H, C$_5$*Me*$_4$); 2.71 (sept, 7.0 Hz, 1H, C*H*Me$_2$); 3.06 (sept, 7.0 Hz, 1H, C*H*Me$_2$); 5.25 (s, 1H, Cp); 6.50 (s, 1H, Cp). ^{13}C (benzene-d_6): δ = 1.22 (Si*Me*$_3$); 1.25 (Si*Me*$_3$); 11.90, 12.61, 14.63, 14.93 (C$_5$*Me*$_4$); 20.30, 22.25, 22.75, 29.39 (CH*Me*$_2$); 29.24, 29.89 (*C*HMe$_2$); 96.28, 99.50, 110.79, 117.79, 112.90, 113.99, 137.07, 143.49, 149.63 (Cp). Anal. Calcd. for $C_{22}H_{34}Zr_1Cl_2$: C, 57.36; H, 7.44. Found C, 57.57; H, 7.14.

Me$_2$ Si(η^5-C$_5$Me$_4$)(η^5-C$_5$H$_2$-2,4-(CHMe$_2$)$_2$)ZrMe$_2$ (8). This compound was prepared in an analogous manner to **3** employing 0.760 g (1.56 mmol) of **7** and 2.5 mL of 1.4 M MeLi solution in diethyl ether yielding 0.560 g (80.4%) of a white solid identified as **8**. ^{1}H (benzene-d_6): δ = 0.440 (s, 3H, Si*Me*$_2$); 0.575 (s, 3H, Si*Me*$_2$); -0.352 (s, 3H, Zr*Me*$_2$); -0.258 (s, 3H, Zr*Me*$_2$); 1.14 (d, 7.0 Hz, 3H); 1.23 (d, 6.8 Hz, 3H); 1.29 (d, 6.9 Hz, 3H); 1.33 (d, 7.0 Hz, 3H); 1.63 (s, 3H, C$_5$*Me*$_4$); 1.79 (s, 3H, C$_5$*Me*$_4$); 1.95 (s, 3H, C$_5$*Me*$_4$); 1.98 (s, 3H, C$_5$*Me*$_4$); 2.54 (sept, 7.0 Hz, 1H, C*H*Me$_2$); 3.03 (sept, 7.0 Hz, 1H, C*H*Me$_2$); 5.04 (s, 1H, Cp), 6.65 (s, 1H, Cp). ^{13}C (benzene-d_6): δ = 1.54 (Si*Me*$_3$); 1.65 (Si*Me*$_3$); 11.36, 11.64, 14.37, 14.53 (C$_5$*Me*$_4$); 20.56, 23.39, 23.89, 29.54 (CH*Me*$_2$); 28.37, 29.72 (*C*HMe$_2$); 32.88 (ZrCH$_3$); 35.93 (Zr-*C*H$_3$) 91.02, 93.77, 109.76, 113.04, 120.94, 123.22, 140.18, 140.49 (Cp).

[Me$_2$ Si(η^5-C$_5$Me$_4$)(η^5-C$_5$H$_2$-2,4-(CHMe$_2$)$_2$)ZrH$_2$]$_2$ (9). This compound was prepared in an analogous manner to **2** employing 0.320 g (0.716 mmol) of **8** and 1 atmosphere of H_2. After stirring for 2 days, the product was collected by filtration and dried *in vacuo* yielding 0.170 g (56.7%) of **9**. ^{1}H (THF-d_8): δ = 0.421 (s, 3H, Si*Me*$_2$); 0.620 (s, 3H, Si*Me*$_2$); 3.87 (d, 20 Hz, 1H, Zr-*H*$_2$); 4.13 (d, 20 Hz, 1H, Zr-*H*$_2$); 1.10 (d, 7.0 Hz, 3H); 1.15 (d, 7.0 Hz, 3H); 1.20 (d, 7.0 Hz, 3H); 1.60 (d, 7.0 Hz, 3H); 1.92 (s, 3H, C$_5$*Me*$_4$); 2.02 (s, 3H, C$_5$*Me*$_4$); 2.23 (s, 3H, C$_5$*Me*$_4$); 2.32 (s, 3H, C$_5$*Me*$_4$); 2.83 (sept, 7.0 Hz, 1H, C*H*Me$_2$); 3.08 (sept, 7.0 Hz, 1H, C*H*Me$_2$); 4.86 (s, 1H, Cp), 5.69 (s, 1H, Cp). Anal. Calcd. for $C_{22}H_{34}Zr_1Cl_2$: C, 62.94; H, 8.64. Found C, 62.07; H, 8.63.

[((Me$_2$Si)$_2$(C$_5$H$_3$)$_2$)Zr]$_3$(μ$_3$-H)$_2$(μ-H)$_3$ (11). In the dry box, a J. Young NMR tube was charged with 10.5 mg of **10** and the sample dissolved in benzene-d_6. On the

vacuum line, the tube was degassed with three-freeze-pump thaw cycles and 1 atmosphere of dihydrogen was admitted at -196 °C. The tube was thawed, shaken and placed into a 100 °C oil bath. After heating for 24 hours, dark green crystals were desposited in the tube and were collected in the dry box for X-ray diffraction.

[$(Me_2Si)_2(\eta^5\text{-}C_5H\text{-}3,5\text{-}(CHMe_2)_2)(\eta^5\text{-}C_5H_2\text{-}4\text{-}CH(CH_3)(CH_2CH_3))]ZrH_2]_2$ (13). In the dry box, a thick walled glass bomb was charged with 0.560 g (1.10 mmol) of **12**. On the vacuum line, cyclohexane was added by vacuum transfer. Upon warming to room temperature, the bomb was then charged with 1 atmosphere of dihydrogen. The bomb was then placed in an 80 °C oil bath and stirred. The reaction was continued for 2 days after which time the contents of the bomb were transferred into a swivel frit assembly. The cyclohexane was removed *in vacuo* and replaced with petroleum ether. Cooling the solution to -80 °C afforded a white solid that was collected by filtration and dried *in vacuo* yielding 0.325 g (61.6%) of **3**. ^{1}H (benzene-d_6): δ = 0.13 ppm (t, 5 Hz, 2H, Zr*H*, bridging); 0.583 (s, 3H, Si*Me*$_2$); 0.604(s, 3H, Si*Me*$_2$); 0.614 (s, 3H, Si*Me*$_2$); 0.638 (s, 3H, Si*Me*$_2$); 1.02 (t, 7 Hz, 3H, CH(CH$_3$)(CH$_2$*CH*$_3$)); 1.78(d, 6.5 Hz, 3H, CH(*CH*$_3$)(CH$_2$CH$_3$)); 1.19 (d, 6.5 Hz, 3H, CH*Me*$_2$); 1.40 (d, 6.5 Hz, 3H, CH*Me*$_2$); 1.61 (d, 6.5 Hz, 3H, CH*Me*$_2$); 1.72 (d, 6.5 Hz, 3H, CH*Me*$_2$); 1.80 (m, 2H, CH(CH$_3$)(C*H*$_2$CH$_3$)); 3.53 (m, 1H, C*H*(CH$_3$)(CH$_2$CH$_3$); 3.14 (sept, 6.5 Hz, 1H, C*H*Me$_2$); 3.66 (sept, 6.5 Hz, 1H, C*H*Me$_2$); 4.25 (t, 5Hz, 2H, Zr*H*, terminal); 5.86 (s, 1H, Cp); 6.56 (s, 1H, Cp); 7.14 (s, 1H, Cp). ^{13}C (benzene-d_6): δ = -0.475 (Si*Me*$_2$); -0.071 (Si*Me*$_2$); 4.16 (Si*Me*$_2$); 4.21 (Si*Me*$_2$); 11.30, 19.34, 22.68, 23.22, 29.79, 30.13, 20.40, 33.79, 34.65 (CHMe$_2$ and CH(CH$_3$)(CH$_2$CH$_3$); 97.88, 99.08, 102.60, 104.20, 109.28, 117.32, 119.09, 139.09, 155.91, 159.62 (Cp). Anal. Calcd. for $C_{24}H_{40}Zr_1Si_2$: C, 60.56; H, 8.47. Found C, 59.54; H, 8.32.

[$(Me_2Si)_2(\eta^5\text{-}C_5H\text{-}3,5\text{-}(CHMe_2)_2)(\eta^5\text{-}C_5H_2\text{-}4\text{-}CH(CH_3)_2]ZrH_2]_2$ (15). In the dry box, a J. Young NMR tube was charged with 10.0 mg (0.0189 mmol) of **14** and the sample was dissolved in benzene-d_6 forming a clear solution. On the vacuum line, the tube was degassed with three freeze-pump thaw cycles. The tube was then cooled to -196 °C and 1 atmosphere of dihydrogen added. The tube was then heated in an 87 °C oil bath and the reaction monitored by NMR spectroscopy. ^{1}H NMR (benzene-d_6): δ = 0.20 ppm (t, 5 Hz, 2H, Zr*H*, bridging); 0.561 (s, 3H, Si*Me*$_2$); 0.601(s, 3H, Si*Me*$_2$); 0.635 (s, 3H, Si*Me*$_2$); 0.681 (s, 3H, Si*Me*$_2$);

0.891 (d, 6.5 Hz, 3H, CH*Me*$_2$); 0.954 (d, 6.5 Hz, 3H, CH*Me*$_2$); 1.12 (d, 6.5 Hz, 3H, CH*Me*$_2$); 1.18 (d, 6.5 Hz, 3H, CH*Me*$_2$); 1.21 (d, 6.5 Hz, 3H, CH*Me*$_2$);1.51 (d, 6.5 Hz, 3H, CH*Me*$_2$); 2.45 (sept, 6.5 Hz, 1H, C*H*Me$_2$); 2.94 (sept, 6.5 Hz, 1H, C*H*Me$_2$); 3.43 (sept, 6.5 Hz, 1H, C*H*Me$_2$); 4.25 (t, 5Hz, 2H, Zr*H*, terminal); 5.73 (s, 1H, Cp); 6.27 (s, 1H, Cp); 7.09 (s, 1H, Cp).

[(Me$_2$Si)$_2$(η^5-C$_5$H-3,5-(CHMe$_2$)$_2$)(η^5-C$_5$H$_2$-4-SiMe$_3$)]ZrMe$_2$ (16). This compound was prepared in an analogous manner as those published for **12** and **14**. ^{1}H NMR (benzene-d_6): δ = -0.142 (s, 6H, Zr*Me*$_2$); 0.392 (s, 9H, Si*Me*$_3$); 0.387 (s, 6H, Si*Me*$_2$); 0.555 (s, 6H, SiMe$_2$); 1.05 (d, 7 Hz, 6H, CH*Me*$_2$); 1.27 (d, 7 Hz, 6H, CH*Me*$_2$); 2.69 (sept, 7Hz, 2H, C*H*Me$_2$); 6.86 (m, 2H, Cp); 6.44 (m, 1H, Cp). ^{13}C NMR (benzene-d_6): δ = 0.94 (Si*Me*$_3$); -1.12 (Si*Me*$_2$); 3.85 (Si*Me*$_2$); 21.39, 29.18 (CH*Me*$_2$); 29.32 (*C*HMe$_2$); 105.34, 111.40, 115.45, 124.68, 134.78, 154.22 (Cp). Anal. Calcd. for $Zr_1Si_3C_{25}H_{44}$ C, 57.73%, H, 8.53%; Found C, 57.90%; H, 8.82%.

[(Me$_2$Si)$_2$(η^5-C$_5$H-3,5-(CHMe$_2$)$_2$)$_2$]ZrMe$_2$ (18). In the drybox, a 25 mL round bottom flask was charged with 2.00 g (2.72 mmol) of **17**. On the vacuum line, approximately 15 mL of ether was added by vacuum transfer. At -80 °C against an Ar counterflow, 4.3 mL (6.00 mmol) of 1.4 M MeLi was added via syringe. The reaction was warmed to room temperature and stirred. With time a white slurry forms. The reaction was stirred for 5 hours and the solvent was removed *in vacuo*.. Toluene was added and the white precipitate was removed by filtration. The toluene was removed *in vacuo* leaving 1.20 g (65%) of a yellow solid identified as **18**. ^{1}H NMR (benzene-d_6): δ = -0.207 (s, 6H, Zr*C*H$_3$); 0.498 (s, 6H, Si*Me*$_2$); 0.616 (s, 6H, Si*Me*$_2$); 1.14 (d, 6 Hz, 12H, CH*Me*$_2$); 1.38 (d, 6 Hz, 12H, CH*Me*$_2$); 2.97 (sept, 6.5 Hz, 4H, C*H*Me$_2$), 6.61 (s, 2H, Cp). ^{13}C NMR (benzene-d_6): δ = 1.61 (Si*Me*$_2$); 6.14 (Si*Me*$_2$); 21.53 (CH*Me*$_2$); 29.30 (CH*Me*$_2$); 29.92 (*C*HMe$_2$); 30.25 (Zr*C*H$_3$); 106.14, 111.53, 153.08 (Cp).

[(Me$_2$Si)$_2$(η^5-C$_5$H-3,5-(CHMe$_2$)$_2$)$_2$]ZrH$_2$ (19). This compound was prepared in an analogous manner to **2** employing 0.950 g (1.69 mmol) of **18** and 4 atmospheres of dihydrogen. The reaction was heated to 87 °C for one week and affords 0.650 g (72.3%) of **19**. ^{1}H NMR (benzene-d_6): δ = -5.649 (m, 2H, Zr*H* (bridging)); -5.205 (m, 1H, Zr*H* (bridging); 0.161 (s, 6H, Si*Me*$_2$); 0.783 (s, 6H, Si*Me*$_2$); 1.18 (d, 7 Hz, 12H, CH*Me*$_2$); 1.22 (d, 7 Hz, 12H, CH*Me*$_2$); 3.16 (sept, 6,5 Hz, 4H, C*H*Me$_2$); 6.23 (s, 2H, Cp). ^{13}C NMR (benzene-d_6): δ = 3.99 (Si*Me*$_2$); 6.73

(Si*Me*$_3$); 23.15 (CH*Me*$_2$); 28.83 (CH*Me*$_2$); 29.64 (CHMe$_2$); 116.44, 118.00, 152.78 (Cp). Anal. Calcd. for $C_{26}H_{44}Zr_1Si_2$: C, 61.96; H, 8.80. Found C, 61.43; H, 8.43.

Solid State Structure for 1. A suitable fragment of **1** was cut from one massive crystal, attached to a glass fiber and centered on an Enraf-Nonius CAD-4 diffractometer under an 85 K stream of N_2 gas. Unit cell parameters were obtained from the setting angles of 25 high-angle reflections. Two equivalent data sets were collected and merged in $P2_1/c$. Three reference reflections were measured every 75 minutes to monitor crystal decay. The structure was solved using direct methods and the difference Fourier maps were used to locate the missing atoms, including hydrogens. A total of 6632 data were refined to R = 0.0342 (GOF = 1.304).[41]

Solid State Structure for 2. A small, clear and colorless crystal of **2** was mounted on a glass fiber with Paratone-N oil. The data was collected on a Bruker Smart 1000 CCD diffractometer under a stream of N_2 gas at 98 K. Four runs of data were collected with 20 second long, -0.20 ° wide ω-scans at four values of ϕ (0, 120, 240 and 300°) with the detector 5 cm (nominal) distant at Θ of -28 °. The initial cell for data reduction was calculated for just under 1000 reflections chosen throughout the data frames. For data processing with SAINT v.602, all defaults were used, except: box size optimization was enabled, periodic orientation matrix updating was disabled, the instrument error was set to a minimum value of 0.001, Laue class integration restraints were not used, the model profiles from all nine areas were blended and for the post-integration global least squares refinement, no constraints were applied. The data were corrected with SADABS v. 2.0 (beta) using a g value of 0.05. No decay correction was needed.

The structure was solved using direct methods and the difference Fourier maps were used to locate all missing atoms, including hydrogens. Refinement of F^2 was against all reflections. A total of 7795 reflections were refined to R = 0.0458 (GOF = 2.286).

Solid State Structure for 5. The crystal was mounted and the data were collected in a manner similar to **2**. Three runs of data were collected with 20 second long, -0.20 ° wide ω-scans at four values of ϕ (0, 120 and 240) with the

detector 5 cm (nominal) distant at Θ of -28 °. The initial cell for data reduction was calculated for just under 1000 reflections chosen throughout the data frames. For data processing with SAINT v. 6.02, all defaults were used, except: box size optimization was enabled, periodic orientation matrix updating was disabled, the instrument error was set to a minimum value of 0.001, Laue class integration restraints were not used, the model profiles from all nine areas were blended and for the post-integration global least squares refinement, no constraints were applied. The data were corrected with SADABS v. 2.0 (beta) using a g value of 0.058. No decay correction was needed.

The structure was solved using direct methods and the difference Fourier maps were used to locate all missing atoms, including hydrogens. Refinement of F^2 was against all reflections. A total of 4312 reflections were refined to R = 0.0610 (GOF = 1.73).

Solid State Structure for 11. The data were collected in the same manner for **1**. Unit cell parameters were obtained from 25 high angle reflections. Two equivalent data sets were collected and merged in $P4_32_12$ (#96). Three reflections were measured every 75 minutes to monitor crystal decay. The structure was solved using direct methods and the difference Fourier maps were used to locate the missing atoms, including hydrogens. A total of 3746 data were refined to *R* = 0.0163 (GOF = 1.627).

References.

1. a) Brintzinger, H.H.; Fischer, D.; Mülhaupt, R.; Reiger, B.; Waymouth, R.M. *Angew. Chem. Int. Ed. Engl.* **1995**, *34*, 1143. b) Bochmann, M. *J. Chem. Soc., Dalton Trans.* **1996**, 255.

2. Hoveyda, A.H.; Morken, J.P. in *The Metallocenes* vol. 2; Togni, A. and Haltermann, L. Eds., Wiley-VCH Publishers, Weinheim, 1988, Chapter 10.

3. a) Waymouth, R.M.; Pino, P. *J. Am. Chem. Soc.* **1990**, *112*, 4911. b) Troutman, M.V.; Appella, D.H.; Buchwald, S.L. *J. Am. Chem. Soc.* **1999**, *121*, 4916.

4. Broene, R.D.; Buchwald, S.L. *J. Am. Chem. Soc.* **1996**, *118*, 11688.

5. Grossman, R.B.; Doyle, R.A.; Buchwald, S.L. *Organometallics* **1991**, *10*, 1501.

6. Cuenca, T.; Galakhov, M.; Royo, B.; Royo, P. *J. Organomet. Chem.* **1996**, *515*, 33.

7. Lee, H.; Desrosiers, P.J.; Guzei, I.; Rheingold, A.L.; Parkin, G. *J. Am. Chem. Soc.* **1998**, *120*, 3255.

8. Diamond, G.M.; Jordan, R.F.; Peterson, J.L. *Organometallics* **1996**, *15*, 4045.

9. Yoder, J.C.; Day, M.W.; Bercaw, J.E. *Organometallics* **1998**, *17*, 4946.

10. Kim, I.; Jordan, R.F. *Macromolecules* **1996**, *29*, 489.

11. a) $[(\eta^5\text{-}C_5H_4\text{-}CH_3)_2ZrH_2]_2$ (3.460 Å): Jones, S.B.; Peterson, J.L. *Inorg. Chem.* **1981**, *20*, 2889. b) $[(\eta^5\text{-}C_5H_4\text{-}CMe_3)_2ZrH_2]_2$ (3.471 Å): Choukroun, R.; Dahan, F.; Larsonneur, A.M.; Samuel, E.; Peterson, J.; Meunier, P.; Sornay, C. *Organometallics* **1991**, *10*, 374. c) $[(\eta^5\text{-}C_5H_4\text{-}SiMe_3)_2ZrH_2]_2$ (3.437 Å): Larsonneur, A.M.; Choukroun, R.; Jaud, J. *Organometallics* **1993**, *12*, 3216. d) $[Me_2Si(\eta^5\text{-}C_5Me_4)_2ZrH_2]_2$ (3.549 Å): Lee, H; Desrosiers, P.J.; Guzei, I.; Rheingold, A.L.; Parkin, G. *J. Am. Chem. Soc.* **1998**, *120*, 3255.

12. Xin, S.; Harrod, J.F.; Samuel, E. *J. Am. Chem. Soc.* **1994**, *116*, 11562.

13. Mitchell, J.P.; Hajela, S.; Brookhart, S.K.; Hardcastle, K.I.; Henling, L.M.; Bercaw, J.E. *J. Am. Chem. Soc.* **1996**, *118*, 1045.

14. Chacon, S.T.; Coughlin, E.B.; Henling, L.M.; Bercaw, J.E. *J. Organomet. Chem.* **1995**, *497*, 171.

15. Chirik, P.J.; Day, M.D.; Bercaw, J.E. *Organometallics* **1999**, *18*, 1873

16. Manriquez, J.M.; McAlister, D.R.; Sanner, R.D.; Bercaw, J.E. *J. Am. Chem. Soc.* **1978**, *100*, 2716.

17. a) Bianchini, C.; Meli, A.; Perruzzini, M.; Vizza, F.; Zanobini, F. *Organometallics* **1989**, *8*, 2080. b) Chaudret, B.; Devillers, J.; Poilblanc, R. *Organometallics* **1985**, *4*, 1727.

18. Fryzuk, M.D.; Johnson, S.A.; Rettig, S.J. *J. Am. Chem. Soc.* **1998**, *120*, 11024.

19. Sanner, R.D.; Duggan, D.M.; McKenzie, T.C.; Marsh, R.E.; Bercaw, J.E. *J. Am. Chem. Soc.* **1976**, *98*, 8358.

20. Sanner, R.D.; Manriquez, J.M.; Marsh, R.E.; Bercaw, J.E. *J. Am. Chem. Soc.* **1976**, *98*, 8351.

21. Roddick, D.M.; Fryzuk, M.D.; Siedler, P.F.; Hillhouse, G.L.; Bercaw, J.E. *Organometallics* **1985**, *4*, 97.

22. a) Fryzuk, M.D.; Love, J.B.; Rettig, S.J.; Young, V.G. *Science* **1997**, *275*, 1445. b) Cohen, J.D.; Fryzuk, M.D.; Loehr, T.M.; Mylvaganam, M.; Rettig, S.J. *Inorg. Chem.* **1998**, *37*, 112.

23. Evans, W.J.; Ulibarri, T.A.; Ziller, J.W. *J. Am. Chem. Soc.* **1988**, *110*, 6877.

24. Allen, F.H.; Kennard, O.; Watson, D.G.; Brammer, L.; Orpen, A.G.; Taylor, R. *J. Chem. Soc., Perkin Trans. 2*, **1987**, S1.

25. a) *trans*-PhN=NPh (114.706 degrees): Bouwstra, J.A.; Schouten, A.; Kroon, J. *Acta Cryst. C.* **1983,** *39*, 1121. b) *trans*-Me_3CN=$NCMe_3$ (112.210 degrees): Argay, G.; Sasvari, K. *Acta Cryst. B.* **1971**, *27*, 1851.

26. Abp = $Me_2Si\{3\text{-}[2\text{-}SiMe_3\text{-}4\text{-}[2\text{-}(2\text{-}CH_3\text{-}C_{10}H_{14})]\text{-}C_5H_2\}_2$. Abrams, M.A. *Ph.D. Thesis*, California Institute of Technology, **1998**.

27. Ligand promoted reductive elimination has been observed in zirconocene alkyl hydride complexes. See McAlister, D.R.; Erwin, D.R.; Bercaw, J.E. *J. Am. Chem. Soc.* **1978**, *100*, 5966.

28. Chernaga, A.; Cook, J.; Green, M.L.H.; Labella, L.; Simpson, S.J.; Souter, J.; Stephens, A.H.H. *J. Chem. Soc., Dalton Trans.* **1997**, 3225.

29. Shin, J.; Parkin, G. *Chem. Comm.* **1999**, 187.

30. Herzog, T.A. *Ph.D. Thesis* California Institute of Technology, **1997**.

31. Cano, A.; Cuenca, T.; Gómez-Sal, P.; Royo, B.; Royo, P. *Organometallics* **1994**, *13*, 1688.

32. Cuenca, T.; Galakhov, M.; Royo, B.; Royo, P. *J. Organomet. Chem.* **1996**, *515*, 33.

33. Gozum, J.E.; Girolami, G.S. *J. Am. Chem. Soc.* **1991**, *113*, 3829.

34. Bown, M. *Acta Cryst. C* **1994**, *50*, 367.

35. Miyake, S.; Bercaw, J.E. *J. Mol. Cat. A* **1998**, *128*, 29.

36. Brandow, C.G.; Wendt, O.F., Bercaw, J.E. *unpublished results*.

37. Burger, B.J.; Bercaw, J.E. in *Experimental Organometallic Chemistry*, ACS Symposium Series, No 357; Wayda, A.L., Darensbourg, M.Y., Eds.; American Chemical Society: Washington, DC 1987; Chapter 4.

38. Marvich, R.H.; Brintzinger, H.H. *J. Am. Chem. Soc.* **1971**, *93*, 2046.

39. Veghini, D.; Day, M.D.; Bercaw, J.E. *Inorg. Chem. Acta* **1998**, *280*, 226.

40. Bulls, A.R. *Ph.D. Thesis*, California Institute of Technology, **1988**.

41. Crystallographic data for **1** have been deposited at the CCDC, 12 Union Road, Cambridge CB2 1EZ, UK, and copies can be obtained on request, free of charge, by quoting the publication citation and the deposition number 114738.

Chapter 3

Ancillary Ligand Effects on Fundamental Transformations in Group 4 Metallocene Chemistry. Kinetics and Mechanism of Olefin Insertion and β-Hydrogen Elimination.

Abstract

Reactions of the metallocene dihydrides, $(R_nCp)_2MH_2$ (R_nCp = alkyl-substituted cyclopentadienyl; M = Zr, Hf), with olefins afford stable zirconocene alkyl hydride adducts of the general formula, $(R_nCp)_2M(CH_2CHR'_2)(H)$ (R' = H, alkyl). For sterically crowded, monomeric dihydrides: $Cp^*_2ZrH_2$ (Cp^* = η^5-C_5Me_5); $Cp^*(\eta^5\text{-}C_5Me_4H)ZrH_2$, $Cp^*(\eta^5\text{-}C_5Me_4\text{-}CH_2CH_3)ZrH_2$, $Cp^*_2HfH_2$ and $Cp^*(\eta^5\text{-}C_5H_3\text{-}1,3\text{-}(CMe_3)_2)HfH_2$, rate constants for olefin insertion have been measured. For $Cp^*_2HfH_2$, the relative rates of olefin insertion have been found to be 1-pentene > styrene > *cis*-2-butene > *trans*-2-butene > isobutene. The rate of isobutene insertion into $Cp^*(\eta^5\text{-}C_5Me_4H)ZrH_2$ is 3.8×10^3 times greater than that for $Cp^*_2ZrH_2$ at 210 K, demonstrating the large steric effect imposed by ancillary ligand substitution for the insertion reaction. A primary kinetic isotope effect of 2.4(3) at 296 K and a linear free energy relationship with correlation to σ (ρ = -0.46(1)) indicate that olefin insertion into a zirconium-hydride bond proceeds via rate determining hydride ($H^{\delta-}$) transfer from the metal to the incipient alkyl. The rates of β-hydrogen elimination for a series of zirconocene alkyl hydride complexes, $(R_nCp)_2Zr(CH_2CHR')(H)$, have been measured via trapping of the intermediate zirconocene dihydride with 4,4-dimethyl-2-pentyne. Primary isotope effects between 3.9-4.5 have been measured at 296 K for a variety of zirconocene isobutyl hydride complexes. A linear free relationship for the phenethyl hydride series, $Cp^*(\eta^5\text{-}C_5Me_4H)Zr(CH_2CH_2\text{-}p\text{-}C_6H_4\text{-}X)(H)$ (X = H, CH_3, CF_3, OCH_3), has been established with a better correlation to σ than σ^+, ρ = -1.80(5). For the series of ziroconocene isobutyl hydride complexes, the rate of β-hydrogen elimination depends on the cyclopentadienyl ligand array, where more substituted metallocenes yield slower rates. Equilibration of a series of $Cp^*(CpR_n)Zr(CH_2CHMe_2)(H)$ and $Cp^*(CpR_n)Zr(CH_2CH_2CH_2CH_3)(H)$ complexes with free olefin has established the relative ground state energies of zirconocene isobutyl and normal butyl complexes. These data in combination with the free energies of activation for β-hydrogen elimination have established the relative transition state energies of each alkyl group for these complexes.

Introduction

Olefin insertion into a metal-hydrogen bond and its microscopic reverse, β-hydrogen elimination from a transition metal alkyl, represent fundamental transformations in organometallic chemistry and constitute key steps in a variety of catalytic processes.[1] Olefin insertion and β-hydrogen elimination have special relevence to metallocene catalyzed olefin polymerization since insertion of an olefin into a metal-hydrogen bond is often the initiation step; subsequent insertions into metal carbon bonds comprise the chain propagation sequence and β-hydrogen elimination has been identified as a major chain termination pathway.[2] The relative rates of these processes determine the chain length of the resulting polymer and hence influence many important polyolefin properties.

Although the effect of metallocene symmetry on polymer stereochemistry is fairly well-understood,[3] a definitive correlation between ancillary ligand substitution and polymer molecular weight has not been established. In fact, the commercialization of current metallocene catalysts is hampered by the low molecular weights of the polymers produced by these catalysts, especially when the polymerization reaction is carried out at plant operating temperatures (60 - 80 °C for polypropylene).[4] End group analysis of these polymers reveals that chain termination occurs primarily by β-hydrogen and β-methyl elimination pathways. Hence, a thorough mechanistic understanding of each of the fundamental transformations related to olefin polymerization may lead to the development of metallocene catalysts that can be tailored to produce polymers with desired stereochemistry and molecular weight.

The details of olefin insertion and β-hydrogen elimination reactions have been the subject of several experimental and theoretical investigations. Early work of Jordan,[5] Watson[6] and Marks[7] has established olefin insertion into a metal alkyl bond as the mode of propagation for d^0 and d^0f^n metal catalyzed polymerizations. However, attempts to gain further insight into the mechanism and rates of olefin binding, insertion and subsequent β-hydrogen elimination reactions have met with limited success. The active species for olefin polymerization is well established as doubly coordinatively unsaturated, 14

electron cationic group 4 metallocene alkyl, but the high activity of these catalysts, and the presence of cocatalysts such as methylalumoxane (MAO) in high concentration prevent a detailed analysis of each of the individual transformations involved during the polymerization reaction.

Previous investigations from our research group have focused on understanding the kinetics and mechanism of both olefin insertion and β-hydrogen elimination in metallocene catalysts. Using both coalesence and magnetization transfer NMR techniques, the kinetics of olefin insertion into a metal hydrogen bond has been examined with a series of group V metallocene complexes of the general formula, $(\eta^5\text{-}C_5R_5)_2M(\eta^2\text{-}CH_2{=}CHR')(H)$ (M = Nb, Ta; R = H, Me; R' = H, CH_3, C_6H_5).[8] For the series of ethylene hydride compounds, increased rates of insertion were observed for niobium ($k_{Nb} > k_{Ta}$) and for less crowded cyclopentadienyl rings ($k_{Cp} > k_{Cp^*}$). Similar effects are also observed in the propylene hydride complexes, although the steric effects dominate the electronic contributions. The rates of olefin insertion for a series of *meta*- and *para*-substituted niobocene styrene hydride complexes have been examined and the electronic effects were found to be primarily inductive in origin. Furthermore, these rates were used to construct a linear free energy relationship that indicated a concerted four center transition state with moderate positive charge development at the β-carbon.

Permethylscandocene complexes, $(\eta^5\text{-}C_5Me_5)_2ScR$ (R = H, alkyl), insert ethylene rapidly at low temperature (-80 °C) without complication from chain transfer from β-hydrogen elimination. Hence, the kinetics of ethylene insertion have been measured for a series of scandium alkyls. The rates of ethylene insertion are reflected by the strength of the scandium-carbon bond, where stronger bonds result in slower rates.[9] The rates of β-hydrogen elimination for a variety of scandium alkyls and phenylethyl complexes have been determined via trapping of the intermediate scandium hydride with 2-butyne.[9] Utilizing these measurements, the transition states for β-hydrogen elimination, and hence that for olefin insertion have been probed by systematically varying the substituent at the β-carbon. In accord with the niobocene styrene hydride complexes, a linear free energy correlation is also found with scandium-phenylethyl series, indicating that the transition state for these processes is quite polar with the electropositive scandium center abstracting hydride (and by extension ($R^{\delta-}$) for

insertion/β-alkyl elimination) of the postively charged β-carbon atom (Figure 1).

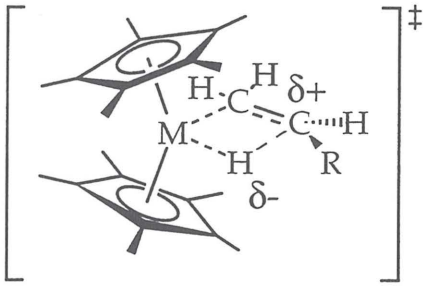

Figure 1. Proposed transition state for olefin insertion and β-hydrogen elimination.

More recent studies have focused on elucidating the rates of chain propagation and transfer in cationic zirconocene catalysts. Erker has reported an experimental estimate for olefin insertion into cationic zirconium allyl fragments[10] whereas Siedle has determined the relative rates of chain propagation and transfer for zirconocene dimethyl/methylalumoxane mixtures.[11] Additionally, numerous theoretical studies have been aimed toward understanding the rates and mechanism of these fundamental transformations.[12] Although the effect of cyclopentadienyl substitution on the stereo- and regiochemical outcome of a metallocene catalyzed polymerization has been well documented,[13,2,3] the influence of cyclopentadienyl sterics on the rates of olefin insertion and β-hydrogen elimination are not well understood. Using 16 electron zirconocene and hafnocene dihydride and alkyl hydride complexes as models for the active polymerization catalyst, we describe our efforts towards understanding the effects of ancillary ligand substitution on olefin insertion and β-hydrogen elimination and, through these studies, reveal the relative contributions of ground and transition state effects on the rates of these processes.

Results

Reactions of the metallocene dihydride complexes, $(CpR_n)_2MH_2$[14] (CpR_n = alkyl substituted cyclopentadienyl; M = Zr, Hf), with olefins such as propylene, 1-butene and isobutene afford stable metallocene alkyl hydride complexes, $(CpR_n)_2M(CH_2CHR'_2)(H)$ (R' = alkyl), in quantitative yield (by NMR) (eq. 1). In general, the remaining metal-hydride bond is unreactive toward excess olefin.[15]

The metallocene alkyl hydride complexes are stable in benzene-d_6 for days at 25 °C.

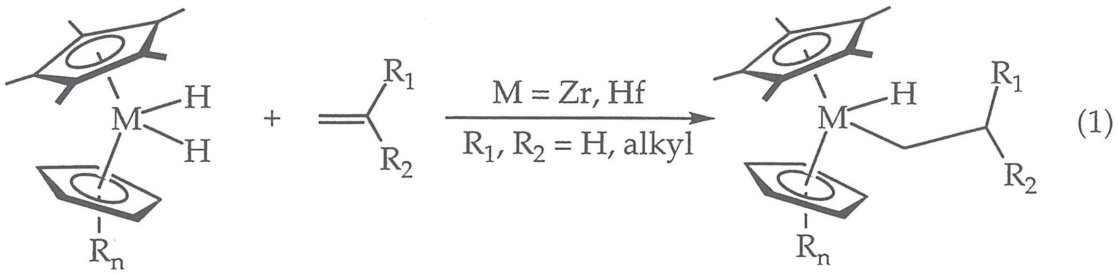

(1)

Kinetic Studies with $Cp^*_2MH_2$ Complexes.

Permethylzirconocene dihydride, $(\eta^5\text{-}C_5Me_5)_2ZrH_2$ (**1**), and permethylhafnocene dihydride, $(\eta^5\text{-}C_5Me_5)_2HfH_2$ (**2**), are monomeric in benzene-d_6 solution and as a result are amenable for kinetic study. Reactions of **1** and **2** with 1,1-disubstituted olefins (*e.g.*, isobutene) and α-olefins are first order in both olefin and the metallocene dihydride (eq. 2). In an attempt to probe olefin steric effects on the rate of insertion, reaction of **1** with a variety of 1,1-disubstituted olefins has been examined. Thus reaction of **1** with isobutene, 2-methyl-1-butene, 2,4-dimethyl-1-pentene, 2,3-dimethyl-1-pentene and α-methylstyrene yields $(\eta^5\text{-}C_5Me_5)_2Zr(CH_2CH(CH_3)_2)(H)$ (**3**), $(\eta^5\text{-}C_5Me_5)_2Zr(CH_2CH(CH_3)(CH_2CH_3))(H)$ (**4**), $(\eta^5\text{-}C_5Me_5)_2Zr(CH_2CH(CH_3)CH_2CH(CH_3)_2)(H)$ (**5**), $(\eta^5\text{-}C_5Me_5)_2Zr(CH_2(CH(CH_3))_2CH_2CH_3)(H)$ (**6**) and $(\eta^5\text{-}C_5Me_5)_2Zr(CH_2CH(CH_3)(C_6H_5))(H)$ (**7**), respectively. Reaction of **1** with 2,4,4-trimethyl-1-pentene produces no reaction. Likewise no alkane is observed upon attempted hydrogenation of this olefin with **1** as the catalyst. The rate constants for these reactions have been measured at 296 K and the results are presented in Table 1.

(2)

Olefin	Metallocene Product	k_{ins} x 10^4 ($M^{-1}sec^{-1}$)
isobutene	**3**	65(3)
2-methyl-1-butene	**4**	24(3)
2,4-dimethyl-1-pentene	**5**	6.3(4)
2,3-dimethyl-1-pentene	**6**	7.3(2)
α-methylstyrene	**7**	14(2)
2,4,4-trimethyl-1-pentene	--	no reaction

Table 1. Rate constants for insertion of disubstituted olefins with **1** at 296 K.

The effect of solvent on the rate of isobutene insertion with **1** has also been examined. The experimentally determined rate constants for the insertion reaction have been measured in a variety of deuterated solvents at 296 K and these values are contained in Table 2.

Solvent	k_{ins} x 10^4 (M^{-1} sec^{-1})
toluene-d_8	65(3)
diethyl ether-d_{10}	35(2)
tetrahydrofuran-d_8	17(5)
pyridine-d_5	no reaction

Table 2. Rate constants as a function of solvent for reaction of **1** with isobutene at 296 K.

Addition of either *cis* or *trans*-2-butene to a toluene-d_8 solution of **1** affords the zirconocene *n*-butyl hydride complex, $(\eta^5\text{-}C_5Me_5)_2Zr(CH_2CH_2CH_2CH_3)(H)$ (**8**) (eq. 3). The zirconocene *sec*-butyl hydride intermediate has not been detected even when the reaction is monitored at -90 °C.[16] These results are contrary to those obtained in related organoactinide complexes, where detection of the

internal alkyl hydride complex has been achieved.[17] Monitoring the reaction between **1** and *trans*-2-butene at low temperatures (T < 250 K) allows for measurement of the rate constant for insertion (Table 3). Likewise, the effect of temperature on the rate of isobutene insertion has also been determined and the rate constants are reported in Table 3. Attempts to measure similar rate constants for the insertion of *cis*-2-butene, propene, styrene and 1-pentene have been unsuccessful due to the rapid rates of these reactions. Trisubstituted olefins such as 3-methyl-2-butene do not react with **1** at elevated temperatures over the course of several days at room temperature.

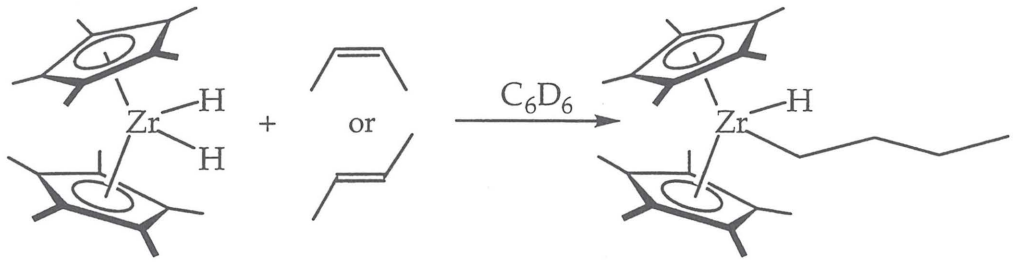

(3)

Temperature (K)	$k_{ins}^{isobutene}$ x 10^4 ($M^{-1}sec^{-1}$)	$k_{ins}^{t\text{-}2\text{-}butene}$ x 10^4 ($M^{-1}sec^{-1}$)
220	---	4.2(1)
240	---	29(2)
250	3.3(1)	69(3)
263	8.5(1)	---
275	19(3)	---
296	65(3)	---

Table 3. Rate constants for reaction of **1** with isobutene and *trans*-2-butene as a function of temperature.

Isobutene, cyclopentene, styrene and 1-pentene react with **2** affording (η^5-$C_5Me_5)_2Hf(CH_2CH(CH_3)_2)(H)$ (**9**), $(C_5Me_5)_2Hf(cyclo\text{-}C_5H_9)(H)$ (**10**), $(C_5Me_5)_2Hf(CH_2CH_2C_6H_5)(H)$ (**11**) and $(C_5Me_5)_2Hf(CH_2(CH_2)_3CH_3)(H)$ (**12**). As with **1**, addition of *cis*- or *trans*-2-butene to **2** affords $(C_5Me_5)_2Hf(CH_2CH_2CH_2CH_3)(H)$ (**13**). In general, the rates of olefin insertion with **2** are slower than those for **1**. For example, the rate constant (296 K) for isobutene insertion with **2** is 2.6 x 10^3 times slower than for **1**. The slower rates of

insertion for **2** permits quantitative determination of olefin insertion rate constants for this series of olefins. The rate constants for insertion of isobutene, *cis*-2-butene, *trans*-2-butene and cyclopentene have been determined over a range of temperatures (Table 4). These data allow for construction of Eyring plots and extraction of the activation parameters for olefin insertion. These values are contained in Table 5. Likewise, the rate constants for insertion of 1-pentene and styrene have been measured at 230 K.

Temperature (K)	$k_{ins}^{isobutene} \times 10^6$ ($M^{-1}sec^{-1}$)	$k_{ins}^{t\text{-}2\text{-}butene} \times 10^6$ ($M^{-1}sec^{-1}$)	$k_{ins}^{c\text{-}2\text{-}butene} \times 10^6$ ($M^{-1}sec^{-1}$)
265	---	---	1200(100)
275	---	---	1900(400)
296	2.5(1)	62(5)	6200(200)
320		220(50)	
340		590(30)	
345	65(3)	---	
362	120(1)	---	

Table 4. Rate constants for reaction **2** with isobutene, *trans*-2-butene and*cis*-2-butene as a function of temperature.

From monitoring the reactions of **1** and **2** with isobutene, *cis*-2-butene and *trans*-2-butene over a range of temperatures, the activation parameters for these reactions have been determined. These values are contained in Table 5.

Compound	Olefin	$\Delta S^{\ddagger a}$	$\Delta H^{\ddagger b}$	$\Delta G^{\ddagger}_{296\ K}{}^{b}$
1	isobutene	-38(3)	9.0(1)	20.2(1)
1	*trans*-2-butene	-29(3)	9.9(1)	18.5(1)
2	isobutene	-43(10)	12.2(2)	24.9(2)
2	*trans*-butene	-45(6)	9.7(1)	23.1(2)
2	cyclopentene	-48(8)	9.6(3)	23.7(3)
2	*cis*-2-butene	-43(8)	7.7(5)	20.4(5)

a. Units = J/mol·K; b. Units = kJ/mol.

Table 5. Activation parameters for reaction of **1** and **2** with a variety of olefins.

Using the experimentally determined rate constants, a quantititative comparison of the rates of insertion for each olefin studied has been obtained from extrapolation of the measured rates to a common temperature of 230 K. The relative rates of insertion are shown in Figure 2.

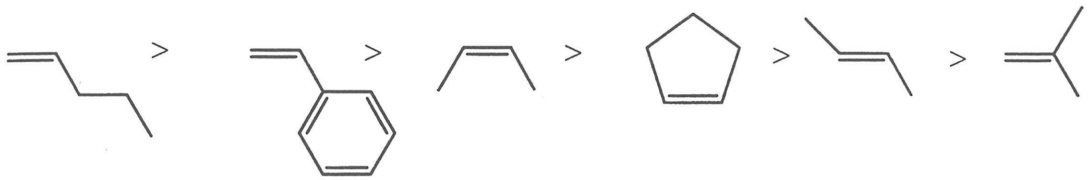

8.2×10^7 4.6×10^6 7.7×10^3 104 38 1

Figure 2. Relative rates olefins insertion with **2** at 230 K.

Isotope Effects on the Rate of Insertion.

Preparation of $(\eta^5\text{-}C_5Me_5)_2ZrD_2$ (**1-d$_2$**) may be accomplished via addition of deuterium gas to **1** at -5 °C. At higher temperatures, incorporation of deuterium into the pentamethylcyclopentadienyl ligands is observed.[14] Mixing equimolar quantities of **1** and **1-d$_2$** in toluene-d_8 followed by addition of isobutene allows for measurement of the kinetic isotope effect for olefin insertion. Measurement of the relative rates of insertion into the Zr-H and Zr-D bond has been achieved by using the integration of the ^{1}H NMR isobutyl methine resonance versus the isobutyl methyl groups (both relative to an internal standard). From this analysis, a kinetic isotope effect of 2.4(3) has been measured at 296 K.

Linear Free Energy Relationship for Insertion of α-Methylstyrene with 1.

Addition of α-methylstyrene to a benzene-d_6 solution of **1** affords $(\eta^5\text{-}C_5Me_5)_2Zr(CH_2CH(CH_3)Ph)(H)$ (**7**) (eq. 4). The ^{1}H NMR spectrum of **7** displays two inequivalent Cp* rings and two diastereotopic C_α protons on the alkyl. Heating a sample of **7** does not result in coalescence of the Cp* or alkyl resonances and eventually reductive elimination of alkane and decomposition of the organometallic complex is observed. However, the clean reaction of **1** with α-methylstyrene lent itself to variations in the *para* position of the incoming

olefin, thus allowing for construction of a free energy relationship for olefin insertion. Addition of 4-fluoro-α-methylstyrene, 4-methyl-α-methylstyrene, 4-methoxy-α-methylstyrene and 4-trifluoromethyl-α-methylstyrene to **1** affords $(\eta^5\text{-}C_5Me_5)_2Zr(CH_2CH(CH_3)\text{-}p\text{-}C_6H_4\text{-}F)(H)$ (**14**), $(\eta^5\text{-}C_5Me_5)_2Zr(CH_2CH(CH_3)\text{-}p\text{-}C_6H_4\text{-}CH_3)(H)$ (**15**), $(\eta^5\text{-}C_5Me_5)_2Zr(CH_2CH(CH_3)\text{-}p\text{-}C_6H_4\text{-}OCH_3)(H)$ (**16**) and $(\eta^5\text{-}C_5Me_5)_2Zr(CH_2CH(CH_3)\text{-}p\text{-}C_6H_4\text{-}CF_3)(H)$ (**17**), respectively (eq. 4). The rates of insertion for each reaction have been measured at 296 K and the observed rate constants are contained in Table 6. Construction of a Hammett plot reveals a better correlation to σ ($r^2 = 0.996$) than σ^+ ($r^2 = 0.667$), with $\rho = -0.46(1)$ (Figure 3).[18]

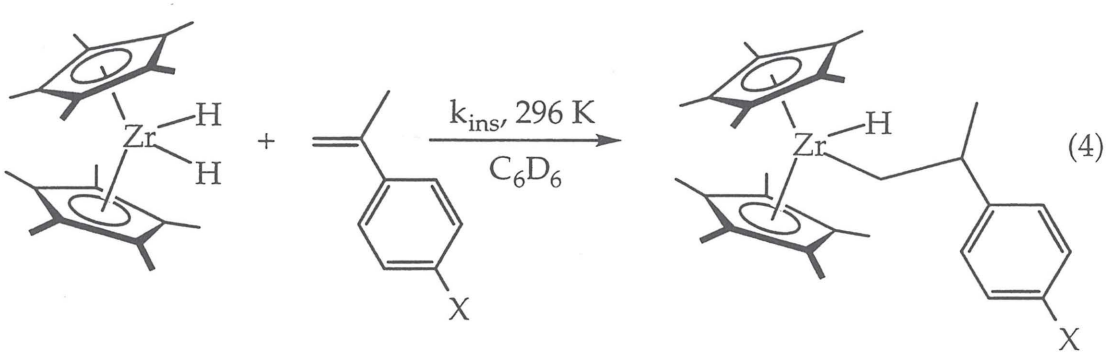

(4)

X = H, F, Me, OCH_3, CF_3

Substituent	$k_{ins} \times 10^5$ ($M^{-1}sec^{-1}$)	σ	σ^+
H	6.92(1)	0	0
F	6.35(2)	0.15	-0.07
OCH_3	7.72(1)	-0.25	-0.78
CH_3	7.47(2)	-0.14	-0.30
CF_3	5.45(2)	0.52	0.08

Table 6. Data for the linear free energy relationship for insertion of *p*-substituted α-methylstyrenes with **1**.

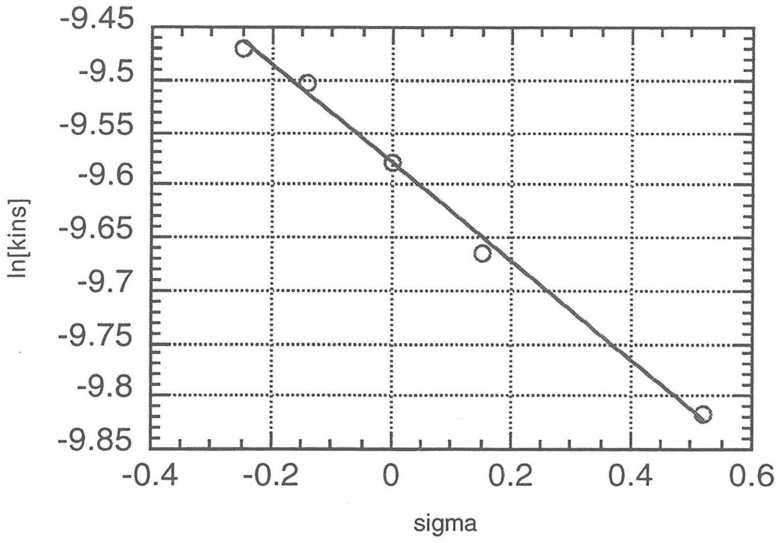

Figure 3. Hammett plot for reaction of **1** with *p*-substituted α-methylstyrenes at 296 K.

Effect of Cyclopentadienyl Substitution on the Rate of Isobutene Insertion.

In addition to **1** and **2**, other monomeric zirconocene and hafnocene dihydrides have been reported.[14] Addition of isobutene to Cp*(η^5-C_5Me_4H)ZrH_2 (**18**) results in quantitative formation of Cp*(η^5-C_5Me_4H)Zr($CH_2CH(CH_3)_2$)(H) (**19**). At 210 K, a rate constant of 3.3(4) x 10^{-2} $M^{-1}sec^{-1}$ has been measured for the rate of isobutene insertion. Attempts to measure the rate of the reaction at higher temperatures have been unsuccessful due to the rapid rate of conversion. Extrapolating the isobutene insertion rate constant for **1** to 210 K using the experimentally determined activation parameters yields a value of 8.7 x 10^{-6} $M^{-1}sec^{-1}$, thus demonstrating that **18** inserts isobutene 3800 times faster than **1**.

Attempts to measure the rate of isobutene insertion for Cp*(η^5-C_5H_3-1,3-$(CMe_3)_2$)ZrH_2 (**20**) and (η^5-C_5H_3-1,3-$(CMe_3)_2$)$_2ZrH_2$ (**21**) have been unsuccessful sinces the rates of insertion are too fast to be measured by low temperature NMR techniques. A rate constant of 5.1(2) x 10^{-3} $M^{-1}sec^{-1}$ has been measured for

the reaction of Cp*(η^5-C_5Me_4-CH_2CH_3)ZrH_2 (**22**) with isobutene affording Cp*(η^5-C_5Me_4-CH_2CH_3)Zr($CH_2CH(CH_3)_2$(H) (**23**) and is approximately the same value as that for the insertion of isobutene with **1**.

Preparation of Cp*(η^5-C_5H_3-1,3-$(CMe_3)_2$)HfH_2 (**24**) has been accomplished via addition of *n*-BuLi to Cp*(η^5-C_5H_3-1,3-$(CMe_3)_2$)$HfCl_2$ under an atmosphere of H_2 as reported for **2**.[19] Reaction of **24** with isobutene results in clean formation of Cp*(η^5-C_5H_3-1,3-$(CMe_3)_2$)Hf($CH_2CH(CH_3)_2$)(H) (**25**). Rate constants for isobutene insertion have been measured between 225 and 270 K and yield activation parameters of $\Delta H^{\ddagger}$ = 11.8(1) kcal/mol and $\Delta S^{\ddagger}$ = -27(5) eu.

Effect of Cyclopentadienyl Substitution on the Regiospecficity of Styrene Insertion.

The influence of cyclopentadienyl substitution on the regiospecificity of olefin insertion has been examined by reaction of styrene with a series of zirconocene dihydride complexes. Reaction of **1** with styrene in benzene-d_6 results in clean formation of (η^5-C_5Me_5)$_2$Zr(CH_2CH_2Ph)(H) (**26**) (eq. 5). The only product observed is that arising from the 1,2 or primary insertion of the carbon-carbon double bond of the olefin. Likewise, reaction of styrene with **20** and **21** affords solely primary insertion products, Cp*(η^5-C_5H_3-$(CMe_3)_2$)Zr(CH_2CH_2Ph) (**27**) and (η^5-C_5H_3-$(CMe_3)_2$)$_2$Zr(CH_2CH_2Ph) (**28**), respectively (Table 7). Reaction of the less substituted zirconocene dihydride, [Cp*(η^5-C_5H_4-CMe_3)ZrH_2]$_2$ (**30**), with styrene yields only the secondary insertion product, Cp*(η^5-C_5H_4-CMe_3)Zr($CH(CH_3)$(Ph)(H) (**30**) as a 1:1 mixture of diastereomers. Confirmation of the regioselectivity of these reactions has been assayed via addition of CH_3OD to a benzene solution of the zirconocene phenethyl hydride. The resulting ethylbenzenes have been analyzed by $^2H\{^1H\}$ NMR spectroscopy and the signals of 1-deutero-ethylbezene and 2-deutero-ethylbenzene determined by integration versus an internal standard.

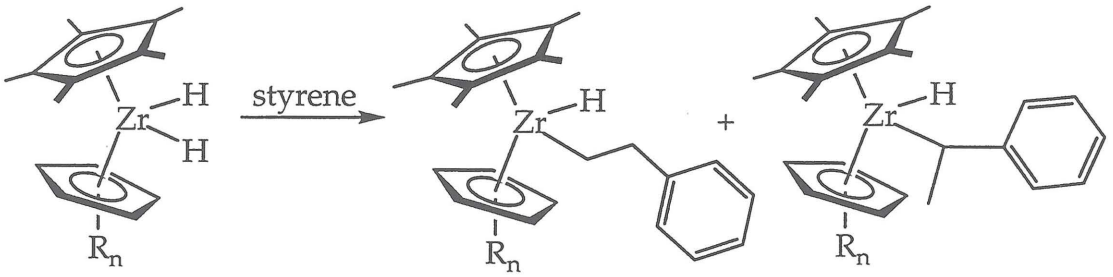

(5)

Addition of styrene to $[Cp^*(THI)ZrH_2]_2$ (**31**) (THI = tetrahydroindenyl), $[(\eta^5\text{-}C_5Me_4H)_2ZrH_2]_2$ (**32**) and $Cp^*(\eta^5\text{-}C_5H_3\text{-}1,3\text{-}(CHMe_2)_2)ZrH_2$ (**33**) results in a mixture of regioisomers depending on the substitution of the metallocene (Table 7). For the "mixed-ring" metallocenes, the 2,1 insertion products are formed as a 1:1 mixture of diastereomers.

Metallocene	1,2-Product (%)	2,1-Product (%)
1	100	0
20	100	0
21	100	0
31	60	40
32	80	20
33	44	56
30	0	100

Table 7. Regiospecificity of styrene insertion with a series of zirconocene dihydrides.

β-Hydrogen Elimination Studies.

Reaction of the zirconocene dihydride complexes with alkynes leads to a variety of products depending on the reaction conditions. Terminal alkynes such as 3,3-dimethyl-1-butyne produce mixtures of products arising from insertion of the alkyne forming the alkenyl hydride complex, as well as those arising from σ-bond metathesis with the hydride, forming the alkynyl complex (eq. 6). Small internal alkynes such as 2-butyne undergo rearrangement to afford crotyl hydride complexes.[20] However, sterically demanding, internal alkynes such as 4,4-dimethyl-2-pentyne (**37**) react with the series of zirconocene dihydrides to yield solely the insertion product, $(CpR_n)_2Zr(CH_3C{=}CH(CMe_3))(H)$. In all cases

examined, only one alkenyl hydride product is observed. Addition of CD_3OD to the series of zirconocene alkenyl-hydride complexes and analysis of the resulting deuterated olefin by $^2H\{^1H\}$ NMR spectroscopy reveals that zirconium center coordinates to C_2 of the acetylene in each case (eq. 7).

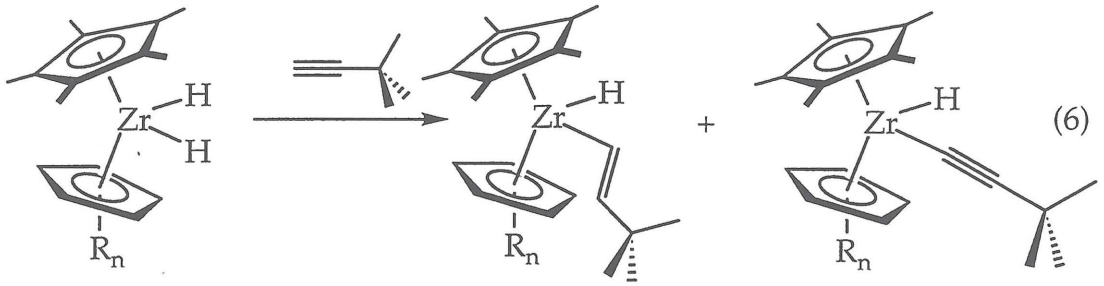

(6)

Reaction of **37** with the zirconocene alkyl hydride complexes also forms the alkenyl hydride complex and free olefin. These products are consistent with β-hydrogen elimination from the alkyl hydride liberating free olefin and the zirconocene dihydride which is then trapped by the acetylene in solution. Under the appropriate conditions (*vide infra*), this reaction may allow for measurement of the rates of β-hydrogen elimination from a series of zirconocene alkyl hydride complexes.

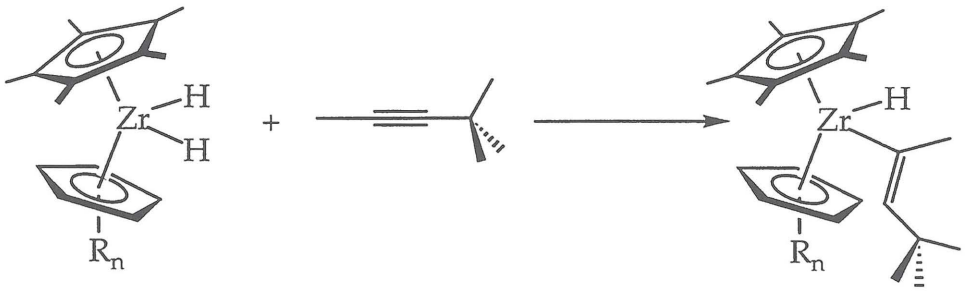

(7)

A series of zirconocene isobutyl hydride complexes has been prepared from addition of isobutene to a benzene-d_6 solution of the zirconocene dihydride. In this manner, Cp*(η^5-C_5H_5)Zr(CH_2CHMe_2)(H) (**38**), Cp*(η^5-C_5H_4-CMe_3)Zr(CH_2CHMe_2)(H) (**39**); Cp*(THI)Zr(CH_2CHMe_2)(H) (**40**), Cp*(η^5-C_5H_2-1,3-$(CHMe_2)_2$)Zr(CH_2CHMe_2)(H) (**41**), Cp*(η^5-C_5H_3-1,3-$(CMe_3)_2$)Zr(CH_2CHMe_2)(H) (**42**), Cp*(η^5-C_5Me_4H)Zr(CH_2CHMe_2)(H) (**19**), (η^5-

$C_5Me_4H)_2Zr(CH_2CHMe_2)(H)$ (**43**) and $Cp^*_2Zr(CH_2CHMe_2)(H)$ (**3**) have been prepared (Figure 4).

The observed rate constants for reaction of **3**, **19**, **38-43** with **37** have been determined and found to be independent of the concentration of **37** over the range of 0.244 to 4.88 M (Table 8). For **3**, 2-butyne was used as the dihydride trap since the reaction of **1** and **37** was not straightforward. This kinetic situation allows for direct measurement of the rate of β-hydrogen elimination ($k_1 = k_{obs}$) since the reverse process (k_{-1}) does not effectively compete with acetylene trapping (Figure 5).

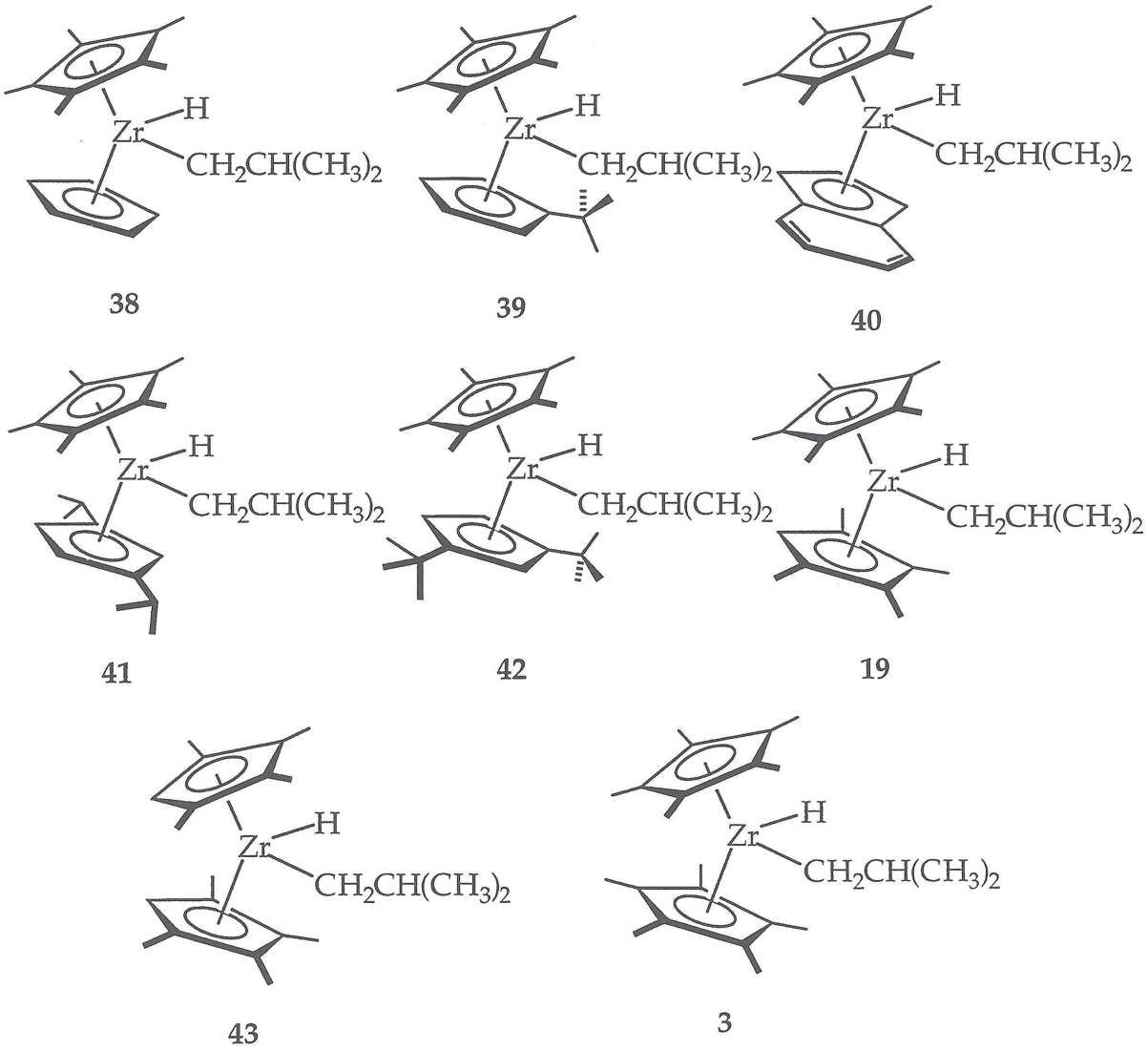

Figure 4. Zirconocene isobutyl hydride complexes.

Further evidence for the dissociative nature of the reaction on the acetylene concentration has been obtained through the use of two different acetylene traps. Reaction of **42** with five equivalents of **37** or 2,2-dimethyl-1-butyne at 268 K forms the alkenyl hydride complexes with observed rate constants of $3.3(4) \times 10^{-4}$ sec^{-1} and $2.7(3) \times 10^{-4}$ sec^{-1}, respectively.

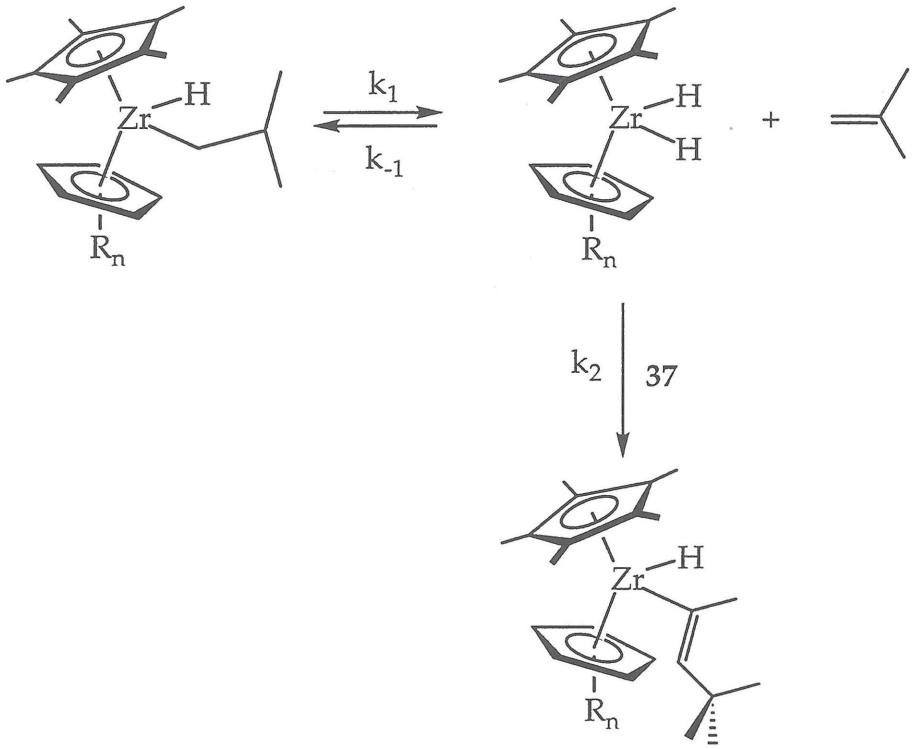

Figure 5. Mechanism for trapping of zirconocene dihydrides with **37**.

Metallocene	[37] (M)[a]	k_{obs} x 10^4 (sec^{-1})
38	0.244	10.6(2)
T = 275 K	0.672	11.2(5)
	0.244	10.3(4)
39	0.244	3.35(4)
T = 275 K	1.37	3.40(5)
	4.88	3.82(9)
40	0.152	10.8(2)
T = 296 K	0.908	10.8(4)
	1.32	10.7(3)
41	1.22	28.4(6)
T = 296 K	0.244	29.8(8)
	1.22	27.0(5)
42	0.122	3.35(5)
T = 296 K	1.37	3.40(2)
	4.88	3.82(8)
19	0.244	0.134(5)
T = 296 K	1.05	0.123(3)
	2.44	0.146(7)
43	0.061	5.44(2)
T = 296 K	0.244	5.43(5)
	0.976	5.26(3)
3	0.244	0.028(4)
T = 296 K	0.650	0.025(6)
	1.10	0.031(5)

a. The estimated errors in the concentrations are ± 5%.
b. Rates measured with 2-butyne

Table 8. Observed rate constants for the reaction of zirconocene isobutyl hydride complexes with **37**.

The rates of β-hydrogen elimination have also been measured as a function of temperature. The activation parameters derived from the experimentally determined rate constants are shown in Table 9. In all cases, the entropy of activation ($\Delta S^{\ddagger}$) is small, further supporting dissociative substitution of the alkyl by the alkenyl (Figure 5).

Complex	ΔS‡ (eu)	ΔH‡ (kcal/mol)	ΔG‡ (kcal/mol) 296 K
38	7.7(8)	21.9(4)	19.6(4)
39	-4.4(4)	18.8(6)	20.1(6)
40	3.1(8)	23.3(3)	21.3(4)
41	-4.1(9)	19.6(7)	20.8(8)
42	-5.19(3)	20.5(3)	22.0(3)

Table 9. Activation parameters for β-hydrogen elimination.

From these data, the relative rates of β-hydrogen elimination as a function of ligand array can be established. All of the reported values are compared to the normalized rate of β-hydrogen elimination for **3** at 296 K. If the experimentally observed rate constant for a given metallocene has not been measured at 296 K, an extrapolated rate constant obtained from the experimentally determined activation parameters is reported. The relative rates of β-hydrogen elimination for the series of zirconocene isobutyl hydride complexes is shown in Figure 6.

Kinetic Isotope Effects for β-Hydrogen Elimination.

Preparation of isotopically labeled zirconocene isobutyl hydride complexes of the general formula, $(CpR_n)_2Zr(CH_2CDMe_2)(D)$, has been accomplished via addition of isobutene to $(CpR_n)_2ZrD_2$.[14] The isotopic purity of all of the compounds has been determined to be > 95% based on ^1H and ^2H NMR spectroscopy. The rates of β-hydrogen elimination for $Cp^*(THI)Zr(CH_2CDMe_2)(D)$ (**40-d$_2$**), $Cp^*(\eta^5\text{-}C_5H_3\text{-}1,3\text{-}(CHMe_2)_2)Zr(CH_2CHMe_2)(H)$ (**41-d$_2$**), $Cp^*(\eta^5\text{-}C_5H_3\text{-}1,3\text{-}(CMe_3)_2)Zr(CH_2CHMe_2)(H)$ (**42-d$_2$**), $Cp^*(\eta^5\text{-}C_5Me_4H)Zr(CH_2CHMe_2)(H)$ (**19-d$_2$**) and $(\eta^5\text{-}C_5Me_4H)_2Zr(CH_2CHMe_2)(H)$ (**43-d$_2$**) have been determined at 296 K by employing **37** as the trap for the intermediate zirconocene dideuteride. Comparison of these rate constants to those determined for protio complexes yields the kinetic isotope effects for β-hydrogen elimination (Table 10).

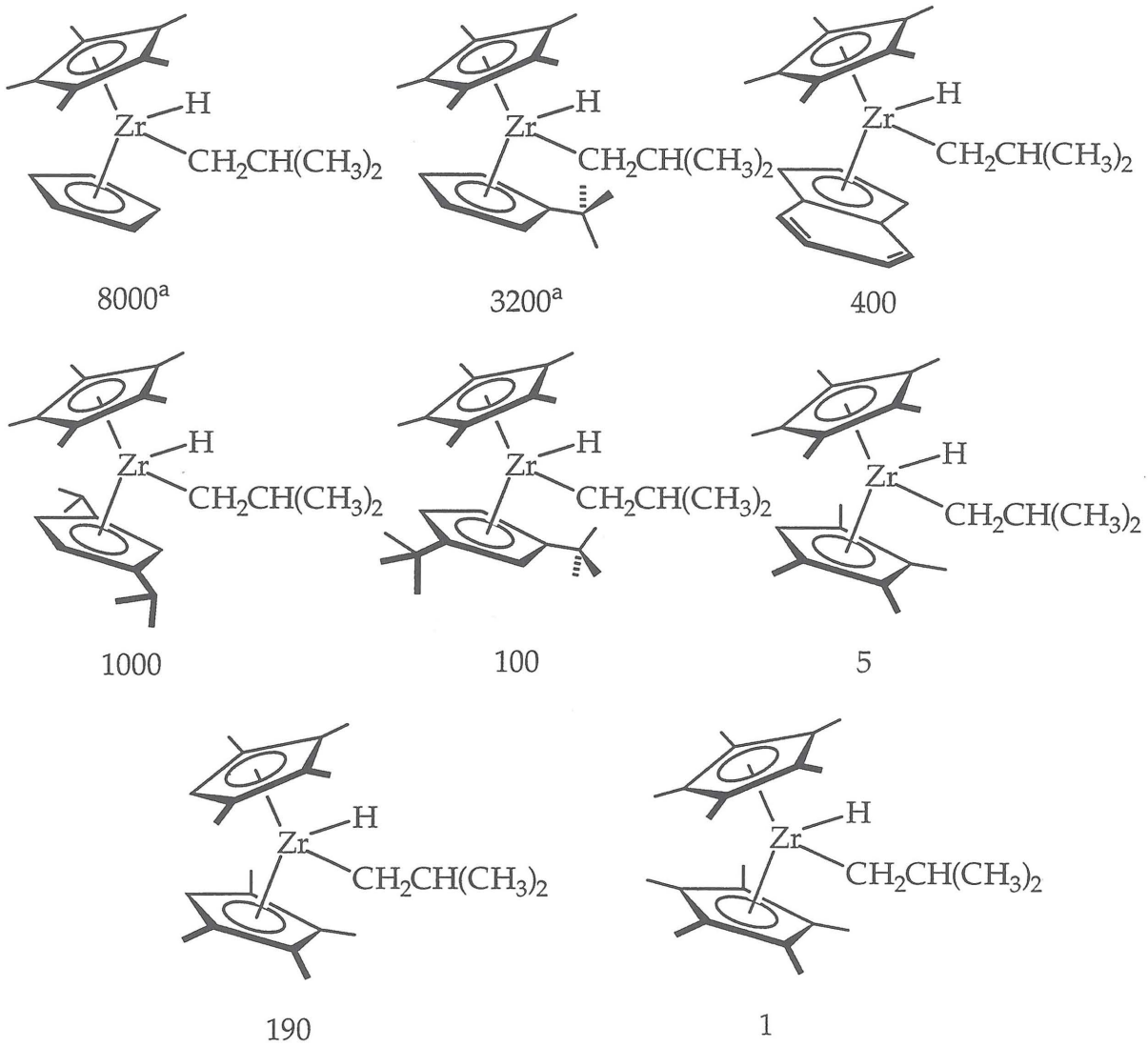

8000[a] 3200[a] 400

1000 100 5

190 1

a. Extrapolated value from experimentally determined activation parameters.

Figure 6. Relative rates of β-hydrogen elimination for a series of zirconocene isobutyl hydrides at 296 K.

Metallocene	k_H (sec^{-1})	k_D (sec^{-1})	k_H/k_D
40-d_2	$1.06(6) \times 10^{-3}$	$2.64(1) \times 10^{-4}$	4.1(2)
41-d_2	$2.8(8) \times 10^{-3}$	$7.10(7) \times 10^{-4}$	3.9(3)
42-d_2	$3.52(9) \times 10^{-4}$	$7.81(10) \times 10^{-5}$	4.5(1)
19-d_2	$1.34(9) \times 10^{-5}$	$3.29(12) \times 10^{-6}$	4.1(3)
43-d_2	$5.38(6) \times 10^{-4}$	$1.34(8) \times 10^{-4}$	4.0(2)

Table 10. Kinetic isotope effects for β-hydrogen elimination at 296 K.

Linear Free Energy Relationship for β-Hydrogen Elimination.

Reaction of **18** with *p*-substituted styrenes affords the phenethyl hydride complexes, $Cp^*(\eta^5\text{-}C_5Me_4H)Zr(CH_2CH\text{-}p\text{-}C_6H_4\text{-}X)(H)$ (X = H, **44**; OCH_3, **45**; CH_3, **46**; CF_3, **47**) (eq. 8). Reaction of each of the phenethyl hydride complexes with **37** as the dihydride trap affords rates of β-hydrogen elimination for each complex. The observed rate constants for these reactions are contained in Table 11. From these data, a linear free energy relationship has been constructed and displays a better correlation to σ ($r^2 = 0.992$) than σ^+ ($r^2 = 0.922$) with a ρ value of -1.80(5).

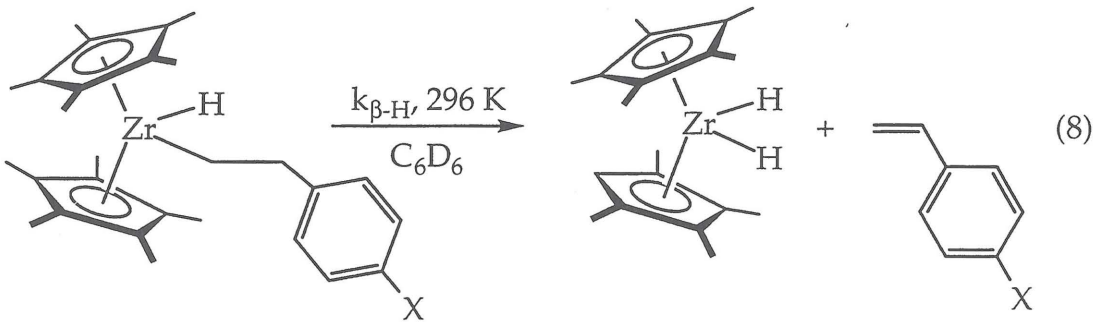

(8)

X = H, **44**; OCH_3, **45**; CH_3, **46**, CF_3, **47**

Compound	$k_{\beta\text{-}H} \times 10^4$ (sec^{-1})	σ	σ^+
44	4.87(9)	0	0
45	8.53(6)	-0.25	-0.78
46	6.94(14)	-0.14	-0.30
47	2.04(15)	0.53	0.08

Table 11. Linear free energy relationship data for $Cp^*(C_5Me_4H)Zr(CH_2CH_2\text{-}p\text{-}C_6H_5\text{-}X)(H)$.

Rates of β-Hydrogen Elimination with Different Alkyls.

The effect of alkyl group on the rate of β-hydrogen elimination has been examined with a series of $Cp^*(\eta^5\text{-}C_5H_4\text{-}CMe_3)Zr(R)(H)$ complexes. Addition of the appropriate olefin to the hydride dimer, **29**, affords the zirconocene alkyl hydride complexes, $Cp^*(\eta^5\text{-}C_5H_4\text{-}CMe_3)Zr(R)(H)$ (R = $CH_2CH_2CMe_3$, **48**;

$CH_2(CH_2)_2CH(CH_3)_2$, **49**; $CH_2CH_2CH_2CH_3$; **50**; cyclopentyl, **51**). As with the zirconocene isobutyl hydride complexes, the rate of substitution of the alkyl ligand by the acetylene is independent of the concentration of **37**. The rates of β-hydrogen elimination have been measured at 296 K and the rate constants are contained in Table 12. The general trend in rate constants for β-hydrogen elimination differ substantially from those observed for olefin insertion with **2**. For example, the cyclopentyl hydride undergoes β-hydrogen elimination approximately 50 times faster than corresponding *n*-butyl hydride complex, whereas for insertion with **2**, 1-butene inserts 10^5 times faster than cyclopentene.

Metallocene	$k_{\beta\text{-}H} \times 10^4$ (sec^{-1})[a]	Relative Rate
48	1.47(8)	1
49	17.8(6)	12.1
50	18.3(5)	12.4
39	90.6(6)	61.6
51	1000(25)	680

a. T= 296 K

Table 12. Rates of β-hydrogen elimination as a function of alkyl ligand.

Ligand Array	$k_{n\text{-}Bu}$ (sec^{-1})	$k_{i\text{-}Bu}$ (sec^{-1})	$k_{n\text{-}Bu}/k_{i\text{-}Bu}$
$[Cp^*(\eta^5\text{-}C_5Me_4H)Zr]$	$7.85(2) \times 10^{-5}$	$1.34(9) \times 10^{-5}$	5.86
$[Cp^*(\eta^5\text{-}C_5H_3\text{-}1,3\text{-}CMe_3)_2Zr]$	$3.35(9) \times 10^{-4}$	$3.5(2) \times 10^{-4}$	0.96
$[Cp^*(\eta^5\text{-}THI)Zr]$	$9.28(1) \times 10^{-4}$	$1.06(6) \times 10^{-3}$	0.875
$[Cp^*(\eta^5\text{-}C_5H_3\text{-}1,3\text{-}(CHMe_2)_2Zr]$	$9.88(2) \times 10^{-4}$	$2.8(8) \times 10^{-3}$	0.357
$[Cp^*(\eta^5\text{-}C_5H_4\text{-}CMe_3)Zr]$	$1.83(5) \times 10^{-3}$	$9.06(6) \times 10^{-3}$	0.201

Table 13. Comparision of the rates of β-hydrogen elimination for a series of zirconocene alkyl hydride complexes.

Since the trend for β-hydrogen elimination for $Cp^*(\eta^5\text{-}C_5H_4\text{-}CMe_3)Zr(R)(H)$ differs from the trend for olefin insertion with **2**, we wished to examine the effect of ancillary ligand substitution on the relative rates of β-hydrogen elimination for a series of *n*-butyl and *i*-butyl hydrides. The observed rate constants for these reactions are contained in Table 13. From these data, a general trend is observed; namely more substituted metallocenes have a ratio of

β-hydrogen elimination rate constants ($k_{n\text{-Bu}}/k_{i\text{-Bu}}$) greater than 1, whereas less substituted metallocenes have $k_{n\text{-Bu}}/k_{i\text{-Bu}}$ less than unity.

Relative Ground State Energies of Zirconocene Alkyl Hydride Complexes.

Addition of five equivalents of 1-butene to the series of zirconocene isobutyl-hydride complexes results in formation of an equilibrium mixture of the zirconocene *i*-butyl hydride and the zirconocene *n*-butyl hydride complexes along with the appropriate amounts of free olefins (eq. 9). Likewise, the equilibrium may be approached from addition of isobutene to the zirconocene *n*-butyl hydride complexes. The experimentally determined equilibrium constants and the corresponding free energy changes for these reactions are reported in Table 14.

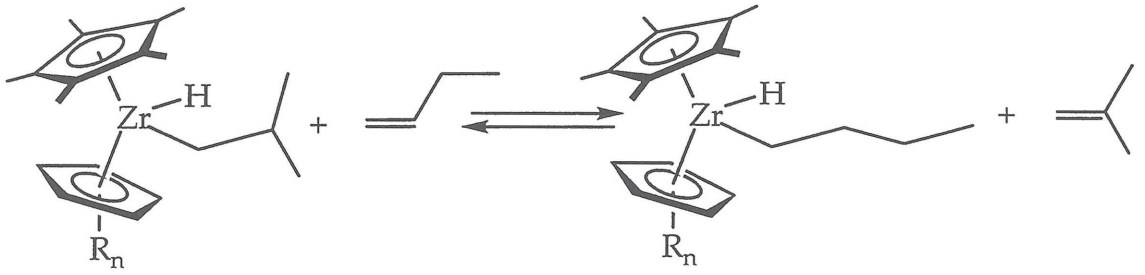

(9)

Ligand Array	$Keq^{296\ K}$	ΔG^{o}_{rxn} (296 K)
$[(\eta^5\text{-}C_5Me_5)_2Zr]$	51(3)	-2.3(2)
$[Cp^*(\eta^5\text{-}C_5Me_4H)Zr]$	43(3)	-2.1(2)
$[Cp^*(\eta^5\text{-}C_5H_3\text{-}1,3\text{-}(CMe_3)_2)Zr]$	25(4)	-1.9(2)
$[Cp^*(\eta^5\text{-}C_5H_3\text{-}1,3\text{-}(CHMe_2)_2)Zr]$	16(2)	-1.7(1)
$[Cp^*(\eta^5\text{-THI})Zr]$	9.6(3)	-1.3(1)
$[Cp^*(\eta^5\text{-}C_5H_4\text{-}CMe_3)Zr]$	9.1(4)	-1.3(1)

Table 14. Equilbrium constants and free energy data for equation 9.

Discussion

Olefin Insertion into $(CpR_n)_2MH_2$

The zirconocene dihydride complexes, $(CpR_n)_2MH_2$, undergo facile reaction with a variety of olefins affording the zirconocene alkyl hydride complexes, $(CpR_n)_2M(R')(H)$ (R, R' = alkyl). For monomeric zirconocene dihydrides, the rates of olefin insertion can be conveniently measured using ^1H NMR spectroscopy. Using these kinetic measurements as a basis for our studies, we have been able to elucidate the mechanism of olefin insertion into neutral, d^0 metallocene dihydride complexes. Furthermore, these experiments allow for careful study of the influence of olefin and cyclopentadienyl sterics on the rates of olefin insertion.

A proposed mechanism for olefin insertion into $(CpR_n)_2ZrH_2$ is shown in Figure 7. The reaction proceeds via initial coordination of the alkene to the metallocene dihydride followed by transfer of hydrogen from the metal center to the incipient metal alkyl. Although the geometry of the olefin dihydride adduct is unknown, we propose that olefin insertion takes place when the olefin occupies the lateral position (*i.e.*, *cis* to only one zirconium hydride) based on preliminary density functional theory calculations with ethylene and Cp_2ZrH_2.[21] Reaction of isobutene with an equimolar mixture of **1** and **1-d$_2$** reveals a kinetic isotope effect of 2.4(3) at 296 K. A normal, primary isotope effect is consistent with a preequilibrium involving rapid coordination and dissociation of olefin followed by rate determining hydride transfer. A similar kinetic profile has been proposed for reactions of olefins with $(\eta^5\text{-}C_5Me_5)_2M(OR)(H)$ (M = Th, U) where primary kinetic isotope effects of 1.4(1) and 1.3(2) have been measured for the insertion of cyclohexene and 1-hexene at 60 °C.[17]

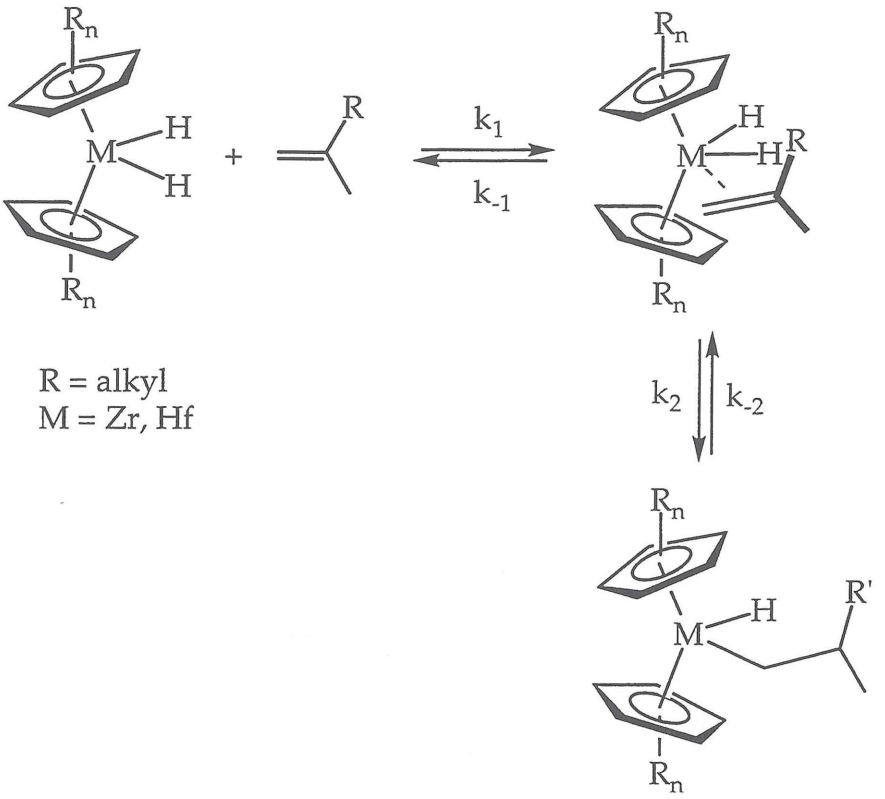

Figure 7. Proposed mechanism for olefin insertion with neutral zirconocene and hafnocene dihydrides.

The effect of solvent on the rate of isobutene insertion has also been measured. As shown in Table 15, the chemical shift of the zirconium hydride and the rate of isobutene insertion correlate with the dielectric constant of the NMR solvent; the reaction proceeds more rapidly in solvents with lower dielectric constants. It has been shown previously that the ^{1}H NMR chemical shift of a group IV metallocene hydride resonance may be used as a measure of ligand binding, where more upfield resonances indicate a greater degree of coordinative saturation about the metal center.[22] For the 16 electron dihydride complex, **1**, the zirconium hydride resonance appears at 7.48 ppm (toluene-d_8) substantially downfield from 0.55 ppm and 1.07 ppm observed for the 18 electron complexes, (η^5-C_5Me_5)$_2$ZrH_2(PF_3) and (η^5-C_5Me_5)$_2$ZrH_2(CO) (both in toluene-d_8).[23] In donor solvents such as THF-d_8, the zirconocene hydride resonance for **1** shifts to 5.75 ppm, implicating a significant contribution from the formally 18 electron solvento complex. Coordination of solvent to the zirconium center decreases the rate of insertion since the incoming olefin can not compete as effectively with the high concentration of competing ligand. A similar solvent

effect has been noted in the related organoactinide complex, where $k_{THF}/k_{toluene} = 0.59$.[17]

Solvent	$k_{ins} \times 10^4$ ($M^{-1}sec^{-1}$)	δ Zr-H (ppm)	Dielectric[a]
toluene-d_8	65(3)	7.48	2.4
diethyl ether-d_{10}	35(2)	7.30	4.3
THF-d_8	17(5)	5.75	7.6
pyridine-d_5	no reaction	5.10	12.3

a. Data taken from *CRC Handbook of Chemistry and Physics* 67th Ed.; CRC Press, Boca Raton, Florida.

Table 15. Rate constants for isobutene insertion as a function of solvent dielectric.

Addition of *para*-substituted α-methylstyrenes, *p*-CH_2=C(CH_3)(C_6H_4-X) (X = H, CH_3, CF_3, OCH_3) to **1** affords the zirconocene alkyl hydrides, **7**, **14-17**. Construction of a linear free energy relationship reveals a better correlation of the observed rate constants with the Hammett constant σ than σ^+ with ρ = -0.46(1). The better correlation to σ is indicative of poor orbital overlap between the empty p orbital on the β-carbon and the π system of the phenyl ring and in the transition state for olefin insertion. Similar observations have been made with permethylniobocene and permethyltantalocene styrene-hydride complexes where ground state crystal structures and the linear free energy relationship indicate that the β-carbon and the π system of the phenyl ring are twisted out of resonance by approximately 30 degrees.[8b] The modest, negative ρ value of -0.46(1) is indicative of a cyclic transition state with little charge separation, with a slight positive charge development at the β carbon of the coordinated olefin, thus implicating transfer of hydrogen as "$H^{\delta-}$". Also consistent with these findings are the highly negative entropies of activation (-30 to -48 e.u.) indicating a highly ordered transition structure for olefin insertion. Therefore, the transition state model developed for the permethylniobocene and tantalocene olefin hydride complexes may be extended to (η^5-$C_5Me_5)_2MH_2$ (Figure 1).

The effect of olefin substitution on the rate of insertion has also been examined with **1** and **2**. Insertion of a variety of 1,1-disubstituted olefins has been examined with **1** at 296 K. In general, increasing the substitution of the olefin descreases the rate of insertion. For example, the rate of isobutene insertion is approximately 10 times faster than that for 2,4-dimethyl-1-pentene.

However, placing a methyl substituent in either the 3 or 4 position of the olefin has little effect on the rate of insertion. This result contrasts with the polymerization activity of $[(EBTHI)Zr\text{-}R]^+$ (EBTHI = ethylene-1,2-*bis*-(η^5-tetrahydroindenyl)) which readily polymerizes 4-substituted α-olefins but displays minimal activity with 3-substituted alkenes.[24] Increasing the substitution of the 4-position of olefin, as in the case of 2,3,4-trimethyl-1-pentene, produces no reaction with the zirconium hydride. Attempts to hydrogenate the olefin in the presence of **1** also results in no reaction, demonstrating the inability of the olefin to insert into the zirconium hydride bond.

Changing the steric disposition of the olefin (*e.g.*, *cis*-2-butene versus isobutene) has dramatic impact on the rate of insertion with **1** and **2**. Internal olefins such as *cis*- and *trans*-2-butene insert much faster than 1,1-disubstituted olefins. For both metallocenes, the rate of *cis*-2-butene insertion is faster than the rate observed for the *trans* isomer with the *cis* isomer reacting with **2** approximately 200 times faster at 230 K than the *trans*. Although the ground state of the *trans* isomer is approximately 0.70 kcal/mol more stable that the *cis*, this energy difference is not enough to account for the observed difference in rates. This difference could either be a result of transition state stabilization imparted by the *cis* olefin isomer or be a result of increased binding of the *cis* isomer to the dihydride forming a higher concentration of the dihydride olefin intermediate which in turn increases the rate of insertion.

The rate of insertion for α-olefins (*e.g.*, 1-pentene, styrene) with **2** is approximately 10^8 times faster than that for 1,1-disubstituted olefins at 230 K. Unfavorable steric interactions between the more substituted isobutene and the bulky pentamethylcyclopentadienyl ligands are responsible for the dramatic difference in rates. These results are in accord with previous studies that demonstrate α-olefins undergo hydrozirconation more rapidly than 1,1-disubstituted olefins.[25] Similar observations have been made in metallocene catalyzed olefin polymerization where it is commonly found that α-olefins undergo insertion at a much greater rate than 1,1-disubstituted olefins.[26]

These results have special relevance to the chain epimerization mechanism proposed by Busico to account for the tacticity dependence on monomer concentration in metallocene-catalyzed isospecific olefin polymerization.[27] The

change in olefin enantioface is accomplished via a series of β-hydrogen elimination and reinsertion steps. A key feature of the mechanism involves in-plane olefin rotation about the π face of the coordinated alkene. It is assumed that once the 1,1-disubstituted olefin is lost from the metal center, it can not compete with the high concentration of monomer present. The results obtained for the insertion of isobutene and 1-pentene with **2** support this assertion. The observed rate difference in the two olefins would not allow reinsertion of the formed polymer chain especially in the presence of such a large excess of α-olefin.

In addition to olefin steric effects, the influence of cyclopentadienyl substitution on the rate of olefin insertion has also been examined. Comparing the rate of isobutene insertion for **1** and **18** at 210 K reveals a 3.8×10^3 fold rate enhancement for the latter. As with the olefin substituent studies, the large rate difference is a result of unfavorable steric interactions between the incoming olefin and the bulky pentamethylcyclopentadienyl rings. Slightly alleviating the steric interactions by replacement of a methyl group with a hydrogen atom greatly enhances the observed rates. Similar effects are observed with **20** and **21** where the reduced steric disposition of ligand results in insertion rates that are too fast to measure with NMR techniques. The rate of isobutene insertion is not changed by replacement of one of the pentamethylcyclopentadienyl methyl groups with an ethyl group as evidenced by the similar rates of isobutene insertion with **1** and **22**.

Cyclopentadienyl substitution also has a large impact on the regiospecificity of styrene insertion. More crowded metallocenes such as **1**, **18**, **20** and **21** proceed with high regioselectivity, yielding solely the 1,2-insertion product. However, more open metallocenes, **31**, **32** and **33**, form mixtures of both 1,2 and 2,1-insertion products and in one case, **29**, only 2,1 insertion products are formed. From these results, it appears that in absence of overriding steric effects, styrene preferrs to insert in a 2,1 fashion, presumably due to electronic stabilization of the metal center by the phenyl ring.[28] However, this electronic stabilization can be offset by unfavorable interactions between the cyclopentadienyl substitution and the alkyl group thus resulting in solely 1,2 insertion products.

The experimentally determined rate constants and resulting activation parameters allow for direct comparison of the insertion barrier for zirconium and hafnium. In general, the barrier for insertion into a zirconium hydrogen bond is approximately 4 kcal/mol lower than that for the corresponding hafnium hydrogen bond. The differences in activation barriers correspond to an approximate rate difference of 10^2. Similar differences in activity have been observed in a variety of zirconium and hafnium catalytic systems[1] and may be attributed to the ground state stabilization of the hafnium complex due to the increased metal hydrogen bond strength.

β-Hydrogen Elimination from $(CpR_n)_2M(R')(H)$ (R, R' = alkyl).

Zirconocene alkyl hydride complexes of the general formula $(CpR_n)_2Zr(R')(H)$ (R, R' = alkyl) undergo facile β-hydrogen elimination as determined by trapping with **37**. Using this kinetic technique, the rates of β-hydrogen elimination for a series of zirconocene isobutyl hydride complexes has been established (Figure 6). In general, more substituted metallocenes display slower rates of β-hydrogen elimination. In comparison to olefin insertion, rates of β-hydrogen elimination are less affected by ancillary ligand substitution. For example, insertion of isobutene with **1** versus **18** results in a 3800-fold rate enhancement. However, in the reverse reaction, β-hydrogen elimination from **3** and **19**, only a 5-fold enhancement in rate is observed.

Since the rates of both olefin insertion and β-hydrogen elimination have been measured for the $[(\eta^5\text{-}C_5Me_5)_2Zr]$ metallocene, the equilibrium constant for the addition of isobutene to **1** can be computed (eq. 10). At 296 K, the equilibrium constant for this reaction is 2.3×10^3, corresponding to a spontaneous reaction with a Gibb's free energy change of -4.6 kcal/mol. Assuming a negative value for the reaction entropy, the insertion of isobutene with **1** is highly exothermic. According to the Hammond postulate,[18] the reaction possesses an "early" transition state, meaning it resembles reactants more than the products. An early transition state magnifies the unfavorable steric interactions between the olefin methyl groups and the pentamethyl-cyclopentadienyl ligand array, resulting in a larger steric effect on the rate of insertion as compared to the rate of β-hydrogen elimination.

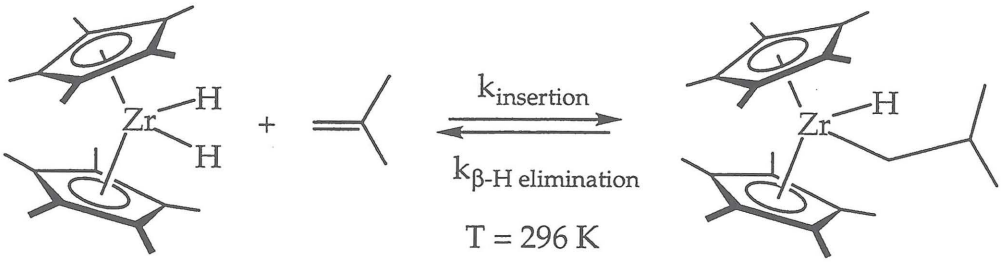

(10)

$K_{eq} = 2.3 \times 10^{-3}\ M^{-1}$

$\Delta G_{rxn} = 4.6$ kcal/mol

Similar cyclopentadienyl steric effects on β-hydrogen elimination have been observed for the polymerization of propylene with metallocene catalysts. Polypropylene produced from Cp_2ZrCl_2/MAO mixtures terminates primarily by β-hydrogen elimination, whereas the polyolefin generated from $Cp^*_2ZrCl_2$/MAO mixtures contains end groups arising from chain termination by β-methyl elimination. The increased rate of β-methyl elimination for the latter system is believed to be a result of inhibition of β-hydrogen elimination by the sterically demanding pentamethylcyclopentadienyl rings (Figure 8).[29]

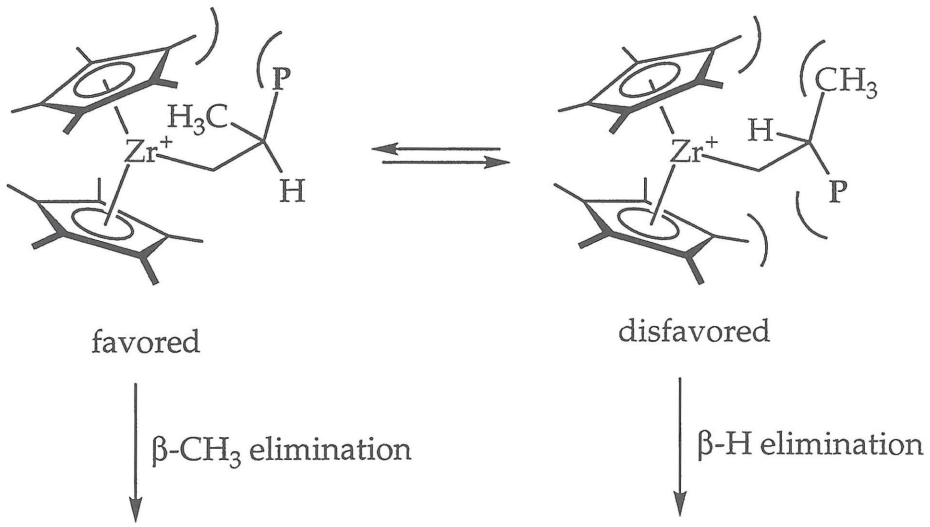

Figure 8. Rationale for preference for β-methyl elimination over β-hydrogen elimination in sterically demanding metallocene catalysts.

The kinetic isotope effects for β-hydrogen elimination have been determined with a series of zirconocene isobutyl hydride complexes, $(CpR_n)_2Zr(CH_2CL(CH_3)_2)(L)$ (L = H or D). In all cases examined, a normal,

primary isotope effect has been obtained (Table 10). These data suggest that β-hydrogen elimination proceeds via rate determining C-H(D) bond cleavage followed by rapid dissociation of the coordinated olefin. The values obtained in this study (~ 4) are larger than those measured for other transition metal systems. A primary kinetic isotope effect of 2.0 has been measured for β-hydrogen elimination in the scandium phenethyl complex, $(\eta^5\text{-}C_5Me_5)_2ScCH_2CH_2C_6H_5$.[9] Likewise, a kinetic isotope effect of 1.6 has been measured for the β-hydrogen elimination in the polymerization of propene with 2-d_1-propene with $[(Me_2Si)_2(\eta^5\text{-}C_5H\text{-}3,5\text{-}(CHMe_2)_2)(\eta^5\text{-}C_5H_2\text{-}4\text{-}CHMe_2)]ZrCl_2$/ methyalumoxane mixtures.[30]

The electronic effects on the rate of β-hydrogen elimination have been examined with a series of *para*-substituted styrene hydride complexes of the general formula, $(\eta^5\text{-}C_5Me_5)(\eta^5\text{-}C_5Me_4H)Zr(CH_2CH_2\text{-}p\text{-}C_6H_5\text{-}X)$ (X = H, Me, OCH_3, CF_3). From the rates of β-hydrogen elimination, a linear free energy relationship has been established. The Hammett plot displays a better correlation to σ than σ^+ with a ρ value of -1.80(5). This value is similar in sign and magnitude to the ρ value of -1.87 obtained for the β-hydrogen elimination of $(\eta^5\text{-}C_5Me_5)_2ScCH_2CH_2\text{-}p\text{-}C_6H_4\text{-}X$.[8]

The kinetic isotope effect and linear free energy data are consistent with β-hydrogen elimination proceeding through the same transition state as olefin insertion; namely a four centered transiton state with slight positive charge development at the β-carbon. Likewise, the rate determining step for β-hydrogen elimination is consistent with being the microscopic reverse of olefin insertion where the rate determining step is scission of the alkyl C-H bond (Figure 7).

Delineation of Ground and Transition State Effects in β-Hydrogen Elimination.

Measurement of the rates of β-hydrogen elimination as well as the relative free energy changes for a variety of zirconocene isobutyl and *n*-butyl hydride complexes allows for the unique opportunity to differentiate between

the relative contributions of ground state and transition state effects for the reaction. From measuring the equilibrium constant and hence free energy change for the addition of both isobutene and 1-butene to a given zirconocene dihydride (Table 14), the relative ground state energies of the two zirconocene alkyl hydride complexes may be established (eq. 11). The change in free energy for the experimentally determined reaction is not the free energy change for the zirconocenes of interest but rather a composite of the relative zirconocene alkyl hydride ground states and the change in free energy for the isomerization of 1-butene to isobutene. Subtraction of the established value of -3.2 kcal/mol[31] for the isomerization of 1-butene to isobutene, the experimentally determined free energy of reaction yields the relative ground state energies of two zirconocene alkyl hydride complexes (Table 16). It is important to note that these calculations allow ordering of the relative ground states of the *n*-butyl hydride as compared to the isobutyl hydride for a given ligand array. Comparison of the ground states of two isobutyl hydride complexes of different ancillary ligation can not be compared with this analysis.

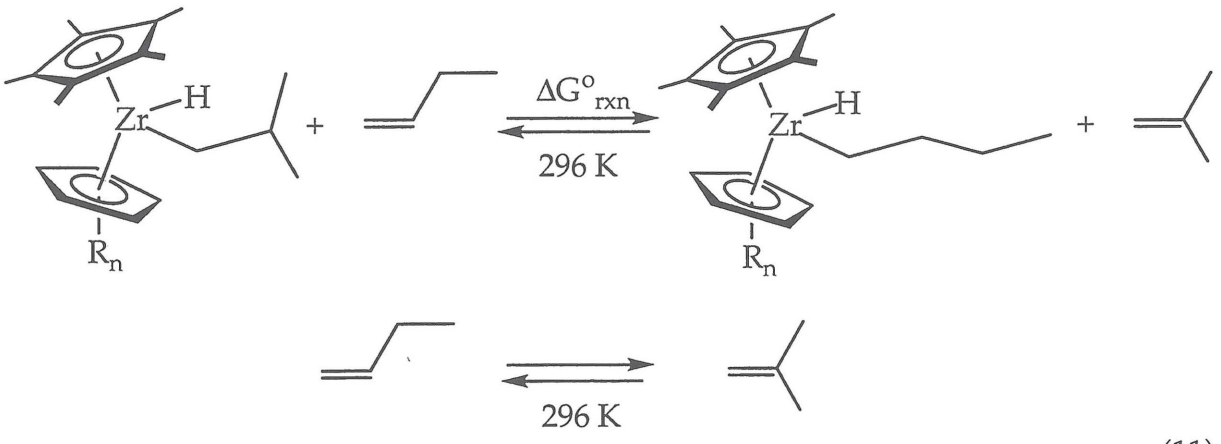

(11)

$\Delta G^o_2 = -3.2$ kcal/mol

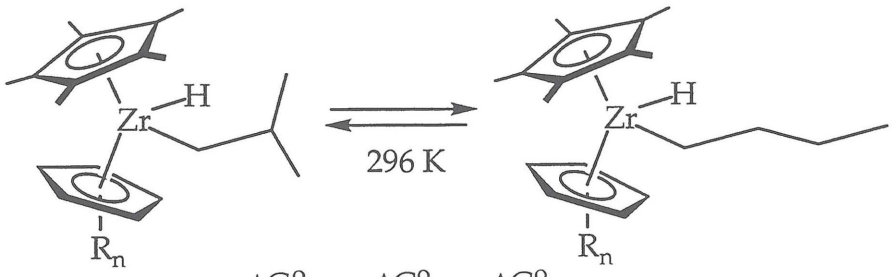

$\Delta G^o_{Zr} = \Delta G^o_{rxn} - \Delta G^o_2$

Ligand Array	ΔG^{o}_{rxn} (kcal/mol)	ΔG^{o}_{Zr} (kcal/mol)
[(η^5-C_5Me_5)$_2$]	-2.3(2)	0.90
[Cp*(η^5-C_5Me_4H)]	-2.1(2)	1.0
[Cp*(η^5-C_5H_3-1,3-CMe_3)$_2$]	-1.9(2)	1.3
[Cp*(η^5-C_5H_3-1,3-$CHMe_2$)$_2$]	-1.7(1)	1.5
[Cp*(THI)]	-1.3(1)	1.9
[Cp*(η^5-C_5H_4-CMe_3)]	-1.3(1)	1.9

Table 16. Relative ground state energies for zirconocene isobutyl and *n*-butyl hydride complexes.

In all cases examined, the zirconocene isobutyl hydride is thermodynamically favored over the corresponding *n*-butyl hydride complex. In an attempt to understand the electronic contribution of this effect, the free energies of formation of isobutane and *n*-butane have been examined. At 296 K, the branched alkane is favored by 1.10 kcal/mol over the linear alkane,[32] in accord with the observed preference for the zirconocene. Previous reports have established a correlation between metal-carbon and carbon-hydrogen bond strengths where the relative energy of the C-H bond may be used to predict the relative strength of the M-C bond.[32] Therefore, the zirconium center, behaving analogously to a hydrogen atom, wishes to form the more stable alkane and therefore prefers the isobutyl hydride over the *n*-butyl hydride.

Although electronic effects are dominant, the ancillary ligand substitution does influence the position of the equilibrium. For less substituted zirconocenes such as [Cp*(η^5-C_5H_4-CMe_3)Zr] and [Cp*(THI)], the electronic contributions dominate since the free energy difference exceeds that for the alkanes.[33] For more crowded members of the series, [(η^5-C_5Me_5)$_2$Zr] and [Cp*(η^5-C_5Me_4H)], steric destabilization of the isobutyl hydride complex is observed. From these data, the energetics of this steric contribution can be estimated to be approximately 1 kcal/mol.

Grubbs[34] has found similar behavior with alkyl-substituted titanocyclobutanes, where the more stable titanocycle is derived from the more stable olefin and is believed to be a result of the structural features of the

metallocycle. Likewise, Wolczanski has found a similar correlation between metal-carbon bond strengths and carbon-hydrogen bond strengths in the equilibration of *tris*-imido zirconium alkyl complexes.[35]

From the experimentally determined rates of β-hydrogen elimination and the relative ground state energies of the zirconocene isobutyl and *n*-butyl hydrides, the relative transition state energies for the β-hydrogen elimination reaction can be determined. Using the Arrhenius relationship, the activation free energy may be calculated for each reaction. Subtraction of the relative ground state contributions for each of the zirconocene alkyl hydrides affords the relative transition state energies for both zirconocene alkyl hydrides for a given ligand array. The relative ground state, activation, and transition state energies are contained in Table 17.

Ligand Array	ΔG^{o}_{Zr}	$\Delta G_{\beta H}^{\ddagger}$ (iBu)	$\Delta G_{\beta H}^{\ddagger}$ (*n*Bu)	$\Delta\Delta G^{\ddagger}$
[Cp*(η^5-C_5Me_4H)]	1.0	23.9	22.9	0
[Cp*(η^5-C_5H_3-1,3-CMe_3)$_2$]	1.3	22.0	22.0	1.3
[Cp*(η^5-C_5H_3-1,3-$CHMe_2$)$_2$]	1.5	21.3	21.4	1.6
[Cp*(THI)]	1.9	20.8	21.4	2.5
[Cp*(η^5-C_5H_4-CMe_3)]	1.9	20.1	21.0	2.8

All energies are given in kcal/mol.

Table 17. Relative ground and transition state energies for zirconocene alkyl hyride complexes.

Based on electronic considerations and the model established for the transition state for β-hydrogen elimination (*vide supra*), the relative energy of a zirconocene isobutyl hydride would be expected to be lower in energy than the corresponding zirconocene *n*-butyl hydride since the more substituted alkyl would better stabilize the developing positive charge on the β-carbon (Figure 8). However, based on steric considerations, the zirconocene *n*-butyl hydride would be favored due to decreased steric interactions with the ligand array. The experimentally determined transition state energy differences indicate that for the sterically crowded metallocene, [Cp*(η^5-C_5Me_4H)Zr], these effects exactly cancel and as a result the isobutyl and *n*-butyl hydride transition states are of equal energy. Thus, the increased rate of β-hydrogen elimination for the *n*-butyl hydride observed for this metallocene is a result of electronic stabilization of the isobutyl hydride in the ground state.

For less substituted metallocenes, the electronically favored isobutyl hydride transition state dominates over the sterically preferred *n*-butyl hydride transition state. This effect increases with decreasing substitution on the metallocene and, as a result, the least crowded metallocene, [Cp*(η^5-C_5H_4-CMe_3)Zr], displays the largest transition state energy difference. From these data, the relative rates of β-hydrogen elimination can be rationalized. For less crowded metallocenes such as [Cp*(η^5-C_5H_4-CMe_3)Zr] and [Cp*(THI)Zr], the electronic stabilization of the isobutyl hydride transition state overcomes the ground state destabilization of *n*-butyl hydride ground state and, as a result, faster rates of isobutyl hydride β-hydrogen elimination are observed. For intermediate metallocenes, these effects are similar, although the transition state effects dominate and faster isobutyl hydride β-hydrogen elimination rates are observed. Only in the most crowded member of the series, [Cp*(η^5-C_5Me_4H)Zr], are the transition state effects overcome by ground state effects.

From these studies, a complete description of the β-hydrogen elimination reaction has been established. The reaction proceeds via rate determining C-H bond scission, forming a four-centered transition state structure which has a build up of positive charge on the β-carbon, resulting in transfer of $H^{\delta-}$ to the metal center. The rate of β-hydrogen elimination is greatly influenced by the structure of the ancillary ligation. For a given alkyl, the rate of β-hydrogen elimination decreases with increasing cyclopentadienyl ligand substitution. When considering β-hydrogen elimination for two different alkyls, both ground state and transition state effects must be considered. The relative ground state energetics may be predicted on electronic grounds from the free energies of the alkanes, although increased cyclopentadienyl substitution perturbs this value. For less substituted metallocenes, the electronic portion of the transition state effect dominates and as a result the most substituted alkyl undergoes more facile β-hydrogen elimination.

Experimental

General Considerations. All air- and moisture-sensitive compounds were manipulated using standard vacuum line, Schlenk or cannula techniques or in a

drybox as described previously.[36] Argon, dinitrogen, dihydrogen and dideuterium gases were purified by passage over columns of MnO on vermiculite and activated molecular sieves. Solvents for air and moisture sensitive reactions were stored under vacuum over titanocene[37] or sodium benzophenone ketyl. NMR solvents: benzene-d_6, toluene-d_8, tetrahydrofuran-d_8, diethyl ether-d_{10} and pyridine-d_5 were purchased from Cambridge Isotope Laboratories. Benzene-d_6 and toluene-d_8 were dried over $LiAlH_4$ and sodium and then stored over titanocene. Tetrahydrofuran-d_8 and diethyl ether-d_{10} were dried over CaH_2 and stored over sodium/benzophenone ketyl. Pyridine-$d_5$was dried over CaH_2. Preparation of **1**,[38] **2**,[18] **3**,[15] **20**, **21**,[14] **22**,[23] **24**,[16] **29**, **31**, **32** and **33**[14] were accomplished as described previously.

Isobutene, 2-methyl-1-butene, 2,4-dimethyl-1-pentene, 2,3-dimethyl-1-pentene and propylene were purchased from Aldrich. Isobutene and propene were dried over Al(*i*-Bu)$_3$ and distilled by vacuum transfer before use. The other olefins were distilled from CaH_2 and stored over $LiAlH_4$. Both *cis*- and *trans*-2-butene were purchased from Matheson and dried over activated 4Å molecular sieves. Styrene and α-methylstyrene were purchased from Aldrich; *p*-fluoro-α-methylstyrene was purchased from Lancaster. All were distilled under reduced pressure from CaH_2 and stored frozen in the drybox. Preparations of *p*-methyl-α-methylstyrene, *p*-trifluoromethyl-α-methylstyrene and *p*-methoxy-α-methylstyrene were accomplished by reaction of $Ph_3P{=}CH_2$ with the appropriate acetophenone as described previously[39] and the resulting product distilled at reduced pressure from CaH_2. Ferrocene used as an internal standard was purchased from Aldrich and sublimed before use.

NMR spectra were recorded on a Bruker AM500 (500.13 MHz for ^1H, 76.77 for ^2H, 125.77 MHz for ^{13}C) spectrometer. All chemical shifts are relative to TMS using ^1H (residual), ^2H or ^{13}C chemical shifts of the solvent as a secondary standard. The temperature of the NMR probe was measured before and after each kinetic run with a standard CH_3OH reference tube.

Kinetics of the Reaction of 1 or 2 with Volatile Olefins. In the dry box, a J. Young NMR tube was charged with 0.50 mL of 0.0488 M (0.0244 mmol) of a stock toluene-d_8 solution of metallocene dihydride containing a known amount of ferrocene. The NMR tube was then attached to the vacuum line via a

calibrated gas volume. The tube was evacuated at -78 °C and 10 equivalents of olefin were charged into the gas bulb by vacuum transfer and the gas condensed in the tube at -78 °C. The NMR probe was calibrated to the desired temperature and the sample was shaken several times just before insertion into the probe. Approximately 10-15 spectra were recorded at regular intervals over the duration of 2-3 half lives. Peak intensities of the ferrocene and metallocene dihydride were measured for each spectrum. The observed rate constants were obtained from slopes of plots of $\ln[Cp^*_2MH_2]$ versus time. Second order rate constants were obtained by dividing the observed psuedo first order rate constants by the concentration of olefin. Activation parameters were obtained by measuring second order rate constants over a temperature range. A plot of $\ln(k/T)$ versus $1/T$ resulted in a slope of $\Delta H^{\ddagger}/R$ and an intercept of $[(\Delta S^{\ddagger}/R) + 23.76]$. Reported errors in the rate constants represent one standard deviation from the least squares fit of the experimental data. These errors were then used to determine the errors in the activation parameters.

Kinetics of the Reaction of 1 with Substituted α-Methylstyrenes. In the dry box, 0.25 mL of 0.096 M stock benzene-d_6 solution of **1** containing a known amount of ferrocene was charged into a J. Young NMR tube. Via microsyringe, 0.25 mL of a benzene-d_6 stock solution of α-methylstyrene was added to the tube and the sample was then immediately frozen in liquid nitrogen. The tube was then quickly thawed and inserted into NMR probe. Approximately 10-15 spectra were recorded at regular intervals over the duration of 2-3 half lives. Work up of the data was carried out as described for the previous experiments.

Determination of β-Hydrogen Elimination Rate Constants. In a typical experiment, a J. Young NMR tube was charged with 0.50 mL of 0.0488 M stock benzene-d_6 or toluene-d_8 solution of zirconocene dihydride containing a known amount of ferrocene. On the vacuum line, the tube was frozen in liquid nitrogen and degassed with three freeze-pump-thaw cycles. Via a 6.9 mL calibrated gas volume, 100 Torr of the desired olefin was added at -196 °C. The tube was thawed and shaken. The ^1H NMR spectrum was then recorded to ensure complete conversion to the alkyl hydride complex had occurred. The tube was reattached to the vacuum line and via a 56.8 mL calibrated gas bulb, the desired amount of **37** was collected in the tube at -196 °C. The tube remained frozen in liquid nitrogen until insertion into the thermostated NMR probe. Approximately

10-15 spectra were recorded over regular intervals over the course of 2-3 half lives. Work up of the data was carried out as described for the previous experiments.

Determination of Equilibrium Constants for Zirconocene Alkyl Hydride Complexes. In a typical experiment, a J. Young NMR tube was charged with 0.50 mL of 0.0488 M stock benzene-d_6 solution containing a known amount of ferrocene. On the vacuum line, the tube was degassed and the appropriate amount of isobutene and 1-butene was then added via calibrated gas volume. The tube was thawed and shaken thoroughly and allowed to stand at room temperature for several hours. The ^{1}H NMR spectrum was then recorded and the equilibrium constant computed from the integration of the various species in solution.

NMR Spectroscopic Data

(η^5-$C_5Me_5)_2Zr(CH_2CH(CH_3)CH_2CH_3)(H)$ (4). ^{1}H NMR (benzene-d_6): δ = 1.92 (s, 30H, $C_5\mathit{Me}_5$); 6.31 (s, 1H, Zr*H*); -0.531 (dd, 1H, $C\mathit{H}_2CH(CH_3)CH_2CH_3$); 0.290 (dd, 1H, $C\mathit{H}_2CH(CH_3)CH_2CH_3$); *not located* ($CH_2C\mathit{H}(CH_3)CH_2CH_3$); 1.36 (m, 2H, $CH_2CH(CH_3)C\mathit{H}_2CH_3$); 0.877 (t, 7 Hz, 3H, $CH_2CH(CH_3)CH_2C\mathit{H}_3$); 1.76 (d, 5 Hz, 3H, $CH_2CH(C\mathit{H}_3)CH_2CH_3$). ^{13}C NMR (benzene-$d_6$): δ = 12.83 ($C_5\mathit{Me}_5$); 118.26 (C_5Me_5); 70.28 ($CH_2CH(CH_3)(CH_2CH_3)$; 31.17 ($CH_2CH(CH_3)(CH_2CH_3)$; 22.87 ($CH_2CH(CH_3)(CH_2CH_3)$; 13.52 ($CH_2CH(CH_3)(CH_2CH_3)$; 29.09 ($CH_2CH(\mathit{C}H_3)(CH_2CH_3)$.

(η^5-$C_5Me_5)_2Zr(CH_2CH(CH_3)CH_2CH(CH_3)_2)(H)$ (5). ^{1}H NMR (benzene-d_6): δ = 1.94 (s, 30H, $C_5\mathit{Me}_5$); 6.39 (s, 1H, Zr*H*); -0.669 (dd, 1H, $C\mathit{H}_2CH(CH_3)CH_2CH(CH_3)_2$); 0.492 (dd, 1H, $C\mathit{H}_2CH(CH_3)CH_2CH(CH_3)_2$); 2.24 (m, 2H,$CH_2C\mathit{H}(CH_3)CH_2CH(CH_3)_2$); 1.12 (m, 2H, $CH_2CH(CH_3)C\mathit{H}_2CH(CH_3)_2$); 2.16 (m, 1H, $CH_2CH(CH_3)CH_2CH(CH_3)_2$); 1.02 (d, 6.5 Hz, 3H, $CH_2CH(C\mathit{H}_3)CH_2CH(CH_3)_2$); 0.98 (d, 6.5 Hz, 6H, $CH_2CH(CH_3)CH_2CH(\mathit{C}H_3)_2$). ^{13}C NMR (benzene-$d_6$): δ = 12.30 ($C_5\mathit{Me}_5$); 12.50 ($C_5\mathit{Me}_5$); 117.34 (C_5Me_5); 117.71 C_5Me_5); 66.60 ($CH_2CH(CH_3)CH_2CH(CH_3)_2$); 39.09 ($CH_2CH(CH_3)CH_2CH(CH_3)_2$); 20.58 ($CH_2CH(CH_3)CH_2CH(CH_3)_2$); 22.64 ($CH_2CH(CH_3)CH_2CH(CH_3)_2$); 35.93 ($CH_2CH(CH_3)CH_2CH(CH_3)_2$); 13.53, 13.62 ($CH_2CH(CH_3)CH_2CH(CH_3)_2$).

(η^5-$C_5Me_5)_2Zr(CH_2CH(CH_3)CH(CH_3)CH_2CH_3)(H)$ (6). ^{1}H NMR (benzene-d_6): δ = 1.93 (s, 30H, C_5Me_5); 6.35 (s, 1H, Zr*H*); -0.386 (dd, 1H, $CH_2CH(CH_3)CH(CH_3)CH_2CH_3$); 0.220 (dd, 1H, $CH_2CH(CH_3)CH(CH_3)CH_2CH_3$); 2.21 (m, 1H, $CH_2CH(CH_3)CH(CH_3)CH_2CH_3$); 1.31 (m, 1H, $CH_2CH(CH_3)CH(CH_3)CH_2CH_3$); 1.18 (m, 2H, $CH_2CH(CH_3)CH(CH_3)CH_2CH_3$); 1.01 (t, 7 Hz, 3H, $CH_2CH(CH_3)CH(CH_3)CH_2CH_3$).

(η^5-$C_5Me_5)_2Zr(CH_2CH(CH_3)(C_6H_5))(H)$ (7). ^{1}H NMR (benzene-d_6): δ = 1.87 (s, 15H, C_5Me_5); 1.94 (s, 15H, C_5Me_5); 6.55 (s, 1H, Zr*H*); -0.944 (dd, 1H, $CH_2CH(CH_3)(C_6H_5)$); -0.969 (dd, 1H, $CH_2CH(CH_3)(C_6H_5)$); 1.56 (t, 6.5 Hz, 1H, $CH_2CH(CH_3)(C_6H_5)$); 1.65 (d, 7 Hz, 3H, $CH_2CH(CH_3)(C_6H_5)$); 7.42 (d, 7.1 Hz, 2H, $CH_2CH(CH_3)$(*ortho*-C_6H_5)); 7.11 (t, 7.5 Hz, 2H, $CH_2CH(CH_3)$(*meta*-C_6H_5)); 7.29 (t, 7.3 Hz, 1H, $CH_2CH(CH_3)$(*para*-C_6H_5)). ^{13}C NMR (benzene-d_6): δ = 12.24 (C_5Me_5); 12.48 (C_5Me_5); 118.44 (C_5Me_5); 118.77 (C_5Me_5); 67.06 ($CH_2CH(CH_3)(C_6H_5)$; 39.45 ($CH_2CH(CH_3)(C_6H_5)$; 30.10 ($CH_2CH(CH_3)(C_6H_5)$; 117.39, 117.65, 119.54, 123.75, 134.51, *1 not located* (C_6H_5).

(η^5-$C_5Me_5)_2Zr(CH_2CH_2CH_2CH_3)(H)$ (8). ^{1}H NMR (benzene-d_6): δ = 1.89 (s, 30H, C_5Me_5); 6.27 (s, 1H, Zr-*H*); 0.159 (t, 9 Hz, 2H, CH_2 $CH_2CH_2CH_3$); 1.24 (m, 2H, CH_2 $CH_2CH_2CH_3$); 1.39 (m, 2H, CH_2 $CH_2CH_2CH_3$); 1.05 (t, 7.3 Hz, 3H, CH_2 $CH_2CH_2CH_3$). ^{13}C NMR (benzene-d_6): δ = 12.09 (C_5Me_5); 113.00 (C_5Me_5); 52.48 ($CH_2CH_2CH_2CH_3$); 31.62 ($CH_2CH_2CH_2CH_3$); 25.57 ($CH_2CH_2CH_2CH_3$); 11.40 ($CH_2CH_2CH_2CH_3$).

(η^5-$C_5Me_5)_2Hf(CH_2CH(CH_3)_2)(H)$ (9). ^{1}H NMR (benzene-d_6): δ = 1.95 (s, 30H, C_5Me_5); 9.76 (s, 1H, Hf-*H*); -0.25 (d, 6.5 Hz, 2H, CH_2 $CH(CH_3)_2$); 2.09 (m, 1H, CH_2 $CH(CH_3)_2$); 1.00 (d, 6Hz, 6H, $CH_2CH(CH_3)_2$). ^{13}C NMR (benzene-d_6): δ = 12.24 (C_5Me_5); 117.52 (C_5Me_5); 76.33 ($CH_2CH(CH_3)_2$); 31.94 ($CH_2CH(CH_3)_2$); 13.63 ($CH_2CH(CH_3)_2$).

(η^5-$C_5Me_5)_2Hf$(*cyclo*-C_5H_9)(H) (10). ^{1}H NMR (benzene-d_6): δ = 1.95 (s, 30H, C_5Me_5); 13.31 (s, 1H, Hf*H*); -0.17, .456, 1.08, 1.93, 2.27 (m, C_5H_9). ^{13}C NMR (benzene-d_6): δ = 12.27 (C_5Me_5); 117.57 (C_5Me_5); 73.17 (C_1-cyclopentene); 29.86 (C_2-cyclopentene); 23.51 (C_3-cyclopentene).

(η^5-$C_5Me_5)_2Hf(CH_2CH_2C_6H_5)(H)$ (11). ^{1}H NMR (benzene-d_6): δ = 1.88 (s, 30H, C_5Me_5); 12.96 (s, 1H, Hf*H*); -0.09 (t, 6.5 Hz, 2H, CH_2 CH_2Ph); 2.22 (t, 6.5 Hz, 2H, CH_2 CH_2Ph); 6.85 (m, 1H, *para*-$CH_2CH_2C_6H_5$); 6.98 (m, 2H, *meta*-$CH_2CH_2C_6H_5$); 7.34 (m, 2H, *ortho*-$CH_2CH_2C_6H_5$). ^{13}C NMR (benzene-d_6): δ = 12.12 (C_5Me_5); 118.26 (C_5Me_5); 62.45 (CH_2CH_2Ph); 30.36 (CH_2CH_2Ph); 125.52 (*para*-C_6H_5); 137.50 (*ortho*-C_6H_5); 150.07 (*meta*-C_6H_5), *1 not located* (*ipso*-C_6H_5).

(η^5-$C_5Me_5)_2Hf(CH_2CH_2CH_2CH_3)(H)$ (12). ^{1}H NMR (benzene-d_6): δ = 1.95 (s, 30H, C_5Me_5); 9.80 (s, 1H, Hf*H*); -0.005 (t, 9 Hz, 2H, CH_2 $CH_2CH_2CH_3$); *not located* (CH_2 $CH_2CH_2CH_3$); 0.981 (m, 2H, CH_2 $CH_2CH_2CH_3$); 1.06 (t, 7.4 Hz, 3H, CH_2 $CH_2CH_2CH_3$). ^{13}C NMR (benzene-d_6): δ = 12.06 (C_5Me_5); 116.97 (C_5Me_5); 62.55 ($CH_2CH_2CH_2CH_3$); 31.50 ($CH_2CH_2CH_2CH_3$); 26.93 ($CH_2CH_2CH_2CH_3$); 14.76 ($CH_2CH_2CH_2CH_3$).

(η^5-$C_5Me_5)_2Hf(CH_2CH_2CH_2CH_2CH_3)(H)$ (13). ^{1}H NMR (benzene-d_6): δ = 1.94 (s, 30H, C_5Me_5); 9.81 (s, 1H, Hf*H*); -0.005 (t, 9 Hz, 2H, CH_2 $CH_2CH_2CH_2CH_3$); *not located* (CH_2 $CH_2CH_2CH_2CH_3$); 0.991 (m, 4H, CH_2 $CH_2CH_2CH_2CH_3$); 1.12 (t, 7.4 Hz, 3H, CH_2 $CH_2CH_2CH_2CH_3$).

(η^5-$C_5Me_5)_2Zr(CH_2CH(CH_3)(C_6H_4$-*p*-F))(H) (14). ^{1}H NMR (benzene-d_6): δ = 1.84 (s, 15H, C_5Me_5); 1.86 (s, 15H, C_5Me_5); 6.31 (s, 1H, Zr*H*); -0.984 (dd, 1H, $CH_2CH(CH_3)(C_6H_4$-*p*-F)); -0.368 (dd, 1H, $CH_2CH(Me)(C_6H_4$-*p*-F)); 2.56 (m, 1H, $CH_2CH(CH_3)(C_6H_4$-*p*-F)); 1.78 (d, 3H, $CH_2CH(CH_3)(C_6H_4$-*p*-F)); 7.19 (m, 2H, $CH_2CH(CH_3)$(*ortho*-C_6H_4-*p*-F)); 6.94 (m, 2H, $CH_2CH(CH_3)$(*meta*-C_6H_4-*p*-F)).

(η^5-$C_5Me_5)_2Zr(CH_2CH(CH_3)(C_6H_4$-*p*-$CH_3$))(H) (15). ^{1}H NMR (benzene-d_6): δ = 1.89 (s, 15H, C_5Me_5); 1.94 (s, 15H, C_5Me_5); 6.54 (s, 1H, Zr*H*); 0.959 (dd, 1H, $CH_2CH(CH_3)(C_6H_4$-*p*-CH_3)); 0.912 (dd, 1H, $CH_2CH(CH_3)(C_6H_4$-*p*-CH_3)); 2.22 (m, 1H, $CH_2CH(CH_3)(C_6H_4$-*p*-CH_3)); 1.19 (d, 7 Hz, 3H, $CH_2CH(CH_3)(C_6H_4$-*p*-CH_3)); 2.16 (s, 3H, $CH_2CH(CH_3)(C_6H_4$-*p*-CH_3)); 6.99 (d, 6 Hz, 2H, $CH_2CH(Me)$(*meta*-C_6H_4-*p*-CH_3)); 7.34 (d, 6 Hz, 2H, $CH_2CH(CH_3)$(*ortho*-C_6H_4-*p*-CH_3)).

(η^5-$C_5Me_5)_2Zr(CH_2CH(CH_3)(C_6H_4$-*p*-$OCH_3$))(H) (16). ^{1}H NMR (benzene-d_6): δ = 1.89 (s, 15H, C_5Me_5); 1.95 (s, 15H, C_5Me_5); 6.53 (s, 1H, Zr*H*); 0.904 (dd, 1H, $CH_2CH(CH_3)(C_6H_4$-*p*-OCH_3)); 0.912 (dd, 1H, $CH_2CH(CH_3)(C_6H_4$-*p*-OCH_3));

1.62 (m, 1H, $CH_2CH(CH_3)(C_6H_4$-*p*-$OCH_3)$); 1.78 (d, 6.5 Hz, 3H, $CH_2CH(CH_3)(C_6H_4$-*p*-$OCH_3)$); 3.34 (s, 3H, $CH_2CH(Me)(C_6H_4$-*p*-$OCH_3)$); 6.92 (d, 6 Hz, 2H, $CH_2CH(Me)$(*meta*-C_6H_4-*p*-$OCH_3)$); 7.34 (d, 6 Hz, 2H, $CH_2CH(Me)$(*ortho*-C_6H_4-*p*-$OCH_3)$).

(η^5-$C_5Me_5)_2Zr(CH_2CH(CH_3)(C_6H_4$-*p*-$CF_3))(H)$ (17). ^{1}H NMR (benzene-d_6): δ = 1.84 (s, 15H, C_5Me_5); 1.92 (s, 15H, C_5Me_5); 6.54 (s, 1H, Zr*H*); -1.11 (dd, 1H, $CH_2CH(CH_3)(C_6H_4$-*p*-$CF_3)$); 0.053 (dd, 1H, $CH_2CH(CH_3)(C_6H_4$-*p*-$CF_3)$); 3.31 (m, 1H, $CH_2CH(CH_3)(C_6H_4$-*p*-$CF_3)$); 1.05 (d, 6.8 Hz, 3H, $CH_2CH(CH_3)(C_6H_4$-*p*-$CF_3)$); 7.24 (d, 6 Hz, 2H, $CH_2CH(Me)$(*meta*-C_6H_4-*p*-$CF_3)$); 7.48 (d, 6 Hz, 2H, $CH_2CH(CH_3)$(*ortho*-C_6H_4-*p*-$CF_3)$).

(η^5-C_5Me_5)(η^5-$C_5Me_4H)Zr(CH_2CH(CH_3)_2)(H)$ (19). ^{1}H NMR (benzene-d_6): δ = 1.91 (s, 15H, C_5Me_5); 1.60, 1.87, 2.10, 2.33 (s, 3H, C_5Me_4H); 4.52 (s, 1H, C_5Me_4H); 6.26 (s, 1H, Zr*H*); -0.445 (dd, 1H, CH_2 $CH(CH_3)_2$); 0.443 (dd, 1H, CH_2 $CH(CH_3)_2$); 2.15 (m, 1H, CH_2 $CH(CH_3)_2$); 0.953 (d, 7 Hz, 3H, $CH_2CH(CH_3)_2$); 1.06 (d, 7 Hz, 3H, $CH_2CH(CH_3)_2$). ^{13}C NMR (benzene-d_6): δ = 12.73 (C_5Me_5); 117.98 (C_5Me_5); 12.17, 12.32, 13.46, 14.56 (C_5Me_4H); 68.38 ($CH_2C(CH_3)_2$); 31.76 ($CH_2CH(CH_3)_2$); 24.47, 29.64 ($CH_2CH(CH_3)_2$); 111.51, 115.70, 119.70, 120.79, 121.63 (Cp).

(η^5-C_5Me_5)(η^5-$C_5Me_4CH_2CH_3)Zr(CH_2CH(CH_3)_2)(H)$ (23). ^{1}H NMR (benzene-d_6): δ = 1.92 (s, 15H, C_5Me_5); 1.76, 1.79, 1.94, 1.98 (s, 3H, $C_5Me_4CH_2CH_3$); 1.85 (q, 6.5 Hz, 2H, $C_5Me_4CH_2CH_3$); 1.90 (t, 7 Hz, 2H, $C_5Me_4CH_2CH_3$); 6.34 (s, 1H, Zr*H*); -0.381 (dd, 1H, CH_2 $CH(CH_3)_2$); 0.053 (dd, 1H, CH_2 $CH(CH_3)_2$); 2.43 (m, 1H, CH_2 $CH(CH_3)_2$); 0.82 (d, 7 Hz, 3H, $CH_2CH(CH_3)_2$); 1.10 (d, 7 Hz, 3H, $CH_2CH(CH_3)_2$).

(η^5-C_5Me_5)(η^5-C_5H_3-$(CMe_3)_2)Hf(CH_2CH(CH_3)_2)(H)$ (25). ^{1}H NMR (benzene-d_6): δ = 1.98 (s, 15H, C_5Me_5); 1.22 (s, 9H, CMe_3); 1.48(s, 9H, CMe_3); 12.98 (s, 1H, Hf*H*); -1.06 (m, 1H, $CH_2CH(CH_3)_2$); 0.75 (m, 1H, $CH_2CH(CH_3)_2$); 2.50 (m, 1H, $CH_2CH(CH_3)_2$); 1.04 (d, 7 Hz, 3H, $CH_2CH(CH_3)_2$); 1.17 (d, 7 Hz, 3H, $CH_2CH(CH_3)_2$); 4.92, 4.62, 6.50 (m, 1H, Cp). ^{13}C NMR (benzene-d_6): δ = 12.71 (C_5Me_5); 116.96 (C_5Me_5); 32.34 (CMe_3); 32.99 (CMe_3); 145.06 (CMe_3); 145.96 (CMe_3); 76.44 ($CH_2CH(CH_3)_2$); 32.34 ($CH_2CH(CH_3)_2$); 24.33 ($CH_2CH(CH_3)_2$); 30.30 ($CH_2CH(CH_3)_2$); 99.86, 104.61, 105.64, *2 not located* (Cp).

(η^5-$C_5Me_5)_2Zr(CH_2CH_2C_6H_5)(H)$ (26). ^{1}H NMR (benzene-d_6): δ = 1.88 (s, 30H, C_5Me_5); *not located* (Zr*H*); 0.54 (t, 6.9 Hz, 2H, CH_2 CH_2Ph); 1.78 (t, 6.3 Hz, 2H, CH_2 CH_2Ph); 7.08 (m, 1H, *para*-$CH_2CH_2C_6H_5$); 7.25 (m, 2H, *meta*-$CH_2CH_2C_6H_5$); 7.40 (m, 2H, *ortho*-$CH_2CH_2C_6H_5$). ^{13}C NMR (benzene-d_6): δ = 12.18 (C_5Me_5); 117.51 (C_5Me_5); 51.79 ($CH_2CH_2C_6H_5$); 26.49 ($CH_2CH_2C_6H_5$); 125.67, 126.15, 138.00, *1 not located* (C_6H_5).

(η^5-C_5Me_5)(η^5-C_5H_3-1,3-$(CMe_3)_2$)$Zr(CH_2CH_2C_6H_5)(H)$ (27). ^{1}H NMR (benzene-d_6): δ = 1.89 (s, 15H, C_5Me_5); 1.16 (s, 9H, CMe_3); 0.956 (s, 9H, CMe_3); 6.49 (s, 1H, Zr*H*); -0.122 (td, 13.9 Hz, 3.8 Hz, 1H, CH_2 CH_2Ph); 0.693 (td, 13.9 Hz, 3.8 Hz, 1H, CH_2 CH_2Ph); 2.48 (td, 13.6 Hz, 4.8 Hz, 1H, CH_2 CH_2Ph); 2.86 (td, 13.6 Hz, 4.8 Hz, 1H, CH_2 CH_2Ph); 7.05 (m, 1H, *para*-$CH_2CH_2C_6H_5$); 7.25 (m, 2H, *meta*-$CH_2CH_2C_6H_5$); 7.31 (m, 2H, *ortho*-$CH_2CH_2C_6H_5$); *not located* (*ipso*-C_6H_5).

(η^5-C_5H_3-1,3-$(CMe_3)_2)_2Zr(CH_2CH_2C_6H_5)(H)$ (28). ^{1}H NMR (benzene-d_6): δ = 1.28, (s, 9H, CMe_3); 1.45 (s, 9H, CMe_3); 5.33 (s, 1H, Zr*H*); 0.55 (t, 10 Hz, 2H, $CH_2CH_2C_6H_5$); 2.76 (t, 10 Hz, 2H, $CH_2CH_2C_6H_5$); 4.85, 5.22, 6.26 (s, 1H, Cp). ^{13}C NMR (benzene-d_6): δ = 32.77 (CMe_3); 32.48 (CMe_3); 141.28 (CMe_3); 144.70 (CMe_3); 60.96 ($CH_2CH_2C_6H_5$); 34.29 ($CH_2CH_2C_6H_5$); 125.56, 126.95, 137.68, *1 not located* (C_6H_5); 97.41, 100.53, 106.63, 114.13, 122.65 (Cp).

(η^5-C_5Me_5)(η^5-C_5H_4-CMe_3)$Zr(CH(C_6H_5)(CH_3))(H)$ (30). ^{1}H NMR (benzene-d_6): δ = 1.75 (s, 15H, C_5Me_5); 1.83 (s, 15H, C_5Me_5); 1.11 (s, 9H, CMe_3); 1.36 (s, 9H, CMe_3);1.37 (s, 1H, Zr*H*); 5.40 (s, 1H, Zr*H*); -0.18 (d, 6.5 Hz, 3H, $CH(C_6H_5)(CH_3)$); 1.86 (d, 6.5 Hz, 3H, $CH(C_6H_5)(CH_3)$); *not located* ($CH(C_6H_5)(CH_3)$); 6.85, 6.89 (m, 1H, *para*-C_6H_5); 7.19, 7.25 (m, 2H, *meta*-C_6H_5); 7.39, 7.44 (m, 2H, *para*-C_6H_5); 3.18, 3.45, 3.66, 4.48, 4.62, 4.72, 4.77, 4.78 (Cp). ^{13}C NMR (benzene-d_6): δ = 12.51, 12.85 (C_5Me_5); 114.30, 114.68, (C_5Me_5); 32.84, 32.88 (CMe_3); 136.62, 145.88 (CMe_3); 39.09, 47.91 ($CH(C_6H_5)(CH_3)$); -7.240, 17.68 (($CH(C_6H_5)(CH_3)$); 112.09, 123.75 (*para*-C_6H_5); 125.71, 126.73 (*ortho*-C_6H_5); 129.16, 132.36 (*meta*-C_6H_5); *2 not located* (*ipso*-C_6H_5); 99.98, 100.03, 100.10, 102.43, 104.08, 105.02, 110.04, 113.79, 120.77, 121.66 (Cp).

(η^5-C_5Me_5)(THI)$Zr(CH_2CH_2C_6H_5)(H)$ (34a). ^{1}H NMR (benzene-d_6): δ = 1.86 (s, 15H, C_5Me_5); 5.89 (s, 1H, Zr*H*); 2.0-2.4 (m, THI); 0.706 (m, 2H, CH_2CH_2Ph); 0.870

(m, 2H, CH_2CH_2Ph); 6.94 (m, 1H, *para*-$CH_2CH_2C_6H_5$); 7.24(m, 2H, *meta*-$CH_2CH_2C_6H_5$); 7.37 (m, 2H, *ortho*-$CH_2CH_2C_6H_5$); 4.13, 4.57, 4.99 (Cp).

(η^5-C_5Me_5)(THI)Zr((CH(C_6H_5)(CH_3))(H) (34b). ^{1}H NMR (benzene-d_6): δ = 1.79 (s, 15H, C_5Me_5); *not located* (Zr*H*); 2.2-2.6 (m, THI); -0.90 (d, 8 Hz, 3H, CH(C_6H_5)(CH_3)); 1.20 (d, 8 Hz, 3H, CH(C_6H_5)(CH_3)); 7.10 (m, 1H, *para*-$CH_2CH_2C_6H_5$); 7.22 (m, 2H, *meta*-$CH_2CH_2C_6H_5$); 7.29 (m, 2H, *ortho*-$CH_2CH_2C_6H_5$); 3.54, 4.58, 4.71, 4.90, *2 not located* (Cp).

(η^5-$C_5Me_4H)_2$Zr($CH_2CH_2C_6H_5$)(H) (35a). ^{1}H NMR (benzene-d_6): δ = 1.79, 1.82, 1.91, 1.99 (s, 6H, C_5Me_4); 6.47 (Zr*H*); 0.38 (t, 6.5 Hz, 2H, CH_2 CH_2Ph); *not located* (CH_2 CH_2Ph); 6.96 (m, 1H, *para*-$CH_2CH_2C_6H_5$); 7.35 (m, 2H, *meta*-$CH_2CH_2C_6H_5$); 7.40 (m, 2H, *ortho*-$CH_2CH_2C_6H_5$).

(η^5-$C_5Me_4H)_2$Zr((CH(C_6H_5)(CH_3))(H) (35b). ^{1}H NMR (benzene-d_6): δ = 1.60, 1.66, 1.73, 1.79, 2.14, 2.15, 2.18, 2.32 (s, 6H, C_5Me_4H); 4.36, *1 not located* (s, 1H, Zr*H*); 0.485, *1 not located* (q, 6 Hz, 1H, C*H*(C_6H_5)(CH_3)); 1.26, *1 not located* (CH(C_6H_5)(CH_3); 4.84, 4.89 (Cp).

(η^5-C_5Me_5)(η^5-C_5H_3-1,3-($CHMe_2)_2$)Zr($CH_2CH_2C_6H_5$)(H) (36a). ^{1}H NMR (benzene-d_6): δ = 1.82 (s, 15H, C_5Me_5); 0.51 (d, 7 Hz. 6H, $CHMe_2$); 0.84 (d, 7 Hz. 3H, $CHMe_2$); 0.88 (d, 7 Hz. 3H, $CHMe_2$); 1.07 (d, 7 Hz. 3H, $CHMe_2$); 2.45 (sept, 6.5 Hz, 1H, C*H*Me_2); 2.59 (sept, 6.5 Hz, 1H, C*H*Me_2); 6.42 (s, 1H, Zr*H*); -0.179 (m, 1H, CH_2 CH_2Ph); 0.82 (m, 1H, CH_2 CH_2Ph); 2.43 (m, 1H, CH_2 CH_2Ph); 2.84 (m, 1H, CH_2 CH_2Ph); 7.06 (m, 1H, *para*-$CH_2CH_2C_6H_5$); 7.29 (m, 2H, *meta*-$CH_2CH_2C_6H_5$); 7.42 (m, 2H, *ortho*-$CH_2CH_2C_6H_5$); 4.89, 5.26, 5.45 (Cp).

(η^5-C_5Me_5)(η^5-C_5H_3-1,3-($CHMe_2)_2$)Zr(CH(C_6H_5)(CH_3))(H) (36b). ^{1}H NMR (benzene-d_6): δ = 1.76 (s, 15H, C_5Me_5); 1.83 (s, 15H, C_5Me_5); 0.68 (d, 7 Hz. 3H, $CHMe_2$); 0.73 (d, 7 Hz. 3H, $CHMe_2$); 1.04 (d, 7 Hz. 3H, $CHMe_2$); 1.06 (d, 7 Hz. 3H, $CHMe_2$); 1.14 (d, 7 Hz. 3H, $CHMe_2$); 1.17 (d, 7 Hz. 3H, $CHMe_2$); 1.21 (d, 7 Hz. 3H, $CHMe_2$); 1.24 (d, 7 Hz. 3H, $CHMe_2$); *not located* (C*H*Me_2); 6.19, *1 not located* (s, 1H, Zr*H*); 4.25, 4.60, 4.63, 4.83, 4.89, 5.76 (Cp).

(η^5-C_5Me_5)(η^5-C_5H_5)Zr($CH_2CH(CH_3)_2$)(H) (38). ^{1}H NMR (benzene-d_6): δ = 1.89 (s, 15H, C_5Me_5); 6.22 (s, 1H, Zr*H*); -1.93 (dd, 1H, CH_2 $CH(CH_3)_2$); 0.25 (dd, 1H,

CH_2 $CH(CH_3)_2$); 2.21 (m, 1H, CH_2 $CH(CH_3)_2$); 1.03 (d, 7Hz, 3H, $CH_2CH(CH_3)_2$); 1.10 (d, 7Hz, 3H, $CH_2CH(CH_3)_2$); 5.74 (s, 5H, C_5H_5). ^{13}C NMR (benzene-d_6): δ = 12.18 (C_5Me_5); 117.62 (C_5Me_5); 71.65 ($CH_2CH(CH_3)_2$); 33.17 ($CH_2CH(CH_3)_2$); 29.91 ($CH_2CH(CH_3)_2$); 28.81 ($CH_2CH(CH_3)_2$); 111.07 (Cp).

$(\eta^5\text{-}C_5Me_5)(\eta^5\text{-}C_5H_4\text{-}CMe_3)Zr(CH_2CH(CH_3)_2)(H)$ (39). ^1H NMR (benzene-d_6): δ = 1.86 (s, 15H, C_5Me_5); 1.34 (s, 9H, CMe_3); 6.22 (s, 1H, Zr*H*); -1.95 (dd, 1H, CH_2 $CH(CH_3)_2$); 0.14 (dd, 1H, CH_2 $CH(CH_3)_2$); 2.41 (m, 1H, CH_2 $CH(CH_3)_2$); 0.97 (d, 7Hz, 3H, $CH_2CH(CH_3)_2$); 0.99 (d, 7Hz, 3H, $CH_2CH(CH_3)_2$); 4.87, 4.92, 5.41, 5.90 (Cp). ^{13}C NMR (benzene-d_6): δ = 12.18 (C_5Me_5); 110.85 (C_5Me_5); 2.31 (CMe_3); 145.60 (CMe_3); 74.39 ($CH_2CH(CH_3)_2$); 33.53 ($CH_2CH(CH_3)_2$); 28.20 ($CH_2CH(CH_3)_2$); 89.75, 98.92, 104.04, 107.98, 109.58 (Cp).

$(\eta^5\text{-}C_5Me_5)$(THI)$Zr(CH_2CH(CH_3)_2)(H)$ (40). ^1H NMR (benzene-d_6): δ = 1.89 (s, 15H, C_5Me_5); 6.24 (s, 1H, Zr*H*); -1.67 (dd, 1H, CH_2 $CH(CH_3)_2$); 0.870 (dd, 1H, CH_2 $CH(CH_3)_2$); 2.17 (m, 1H, CH_2 $CH(CH_3)_2$); 0.975 (d, 7 Hz, 3H, $CH_2CH(CH_3)_2$); 1.04 (d, 7 Hz, 3H, $CH_2CH(CH_3)_2$); 2.49, 2.55, 2.69, 2.78 (m, THI),4.70, 4.98, 5.61 (m, 1H, Cp). ^{13}C NMR (benzene-d_6): δ = 12.70 (C_5Me_5); 117.39 (C_5Me_5); 24.32, 25.63, 26.18 28.47 (THI), 87.95 ($CH_2C(CH_3)_2$); 34.33 ($CH_2C(CH_3)_2$); 30.21 ($CH_2C(CH_3)_2$); 103.46, 105.21, 111.86, 126.45, 127.93 (Cp).

$(\eta^5\text{-}C_5Me_5)(\eta^5\text{-}C_5H_3\text{-}1,3\text{-}(CHMe_2)_2)Zr(CH_2CH(CH_3)_2)(H)$ (41). ^1H NMR (benzene-d_6): δ = 1.92 (s, 15H, C_5Me_5); 6.34 (s, 1H, Zr*H*); 1.10 (d, 7 Hz. 3H, $CHMe_2$); 1.23 (d, 7 Hz. 3H, $CHMe_2$); 1.30 (d, 7 Hz. 3H, $CHMe_2$); 1.34 (d, 7 Hz. 3H, $CHMe_2$); 2.79 (sept, 6.5 Hz, 1H, $CHMe_2$); 3.25 (sept, 6.5 Hz, 1H, $CHMe_2$); -0.359 (dd, 1H, CH_2 $CH(CH_3)_2$); 0.220 (dd, 1H, CH_2 $CH(CH_3)_2$); 2.22 (m, 1H, CH_2 $CH(CH_3)_2$); 0.965 (d, 7Hz, 6H, $CH_2CH(CH_3)_2$); 4.74, 4.85, 5.94 (m, 1H, C_5H_3-1,3-$CHMe_2$). ^{13}C NMR (benzene-d_6): δ = 12.89 (C_5Me_5); 117.18 (C_5Me_5); 71.82 (CH_2CMe_2); 21.89, 22.64, 26.60, 27.34, 28.29, 29.07, 29.68, 30.48, 31.28 ($CHMe_2$, CH_2CMe_2); 88.31, 95.92, 100.52, 109.56, 123.00 (Cp).

$(\eta^5\text{-}C_5Me_5)(\eta^5\text{-}C_5H_3\text{-}1,3\text{-}(CMe_3)_2)Zr(CH_2CH(CH_3)_2)(H)$ (42) . ^1H NMR (benzene-d_6): δ = 1.88 (s, 15H, C_5Me_5); 6.48 (s, 1H, Zr*H*); 0.956 (s, 9H, CMe_3); 1.23 (s, 9H, CMe_3); -0.825 (dd, 1H, CH_2 $CH(CH_3)_2$); -0.836 (dd, 1H, CH_2 $CH(CH_3)_2$); 2.31 (m, 1H, CH_2 $CH(CH_3)_2$); 0.956 (d, 7 Hz, 6H, $CH_2CH(CH_3)_2$); 4.59, 4.75, 4.79 (m, 1H, C_5H_3-1,3-$(CMe_3)_2$). ^{13}C NMR (benzene-d_6): δ = 12.89 (C_5Me_5); 117.86

(C_5Me_5); 32.06 (CMe_3); 33.03 (CMe_3); 2 *not located* (CMe_3); 70.44 ($CH_2CH_2(CH_3)_2$); 31.90 ($CH_2CH_2(CH_3)_2$); 31.32 ($CH_2CH_2(CH_3)_2$); 29.98 ($CH_2CH_2(CH_3)_2$); 99.87,103.77, 105.82, 106.71, 116.87 (Cp).

(η^5-$C_5Me_4H)_2Zr(CH_2CH(CH_3)_2)(H)$ (43). ^{1}H NMR (benzene-d_6): δ = 2.01, 2.07 (s, 12H, C_5Me_4H); 5.10 (s, 2H, C_5Me_4H); 5.96 (s, 1H, Zr*H*); -0.06 (d, 6.8 Hz, 2H, CH_2 $CH(CH_3)_2$); 2.28 (m, 1H, CH_2 $CH(CH_3)_2$); 1.03 (d, 6 Hz, 6H, $CH_2CH(CH_3)_2$). ^{13}C NMR (benzene-d_6): δ = 12.49, 13.14, 13.72, 14.22 (C_5Me_4H); 75.33 ($CH_2CH(CH_3)_2$); 31.17 ($CH_2CH(CH_3)_2$); 30.21 ($CH_2CH(CH_3)_2$); 108.37, 116.98, 117.45, 121.25, 121.76 (Cp).

(η^5-C_5Me_5)(η^5-C_5Me_4H)$Zr(CH_2CH_2C_6H_5)(H)$ (44). ^{1}H NMR (benzene-d_6): δ = 1.85 (s, 15H, C_5Me_5); 1.81, 1.84 (s, 6H, C_5Me_4H); 5.28 (bs, 1H, Zr*H*); -0.131 (m, 1H, CH_2 CH_2Ph); 0.470 (m, 1H, CH_2 CH_2Ph); *not located* (CH_2 CH_2Ph); 7.10 (m, 1H, *para*-$CH_2CH_2C_6H_5$); 7.24 (m, 2H, *meta*-$CH_2CH_2C_6H_5$); 7.42 (m, 2H, *ortho*-$CH_2CH_2C_6H_5$); 4.48 (Cp). ^{13}C NMR (benzene-d_6): δ = 12.56 (C_5Me_5); 116.59 (C_5Me_5); 11.67, 12.19, 13.33, 14.71 (C_5Me_4H); 47.14 (CH_2CH_2Ph); 22.68 (CH_2CH_2Ph); 96.10, 105.77, 119.62, 2 *not located* (Cp); 122.42 (*para*-C_6H_5); 125.86 (*ortho*-C_6H_5); 129.40 (*meta*-C_6H_5); *1 not located* (*ipso*-C_6H_5).

(η^5-C_5Me_5)(η^5-C_5Me_4H)$Zr(CH_2CH_2(C_6H_4$-*p*-$OCH_3))(H)$ (45). ^{1}H NMR (benzene-d_6): δ = 1.86 (s, 15H, C_5Me_5); 1.71, 1.77, 2.06, 2.10 (s, 6H, C_5Me_4H); 5.06 (s, 1H, Zr*H*); 0.51 (m, 2H, $CH_2CH_2C_6H_5$-*p*-OCH_3); 1.52 (m, 2H, $CH_2CH_2C_6H_5$-*p*-OCH_3); 3.24 (s, 3H, $CH_2CH_2C_6H_5$-*p*-OCH_3); 6.88 (d, 8.6 Hz, 2H, CH_2CH_2-*meta*-C_6H_5-*p*-OCH_3); 7.36 (d, 8.6 Hz, 2H, CH_2CH_2-*ortho*-C_6H_5-*p*-OCH_3), 4.49 (Cp). ^{13}C NMR (benzene-d_6): δ = 12.56 (C_5Me_5); 114.32 (C_5Me_5); 11.62, 12.23, 13.26, 14.78 (C_5Me_4H); 55.14 ($CH_2CH_2(C_6H_4$-*p*-$OCH_3)$); 20.35 ($CH_2CH_2(C_6H_4$-*p*-$OCH_3)$); 45.25 (C_6H_4-OCH_3); 105.56, 113.05, 116.18, 116.72, 117.09 (Cp); 122.01 (*ortho*-C_6H_4-*p*-OCH_3); 127.45 (*para*-C_6H_4-*p*-OCH_3); 130.32 (*meta*-C_6H_4-*p*-OCH_3); 159.16 (*ipso*-C_6H_4-*p*-OCH_3).

(η^5-C_5Me_5)(η^5-C_5Me_4H)$Zr(CH_2CH_2(C_6H_4$-*p*-$CH_3))(H)$ (46). ^{1}H NMR (benzene-d_6): δ = 1.86 (s, 15H, C_5Me_5); 1.69, 1.79, 2.04, 2.11 (s, 6H, C_5Me_4H); 5.62 (bs, 1H, Zr*H*); 0.510 (m, 2H, $CH_2CH_2C_6H_5$-*p*-CH_3); 1.57 (m, 2H, $CH_2CH_2C_6H_5$-*p*-CH_3); 6.94 (d, 8.6 Hz, 2H, CH_2CH_2-*meta*-C_6H_5-*p*-CH_3); 7.37 (d, 8.6 Hz, 2H, CH_2CH_2-*ortho*-C_6H_5-*p*-CH_3), 4.48 (Cp). ^{13}C NMR (benzene-d_6): δ = 12.57 (C_5Me_5); 116.27

(C_5Me_5); 11.66, 12.19, 13.30, 14.76 (C_5Me_4H); 58.03 ($CH_2CH_2(C_6H_4$-*p*-$OCH_3)$); 29.21 ($CH_2CH_2(C_6H_4$-*p*-$OCH_3)$); 38.06 (C_6H_4-CH_3); 113.04, 116.57, 116.84, 117.29, 117.82 (Cp); 122.28 (*ortho*-C_6H_4-*p*-CH_3); 137.97 (*para*-C_6H_4-*p*-CH_3); 143.97 (*meta*-C_6H_4-*p*-OCH_3); 159.03x (*ipso*-C_6H_4-*p*-CH_3).

(η^5-C_5Me_5)(η^5-C_5Me_4H)Zr($CH_2CH_2(C_6H_4$-*p*-CF_3))(H) (47). ^{1}H NMR (benzene-d_6): δ = 1.84 (s, 15H, C_5Me_5); 1.63, 1.77, 1.95, 2.16 (s, 6H, C_5Me_4H); 4.82 (s, 1H, Zr*H*); -0.237 (m, 1H, $CH_2CH_2C_6H_5$-*p*-CF_3); 0.334 (m, 1H, $CH_2CH_2C_6H_5$-*p*-CF_3); 1.51 (m, 2H, $CH_2CH_2C_6H_5$-*p*-CF_3); 7.19 (d, 8.6 Hz, 2H, CH_2CH_2-*meta*-C_6H_5-*p*-CF_3); 7.48 (d, 8.6 Hz, 2H, CH_2CH_2-*ortho*-C_6H_5-*p*-CF_3), 4.48 (Cp). ^{13}C NMR (benzene-d_6): δ = 12.50 (C_5Me_5); 116.16 (C_5Me_5); 11.71, 12.06, 13.45, 14.54 (C_5Me_4H); 49.30 ($CH_2CH_2C_6H_4$-*p*-CF_3); 25.23 ($CH_2CH_2C_6H_4$-*p*-CF_3); 32.84 (q, 28 Hz, ($CH_2CH_2C_6H_4$-*p*-CF_3); 106.29, 114.88, 115.87, 117.32, 119.43 (Cp); 125.67, 125.96, 141.44, *3 not located* ($CH_2CH_2C_6H_4$-*p*-CF_3). ^{19}F NMR (benzene-d_6): δ = -62.19 ppm (CF_3).

(η^5-C_5Me_5)(η^5-C_5H_4-CMe_3)Zr($CH_2CH_2C(CH_3)_3$)(H) (48). ^{1}H NMR (benzene-d_6): δ = 1.89 (s, 15H, C_5Me_5); 1.47 (s, 9H, C_5H_4-CMe_3); *not located* (s, 1H, Zr*H*); -0.99 (m, 1H, $CH_2CH_2CMe_3$); 0.30 (m, 1H, $CH_2CH_2CMe_3$); 2.32 (m, 2H, $CH_2CH_2CMe_3$); 1.04 (s, 9H, $CH_2CH_2CMe_3$); 4.91 (m, 2H, Cp); 5.00 (m, 1H, Cp); 5.90 (m, 2H, Cp). ^{13}C NMR (benzene-d_6): δ = 12.58 (C_5Me_5); 116.34 (C_5Me_5); 32.84 (CMe_3); 29.90 (CMe_3); 146.06 (CMe_3); 1 *not located* (CMe_3); 49.98 ($CH_2CH_2CMe_3$); 35.94 ($CH_2CH_2CMe_3$); 102.68, 104.01, 107.25, 109.89, 120.76 (Cp).

(η^5-C_5Me_5)(η^5-C_5H_4-CMe_3)Zr($CH_2CH_2CH_2CH(CH_3)_2$)(H) (49). ^{1}H NMR (benzene-d_6): δ = 1.83 (s, 15H, C_5Me_5); 1.41 (s, 9H, C_5H_4-CMe_3); 5.39 (s, 1H, Zr*H*); -0.450 (m, 1H, $CH_2CH_2CH_2CH(CH_3)_2$); -0.450 (m, 1H, $CH_2CH_2CH_2CH(CH_3)_2$); 0.651 (m, 2H, $CH_2CH_2CH_2CH(CH_3)_2$); 0.589 (m, 2H, $CH_2CH_2CH_2CH(CH_3)_2$); 2.56 (m, 1H, $CH_2CH_2CH_2CH(CH_3)_2$); 0.999 (d, 6Hz, 6H, $CH_2CH_2CH_2CH(CH_3)_2$); 4.22, 4.91, 5.34, 5.98 (m, 1H, Cp). ^{13}C NMR (benzene-d_6): δ = 12.46 (C_5Me_5); 112.77 (C_5Me_5); 32.09 (CMe_3); 139.36 (CMe_3); 56.14 ($CH_2(CH_2)_2CH(CH_3)_2$); 18.39, 22.29 ($CH_2(CH_2)_2CH(CH_3)_2$) 32.78 ($CH_2(CH_2)_2CH(CH_3)_2$); 23.45 ($CH_2(CH_2)_2CH(CH_3)_2$; 103.56, 105.92, 109.53, 115.77, 118.64 (Cp).

(η^5-C_5Me_5)(η^5-C_5H_4-CMe_3)Zr($CH_2CH_2CH_2CH_3$)(H) (50). ^{1}H NMR (benzene-d_6): δ = 1.82 (s, 15H, C_5Me_5); 1.40 (s, 9H, CMe_3); 5.94 (s, 1H, Zr*H*); -0.504 (dd, 1H, $CH_2CH_2CH_2CH_3$); -0.02 (dd, 1H, $CH_2CH_2CH_2CH_3$); 1.26 (m, 2H, $CH_2CH_2CH_2CH_3$); 0.650 (m, 2H, $CH_2CH_2CH_2CH_3$); 1.06 (t, 7Hz, 3H, $CH_2CH_2CH_2CH_3$); 4.23, 4.88, 4.91, 5.33 (Cp). ^{1}H NMR (benzene-d_6): δ = 12.35 (C_5Me_5); 115.38 (C_5Me_5); 32.49 (CMe_3); 156.10 (CMe_3); 46.58 ($CH_2CH_2CH_2CH_3$); 29.56 ($CH_2CH_2CH_2CH_3$); 18.66 ($CH_2CH_2CH_2CH_3$); 12.71 ($CH_2CH_2CH_2CH_3$); 101.09, 103.48, 104.00, 105.83, 109.43 (Cp).

(η^5-C_5Me_5)(η^5-C_5H_4-CMe_3)Zr(*cyclo*-C_5H_9)(H) (51). ^{1}H NMR (benzene-d_6): δ = 1.76 (s, 15H, C_5Me_5); 1.40 (s, 9H, C_5H_4-CMe_3); 5.71 (s, 1H, Zr*H*); -0.512, 0.105, 1.13, 1.93, 2.31 (m, C_5H_9); 4.73, 4.89, 4.96, 5.83 (m, 1H, Cp). ^{13}C NMR (benzene-d_6): δ = 12.42 (C_5Me_5); 114.16 (C_5Me_5); 32.89 (CMe_3); 146.33 (CMe_3); 47.65 (*ipso*-C_5H_9); 23.51, 29.23, 34.10, 37.53 (C_5H_9); 99.90, 103.00, 104.41, 109.96, 125.51 (Cp).

(η^5-C_5Me_5)(η^5-C_5H_5)Zr($C(CH_3)$=C(H)(CMe_3))(H) (52). ^{1}H NMR (benzene-d_6): δ = 1.81 (s, 15H, C_5Me_5); 3.51 (s, 1H, Zr*H*); 1.10 (s, 9H, $C(CH_3)$=C(H)(CMe_3)); 2.45 (s, 3H, $C(CH_3)$=C(H)(CMe_3); 3.45 (s, 1H, $C(CH_3)$=C(*H*)(CMe_3); 5.48 (Cp). ^{13}C NMR (benzene-d_6): δ = 12.57 (C_5Me_5); 114.39 (C_5Me_5); 30.77 ($C(CH_3)$=C(CMe_3)(H)); *not located* ($C(CH_3)$=C(*C*Me_3)(H)); 3.68 ($C(CH_3)$=C(CMe_3)(H)); 186.82 ($C(CH_3)$=C(CMe_3)(H)); 95.71 (Cp).

(η^5-C_5Me_5)(η^5-C_5H_4-CMe_3)Zr($C(CH_3)$=C(H)(CMe_3))(H) (53). ^{1}H NMR (benzene-d_6): δ = 1.81 (s, 15H, C_5Me_5); 1.41 (s, 9H, C_5H_4-CMe_3); 3.54 (s, 1H, Zr*H*); 1.14 (s, 9H, $C(CH_3)$=C(H)(CMe_3)); 2.49 (s, 3H, $C(CH_3)$=C(H)(CMe_3); 3.48 (s, 1H, $C(CH_3)$=C(*H*)(CMe_3); 4.52, 5.00, 5.08, 5.81 (Cp). ^{13}C NMR (benzene-d_6): δ = 12.42 (C_5Me_5); 114.17 (C_5Me_5); 33.32 (CMe_3); 32.81 (CMe_3); 150.46 (CMe_3); 150.59 (CMe_3); 12.68 ($C(CH_3)$=C(CMe_3)(H)); 190.23 ($C(CH_3)$=C(CMe_3)(H)); 20.52 ($C(CH_3)$=C(CMe_3)(H)); 95.65, 95.94, 98.55, 99.07, 104.03 (Cp).

(η^5-C_5Me_5)(THI)Zr($C(CH_3)$=C(H)(CMe_3))(H) (54). ^{1}H NMR (benzene-d_6): δ = 1.84 (s, 15H, C_5Me_5); 0.80-1.10 (m, THI); 3.84 (s, 1H, Zr*H*); 1.24 (s, 9H, $C(CH_3)$=C(H)(CMe_3)); 2.49 (s, 3H, $C(CH_3)$=C(H)(CMe_3); 3.70 (s, 1H, $C(CH_3)$=C(*H*)(CMe_3); 4.98, 5.08, 5.55 (Cp). ^{13}C NMR (benzene-d_6): δ = 12.60 (C_5Me_5); 114.31 (C_5Me_5); 31.90 (CMe_3); 159.11 (CMe_3); 3.77 ($C(CH_3)$=C(CMe_3)(H)); 187.12 ($C(CH_3)$=C(CMe_3)(H)); 20.17

($C(CH_3)$=$C(CMe_3)$(H)); 23.94, 24.58, 24.70, 26.86 (THI); 92.75, 100.32, 100.84, 101.83, 106.21 (Cp).

(η^5-C_5Me_5)(η^5-C_5H_3-1,3-($CHMe_2$)$_2$)Zr($C(CH_3)$=C(H)(CMe_3))(H) (55). ^{1}H NMR (benzene-d_6): δ = 1.85 (s, 15H, C_5Me_5); 3.68 (s, 1H, Zr*H*); 1.06 (d, 7 Hz. 3H, $CHMe_2$); 1.28 (d, 7 Hz. 3H, $CHMe_2$); 1.34 (d, 7 Hz. 3H, $CHMe_2$); 1.41 (d, 7 Hz. 3H, $CHMe_2$); 2.75 (sept, 6.5 Hz, 1H, $CHMe_2$); 3.20 (sept, 6.5 Hz, 1H, $CHMe_2$); 1.18 (s, 9H, $C(CH_3)$=C(H)(CMe_3)); 2.48 (s, 3H, $C(CH_3)$=C(H)(CMe_3); 86.25 ($C(CH_3)$=$C(CMe_3)$(H)); 3.34 (s, 1H, $C(CH_3)$=C(*H*)(CMe_3); 4.65, 4.74, 4.98 (m, 1H, C_5H_3-1,3-(CMe_3)$_2$). ^{13}C NMR (benzene-d_6): δ = 12.95 (C_5Me_5); 117.29 (C_5Me_5); 25.21, 25.48, 27.05, 27.26 ($CHMe_2$); 30.22, 21.14 ($CHMe_2$); 30.97 (CMe_3); 139.72 (CMe_3); 3.73 ($C(CH_3)$=C(CMe_3)(H)); *not located* ($C(CH_3)$=$C(CMe_3)$(H)); 21.90 ($C(CH_3)$=$C(CMe_3)$(H)) 88.37, 99.72, 99.42, 104.73, 114.49 (Cp).

(η^5-C_5Me_5)(η^5-C_5H_3-1,3-(CMe_3)$_2$)Zr($C(CH_3)$=C(H)(CMe_3))(H) (56). ^{1}H NMR (benzene-d_6): δ = 1.85 (s, 15H, C_5Me_5); 3.56 (s, 1H, Zr*H*); 1.17 (s, 9H, C_5H_5-1,3-(CMe_3)$_2$)); 1.55 (s, 9H, C_5H_5-1,3-(CMe_3)$_2$); 1.22 (s, 9H, $C(CH_3)$=C(H)(CMe_3)); 2.55 (s, 3H, $C(CH_3)$=C(H)(CMe_3); 3.34 (s, 1H, $C(CH_3)$=C(*H*)(CMe_3); 4.49, 4.68, 4.95 (m, 1H, C_5H_3-1,3-(CMe_3)$_2$). ^{13}C NMR (benzene-d_6): δ = 13.06 (C_5Me_5); 119.88 (C_5Me_5); 32.88 (CMe_3); 32.20 (CMe_3); 114.16 (CMe_3); 117.44 (CMe_3); 31.88 (CMe_3); 136.18 (CMe_3); 3.83 ($C(CH_3)$=C(CMe_3)(H)); 167.31 ($C(CH_3)$=$C(CMe_3)$(H)); 28.04 ($C(CH_3)$=$C(CMe_3)$(H)); 100.99, 105.46, 109.02, *2 not located* (Cp).

(η^5-C_5Me_5)(η^5-C_5Me_4H)Zr($C(CH_3)$=C(H)(CMe_3))(H) (57). ^{1}H NMR (benzene-d_6): δ = 1.85 (s, 15H, C_5Me_5); 1.86, 1.88, 1.91, 2.01 (s, 3H, C_5Me_4 H); 4.47 (s, 1H, Zr*H*); 4.47 (s, 1H, C_5Me_4 *H*); 1.21 (s, 9H, $C(CH_3)$=C(H)(CMe_3)); 2.46 (s, 3H, $C(CH_3)$=C(H)(CMe_3); 3.53 (s, 1H, $C(CH_3)$=C(*H*)(CMe_3). ^{13}C NMR (benzene-d_6): δ = 12.71 (C_5Me_5); 114.47 (C_5Me_5); 11.83, 12.41, 12.89, 13.32 (C_5Me_4H); 31.66 (CMe_3); 150.89 (CMe_3); 15.45 ($C(CH_3)$=C(CMe_3)(H)); 162.71 ($C(CH_3)$=$C(CMe_3)$(H)); 18.41 ($C(CH_3)$=$C(CMe_3)$(H)); 98.57, 102.25, 105.49, 122.54, *1 not located* (Cp).

(η^5-C_5Me_4H)$_2$Zr($C(CH_3)$=C(H)(CMe_3))(H) (58). ^{1}H NMR (benzene-d_6): δ = 2.12, 2.21 (s, 6H, C_5Me_4H); 5.15 (s, 2H, C_5Me_4H); 3.73 (s, 1H, Zr*H*); 1.24 (s, 9H, $C(CH_3)$=C(H)(CMe_3)); 2.46 (s, 3H, $C(CH_3)$=C(H)(CMe_3); 3.35 (s, 1H, $C(CH_3)$=C(*H*)(CMe_3). ^{13}C NMR (benzene-d_6): δ = 12.11, 12.84, 13.96, 13.54

(C_5Me_4H); 88.33 (Zr-C(CH_3)=*C*(H)(CMe_3)); 187.30 (Zr-*C*(CH_3)=C(H)(CMe_3)); 31.56 (Zr-C(CH_3)=C(H)(*C*Me_3)); 143.72 (Zr-C(CH_3)=C(H)(*C*Me_3)); 18.64 (Zr-C(*C*H_3)=C(H)(CMe_3)); 98.95, 111.28, 114.82, 116.97, 120.26 (Cp).

(η^5-C_5Me_5)(η^5-C_5H_5)Zr($CH_2CH_2CH_2CH_3$)(H) (59). ^{1}H NMR (benzene-d_6): δ = 1.73 (s, 15H, C_5Me_5); 6.21 (s, 1H, Zr*H*); -0.09 (dd, 1H, C*H*$_2$ $CH_2CH_2CH_3$); 0.577 (dd, 1H, C*H*$_2$ $CH_2CH_2CH_3$); 1.92 (m, 2H, CH_2 C*H*$_2$$CH_2CH_3$); 0.88 (m, 2H, CH_2 CH_2C*H*$_2$$CH_3$); 1.05 (t, 7.3 Hz, 3H, CH_2 CH_2CH_2C*H*$_3$), 5.91 (s, 5H Cp). ^{13}C NMR (benzene-d_6): δ = 12.65 (C_5Me_5); 116.81 (*C*$_5$Me$_5$); 56.71 ($CH_2CH_2CH_2CH_3$); 31.50 ($CH_2CH_2CH_2CH_3$); 24.95 ($CH_2CH_2CH_2CH_3$); 14.33 (*C*$H_2CH_2CH_2CH_3$); 107.16 (Cp).

(η^5-C_5Me_5)(η^5-C_5H_3-1,3-($CHMe_2$)$_2$)Zr($CH_2CH_2CH_2CH_3$)(H) (60). ^{1}H NMR (benzene-d_6): δ = 1.84 (s, 15H, C_5Me_5); 5.38 (s, 1H, Zr*H*); 1.19, 1.24, 1.42, 1.50 (d, 7Hz, 3H, CH*Me*$_2$); 2.78, 3.20 (sept, 6.5Hz, 1H, C*H*Me$_2$); -0.401 (m, 2H, C*H*$_2$ $CH_2CH_2CH_3$); *not located* (CH_2 C*H*$_2$$CH_2CH_3$); 1.06 (m, 2H, CH_2 CH_2C*H*$_2$$CH_3$); 0.870 (t, 7.3 Hz, 3H, CH_2 CH_2CH_2C*H*$_3$); 3.95, 4.88, 5.01 (m, 1H, Cp).

(η^5-C_5Me_5)(THI)Zr($CH_2CH_2CH_2CH_3$)(H) (61). ^{1}H NMR (benzene-d_6): δ = 1.86 (s, 15H, C_5Me_5); 5.95 (s, 1H, Zr*H*); -0.501 (m, 2H, C*H*$_2$ $CH_2CH_2CH_3$); 1.40 (m, 2H, CH_2 C*H*$_2$$CH_2CH_3$); 0.82 (m, 2H, CH_2CH_2C*H*$_2$$CH_3$); 1.10 (t, 7.0 Hz, 3H, CH_2 CH_2CH_2C*H*$_3$), 4.75, 5.02, 5.20 (m, 1H, Cp). ^{13}C NMR (benzene-d_6): δ = 12.15 (C_5Me_5); 117.92 (*C*$_5$Me$_5$); 23.84, 25.01, 25.25, 25.93 (THI); 53.40 ($CH_2CH_2CH_2CH_3$); 47.52 ($CH_2CH_2CH_2CH_3$); 31.73 ($CH_2CH_2CH_2CH_3$); 14.32 (*C*$H_2CH_2CH_2CH_3$); 107.65, 110.40, 111.60, 125.13, 125.76 (Cp).

(η^5-C_5Me_5)(η^5-C_5Me_4H)Zr($CH_2CH_2CH_2CH_3$)(H) (62). ^{1}H NMR (benzene-d_6): δ = 1.88 (s, 15H, C_5Me_5); 1.71, 1.81, 1.91, 2.08 (s, 3H, C_5Me_4 H); 4.47 (s, 1H, C_5Me_4H); 4.76 (s, 1H, Zr*H*); 0.057 (dd, 1H, C*H*$_2$ $CH_2CH_2CH_3$); 0.161 (dd, 1H, C*H*$_2$ $CH_2CH_2CH_3$); *not located* (CH_2C*H*$_2$$CH_2CH_3$); 1.43 (m, 2H, CH_2 CH_2C*H*$_2$$CH_3$); 1.08 (t, 6.5 Hz, 3H, $CH_2CH_2CH_2$C*H*$_3$). ^{13}C NMR (benzene-d_6): δ = 12.60 (C_5Me_5); 115.71 (*C*$_5$Me$_5$); 11.67; 12.18; 12.30; 13.12 (C_5Me_4 H); 43.66 (*C*$H_2CH_2CH_2CH_3$); 27.86 ($CH_2CH_2CH_2CH_3$); 16.09 ($CH_2CH_2CH_2CH_3$); 15.06 (*C*$H_2CH_2CH_2CH_3$); 105.44; 115.56; 116.47; 116.89; 117.52 (Cp).

(η^5-C_5Me_5)(η^5-C_5H_3-1,3-(CMe_3)$_2$)Zr($CH_2CH_2CH_2CH_3$)(H) (63). ^{1}H NMR (benzene-d_6): δ = 1.72 (s, 15H, C_5Me_5); 1.10, 1.31 (s, 9H, CMe_3); 5.51 (s, 1H, Zr*H*); 0.14 (m, 2H, CH_2 $CH_2CH_2CH_3$); 0.652 (m, 2H, $CH_2CH_2CH_2CH_3$); 0.753 (m, 2H, $CH_2CH_2CH_2CH_3$); 943 (t, 7Hz, 3H, $CH_2CH_2CH_2CH_3$); 4.43, 4.60, 4.65 (m, 1H, Cp). ^{13}C NMR (benzene-d_6): δ = 13.06 (C_5Me_5); 113.86 (C_5Me_5); 32.86 (CMe_3); 35.00 (CMe_3); 142.62 (CMe_3); 140.92 (CMe_3); 42.13 ($CH_2CH_2CH_2CH_3$); 31.31 ($CH_2CH_2CH_2CH_3$); 27.38 ($CH_2CH_2CH_2CH_3$); 13.61 ($CH_2CH_2CH_2CH_3$); 100.99; 105.52; 109.05; 110.16; 111.99 (Cp).

References.

1. Crabtree, R.H. *The Organometallic Chemistry of the Transition Metals*, 2nd Ed; Wiley, New York, 1994; Chapters 7, 9.

2. Brintzinger, H.H.; Fischer, D.; Mülhaupt, R.; Rieger, B.; Waymouth, R.M. *Angew. Chem. Int. Ed. Engl.* **1995**, *34*, 1143.

3. a) Gilchrist, J.H.; Bercaw, J.E. *J. Am. Chem. Soc.* **1996**, *118*, 12021. b) Herzog, T.A.; Zubris, D.L.; Bercaw, J.E. *J. Am. Chem. Soc.* **1996**, *118*, 11988 and references therein.

4. Resconi, L.; Camurati, I.; Sudmeijer, O. *Topics In Catalysis* **1999**, *7*, 145.

5. a) Jordan, R.F.; Dasher, W.E.; Echols, S.F. *J. Am. Chem. Soc.* **1986**, *108*, 1718. b) Jordan, R.F.; Bajgur, C.S.; Willet, R.; Scott, B. *J. Am. Chem. Soc.* **1986**, *108*, 7410.

6. Watson, P.L. *J. Am. Chem. Soc.* **1982**, *104*, 337.

7. Jeske, G.; Lauke, H.; Mauerman, H.; Swepston, P.N.; Shuman, H.; Marks, T.J. *J. Am. Chem. Soc.* **1985**, *107*, 8091.

8. a) Doherty, N.M.; Bercaw, J.E. *J. Am. Chem. Soc.* **1985**, *107*, 2670. b) Burger, B.J.; Santarsiero, B.D.; Trimmer, M.S.; Bercaw, J.E. *J. Am. Chem. Soc.* **1988**, *110*, 3134.

9. Burger, B.J.; Thompson, M.E.; Cotter, W.D.; Bercaw, J.E. *J. Am. Chem. Soc.* **1990**, *112*, 1566.

10. Karl J.; Dahlmann M.; Erker G.; Bergander K. *J. Am. Chem. Soc.* **1998**, *120*, 5643.

11. Siedle, A.R.; Lamanna, W.M.; Newmark, R.A.; Schroepfer, J.N. *J. Mol. Cat. A* **1998**, *128*, 257.

12. a) Woo, T.K.; Margl, P.M.; Lohrenz, J.C.W.; Blöchl, P.E.; Ziegler, T. *J. Am. Chem. Soc.* **1996**, *118*, 13021. b) Richardson, D.E.; Alameddin, N.G.; Ryan, M.F.; Hayes, T.; Eyler, J.R.; Siedle, A.R. *J. Am. Chem. Soc.* **1996** *118*, 11244. c) Froese,

R.D.J.; Musaev, D.G.; Matsubara, T.; Morokuma, K.J. *Organometallics* **1997**, *16*, 2514 and references cited therein.

13. a) Toto, M.; Cavallo, L.; Corradini, P.; Moscardi, G.; Resconi, L.; Guerra, G. *Macromolecules* **1998**, *31*, 3431.

14. Chirik, P.J.; Day, M.W.; Bercaw, J.E. *Organometallics* **1999**, *18*, 1873.

15. Addition of one equivalent of ethylene to $[(CpR_n)_2ZrH_2]_2$ results in clean formation of $(CpR_n)_2Zr(CH_2CH_3)(H)$. However, addition of excess ethylene results in reductive elimination of ethane and formation of the zirconocyclopentane. McAlister, D.R.; Erwin, D.R.; Bercaw, J.E. *J. Am. Chem. Soc.* **1978**, *100*, 5966.

16. Chirik, P.J.; Day, M.W.; Labinger, J.A.; Bercaw, J.E. *J. Am. Chem. Soc.* **1999**, *121*, 10308.

17. Lin, Z.; Marks, T.J. *J. Am. Chem. Soc.* **1990**, *112*, 5515.

18. Values for σ and σ^+ were taken from Isaacs, N.S. *Physical Organic Chemistry*, John Wiley and Sons: New York, 1986, p. 131.

19. Roddick, D.M.; Fryzuk, M.D.; Seidler, P.F.; Hillhouse, G.L.; Bercaw, J.E. *Organometallics* **1985**, *4*, 97.

20. McDade, C.; Bercaw, J.E. *J. Organomet. Chem.* **1985**, *279*, 281.

21. Brandow, C.G.; Bercaw, J.E. *unpublished results*.

22. Bercaw, J.E. in *Transition Metal Hydrides*, Advances in Chemistry Series, Chapter 10.

23. Manriquez, J.M.; McAlister, D.R.; Sanner, R.D.; Bercaw, J.E. *J. Am. Chem. Soc.* **1978**, *100*, 2716.

24. Stehling, U.; Diebold, K. R.; Roll, W.; Brintzinger, H.H.; Jungling, S.; Mülhaupt, R.; Langhauser, F. *Organometallics* **1994**, *13*, 964.

25. Labinger, J.A. In *Comprehensive Organic Synthesis*; Trost, B.M.; Fleming, I., Eds.; Pergamon Press: Oxford, 1991; Chapter 3.9.

26. Busico, V.; Cippullo, R. *J. Am. Chem. Soc.* **1994**, *116*, 9329.

27. Busico, V.; Caporaso, L.; Cippulo, R.; Landriani, L.; Angelini, G.; Margonelli, A.; Segre, A.L. *J. Am. Chem. Soc.* **1996**, *118*, 2105.

28. Nelson, J.E.; Bercaw, J.E.; Labinger, J.A. *Organometallics* **1989**, *8*, 2404 and references therein.

29. Resconi, L.; Piemontesi, F.; Franciscono, G.; Abis, L.; Fiorani, T. *J. Am. Chem. Soc.* **1992**, *114*, 1025.

30. Veghini, D.; Henling, L.M.; Burkhardt, T.J.; Bercaw, J.E. *J. Am. Chem. Soc.* **1999**, *121*, 564.

31. Benson, S.W. *Thermochemical Kinetics* 2nd Ed.; Wiley and Sons, New York, 1976.

32. a) Bryndza, H.E.; Fong, L.K.; Paciello, R.A.; Tam, W.; Bercaw, J.E. *J. Am. Chem. Soc.* **1987**, *109*, 1444. b) Labinger, J.A.; Bercaw, J.E. *Organometallics* **1988**, *7*, 926.

33. Although a correlation exists between M-C and C-H bond strengths, it is not absolute, and as a result values may exceed the differences in alkane free energies.

34. Straus, D.A.; Grubbs, R.H. *Organometallics* **1982**, *1*, 1658.

35. Schaller, C.P.; Cummins, C.C.; Wolczanski, P.T. *J. Am. Chem. Soc.* **1996**, *118*, 591.

36. Burger, B.J.; Bercaw, J.E. In *Experimental Organometallic Chemistry*; ACS Symposium Series No. 357; Wayda, A.L.; Darensbourg, M.Y. Eds.; American Chemical Society: Washington, DC 1987; Chapter 4.

37. Marvich, R.H.; Brintzinger, H.H. *J. Am. Chem. Soc.* **1971**, *93*, 2046.

38. Schock, L.E.; Marks, T.J. *J. Am. Chem. Soc.* **1988**, *110*, 7701.

39. Vogel, A.I. *Vogel's Textbook of Practical Organic Chemistry* 5th Ed.; John Wiley and Sons, New York, 1989 pp. 495-498.

Chapter 4

Alkyl Rearrangement Processes in Organozirconium Complexes. Observation of Internal Alkyl Complexes during Hydrozirconation.*

Abstract

Isotopically labeled alkyl zirconocene complexes of the general formula, $(CpR_n)_2Zr(CH_2CDR'_2)(X)$ (CpR_n = alkyl-substituted cyclopentadienyl; R' = H, alkyl group; X = H, D, Me), undergo isomerization of the alkyl ligand as well as exchange with free olefin in solution under ambient conditions. Increasing the substitution on the Cp ring results in slower isomerization reactions, but these steric effects are small. In contrast, changing X has a very large effect on the rate of isomerization. Pure σ-bonding ligands such as methyl and hydride promote rapid isomerization, whereas π-donor ligands inhibit β-H elimination and hence alkyl isomerization. For $(\eta^5\text{-}C_5H_5)_2Zr(R)(Cl)$, internal alkyl complexes have been observed for the first time. The rate of isomerization depends on the length of the alkyl: longer alkyl chains (heptyl, hexyl) isomerize faster than shorter chains (butyl). The transient intermediate species have been identified by a combination of isotopic labeling and ^1H, ^2H and ^{13}C NMR experiments. The solid state structure of the zirconocene cyclopentyl-chloride complex, $Cp_2Zr(\textit{cyclo}\text{-}C_5H_9)(Cl)$, has been determined by X-ray diffraction.

Introduction

Alkyl complexes play a central role in organotransition metal chemistry in both catalytic and stoichiometric transformations.[1] The preferences (kinetic and/or thermodynamic) of a transition metal to bond to a terminal or a internal carbon atom of an alkyl ligand often determine the selectivity and productivity of a system. However, delineation of the factors that govern these preferences is by no means straightforward. The identity of the transition metal, coordination environment and ancillary ligation all influence the relative stabilities for terminal versus internal alkyl complexes.[2]

Alkyl isomerization has special relevance, both historical and practical, in group 4 metallocene chemistry. The original studies by Schwartz and coworkers[3] reported the hydrozirconation of internal olefins with $[Cp_2Zr(H)(Cl)]_n$ as yielding solely terminal products. This hydrometallation-isomerization protocol allows for functionalization of otherwise unactivated methyl groups and has found widespread synthetic utility.[4]

More recently, alkyl isomerization reactions have been found to influence the stereo- and regiochemical outcome of group 4 metallocene-catalyzed olefin polymerizations.[5] The degree of isotacticity of the polypropylene produced from a variety of C_2-symmetric zirconocene catalysts has been shown to decrease with decreasing monomer concentration.[6] The explanation for this behavior is an alkyl isomerization process that competes with olefin insertion at low monomer concentrations. Isomerization of a "2,1"-inserted monomer unit producing a "3,1"-regiomistake has also been identified (eq. 1).[7] Despite efforts to suppress both of these pathways, the origins of alkyl isomerization and the identity of the mechanisms and their rate limiting steps have remained elusive.

$$M\text{—}P \xrightarrow{CH_3CH=CH_2} \underset{\text{"2,1" misinsertion}}{M\text{—}\overset{\overset{CH_3}{|}}{C}HCH_2P} \longrightarrow \underset{\text{"3,1" misinsertion}}{M\text{—}CH_2CH_2CH_2P} \qquad (1)$$

In this report we describe direct observation of the alkyl isomerization process in several neutral zirconocene complexes of the form $(CpR_n)_2Zr(CH_2CHR'_2)(X)$ (X = H, Me, Cl; CpR_n = alkyl substituted η^5-cyclopentadienyl; R' = H or alkyl). Factors that affect the facility of the isomerization process are disclosed. Additionally, evidence for involvement of free olefin in the mechanism of alkyl isomerization is presented.

Results

Rearrangement of Labeled Alkyls Obtained from Hydrozirconation of Terminal Olefins.

Zirconocene alkyl-hydride complexes are prepared via addition of the appropriate olefin to the zirconocene dihydride.[8,9] This synthetic protocol allows facile incorporation of isotopic labels into the zirconocene alkyl-hydride complex (eq. 2).

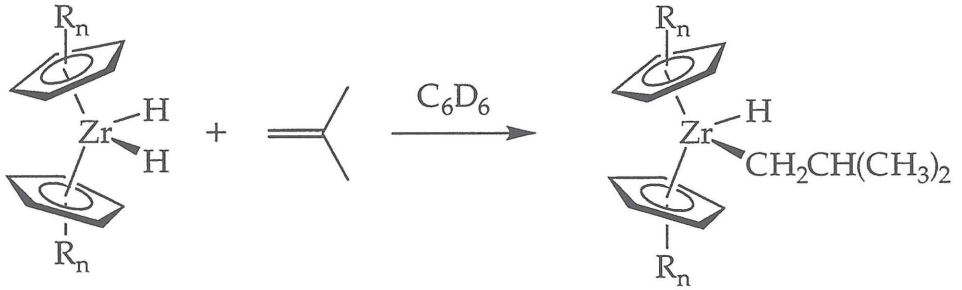

(2)

$CpR_n = (\eta^5\text{-}C_5Me_5)$, Cp* (**1**)

$CpR_n = (\eta^5\text{-}C_5Me_4H)$ (**2**)

Thus, reaction of substituted zirconocene dideuterides, $(CpR_n)_2ZrD_2$ (CpR_n = (η^5-C_5Me_5) (Cp*), (η^5-C_5Me_4H)) with isobutylene in benzene solution affords specifically labeled complexes, $(CpR_n)_2Zr(CH_2CDMe_2)(D)$ in quantitative yield (^{1}H NMR). In benzene solution $Cp^*_2Zr(CH_2CDMe_2)(D)$ undergoes isotopic rearrangement affording both $Cp^*_2Zr(CHDCHMe_2)(D)$ and $Cp^*_2Zr\{CH_2CH(CH_2D)(CH_3)\}(D)$ (eq. 3).[10] $(\eta^5\text{-}C_5Me_4H)_2Zr(CH_2CDMe_2)(D)$ exhibits similar behavior.

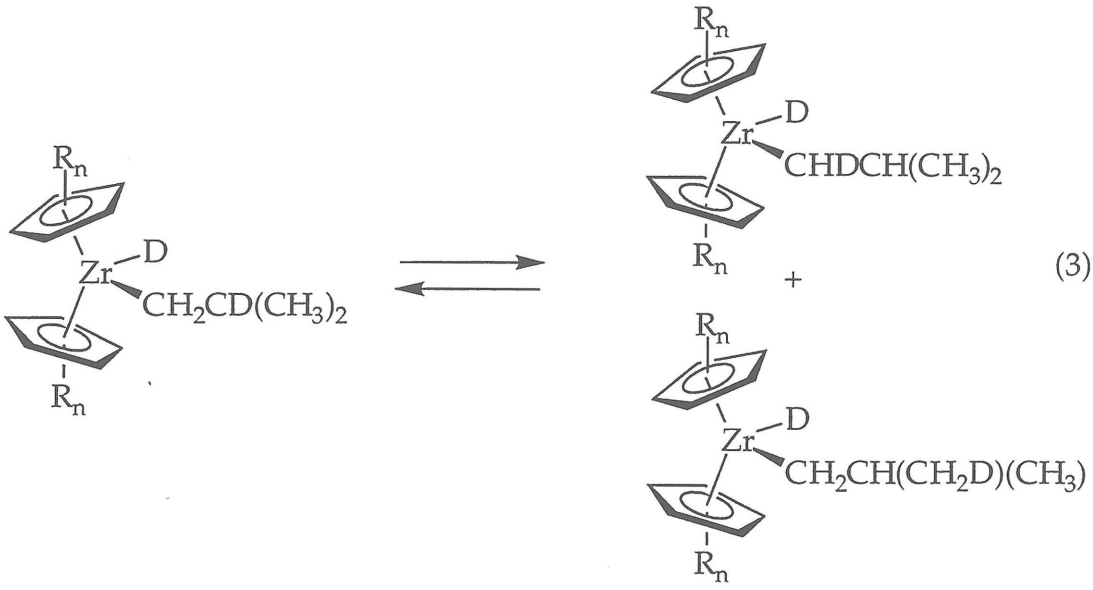

(3)

Moreover, addition of propylene to a benzene solution of pure $Cp^*_2Zr(CH_2CDMe_2)(D)$ or $(\eta^5\text{-}C_5Me_4H)_2Zr(CH_2CDMe_2)(D)$ results in rapid exchange between free olefin and coordinated alkyl.

By following the kinetics of these reactions using $\{^1H\}^2H$ NMR spectroscopy, a rate constant of $1.0(4) \times 10^{-8}$ s^{-1} has been measured for the rearrangement of $Cp^*_2Zr(CH_2CDMe_2)(D)$ to $Cp^*_2Zr(CHDCHMe_2)(D)$ and $Cp^*_2Zr\{CH_2CH(CH_2D)(CH_3)\}(D)$ at 296K. The corresponding rate constant for $(\eta^5\text{-}C_5Me_4H)_2Zr(CH_2CDMe_2)(D)$ is $4.3(4) \times 10^{-7}$ sec^{-1} at 296 K in equal amounts. No measureable equilibrium isotope effects was observed. Several other zirconocene isobutyl-deuteride complexes were examined (*e. g.*, $Cp^*(\eta^5\text{-}C_5H_4\text{-}CMe_3)Zr(CH_2CDMe_2)(D)$, $Cp^*CpZr(CH_2CDMe_2)(D)$), but reliable kinetic data could not be obtained.

Reaction of $(CpR_n)_2ZrH_2$ with one equivalent of $^{13}CH_2{=}CHCH_3$ results in quantitative formation (^1H NMR) of $(CpR_n)_2Zr(^{13}CH_2CH_2CH_3)(H)$. Addition of excess propylene or other α-olefins results in reductive elimination of propane and formation of products derived from the resulting $[(CpR_n)_2Zr(II)]$.[11] Monitoring a benzene-d_6 solution of $Cp^*_2Zr(^{13}CH_2CH_2CH_3)(H)$ by ^{13}C NMR spectroscopy reveals isomerization affording $Cp^*_2Zr(CH_2CH_2{}^{13}CH_3)(H)$ (eq. 4) with a $k^{296K} = 1.2 \times 10^{-4}$ s^{-1}. Similar isomerizations are observed for $(\eta^5\text{-}C_5Me_4H)_2Zr(^{13}CH_2CH_2CH_3)(H)$ to $(\eta^5\text{-}C_5Me_4H)_2Zr(CH_2CH_2{}^{13}CH_3)(H)$ ($k^{296K} = 1.1 \times 10^{-3}$ s^{-1}) and for $Cp^*(\eta^5\text{-}C_5H_4\text{-}CMe_3)Zr(^{13}CH_2CH_2CH_3)(H)$ to

$Cp^*(\eta^5\text{-}C_5H_4\text{-}CMe_3)Zr(CH_2CH_2{}^{13}CH_3)(H)$; the rate of the latter is too fast to measure using simple NMR spectral monitoring.

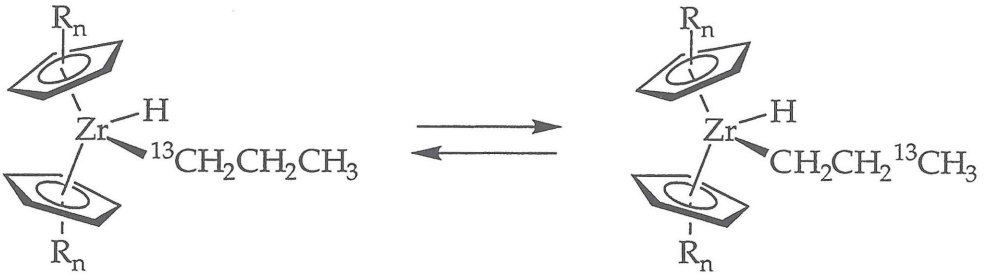

(4)

To determine the effect of the "spectator" ligand (hydride in the examples above) on the rate of alkyl isomerization, several alkyl complexes derived from Schwartz's reagent, $[Cp_2Zr(H)(Cl)]_n$[12] (**3**) were prepared. Although **3** is an insoluble polymeric material, its reaction with olefins affords soluble, well-characterized zirconocene alkyl-chloride complexes, $Cp_2Zr(R)(Cl)$.[13] Thus reaction of **3** with isobutylene, 1-butene, ethylene and propylene affords $Cp_2Zr(CH_2CHMe_2)(Cl)$ (**7**), $Cp_2Zr(CH_2CH_2CH_2CH_3)(Cl)$ (**4**), $Cp_2Zr(CH_2CH_3)(Cl)$ (**5**) and $Cp_2Zr(CH_2CH_2CH_3)(Cl)$ (**6**). Benzene solutions of $Cp_2Zr(CH_2CHDCH_2CH_3)(Cl)$ and $Cp_2Zr(CH_2CH_2D)(Cl)$, prepared from $[Cp_2Zr(D)(Cl)]_n$ and the appropriate olefin, display a single peak in the $\{^1H\}^2H$ NMR spectrum. No change is observed over the course of one week at 296 K. Thus, there is no evidence for rearrangement of these terminal alkyls via β-H elimination under these conditions (eq. 5). Likewise, a solution of $Cp_2Zr(^{13}CH_2CH_2CH_3)(Cl)$ does not undergo isotopic rearrangement at 296 K.

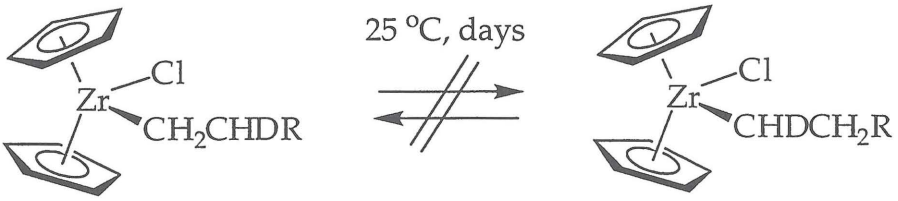

(R = H, CH_2CH_3)

(5)

Furthermore, addition of five equivalents of $^{13}CH_2{=}CHCH_3$ to a solution of $Cp_2Zr(CH_2CH_2CH_3)(Cl)$ (**7**) in benzene-d_6 resulted in no incorporation of ^{13}C into the propyl group over the course of one week (eq. 6).

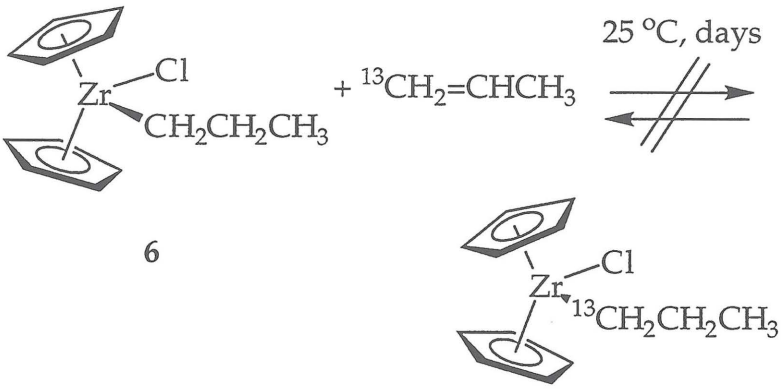

(6)

Reaction of $[Cp_2Zr(CH_3)(\mu_2\text{-}H)]_2$[14] with $^{13}CH_2=CHCH_3$ affords $Cp_2Zr(CH_3)(^{13}CH_2CH_2CH_3)$ in quantitative yield (^{1}H NMR). Over the course of three hours at room temperature, $Cp_2Zr(CH_3)(^{13}CH_2CH_2CH_3)$ isomerizes to $Cp_2Zr(CH_3)(CH_2CH_2{}^{13}CH_3)$ (eq. 7).

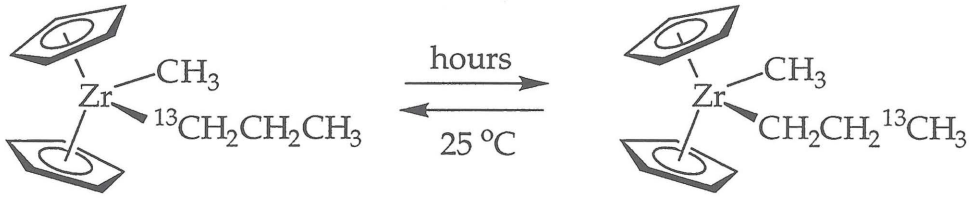

(7)

Addition of $^{13}CH_2=CHCH_3$ to a benzene solution of $[Cp_2ZrH_2]_n$ results in formation of dimeric $[Cp_2Zr(^{13}CH_2CH_2CH_3)(\mu_2\text{-}H)]_2$, which undergoes isomerization to $[Cp_2Zr(CH_2CH_2{}^{13}CH_3)(\mu_2\text{-}H)]_2$ over five days at room temperature.

Hydrozirconation of internal olefins with $[Cp_2Zr(H)(Cl)]_n$.

$Cp_2Zr(cyclo\text{-}C_5H_9)(Cl)$ (**8**) and $Cp_2Zr(cyclo\text{-}2\text{-}D\text{-}C_5H_8)(Cl)$ are obtained from addition of cyclopentene to a solution of **3** or **3-*d*** in either benzene or diethyl ether. The unlabeled complex has been isolated as bright yellow crystals that are stable under vacuum. Cooling an Et_2O solution of **8** to -40 °C affords clear yellow crystals suitable for X-ray diffraction. As shown in Figure 1, the cyclopentyl ligand adopts an envelope conformation and is contained in the metallocene wedge.

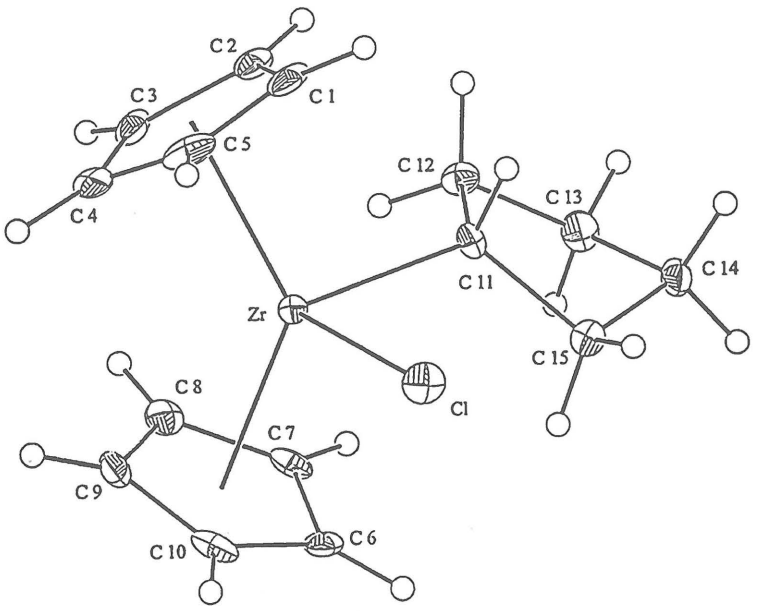

Figure 1. Molecular Structure of $Cp_2Zr(cyclo\text{-}C_5H_9)(Cl)$ (**8**) (50% probability ellipsoids). Selected bond distances (Å): Zr-Cent(1), 2.2305(7); Zr-Cent(2), 2.2094(7); Zr-C(11), 2.276(5); Zr-Cl, 2.4373(18). Bond angles (deg): Cent(1)-Zr-Cent(2), 130.83(3); C(11)-Zr-Cl, 93.85(13). Cent(1) is the centroid formed by C(1), C(2), C(3), C(4) and C(5). Cent(2) is the centroid formed by C(6), C(7), C(8), C(9) and C(10).

The $\{^1H\}^2H$ NMR spectrum of a benzene solution of $Cp_2Zr(cyclo\text{-}2\text{-}D\text{-}C_5H_8)(Cl)$ containing a ten-fold excess of cyclopentene initially exhibits only one resonance at $\delta = 1.43$ ppm, corresponding to deuterium at the 2-position of the cyclopentyl ligand. After 12 hours at 296 K, a new peak appears at $\delta = 2.19$ ppm that has been identified as free cyclopentene-3-d_1. Over a period of five days, deuterium appears in the remaining positions of the Zr-bound cyclopentyl ring and the free cyclopentene.

Reaction of **3** with *cis*-2-butene has also been studied by ^1H NMR spectroscopy. After 35 minutes at room temperature, the NMR spectrum displays resonances attributable to $Cp_2Zr\{CH(CH_3)CH_2CH_3\}(Cl)$ (**9**) as shown in Figure 2. Over the course of hours at room temperature, the peaks for **9** are replaced by resonances for $Cp_2Zr(CH_2CH_2CH_2CH_3)(Cl)$ (**4**) (eq. 8). Changing the solvent from benzene to THF has no discernible effect on the rate of isomerization. During the isomerization of **9** to **4**, formation of *trans*-2-butene is observed by NMR. Furthermore, addition of 1-pentene to a mixture containing

only **9** and **4** results in buildup of $Cp_2Zr(CH_2CH_2CH_2CH_2CH_3)(Cl)$ (**10**) during the course of isomerization.

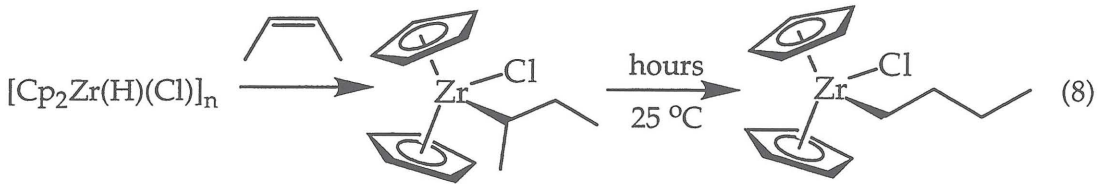

(8)

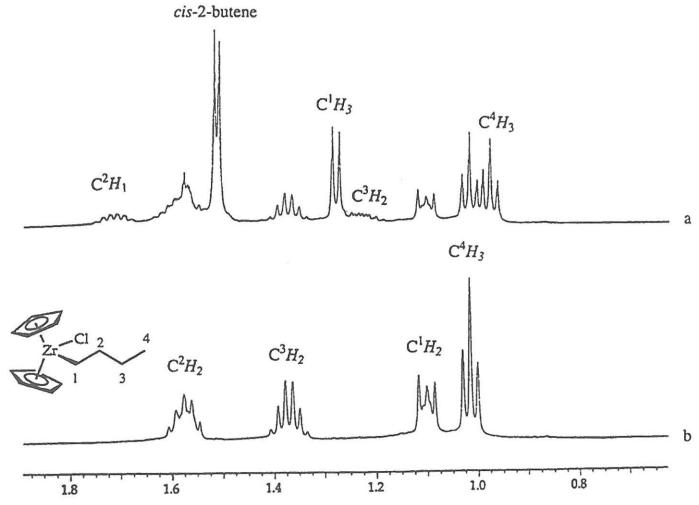

Figure 2. 500-MHz ^1H NMR spectra of the butyl resonances following hydrozirconation of *cis*-2-butene (a) after 6 h and (b) 3 days.

Twenty minutes after reaction of **3-*d*** with *cis*-2-butene (benzene-d_6, 296 K) in benzene solution, the $\{^1H\}^2H$ NMR spectrum displays a singlet at $\delta = 1.20$ ppm, assigned to the β-deuterium of $Cp_2Zr\{CH(CH_3)CHDCH_3\}(Cl)$. Over the course of several hours at this temperature, singlets at 1.31 ppm and 1.47 ppm appear in an approximately 2:1 ratio with gradual disappearance of the resonance at 1.20 ppm. No further change in the ^1H NMR spectrum is observed even after weeks at room temperature. The peaks at 1.31 ppm and 1.47 ppm are assigned to the deuterons at position C_3 and C_2, respectively, of **4** (eq. 9). No signal attributable to deuterium in the terminal positions (C_1 and C_4) of **4** is observed.

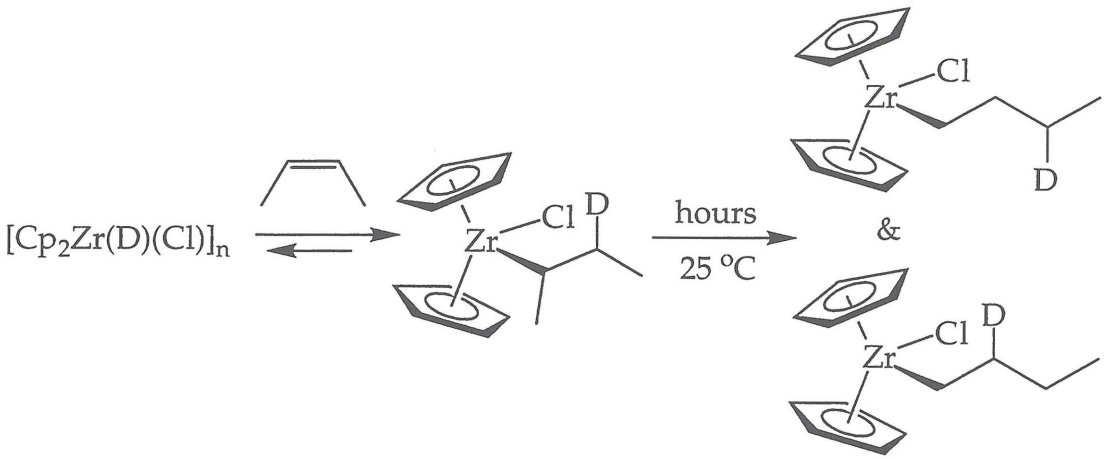

(9)

Reactions of $[Cp_2Zr(H)(Cl)]_n$ (**3**) with several longer chain olefins have also been examined. Monitoring the reaction of **3** with *cis*-2-hexene, *trans*-2-hexene and *trans*-3-hexene by ^1H NMR reveals that internal alkyl complexes are likely present at early conversion times, but the identity and relative amounts of these species could not be definitively established due to the complexity of the ^1H NMR spectra. In the expectation that the ^{13}C NMR spectra would be a much more readily interpretable, 1-^{13}C-*cis*-2-heptene, *cis*-$^{13}CH_3CH{=}CHCH_2CH_2CH_2CH_3$, was prepared by addition of $^{13}CH_3I$ to $LiC{\equiv}CCH_2CH_2CH_2CH_3$ in liquid ammonia, followed by hydrozirconation of the alkyne and quenching with H_2O.

The ^{13}C NMR spectrum (Figure 3) for the reaction of **3** with *ca.* 1.3 equivalents of *cis*-$^{13}CH_3CH{=}CHCH_2CH_2CH_2CH_3$ in benzene-d_6 after 10 minutes at 296 K exhibits a resonance at $\delta = 23.45$ attributable to $Cp_2Zr\{CH(^{13}CH_3)(CH_2)_4CH_3\}(Cl)$ and additional resonances at $\delta = 56.0$ ppm and $\delta = 14.7$ ppm, assigned to C_1 of $Cp_2Zr\{^{13}CH_2(CH_2)_5CH_3\}(Cl)$ and C_7 of $Cp_2Zr\{CH_2(CH_2)_5{}^{13}CH_3\}(Cl)$, respectively. The resonance due to $Cp_2Zr\{CH(^{13}CH_3)(CH_2)_4CH_3\}(Cl)$ grows in to a maximum relative intensity of *ca.* 50% over a period of about 5 hours, then decreases as those attributable to $Cp_2Zr\{^{13}CH_2(CH_2)_5CH_3\}(Cl)$ and C_7 of $Cp_2Zr\{CH_2(CH_2)_5{}^{13}CH_3\}(Cl)$ continue to grow until after about 48 hours, they are the only resonances attributable to an organometallic compound. During this period, their ratio remains constant at 85:15 (eq. 10).[15]

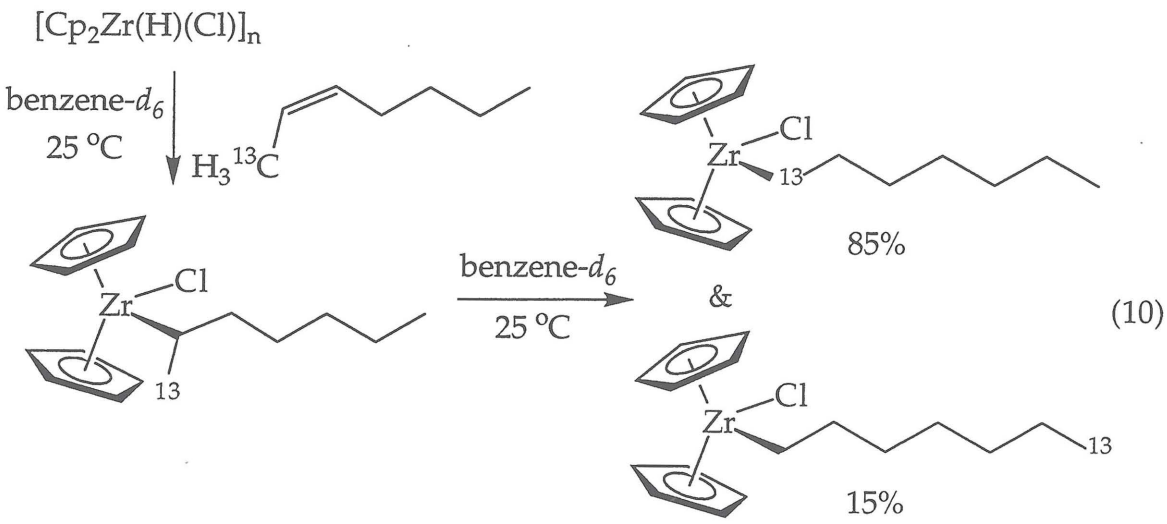

(10)

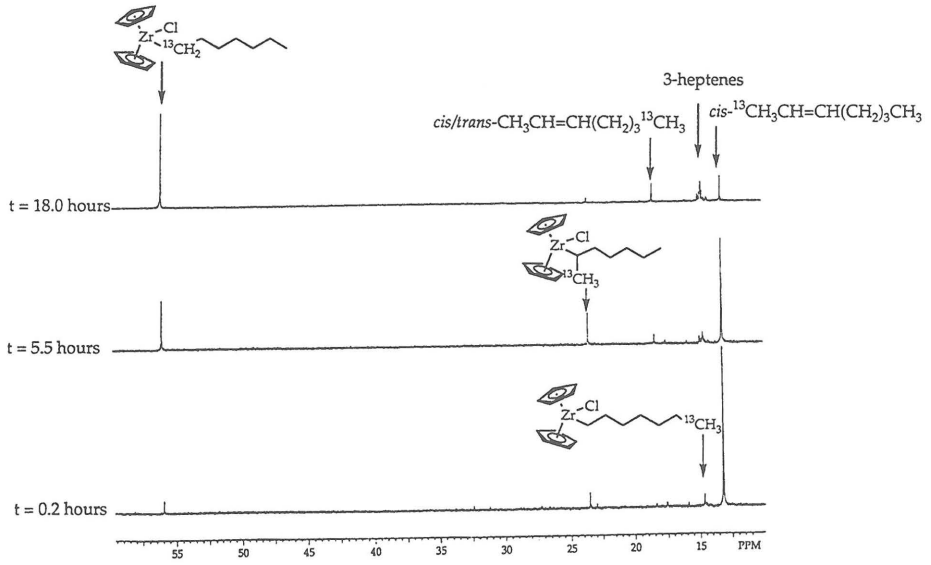

Figure 3. 125.77-MHz $\{^1H\}^{13}C$ NMR spectra of the heptyl resonances following hydrozirconation of *cis*-$^{13}CH_3CH{=}CHCH_2CH_2CH_2CH_3$. Conversion of $Cp_2Zr\{CH(^{13}CH_3)(CH_2)_4CH_3\}(Cl)$ to other isomers is observed, predominantly $Cp_2Zr\{^{13}CH_2(CH_2)_5CH_3\}(Cl)$ and C_7 of $Cp_2Zr\{CH_2(CH_2)_5{}^{13}CH_3\}(Cl)$.

For confirmation of these assignments, the hydrozirconation of unlabeled *cis*-2-heptene was carried out in toluene-d_8 for three hours at 296 K, and the reaction was then cooled to -50 °C to prevent further isomerization. The ^{13}C NMR spectrum of the reaction mixture was recorded at this temperature (Figure

4). Evident are 14 resonances that correspond to heptyl resonances of two organozirconium complexes, assigned as $Cp_2Zr\{CH_2(CH_2)_5CH_3\}(Cl)$ and $Cp_2Zr\{CH(CH_3)(CH_2)_4CH_3\}(Cl)$. Perhaps the most informative feature of the spectrum is the region between 50 and 60 ppm, where carbons directly bound to zirconium generally resonate. In this region, only two peaks are observed, one at $\delta = 56.0$ ppm assigned to C_1 of $Cp_2Zr\{CH_2(CH_2)_5CH_3\}(Cl)$ and the other at $\delta =$ 59.8 ppm assigned to methine carbon of $Cp_2Zr\{CH(CH_3)(CH_2)_4CH_3\}(Cl)$.

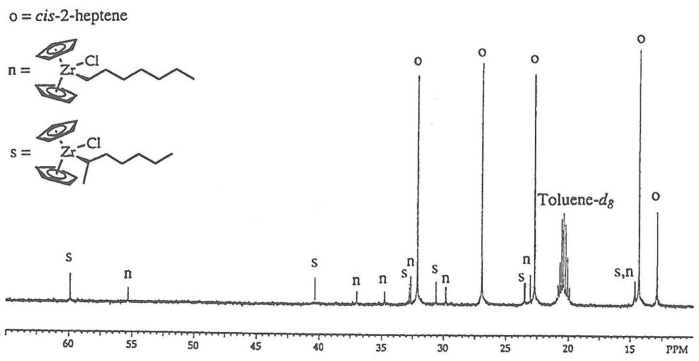

Figure 4. Upfield region of the 125.77 MHz $\{^1H\}^{13}C$ NMR spectrum obtained at 240 K, following hydrozirconation of *cis*-2-heptene with **3**.

In addition to peaks corresponding to $Cp_2Zr\{^{13}CH_2(CH_2)_5CH_3\}(Cl)$, $Cp_2Zr\{CH_2(CH_2)_5{}^{13}CH_3\}(Cl)$ and $Cp_2Zr\{CH(^{13}CH_3)(CH_2)_4CH_3\}(Cl)$, the ^{13}C NMR spectrum shown in Figure 3 exhibits resonances assigned to terminally ^{13}C-labeled isomeric internal heptenes, based on comparison to authentic samples, along with smaller signals believed to be due to singly ^{13}C-labeled isomeric 3-heptenes (eq. 11). The largest peak at $\delta = 18.3$ ppm corresponds to both 7-^{13}C-*cis*-2-heptene and 7-^{13}C-*trans*-2-heptene.

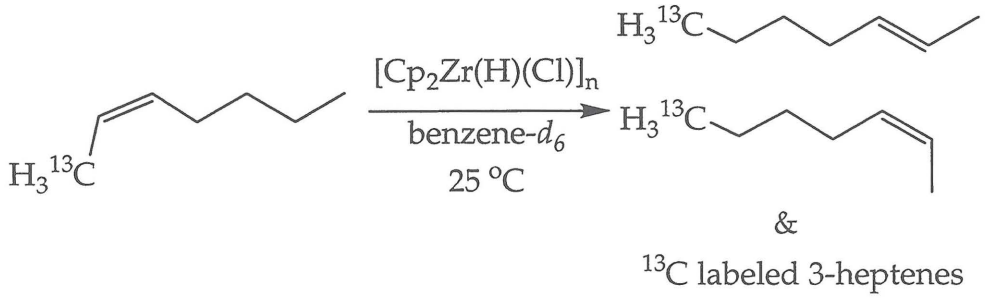

(11)

The course of hydrozirconation of *cis*-2-butene in benzene solution was also followed by quenching with CH_3OD at various time intervals (eq. 12); results are given in Table 1.

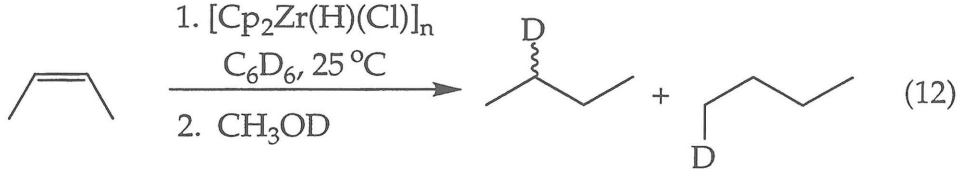

(12)

$\{^1H\}^2H$ NMR spectroscopy reveals that at short reaction times (up to about 20 minutes) only 2-deuterobutane is formed, whereas with longer reaction times increasing amounts of 1-deuterobutane is obtained. The time variation of the ratios 1- and 2-deuterated butanes is consistent with the rate of isomerization of $Cp_2Zr\{CH(CH_3)CH_2CH_3\}(Cl)$ to $Cp_2Zr(CH_2CH_2CH_2CH_3)(Cl)$ as monitored directly by ^1H NMR (*vide supra*).

For the hydrozirconation of longer internal olefins such as *cis*-2-pentene and *cis*-2-heptene in benzene solution, quenching after one hour with CH_3OD results in solely *terminally* deuterated alkane. The $^2H\{^1H\}$ NMR spectra of the deuterated alkanes obtained after 1 hour of hydrozirconation are shown in Figure 5. These results suggest that rearrangements of the internal to the primary alkyls are relatively rapid, in contrast to the conclusions obtained by directly monitoring the reaction of **3** with *cis*-$^{13}CH_3CH{=}CHCH_2CH_2CH_2CH_3$ by ^{13}C NMR spectroscopy. In an attempt to reconcile this discrepancy, addition of 10 mol percent CH_3OD was added to the hydrozirconation of *cis*-2-heptene after 1 hour and the reaction monitored by low temperature ^{13}C NMR spectroscopy; $Cp_2Zr\{CH_2(CH_2)_5CH_3\}(Cl)$ is the only (remaining) heptylzirconium product observed. However, when an identical experiment is performed with *cis*-2-butene, both internal and terminal organozirconium products are observed in the ^{13}C NMR spectrum, also in agreement with the corresponding quenching experiment. Since after 1 hour the hydrozirconation of *cis*-2-heptene with insoluble **3** results in relatively low conversion of the olefin to the zirconium alkyl as compared to the hydrozirconation of *cis*-2-butene, we sought to remove unreacted **3** from the reaction mixture before the addition of methanol. Removal of unreacted **3** can be accomplished by filtration, resulting in a clear

yellow solution. Addition of CH_3OD to the filtrate, followed by analysis by $\{^1H\}^2H$ NMR, reveals that both internally and terminally deuterated heptanes are produced. In order to further demonstrate the effects of unreacted **3** on the quenching of hydrozirconation reactions, addition of *cis*-2-butene to a twofold excess of **3** followed by quenching with CH_3OD after 1 hour results in a substantial increase in the amount of terminally deuterated butane as compared to the stoichiometric reaction.

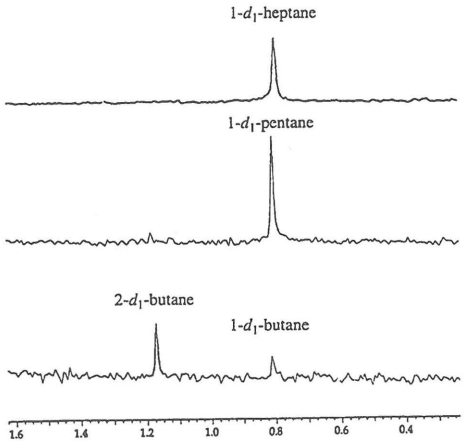

Figure 5. 76.77 MHz $\{^1H\}^2H$ NMR spectra of deuterated alkanes produced by treatment of **3** with *cis*-2-butene, *cis*-2-pentene and *cis*-2-heptene, followed by a CH_3OD quench.

Discussion

Rearrangements of isotopically labeled $(CpR_n)_2Zr(CH_2CHR'_2)(H)$. Complexes of the general formula $(CpR_n)_2Zr(CH_2CHR_2')(H)$ (R, R', R" = alkyl, H) are readily prepared from $(CpR_n)_2ZrH_2$ and the appropriate olefin, CH_2=CR'R". We have previously shown that although these complexes are stable in solution at 296 K, they undergo facile, reversible β-H elimination.[9] Using methyl-*tert*-butylacetylene to rapidly trap $(CpR_n)_2ZrH_2$, rate constants for β-H elimination have been measured for the $(CpR_n)_2Zr(CH_2CHR_2')(H)$ (CpR_n = (η^5-C_5Me_5) (Cp*), (η^5-C_5Me_4H)) systems examined here, as well as for several other substituted zriconocenes.[16] Whereas isotopically labeled alkyl complexes undergo rearrangement under the same conditions, the rates of rearrangement are 10^3 to 10^4 times slower than β-H elimination.

A proposed mechanism for deuterium migration in $Cp^*_2Zr(CH_2CDMe_2)D$ is shown in Scheme 1; similar paths can account for all the isotopic rearrangements observed. Following β-H elimination and olefin reorientation, either through intramolecular olefin rotation or by dissociation and recoordination in the opposite direction, β-H migratory insertion affords secondary or tertiary alkyl-hydride species. Since all alkyl-hydride complexes studied undergo very rapid exchange with free olefin, we favor the olefin dissociation pathway, although the presence of an olefin-dihydride intermediate which undergoes olefin rotation faster than dissociation can not be ruled out definitively. The secondary or tertiary alkyl-hydride intermediate then undergoes β-H elimination and readdition to form the primary alkyl with the label in a new position.

A mechanism similar to that shown in Scheme 1 has been proposed by Busico to account for the tacticity dependence on monomer concentration in metallocene catalyzed olefin polymerization, where lower propylene pressures result in decreased stereospecificity.[6c] At low propylene concentrations, epimerization at the methine carbon of the last inserted monomer unit competes with olefin insertion, hence decreasing the isotacticity of the resulting polypropylene. A sequence of β-H elimination and reinsertion steps leads to formation of the *tertiary*-alkyl intermediate $[Zr\text{-}C(CH_3)_2\mathbf{P}]$ ($\mathbf{P}$ = polymer chain), which may β-H eliminate from either methyl group to reform the original $[ZrCH_2CH(CH_3)\mathbf{P}]$ or the enantiomeric equivalent. Busico favors the olefin rotation pathway over the free olefin route, since it is commonly accepted that α-olefins undergo insertion at a much greater rate than the corresponding *gem*-disubstituted olefins.[6]

The rate of alkyl isomerization is influenced by the degree of substitution on the cyclopentadienyl ligands: more substituted cyclopentadienyl ligands slow the rate of the reaction.[9] For the ^{13}C-labeled propyl-hydride complexes, the relative rate of isotopic rearrangement is $[Cp^*(\eta^5\text{-}C_5H_4\text{-}CMe_3)Zr] > [(\eta^5\text{-}C_5Me_4H)_2Zr] > [Cp^*_2Zr]$. Similarly, the rate of deuterium scrambling in the labeled isobutyl-deuteride complexes is $[(\eta^5\text{-}C_5Me_4H)_2Zr] > [Cp^*_2Zr]$. In both cases, the effect of changing the cyclopentadienyl substitution has a relatively modest effect on the rate of isotopic rearrangement. For example, the rate

Scheme 1

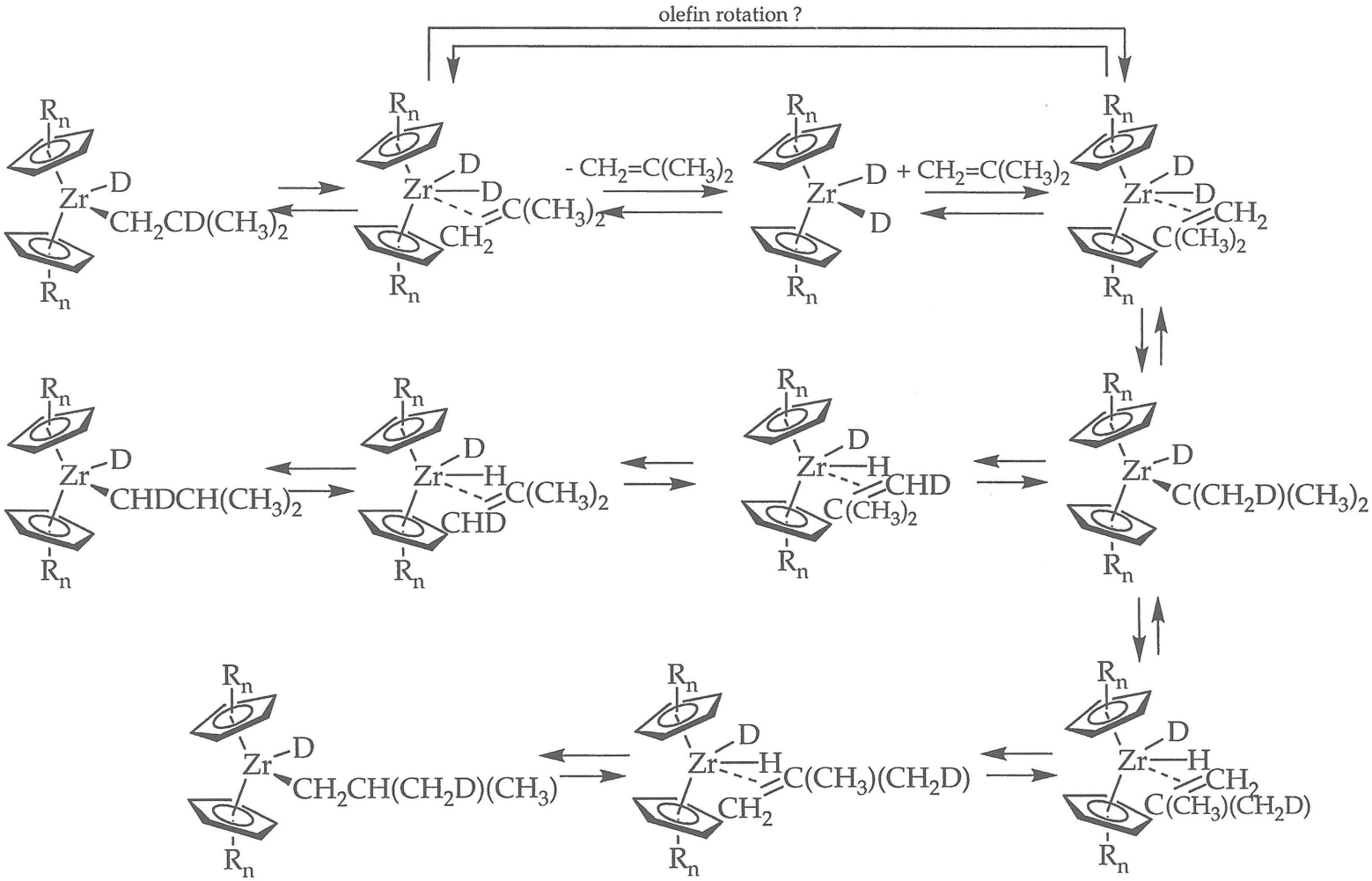
olefin rotation ?
- CH2=C(CH3)2
+ CH2=C(CH3)2
Rn
Zr
D
H
CH2CD(CH3)2
C(CH3)2
CH2
CHDCH(CH3)2
CHD
C(CH2D)(CH3)2
CH2CH(CH2D)(CH3)
C(CH3)(CH2D)

enhancement from removing two methyl groups results in a 40-fold increase in the rate constant at 296 K.

Since the rates for olefin insertion and β-H elimination are more than two orders of magnitude faster than isotopic rearrangement, we conclude that the formation of the more substituted alkyl complex (either secondary or tertiary) is the rate determining step in the isomerization process of Scheme 1. This assertion is supported by the failure to observe any intermediate internal alkyl complex in these systems. We have observed similar behavior for the addition of *cis*-2-butene to $Cp^*_2ZrH_2$, where the addition of the zirconium hydride bond is much slower than isomerization of the internal alkyl to the final, only observable terminal product, $Cp^*_2Zr(CH_2CH_2CH_2CH_3)(H)$.[9]

The rate constant at 296 K for β-H elimination of the isobutyl ligand from $Cp^*_2Zr(CH_2CHMe_2)(H)$ is much greater than the rate constant for the isomerization ($k_{\beta\text{-}H} = 2.8 \times 10^{-6}\ s^{-1}$; $k_{isom} = 1.0 \times 10^{-8}\ s^{-1}$; $k_{\beta\text{-}H}/k_{isom} = 280$) for $Cp^*_2Zr(CH_2CDCMe_2)(D)$ to $Cp^*_2Zr(CHDCHMe_2)(D)$ and $Cp^*_2Zr(CH_2CH(CH_2D)(CH_3))(D)$.[9] By comparion, for the related propyl-hydride complex $Cp^*_2Zr(^{13}CH_2CH_2CH_3)(H)$, these rates are much greater and ratio rates less, ($k_{\beta\text{-}H} = 1.1 \times 10^{-3}\ s^{-1}$; $k_{isom} = 1.2 \times 10^{-4}\ s^{-1}$; $k_{\beta\text{-}H}/k_{isom} = 11$).[9] These data indicate that the isopropyl hydride intermediate is more accessible than the corresponding *tert*-butyl-hydride intermediate (**A** in Scheme 1). Apparently, the presence of an additional methyl group in the case of the *tert*-butyl intermediate sterically disfavors its formation relative to the isopropyl complex, which then in turn decreases the rates of isomerization (as well as β-H elimination).

Rearrangements of $Cp_2Zr(CH_2CHR'_2)(X)$ (R' = H, Me, Et; X = H, Me, Cl).

Changing the "spectator" ligand in the metallocene wedge from hydride to other one electron ("X-type") ligands has a relatively larger effect on the rates of β-H elimination and alkyl isomerization. Whereas $Cp^*(C_5H_4\text{-}CMe_3)Zr(CH_2CHR'_2)(H)$ (R' = H, Me, Et) undergo facile β-H elimination at 296 K, the corresponding compounds $Cp_2Zr(CH_2CHR'_2)(Cl)$ (R' = H, Me, Et) are stable to β-H elimination/olefin rotation/reinsertion, as

demonstrated by the lack of deuterium scrambling and lack of isotopic rearrangement for $Cp_2Zr(^{13}CH_2CH_2CH_3)(Cl)$. The observation that $Cp_2Zr(CH_2CH_2CH_3)(Cl)$ does not exchange with $^{13}CH_2{=}CHCH_3$ also is in agreement with the very stable nature of these alkyl/chloro complexes. A general lack of β-H elimination from primary alkyl complexes of the type $Cp_2Zr(CH_2CHR'_2)(Cl)$ was originally proposed by Schwartz,[18] based on the absence of alkyl exchange with olefins in the related cyclohexylmethyl complex, $Cp_2Zr(CH_2\text{-}\textit{cyclo}\text{-}C_6H_{11})(Cl)$.

In order to establish whether this effect is steric or electronic in origin, the labeled propyl-methyl complex $Cp_2Zr(^{13}CH_2CH_2CH_3)(CH_3)$ was prepared.[17] Isotopic rearrangement is observed over the course of three hours at 296 K. Since methyl and chloride are approximately isosteric, the difference in reactivity must therefore be due to electronic properties, most likely the π-donating ability of the chloride ligand. Lone electron pair donation from Cl into the $1a_1$ zirconocene orbital formally completes the 18-electron zirconocene valence shell, and hence, unlike $Cp_2Zr(CH_2CHR'_2)(X)$ (X = H, CH_3), there is no (strictly) empty orbital for β-H elimination.[18] Moreover, alkyl isomerization initiated by β-H elimination should be very facile for zirconocene cations, $[Cp_2Zr(CH_2CHR'_2)]^+$, since formally there are two vacant orbitals.[19]

We considered the possibility that small, undetectable amounts of the dihydride complex, $[Cp_2ZrH_2]_n$, might promote propyl isomerization for $Cp_2Zr(^{13}CH_2CH_2CH_3)(CH_3)$, since preparation of $[Cp_2Zr(CH_3)(H)]_2$ involves hydrogenation of Cp_2ZrMe_2. $[Cp_2Zr(^{13}CH_2CH_2CH_3)(H)]_2$ was therefore prepared via treatment of $[Cp_2ZrH_2]_n$ with $^{13}CH_2{=}CHCH_3$. Isotopic rearrangement for $[Cp_2Zr(^{13}CH_2CH_2CH_3)(H)]_2$ does occur over the course of 5 days at 296 K, but at a rate much slower than observed for $Cp_2Zr(^{13}CH_2CH_2CH_3)(CH_3)$. The slow isomerization rate for $[Cp_2Zr(^{13}CH_2CH_2CH_3)(H)]_2$ is attributed to its dimeric nature in solution. Schwartz[20] has previously reported the robust nature of these alkyl-hydride complexes, a result of their strong bridging hydride interactions. Presumably, the dimeric alkyl-hydride must dissociate into the 16-electron monomeric species in order to undergo β-H elimination, eventually resulting in isotopic scrambling.

Hydrozirconation of Internal Olefins and Isomerization of Internal Alkyls.

In contrast to primary alkyl complexes of $Cp_2Zr(R)(Cl)$, internal acyclic and cyclic alkyl complexes readily undergo β-H elimination and alkyl isomerization reactions. The formation of terminal products from hydrozirconation of internal olefins was a striking observation in early studies.[3,4] It is this behavior that has made hydrozirconation a valuable synthetic tool for a variety of transformations.[4] The order of reactivity based on qualitative observations is: terminal alkene > internal alkene > exocyclic alkene > cyclic alkene ≈ trisubstituted alkene.[4c] For example, only the zirconium-2-cyclohexenylethyl complex is observed upon the hydrozirconation of vinylcyclohexene.[21] Isomerization of the internal alkyl adduct is generally believed to be much faster than its initial formation by reaction of internal olefin with polymeric **3**, since no internally substituted products are isolated from treatment of the organozirconium complex with various electrophiles. For example, the hydrozirconation of (Z)-5-decene at 40 °C for 4 hours, followed by addition of D_2O, resulted in formation of up to 70% 1-d_1-decane, with the remaining products identified as internal decenes; no internally deuterated decanes were detected.[22] Tertiary alkylzirconium complexes, e.g., $Cp_2Zr(CMe_3)(Cl)$, appear to be generally inaccessible even as intermediates. Attempted hydrozirconation of an internal alkene which is capped at both ends with *tert*-butyl groups yields only isomerized alkene.[18]

Direct analysis of the hydrozirconation of *cis*-2-butene by high field ^1H NMR spectroscopy has now provided the first observation of a transient zirconium internal alkyl complex, $Cp_2Zr(CH(CH_3)CH_2CH_3)(Cl)$ (**9**).[23] The isomerization of **9** to $Cp_2Zr(CH_2CH_2CH_2CH_3)(Cl)$ (**4**) occurs over the course of several hours at 296 K, which is slower than the time required for the complete reaction of $[Cp_2Zr(H)(Cl)]_n$ (**3**). Clearly, the rate of alkyl isomerization in the butyl case is not as rapid as previously believed.

The hydrozirconation of *cis*-2-butene with **3-d** also confirms the formation of **9**. The $^2H\{^1H\}$ NMR spectrum initially displays one peak, attributable to the β-deuterium of $Cp_2Zr(CH(CH_3)CHDCH_3)(Cl)$.[24] The proposed mechanism for isomerization of $Cp_2Zr(CH(CH_3)CHDCH_3)(Cl)$ to $Cp_2Zr(CH_2CH_2CHDCH_3)$-(Cl) and $Cp_2Zr(CH_2CHDCH_2CH_3)(Cl)$ is shown in Scheme 2. After addition of

Scheme 2

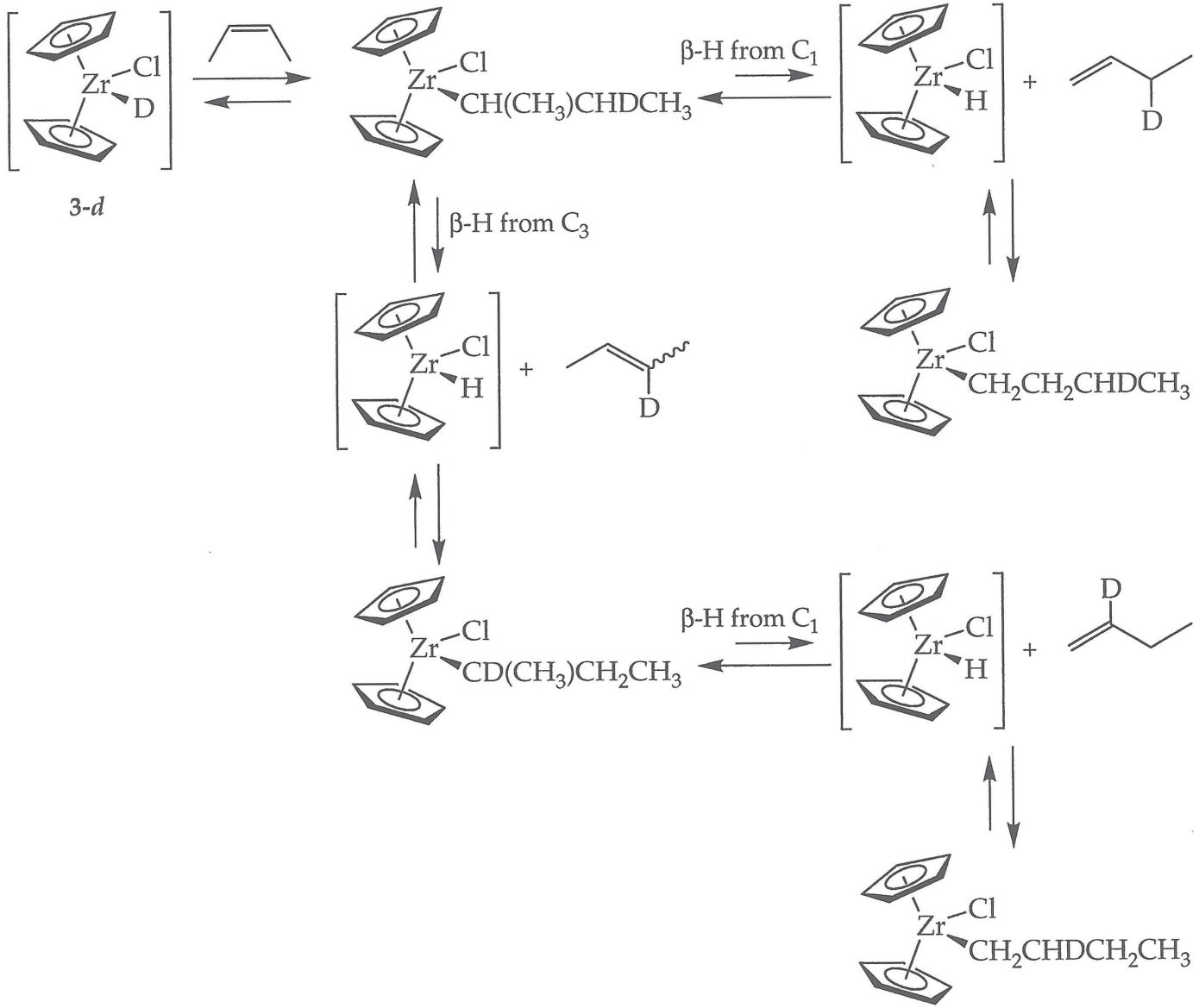
Zr
Cl
D
3-*d*
CH(CH3)CHDCH3
β-H from C1
H
+
β-H from C3
CH2CH2CHDCH3
CD(CH3)CH2CH3
CH2CHDCH2CH3

the olefin, the internal alkyl complex can β-H eliminate from either C_1 or C_3. If β-H elimination occurs from C_1, [$Cp_2Zr(H)(Cl)$] and 3-d_1-1-butene are formed, which then undergo insertion to form $Cp_2Zr(CH_2CH_2CHDCH_3)(Cl)$. If β-H elimination occurs from C_3, liberation of *cis*- or *trans*-2-d_1-2-butene occurs with formation of [$Cp_2Zr(H)(Cl)$]. The 2-butenes then reinsert, forming another internal alkyl complex, now with deuterium on the carbon bound directly to zirconium. This then undergoes β-H elimination from C_1 to generate 2-d_1-1-butene which then inserts forming $Cp_2Zr(CH_2CHDCH_2CH_3)(Cl)$. The ratio of $Cp_2Zr(CH_2CH_2CHDCH_3)(Cl)$ to $Cp_2Zr(CH_2CHDCH_2CH_3)(Cl)$ is approximately 2:1 during the isomerization reaction, indicating that β-H elimination from C_1 is favored over elimination from C_3. No deuteration in the α or ω positions of **4** is observed, consistent with the static nature of primary alkyls, since those isotopomers are only accessed by further rearrangement of $Cp_2Zr(CH_2CH_2CHDCH_3)(Cl)$ or $Cp_2Zr(CH_2CHDCH_2CH_3)(Cl)$.

The detection of *trans*-2-butene during isomerization of **9** to **4** suggests the intermediacy of [$Cp_2Zr(H)(Cl)$] and free olefin, rather than olefin-hydride intermediates that undergo intramolecular olefin rotation. This conclusion is further supported by the addition of 1-pentene to a mixture of **9** and **4**. By the time **9** is completely gone, the pentyl-chloride complex, $Cp_2Zr(CH_2CH_2CH_2CH_2CH_3)(Cl)$, is observed along with **4** (Scheme 3). Facile olefin exchange is not surprising for a d^0 metal complex that is not capable of stabilizing π-back donation.

Scheme 3

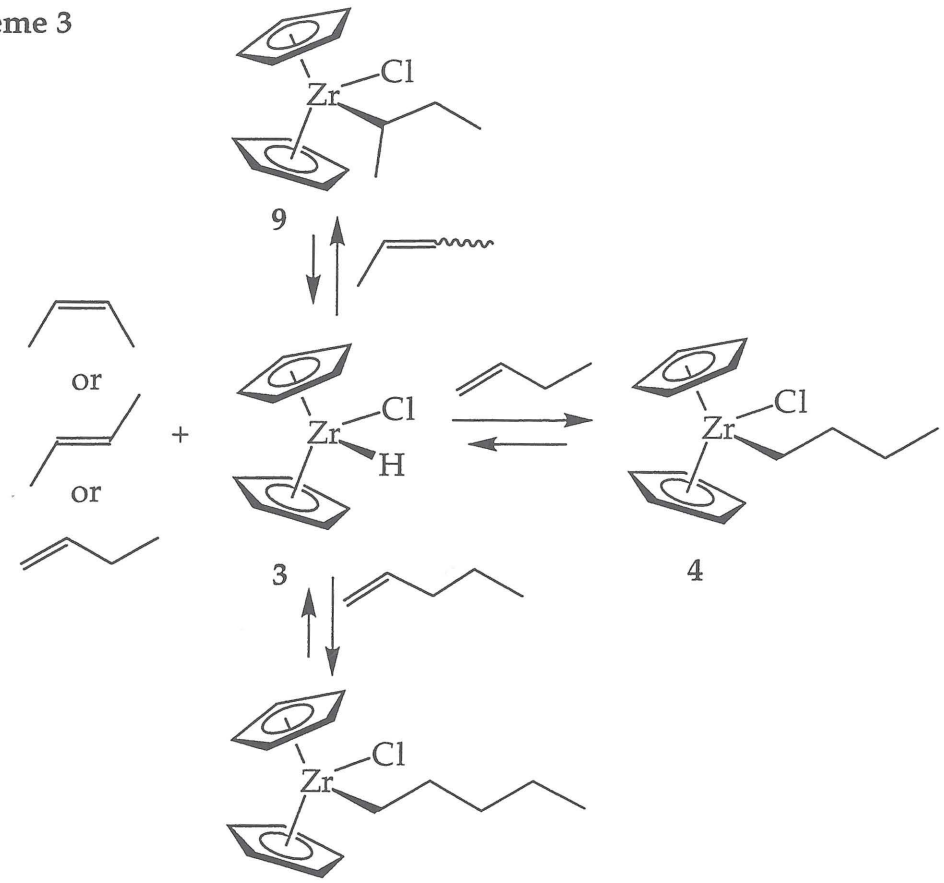

The isomerization of the deuterium-labeled cyclopentyl-chloride complex $Cp_2Zr(cyclo\text{-}2\text{-}D\text{-}C_5H_8)(Cl)$ also supports a free olefin pathway in alkyl isomerization. The fact that deuterium appears in free cyclopentene (cyclopentene-3-d_1) *before* it appears in positions other than the 2 position of **8** demonstrates that β-H elimination and liberation of free cyclopentene is the favored pathway over intramolecular olefin rotation and reinsertion (Scheme 4). Note that the absence of cyclopentene-1-d_1 is consistent with Scheme 4, since both the addition and elimination of Zr-H follow strict *syn* stereochemistry.

Alkyl length clearly has a significant effect on the rate of isomerization of internal alkyls. Hydrozirconation of *cis*-$^{13}CH_3CH{=}CHCH_2CH_2CH_2CH_3$ demonstrates that alkyl isomerization of the internal heptyl-chloride complex is faster than that of the corresponding butyl complex, since $Cp_2Zr\{CH(^{13}CH_3)(CH_2)_4CH_3\}(Cl)$ disappears in less than 24 hours whereas **9** persists for several days. Isomerization of $Cp_2Zr\{CH(^{13}CH_3)(CH_2)_4CH_3\}(Cl)$ produces both $Cp_2Zr\{^{13}CH_2(CH_2)_5CH_3\}(Cl)$ and $Cp_2Zr\{CH_2(CH_2)_5{}^{13}CH_3\}(Cl)$, consistent with isomerization in both directions down the alkyl chain, while ^{13}C

NMR spectroscopy reveals that only one internal alkyl complex, $Cp_2Zr\{CH(^{13}CH_3)(CH_2)_4CH_3\}(Cl)$, is formed in appreciable concentration. Formation of $Cp_2Zr\{CH_2(CH_2)_5{}^{13}CH_3\}(Cl)$ implies the intermediacy of 3- and 4-heptyl zirconium complexes, although we have been unable to detect these complexes spectroscopically. Based on this evidence, we propose that the rate of isomerization for 3- and 4-heptyl complexes is rapid, such that only the 2-isomer can be observed. Unfavorable steric interactions between alkyl chains longer than methyl and the chloride ligand in the 3- and 4-heptyl zirconocene presumably results in destabilization and hence faster rates of isomerization. Although reliable force fields are not available, molecular mechanics[25] calculations support this assertion. Of the internal alkyl complexes, $Cp_2Zr\{CH(CH_3)(CH_2)_4CH_3\}(Cl)$ was found to be approximately 2 kcal·mol^{-1} more stable than $Cp_2Zr\{CH(CH_2CH_2CH_2CH_3)(CH_2CH_3)\}(Cl)$, which in turn is about 3 kcal·mol^{-1} more stable than $Cp_2Zr\{CH(CH_2CH_2CH_3)_2\}(Cl)$.

In addition to directly observing internal alkyl complexes by NMR spectroscopy, we have looked for these species in quenching reactions. Hydrozirconation of *cis*-2-butene followed by addition of CH_3OD affords mixtures of internally and terminally deuterated alkanes. For hydrozirconation in the presence of excess *cis*-2-butene, internally deuterated butanes are observed for up to 48 hours, much longer than previously reported.[4c] The ratio of internally to terminally deuterated butanes obtained from the quenching experiments corresponds roughly to the amounts of internal and terminal butyl organozirconium complexes that were detected by direct NMR observation.

Scheme 4

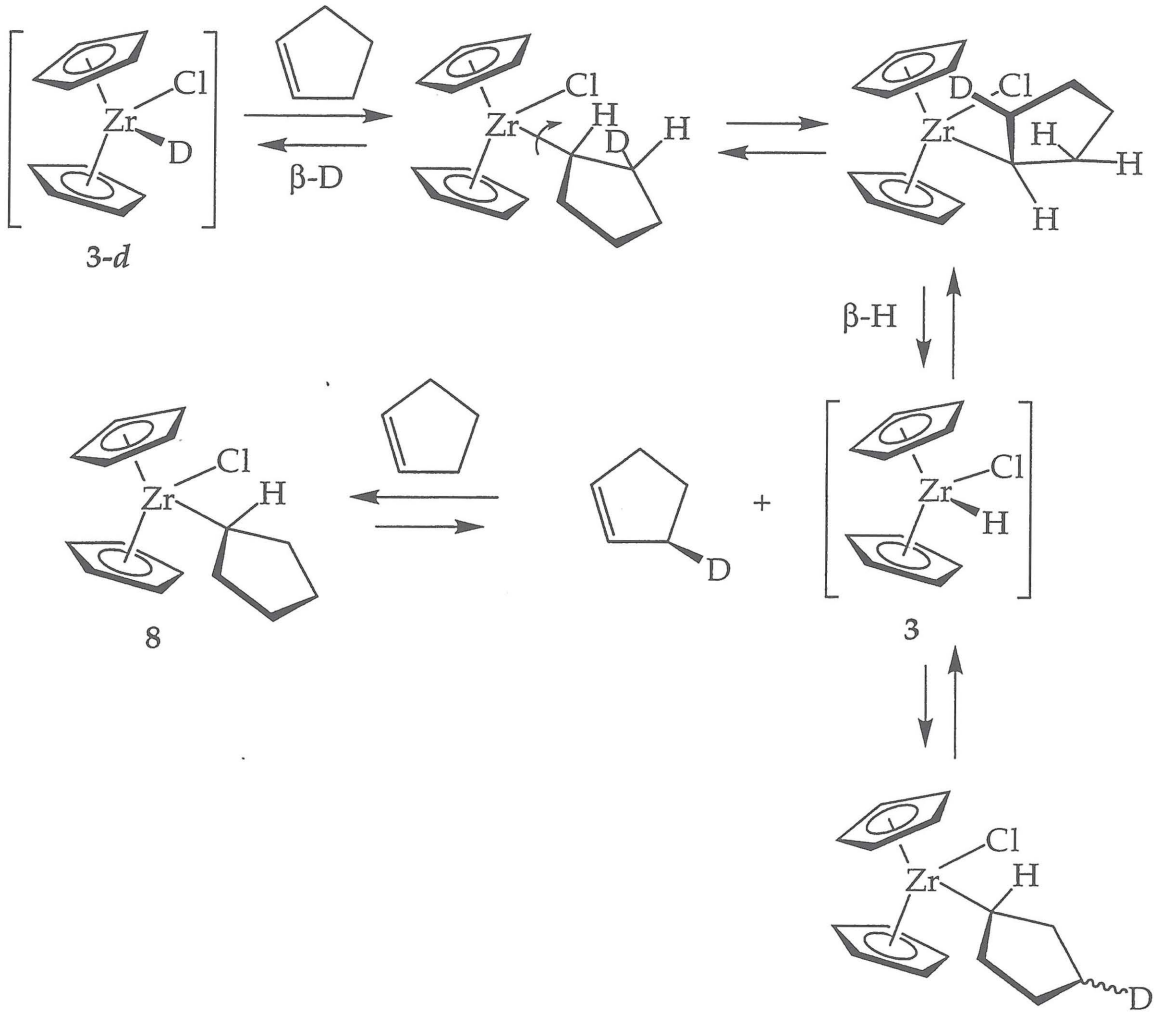

By contrast, addition of CH_3OD to reactions of $[Cp_2Zr(H)(Cl)]_n$ with *cis*-2-pentene or *cis*-2-heptene results in *only* terminally deuterated alkanes. These results appear inconsistent with those obtained by monitoring the reaction by NMR spectroscopy. To resolve the discrepancy we first examined the solution obtained from hydrozirconation of *cis*-2-heptene for one hour followed by addition of 10 mol percent of CH_3OD by ^{13}C NMR. Only terminal zirconium heptyl complex was detected, suggesting methanol somehow catalyzes the isomerization of $Cp_2Zr\{CH(CH_3)(CH_2)_4CH_3\}(Cl)$ to $Cp_2Zr\{CH_2(CH_2)_5CH_3\}(Cl)$. By comparison, after hydrozirconation of *cis*-2-butene followed by addition of 10 mol percent of methanol, both **9** and **4** are observed by low temperature ^{13}C

NMR spectroscopy, so that methanol does not promote isomerization in this case.

Why might $Cp_2Zr\{CH(CH_3)CH_2CH_3\}(Cl)$ and $Cp_2Zr\{CH(CH_3)(CH_2)_4CH_3\}(Cl)$ behave differently? Qualitative comparison of the relative rates of hydrozirconation reveals that *cis*-2-butene reacts more rapidly than *cis*-2-heptene with $[Cp_2Zr(H)(Cl)]_n$ (**3**). This is in accord with previous observations that longer olefins undergo hydrozirconation at a slower rate than their less sterically crowded counterparts.[5c] Thus, after one hour there is considerably more unreacted $[Cp_2Zr(H)(Cl)]_n$ during the hydrozirconation of *cis*-2-heptene than for *cis*-2-butene. We therefore postulate that methanol might react with the residual **3**, forming a small amount of an organozirconium species that catalyzes the isomerization of internal alkyl to terminal complex.

To test this hypothesis, we carried out the hydrozirconation of *cis*-2-heptene for one hour followed by removal of unreacted **3** by filtration and addition of CH_3OD to the clear yellow filtrate. In this case $\{^1H\}^2H$ NMR spectroscopy showed formation of *both* internally and terminally deuterated heptanes (*ca.* 40:60, respectively). In the complementary experiment, hydrozirconation of *cis*-2-butene in the presence of *excess* **3** followed by quenching with CH_3OD results in enrichment of 1-d_1-butane (Table 1), presumably due to an increased concentration of the (as yet unidentified) isomerization catalyst.

These results are consistent with the previous observations for the hydrozirconation of internal olefins yielding only terminally substituted products. This behavior has made **3** a valuable synthetic tool for the functionalization of otherwise unreactive C-H bonds. Typically hydrozirconation reactions are performed using elevated temperatures and/or until a homogenous solution is obtained thus allowing isomerization of all internal alkyl adducts to the more stable terminal organozirconium complex. However, the isomerization of the internal alkyl adduct is not as rapid as previously reported and internally functionalized alkanes can be prepared under the appropriate conditions. Our results demonstrate that in addition to long reaction times, addition of electrophiles such as H^+ in the presence of unreacted **3**

can promote alkyl isomerization. These results in concert offer an explanation for the lack of previous identification of internal alkyl adducts.

Experimental

General Considerations. All air and moisture sensitive compounds were manipulated using standard vacuum line, Schlenk or cannula techniques or in a dry box under a nitrogen atmosphere as described previously.[26] Argon, dinitrogen, dihydrogen and dideuterium gases were purified by passage over columns of MnO on vermiculite and activated molecular sieves. Solvents for air and moisture sensitive reactions were stored under vacuum over titanocene.[27] Preparations of $Cp^*_2ZrH_2$,[28] $[Cp^*(\eta^5\text{-}C_5H_4\text{-}CMe_3)ZrH_2]_2$, $(\eta^5\text{-}C_5Me_4H)_2ZrH_2$, $[Cp_2Zr(CH_3)(H)]_2$,[14] $[Cp_2Zr(Cl)(H)]_n$[12], $[Cp_2Zr(Cl)(D)]_n$[12], $[Cp_2ZrH_2]_n$[15] were carried out as described previously. NMR solvents: benzene-d_6, toluene-d_8 and tetrahydrofuran-d_8 were purchased from Cambridge Isotope Laboratories. Benzene-d_6 and toluene-d_8 were dried over $LiAlH_4$ and sodium and then stored over titanocene. Tetrahydrofuran-d_8 was dried over CaH_2 and stored over sodium/benzophenone ketyl. $^{13}CH_2{=}CHCH_3$ was purchased from Cambridge Isotope Laboratories and distilled on the vacuum line before use. $^{13}CH_3I$ and CH_3OD were purchased from Cambridge Isotope Laboratories and used as received. Ethylene was purchased from Matheson and passed through a trap maintained at -78 °C before use. Isobutene, *cis*-2-butene and propene were purchased from Aldrich, dried over $Al(i\text{-}Bu)_3$ and stored over 4Å molecular sieves. 1-Pentene, 1-hexene, *cis*- and *trans*-2-hexene, *trans*-3-hexene and cyclopentene were purchased from Aldrich, distilled from $LiAlH_4$ and stored over CaH_2. 2-pentyne was purchased from Lancaster and used as received.

NMR spectra were recorded on a Bruker AM500 (500.13 MHz for ^1H, 76.77 for ^2H, 125.77 MHz for ^{13}C) spectrometer. All chemical shifts are relative to TMS using ^1H (residual), ^2H or ^{13}C chemical shifts of the solvent as a secondary standard. For ^{13}C NMR experiments, 10 second relaxation delays were used to obtain reliable integration data. Elemental analyses were carried out at the Caltech Elemental Analysis Facility by Fenton Harvey. Many of the alkyl complexes reported either decompose or form oils upon attempted isolation, thereby precluding elemental analysis.

$Cp^*_2Zr(CH_2CDMe_2)(D)$ (1). In the dry box, a J. Young NMR tube was charged with 0.50 mL of a 0.0488 M stock solution (0.0244 mmol) of $Cp^*_2ZrH_2$ and 0.094 M Cp_2Fe in benzene-d_6. On the vacuum line, the solution was frozen and degassed with three freeze-pump-thaw cycles. The tube was then fully submerged in liquid nitrogen and 1 atmosphere of D_2 was admitted. The tube was thawed, shaken and rotated at room temperature for 5 minutes after which time the solution was again frozen and the tube evacuated. Via a 6.9 mL calibrated gas volume, 76 Torr (0.028 mmol) of isobutene was added at -196 °C. The tube was then thawed and shaken and monitored by ^1H NMR spectroscopy. ^1H NMR (benzene-d_6): δ = 1.93 (s, 30 H, Cp*), -0.049 (s, 2H, CH_2CDMe_2), 1.02 (s, 6H, CH_2CDMe_2). ^2H NMR (benzene): δ = 6.36 (s, 1D, Zr-*D*), 1.91 (s, 1D, CH_2CDMe_2).

Isomerization of 1 and 2 as monitored by $\{^1H\}^2H$ NMR. In the dry box, a flame-sealable NMR tube was charged with 0.50 mL of a 0.166 M stock solution **1** or **2** containing 10 µL of benzene-d_6 in C_6H_6. On the vacuum line, the solution was frozen and degassed with three freeze-pump-thaw cycles. The entire tube was then immersed in liquid nitrogen and 1 atmosphere of D_2 was admitted. The tube was thawed and rotated. After five minutes, the tube was again frozen and isobutene (230 Torr, 6.9 mL, 0.085 mmol) was added via calibrated gas volume. The tube was then sealed with a torch, thawed and placed in a thermostated bath. Approximately 8-10 spectra were recorded at regular intervals during the course of the reaction and the intensity of each peak was measured by integration versus the internal standard. The rate of the reaction was then plotted as an approach to equilibrium as described previously.[29]

$(\eta^5\text{-}C_5Me_4H)_2Zr(CH_2CDMe_2)(D)$ (2). This compound was prepared in the same manner as **1**. ^1H NMR (benzene-d_6): δ = 2.13 (s, 6H, C_5Me_4H), 2.07 (s, 6H, C_5Me_4H), 1.99 (s, 6H, C_5Me_4H), 1.94 (s, 6H, C_5Me_4H), 5.11 (s, 2H, C_5Me_4H), -0.07 (s, 2H, CH_2CDMe_2), 1.03 (s, 6H, CH_2CDMe_2). ^2H (benzene): δ = 5.93 (s, 1D, Zr-*D*), 2.23 (s, 1D, CH_2CDMe_2).

$Cp^*_2Zr(CH_2CH_2CH_3)(H)$. In the dry box, a J. Young NMR tube was charged with 7.0 mg (0.019 mmol) of $Cp^*_2ZrH_2$ and 0.50 mL benzene-d_6 added forming a clear solution. On the vacuum line, the tube was degassed with three

freeze-pump-thaw cycles. Via 6.9 mL calibrated gas bulb, 52 Torr (0.019 mmol) of CH_2=CH_2CH_3 was added at -196 °C. The solution was then thawed and the tube shaken. With shaking the solution turns from colorless to yellow. ^{1}H NMR (benzene-d_6): δ = 1.94 (s, 30 H, Cp*), -0.25 (m, 2H, $CH_2CH_2CH_3$), 1.86 (m, 2H, $CH_2CH_2CH_3$), 1.86 (t, ,7Hz, 3H, $CH_2CH_2CH_3$) . **Cp*$_2$Zr(^{13}CH$_2$CH$_2$CH$_3$)(H).** ^{13}C{^{1}H} NMR (benzene-d_6): δ = 55.15 ($CH_2CH_2CH_3$), 20.98 ($CH_2CH_2CH_3$).

(η^5-C$_5$Me$_4$H)$_2$Zr(CH$_2$CH$_2$CH$_3$)(H). This compound was prepared in the same manner as **1** using 8.0 mg (0.024 mmol) of (η^5-$C_5Me_4H)_2ZrH_2$ and 70 Torr (0.026 mmol) of CH_2=CH_2CH_3. ^{1}H NMR (benzene-d_6): δ = 2.26 (s, 6H, C_5Me_4H), 2.14 (s, 6H, C_5Me_4H), 2.08 (s, 6H, C_5Me_4H), 1.98 (s, 6H, C_5Me_4H), 5.43 (s, 2H, C_5Me_4H), -0.60 (m, 2H, $CH_2CH_2CH_3$), 2.29 (m, 2H, $CH_2CH_2CH_3$), 0.94 (t, 7 Hz, 3H, $CH_2CH_2CH_3$). **(η^5-C$_5$Me$_4$H)$_2$Zr(^{13}CH$_2$CH$_2$CH$_3$)(H).** ^{13}C{^{1}H} NMR (benzene-d_6): δ = 55.74 ($CH_2CH_2CH_3$), 20.24 ($CH_2CH_2CH_3$).

Isomerization of Cp*$_2$Zr(^{13}CH$_2$CH$_2$CH$_3$)(H) and (η^5-C$_5$Me$_4$H)$_2$Zr(^{13}CH$_2$CH$_2$CH$_3$)(H) by ^{13}C NMR Analysis. In the dry box, a J. Young NMR tube was charged with 0.50 mL of 0.166 M stock solution of metallocene in benzene-d_6. On the vacuum line, the solution was frozen and degassed with three freeze-pump-thaw cycles. While frozen in liquid nitrogen, $^{13}CH_2$=$CHCH_3$ was added to the tube via 6.9 mL calibrated gas volume. The tube was sealed, rotated several times and then placed in the temperature calibrated NMR probe. Approximately 8-10 spectra were recorded at regular intervals during the course of the reaction. The intensity of each peak was determined by integration and the kinetics plotted as an approach to equilibrium.

Cp*(C$_5$H$_4$-CMe$_3$)Zr(CH$_2$CH$_2$CH$_3$)(H). This compound was prepared in the same manner as **1** using 6.8 mg (0.0196 mmol) of [Cp*(C_5H_4-CMe_3)ZrH_2]$_2$ and 52 Torr (0.0196 mmol) of $^{13}CH_2$=$CHCH_3$. ^{1}H NMR (benzene-d_6): δ = 1.82 (s, 15H, Cp*), 1.40 (s, 9H, C_5H_4-CMe_3), 5.32, 4.91, 4.88, 4.20 (m, C_5H_4-CMe_3), 5.94 (s, 1H, Zr-*H*), -0.50 (m, 2H, $CH_2CH_2CH_3$), 2.10 (m, $CH_2CH_2CH_3$), 1.07 (t, 6 Hz, 3H, $CH_2CH_2CH_3$).**Cp*(C$_5$H$_4$-CMe$_3$)Zr(^{13}CH$_2$CH$_2$CH$_3$)(H).** ^{13}C{^{1}H} NMR (benzene-d_6): d = 55.07 ($CH_2CH_2CH_3$), 21.33 ($CH_2CH_2CH_3$).

$Cp_2Zr(CH_2CHMe_2)(Cl)$. In the dry box, a J. Young NMR tube was charged with 9.0 mg (0.035 mmol) of **3** and benzene-d_6 added. On the vacuum line, the tube was frozen in liquid nitrogen and degassed with three freeze-pump-thaw cycles. Via calibrated gas volume, 108 Torr (0.040 mmol) of isobutene was added at -196 °C. The tube was thawed and rotated. With time, dissolution of **3** was observed with formation of a bright yellow solution. ^{1}H NMR (benzene-d_6): δ = 6.24 (s, 10H, C_5H_5), 0.968 (d, 6.4 Hz, 2H, CH_2CHMe_2), 2.20 (sept., 6.5 Hz, 1H, CH_2CHMe_2), 0.849 (d, 6.5 Hz, 6H, CH_2CHMe_2). ^{13}C NMR (benzene-d_6): δ = 110.94 (C_5H_5); 50.27 (CH_2CHMe_2); 38.44 (CH_2CHMe_2); 13.79 (CH_2CHMe_2).

$Cp_2Zr(CH_2CH_2CH_2CH_3)(Cl)$. In the dry box, a J. Young NMR tube was charged with 15.0 mg (0.058 mmol) of **3** and benzene-d_6 added. On the vacuum line, the tube was degassed with three freeze-pump-thaw cycles. Via calibrated gas bulb, 165 Torr (0.061 mmol) of 1-butene was added at -196 °C. The solution was then thawed, and the tube shaken. With shaking the white solid dissolves forming a yellow solution. ^{1}H NMR (benzene-d_6): δ = 5.77 (s, 10H, C_5H_5), 1.10 (m, 2H, $CH_2CH_2CH_2CH_3$), 1.58 (pent., 7.2 Hz, 2H, $CH_2CH_2CH_2CH_3$), 1.37 (m, 7.3 Hz, 2H, $CH_2CH_2CH_2CH_3$), 1.02 (t, 7.3 Hz, 3H, $CH_2CH_2CH_2CH_3$). ^{13}C NMR (benzene-d_6): δ = 112.86 (C_5H_5), 55.55 ($CH_2CH_2CH_2CH_3$), 37.16 ($CH_2CH_2CH_2CH_3$), 29.72 ($CH_2CH_2CH_2CH_3$), 14.38 ($CH_2CH_2CH_2CH_3$).

$Cp_2Zr(CH_2CHDCH_2CH_3)(Cl)$. A sample was prepared in an identical manner to that described above with 35.0 mg (0.135) of **3-d**. $\{^1H\}^2H$ NMR (benzene): δ = 1.51 (s, 1D, $CH_2CDHCH_2CH_2CH_3$).

$Cp_2Zr(CH_2CH_3)(Cl)$. In the dry box, a J. Young NMR tube was charged with 14.0 mg (0.054 mmol) of **3** and benzene-d_6 added. On the vacuum line, the tube was degassed with three freeze-pump-thaw cycles. Via 6.9 mL calibrated gas bulb, 250 Torr (0.092 mmol) of ethylene was added at -196 °C after passage through a -80 °C trap. The solution was then thawed and the tube shaken. With shaking the white solid dissolves forming a yellow solution. ^{1}H NMR (benzene-d_6): δ = 5.76 (s, 10H, C_5H_5), 1.09 (q, 7.6 Hz, 2H, CH_2CH_3), 1.44 (t, 7.65 Hz, CH_2CH_3). ^{13}C NMR (benzene-d_6): δ = 111.57 (C_5H_5); 56.10 (CH_2CH_3); 14.70 14.70 (CH_2CH_3);

$Cp_2Zr(CH_2CH_2D)(Cl)$. A sample was prepared in an identical manner to that described above with 57.0 mg (0.220) of **3-d**. $\{^1H\}^2H$ NMR (benzene) δ = 1.38 (s, 1D, CH_2CH_2D).

$Cp_2Zr(CH_2CH_2CH_3)(Cl)$. In the dry box, a J. Young NMR tube was charged with 5.0 mg (0.014 mmol) of **3** and benzene-d_6 added. On the vacuum line, the tube was degassed with three freeze-pump-thaw cycles. Via calibrated gas bulb, 60 Torr (0.022 mmol) of CH_2=$CHCH_3$ was added at -196 °C. The solution was then thawed and the tube shaken. With shaking the white solid dissolves forming a yellow solution. ^1H NMR (benzene-d_6): δ = 5.77 (s, 10H, C_5H_5), 1.09 (m, 2H, $CH_2CH_2CH_3$), 1.50 (m, 2H, $CH_2CH_2CH_3$), 1.01 (t, 7 Hz, 3H, $CH_2CH_2CH_3$). **$Cp_2Zr(^{13}CH_2CH_2CH_3)(Cl)$.** ^{13}C NMR (benzene-d_6): δ = 58.72 ($CH_2CH_2CH_3$).

$Cp_2Zr(cyclo\text{-}C_5H_9)(Cl)$. In the dry box, a 25 mL round bottom flask equipped with stir bar was charged with 0.430 g (1.67 mmol) of **3** and a 180° needle valve was attached. On the vacuum line, approximately 10 mL of Et_2O was added by vacuum transfer at -78 °C. While at -78 °C, 400 Torr of cyclopentene was added. The reaction was backfilled with argon and warmed to room temperature with stirring. Over the course of several hours, a clear yellow solution forms. The reaction was continued for 12 hours and then all volatiles were removed *in vacuo*. The reaction flask was transferred onto a swivel frit assembly and the yellow solid extracted with Et_2O. The Et_2O was removed in vacuo leaving a yellow solid. The solid was recrystallized from Et_2O at -40 °C in the dry box freezer. Yield of product: 0.350 g (63.5%). ^1H NMR (benzene-d_6): δ = 5.79 (s, 10H, C_5H_5), 1.59 (m, 1H, C_5H_9), 1.67 (m, 2H, C_5H_9), 1.46 (m, 2H, C_5H_9), 1.45 (m, 2H, C_5H_9), 1.92 (m, 2H, C_5H_9). Anal. for $C_{15}H_{19}Zr_1Cl_1$: C: 55.27% H: 5.87%. Found C: 54.97%, H: 5.90%.

$Cp_2Zr(CH_3)(CH_2CH_2CH_3)$. In the dry box, a J. Young NMR tube was charged with 5.0 mg (0.021 mmol) of $[Cp_2Zr(CH_3)(H)]_2$ and benzene-d_6 added. On the vacuum line, the tube was degassed with three freeze-pump-thaw cycles. Via 6.9 mL calibrated gas bulb, 60 Torr (0.022 mmol) of $^{13}CH_2$=$CHCH_3$ was added at -196 °C. The solution was then thawed and the tube shaken. With shaking the white solid dissolves forming a yellow solution. The sample was placed in the NMR probe and monitored by ^{13}C and ^1H NMR spectroscopy. ^1H NMR

(benzene-d_6): δ = 5.71 (s, 10H, C_5H_5), 0.113 (s, 3H, Zr-CH_3), 0.518 (m, 2H, $CH_2CH_2CH_3$), 1.66 (m, 2H, $CH_2CH_2CH_3$), 1.03 (t, 6.8 Hz, 3H, $CH_2CH_2CH_3$). **$Cp_2Zr(CH_3)(^{13}CH_2CH_2CH_3)$.** ^{13}C NMR (benzene-d_6): δ = 57.72 ($CH_2CH_2CH_3$), 27.34 ($CH_2CH_2CH_3$).

Addition of *cis*-2-Butene to 3. Identification of 9. In the dry box, a J. Young NMR tube was charged with 14.0 mg (0.054 mmol) of **3** and benzene-d_6 added. On the line the tube was degassed with three freeze-pump-thaw cycles. Via calibrated gas volume, 220 torr (0.081 mmol) of *cis*-2-butene added at -196 °C. The tube was thawed and shaken. With time, the white solid dissolves forming a clear yellow solution. ^1H NMR (benzene-d_6) **9**: δ = 5.78 (s, 10H, C_5H_5), 1.27 (d, 6.9 Hz, 3H, $CH(CH_3)CH_2CH_3$), 1.22 (m, 2H, $CH(CH_3)CH_2CH_3$), 1.72 (m, 1H, $CH(CH_3)CH_2CH_3$), 0.973 (t, 7.1 Hz, 3H, $CH(CH_3)CH_2CH_3$). ^{13}C NMR (benzene-d_6): δ = 112.50 (C_5H_5), 62.86 ($CH(CH_3)CH_2CH_3$), 33.46 $CH(CH_3)CH_2CH_3$), 22.74 ($CH(CH_3)CH_2CH_3$), 15.74 ($CH(CH_3)CH_2CH_3$).

Addition of 1-Pentene to 9. In the dry box, a J. Young NMR tube was charged with 8.0 mg (0.031 mmol) of **3** and benzene-d_6 added. On the vacuum line, the tube was degassed with three freeze-pump-thaw cycles. Via calibrated gas volume, 90 Torr (0.033 mmol) of *cis*-2-butene was added. The tube was sealed and the solution thawed. The tube was rotated for until all solid had dissolved (~3 hours). The NMR spectrum was recorded to verify the disappearance of starting materials. The tube was again placed on the vacuum line and via calibrated gas volume, 90 Torr (0.033 mmol) of 1-pentene was added. The solution was thawed and the tube shaken. ^1H NMR spectra were then recorded in several intervals over the course of 24 hours.

Preparation of 1-^{13}C-2-heptyne. In the dry box, a 100 mL round bottom flask equipped with stir bar was charged with 2.00 g (22.7 mmol) [Li][C≡$CCH_2CH_2CH_2CH_3$] and a 180° needle valve was attached. On the vacuum line, the flask assembly was evacuated and ~30 mL ammonia was condensed onto the white solid at -78 °C. Against an Ar counterflow, 3.18 g (22.7 mmol) $^{13}CH_3I$ was added via syringe with stirring. The reaction mixture was warmed to -50 °C and the clear, colorless solution was stirred forming a white precipitate. The reaction was stirred for 2 hours after which time the reaction was warmed to 0 °C and the NH_3 allowed to escape via an oil bubbler. In air, 10

mL of water was added and the organic layer collected. Clear organic layer was dried over $MgSO_4$, followed by CaH_2. Product was identified as 1-^{13}C-2-heptyne by comparison to the ^{1}H and ^{13}C NMR spectra of the authentic material. Yield 1.80 g (82.5 %).

Preparation of 1-^{13}C-*cis*-2-heptene. In the dry box, a 100 mL round bottom flask equipped with stir bar was charged with 3.67 g (14.5 mmol) of $Cp_2Zr(H)(Cl)$ and a 180° needle valve was attached. On the vacuum line, approximately 25 mL of Et_2O was added by vacuum transfer. Against an Ar counterflow at -80 °C, 1-^{13}C-2-heptyne was added via syringe. The reaction was warmed to room temperature and stirred for 2 days. With time, the white suspension turned into a cloudy yellow solution. The reaction was quenched at 0 °C by addition of 10 mL H_2O. An additional 50 mL of water was added and the organic layer collected and dried over $MgSO_4$. Ether was removed by atmospheric distillation. The clear, colorless liquid product was then distilled from CaH_2 and then vacuum transferred from $LiAlH_4$. Yield: 0.340 g (24%). The product was characterized by comparison of the ^{1}H and ^{13}C NMR spectra with authentic samples.

Reaction of 3 with 1-^{13}C-*cis*-2-heptene. In the dry box, a screw-capped NMR tube was charged with 10.0 mg (0.0394 mmol) of **3** and benzene-d_6 added. To the tube, 45 µL of a 1.0 M stock solution of 1-^{13}C-*cis*-2-heptene in benzene-d_6 was added. The tube was shaken and placed in the NMR probe. Spectra were recorded over the course of 44 hours.

Hydrozirconation of *cis*-2-butene and *cis*-2-heptene: CH_3OD Quench. In the dry box, a J. Young NMR tube was charged ~25 mg of **3**, and C_6H_6 and 10 µL of benzene-d_6 added. On the vacuum line, the solution was frozen in liquid nitrogen and the tube evacuated. Via calibrated gas volume, olefin was added to the tube at -196 °C. The solution was frozen and rotated continuously at room temperature for the 12 hours. The solution was then frozen in liquid nitrogen and 20 µL of CH_3OD was added via microsyringe. The tube was capped, thawed and shaken. The yellow solution turns clear with formation of white precipitate. The {^{1}H}^{2}H NMR spectrum was then recorded and the amount of internally deuterated alkane versus terminally deuterated alkane was determined by integration.

Hydrozirconation of *cis*-2-heptene - CH_3OD Quench: Identification of Internal Heptanes. An identical procedure to that described above was followed except that after one hour, the reaction mixture was passed through a syringe filter in the dry box to remove any unreacted **3**. The clear yellow solution was frozen at -196 °C, CH_3OD added and the tube was capped, thawed and shaken and the $\{^1H\}^2H$ NMR spectrum was recorded.

Structure Determination for 8. A suitable fragment was cut from a single crystal of **8**, attached to a glass fiber and centered on an Enraf-Nonius CAD-4 diffractometer under an 85 K stream of N_2 gas. Unit cell parameters were obtained from the setting angles of 25 high angle reflections. Two equivalent data sets were collected and merged in $P2_12_12_1$. Three reference reflections were measured every 75 minutes to monitor crystal decay. The structure was solved using direct methods and the difference Fourier maps were used to locate all missing atoms, including hydrogens. 5917 data were refined to R = 0.0287 (GOF = 1.78).

Acknowledgments. This work has been supported by USDOE Office of Basic Energy Sciences (Grant No. DE-FG03-85ER13431) and Exxon Chemicals America.

Supplementary Information Available: ORTEP drawings showing the complete atom labeling schemes, cell and crystal packing diagrams, tables of atomic coordinates, complete bond distances and angles and anisotropic diplacement parameters for **8**.[30] See any masthead page for ordering or Internet access instructions.

References.

* The work in this chapter has been published previously. See Chirik, P.J.; Day, M.W.; Labinger, J.A.; Bercaw, J.E. *J. Am. Chem. Soc.* **1999**, *121*, 10308.

1. Collman, J.P.; Hegedus, L.S.; Norton, J.R.; Finke, R.G. *Principles and Applications of Organotransition Metal Complexes*: University Science Books, Mill Valley, CA, 1987.

2. For a recent example of phosphine ligand effects on rhodium-catalyzed hydroformylation see: Casey, C.P.; Paulsen, E.L.; Beuttenmueller, E.W.; Proft, B.R.; Matter, B.A.; Powell, D.R. *J. Am. Chem. Soc.* **1999**, *121*, 63.

3. (a) Hart, D.W.; Schwartz, J. *J. Am. Chem. Soc.* **1974**, *96*, 8115.
(b) Schwartz, J.; Labinger, J.A. *Angew. Chem. Int. Ed. Engl.* **1976**, *15*, 333.

4. (a) Negishi, E.; Takahashi, T. *Synthesis* **1988**, 1.
(b) Wipf, P.; Takahashi, H.; Zhuang, N. *Pure and Appl. Chem.* **1998** *70*, 1077.
(c) Labinger, J.A. In *Comprehensive Organic Synthesis*. Trost, B.M.; Fleming, I. Eds. Pergamon Press, Oxford (1991), Chapter 3.9.

5. Brintzinger, H.H.; Fischer, D.; Mülhaupt, R.; Reiger, B.; Waymouth, R.M. *Agnew. Chem. Int. Ed. Engl.* **1995**, *34*, 1143.

6. (a) Busico, V.; Cipullo, R. *J. Am. Chem. Soc.* **1994**, *116*, 9329.
(b) LeClerc, M.; Brintzinger, H.H. *J. Am. Chem. Soc.* **1995**, *117*, 1651.
(c) Busico, V.; Caporaso, L.; Cipullo, R.; Landriani, L.; Angelini, G.; Margonelli, A.; Segre, A.L. *J. Am. Chem. Soc.* **1996**, *118*, 2105.

7. Busico, V.; Cipullo, R.; Chadwick, J.C.; Modder, J.F.; Sudmeijer, O. *Macromolecules* **1994**, *27*, 7538.

8. Chirik, P.J.; Day, M.W.; Bercaw, J.E. *Organometallics*, **1999**, *18*, 1873.

9. Chapter 3.

10. Exchange between the hydride ligand and the coordinated alkyl is also observed, producing complexes with two deuterium labels in the isobutyl group and hydrogen on zirconium.

11. McAlister, D.R.; Erwin, D.K.; Bercaw, J.E. *J. Am. Chem. Soc.* **1978**, *100*, 5966.

12. Buchwald, S.J.; LaMaire, S.J.; Nielson, R.B.; Watson, B.T.; King, S.M. *Tetrahedron Lett.* **1987**, *28*, 3895.

13. (a) Nelson, J.E.; Bercaw, J.E.; Labinger, J.A. *Organometallics* **1989**, *8*, 2404.
(b) Erker, G.; Kropp, K.; Atwood, J.L.; Hunter, W.E. *Organometallics* **1983**, *2*, 1555.
(c) Gibson, T. *Organometallics* **1987**, *6*, 918.

14. Jordan, R.F.; Bajgur, C.S.; Dasher, W.E.; Rheingold, A.L. *Organometallics* **1987**, *6*, 1041.

15. A small amount of $Cp_2Zr\{(CH(CH_3)(CH_2)_4{}^{13}CH_3\}(Cl)$ may be formed during the isomerization reaction, but we are unable to detect such a species due to overlapping ^{13}C NMR resonances (see Figure 4).

16. Burger, B.J.; Thompson, M.E.; Cotter, W.D.; Bercaw, J.E. *J. Am. Chem. Soc.* **1990**, *112*, 1566.

17. This complex slowly decomposes in solution over the course of several days at room temperature. Access to Zr(II)-derived compounds from dialkyl zirconocenes has been noted previously. See, for example,

Negishi, E.I.; Montchamp, J.L. in *Metallocenes, Vol. 1;* Togni A.; Halterman, R.L., Eds.; VCH: Weinheim, 1998, Chapter 5.

18. Lauher, J.W.; Hoffman, R. *J. Am. Chem. Soc.* **1976**, *98*, 1729.

19 Current studies are underway to measure the rates of isomerization in related alkyl zirconocene cations. Wendt, O.F.; Bercaw, J.E., unpublished results.

20. Gell, K. I.; Posin, B.; Schartz, J.; Williams, G. M. *J. Am. Chem. Soc.* **1982**, *104*, 1840.

21. Negishi, E.; Miller, J.A.; Yoshida, T. *Tetrahedron Lett.* **1984**, *25*, 3407.

22. Annby, U.; Alvhäll, J.; Gronowitz, S.; Hallberg, A. *J. Organomet. Chem.* **1989**, *377*, 75.

23. Secondary alkyls have been observed for styrene and other related aryl substrates: see reference 13a.

24. Relative rates of isomerization suggest that a detectable amount of **13-d$_2$** should form during isomerization to **8-d$_2$**. To date, we have been unable to detect such an intermediate by $^2H\{^1H\}$ NMR.

25. Molecular mechanics calcuations (MM2 level) were performed using CAChe molecular modeling software using the structural parameters obtained from the solid state structure of **11**.

26. Burger, B.J.; Bercaw, J.E. In *Experimental Organometallic Chemistry*; ACS Symposium Series No. 357; Wayda, A.L.; Darensbourg, M.Y. Eds.; American Chemical Society: Washington, DC 1987; Chapter 4.

27. Marvich, R.H.; Brintzinger, H.H. *J. Am. Chem. Soc.* **1971**, *93*, 2046.

28. Schock, L.E.; Marks, T.J. *J. Am. Chem. Soc.* **1988**, *110*, 7701.

29. Moore, J.W.; Pearson, R.G. *Kinetics and Mechanism*, 3rd Ed; John Wiley & Sons, New York (1981) p. 307.

30. Crystallographic data have been deposited at CCDC, 12 Union Road, Cambridge CB2 1EZ, UK, and copies can be obtained on request free of charge, by quoting the publication citation and the deposition number 114941.

Chapter 5

Kinetic Isotope Effects for β-Methyl Elimination. Experimental Observation of γ-Agostic Interactions during the Ziegler-Natta Polymerization of Olefins.

Abstract

Preparation of isotopically labeled zirconocene-neopentyl methyl complexes of the general formula, $(CpR_n)_2Zr(CH_3)(CH_2C(CH_3)_2CD_3)$ (CpR_n = alkyl substituted cyclopentadienyl), has been accomplished via salt metathesis of d_3-$LiCH_2C(CH_3)_2CD_3$ with $(CpR_n)_2Zr(CH_3)(Cl)$. Addition of $B(C_6F_5)_3$ to $(CpR_n)_2Zr(CH_3)(CH_2C(CH_3)_2CD_3)$ results in β-methyl elimination forming the ion-pair species, $[(CpR_n)_2ZrMe][MeB(C_6F_5)_3]$, along with isotopomers of isobutene. Comparison of the relative amounts of d_3 to d_0-isobutene affords the kinetic isotope effect for β-methyl elimination. For $Cp_2Zr(CH_3)(CH_2C(CH_3)_2CD_3)$, a kinetic isotope effect of 1.40(2) has been measured at 296 K. Normal secondary kinetic isotope effects have been observed for a total of five metallocenes and the magnitude of these effects is essentially invariant with ligand array. These effects are indicative of γ-agostic assistance in the transition state for β-methyl elimination.

Introduction

Agostic interactions,[1] whereby a C-H sigma bond forms a three-center, two electron covalent bond to a transition metal center are now ubiquitous in organometallic chemistry and have been identified in many catalytic reactions.[2] In metallocene-catalyzed olefin polymerization, agostic interactions are believed to play a central role in lowering the activation barriers for olefin insertion[3] as well as increasing degrees of stereospecificity.[4] Experimental observation of α-agostic interactions during olefin insertion into a metal carbon bond (Figure 1) was first achieved using isotopic perturbation of stereochemistry[5] during the catalytic hydrocyclization of *trans*-deuterated α, ω-dienes with scandocene and yttrocene catalysts.[6,7] More recent studies by Brintzinger have identified α-agostic interactions during the hydrodimerization of deuterated 1-hexene[8] as well as during the polymerization of (*E*) and (*Z*)-propene-d_1 with *ansa*-zirconocene catalysts.[9] The β-agostic ground state structure has been identified in a number of group 3[10] and group 4 metallocenes and is believed to be the catalyst resting state during polymerization.[11]

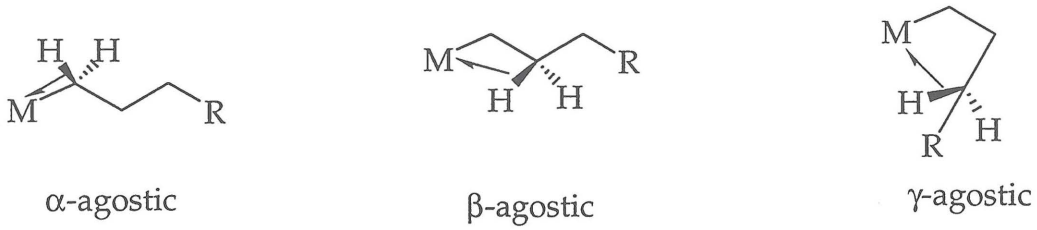

Figure 1. Types of agostic interactions.

In addition to these interactions, γ-agostic structures have also been proposed in several Ziegler-Natta polymerization systems. Theoretical studies have identified γ-agostic alkyls as kinetic products following olefin insertion[12] as well as possible resting states for the active species.[13] Experimental observation of γ-agostic interactions has been achieved in the solid state structures of $Cp^*_2YCH(SiMe_3)_2$ ($Cp^* = C_5Me_5$), $Cp^*_2YN(SiMe_3)_2$,[14] and $RuCl_2(PPh_3)(N(SiMe_3)C(Ph)(NH(PPh_2)))$[15] and by NMR chemical shifts in tantalum carborane complexes.[16]

β-Methyl elimination (eq. 1) is well suited for experimental detection of γ-agostic interactions, being the microscopic reverse of olefin insertion into a metal methyl bond and as a result must access the same transition state. Chain termination by β-methyl elimination has been identified in several olefin polymerization systems[17] and has also been observed in organoscandium complexes.[18] Horton has described the preparation of $[(CpR_n)_2Zr(CH_2CMe_3)][CH_3B(C_6F_5)_3]$ ($CpR_n = C_5H_5, C_5Me_5$) which undergoes β-methyl elimination resulting in formation of isobutene and $[(CpR_n)_2Zr(Me)][MeB(C_6F_5)_3]$.[19] Due to their utility in olefin polymerization,[20] we felt that isotopic modification of the complexes originally described by Horton would be a logical choice to identify γ-agostic interactions in metallocene polymerization catalysts.

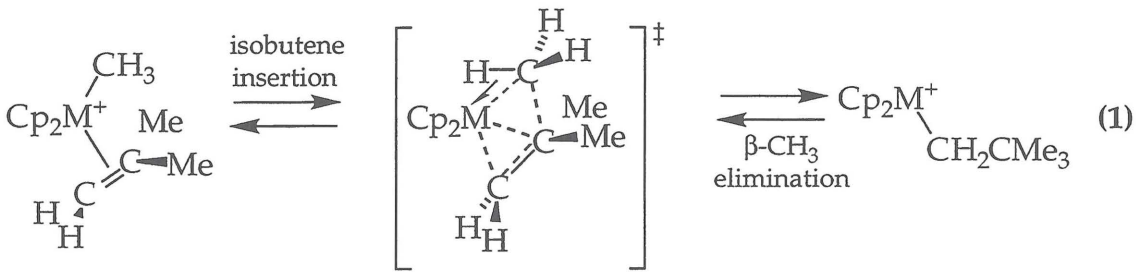

Results and Discussion

The strategy employed for the synthesis of isotopically labeled zirconocene neopentyl methyl complexes involved initial preparation of the zirconocene methyl chloride complexes followed by salt metathesis with labeled neopentyl lithium affording the desired zirconocene methyl neopentyl complex. Preparation of $Cp_2Zr(CH_3)(Cl)$ has been accomplished according to literature procedures[21] whereas $Cp^*_2Zr(CH_3)(Cl)$, $Cp^*(C_5Me_4)Zr(CH_3)(Cl)$, *rac*-(EBI)$Zr(CH_3)(Cl)$ and $ThpZr(CH_3)(Cl)$ were prepared via slow addition of one equivalent of HCl to the corresponding dimethyl complex (eq. 2).[22]

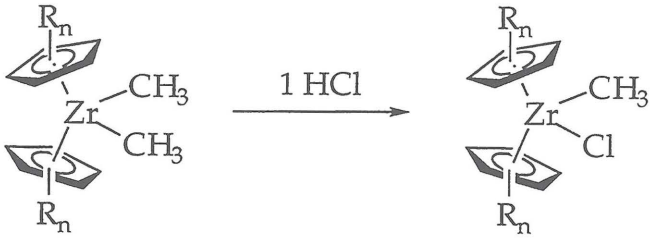

(2)

Preparation of $LiCH_2C(CH_3)_2CD_3$ proceeded via alkylation of ethyl isobutyrate with CD_3I followed by reduction of the ester to the alcohol via addition of lithium aluminum hydride (eq. 3). Conversion of $CD_3(CH_3)_2CCH_2OH$ to the bromide was accomplished with addition of Ph_3PBr_2 which is formed *in situ* by addition of Br_2 to triphenylphosphine. Lithium-halogen exchange in refluxing petroleum ether affords $LiCH_2C(CH_3)_2CD_3$ in modest yield. Addition of $LiCH_2C(CH_3)_2CD_3$ to the zirconocene methyl-chloride complexes affords the desired dialkyl complexes. In this manner, $Cp_2Zr(CH_2C(CH_3)_2CD_3)(Me)$ (**1**), $Cp^*_2Zr(CH_2C(CH_3)_2CD_3)(Me)$ (**2**), $Cp^*(C_5Me_4H)Zr(CH_2C(CH_3)_2CD_3)(Me)$ (**3**), *rac*-$(EBI)Zr(CH_2C(CH_3)_2CD_3)(Me)$ (**4**) and $ThpZr(CH_2C(CH_3)_2CD_3)(Me)$ (**5**) have been prepared in >95% isotopic purity.[22]

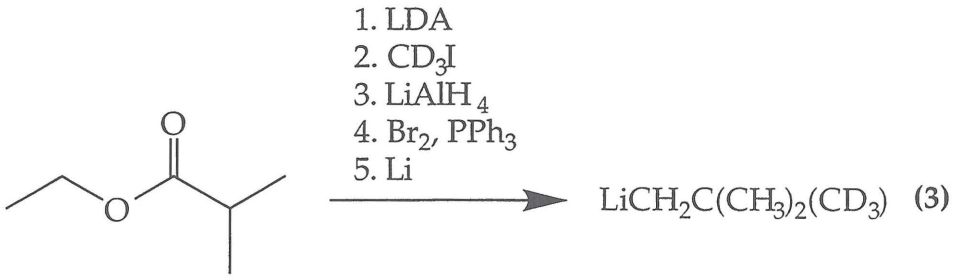

(3)

Slow cooling of a diethyl ether solution of **1** affords yellow columns that are suitable for X-ray diffraction. The molecular structure of **1** is shown in Figure 2 and displays a commonly observed coordination mode for zirconocenes. All of the hydrogen atoms have been located in the difference map and have been refined. No ground state γ-agostic interactions are observed since the closest zirconium-γ-hydrogen distance found in **1** is 3.774 Å.

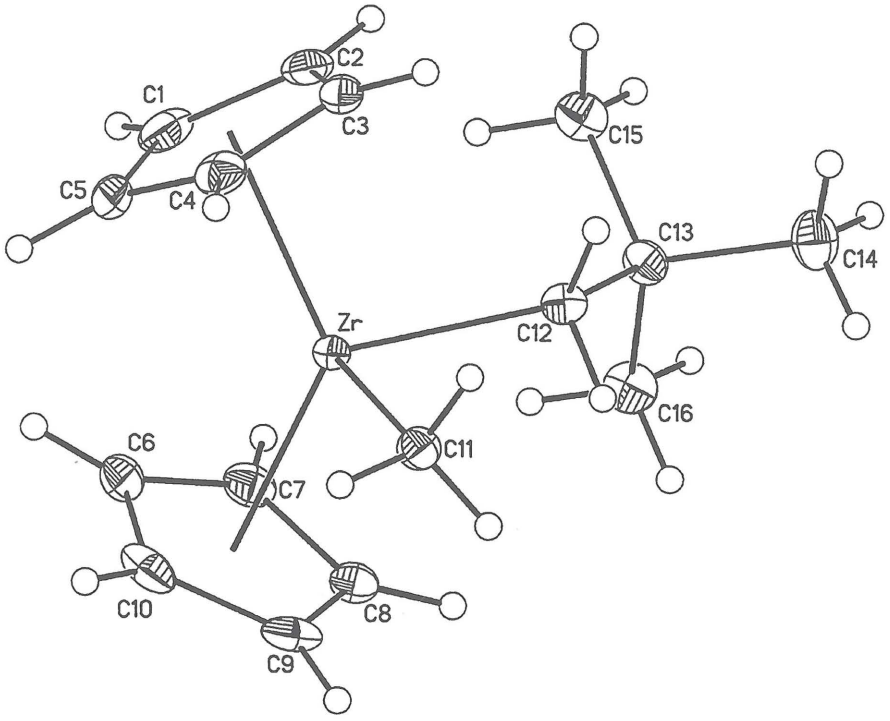

Figure 2. Molecular structure of $Cp_2Zr(CH_2CMe_3)(CH_3)$ (**1**) with 50% probability ellipsoids. Selected bond lengths (Å): Zr-Cent(1), 2.232; Zr-Cent(2), 2.234; Zr-C(11), 2.2980(13); Zr-C(12), 2.2719(12). Bond angles (deg): Cent(1)-Zr-Cent(2), 130.6; C(11)-Zr-C(12), 94.99. Cent(1) is the centroid formed by C(1), C(2), C(3), C(4) and C(5). Cent(2) is the centroid formed by C(6), C(7), C(8), C(9) and C(10).

Time (min)	%-isobutene-d_0	%-isobutene-d_3	%-isobutene-d_6	Total Isobutene (mmol)	% Conversion
2.0	26.7	73.3	< 0.1	1.60×10^{-3}	2.48
10.0	26.1	73.9	< 0.1	1.93×10^{-2}	29.9
18.0	26.1	73.9	< 0.1	3.14×10^{-2}	48.6
26.0	26.2	73.8	< 0.1	4.10×10^{-2}	63.6
45.0	27.2	72.5	0.2	4.94×10^{-2}	76.6
120.0	33.8	64.4	1.8	5.14×10^{-2}	79.7

Table 1. Distribution of isotopomers for the β-methyl elimination for **1** at 296 K.

Reaction of **1** with $B(C_6F_5)_3$ results in β-methyl elimination initially forming d_3 and d_0-isobutene along with $[Cp_2ZrMe][MeB(C_6F_5)_3]$. Monitoring the headspace of the reaction by GC/MS allows for quantification of each of the isotopomers produced. Control experiments determining the detector response to different isotopomers of isobutene have been performed. Plots of detector response versus concentration of d_0 and d_8-isobutene ranging from 0.5 M to 2.0 M have been constructed in order to determine the isotope effect, if any, on fragmentation. The detector response for d_0-isobutene (slope = 416 response/M; $R^2 = 0.992$) is almost identical to that for the d_8 isotopomer (slope = 410 response/M; $R^2 = 0.989$).

At early reaction times during the β-methyl elimination of **1**, only d_0- and d_3-isobutene are detected, but as the reaction progresses d_6-isobutene gradually appears (Table 1). Competing reactions such as allylic activation of the isobutene by $[Cp_2ZrCH_3][MeB(C_6F_5)_3]$ at longer reaction times complicates the observed values of the kinetic isotope effect (Figure 3).[19] Likewise, competing insertion of d_3-isobutene into $[Cp_2ZrCD_3][MeB(C_6F_5)_3]$ followed by β-methyl elimination accounts for formation of the d_6 isotopomer (Figure 4). As a result, all kinetic isotope effects reported are from early conversion where the reaction is devoid of these competing processes.

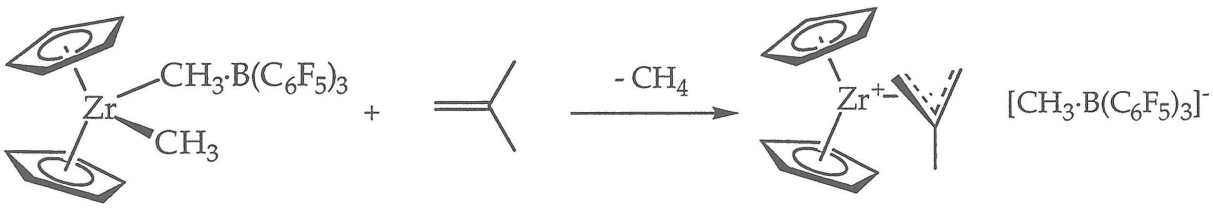

Figure 3. Allylic activation of isobutene by zirconocene methyl cations forming zirconocene crotyl complexes.

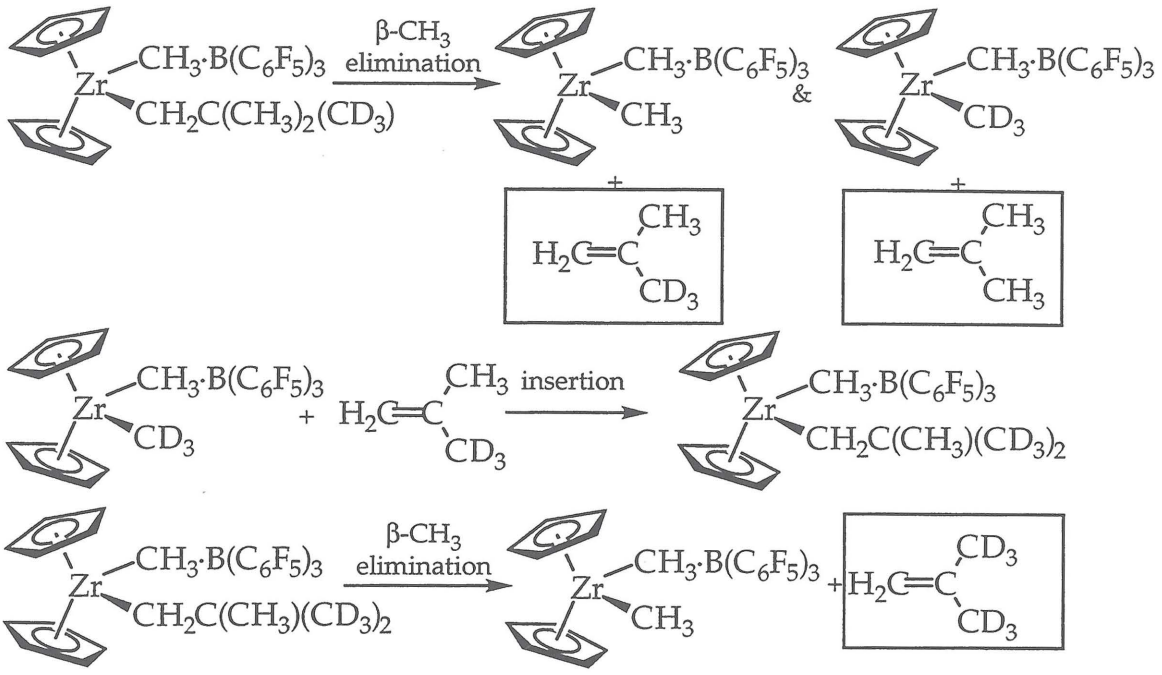

Figure 4. Reversible β-methyl elimination and olefin insertion to form d_6-isobutene.

For **1**, a normal, secondary kinetic isotope effect (k_H/k_D) of 1.40(2) is observed at 296 K. A normal isotope effect is consistent with a transition state γ-agostic interaction during C-C bond breaking. Moreover, this transition state effect is consistent with the α-agostic transition state observed for olefin insertion.[6] If the γ-agostic interaction were to occur primarily in the ground state, an inverse kinetic isotope effect would be expected due to the relative stability of the C-H agostic methyl group versus the C-D fragment.[26] However, a normal secondary isotope effect is not sufficient to rule out rapid interconversion between C-H and C-D ground state structures. However, the lack of a substantial ground state interaction is consistent with strong ion-pair formation observed previously by Horton based on ^{19}F NMR chemical shifts.[19] It should also be noted that similar, normal secondary hyperconjugative isotope effects have been observed in carbonium ion rearrangements.[23]

The effect of temperature on the kinetic isotope effects during the β-methyl elimination reaction has been studied with **1**. As the temperature is raised, the value of the isotope effect decreases. At 5 °C, a k_H/k_D = 1.49(6) has been measured whereas at 35 °C, a k_H/k_D = 1.35(3) is observed. The

temperature dependence of the isotope effect is consistent with a transition state γ-agostic interaction.[23]

Reaction of **2-5** with $B(C_6F_5)_3$ also results in β-methyl elimination and formation of d_0 and d_3-isobutene. As with **1**, normal kinetic isotope effects are observed at 296 K (Table 2) and at early reaction times. For **1-4**, the value of the kinetic isotope effect is essentially invariant with catalyst structure. However, for the doubly-silylene linked **5**, a smaller kinetic isotope effect of 1.28(6) is observed. In all cases, d_6 -isobutene is observed at longer reaction times indicative of reversible olefin insertion (Figure 3).

Complex	k_H/k_D (296 K)
$[Cp_2Zr(d_3\text{-Np})][MeB(C_6F_5)_3]$	1.40(2)
$[Cp^*(C_5Me_4H)Zr(d_3\text{-Np})][MeB(C_6F_5)_3]$	1.38(2)
$[Cp^*_2Zr(d_3\text{-Np})][MeB(C_6F_5)_3]$	1.43(5)
rac-(EBI)$Zr(d_3\text{-Np})][MeB(C_6F_5)_3]$	1.49(4)
$THPZr(d_3\text{-Np})][MeB(C_6F_5)_3]$	1.28(6)

Table 2. Kinetic isotope effects for β-methyl elimination with a series of zirconocene catalysts.

Conclusions

In summary, the first experimental observation of a γ-agostic interaction has been achieved during the β-methyl elimination of isotopically labeled isobutene from zirconocene neopentyl cations. From the magnitude of these effects, it appears that these interactions occur primarily in the transition state and are essentially independent of ancillary ligation. Since β-methyl elimination is the microscopic reverse of olefin insertion, the observed isotope effects are consistent with previous studies that have identified α-agostic interactions in the transition state for olefin insertion.

Experimental

General Considerations. All air- and moisture-sensitive compounds were manipulated using standard vacuum line, Schlenk, or cannula techniques or in a drybox under a nitrogen atmosphere as described previously.[24] Argon, dinitrogen, dihydrogen, and dideuterium gases were purified over columns of MnO on vermiculite and activated molecular sieves. Solvents for air- and moisture-sensitive reactions were stored under vacuum over titanocene. Benzene-d_6 and toluene-d_8 were purchased from Cambridge Isotope Laboratories. Both solvents were dried over $LiAlH_4$ and sodium and then stored over titanocene. Ethylisobutyrate, lithium diispropylamide and bromine were purchased from Aldrich and used as received. Anhydrous hydrochloric acid was purchased from Aldrich and was subject to three freeze-pump-thaw cycles at -196 °C before use. Lithium turnings were purchased from Strem and stored under argon. Preparation of d_8-isobutene was accomplished via dehydration of $(CD_3)_3COD$ (Cambridge) with phosphoric acid. Preparation of (EBI)$ZrMe_2$,[25] $Cp_2Zr(Me)(Cl)$,[21] $Cp^*_2ZrMe_2$, $Cp^*(C_5Me_4H)ZrMe_2$,[26] THP$ZrMe_2$[27] were prepared as described previously.

NMR spectra were recorded on Bruker AM500 (500.13 MHz for ^1H, 76.77 for ^2H, 125.77 MHz for ^{13}C), JEOL Delta 400 or Varian Inova 500 spectrometers. All ^1H, ^2H and ^{13}C NMR chemical shifts are relative to TMS using ^1H (residual), ^2H or ^{13}C chemical shifts of the solvent as a secondary standard. Elemental analyses were carried out at the Caltech Elemental Analysis Facility by Fenton Harvey.

GC-MS isotopic analyses were performed on a Hewlett-Packard 5972 mass spectrometer (Hewlett Packard Co., Palo Alto, California) equipped with a Hewlett Packard model 5980 Series II gas chromatograph. Separations were achieved on a 100% dimethylpolysiloxane capillary column (60 m, 0.32 mm i.d., 5 m film thickness; Rtx®-1 Crossbond, Restek Corporation, Bellefonte, PA). Electronic pressure control was used to maintain a constant column flow of 2 mL/min. Injections were performed in split mode with a 30:1 split ratio. The column temperature was programmed from 110 °C (2 min hold) to 185 °C at 25

°C/min and then to 230 °C at 50 °C/min for 2 minutes. The second ramp was to clear benzene or toluene from the column.

The mass spectrometer was operated in the electron-impact mode with an electron energy of 70 eV at 15 Amperes emission current. The electron multiplier was operated at 2012 volts. The quadrapole was scanned from 100 to 15 m/z at a rate of 7.85 times per second. The detector response to the isotopomers of isobutene was calibrated by making stock solutions of d_0 and d_8-isobutene and determining their reponse over a concentration range of 0.5 M to 2.0 M and was found to be identical for both isotopomers. Furthermore, solutions of pure d_0 and d_3-isobutene were mixed and found to have additive responses. Determination of the amounts of d_0 (56 amu), d_3 (59 amu) and d_6 (62 amu) isobutene were integrated relative to an internal pentane standard (43 amu).

Preparation of Ethyl-d_3-2,2-Dimethylbutyrate. In the dry box, a three necked round bottom flask equipped with a magnetic stir bar was charged with 11.3 g (0.105 mol) of lithium diisopropylamide. A reflux condensor, inlet valve and an addition funnel were attached to the flask. On the Schlenk line, the flask assembly was purged with Ar for 10 minutes. Approximately 200 mL of THF was added via cannula forming a brown solution. The addition funnel was charged with 12.0 g (0.103 mol) of ethylisobutyrate and 10 mL of THF. The solution of ester was added slowly to the reaction mixture at -78 °C over the course of 10 minutes. The reaction mixture was stirred at -78 °C for one hour. Into the addition funnel, 14.9 g (0.105 mmol) of CD_3I was charged along with 10 mL of THF. The solution was dripped into the reaction mixture over the course of 15 minutes. The reaction mixture was maintained at -78 °C for an additional 30 minutes and then warmed to room temperature and stirred for 8 hours. With time, a milky yellow/white reaction mixture forms. The reaction mixture was poured into 500 mL of brine and the organic layer was collected. The aqueous layer was washed with three 50 mL portions of ether and the organic layers were combined and dried over $MgSO_4$. The ether solution was filtered and the solvent was removed via rotovap. The clear, colorless liquid was distilled at 135 °C and atmospheric pressure yielding 7.03 g (52.4%) of product. The product was identified as d_3- ethyl-2,2-dimethylbutyrate by comparison of the ^1H and ^{13}C NMR spectra of an authentic sample.

Preparation of d_3-Neopentyl Alcohol. A three necked, 500 mL round bottom flask equipped with magnetic stir bar was charged with 3.00 g (79.0 mmol) $LiAlH_4$ and a reflux condensor, addition funnel and a gas inlet were attached. On the Schlenk line, the assembly was purged with Ar for approximately 20 minutes. Via cannula, approximately 200 mL of Et_2O was added. Into the addition funnel, 5.50 g (42 mmol) of d_3- ethyl-2,2-dimethylbutyrate was charged along with 50 mL of Et_2O. The ester solution was slowly dripped into the $LiAlH_4$ slurry over the course of 30 minutes. The reaction mixture was stirred overnight. The reaction was quenched via slow and careful addition of 3.0 mL of H_2O, followed by 15 mL of 15% NaOH and then finally 3 mL of H_2O. The organic layer was collected by filtration and was washed three times with H_2O. The organic layer was dried over Na_2SO_4 and the solvent removed by rotovap leaving a clear liquid. The product was purified by atmospheric distillation at 56 ^oC, yielding 3.40 g (89%) of d_3-neopentyl alcohol. The product was identified as d_3-neopentyl alcohol by comparison of ^1H and ^{13}C NMR spectra with an authentic sample of $(CH_3)_3CCH_2OH$.

Preparation of d_3-Neopentyl Bromide. An argon purged 250 mL three necked flask equipped with magnetic stir bar was charged with 9.42 g (35.9 mmol) of PPh_3. Approximately 100 mL of dimethylformamide was added by cannula. The flask was cooled to 0 ^oC and 5.7 g (35.6 mmol) of Br_2 was added slowly via syringe. A white cloudy reaction mixture forms. The reaction mixture was warmed to room temperature and stirred for 30 minutes. Via syringe, a 50 mL solution of 3.00 g (32.9 mmol) of d_3-NpOH was added. With addition of alcohol, the solid dissolves forming a yellow solution. The reaction was stirred at room temperature for 16 hours. A distillation head was then attached to the flask and the product was distilled out of the reaction mixture at 150 ^oC and atmospheric pressure. The product was washed with water three times and dried over Na_2SO_4 yielding 1.75 g (34.5%) of a clear liquid identified as d_3-NpBr by comparison to an authentic sample of $(CH_3)_3CCH_2Br$.

Preparation of d_3-NpLi. A 100 mL flask equipped with stir bar was charged with fresh lithium turnings. Via cannula, approximately 50 mL of petroleum ether was added. Against an argon counterflow, 1.50 g (9.74 mmol) d_3-NpBr was added via syringe. The reaction mixture was refluxed for one week after which

time a milky white slurry formed. The flask was transferred onto a swivel frit assembly and filtered. The petroleum ether was removed *in vacuo* leaving 0.650 g (82.3 %) of a white powder identified as d_3-NpLi based on comparison to an authentic sample of $(CH_3)_3CCH_2Li$.

Preparation of $Cp_2Zr(d_3\text{-Np})(CH_3)$ (1). In the dry box, a 25 mL round bottom flask was charged with 0.466 g (1.71 mmol) of $Cp_2Zr(CH_3)(Cl)$ and 0.139 g (1.71 mmol) of d_3-NpLi and attached to a swivel frit assembly. On the vacuum line, approximately 10 mL of Et_2O was added by vacuum transfer. The orange reaction mixture was warmed to room temperature and stirred for 16 hours. The white precipitate was removed by filtration and washed three times with Et_2O. The solvent was removed *in vacuo* leaving an orange oily soild. The oily solid was recrystallized from cold petroleum ether yielding 0.400 g (75.3%) of a yellow powder identified as **1** based on comparision to literature data. $^2H\{^1H\}$ NMR: δ = 1.02 ppm.

Preparation of $Cp^*(C_5Me_4H)Zr(CH_3)(Cl)$. In the dry box, a 25 mL round bottom flask equipped with stir bar was charged with 0.290 g (0.767 mmol) of $Cp^*(C_5Me_4H)ZrMe_2$ and attached to a 43.48 mL calibrated gas volume. On the vacuum line, approximately 10 mL of petroleum ether was added by vacuum transfer. The gas bulb was charged with 330 torr (0.767 mmol) of anhydrous HCl. The HCl was added to the solution at room temperature. The reaction mixture was stirred for 13 hours over which time a white precipitate forms. The flask was tranferred onto a swivel frit and the white solid collected by filtration and washed with petroleum ether. Solid dried *in vacuo* leaving 0.200 g (65.4%) of $Cp^*(C_5Me_4H)Zr(CH_3)(Cl)$. ^1H NMR (benzene-d_6) δ = 1.81 (s, 15H, $C_5\mathit{Me}_5$), 2.10 (s, 3H, $C_5\mathit{Me}_4H$), 1.92 (s, 3H, $C_5\mathit{Me}_4H$), 1.76 (s, 3H, $C_5\mathit{Me}_4H$), 1.45 (s, 3H, $C_5\mathit{Me}_4H$), 4.73 (s, 3H, $C_5Me_4\mathit{H}$), -0.02 (s, 3H, Zr*Me*) . ^{13}C NMR (benzene-d_6) 12.39 ($C_5\mathit{Me}_5$), 12.04, 12.11, 12.72, 12.82 ($C_5\mathit{Me}_4H$), 107.46 (C_5Me_5), 106.45, 105.59, 119.81 (C_5Me_4H), 2 peaks *not located* , 38.06 (Zr*Me*). Anal. Calcd. for $Zr_1C_{20}H_{31}Cl_1$: C, 60.34 H, 7.85. Found C, 60.72 H, 8.29.

Preparation of $Cp^*_2Zr(Me)(Cl)$. In the dry box, a 50 mL flask was charged with 0.740 g (1.89 mmol) of $Cp^*_2ZrMe_2$ and attached to a calibrated gas volume. On the vacuum line, approximately 25 mL of petroleum ether was added by vacuum transfer forming a clear solution. The 104 mL bulb was charged with 340 torr

(1.90 mmol) of anhydrous HCl. The gas was added to the flask at room temperature and the reaction stirred for 3 days over which time a white precipitate formed. Flask transferred onto a swivel frit assembly and the solid collected by filtration and washed with petroleum ether. The solid was dried *in vacuo* affording 0.450 g (58%) of $Cp^*_2Zr(CH_3)Cl$. ^1H NMR (benzene-d_6) δ = 1.80 (s, 30H, C_5Me_5), 0.00 (s, 3H, Zr*Me*). Anal. Calcd. for $Zr_1C_{21}H_{33}Cl_1$: C, 61.20 H, 8.07. Found C, 60.94 H, 8.15.

Preparation of $Cp^*_2Zr(d_3\text{-Np})(CH_3)$ (2). In the dry box a 25 mL round bottom flask was charged with 0.200 g (.485 mmol) of $Cp^*_2Zr(Me)Cl$ and 0.039 (0.485 mmol) d_3-NpLi. The flask was then attached to a fine swivel frit assembly. On the vacuum line, toluene was added by vacuum transfer. The reaction was warmed to room temperature and stirred for 2 days. The solvent was removed *in vacuo* and the resulting yellow solid was extracted with petroleum ether. The solid was recrystallized from petroleum ether at -80 °C affording 0.110 g (50.4%) identified as $Cp^*_2Zr(d_3\text{-Np})(CH_3)$ based on literature data.[19] ^2H NMR (benzene): 1.09 ppm.

Preparation of $Cp^*(C_5Me_4H)Zr(d_3\text{-Np})(CH_3)$ (3). In the dry box, a 25 mL flask was charged with 0.140 g (0.351 mmol) of $Cp^*(C_5Me_4H)Zr(Me)(Cl)$ and 0.028 g (0.351 mmol) of d_3-NpLi. The flask was attached to a fine swivel frit assembly. On the vacuum line, approximately 10 mL of toluene was added by vacuum transfer. The reaction was warmed to room temperature and stirred for 3 days over which time a yellow solution and white precipitate formed. The toluene was removed *in vacuo* and petroleum ether added by vacuum transfer. The white precipitate was removed by filtration and the solvent removed *in vacuo* leaving a yellow oil. Attempts to crystallize the oil by slow cooling of ether or petroleum ether solution were not successful. ^1H NMR (benzene-d_6) δ = 1.80 (s, 15H, Cp*), 2.15 (s, 3H, C_5Me_4H), 2.09 (s, 3H, C_5Me_4H), 1.98 (s, 3H, C_5Me_4H), 1.85 (s, 3H, C_5Me_4H), 4.60 (s, 3H, C_5Me_4H), 1.12 (s, 6H, $ZrCH_2C(CH_3)_2(CD_3)$), 0.21 (d, 1H, 10 Hz, $ZrCH_2C(CH_3)_2(CD_3)$; -0.02 (d, 1H, 10 Hz, $ZrCH_2C(CH_3)_2(CD_3)$, -0.37 (s, 3H, Zr*Me*). ^2H NMR (benzene) δ = 1.10. Isolation as an oil prevented elemental analysis.

Preparation of *rac*-(EBI)Zr(d_3-Np)(CH_3) (4). In the dry box, a 25 mL round bottom flask was charged with 0.150 g (0.376 mmol) of *rac*-(EBI)Zr(Me)(Cl) and

0.031 g (0.376 mmol) of d_3-NpLi. The flask was attached to a medium swivel frit assembly. On the vacuum line, approximately 10 mL of Et_2O was added by vacuum transfer and warmed to room temperature. The reaction was stirred for 24 hours over which time an orange solution and white precipitate formed. The white solid was removed by filtration and the solvent removed *in vacuo* leaving an orange solid. The solid was dried *in vacuo* affording 0.080 g (49.0%). ^{1}H NMR (benzene-d_6) δ = -1.98 (d, 6 Hz, 1H, $CH_2C(CH_3)_2CD_3$); -0.02 (d, 6 Hz, 1H, $CH_2C(CH_3)_2CD_3$); -0.95 (s, 3H, $ZrCH_3$); 0.87 (s, 6H, $ZrCH_2C(CH_3)_2CD_3$); 2.65 (m, 2H, CH_2CH_2, EBI); 2.82 (m, 2H, CH_2CH_2, EBI); 5.55 (m, 1H, Cp, EBI); 5.63 (m, 1H, Cp, EBI); 5.76 (m, 1H, Cp, EBI); 6.40 (m, 1H, Cp, EBI); 6.8-7.4 (m, benzo, EBI). ^{2}H NMR (benzene) δ = 0.85 ($ZrCH_2C(CH_3)_2CD_3$). Anal. Calcd. for $Zr_1C_{26}H_{30}D_3Cl_1$: C, 66.13 H, 7.04. Found C, 65.73 H, 7.26.

Preparation of ThpZr(CH$_3$)(Cl). In the dry box, a 25 mL round bottom flask was charged with 0.330 g (.735 mmol) of ThpZrMe$_2$ and the flask attached to a 43.48 mL calibrated gas volume. On the vacuum line, petroleum ether was added by vacuum transfer and the solution warmed to room temperature. The gas bulb was charged with 314 torr (0.735 mmol) of anhydrous HCl. The HCl was added at room temperature and the reaction stirred for 3 days over which time a white solid precipitated from solution. The precipitate was collected by filtration and washed with cold ether. The solid was dried *in vacuo* affording 0.280 g (82%) of a white solid identified as ThpZr(Me)(Cl). ^{1}H NMR (benzene-d_6) δ = 0.348 (s, 3H, Me_2Si); 0.549 (s, 3H, Me_2Si); 0.791 (s, 3H, Me_2Si); 0.814 (s, 3H, Me_2Si); 0.161 (s, 3H, Zr*Me*); 0.840 (d, 7 Hz, 3H, CHMe_2); 1.10 (d, 7 Hz, 3H, CHMe_2); 1.24 (d, 7 Hz, 3H, CHMe_2); 1.39 (d, 7 Hz, 3H, CHMe_2); 2.61 (sept, 7 Hz, 1H, C*H*Me$_2$); 2.91 (sept, 7 Hz, 1H, C*H*Me$_2$); 6.31 (m, 1H, Cp); 6.40 (m, 1H, Cp), 6.59 (m, 1H, Cp); 6.69 (m, 1H, Cp). ^{13}C (benzene-d_6) δ = -0.1865, -0.689, 3.59, 3.63 (Me_2Si), 31.62 ($ZrCH_3$), 28.82, 28.97, 29.38, 29.60 (CHMe_2), 21.23, 21.00 (*CH*Me$_2$), 104.41, 111.18, 112.27, 114.65, 116.71, 128.68, 132.21, 133.74, 157.27, 160.03 (Cp). Anal. Calcd. for $Zr_1C_{21}H_{33}Cl_1Si_2$: C, 53.86 H, 7.10. Found C, 52.72 H, 7.49.

Preparation of ThpZr(d_3-Np)(CH$_3$) (5). In the dry box, a 25 mL round bottom flask equipped with magnetic stir bar was charged with 0.200 g (0.426 mmol) of ThpZr(Me)(Cl) and 0.0345 g (0.426 mmol) of d_3-NpLi. The flask was attached to a fine swivel frit and on the vacuum line 10 mL of Et_2O was added by vacuum transfer. The reaction mixture was warmed to room temperature and stirred for

24 hours over which time a yellow solution and white precipitate formed. The precipitate was removed by filtration and washed with several portions of ether. The solvent was removed *in vacuo* leaving a dark sticky solid. Recrystallization from cold petroleum ether afforded 0.120 g (51.5 %) of a white solid identified as ThpZr(d_3-Np)(Me). ^{1}H NMR (benzene-d_6) δ = 0.093 (s, 3H, Me_2Si); 0.378 (s, 3H, Me_2Si); 0.516 (s, 3H, Me_2Si); 0.528 (s, 3H, Me_2Si); 0.5750 (s, 6H, Zr-$CH_2C(CH_3)_2CD_3$); 0.127 (s, 2H, $ZrCH_2C(CH_3)_2CD_3$); 0.944 (d, 7 Hz, 3H, $CHMe_2$); 1.07 (d, 7 Hz, 3H, $CHMe_2$); 1.25 (d, 7 Hz, 3H, $CHMe_2$); 1.42 (d, 7 Hz, 3H, $CHMe_2$), 2.62 (sept, 7 Hz, 1H, $CHMe_2$), 2.95 (sept, 7 Hz, 1H, $CHMe_2$), 6.34 (m, 1H, Cp); 6.45 (m, 1H, Cp); 6.63 (m, 1H, Cp); 6.72 (m, 1H, Cp). Anal. Calcd. for $Zr_1C_{26}H_{41}D_3Si_2$: C, 61.59 H, 9.34. Found C, 60.92 H, 9.29.

General Procedure for Isotope Effect Measurements. In a typical experiment, 20.0 mg (0.0645 mmol) of **1** was dissolved in 2.0 mL of a stock solution of benzene containing 0.2% (by weight) of pentane. Similarly, 36.0 mg (0.0703 mmol) of $B(C_6F_5)_3$ was dissolved in 1.0 mL of stock benzene solution. In the dry box, the zirconium solution was charged into a 50 mL round bottom flask equipped with a side arm and a septum port. The side arm of the flask was charged with the solution of $B(C_6F_5)_3$. The flask was placed in a thermostated bath of ethylene glycol and equilibrated to the desired temperature. The $B(C_6F_5)_3$ solution was added to the rapidly stirred zirconium solution at which time a canary yellow solution formed. The reaction was monitored by withdrawing 100 μL of gas from the reaction vessel and injecting it into the GC/MS instrument.

Structure Determination for 1. A section was cut from a yellow column and mounted on a glass fiber with Paratone-N oil. The data was collected on a Bruker Smart 1000 CCD diffractometer under a stream of N_2 gas at 98 K. Three runs of data were collected with 20 second long, -0.20 ° wide ω-scans at three values of ϕ (0, 120 and 240°) with the detector 5 cm (nominal) distant at Θ of -28 °. The initial cell for data reduction was calculated for just under 1000 reflections chosen throughout the data frames. For data processing with SAINT v.602, all defaults were used, except: box size optimization was enabled, periodic orientation matrix updating was disabled, the instrument error was set to zero, Laue class integration restraints were not used, the model profiles from all nine

areas were blended and for the post-integration global least squares refinement, no constraints were applied. The data were corrected with SADABS v. 2.0 (beta) using default parameters except that the scale factor esd was set to a minimum value of 0.001. On the three .raw files the g values converged to 0.0428. No decay correction was needed.

The structure was solved using direct methods and the difference Fourier maps were used to locate all missing atoms, including hydrogens. No reflections were specifically omitted from the final processed dataset; 2095 reflections were rejected, with 33 space group-absence violations and 32 inconsistent reflections. Refinement of F^2 was against all reflections. A total of 3299 reflections were refined to R = 0.0219 (GOF = 2.581).

References.

1. a) Brookhart, M.; Green, M.L.H. *J. Organomet. Chem.* **1983**, *250*, 395. b) Brookhart, M.; Green, M.L.H.; Wong, L.L. *Prog. Inorg. Chem.* **1988**, *36*, 1.

2. Grubbs, R.H.; Coates, G.W. *Acc. Chem. Res.* **1996**, *29*, 85.

3. Prosenc, M.H.; Janiak, C.; Brintzinger, H.H. *Organometallics* **1992**, *11*, 4036.

4. Röll, W.; Brintzinger, H.H.; Rieger, B.; Zolk, R. *Angew. Chem. Int. Ed. Engl.* **1990**, *29*, 279.

5. Clawson, L.; Soto, J.; Buchwald, S.L.; Steigerwald, M.L., Grubbs, R.H. *J. Am. Chem. Soc.* **1985**, *107*, 3377.

6. Piers, W.E.; Bercaw, J.E. *J. Am. Chem. Soc.* **1990**, *112*, 9406.

7. Burger, B.J.; Cotter, W.D.; Coughlin, E.B.; Chacon, S.T.; Hajela, S.; Herzog, T.; Köhn, R.; Mitchell, J.; Piers, W.E.; Shapiro, P.J.; Bercaw, J.E. In *Ziegler Catalysts*; Fink, G.; Mülhaupt, R.; Brintzinger, H.H., Eds.; Springer-Verlag: Berlin, 1995; pp. 317-331.

8. Krauledat, H.; Brintzinger, H.H. *Agnew. Chem. Int. Ed. Engl.* **1990**, *29*, 1412.

9. LeClerc, M.K.; Brintzinger, H.H. *J. Am. Chem. Soc.*. **1995**, *117*, 1651.

10. Burger, B.J.; Thompson, M.E.; Cotter, W.D.; Bercaw, J.E. *J. Am. Chem. Soc.* **1990**, *112*, 1566.

11. a) Guo, Z.; Swenson, D.C.; Jordan, R.F. *Organometallics* **1994**, *13*, 1424. b) Jordan, R.F.; Bradley, P.K.; Baenziger, N.C.; LaPointe, R.E. *J. Am. Chem. Soc.* **1990**, *112*, 1289.

12. a) Woo, T.K.; Fan, L.; Ziegler, T. *Organometallics* **1994**, *13*, 2252. b) Woo, T.K.; Fan, L.; Ziegler, T. *Organometallics* **1994**, *13*, 432. c) Fan, L.; Harrison, D.; Woo, T.K.; Ziegler, T. *Organometallics* **1995**, *14*, 2018. d) Kawamura-Kuribayashi, H.; Koga, N.; Morokuma, K. *J. Am. Chem. Soc.* **1992**, *114*, 8687. e) Kawamura-Kuribayashi, H.; Koga, N.; Morokuma, K. *J. Am. Chem. Soc.* **1992**, *114*, 2359. f) Meier, R.J.; van Doremaele, G.H.J.; Iarlori, S.; Buda, F. *J. Am. Chem. Soc.* **1994**, *116*, 7274. g) Yu, Z.; Chien, J.C.W. *J. Poly. Sci. Part A: Poly. Chem.* **1995**, *33*, 1085.

13. a) Woo, T.K.; Margl, P.M.; Lohrenz, J.C.W.; Blöchl, P.E.; Ziegler, T. *J. Am. Chem. Soc.* **1996**, *118*, 13021. b) Lohrenz, J.C.W.; Woo, T.K.; Ziegler, T. *J. Am. Chem. Soc.* **1995**, *117*, 12793.

14. den Haan, K.H.; de Boer, J.L.; Teuben, J.H.; Spek, A.L.; Kojic-Prodic, B.; Hays, G.R.; Huis, R. *Organometallics* **1986**, *5*, 1726.

15. Wong, W.K.; Jaing, T.; Wong, T.K. *J. Chem. Soc. Dalton Trans.* **1995**, 3087.

16. Boring, E.; Sabat, M.; Finn, M.G.; Grimes, R.N. *Organometallics* **1998**, *17*, 3865.

17. Resconi, L.; Piemontesi, F.; Fraciscono, G.; Abis, L.; Fiorani, T. *J. Am. Chem. Soc.* **1992**, *114*, 362.

18. Hajela, S.H.; Bercaw, J.E. *Organometallics* **1994**, *13*, 1147.

19. Horton, A.D. *Organometallics* **1996**, *15*, 2675.

20. Brintzinger, H.H.; Fischer, D.; Mülhaupt, R.; Rieger, B.; Waymouth, R.M. *Angew. Chem. Int. Ed. Engl.* **1995**, *34*, 1143.

21. Surtees, J.R. *J. Chem. Soc. Chem. Comm.* **1965**, 567.

22. EBI = ethylene-*bis*-indenyl; THP = $(Me_2Si)_2(\eta^5\text{-}C_5H_3)(\eta^5\text{-}C_5H\text{-}3,5\text{-}(CHMe_2)_2)$

23. Isaacs, N.S. *Physical Organic Chemistry*, John Wiley and Sons: New York, 1986.

24. Burger, B.J.; Bercaw, J.E. In *Experimental Organometallic Chemistry*; ACS Symposium Series No. 357; Wayda, A.L.; Darensbourg, M.Y. Eds.; American Chemical Society: Washington, DC 1987; Chapter 4.

25. Kim, I.; Jordan, R.F. *Macromolecules* **1996**, *26*, 489.

26. Chirik, P.J.; Day, M.D.; Bercaw, J.E. *Organometallics* **1999**, *18*, 1873.

27. Veghini, D.; Day, M.D.; Bercaw, J.E. *Inorg. Chem. Acta* **1998**, *280*, 226.

28. A ground state β-agostic interaction has been used to explain the observed inverse kinetic isotope effect in the cobalt-catalyzed polymerization of ethylene. Tanner, M.J.; Brookhart, M.; Desimone, J.M. *J. Am. Chem. Soc.* **1997**, *119*, 7617.

Chapter 6

Preparation and Characterization of *Ansa*-Tantalocene Derivatives as Transition State Models for Metallocene Olefin Polymerization Catalysts.

Abstract

Preparation of *ansa*-tantalocene complexes is described. Reaction of distannylated singly silylene-bridged cyclopentadienyl ligands with $TaCl_5$ yields tantalocene trichloride complexes of the general formula, $Me_2Si(\eta^5\text{-}C_5H_4)(\eta^5\text{-}C_5H_2\text{-}R_2)TaCl_3$ (R = H, alkyl). Reduction of the tantalocene trichlorides with $LiAlH_4$ followed by hydrolysis with aqueous ammonium chloride affords the corresponding tantalocene trihydride complexes. Thermolysis of the tantalocene trihydride complexes with phosphines, carbon monoxide and olefins affords the ligand-hydride complexes. The stereochemistry of the resulting products is dependent on both the steric disposition of the ancillary ligation and the incoming ligand, where increased substitution results in higher degrees of selectivity. Reduction of the tantalocene trichloride complexes with zinc dust affords the tantalocene dichloride complexes. Addition of an excess of Grignard reagents of the general form, RCH_2CH_2MgX (R = H, CH_3, C_6H_5; X = Cl, Br), affords the tantalocene olefin-hydride complexes. For $Me_2Si(\eta^5\text{-}C_5H_4)(\eta^5\text{-}C_5H_3\text{-}CHMe_2)Ta(\eta^2\text{-}CH_2CH_2)(H)$, the predominant isomer (95%) is the one in which the ethylene ligand is coordinated in the open portion of the metallocene wedge. Similar results have been obtained with tantalocene styrene-hydrides and propylene-hydrides. For each metallocene studied, the substitution on the cyclopentadienyl ring directs the coordination of the olefin as to minimize unfavorable steric interactions. The selectivities observed in olefin and phosphine coordination correlate with the specificity of the corresponding zirconocene polymerization catalyst. Both singly and doubly silylene-bridged tantalocene trimethyl complexes have been prepared from reaction of the deprotonated cyclopentadienyl ligand with $TaCl_2Me_3$. The singly-bridged, $Me_2Si(\eta^5\text{-}C_5H_4)(\eta^5\text{-}C_5H_2\text{-}2,4\text{-}(CHMe_2)_2)Ta(CH_3)_3$ displays the expected η^5, η^5 coordination of the cyclopentadienyl ligands, whereas for $Me_2C(\eta^5\text{-}C_5H_4)$(Fluorenyl)$TaMe_3$ and $Me_2C(\eta^5\text{-}C_5H_4)$(Fluorenyl)$TaMe_2F$, η^1-coordination is observed for the fluorenyl ligand. The doubly silylene-bridged, $(Me_2Si)_2(\eta^5\text{-}C_5H_2\text{-}4\text{-}SiMe_3)(\eta^2\text{-}C_5H\text{-}3,5\text{-}(CHMe_2)_2)Ta(CH_3)_3$ displays an unsual dihapticity for the cyclopentadienyl ligand due to unfavorable steric interactions between the tantalum methyl groups and the dimethylsilylene linkers.

Introduction

Stereospecific olefin polymerization promoted by group 3 and 4 *ansa*-metallocene catalysts represents one of the most enantioselective chemical transformations known.[1] Elucidation of the steric and electronic factors that control this remarkable selectivity may aid in the design of new catalysts and also result in the development of new asymmetric transformations. Considerable effort has been devoted toward understanding the nature of the transition state for the C-C bond forming step in metallocene catalysts. From these studies general features common to all metallocene systems have been elucidated. Electronically, it is well accepted that a 14 electron metallocene alkyl with 2 vacant orbitals is required; one orbital is used to accommodate the incoming olefin, while the other allows for α-agostic assistance[2] in the transition state for carbon-carbon bond formation (Figure 1).[3]

M = Sc, Y, lanthanide
R' = hydride or alkyl

M = Ti, Zr, Hf
R' = hydride or alkyl
X^- = weakly coordinating anion

Figure 1. Doubly coordinatively unsaturated, 14 electron metallocene catalysts for olefin polymerization.

In addition to electronic effects, considerable effort has been devoted toward understanding the key steric interactions in the olefin insertion transition state. Calculations by Corradini[4] demonstrate that the enantiofacial approach of the olefin is determined by the metal alkyl unit, such that the olefin substituent is placed in a *trans*-relationship with the β-carbon of the metal alkyl. The metal alkyl is believed to orient itself toward the most open portion of the metallocene framework (Figure 2). The first experimental evidence in support of this model

was provided by Pino.[5] Hydrooligomerization of α-olefins with optically pure ethylene *bis*(4,5,6,7-tetrahydroindenyl) zirconium dichloride (EBTHIZrCl$_2$) produced chiral hydrotrimers and hydrotetramers with the predicted absolute configurations.[6] More recently, Gilchrist and Bercaw[7] were able to determine the stereoselectivity of yttrium-hydride and yttrium-pentyl additions to carbon-carbon double bonds. Optically active deutero-1-pentenes were prepared and used to evaluate the stereoselectivity of olefin insertion into Y-H and Y-pentyl bonds with an optically pure yttrocene. From these studies it was determined that insertions into yttrium-hydride bonds proceed with modest selectivity (34% ee) whereas insertions into yttrium-alkyl bonds proceed with very high levels (> 95% ee) of enantioselectivity. In both the Pino and Bercaw studies, insertion into the metal-hydride occurs with the opposite enantioselectivity of the insertion into the metal alkyl.

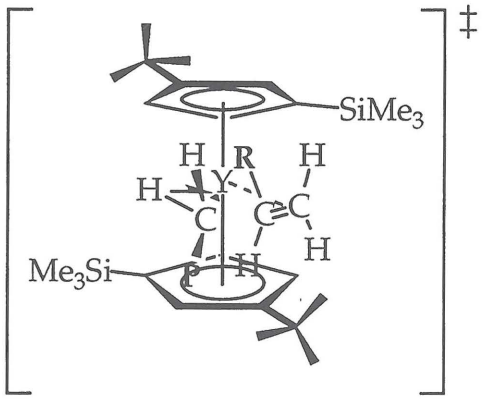

Figure 2. Model for the olefin insertion transition state in chiral yttrocene catalysts.

The stereochemical model developed in the C_2-symmetric isospecific systems has since been extended to include C_s-symmetric syndiospecific catalysts.[8] In these systems, the favored transition state geometry for two classes of syndiospecific catalysts is shown in Figure 3. In these metallocenes, the growing polymer chain extends away from the less sterically demanding cyclopentadienyl moiety thus forcing the propylene methyl group down toward the more sterically demanding ligand assuming the *trans* relationship between the coordinated olefin and the growing polymer chain dominates. In both cases shown, the sterically demanding ligand contains an open region to accommodate the methyl substituent on the incoming monomer.

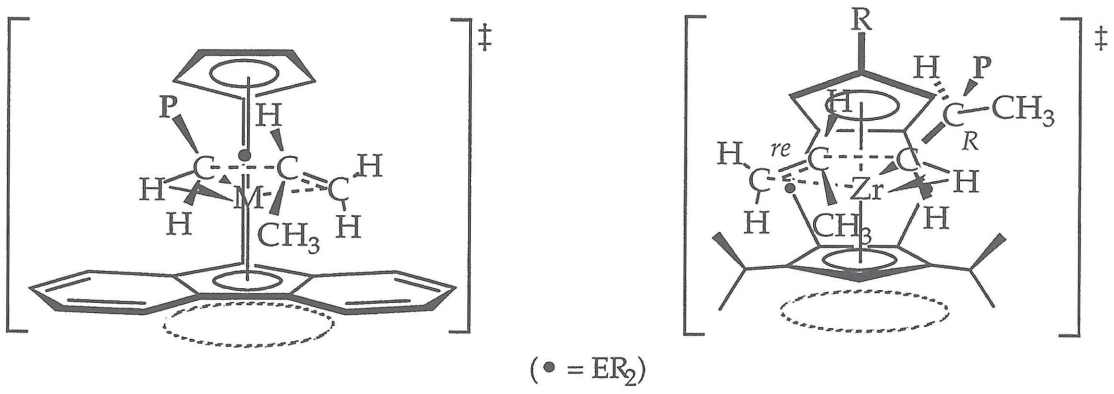

Figure 3. Proposed transition state for syndiospecific metallocene catalysts.

Although these proposals have been sucessful in explaining the high levels of stereocontrol observed with C_2 and C_s symmetric catalysts, some metallocenes operate with relatively high levels of enantiofacial selectivity that can not be readily explained with current transition state models. One such class of metallocenes are the monosubstituted singly silylene-bridged $Me_2Si(\eta^5\text{-}C_5H_4)(\eta^5\text{-}C_5H_3\text{-}3\text{-}R)ZrCl_2$ (R = CMe_3, $CHMe_2$) complexes originally reported by Miya,[9] which polymerize propylene with [mmmm] contents exceeding 70% (Figure 4).

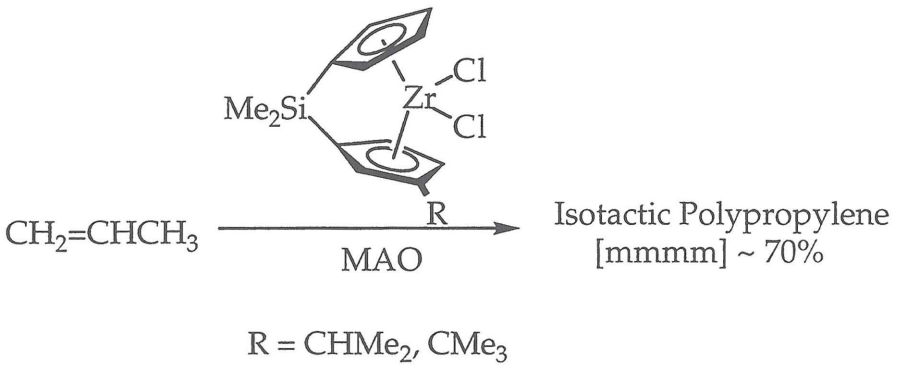

Figure 4. Isotactic polypropylene produced by C_1-symmetric metallocene catalysts.

One approach to modeling the carbon-carbon bond forming transition state of a group 4 metallocene catalyst is to prepare the analogous *ground state* group 5 (M = Nb, Ta) metallocene olefin-alkyl complex. The niobocene and tantalocene complexes can access a formally M(III), d^2 resonance structure (Figure 5) which stabilizes the bound olefin through π-backbonding interactions. Once prepared, conventional NMR and X-ray diffraction experiments may be

used to determine the relative disposition of the bound olefin and the metal-alkyl fragment with respect to the ancillary ligation. This approach has been used to elucidate the kinetics and mechanism of olefin insertion into metal-hydride bonds with *bis*-cyclopentadienyl and *bis*-pentamethylcyclopentadienyl niobocene and tantalocene olefin-hydride complexes.[10]

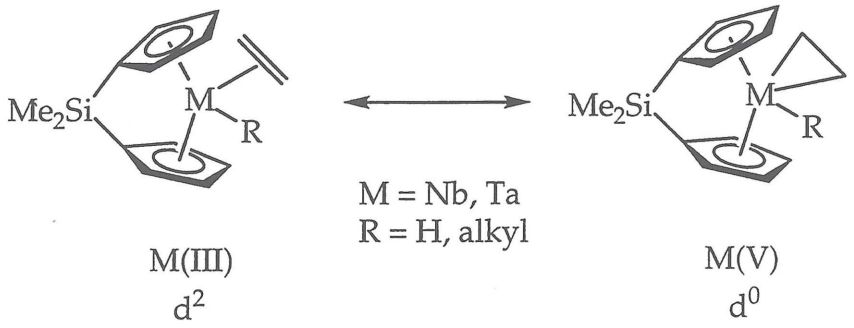

Figure 5. Resonance structures of niobocene and tantalocene olefin hydride complexes.

Reports of group 5 *ansa* metallocenes have been quite limited. Green has reported the synthesis and solution NMR dynamics of a series of carbon-bridged unsubstituted niobocene dichloride and borohydride complexes.[11] Similar silicon-bridged *ansa*-niobocene dichloride and acetylene-chloride complexes have also been prepared.[12] Hermann has reported the synthesis *ansa*-niobocene and *ansa*-tantalocene amide and imido complexes via traditional salt metathesis and amine elimination methodologies.[13] Parkin[14] has prepared $Me_2Si(C_5Me_4)_2TaCl_3$ via tin elimination and was also able to prepare the corresponding tantalocene trihydride complex via reduction of the trichloride with $LiAlH_4$ followed by hydrolysis. Thermolysis of the trihydride in the presence of ethylene afforded $Me_2Si(C_5Me_4)_2Ta(\eta^2\text{-}CH_2CH_2)(H)$ which has been characterized by X-ray crystallography.

Results and Discussion

Tantalum Trihydride Complexes

Initially, our synthetic efforts focused on a general route for the preparation of *ansa*-tantalocene complexes and on the development of methods for further synthetic elaboration of these compounds to the desired olefin-

hydride and olefin-alkyl tantalocenes. The first synthetic targets were tantalocene trichloride complexes since Parkin's successful synthesis of $Me_2Si(C_5Me_4)_2Ta(\eta^2\text{-}CH_2CH_2)(H)$ involved straightforward preparation of the $Me_2Si(C_5Me_4)_2TaCl_3$.[14]

Reaction of two equivalents of *n*-Bu_3SnCl with $Li_2[Me_2Si(\eta^5\text{-}C_5H_4)_2]$ (Li_2Sp) affords the distannylated cyclopentadiene derivative, $[Me_2Si(\eta^5\text{-}C_5H_4)_2][SnBu_3]_2$ (**1**), as a bright yellow oil. Addition of $TaCl_5$ to a diethyl ether solution of **1** results in precipitation of a red solid identified as $Me_2Si(\eta^5\text{-}C_5H_4)_2TaCl_3$ (**2**) based on ^1H NMR spectroscopy. Compound **2** is soluble in THF but insoluble in most other common laboratory solvents. Over time, **2** initiates the polymerization of THF so special care should be taken when preparing such solutions. Reduction of **2** with $LiAlH_4$ followed by hydrolysis with saturated NH_4Cl solution affords the tantalum trihydride complex, $SpTaH_3$ (**3**) (eq. 1). Quenching the reaction mixture with distilled water results in a mixture of products, presumably arising from ligand degradation resulting from hydrolysis of the dimethyl silylene linker. The presence of an acid buffer such as NH_4Cl maintains a minimal concentration of base thus allowing for isolation of a clean product. In addition to the typical ligand resonances, the ^1H NMR spectrum of **3** in benzene-d_6 displays a triplet at 0.20 ppm for the central tantalum hydride and a doublet at -1.87 ppm for the lateral tantalum hydrides. These values are typical for tantalocene hydride resonances.[15]

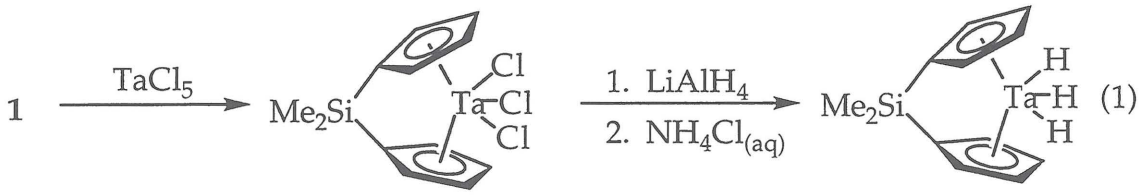

(1)

2 **3**

This synthetic methodology has been extended to include the preparation of more substituted tantalocene trichloride and trihydride complexes. Addition of $TaCl_5$ to an Et_2O solution of $[Me_2Si(C_5H_4)(C_5H_3\text{-}3\text{-}CHMe_2)][SnBu_3]_2$ ($[iPrSp][SnBu_3]_2$), $[Me_2Si(C_5H_4)(C_5H_2\text{-}2,4\text{-}(CHMe_2)_2][SnBu_3]_2$ ($[iPr_2Sp][SnBu_3]_2$) and $[Me_2Si(C_5H_4)(C_5H_3\text{-}3\text{-}CMe_3)][SnBu_3]_2$ ($[tBuSp][SnBu_3]_2$) results in precipitation of iPrSp$TaCl_3$ (**4**), $iPr_2SpTaCl_3$ (**5**) and tBuSp$TaCl_3$ (**6**) respectively.

As with the parent trichloride complex, **4**, **5** and **6** undergo reduction with $LiAlH_4$ followed by subsequent hydrolysis with aqueous NH_4Cl to yield iPrSpTaH$_3$ (**7**), iPr$_2$SpTaH$_3$ (**8**) and tBuSpTaH$_3$ (**9**). Each trihydride complex displays upfield lateral hydride resonances (~ -1 to -2 ppm) as well as resonances for the central tantalum hydride (~ 0 to 1 ppm) in the ^{1}H NMR spectrum.

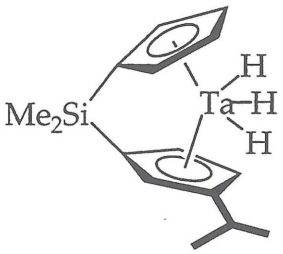

6

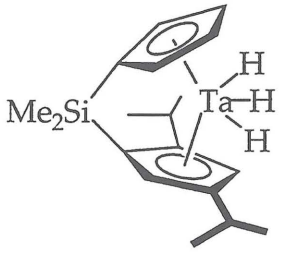

7

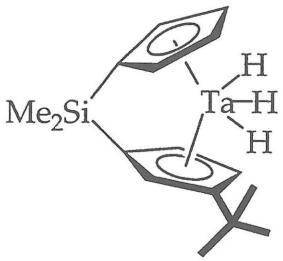

8

Attempts to metallate highly substituted, sterically demanding stannylated cyclopentadienyl ligands have been unsuccessful. No tractable tantalocene trichloride complexes have been obtained from the reaction of [Me$_2$Si(C$_5$H$_4$)(C$_5$H$_2$-(CMe$_3$)$_2$)][SnBu$_3$]$_2$ {[tBu$_2$Sp][Bu$_3$Sn]$_2$} and [Me$_2$Si(C$_5$H$_2$-(CHMe$_2$)$_2$)$_2$][SnBu$_3$]$_2$ {[Ip][Bu$_3$Sn]$_2$} with $TaCl_5$. Likewise, indenyl and fluorenyl substituted ligands such as [EBI][SnBu$_3$]$_2$(EBI = ethylene-*bis*-indenyl) and [Me$_2$C(C$_5$H$_4$)(fluorenyl)][SnBu$_3$]$_2$ do not produce the desired tantalocene trichloride complexes after stirring with $TaCl_5$ for several days.

The trihydride complexes: **3**, **7**, **8**, and **9** display a wealth of reaction chemistry with a variety of unsaturated organic molecules. Heating a benzene-d_6 solution of **3** to 87 °C under an atmosphere of carbon monoxide results in quantitative formation of the carbonyl hydride complex, SpTa(CO)(H) (**10**) (eq. 2). The hydride ligand displays a single downfield resonance at -5.68 ppm, substantially shifted from the starting tantalocene trihydride complex. In a similar manner, **7**, **8** and **9** react with carbon monoxide over the course of several hours at 87 °C to afford the carbonyl-hydride complexes, iPrSpTa(CO)(H) (**11**), iPr$_2$SpTa(CO)(H) (**12**) and tBuSpTa(CO)(H) (**13**). For **11** and **12**, equimolar mixtures of isomers are formed, implying that the linear carbon monoxide molecule is not sufficient in differentiating the steric environments of each side of the metallocene wedge. For **13**, a 88:12 ratio of two carbonyl-hydride products is

formed, suggesting that the *tert*-butyl substituted ligand is more sterically conjested than its isopropyl substituted counterparts.

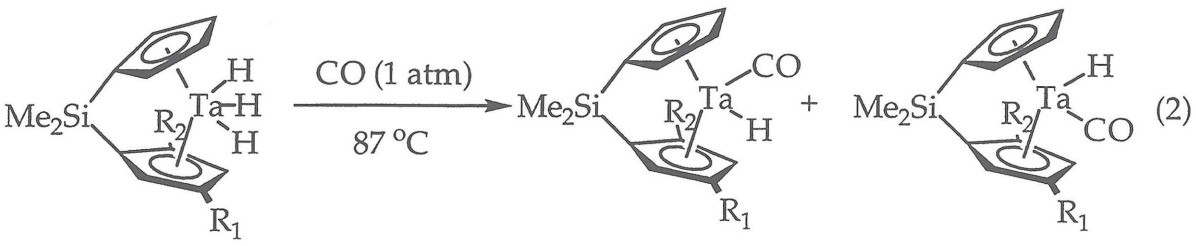

(2)

$R_1 = R_2 = H$: **3**
$R_1 = CHMe_2$, $R_2 = H$: **7**
$R_1 = R_2 = CHMe_2$: **8**
$R_1 = CMe_3$, $R_2 = H$: **9**

Reaction of **3** with excess ethylene at 87 °C affords the tantalum ethylene-ethyl complex, $SpTa(\eta^2\text{-}CH_2CH_2)(CH_2CH_3)$ (**14**), in quantitative yield (eq. 3). Allowing a benzene-d_6 solution of **14** to stand at room temperature results in a mixture of **14**, $SpTa(\eta^2\text{-}CH_2CH_2)(H)$ (**15**) and free ethylene. Formation of **15** arises from loss of ethylene forming a transient Ta(III) ethyl complex which undergoes β-hydrogen elimination. Formation of ethylene-ethyl complexes from thermolysis of Cp_2MH_3 (M = Nb, Ta) in the presence of ethylene has been observed previously.[16] The kinetics of the reaction of **6** with ethylene have been measured at 87 °C. As shown in Table 1, the rate of reaction is independent of the concentration of ethylene (0.196 M to 1.27 M) consistent with rate determining reductive elimination of dihydrogen forming a Ta(III) monohydride, followed by rapid coordination of ethylene, insertion into the tantalum-hydride and coordination of another ethylene equivalent. For comparison, $Me_2Si(C_5Me_4)_2TaH_3$ reacts with ethylene at 90 °C with a rate constant of $9.8(9) \times 10^{-4}$ sec^{-1} forming $Me_2Si(C_5Me_4)_2Ta(\eta^2\text{-}CH_2{=}CH_2)(H)$.[14] Similarly, reaction of $Cp^*_2TaH_3$ ($Cp^* = \eta^5\text{-}C_5Me_5$) with ethylene at 90 °C results in $Cp^*_2Ta(\eta^2\text{-}CH_2{=}CH_2)(H)$ with a rate constant of 2.5×10^{-7} sec^{-1}.[17] These results indicate that the *ansa*-bridge influences the rate of reductive elimination more than cyclopentadienyl substitution.

The effect of an *ansa*-bridge on rates of reductive elimination has been studied by Parkin.[14] Reductive elimination from *ansa*-tantalocene trihydride complexes was found to be approximately 4000 times greater than

corresponding unlinked *bis*-pentamethylcylopentadienyl complexes. The origin of the striking difference is believed to be reduced electron donating capability of the cyclopentadienyl rings in the *ansa* complex. This results in destabilization of the ground state Ta(V) trihydride with respect to the Ta(III) monohydride intermediate and thus increases the rate of reductive elimination.

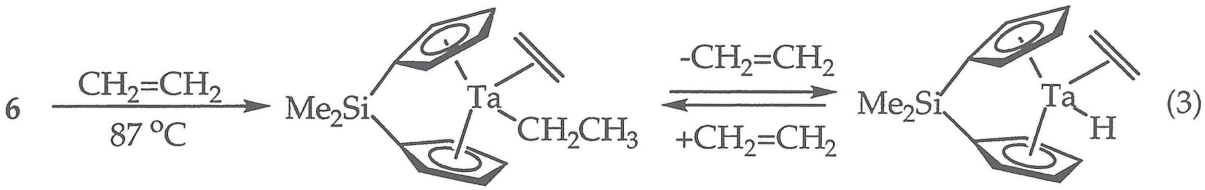

(3)

14 **15**

[Ethylene] (M)	$k_{obs}^{360\ K} \times 10^4$ (sec^{-1})
0.196	1.23(4)
0.635	1.26(2)
1.27	1.13(6)

Table 1. Measured rate constants for the reaction of **6** with ethylene forming **14**.

Using dynamic NMR techniques, an experimental estimate for the rate of ethylene insertion for **15** can be established. At 85 °C, the dimethylsilylene peaks for **15** coalesce, corresponding to a rate constant of 480(10) sec^{-1}. This rate constant is a composite of the rate of olefin insertion and site interconversion since equivalencing both sides of the metallocene wedge can only be accomplished when both of these processes are occurring. The rate of insertion can, in principle, be measured independently using magnetization transfer or line broadening techinques, but these experiments have not been sucessful. For comparison, the rate constant for ethylene insertion with $Me_2Si(C_5Me_4)_2Ta(\eta^2\text{-}CH_2{=}CH_2)(H)$ has been found to be 1.83×10^3 sec^{-1} at 100 °C corresponding to a free energy of activation of 16.3 kcal/mol.[14] The corresponding site interconversion barrier has also been measured for $Me_2Si(C_5Me_4)_2Ta(\eta^2\text{-}CH_2{=}CH_2)(H)$ and found to be 0.70 kcal/mol. The observed insertion rate for the *ansa* complex is significantly faster than the value of 2.3 sec^{-1} measured for $Cp^*_2Ta(\eta^2\text{-}CH_2{=}CH_2)(H)$ at 100 °C. Assuming the barrier for site interconversion is small, it appears that the rate of insertion for **15** is similar to

that observed for $Me_2Si(C_5Me_4)_2Ta(\eta^2\text{-}CH_2{=}CH_2)(H)$, thus indicating that the rate of olefin insertion is influenced more by the presence of an *ansa* bridge rather than cyclopentadienyl substitution.

Reaction of **7**, **8** and **9** with ethylene results in a mixture of isomeric ethylene-ethyl and ethylene-hydride complexes. The lack of symmetry in these molecules coupled with the isomeric products formed has complicated identification of each compound. As a result, the reactivity of the tantalocene trihydride complexes with phosphine ligands has been examined. Through systematic variation in the steric properties of the phosphine, the selectivity for coordination to each side of the metallocene wedge may be determined. Additionally, the resulting tantalocene phosphine-hydride complexes are not expected to undergo further insertion reactions.

Thermolysis of **7** with excess PMe_3 at 87 °C affords two isomeric phosphine-hydride complexes, $iPrSpTa(PMe_3)(H)$ (**16a**, **16b**) (eq. 4). After one hour of heating, the product mixture contains 85% **16a** and 15% **16b**. The identity of each isomer has been established using NOE difference NMR spectroscopy. For the major isomer, **16a**, a strong NOE enhancement in the isopropyl methyl and methine hydrogens of the cyclopentadienyl ligand is observed upon irradiation of the tantalum hydride. Moreover, irradiation of the trimethylphosphine ligand does not result in an NOE enhancement in the isopropyl methine hydrogen thus indicating that the phosphine ligand resides in the open portion of the metallocene wedge. Continued heating of the sample over the course of 19 hours affords solely the major isomer, **16a**.

Increasing the steric disposition of the phosphine ligand also affects the selectivity of the reaction. Reaction of **7** with PEt_3 at 87 °C affords only one isomer of the phosphine-hydride complex, $iPrSpTa(PEt_3)(H)$ (**17**). Contrary to the results with carbon monoxide, phosphine ligands are useful for differentiating the steric disposition of each side of the metallocene wedge. Larger phosphines such as PEt_3 are more effective than PMe_3 in selectively binding to the more open portion of the metallocene. In both cases, the isopropyl substituent is quite effective in directing the coordination of the phosphine to the tantalum center.

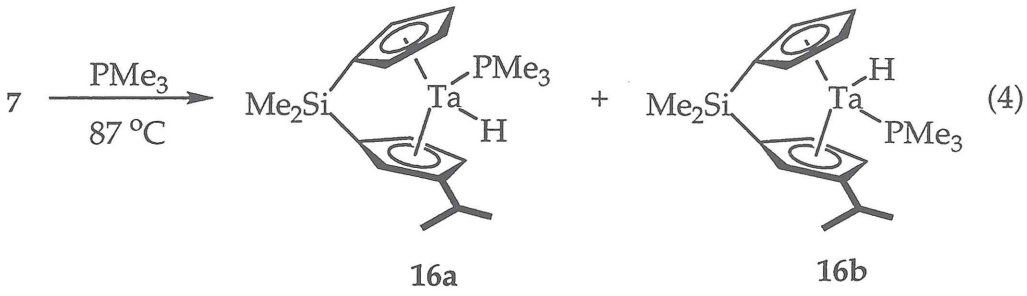

16a **16b**

The tantalocene trihydride, **8**, undergoes clean reaction with trimethylphosphine at 87 °C resulting in a mixture of two isomeric phosphine-hydride products, $iPr_2SpTa(PMe_3)(H)$ (**18a, 18b**) (eq. 5). At early reaction times (*e.g.*, 1 hour), an approximately equimolar mixture of the two isomers is present (Table 2). As the reaction progresses, **18b** becomes the predominant isomer in solution eventually becoming the only product present. Similar reactivity is observed for the thermolysis of **8** in the presence of PEt_3. However, the more bulky triethylphosphine perturbs the product distribution more than PMe_3 as evidenced by the 21:79 ratio of **19a**:**19b** at only 30% conversion (Table 2). In both cases, assignments of each isomer are based upon NOE difference NMR spectroscopy. For both phosphines, the preferred isomer is the one in which the phosphine ligand resides on the side of the metallocene wedge with the 4-isopropyl substituent. Coordination of the phosphine on the narrow, hence more sterically conjested side of the tantalocene wedge with the 2-isopropyl substituent is disfavored, hence the minor isomer slowly converts to the major with continued heating.

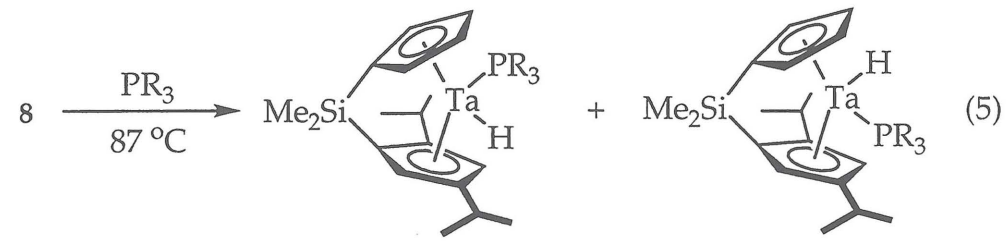

$R = CH_3$ **18a** **18b**

$R = CH_2CH_3$ **19a** **19b**

Phosphine	Time (hrs)	% Conversion	% 18a[1]	% 18b
PMe_3	1.0	26	44	56
	3.0	52	45	55
	5.75	87	39	61
	10	100	24	76
	23	100	0	100
PEt_3	1.3	30	21	79
	4.5	78	5	95

1. For PEt_3, the products are **19a** and **19b** respectively.

Table 2. Reaction of **8** with PR_3 at 87 °C.

Thermolysis of **9** in the presence of PMe_3 affords solely one isomer of tBuSpTa(PMe_3)(H) (**20**). NOE difference NMR spectroscopy reveals that the observed isomer is the one in which the phosphine is coordinated away from the *tert*-butyl substituent in the metallocene wedge. As with the [iPrSp] ligand system, single substitution with a *tert*-butyl group is effective in directing the coordination of the phosphine ligand.

Preparation of Tantalocene Olefin-Hydride Complexes

Due to the recurring problem of over alkylation upon thermolysis of the tantalocene trihydrides with olefins, a cleaner route to the desired olefin-hydride and olefin-alkyl complexes was desired. Previous studies have shown that the Ta(IV) complex, $Cp^*_2TaCl_2$, undergoes clean reaction with a variety of Grignard reagents such as ethylmagnesium bromide and phenethylmagnesium bromide to yield olefin-hydride complexes.[17] For this reason, a route to *ansa*-Ta(IV) dichloride complexes has been pursued.

Addition of zinc dust to a THF solution of **2** results in formation of green solution which thickens over time. Further inspection reveals that polymerization of the THF solvent accompanies the reduction of the tantalum complex. To avoid this complication, the reaction was repeated in dimethoxyethane (DME) and a green powder identified as $SpTaCl_2$ (**21**) has been isolated in 88% yield (eq. 6). Reduction of **4**, **5** and **6** with zinc dust also proceeds

smoothly in DME resulting in $iPrSpTaCl_2$ (**22**), $iPr_2SpTaCl_2$ (**23**) and $tBuSpTaCl_2$ (**24**) respectively. Each of the tantalum dichloride complexes display a diagnostic eight line (^{181}Ta, 99.99% S = 7/2) EPR spectrum (g = 1.94), consistent with a d^1, Ta(IV) complex (Figure 6).

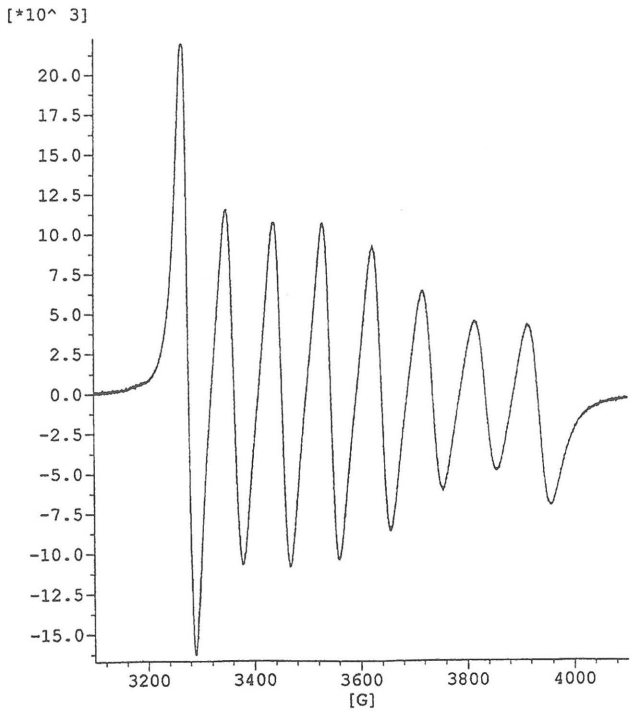

Figure 6. EPR spectrum of **23** in dichloromethane at 296 K.

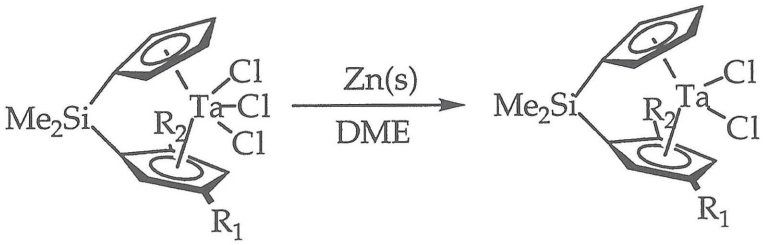

(6)

$R_1 = R_2 = H$: **21**
$R_1 = CHMe_2$, $R_2 = H$: **22**
$R_1 = R_2 = CHMe_2$: **23**
$R_1 = CMe_3$, $R_2 = H$: **24**

Reaction of **21** with 2.2 equivalents of CH_3CH_2MgBr affords an orange solution and brown precipitate, consistent with disappearance of the Ta(IV) complex. However, attempts to isolate a tractable product from the reaction mixture have been unsuccessful. Similarly, addition of $PhCH_2CH_2MgBr$ to **21** results in no tractable product.

Addition of 2.2 equivalents of CH_3CH_2MgBr to a ethereal slurry of **22** also results in formation of an orange solution and brown precipitate. However, in this case a yellow oil identified as iPrSpTa(η^2-CH_2CH_2)(H) (**25**) has been isolated (eq. 7). Presumably one equivalent of the ethyl Grignard reagent serves to reduce the tantalum dichloride complex to the Ta(III) chloride which subsequently undergoes alkylation by a second equivalent of Grignard reagent to produce the punative Ta(III) intermediate, iPrSpTaCH_2CH_3, which then undergoes β-hydrogen elimination affording **25** (eq. 7).[17]

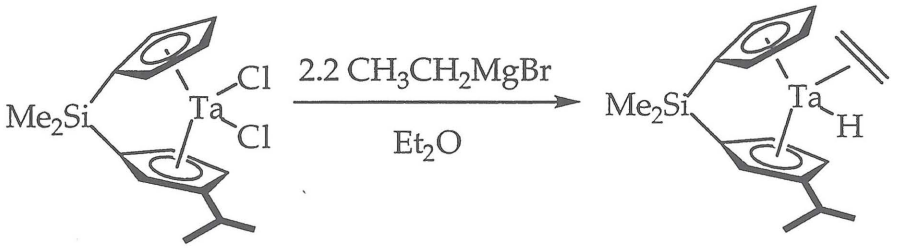

(7)

25

The ^1H NMR spectrum of **25** indicates that predominantly one isomer of the ethylene-hydride complex forms upon alkylation. A diagnostic upfield resonance (δ = -2.70 ppm) is observed for the tantalum hydride of the major isomer. NOE difference NMR experiments confirm that the preferred isomer is the one in which the ethylene ligand resides in the open portion of the metallocene wedge away from the isopropyl substituent. Irradiation of the ethylene resonance at 0.51 ppm results in an NOE enhancement of the tantalum hydride, thus indicating it is the *endo* ethylene hydrogens.[18] Selective irradiation of the isopropyl doublets and the isopropyl methine resonances result in a strong NOE to the tantalum hydride and a weak NOE to the *endo* ethylene peak. These data strongly suggest that the isomer formed is the one in which the ethylene is away from the isopropyl substituent.

Heating a benzene-d_6 solution of **25** results in broadening of the signals observed for the tantalum-hydride, the cyclopentadienyl hydrogens and the isopropyl methine hydrogen. The broadening of the NMR signals is indicative of olefin insertion and β-hydrogen elimination occurring on the NMR timescale (eq. 8). Attempts to quantify the rate of insertion using magnetization transfer NMR techniques have been unsuccessful. The same isomeric distribution is observed during heating and upon cooling to 25 °C, indicating the observed isomeric preference is indeed thermodynamic and not kinetic products arising from the alkylation procedure.

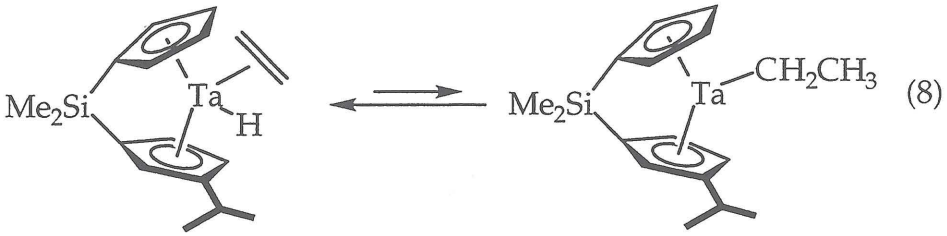

(8)

Addition of 2.2 equivalents of $CH_3CH_2CH_2MgBr$ to **22** results in formation of four of the eight possible iPrSp(η^2-CH_2CHCH_3)(H) isomers. The distribution of the propylene-hydride isomers is 63.7% (**26a**), 20.6% (**26b**), 13.0% (**26b**) and 2.6% (**26d**). NOE difference spectroscopy indicates that the major isomer is the one in which the propylene is coordinated in an *endo* fashion on the open side of the metallocene wedge with the methyl group pointed toward the less substituted cyclopentadiene (Figure 7).

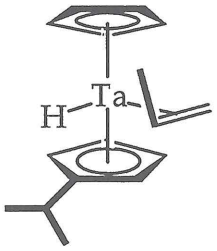

Figure 7. The major isomer for **26**.

Similar reactivity is observed upon addition of phenethylmagnesium chloride to **21**. Of the 8 styrene-hydride isomers possible, three iPrSpTa(η^2-CH_2CHPh)(H) complexes are observed after purification. Two major isomers (**27a**, **27b**) are observed in a 60:40 ratio and constitute 91% of the product distribution,

whereas one trace isomer (**27c**) forms the remainder of the product mixture. Each of the styrene-hydride isomers displays an upfield tantalum hydride resonance in the ^{1}H NMR spectrum (**27a** = -1.52 ppm, **27b** = -1.69 ppm, **27c** = -1.74 ppm). Recrystallization of the reaction mixture affords yellow needles that are suitable for X-ray diffraction. The results of the X-ray diffraction experiment are shown in Figure 8. The ^{1}H NMR spectrum of the single crystals of **27b** in benzene-d_6 indicate that the crystal structure represents the styrene hydride isomer that constitutes 40% of the product mixture. The benzene-d_6 solution of **27b** rapidly equilibrates ($t_{1/2}$ ~ 30 minutes) at 296 K the 60:40 mixture of the major isomers and also contains a trace amount of the minor isomer, **27c**.

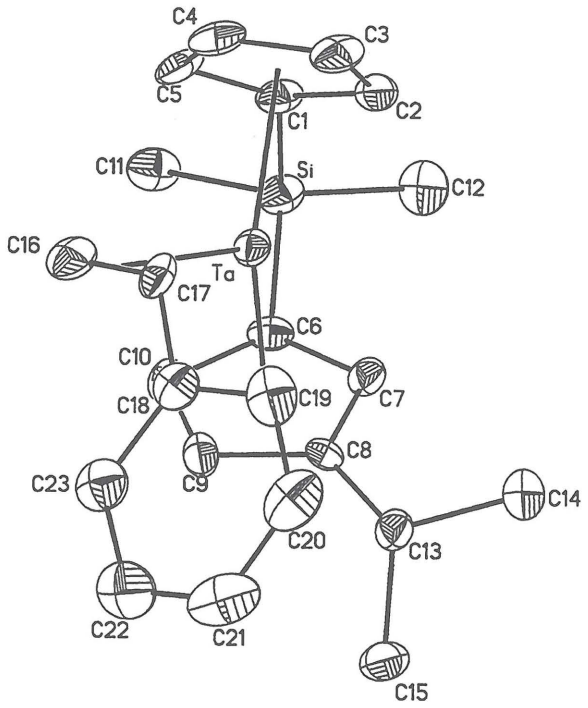

Figure 8. Molecular structure of **27b** with 50% probability ellipsoids and atom labeling scheme.

The solid state structure for the minor tantalocene styrene-hydride complex, **27b**, reveals the expected η^2-coordination of the styrene ligand. Although the tantalum hydride was not located in the difference map, the orientation of the styrene is clearly on the side of the metallocene wedge away from the isopropyl group (Figure 9). The isopropyl group orients itself such that the methine hydrogen points towards the phenyl group of the coordinated styrene ligand, thus minimizing unfavorable steric interactions between the olefin substituent and the ancillary ligand substitution. The C(16)-C(17) bond

distance is 1.4196(89) Å which is typical for group V olefin-hydride complexes.[10] The phenyl group on the styrene ligand is twisted 6.2 ° from the olefin plane [C(16)-C(17)-C(18)], which is reduced substantially from the 32 ° observed for $(\eta^5\text{-}C_5Me_5)_2Nb(\eta^2\text{-}CH_2CHC_6H_5)(H)$.[10]

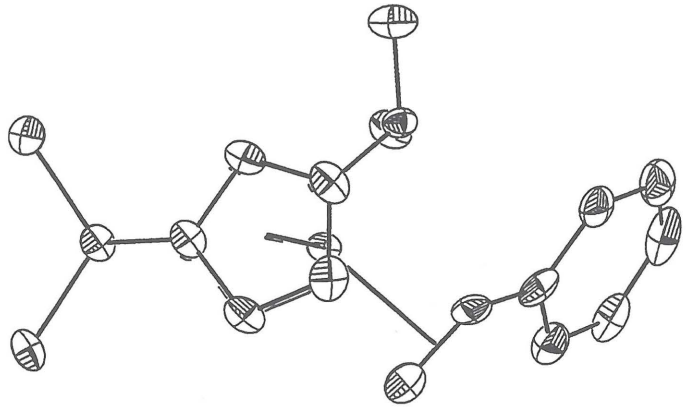

Figure 9. Top view of **27b** with 50% probability ellipsoids.

Major Isomer (60%) Minor Isomer (40%)

Figure 10. The two predominant isomers of **27**.

NOE difference NMR experiments on the mixture of isomers reveals that the major isomer, **27a**, is the one where the styrene is coordinated in the open portion of the metallocene wedge with the phenyl group oriented toward the unsubstituted cyclopentadienyl ring (Figure 10). The major isomers are the same for the propylene-hydride and styrene-hydride complexes thus demonstrating the stereodirecting ability of the isopropyl substituted ligand. Comparing the major and minor isomers of **27** indicates a 20% de for insertion into the tantalum-hydride, in accord with previous studies that demonstrate low selectivities for metallocene hydride insertions.[7] Although the enantiofacial preference for olefin

coordination is poor, the site selectivity is quite good, where at least 91% of the olefin coordination occurs away from the isopropyl substituent.

The rapid equilibration of the styrene-hydride isomers can take place by three mechanisms (Figure 11). The first pathway involves olefin insertion into the tantalum hydride followed by β-hydrogen elimination to generate the thermodynamic distribution of isomers. The second pathway generates a tantalum(III) hydride from dissociation of the styrene followed by recoordination thus equilibrating the isomers. Finally, a pathway involving rotation about π-face of olefin is also possible. This pathway can only generate one other isomer (*exo*, phenyl substituent towards Cp) in addition to **27b.** Since the isomer is not observed, this pathway has been ruled out.

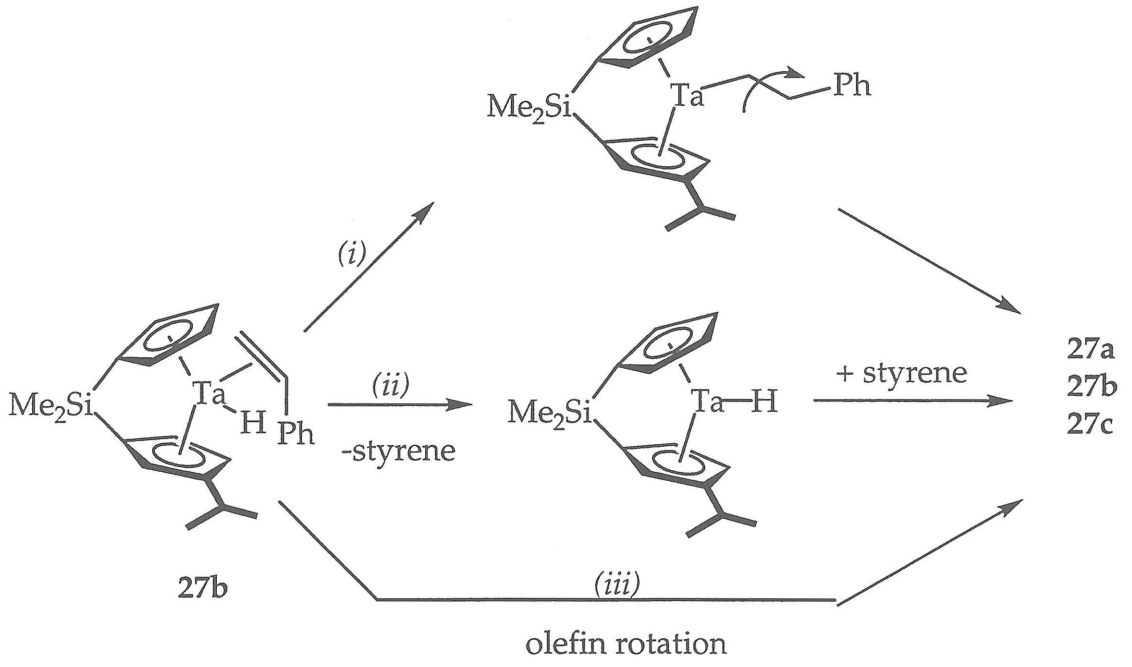

Figure 11. Possible mechanisms for styrene-hydride isomer interconversion.

In an attempt to distinguish between the two remaining pathways shown in Figure 11, olefin exchange experiments have been conducted. Addition of $^{13}CH_2=^{13}CH_2$ to a benzene-d_6 solution of **25** results in incorporation of the labeled olefin over the course of three days (eq. 9). Similarly, addition of ethylene to the isomeric mixture of styrene-hydride complexes results in formation of **25** over the course a week at 296 K. The ethylene-hydride isomer

formed from addition of ethylene to **27** is the same as the one prepared from the alkylation of **22**. Since olefin exchange is slow with respect to isomerization of **27b**, the process by which the pure styrene-hydride isomer converts to the thermodynamic mixture appears to be olefin insertion/β-hydrogen elimination (pathway *(i)*, Figure 11).

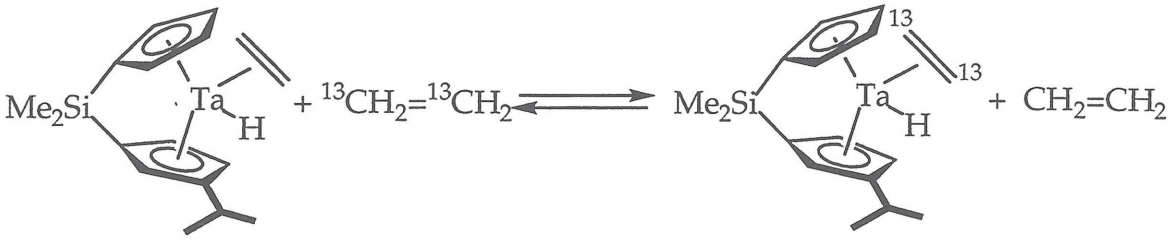

(9)

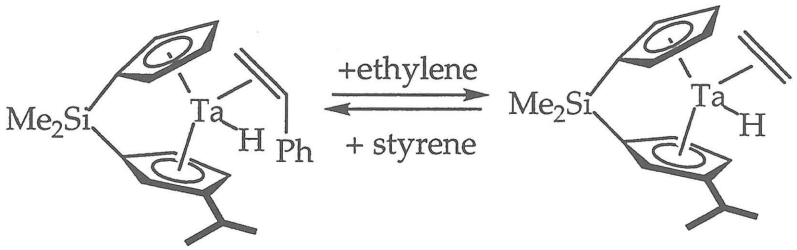

Reaction of 2.2 equivalents of CH_3CH_2MgBr to **23** results in a mixture of ethylene-hydride products, $iPr_2SpTa(\eta^2\text{-}CH_2CH_2)(H)$ (**28a**, **28b**), with the major isomer constituting 78% of the product mixture (eq. 10). NOE difference NMR experiments reveal that the major isomer, **28a**, is the one where the ethylene ligand resides in the open portion of the metallocene wedge, on the side of the molecule with the 4-isopropyl substituent. These results are consistent with the major isomer in the phosphine-hydride complexes, **18a** and **19a**. The steric differentiation between the two sides of the metallocene wedge is not as pronounced as with the iPrSp ligand since in this case two ethylene-hydride isomers are formed whereas with the monosubstituted ligand only one ethylene-hydride is observed. These results are consistent with the results obtained from the olefin polymerization experiments, where monosubstituted ligand arrays produce mainly isotactic polypropylene and the disubstituted ligands produce atactic polypropylene.

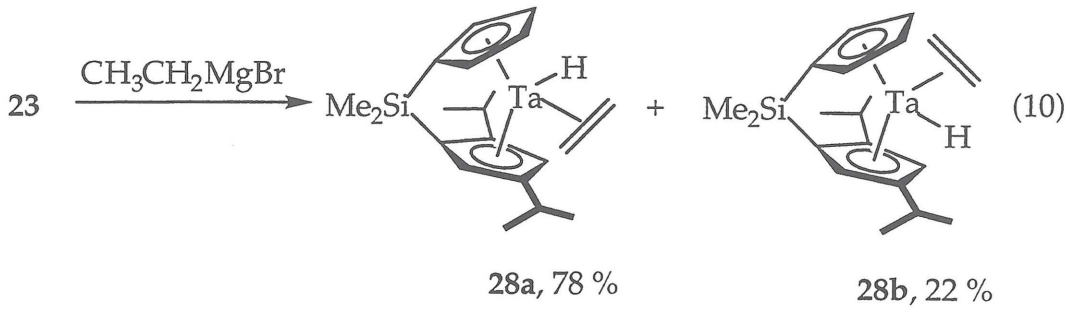

28a, 78 % **28b**, 22 %

Attempts to prepare clean propylene-hydride complexes with the [iPr$_2$Sp] ligand framework have not been successful. Addition of 2.2 equivalents of $CH_3CH_2CH_2MgBr$ to **23** does result in formation of a yellow oil consistent with formation of an olefin-hydride complex. Although the ^{1}H NMR spectrum in benzene-d_6 displays peaks indicative of the desired propylene-hydride complex, the product is not sufficiently pure to allow for definitive assignment.

Preparation of the styrene-hydride complex, iPr$_2$SpTa(η^2-CH_2CHPh)(H) (**29**), has been accomplished via addition of phenethylmagnesium chloride to a diethyl ether solution of **23** (eq. 11). Analysis of the product mixture by ^{1}H NMR spectroscopy indicates that four isomers are formed. The isomer distribution consists of two major isomers formed in 55:45 ratio constituting 87% of the styrene-hydride products. Two minor isomers composing 13% of the product mixture are formed in equal amounts. Recrystallization of the reaction mixture from cold petroleum ether affords yellow needles that are suitable for X-ray diffraction. The solid state structure of one isomer of the styrene-hydride complex is shown in Figure 12. Dissolving the crystals in benzene-d_6 reveals that the isomer that crystallizes is the major isomer formed. Monitoring the solution over time by ^{1}H NMR spectroscopy reveals that the pure **29a** undergoes rapid isomerization (~ 30 minutes at 296 K) to the thermodynamic mixture of styrene-hydride products. The major isomer, **29a**, is the one in which is the styrene ligand resides in the open portion of the metallocene wedge consistent with the major isomer formed in the ethylene-hydride complex and in the phosphine-hydride complexes. The phenyl group of the styrene ligand is directed away from the bulky isopropyl groups and towards the unsubstituted cyclopentadienyl ligand.

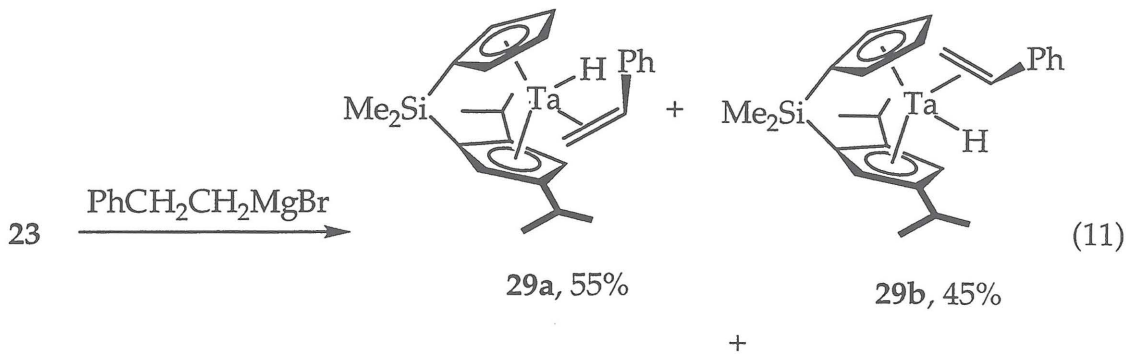

(11)

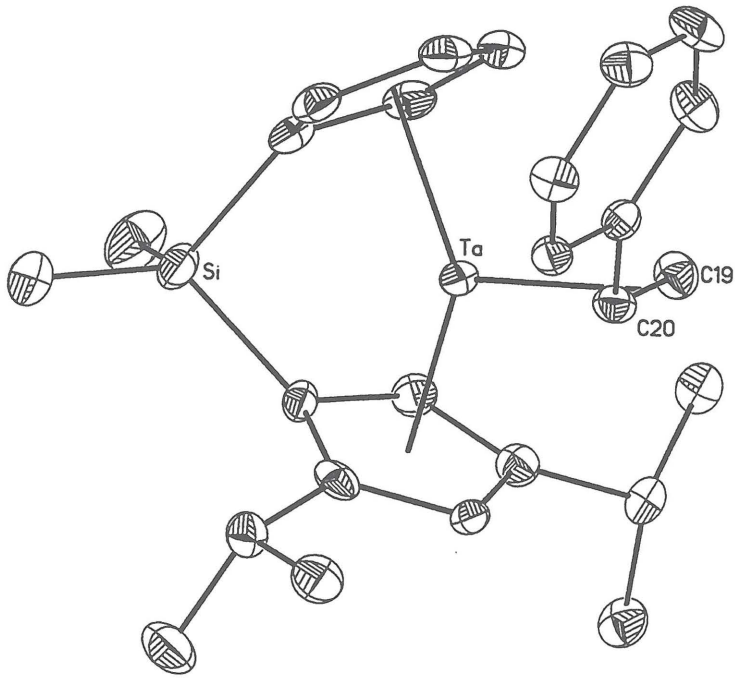

Figure 12. Partially labeled view of the molecular structure of **29a** with 50% probability ellipsoids. Hydrogen atoms are omitted for clarity.

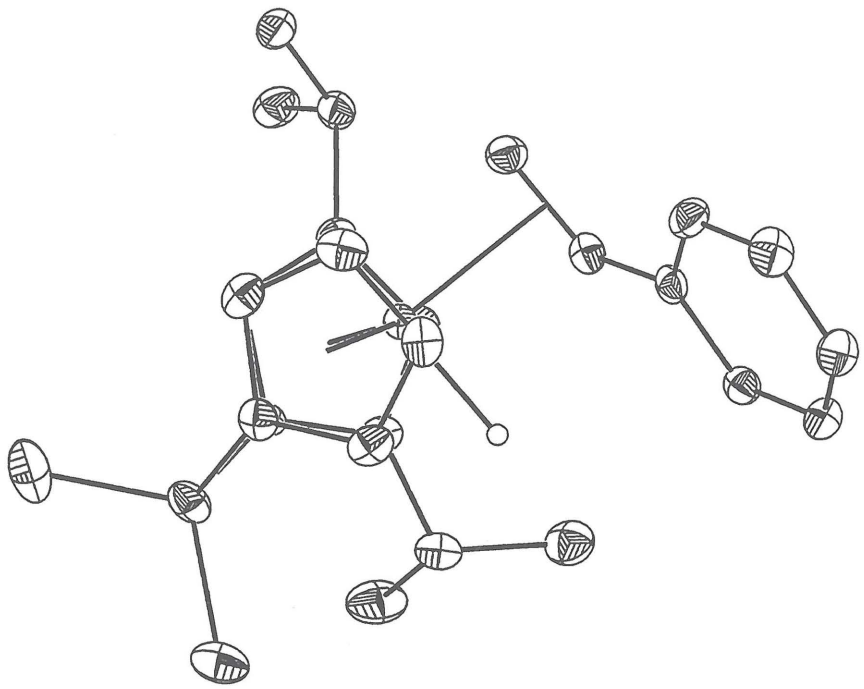

Figure 13. Top view of **29a** with 50% probability ellipsoids.

For the **29a**, all of the hydrogens, including the tantalum-hydride, have been located in the difference Fourier map. The hydride is coordinated on the side of wedge with the 2-isopropyl substituent. The Ta-H distance of 1.72 Å observed in **29a** is typical for terminal hydrides of group V metallocenes. For example, a Nb-H distance of 1.75(3) Å has been determined for $Cp^*_2Nb(CH_2{=}CHPh)(H)$[10b] while the Ta-H bond distances in Cp_2TaH_3 are 1.769(8), 1.775(9), and 1.777(9) Å.[19] As with **27b**, the coordinated styrene displays a C(19)-C(20) distance of 1.451(5) Å and the plane of the phenyl ring is twisted only 3.2 ° with respect to the olefin framework. The 2-isopropyl substituent is rotated such that the methine hydrogen is oriented towards the dimethylsilylene linker. This conformation places one isopropyl methyl group up toward the metallocene wedge. The 4-isopropyl group, being sufficiently removed from the dimethyl silylene linker, orients its methine hydrogen toward the metallocene wedge thus minimizing steric interactions between the coordinated styrene and the ancillary ligand substitution.

Alkylation of **24** with $PhCH_2CH_2MgCl$ in diethyl ether affords a yellow solid identified as one isomer of $tBuSpTa(\eta^2\text{-}CH_2CHPh)(H)$ (**30**). Slow cooling of

a petroleum ether solution of **30** deposits yellow blades that are suitable for X-ray diffraction. The solid state structure of **30**, shown in Figures 14 and 15, reveals the isomer formed is the *endo* isomer where the styrene ligand is on the more open portion of the metallocene wedge with the phenyl ring oriented away from the bulky *tert*-butyl substituent. The tantalum hydride has been located in the difference map and displays a Ta-H bond length of 1.81 Å. The C(17)-C(18) bond length of 1.445(9) Å and the 4.2 ° twist to the phenyl ring with respect to the plane of the olefin is consistent with the other *ansa*-tantalocene styrene hydride complexes.

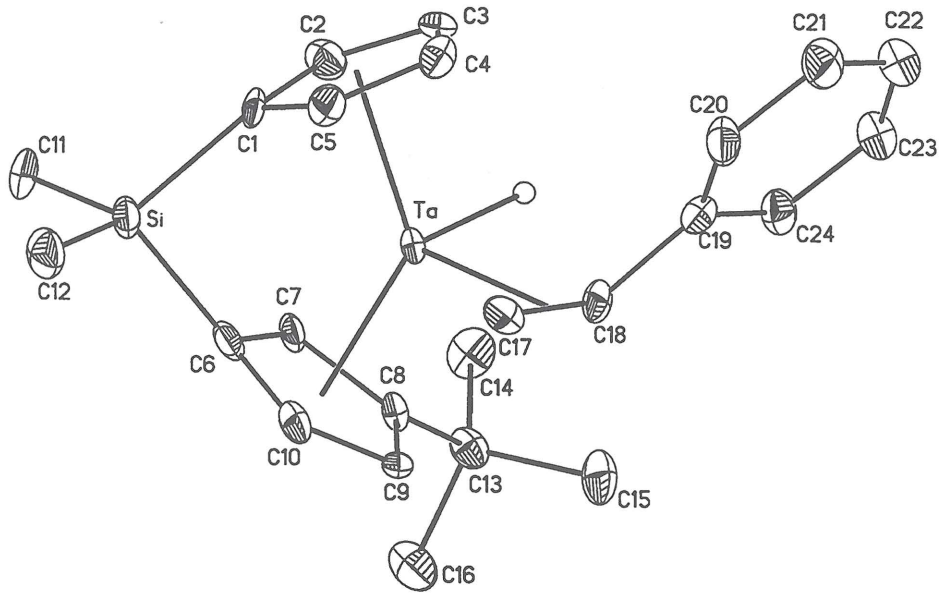

Figure 14. Molecular structure of **30** with 50% probability ellipsoids and atom labeling scheme.

The olefin-hydride complexes prepared reveal the effect of ancillary ligand substitution on the stereochemistry of olefin coordination. For [iPrSpTa], the isopropyl group is quite effective in directing coordination of ethylene such that the olefin coordinates away from the alkyl substituent 95% of the time. This result is quite surprising, since minimal steric interaction between the isopropyl substituent and the ethylene ligand would be expected. Similar directing effects are observed in iPrSpTa(η^2-$CH_2CHC_6H_5$)(H) complexes. Although only 20% diastereoselectivity is observed, the isopropyl group is effective in directing the styrene toward the open portion of the metallocene wedge. Increasing the steric

bulk of the ligand with tBuSpTa(η^2-$CH_2CHC_6H_5$)(H) results in even greater selectivity. Since the isopropyl substituent in [iPrSpTa] rotates the methine hydrogen toward the olefin, coordination of the styrene with the phenyl group oriented toward and away from the monosubstituted cyclopentadienyl ring is observed. However, in the [tBuSpTa] case, the *tert*-butyl group can only position a methyl group toward the olefin substituent and hence only one isomer is formed upon coordination of olefin.

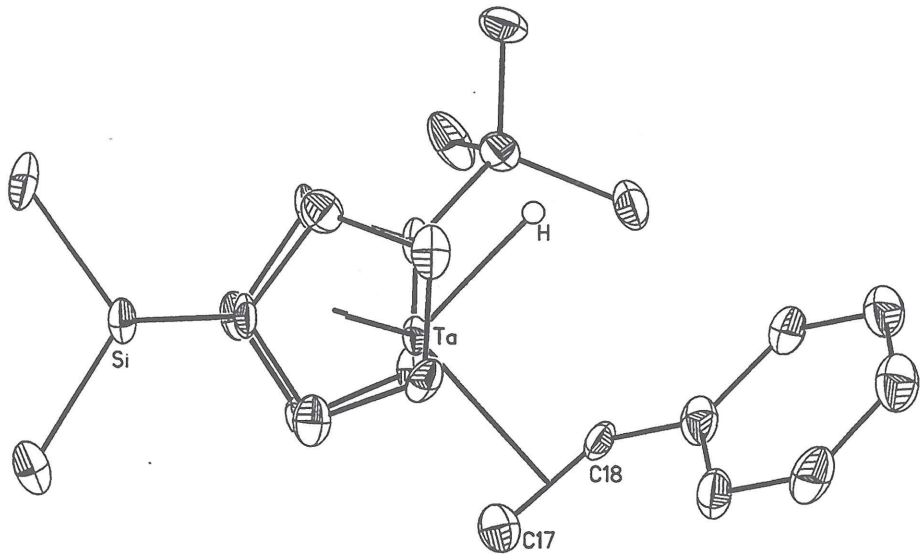

Figure 15. Top view of **30** with 50% probability ellipsoids.

In the disubstituted, [iPr_2SpTa] system, different selectivities for olefin coordination are observed. In this case, styrene-hydride isomers where the phenyl group is oriented away from the isopropyl substituents constitute 87% of the product mixture. Although the selectivity between different sides of the metallocene wedge is poor (55:45), the isopropyl groups are effective in directing the olefin substituent toward the less substituted cyclopentadienyl ring. Interestingly, in all cases studied, *endo* styrene-hydride products dominate. This contrasts previous results in *bis*-cyclopentadienyl tantalum and niobium complexes where approximately equal amounts of each isomer are observed.[10] For the *ansa*-tantalocenes, unfavorable steric interactions between the dimethylsilylene linker and the *exo*-alkyl substituent disfavor formation of *exo*-isomers.

In combination, the results indicate that ancillary ligand substitution in C_1 symmetric tantalocene olefin-hydride complexes is effective in directing the coordination of an olefin. The dimethylsilylene linker is effective in disfavoring the formation of *exo*-isomers while the cyclopentadienyl substitution directs the olefin toward a particular side of the metallocene wedge.

Preparation of Tantalum Trimethyl Complexes

Having successfully modeled the transition state geometry for the olefin-hydride transition state for C_1-symmetric ligands, we turned our attention to the preparation of olefin-alkyl complexes in order to understand the transition state for carbon-carbon bond formation. Based on theoretical predictions and studies with chiral yttrocene and zirconocene catalysts, we anticipate the geometry for the carbon-carbon bond forming transition state to have the opposite enantiofacial preference than the olefin-hydride transition state.[4-7] In order to prepare our target molecules, several synthetic strategies have been devised.

Previous reports from Schrock and our laboratory have shown that cyclopentadienyl tantalum trimethyl complexes can be converted to the ethylene-methyl complex (Figure 16).[20] Following preparation of the trimethyl complex, abstraction of one methyl group with trityl tetrafluoroborate results in formation of the tantalocene dimethyl cation. Subsequent deprotonation of one of the methyl groups with strong base affords the tantalocene methylidene-methyl complex. Bimolecular decomposition of the methylidene-methyl complex takes place over the course of hours at room temperature liberating an equivalent of an unidentified Ta(III) compound and generating $Cp_2Ta(\eta^2\text{-}CH_2{=}CH_2)(CH_3)$.

Our group has recently extended this methodology to include *ansa*-tantalocene complexes.[21] Conversion of $SpTaMe_3$ to $SpTa(\eta^2\text{-}CH_2{=}CH_2)(CH_3)$ has been accomplised using the procedure outlined in Figure 16. We therefore decided to prepare *ansa*-tantalum trimethyl complexes with the hope of being able to convert these compounds to the corresponding olefin-methyl complexes.

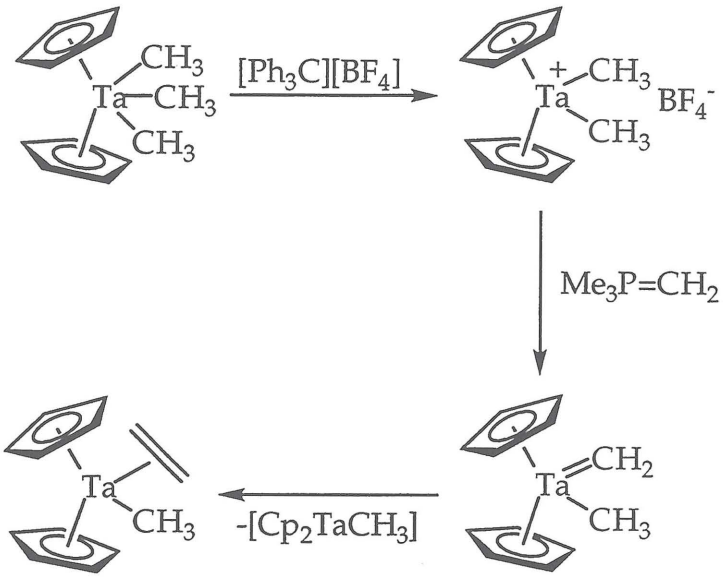

Figure 16. Synthetic route for the preparation of $Cp_2Ta(\eta^2\text{-}CH_2{=}CH_2)(CH_3)$.

Slow addition of a THF solution of $Li_2[iPr_2Sp]$ to a THF solution of $TaCl_2Me_3$ at -80 °C, results in clean formation of the tantalum trimethyl complex, $iPr_2SpTaMe_3$ (**31**), in good yield.[22] Slow cooling of a diethyl ether solution of **31** yields crystals suitable for X-ray diffraction. The solid state structure of **31** is shown in Figures 17 and 18. The tantalocene displays the expected η^5 hapticity for both cyclopentadienyl rings. The tantalum methyl groups are located in the plane of the metallocene wedge and display slightly long tantalum-methyl bond lenghts of 2.3253(71) Å (Ta-C(19)), 2.2875(66) Å (Ta-C(20)) and 2.3730(88) Å (Ta-C(21)).[23] The elongated thermal ellipsoid for C(20) is a result of crystal twinning and may be a ghost image of another tantalum center. The dimethylsilylene linker in **31** is rotated to one side of the metallocene wedge. As with **29a**, the 2-isopropyl substituent rotates the methine hydrogen toward the dimethylsilylene linker to avoid unfavorable steric interactions. This places one isopropyl methyl group toward the metallocene wedge, thus rotating the tantalum methyl groups toward one side of the metallocene.

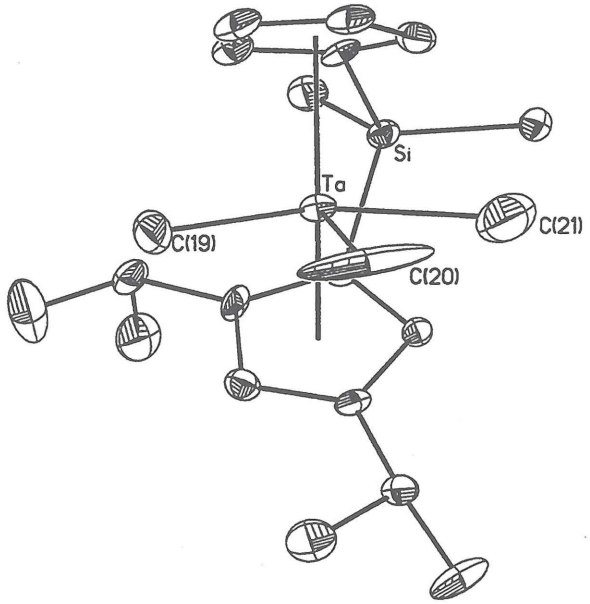

Figure 17. Molecular structure of **31** with 50% probability ellipsoids with partial atom labeling scheme. Hydrogen atoms omitted for clarity.

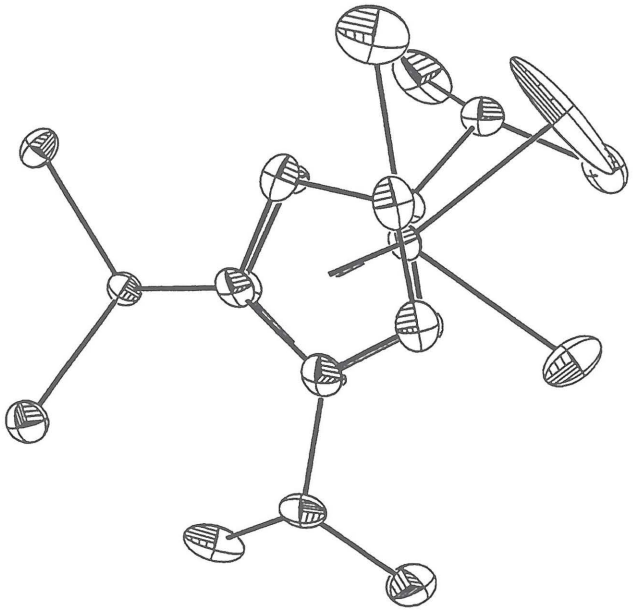

Figure 18. Top view of the solid state structure of **31** with 50% probability ellipsoids. Hydrogen atoms omitted for clarity.

Abstraction of one of the tantalum methyl groups can be accomplished via additon of $[Ph_3C][BF_4]$ to **31** yielding $[iPr_2SpTaMe_2][BF_4]$ (**32**) as a bright yellow solid. Deprotonation of one of the methyl groups proceeds readily with addition of $LiCH(SiMe_3)_2$ affording only one isomer of the methylidene-methyl complex, $iPr_2SpTa(CH_2)(CH_3)$ (**33**). Attempts to deprotonate **32** with other bases such as $LiCH_2SiMe_3$ and $LiN(SiMe_3)_2$ result in formation of **33** although the reaction is not as clean and reproducible as with $LiCH(SiMe_3)_2$. The ^1H NMR spectrum of **33** in benzene-d_6 displays two doublets at 10.22 and 10.30 ppm for the $Ta{=}CH_2$ fragment. Over the course of 12 hours in solution, **33** converts to one isomer of $iPr_2SpTa(\eta^2\text{-}CH_2CH_2)(CH_3)$ (**34**) (Figure 19). For comparison, the unsubstituted complex, $SpTa(=CH_2)(CH_3)$, converts to the ethylene-methyl complex in minutes at 296 K. The instability of both **33** and **34** has not allowed for characterization of the observed isomer by NOE difference NMR spectroscopy. The increased time required for **33** to convert to **34** is consistent with a bimolecular mechanism proposed by Schrock, since the increased steric disposition of the $[iPr_2Sp]$ increases the stability of **33** compared to $SpTa(CH_2)(CH_3)$.

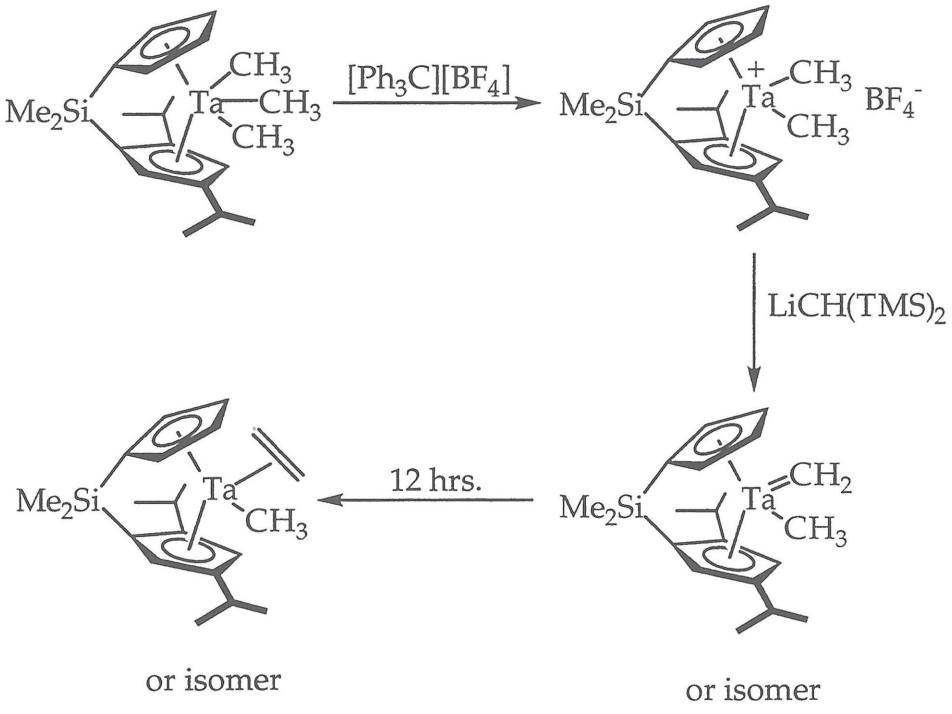

Figure 19. Preparation of **34**.

The synthetic methodology used for the preparation **31** has been extended to include other ligand arrays. The isopropylidene bridged cyclopentadienyl-fluorenyl ligand, $Me_2C(C_5H_4)$(Fluorenyl), when coordinated to zirconium and hafnium results in catalysts that are efficient in producing syndiotactic polypropylene.[24] The proposed mechanism for syndiospecific polymerization requires alternating, stereoregular propylene insertions. In order to evaluate these proposals, we felt that this ligand system would be well-suited for coordination to tantalum in an attempt to model the transition state for syndiospecific olefin polymerization.

Reaction of $Li_2[Me_2C(C_5H_4)(Fluorenyl)]$ with $TaCl_2Me_3$ in toluene affords a golden solid identified as $Me_2C(C_5H_4)(Fluorenyl)TaMe_3$ (**35**) (eq. 12). In a similar manner, reaction of $Li_2[Ph_2C(C_5H_4)(Fluorenyl)]$ with $TaCl_2Me_3$ yields $Ph_2C(C_5H_4)(Fluorenyl)TaMe_3$ (**36**) (eq. 12). The ^1H NMR spectrum of **36** displays 5 inequivalent phenyl resonances indicating restricted rotation about the phenyl-carbon bond. Similar solution behavior has been noted in similar zirconocene complexes.[25] Recrystallization of **35** from a cold mixture of CH_2Cl_2/Et_2O affords crystals suitable for X-ray diffraction, and the solid state structure is shown in Figure 20.

The solid state structure of **35** reveals an η^1 coordination of the flourenyl ligand. The average carbon-carbon bond distance in the η^5 coordinated cyclopentadienyl ring is 1.41(1) Å whereas the five membered ring in the flourenyl ligand displays long and short carbon-carbon bonds, consistent with η^1 coordination. For example, the C(9)-C(21) distance of 1.5016(13) Å suggests substantial single bond character whereas the 1.4167(45) Å and 1.4166(48) Å bond distances for C(10)-C(15) and C(16)-C(21) are indicative of carbon-carbon double bonds. The central tantalum methyl group, C(24), is colinear with the centroid formed with the cyclopentadienyl ring and is 2.2095(34) Å away from the metal center.

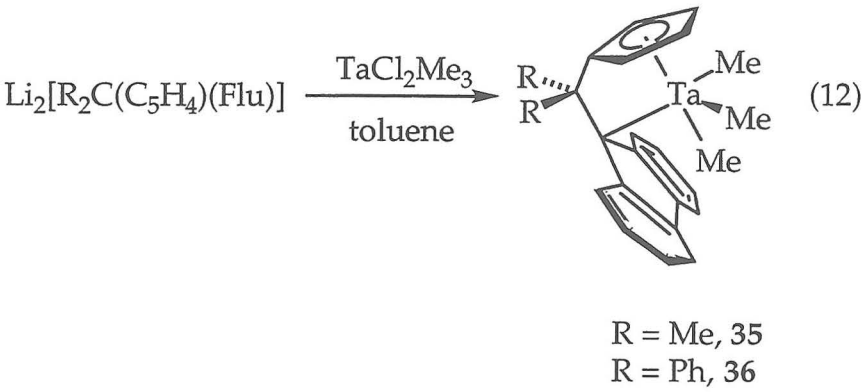

R = Me, **35**
R = Ph, **36**

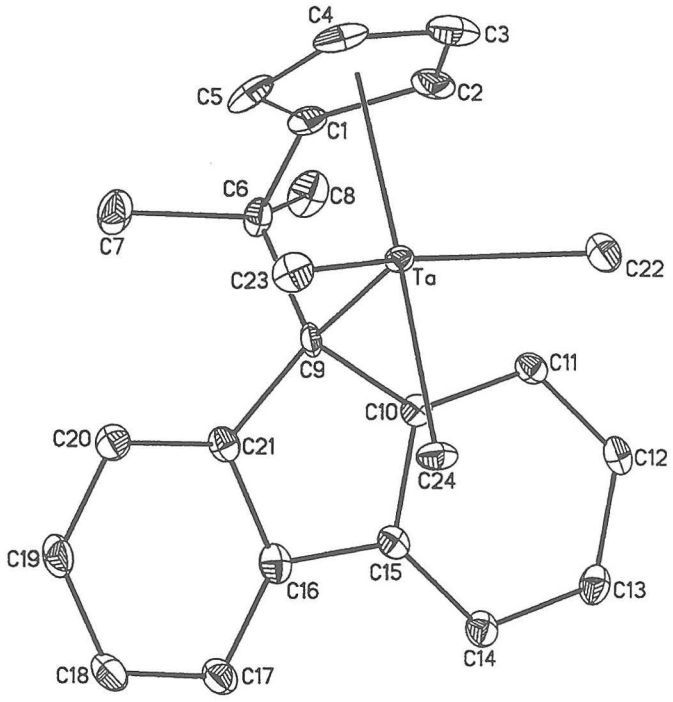

Figure 20. Molecular structure of **35** with 50% probability ellipsoids and atom labeling scheme. Hydrogens omitted for clarity.

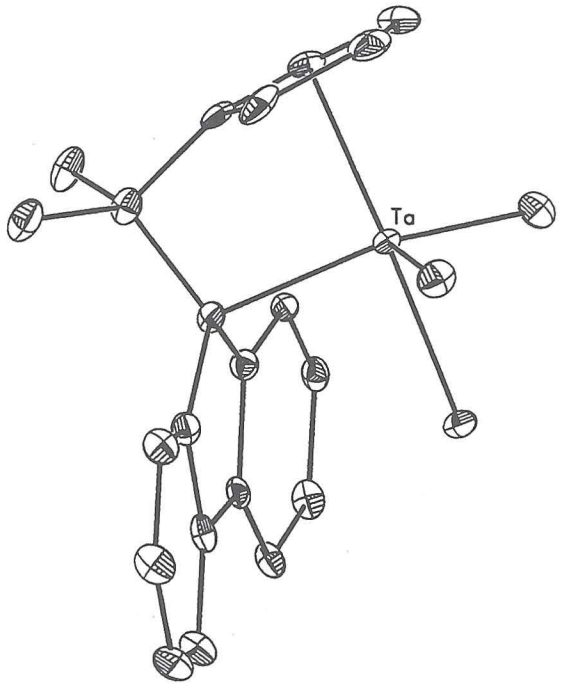

Figure 21. Side view of **35** with 50% probability ellipsoids. Hydrogens omitted for clarity.

In the batch of yellow crystals of **35**, a small amount (~ 5%) of an orange crystalline material suitable for X-ray diffraction was observed. The solid state structure of the orange material (**35a**) is shown in Figure 22 and reveals a bridged, dinuclear species where one ligand spans two [$TaClMe_3$] fragments. Both the cyclopentadienyl and fluorenyl ligands are coordinated in the expected η^5 fashion. The planes of the cyclopentadienyl and fluorenyl rings are oriented 90 ° with respect to each other. Typical tantalum-methyl bond distances {Ta(2)-C(25): 2.1877(88) Å, Ta(2)-C(26): 2.1678(112) Å, Ta(2)-C(27): 2.1890(83) Å} and tantalum-chloride bond distances {Ta(2)-Cl(2): 2.3578(5) Å} are observed for the fluorenyl portion of the molecule.[24] The methyl groups bonded to Ta(1) are slightly disordered with Cl(1) and hence a small ellipsoid and slightly longer bond length (2.2682 Å) is observed for C(22).

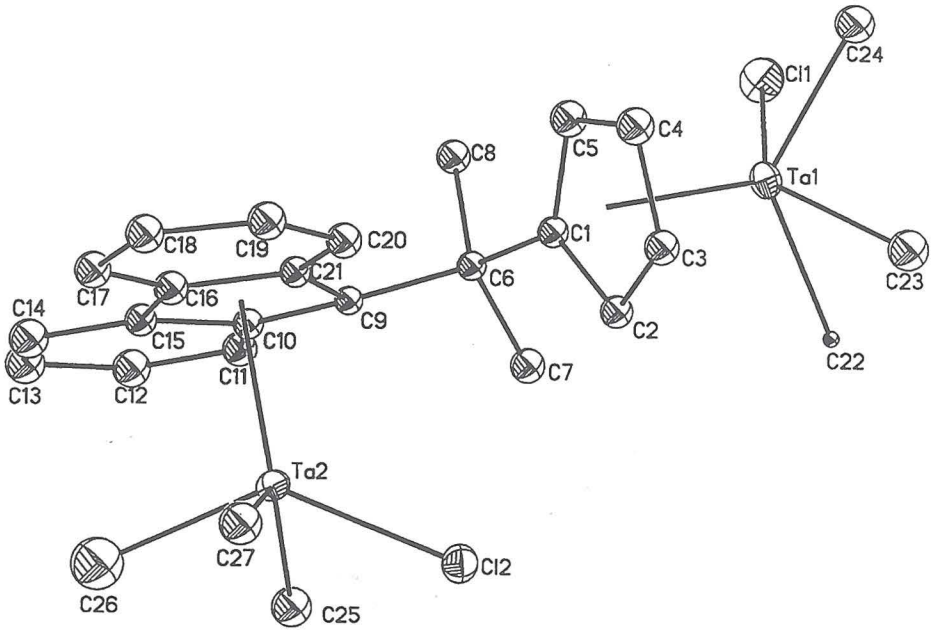

Figure 22. Molecular structure of **35a** with atom labeling scheme and 50% probability ellipsoids. Hydrogen atoms omitted for clarity.

A more sterically expansive version of the isopropylidene-linked cyclopentadienyl, fluorenyl ligand employing 1,1,4,4,7,7,10,10-octamethyl-1,2,3,4,7,8,9,10-octahydrodibenzo [b,h] fluorene (Oct) has been prepared and has been found to be useful in syndiospecific olefin polymerization.[25] Addition of $TaCl_2Me_3$ to a THF solution of $Li_2[Me_2C(C_5H_4)(Oct)]$ produces a brown solid that has been identified as $Me_2C(C_5H_4)(Oct)TaMe_3$ (**37**) on the basis of NMR spectroscopy. Unfortunately, single crystals suitable for diffraction have not been obtained and therefore the hapticity of the Oct fragment has not been determined.

Addition of HBF_4 to **35** at low temperature in toluene solution results in formation of methane and a red solid. A combination of NMR spectroscopy and X-ray crystallography reveal that the product of this reaction is not the desired dimethyl cation, $[Me_2C(C_5H_4)(Fluorenyl)TaMe_2][BF_4]$, but rather the neutral tantalocene dimethyl fluoride complex, $Me_2C(C_5H_4)(Flu)TaMe_2F$ (**38**), which arises from fluoride abstraction from BF_4^- by the dimethyl cation (eq. 13). The solid state structure for **38** is shown in Figure 23. Preparation of **38** can also be accomplished via addition of $[Ph_4C][BF_4]$ to **35**, although the reaction is not as

clean as the protonation with HBF_4. Abstraction of fluoride from BF_4^- demonstrates the increased Lewis acidity of the *ansa*-metallocene with the η^1-fluorenyl ligand as compared to Cp_2TaMe_3 and **31**.

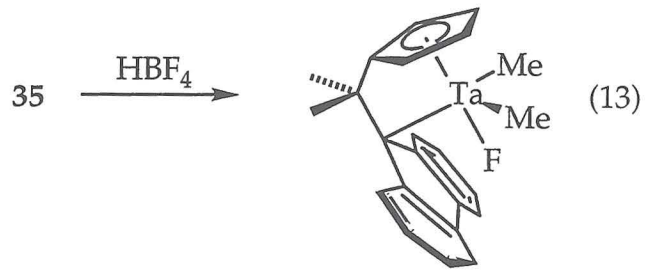

(13)

The solid state structure of **38** is analogous to that observed with **35**. The flouride ligand is colinear with the tantalum cylopentadienyl centroid and is bonded 1.9133(16) Å away from the metal center. As with **35**, the five membered portion of the fluorenyl ring displays carbon-carbon bond distances consistent with isolated single {C(9)-C(21): 1.5046(39) Å, C(9)-C(10): 1.489(39) Å; C(15)-C(16): 1.4527(11) Å)} and double bonds {C(10)-C(15): 1.4056(41), C(16)-C(21): 1.4148(39) Å)}.

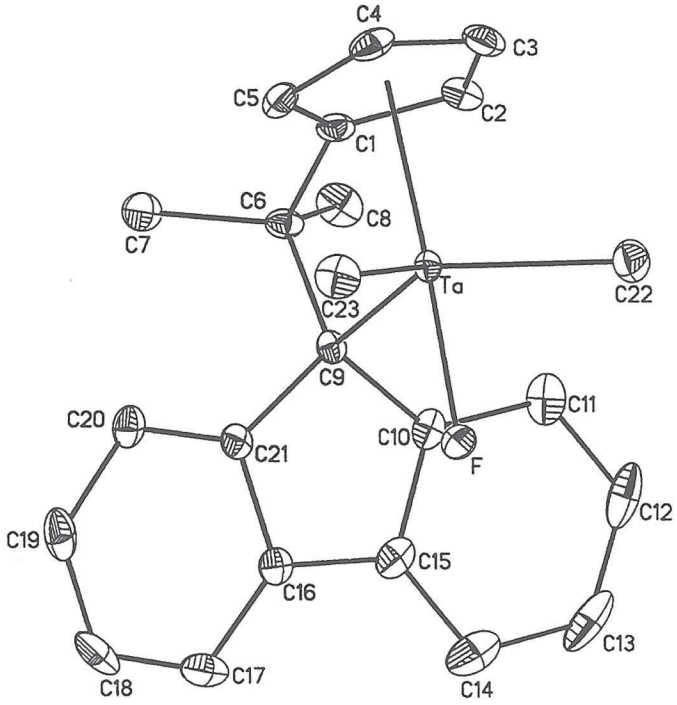

Figure 23. Molecular structure of **38** with 50% probability ellipsoids and atom labeling scheme. Hydrogen atoms omitted for clarity.

Stirring **35** with excess $ZnCl_2$ results in formation of a red powder identified as $Me_2C(C_5H_4)$(Fluorenyl)$TaMe_2Cl$ (**39**) (eq. 14). Addition of excess $ZnCl_2$ does not chlorinate the remaining tantalum methyl groups. Similar results have been observed by Bazan for reaction of (TBM)$TaMe_3$ (TBM = tribenzylidenemethane) with $ZnCl_2$.[26] Preparation of **39** can also be accomplished via addition of one equivalent of anhydrous HCl to **35**. Interestingly, addition of excess HCl to **39** does not result in protonation of the lateral tantalum methyl groups but rather protonates the fluorenyl ligand, yielding the piano stool complex, Me_2(FluorenylH)(η^5-C_5H_4)$TaMe_2Cl$. Attempts to remove the chloride ligand from **39** with $AgBF_4$, AgOTf or $NaBPh_4$ have been unsuccessful.

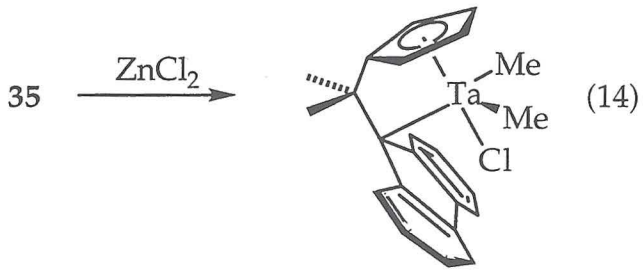

(14)

In addition to the cyclopentadienyl-fluorenyl ligand system, attempts to prepare doubly silylene-linked *ansa* tantalocene olefin-hydride and olefin-alkyl products have been pursued. These ligands have been shown to promote syndiotactic polymerization of propylene when coordinated to group 4 metals.[8] Reaction of $K_2[(Me_2Si)_2(C_5H$-2,4-$(CHMe_2)_2)(C_5H_2$-4-$SiMe_3)]$ (TMSThp) with $TaCl_2Me_3$ in Et_2O followed by filtration and recrystallization affords the tantalocene trimethyl complex, TMSThp$TaMe_3$ (**40**), as a light sensitive, golden yellow solid. Slow cooling of an Et_2O solution of **40** affords crystals that are suitable for X-ray diffraction. The solid state structure of **40** is shown in Figure 24.

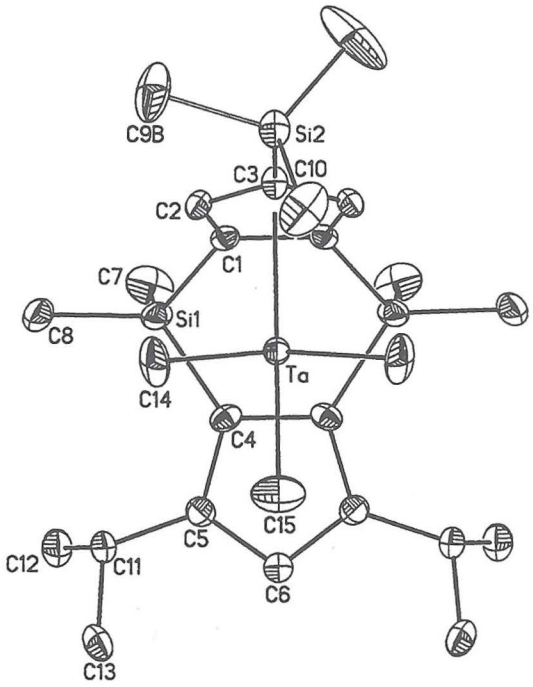

Figure 24. Molecular structure of **40** with 50% probability ellipsoids and atom labeling scheme as viewed in the equitorial plane. Selected bond lengths (Å): Ta-Cent(1), 2.131; Ta-Cent(2), 2.378. Bond angles (deg): Cent(1)-Ta-Cent(2), 96.9. Cent(1) is the centroid formed by C(1), C(2), C(3), C(1A), C(2A) and Cent(2) is the centroid formed by C(4) and C(4A).

Yellow blades of **40** crystallize in the orthorombic space group P_{nma} and contain a mirror plane of symmetry containing the tantalum atom, the cyclopentadienyl centroids and the central tantalum methyl group. The metallocene displays an unusual η^5, η^2 coordination of the cyclopentadienyl groups. The centroid formed by the η^5-cyclopentadienyl ring and the central tantalum methyl group (C15) are colinear. No significant deviations (1.40-1.43 Å) in the carbon-carbon bond lengths are observed in the two cyclopentadienyl rings. Typical tantalum-methyl group distances are observed, with Ta-C(14) being 2.2026(60) Å and Ta-C(15) being 2.2114(90) Å.

Dihapto coordination of a cyclopentadienyl ring, although rare, has been observed in other transition metal and main group complexes. Green[27] has determined the solid state structure of $(\eta^5\text{-}C_5H_5)_2Ti(\eta^2\text{-}C_5H_5)$ by X-ray diffraction. The dihapto cyclopentadienyl ring has no significant deviations in the carbon-carbon bond distances, each being 1.42-1.44 Å. Shapiro has identified a

number of cyclopentadienyl aluminum compounds that display η^2 cyclopentadienyl ring coordination.[28] Molecular structure determinations, NMR spectroscopic measurements and theoretical calculations indicate that in the absence of Lewis bases or π-bonding substituents, the η^2 geometry of the cyclopentadienyl ring is preferred.

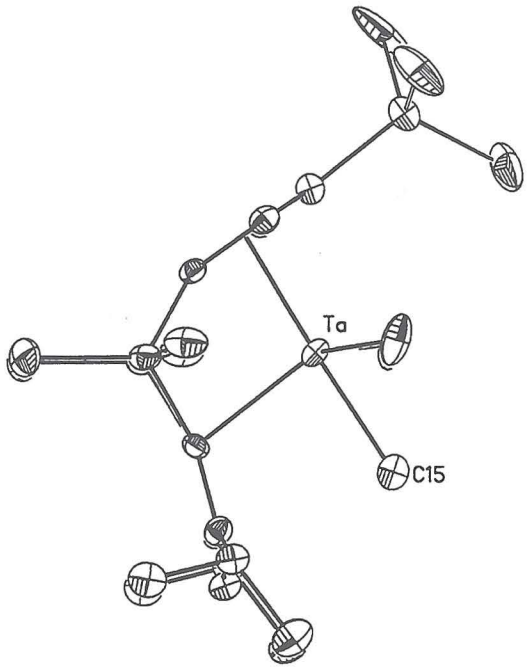

Figure 25. Side view of **40** with 50% probability ellipsoids.

The reactivity of **40** has been briefly explored. Addition of one equivalent of HCl results in protonation of the central methyl group resulting in the C_s symmetric, TMSThpTaMe_2Cl (**41**) (eq. 15). Exposure of **36** to an atmosphere of dihydrogen results in rapid decomposition. Likewise, reaction of [Ph_3][BF_4] with **36** results in decomposition. Addition of PMe_3 produces no reaction even at elevated temperatures.

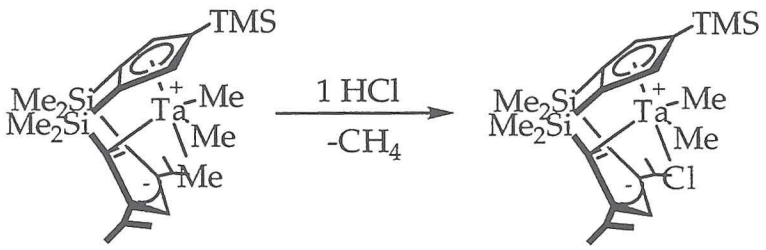

(15)

Reactivity of Olefin-Hydride Complexes

Another synthetic approach to the desired olefin-alkyl complexes is to trap a Ta(III) alkyl species with an olefin such as ethylene or propylene. Previous work has demonstrated that reaction of $Cp^*_2Nb(\eta^2\text{-}CH_2{=}CH_2)(H)$ with carbon monoxide and methylisocyanide results in formation of $Cp^*_2Nb(CH_2CH_3)(L)$ (L = CO, CH_3NC)[10] thus suggesting that trapping of the punantive M(III) alkyl is synthetically feasible. Tebbe[16] has shown that thermolysis of Cp_2MH_3 (M = Nb, Ta) in the presence of excess ethylene affords $Cp_2M(CH_2CH_3)(\eta^2\text{-}CH_2{=}CH_2)$, demonstrating the ability of ethylene to trap the M(III) intermediate.

Addition of ethylene to **25** at room temperature results in slow olefin exhange rather than trapping of a Ta(III) ethyl species (*vide supra*). Heating a benzene-d_6 solution of **25** in the presence of ethylene does produce one isomer of the desired iPrSpTa$(CH_2CH_3)(\eta^2\text{-}CH_2{=}CH_2)$ (**42**). However, upon standing, **42** undergoes loss of ethylene affording a mixture of **42** and **45** thus preventing definitive characterization of the tantalocene olefin alkyl.

In a similar experiment, excess styrene (> 15 equivalents) has been added to **30**. No reaction is observed at 25 °C after one week. Heating the reaction mixture to 87 °C for several days results in formation of a very small amount (~ 5%) of the desired tantalocene styrene phenylethyl complex (eq. 16). In an attempt to increase the equilibrium concentration of the desired olefin alkyl complex, pentafluorostyrene has been added to **30**. It was hypothesized that fluorination of the phenyl ring would lower the energy of the π^* molecular orbital of the C=C double bond which in turn would increase the metal to olefin backbonding interaction thus shifting the equilibrium toward the olefin alkyl complex. Unfortunately, heating **30** with pentafluorostyrene for one week produced no desired product.

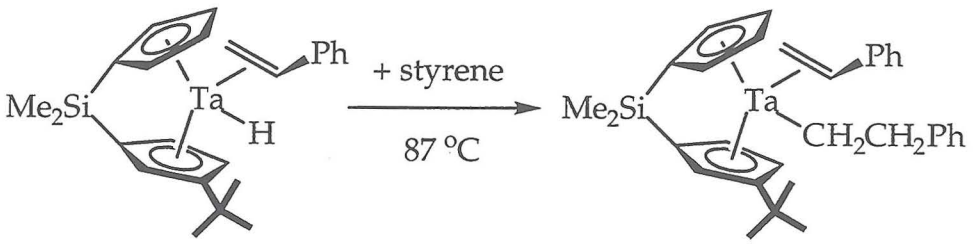

30

or isomer (16)

trace amounts

Since addition of olefin to the tantalocene olefin hydride complexes has not produced any of the target complexes, addition of other smaller neutral ligands has been attempted. Addition of 15 equivalents of PMe_3 to **30** produces no reaction over the course of several days at 25 °C. Heating the reaction mixture to 87 °C results no desired product; only a small amount (~ 5%) of exchange of PMe_3 for coordinated styrene is observed (eq. 17).

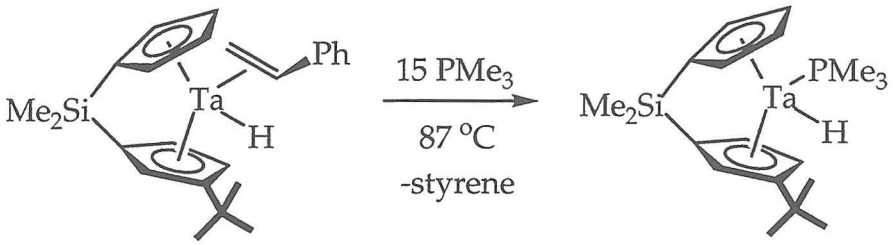

30 **20** (17)

(~ 5% conversion)

Addition of 1 atmosphere of carbon monoxide to **30** at 87 °C results in formation of **13** and tBuSpTa(CH_2CH_2Ph)(CO) (eq. 18). The identity of the phenyl ethyl carbonyl has yet to be established by NOE difference NMR spectroscopy. Similar results have been obtained in related permethylniobocene olefin-hydride complexes.

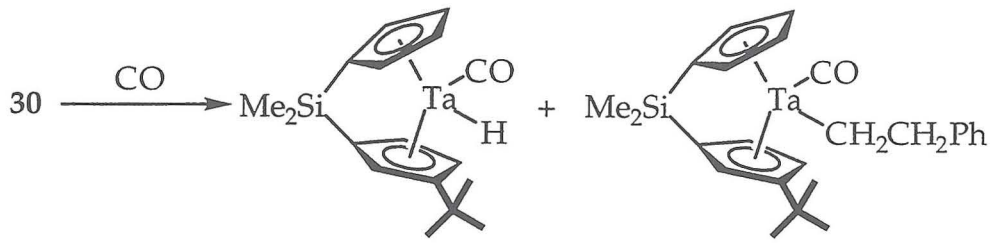

(18)

or isomer

Conclusions

A variety of singly silylene-bridged tantalocene trichloride complexes has been prepared via tin elimination from the distannylated cyclopentadienyl ligands. Reduction of the trichloride complexes followed by hydrolysis results in formation of the tantalocene trihydride complexes. At elevated temperatures, the tantalum trihydride complexes undergo clean reaction with a variety of ligands such as phosphines, carbon monoxide and olefins to yield the ligand-hydride species, $Me_2Si(C_5H_4)(C_5H_2\text{-}R_1\text{-}R_2)Ta(H)(L)$ (L = PR_3, CO, ethylene) species. For C_1 -symmetric metallocenes, the isomeric distribution of the product mixture is dependent on both cyclopentadienyl substitution and on the nature of the incoming ligand. In both cases, increased steric bulk results in higher selectivities.

Reduction of the tantalocene trichloride complexes with zinc dust results in formation of the Ta(IV) dichloride species. These compounds undergo alkylation with addition of excess Grignard reagents, forming olefin-hydride complexes. For iPrSpTa(η^2-CH_2=CH_2)(H), one isomer is observed and has been determined to be the one in which the olefin coordinates to the open side of the metallocene wedge away from the isopropyl substituent. Similar results have been obtained with styrene-hydrides and propylene-hydrides. For each ligand array, the styrene-hydride complexes have been characterized by X-ray crystallography. In the case of $iPr_2SpTa(\eta^2\text{-}CH_2\text{=}CHPh)(H)$ and tBuSpTa(η^2-CH_2=CHPh)(H) , the major isomer has been crystallized and is the *endo* isomer in which the phenyl substitutuent orients to avoid interactions with the ligand alkyl groups. For iPrSpTa(η^2-CH_2=CHPh)(H), the minor isomer crystallizes from solution but upon dissolution in benzene converts to the thermodynamic

mixture of products. In all cases studied, the ancillary ligand substitution is effective in directing the coordination of the olefin.

A variety of singly and doubly bridged *ansa*-tantalocene trimethyl complexes have been prepared and structurally characterized. For fluorenyl substituted ligands, the fluorenyl ligand adopts an η^1 hapticity upon coordination to tantalum. For the doubly silylene bridged tantalocene, TMSThpTaMe$_3$, an unusual η^2 coordinated cyclopentadienyl ring is observed. In one case, iPr$_2$SpTaMe$_3$, the trimethyl complex has been converted to a desired olefin-alkyl complex, iPr$_2$SpTa(η^2-CH$_2$=CH$_2$)(CH$_3$).

Experimental

General Considerations. All air- and moisture-sensitive compounds were manipulated using standard vacuum line, Schlenk or cannula techniques or in a drybox under a nitrogen atmosphere as described previously.[29] Argon, dinitrogen and dihydrogen gases were purified by passage over columns of MnO on vermiculite and activated molecular sieves. Toluene and petroleum ether were distilled from sodium and stored under vacuum over titanocene.[30] Tetrahydrofuran, dimethoxyethane and ether were distilled from sodium benzophenone ketyl. Tetrahydrofuran-d_8 was distilled from sodium benzophenone ketyl and stored over 4Å molecular sieves. Dichloromethane-d_2 was distilled from CaH$_2$. TaCl$_5$, (*n*-Bu)$_3$SnCl, 1.0 M LiAlH$_4$ in diethyl ether, 3.0 CH$_3$CH$_2$MgBr in diethyl ether, 2.0 M CH$_3$CH$_2$CH$_2$MgCl in diethyl ether, 1.0 M PhCH$_2$CH$_2$MgBr in THF, 54% HBF$_4$ in diethyl ether, PMe$_3$ and PEt$_3$ were purchased from Aldrich and used as received. Carbon monoxide was purchased from Matheson, and anhydrous hydrochloric acid was purchased from Aldrich. Zinc dust and ZnCl$_2$ were purchased from Strem Chemical and dried at 100 °C under high vacuum. Ethylene was purchased from Matheson and passed through a dry ice trap immediately before use. All dilithio salts of ligands were prepared according to standard procedures[31] while TaCl$_2$Me$_3$ was prepared according to literature procedures.[20]

NMR spectra were recorded on a JEOL GX-400 (^{1}H, 399.78 MHz, ^{13}C, 100.53 MHz, ^{31}P, 161.9 MHz, ^{19}F, 376.1 MHz) or a Varian Inova 500 (^{1}H, 500.13 MHz, ^{13}C, 125.77 MHz). All chemical shifts are relative to TMS for ^{1}H (residual) and ^{13}C (solvent as a secondary standard and H_3PO_4 for ^{31}P). Nuclear Overhauser Difference experiments were carried out on a Varian Inova 500 MHz spectrometer. Elemental analyses were carried out at the Caltech Analytical Facility by Fenton Harvey or by Midwest Microlab, Indianapolis, Indiana.

$[Me_2Si(C_5H_4)_2][n\text{-}Bu_3Sn]_2$ (1). In the dry box, a 100 mL round bottom flask was charged with 3.50 g (17.5 mmol) of $Li_2[Me_2Si(\eta^5\text{-}C_5H_4)_2]$. The white solid was slurried in 30 mL of Et_2O. Via pipette, 11.97 g (36.8 mmol) of *n*-Bu_3SnCl was added over the course of 15 minutes. The reaction flask was then attached to a swivel frit assembly and stirred for 3 days at room temperature. The yellow Et_2O solution was filtered and the white precipitate washed with recycled Et_2O. The Et_2O was removed *in vacuo* leaving a 12.5 g (92.5%) of a yellow oil identified as **1**. ^{1}H NMR (benzene-d_6): δ = 0.162 (s, 6H, Si*Me*$_2$); 0.760 (t, 7 Hz, 18H, Sn-$CH_2CH_2CH_2CH_3$); 1.10 (m, 12H, Sn*Bu*$_3$); 1.13 (m, 12H, Sn*Bu*$_3$); 1.41 (m, 12H, Sn*Bu*$_3$); 5.96 (m, 4H, Cp); 6.58 (m, 4H, Cp). ^{13}C NMR (benzene-d_6): δ = 0.595 (Si*Me*$_2$); 12.23 (Sn*Bu*$_3$); 14.37 (Sn*Bu*$_3$); 17.92 (Sn*Bu*$_3$); 28.32 (Sn*Bu*$_3$); 109.96, 133.24, 133.46 (Cp).

$Me_2Si(\eta^5\text{-}C_5H_4)_2TaCl_3$ (2). In the dry box, 5.60 g (7.30 mmol) of **1** was charged into a 100 mL round bottom flask and dissolved in approximately 50 mL of Et_2O, forming a clear solution. Small portions of $TaCl_5$ (2.61 g; 7.30 mmol) were then added slowly to the reaction mixture. A red solid forms upon addition of $TaCl_5$. The flask was attached to a swivel frit assembly and the reaction mixture stirred for 12 hours. The solid was collected by filtration and was washed with small portions of Et_2O. The red solid was dried *in vacuo* yielding 2.80 g (81%) of **2**. ^{1}H NMR (THF-d_8): δ = 0.97 ppm (s, 6H, Si*Me*$_2$); 6.52 (m, 4H, Cp); 7.71 (m, 4H, Cp). ^{13}C NMR (THF-d_8): δ = 12.38 (Si*Me*$_2$); 115.21, 134.74, *1 not located* (Cp).

$Me_2Si(\eta^5\text{-}C_5H_4)_2TaH_3$ (3). In the dry box, 1.00 g (2.02 mmol) of **2** is charged into a round bottom flask and attached to a medium swivel frit assembly. On the vacuum line, approximately 15 mL of Et_2O was added by vacuum transfer. At -80 °C, 15.0 mL (15 mmol) of 1.0 M $LiAlH_4$ solution was added via syringe against an argon counterflow. With addition, a yellow solid forms. The reaction

mixture was warmed to room temperature and stirred overnight. Via syringe, 2.0 mL of saturated NH_4Cl solution was added at 0 °C. With addition of the NH_4Cl solution an exothermic reaction and formation of white precipitate ensued. The reaction mixture was stirred for 1 hour and then filtered. The white solid was washed with Et_2O several times. The Et_2O was removed *in vacuo* leaving 0.260 g (33%) of a white solid identified as **3**. ^1H NMR (benzene-d_6): δ = -1.95 (d, -0.04, 15 Hz, 2H Ta-*H*); 0.02 (t, 10 Hz, 1H, Ta-*H*); -0.04 (s, 6H, Si*Me*$_2$); 4.84 (m, 4H, Cp); 5.36 (m, 4H, Cp).

$Me_2Si(\eta^5\text{-}C_5H_4)(\eta^5\text{-}C_5H_3\text{-}3\text{-}CHMe_2)TaCl_3$ (4). Prepared in an analogous manner to **2** with 4.90 g (6.06 mmol) of $[Me_2Si(\eta^5\text{-}C_5H_4)(\eta^5\text{-}C_5H_3\text{-}CHMe_2)][Sn(n\text{-}Bu)_3]_2$ and 2.17 g (6.05 mmol) of $TaCl_5$ affording 2.00 g (64%) of **4**. ^1H NMR (THF-d_8): 0.895 (s, 3H, Si*Me*$_2$); 0.961 (s, 3H, Si*Me*$_2$); 1.29 (d, 6.5 Hz, 3H, CH*Me*$_2$); 1.37 (d, 6.5 Hz, 3H, CH*Me*$_2$);. 2.87 (sept, 7 Hz, 1H, C*H*Me$_2$); 6.28, 6.56, 6.97, 7.28, 7.35, 7.61, 7.79 (m, 1H, Cp). ^{13}C NMR: (THF-d_8): δ = -5.20 (Si*Me*$_2$), -5.48 (Si*Me*$_2$), 20.77 (CH*Me*$_2$), 24.44 (CH*Me*$_2$), 30.52 (C*H*Me$_2$), 115.34, 116.56, 116.78, 135.42, 138.29, 138.47 (Cp).

$[Me_2Si(C_5H_4)(C_5H_2\text{-}2,4\text{-}(CHMe_2)_2)][n\text{-}Bu_3Sn]_2$. Prepared in an analogous manner to **1** with 3.80 g (13.6 mmol) of $Li_2[Me_2Si(C_5H_4)(C_5H_2\text{-}(CHMe_2)_2]$ and 9.70 g (29.4 mmol) of *n*-Bu_3SnCl affording 10.5 g (90.5%) of $Me_2Si(C_5H_4)(C_5H_2\text{-}(CHMe_2)_2)][n\text{-}Bu_3Sn]_2$. ^1H NMR(CD_2Cl_2): δ = 0.02 (s, 3H, Si*Me*$_2$); 0.30 (s, 3H, Si*Me*$_2$); 0.81 (t, 7 Hz, 18H, Sn*Bu*$_3$); 0.89 (t, 7 Hz, 18H, Sn*Bu*$_3$); 1.1-1.6 (m, Sn*Bu*$_3$); 2.60 (sept, 7Hz, 1H; C*H*Me$_2$); 2.69 (sept, 7 Hz, 1H; C*H*Me$_2$); 5.30 (m, 1H, Cp); 5.55 (m, 1H, Cp); 5.91 (m, 1H, Cp); 6.02 (m, 1H, Cp); 6.10 (m, 1H, Cp).

$Me_2Si(\eta^5\text{-}C_5H_4)(\eta^5\text{-}C_5H_2\text{-}2,4\text{-}(CHMe_2)_2)TaCl_3$ (5). Prepared in an analogous manner to **2** with 6.50 g (7.58 mmol) of $[Me_2Si(\eta^5\text{-}C_5H_4)(\eta^5\text{-}C_5H_2\text{-}(CHMe_2)_2)][n\text{-}Bu_3Sn]_2$ and 2.70 g (7.54 mmol) of $TaCl_5$ affording 2.54 (60%) of **5**. ^1H NMR (CD_2Cl_2): δ = 0.05 (s, 3H, Si*Me*$_2$); 0.30 (s, 3H, Si*Me*$_2$); 2.64 (sept; 7H, 1H, C*H*Me$_2$); 2.72 (sept; 7 Hz, 1H, C*H*Me$_2$); 5.31 (m, 1H, Cp); 5.57 (m, 1H, Cp); 5.92 (m, 1H, Cp); 6.42 (m, 1H, Cp); 6.49 (m, 1H, Cp); 6.58 (m, 1H, Cp). Anal. Cald. for $Ta_1Si_1C_{18}H_{26}Cl_3$ C, 38.76%, H, 4.70%; Found C, 37.96%; H, 4.55%.

$[Me_2Si(C_5H_4)(C_5H_3\text{-}3\text{-}CMe_3)][n\text{-}Bu_3Sn]_2$. Prepared in an analogous manner to **1** with 3.00 g (11.7 mmol) of $Li_2[Me_2Si(C_5H_4)(C_5H_3\text{-}3\text{-}(CMe_3))]$ and 8.10 g (24.5

mmol) of *n*-Bu_3SnCl affording 8.73 g (90%) of $[Me_2Si(C_5H_4)(C_5H_3\text{-}3\text{-}(CMe_3))][SnBu_3]_3$. ^1H NMR (benzene-d_6): δ = 0.42 (s, 3H, Si*Me*$_2$); 0.45 (s, 3H, Si*Me*$_2$); 1.45 (s, 9H, C*Me*$_3$); 0.90-1.10, 1.30-1.65 (m, Sn*Bu*$_3$); 5.75, 5.81, 6.24, 6.56, 6.73, 6.88, 6.92 (m, 1H, Cp). ^{13}C NMR (benzene-d_6): 11.72, 12.17 (Si*Me*$_2$); 30.11 (C*Me*$_3$); 154.45 (*C*Me$_3$); 14.26, 17.71, 27.45, 28.00, 28.22, 28.55, 29.85, 32.00 (Sn*Bu*$_3$); 97.54, 98.67, 103.59, 115.63, 121.51, 126.86, 132.29, 132.98, *2 not located* (Cp).

$Me_2Si(\eta^5\text{-}C_5H_4)(\eta^5\text{-}C_5H_3\text{-}3\text{-}(CMe_3))TaCl_3$ (6). Prepared in an analogous manner to **2** with 4.55 g (5.47 mmol) of $[Me_2Si(C_5H_4)(C_5H_3\text{-}(CMe_3)][Sn(n\text{-}Bu)_3]_2$ and 1.96 g (5.47 mmol) of $TaCl_5$ affording 1.50 g (51.7%) of **6**. ^1H NMR (THF-d_8): δ = 1.113 (s, 3H, Si*Me*$_2$); 1.17 (s, 3H, Si*Me*$_2$); 1.40 (s, 9H, C*Me*$_3$); 6.23, 6.38, 6.69, 7.27, 7.64, 7.80 (s, 1H, Cp). ^{13}C NMR (THF-d_8): -1.68, -0.27 (Si*Me*$_3$); 33.34 (C*Me*$_3$); 151.71 (*C*Me$_3$); 109.52, 112.83, 118.90, 120.72, 124.61, 131.82, 144.62, *3 not located* (Cp). Anal. Cald. for $Ta_1Si_1C_{16}H_{22}Cl_3$ C, 36.28%, H, 4.19%; Found C, 35.75%; H, 3.55%.

$Me_2Si(\eta^5\text{-}C_5H_4)(\eta^5\text{-}C_5H_3\text{-}3\text{-}CHMe_2)TaH_3$ (7). Prepared in an analogous manner to **3** employing 1.00 g (1.94 mmol) of **4** and 14.5 mL (14.5 mmol) of 1 M $LiAlH_4$ and quenched with 2.0 mL of saturated NH_4Cl solution yielding 0.257 g (31.8%) of a white solid identified as **7**. ^1H (benzene-d_6): δ = -0.002 (s, 3H, Si*Me*$_2$), -0.05 (s, 3H, Si*Me*$_2$), 1.2 (d, 6 Hz, 6H, CH*Me*$_2$), 2.73 (sept, 7 Hz, C*H*Me$_2$), 4.83, 4.91, 5.03, 5.05, 5.22, 5.28, 5.51 (m, 1H, Cp), -1.64 (dd, 11.5 Hz, 12 Hz, 1H, Ta*H*), -1.80 (dd, 11 Hz, 12 Hz, 1H, Ta*H*), 0.52 (t, 12 Hz, Ta*H*). ^{13}C (benzene-d_6): δ = -5.93 (*Me*$_2$Si), -4.66 (*Me*$_2$Si), 24.39 (CH*Me*$_2$), 25.04 (CH*Me*$_2$), 28.54 (CHMe$_2$), 88.08, 88.97, 89.21, 90.52, 93.69, 94.27, 97.66, 3 *not located* (Cp).

$Me_2Si(\eta^5\text{-}C_5H_4)(\eta^5\text{-}C_5H_2\text{-}2,4\text{-}(CHMe_2)_2)TaH_3$ (8). Prepared in an analogous manner to **3** employing 0.900 g (1.61 mmol) of **5** and 11.8 mL of 1.0 M $LiAlH_4$. The reaction was quenched with 1.6 mL of saturated NH_4Cl solution affording 0.235 g (32.1%) of **8** as a yellow oil. ^1H NMR (benzene-d_6): δ = 0.13 (s, 3H, Si*Me*$_2$), 0.26 (s, 3H, Si*Me*$_2$), 1.16 (d, 6 Hz, 3H, CH*Me*$_2$), 1.29 (d, 6 Hz, 6H, CH*Me*$_2$), 1.42 (d, 6 Hz, 3H, CH*Me*$_2$), 2.68 (sept, 7 Hz, 1H, C*H*Me$_2$), 2.88 (sept, 7 Hz, 1H, C*H*Me$_2$), 4.69, 4.73, 5.11, 5.18, 5.21, 5.70 (bs, 1H, Cp), 0.75 (t, 12 Hz, 1H, Ta*H*), -1.76 (m, 1H, Ta*H*), -1.48 (m, 1H, Ta*H*). ^{13}C NMR (toluene-d_8): -3.69 (Si*Me*$_2$), -3.72 (Si*Me*$_2$), 21.06 (CH*Me*$_2$), 24.13 (CH*Me*$_2$), 24.65 (CH*Me*$_2$), 28.24

(CH*Me*$_2$), 29.42 (CHMe$_2$), 30.17(CHMe$_2$), 62.93, 68.04, 86.22, 87.86, 88.74, 92.58, 92.67, 98.51, 126.24, 129.03 (Cp).

Me$_2$Si(η^5-C$_5$H$_4$)(η^5-C$_5$H$_3$-3-(CMe$_3$))TaH$_3$ (9). Prepared in an analogous manner to **3** employing 0.760 g (1.43 mmol) of **6** and 10.2 mL of 1.0 M LiAlH$_4$. The reaction was quenched with 1.75 mL of saturated NH$_4$Cl solution affording 0.250 g (37.5 %) of **9**. ^{1}H NMR (benzene-d_6): δ = -1.79 (m, 1H, Ta-*H*); -1.88 (m, 1H, Ta-*H*); 0.276 (t, 11 Hz, 1H, Ta-*H*); -0.027 (s, 3H, Si*Me*$_2$); -0.001 (s, 3H, Si*Me*$_2$); 1.27 (s, 9H, C*Me*$_3$); 4.762, 4.766, 4.902, 4.982, 5.187, 5.263, 5.451 (m, 1H, Cp). ^{13}C NMR (benzene-d_6): δ = -5.604 (Si*Me*$_2$); -4.776 (Si*Me*$_2$); 32.661 (C*Me*$_3$); 138.224 (CMe$_3$); 87.17, 89.23, 89.53, 90.72, 93.24, 94.36, 97.35, *3 not located* (Cp).

Me$_2$Si(η^5-C$_5$H$_4$)$_2$Ta(CO)(H) (10). In the dry box, a J. Young NMR tube was charged with 10.0 mg (0.027 mmol) of **3** and the sample was dissolved in C$_6$D$_6$ forming a clear solution. On the vacuum line, carbon monoxide gas was passed through a trap of liquid nitrogen and 1 atmosphere was charged into the NMR tube. The tube was sealed and heated to 87 ^{o}C for 48 hours resulting a red solution and a quantitive yield of **10**. Attempts to isolate the material in the solid state have been unsuccessful. ^{1}H NMR (benzene-d_6): δ = -5.72 ppm (s, 1H, Ta-*H*); -0.29 (s, 3H, Si*Me*$_2$); -0.18 (s, 1H, Si*Me*$_2$); 4.09, 4.41, 4.74, 5.73 (m, 1H, Cp). IR (benzene-d_6): 1895.5 cm^{-1}.

Me$_2$Si(η^5-C$_5$H$_4$)(η^5-C$_5$H$_3$-3-CHMe$_2$)Ta(CO)(H) (11). The sample was prepared in an analogous manner to **10** with 10.0 mg (0.024 mmol) of **7** and 1 atmosphere of CO and was heated for 8 hours resulting in quantitative formation of two isomers of **11**. ^{1}H NMR (benzene-d_6): δ = -5.32 (s, 1H, Ta-*H*); -5.70 (s, 1H, Ta-*H*); -0.221 (s, 3H, Si*Me*$_2$); -0.198 (s, 3H, Si*Me*$_2$); -0.172 (s, 3H, Si*Me*$_2$); -0.137 (s, 3H, Si-*Me*$_2$); 1.07 (d, 7Hz, 3H, CH*Me*$_2$); 1.09 (d, 7 Hz, 3H CH*Me*$_2$); 1.16 (d, 7 Hz, 3H, CH*Me*$_2$); 1.17 (d, 7 Hz, 3H, CH*Me*$_2$); 2.42 (sept; 7 Hz, 1H, C*H*Me$_2$); 2.66 (sept; 7 Hz, 1H, C*H*Me$_2$); 3.32, 3.81, 4.10, 4.16, 4.25, 4.70, 4.43, 4.52, 4.60, 4.62, 4.65, 4.69, 4.80, 5.69 (m, 1H, Cp). ^{13}C NMR (benzene-d_6): δ = -6.24, -6.08, -4.50, -4.29 (Si*Me*$_2$); 24.55, 24.89, 27.13, 28.55 (CH*Me*$_2$); 29.06, 29.13 (*C*HMe$_2$); 76.27, 77.41, 77.65, 79.42, 80.50, 81.34, 81.69, 82.82, 83.38, 85.99, 85.99, 89.60, 90.23, 90.99, 101.02, 103.46, 104.26, 121.40, 126.16, 128.84, 138.34 (Ta-*C*O) *not located*. IR (benzene-d_6): 1901.4 cm^{-1}.

$Me_2Si(\eta^5\text{-}C_5H_4)(\eta^5\text{-}C_5H_2\text{-}2,4\text{-}(CHMe_2)_2)Ta(CO)(H)$ (12). The sample was prepared in an analogous manner to **10** with 10.0 mg (0.022 mmol) of **8** and 1 atmosphere of CO and was heated for 8 hours resulting in quantitative formation of two isomers of **12**. ^{1}H NMR (benzene-d_6): δ = -5.57 (s, 1H, Ta-*H*); -4.95 (s, 1H, Ta-*H*); -0.13 (s, 3H, Si*Me*$_2$); -0.08 (s, 3H, Si*Me*$_2$); 0.12 (s, 3H, Si*Me*$_2$); 0.20 (s, 3H, Si*Me*$_2$); 1.12 (d, 7 Hz, 3H, CH*Me*$_2$); 1.20 (d, 7 Hz, 3H, CH*Me*$_2$); 1.31 (d, 7 Hz, 3H, CH*Me*$_2$); 1.41 (d, 7 Hz, 3H, CH*Me*$_2$); 1.89 (sept, 7 Hz, 1H; C*H*Me$_2$); 2.47 (sept, 7 Hz, 1H; C*H*Me$_2$); 2.50 (sept, 7 Hz, 1H, C*H*Me$_2$); 2.74 (sept, 7 Hz, 1H; C*H*Me$_2$); 3.68, 3.95, 4.34, 4.43, 4.48, 4.53, 4.60, 4.67, 4.72, 4.81, 4.86, 5.59, 5.77, 5.95 (m, 1H, Cp). ^{13}C NMR (benzene-d_6): δ = -5.555, -4.303, -3.152, -1.518 (Si*Me*$_2$); 13.96, 22.44, 24.02, 24.73, 26.91, 28.31, 28.68, 28.85 (CH*Me*$_2$); 29.01, 30.09, 30.31, 31.49 (*C*HMe$_2$); 77.62, 79.16, 79.36, 79.96, 80.24, 88.52, 88.71, 89.04, 94.71, 96.17, 96.17, 96.78, 98.89, 101.45, 104.15, 109.21, 112.60, 118.74, 119.94, *2 not located* (Cp); 202.04, 203.62 (Ta-*C*O). IR (benzene-d_6): 1895.5 cm^{-1}.

$Me_2Si(\eta^5\text{-}C_5H_4)(\eta^5\text{-}C_5H_3\text{-}3\text{-}CMe_3)Ta(CO)(H)$ (13). The sample was prepared in an analogous manner to **10** with 10.0 mg (0.021 mmol) of **9** and 1 atmosphere of CO and was heated for 8 hours resulting in quantitative conversion to two isomers of **13**.

Major Isomer: ^{1}H NMR (benzene-d_6): δ = -5.51 (s, 1H, Ta-*H*); -0.180 (s, 3H, Si*Me*$_2$); -0.177 (s, 3H, Si*Me*$_2$); 1.29 (s, 9H, C*Me*$_3$); 3.79, 4.16, 4.29, 4.44, 4.52, 4.79, 5.72 (m, 1H, Cp). ^{13}C NMR (benzene-d_6): δ = -4.82 (Si*Me*$_2$); -6.43 (Si*Me*$_2$); 32.04 (C*Me*$_3$); 143.11 (*C*Me$_3$); 75.94, 77.18, 79.47, 82.23, 85.34, 88.58, 89.69, 103.80, *2 not located* (Cp); 197.80 (Ta-*C*O).

Minor Isomer: ^{1}H NMR (benzene-d_6): δ = -5.43 (s, 1H, Ta-*H*); -0.140 (s, 3H, Si*Me*$_2$); -0.160 (s, 3H, Si*Me*$_2$); 1.27 (s, 9H, C*Me*$_3$); 3.80, 4.38, 4.47, 5.04, 5.42, 5.47, 5.76 (m, 1H, Cp). ^{13}C NMR (benzene-d_6): δ = -4.99 (Si*Me*$_2$); -3.37 (Si*Me*$_2$); 32.21 (C*Me*$_3$); 142.47 (*C*Me$_3$); 78.60, 81.27, 83.51, 87.54, 87.73, 91.41, 91.33, 102.37, *2 not located* (Cp); *not located* (Ta-*C*O).

$Me_2Si(\eta^5\text{-}C_5H_4)_2Ta(\eta^2\text{-}CH_2CH_2)(CH_2CH_3)$ (14). In the dry box, a J. Young NMR tube was charged with 10.0 mg (0.0255 mmol) of **3** and the solid dissolved in C_6D_6. On the vacuum line, the tube was degassed with three freeze-pump-

thaw cycles and 0.255 mmol of ethylene added via a calibrated gas volume. The tube was thawed and then heated to 87 °C for three hours. Attempts to isolate this complex in the solid state lead to decomposition. ^{1}H NMR (benzene-d_6): -0.02 (s, 3H, SiMe_2); 0.10 (s, 3H, SiMe_2); 0.78 (t, 11 Hz; 2H; CH_2=CH_2); 1.75 (t, 11 Hz; 2H; CH_2=CH_2); 1.35 (q, 7 Hz; 2H; CH_2CH_3); 1.33 (t, 7 Hz; 3H; CH_2CH_3); 3.62; 4.81; 5.19; 5.27 (m, 1H, Cp).

$Me_2Si(\eta^5\text{-}C_5H_4)_2Ta(\eta^2\text{-}CH_2CH_2)(H)$ (15). Complex **15** has been observed by ^{1}H NMR spectrscopy as component of an equilibrium with **14** and free ethylene. ^{1}H NMR (benzene-d_6): δ = -2.97 (s, 1H, Ta-*H*) ; 0.01 (s, 3H, SiMe_2); 0.12 (s, 3H, SiMe_2); 0.48 (t, 11 Hz, 2H, CH_2=CH_2); 1.08 (t, 11 Hz, 2H, CH_2=CH_2); 3.34; 4.28; 5.39; 5.82 (m, 1H, Cp).

$Me_2Si(\eta^5\text{-}C_5H_4)(\eta^5\text{-}C_5H_3\text{-}3\text{-}CHMe_2)Ta(PMe_3)(H)$ (16a,b). NMR Scale: In the dry box, a J. Young NMR tube was charged with 11.4 mg (0.0276 mmol) of **8** and the sample dissolved in C_6D_6. On the vacuum line, the tube was frozen in liquid nitrogen and degassed. Via calibrated 7.0 mL gas volume, 260 torr (0.968 mmol) of PMe_3 was added. The tube was thawed and shaken and then heated to 87 °C and monitored over time by ^{1}H and ^{31}P NMR spectroscopy. Preparative Scale: In the dry box, a 25 mL thick-walled glass vessel equipped with a magnetic stirring bar was charged with 70.0 mg (0.170 mmol) of **8**. On the vacuum line, the bomb was evacuated and approximately 5 mL of toluene was added by vacuum transfer at -78 °C. The bomb was then attached to a 200 mL calibrated volume and 80 torr (0.850 mmol) of PMe_3 was added. The reaction mixture was heated to 87 °C for 36 hours. The contents of the thick-walled vessel were transferred into a swivel frit assembly and the toluene was removed *in vacuo* leaving a red oil. Attempts to recrystallize the product from petroleum ether or diethyl ether have been unsuccessful. NMR analysis reveals that **16a** is the only isomer present. UV-VIS (toluene): 452.1 nm, ε ~ 5000 M^{-1} cm^{-1}.
16a: ^{1}H NMR (benzene-d_6): δ = -7.89 (d, 21.5 Hz, 1H, Ta-*H*); -0.084 (s, 3H, SiMe_2); -0.042 (s, 3H, SiMe_2); 1.00 (d, 7.5 Hz, 9H, PMe_3); 1.29 (d, 6.5 Hz, 3H, CHMe_2); 1.39 (d, 6.5 Hz, 3H, CHMe_2); 2.79 (sept, 7 Hz, 1H, C*H*Me_2); 4.24, 4.26, 4.37, 4.66, 4.72, 4.80, 5.72 (m, 1H, Cp). ^{13}C NMR (benzene-d_6): δ = -5.35, -3.29 (SiMe_2); 25.81, 26.00, 29.47 (CHMe_2); 29.47 (C*H*Me_2); 25.27 (d, 20 Hz, PMe_3); 64.92, 66.58, 75.02, 75.67, 91.25, 92.64, 101.54, 135.25, 2 *not located* (Cp). ^{31}P NMR (benzene-d_6): δ = -26.52.

16b: ^{1}H NMR (benzene-d_6): δ = -8.20 (d, 20 Hz, 1H, Ta-*H*); -0.06 (s, 3H, Si*Me*$_2$); -0.01 (s, 3H, Si*Me*$_2$); 1.01 (d, 8 Hz, 9H, P*Me*$_3$); 1.20 (d, 6.5 Hz, 3H, CH*Me*$_2$); 1.27 (d, 6.5 Hz, 3H, CH*Me*$_2$); 2.60 (sept, 7 Hz, 1H, C*H*Me$_2$); 4.20; 4.37; 4.84; 5.01; 5.20, *3 not located* (m, 1H, Cp). ^{31}P NMR (benzene-d_6): δ = -26.10.

$Me_2Si(\eta^5\text{-}C_5H_4)(\eta^5\text{-}C_5H_3\text{-}3\text{-}CHMe_2)Ta(PEt_3)(H)$ (17). In the dry box, a J. Young NMR tube was charged with 10.0 mg (0.242 mmol) of **8** and the sample was dissolved in C_6D_6. In the dry box, 15.0 μL (0.158 mmol) of PEt_3 was added to the tube via microsyringe. The tube was heated in an 87 °C oil bath and the progress of the reaction monitored by ^{1}H and ^{31}P NMR spectroscopy. ^{1}H NMR (benzene-d_6): δ = -8.03 (d, 21.5 Hz, 1H, Ta-*H*); -0.028 (s, 3H, Si*Me*$_2$); 0.012 (s, 3H, Si*Me*$_2$); 0.779 (m, 9H, P*Et*$_3$); 0.939 (m, 6H, P*Et*$_3$); 1.30 (d, 6.5 Hz, 3H, CH*Me*$_2$); 1.39 (d, 6.5 Hz, 3H, CH*Me*$_2$); 2.77 (sept, 7 Hz, 1H, C*H*Me$_2$); 3.85; 4.20; 4.24; 4.59; 4.73; 4.80; 5.63 (m, 1H, Cp). ^{13}C NMR (benzene-d_6): δ = -5.35, -3.14 (Si*Me*$_2$); 24.93, 25.42 (CH*Me*$_2$); 29.42 (*C*HMe$_2$); 28.85 (d, 85 Hz, P(CH_2CH_3)$_3$); 8.46 (P(CH_2CH_3)$_3$); 66.22, 68.15, 74.07, 74.39, 91.20, 93.32, 101.05, 134.92, 146.12, 150.39. ^{31}P (benzene-d_6): δ = -17.60. UV-VIS (toluene): 454.6 nm, ε ~ 5000 M^{-1} cm^{-1}.

$Me_2Si(\eta^5\text{-}C_5H_4)(\eta^5\text{-}C_5H_2\text{-}2,4\text{-}(CHMe_2)_2)Ta(PMe_3)(H)$ (18a,b). In the dry box, 0.06 mL of a 0.235 M stock solution of **8** in C_6D_6 was charged into a J. Young NMR tube. On the line, the tube was frozen in liquid nitrogen and degassed. Via 43.48 mL calibrated gas volume, 30 torr of PMe_3 was added. The tube was placed in an 87 °C oil bath and monitored by ^{1}H and ^{31}P NMR spectroscopy. **18a**: ^{1}H NMR (benzene-d_6): δ = -7.83 (d, 31 Hz; 1H, Ta-*H*). ^{31}P (benzene-d_6): δ = -26.92. **18b:** ^{1}H NMR (benzene-d_6): δ = -8.13 (d, 31 Hz, 1H, Ta-*H*); -0.62 (s, 3H, Si*Me*$_2$); 0.785 (s, 3H, Si*Me*$_2$); 1.07 (d, 8 Hz, 9H, P*Me*$_3$); 1.24, 1.29 (d, 7 Hz, 3H, 4-CH*Me*$_2$); 1.37; 1.38 (d, 7 Hz, 3H, 2-CH*Me*$_2$); 2.43 (sept, 6.5 Hz; 1H; 2-C*H*Me$_2$); 2.75 (sept, 6.5 Hz; 1H; 4-C*H*Me$_2$); 4.23, 4.31, 4.46, 4.62, 4.75, 5.22 (m, 1H, Cp). ^{13}C (benzene-d_6): δ = -3.77, 2.34 (Si*Me*$_2$); 46.50 (d, 490 Hz, P*Me*$_3$); 24.06; 24.79; 25.53; 29.65; 30.44; 32.56 (CH*Me*$_2$); 71.59; 71.63; 72.26; 79.75; 80.15; 93.34; 95.30;; 100.33; 100.63; *1 not located* (Cp) ^{31}P (benzene-d_6): δ = -29.09.

$Me_2Si(\eta^5\text{-}C_5H_4)(\eta^5\text{-}C_5H_2\text{-}2,4\text{-}(CHMe_2)_2)Ta(PEt_3)(H)$ (19a,b). In the dry box, 0.05 mL of a 0.235 M stock solution of **8** in C_6D_6 was charged into a J. Young NMR tube. Via microsyringe, 7.0 mg (0.059 mmol) of PEt_3 was added to the tube. The tube was heated to 87 °C and the progress of the reaction monitored by ^{1}H and

^{31}P NMR spectroscopy. **19a:** ^{1}H NMR (benzene-d_6): δ = -7.80 (d, 20 Hz, 1H, Ta-*H*); **19b:** ^{1}H NMR (benzene-d_6): δ = -8.25 (d, 20 Hz, 1H, Ta-*H*); -0.05 (s, 1H, Si*Me*$_2$); 0.21 (s, 1H, Si*Me*$_2$); 0.85 (m, 9H, P*Et*$_3$); 1.16 (m, 6H, P*Et*$_3$); 1.02, 1.06 (d, 6.5 Hz, 3H, CH*Me*$_2$); 1.46; 1.50 (d, 6.5 Hz, 3H, CH*Me*$_2$); 2.62; 2.71 (sept, 7 Hz, 1H, C*H*Me$_2$); 4.28; 4.36; 4.41; 4.63; 4.65; 4.80; 4.92; (m, 1H, Cp). ^{31}P (benzene-d_6): δ = -17.65.

$Me_2Si(\eta^5\text{-}C_5H_4)(\eta^5\text{-}C_5H_3\text{-}3\text{-}CMe_3)Ta(PMe_3)(H)$ (20). The sample was prepared in an analogous manner to **16** employing 10.0 mg (0.021 mmol) of **8** and 30 torr of PMe$_3$ was added via a 43.48 mL calibrated gas volume. The tube was placed in an 87 °C oil bath and monitored by ^{1}H and ^{31}P NMR spectroscopy. ^{1}H NMR (benzene-d_6): δ = -7.960 (d, 20.5 Hz, Ta-*H*); -0.048 (s, 3H, Si*Me*$_2$); -0.006 (s, 3H, Si*Me*$_2$); 1.02 (d, 7 Hz, 9H, P*Me*$_3$); 1.44 (s, 9H, C*Me*$_3$); 3.87, 3.92, 4.16, 4.19, 4.66, 4.75, 5.84 (m, 1H, Cp). ^{13}C NMR (benzene-d_6): δ = -5.78 (Si*Me*$_2$); -3.52 (Si*Me*$_2$); 32.45 (C*Me*$_3$); 140.86 (*C*Me$_3$); 47.12 (d, 695 Hz, P*Me*$_3$); 64.29, 65.66, 74.21, 75.79, 88.62, 90.47, 101.97 (Cp). ^{31}P (benzene-d_6): δ = -28.61.

$Me_2Si(\eta^5\text{-}C_5H_4)_2TaCl_2$ (21). In the dry box, a fine swivel frit assembly was charged with 0.716 g (1.51 mmol) of **2** and 0.098 g (1.51 mmol) of Zn dust. On the vacuum line, the frit assembly was evacuated and approximately 25 mL of DME was added by vacuum transfer at -78 °C. The reaction was stirred and slowly warmed to room temperature. After 4 hours, a forest green reaction mixture forms. After stirring for 16 hours, the green DME solution was filtered and the remaining solid was washed three times with recycled solvent. The DME was removed *in vacuo* leaving a green oily solid. Addition of Et_2O afforded a green precipitate that was collected by filtration and dried *in vacuo* leaving 0.580 g (88%) of **20**. EPR (CH_2Cl_2): g_{iso} = 1.98; a_{iso}= 101.9 G.

$Me_2Si(\eta^5\text{-}C_5H_4)(\eta^5\text{-}C_5H_3\text{-}3\text{-}CHMe_2)TaCl_2$ (22). This compound was prepared in an analogous manner to **21** employing 0.960 g (1.86 mmol) of **4** and 0.121 g (1.86 mmol) of Zn dust affording 0.600 g (67.1%) of a green solid identified as **22**. EPR (CH_2Cl_2): g_{iso} = 1.94; a_{iso} = 101.3 G.

$Me_2Si(\eta^5\text{-}C_5H_4)(\eta^5\text{-}C_5H_2\text{-}2,4\text{-}(CHMe_2)_2)TaCl_2$ (23). This compound was prepared in an analogous manner to **21** employing 2.47 g (4.43 mmol) of **5** and

0.288 g (4.43 mmol) of Zn dust affording 2.20 g (95.1%) of a green solid identified as **23**. Sublimation at 140 °C and 10^{-4} torr affords analytically pure material. Anal. Cald. for $Ta_1Si_1C_{15}H_{20}Cl_2$ C, 37.51%, H, 4.20%; Found C, 37.28%; H, 4.23%. EPR (CH_2Cl_2): g_{iso} = 1.94 ; a_{iso} = 92.9 G.

$Me_2Si(\eta^5\text{-}C_5H_4)(\eta^5\text{-}C_5H_3\text{-}3\text{-}CMe_3)TaCl_2$ (24). This compound was prepared in an analogous manner to **21** employing 1.00 g (1.73 mmol) of **6** and 0.115 g (1.73 mmol) of Zn dust affording 0.726 g (78.5%) of a green solid identified as **24**. Anal. Cald. for $Ta_1Si_1C_{16}H_{22}Cl_2$ C, 38.88%, H, 4.49%; Found C, 37.55%; H, 4.36%. EPR (CH_2Cl_2): g_{iso} = 1.94; a_{iso} = 101.2 G.

$Me_2Si(\eta^5\text{-}C_5H_4)(\eta^5\text{-}C_5H_3\text{-}3\text{-}CHMe_2)Ta(\eta^2\text{-}CH_2CH_2)(H)$ (25). In the dry box, a fine swivel frit assembly was charged with 0.300 g (0.625 mmol) of **22**. On the vacuum line, approximately 25 mL of Et_2O was added by vacuum transfer. At -80 °C, against an Ar counterflow, 1.00 mL of a 3.0 M CH_3CH_2MgBr solution was added by syringe. The reaction mixture was stirred and slowly warmed to room temperature. After 2 hours, an orange solution and brown precipitate form. The reaction mixture was stirred for 16 hours after which time the Et_2O was removed and replaced with 10 mL of petroleum ether. The product was extracted several times with petroleum ether. The solvent removed *in vacuo* leaving a yellow oil identified as **25**. ^1H NMR (benzene-d_6): δ = -2.72 (s, 1H, Ta-*H*); 0.19 (s, 3H, Si*Me*$_2$); 0.30 (s, 3H, Si*Me*$_2$); 0.51 (m, 2H, C*H*$_2$=CH$_2$, endo); 1.10 (m, 2H, CH$_2$=C*H*$_2$, exo); 1.23 (d, 7 Hz, 3H, CH*Me*$_2$); 1.29 (d, 7 Hz, 3H, CH*Me*$_2$); 2.90 (sept, 7 Hz, 1H, C*H*Me$_2$); 3.40, 4.32, 4.42, 4.47, 5.35 (2H), 5.94 (m, 1H, Cp). ^{13}C NMR (benzene-d_6): δ = -6.92 (Si*Me*$_2$); -4.10 (Si*Me*$_2$); 11.87 (CH$_2$=CH$_2$, endo); 30.10 (*C*H$_2$=CH$_2$, exo); 23.65 (CH*Me*$_2$); 25.73 (CH*Me*$_2$); 28.45 (CHMe$_2$); 80.62, 82.38; 91.90; 93.26; 102.10; 104.05; 105.49, *3 not located* (Cp).

$Me_2Si(\eta^5\text{-}C_5H_4)(\eta^5\text{-}C_5H_3\text{-}3\text{-}CHMe_2)Ta(\eta^2\text{-}CH_2CHCH_3)(H)$ (26). In the dry box, a fine swivel frit assembly was charged with 0.225 g (0.514 mmol) of **22**. On the vacuum line, approximately 25 mL of Et_2O was added by vacuum transfer. At -80 °C, against an Ar counterflow, 2.0 M $CH_3CH_2CH_2MgCl$ solution in diethyl ether was added via syringe. The reaction mixture was stirred and slowly warmed to room temperature. With warming an orange solution and brown precipitate forms. The reaction was stirred for 24 hours and the Et_2O was removed *in vacuo* and replaced with petroleum ether. The product was extracted

several times with petroleum ether. The solvent was removed *in vacuo* leaving a thick orange oil identified as **26**. Major Isomer (63.7%) ^{1}H NMR (benzene-d_6): δ = -2.71 (s, 1H, Ta-*H*); 0.04 (s, 3H, Si*Me*$_2$); 0.12 (s, 3H, Si*Me*$_2$); 1.23 (d, 7 Hz, 3H; CH*Me*$_2$); 1.30 (d, 7 Hz, 3H, CH*Me*$_2$); 2.89 (sept, 6.5 Hz, 1H, C*H*Me$_2$); 0.44 (dd, 10 Hz, 6 Hz, 1H, C*H*$_2$=CHCH$_3$); 0.87 (dd, 10 Hz, 6 Hz, 1H; C*H*$_2$=CHCH$_3$); 1.01 (m, 1H, CH$_2$=C*H*CH$_3$); 2.21 (d, 6.5 Hz, 3H; CH$_2$=CHC*H*$_3$); 3.37; 3.79; 4.40; 4.56; 5.15; 5.57; 5.59 (m, 1H, Cp). ^{13}C NMR (benzene-d_6): δ = -6.63 (Si*Me*$_2$); -4.27 (Si*Me*$_2$); 30.17 (CH$_2$=CHCH$_3$), 28.77 (CH$_2$=CHCH$_3$); 24.23 (CH$_2$=CHCH$_3$); 21.63 (CH*Me*$_2$); 21.76 (CH*Me*$_2$); 29.03 (C*H*Me$_2$); 81.62; 83.10; 81.31; 91.39; 104.37; 106.70; 106.81; *3 not located* (Cp).

Minor Isomer (20.6 %), ^{1}H NMR (benzene-d_6): δ = -2.65 (s, 1H, Ta-*H*); 0.10 (s, 3H, Si*Me*$_2$); 0.15 (s, 3H, Si*Me*$_2$); 1.25 (d, 7 Hz, 3H; CH*Me*$_2$); 1.27 (d, 7 Hz, 3H; CH*Me*$_2$); 2.80 (sept, 6.5 Hz, 1H; C*H*Me$_2$); *3 propylene resonances not located*; 2.25 (d, 6.5 Hz, 3H; CH$_2$=CHC*H*$_3$); 3.30; 3.65; 4.36; 4.37; 5.18; 5.36; 5.91; (m, 1H, Cp); ^{13}C NMR (benzene-d_6): δ = -7.01 (Si*Me*$_2$); -3.44 (Si*Me*$_2$); 29.69 (CH$_2$=CHCH$_3$); 23.85 (CH$_2$=CHCH$_3$); 25.98 (CH$_2$=CHCH$_3$); 21.28 (CH*Me*$_2$); 22.52 (CH*Me*$_2$); 27.76 (C*H*Me$_2$); 79.50; 84.81; 91.02; 94.26; 98.10; 99.34; 107.38; *3 not located* (Cp).

Me$_2$Si(η^5-C$_5$H$_4$)(η^5-C$_5$H$_3$-3-CHMe$_2$)Ta(η^2-CH$_2$CHPh)(H) (27). This compound was prepared in a similar manner to **25** employing 0.400 g (0.914 mmol) of **22** and 2.28 mL of 1.0 M PhCH$_2$CH$_2$MgBr in THF solution. A golden yellow solid (0.120 g) sample of **27** was obtained by slow cooling of a petroleum ether solution followed by filtration. Anal. Cald. for Ta$_1$Si$_1$C$_{23}$H$_{29}$ C, 53.69%, H, 5.68%; Found C, 53.12%; H, 5.82%.

Major Isomer (54%) ^{1}H NMR: (benzene-d_6): δ = -1.53 (s, 1H, Ta-*H*); -0.03 (s, 3H, Si*Me*$_2$); 0.09 (s, 3H, Si*Me*$_2$); 1.26 (d, 7 Hz, 3H; CH*Me*$_2$); 1.34 (d, 7 Hz, 3H; CH*Me*$_2$); 2.92 (sept, 6.5 Hz, 1H; C*H*Me$_2$); 3.56 (m, 1H; C*H*$_2$=CHPh, *cis*); 3.59 (m, 1H; C*H*$_2$=CHPh, *trans*); 3.10 (t, 10 Hz. 1H; CH$_2$=C*H*Ph); 4.29; 4.33; 5.17; 5.23; 5.28; 5.56; 5.61 (m, 1H, Cp). ^{13}C NMR (benzene-d$_6$): δ = -6.75 (Si*Me*$_2$); -4.36 (Si*Me*$_2$); 13.77 (CH$_2$=CHPh); 30.11 (CH$_2$=*C*HPh); 21.70 (C*Me*$_2$); 24.26 (CH*Me*$_2$); 29.09 (C*H*Me$_2$); 83.12; 86.05; 93.46; 95.19; 105.34; 110.55; *4 not located* (Cp). 121.90 (C$_6$H$_5$, *meta*); 136.79 (C$_6$H$_5$, *ortho*); 154.81 (C$_6$H$_5$, *para*) *1 not located* (C$_6$H$_5$, *ipso*).

Minor Isomer (36%) ^{1}H NMR: (benzene-d_6): δ = -1.69 (s, 1H, Ta-*H*); -0.01 (s, 3H, Si*Me*$_2$); 0.093 (s, 3H, Si*Me*$_2$); 1.25 (d, 7 Hz, 3H; CH*Me*$_2$); 0.76 (d, 7 Hz, 3H; CH*Me*$_2$); 1.76 (sept, 6.5 Hz, 1H; C*H*Me$_2$); 3.48 (m, 1H; C*H*$_2$=CHPh, *cis*); 3.48 (m, 1H; C*H*$_2$=CHPh); 3.10 (t, 10 Hz, 1H; CH$_2$=C*H*Ph); 4.24; 4.29; 4.32; 5.21; 5.27; 5.62; 6.04 (m, 1H, Cp). ^{13}C NMR (benzene-d_6): δ = -6.92 (Si*Me*$_2$); -4.10 (Si*Me*$_2$); 14.26 (*C*H$_2$=CHPh); 28.65 (CH$_2$=*C*HPh); 24.22 (*C*Me$_2$); 25.48 (CH*Me*$_2$); 26.31 (*C*HMe$_2$); 80.72; 84.27; 94.67; 95.66; 104.79; 106.37; 107.73; 110.34 (Cp), 121.54 (C$_6$H$_5$, *meta*); 138.88 (C$_6$H$_5$, *ortho*); 153.84 (C$_6$H$_5$, *para*); *1 not located* (C$_6$H$_5$, *ipso*).

Trace Isomer (10%) ^{1}H NMR: (benzene-d_6): δ = -1.74 (s, 1H, Ta-*H*); -0.04 (s, 3H, Si*Me*$_2$); 0.06 (s, 3H, Si*Me*$_2$); 0.92 (d, 7 Hz, 3H; CH*Me*$_2$); 1.13 (d, 7 Hz, 3H; CH*Me*$_2$); 2.40 (sept, 6.5 Hz, 1H; C*H*Me$_2$); *not located* (m, 1H; C*H*$_2$=CHPh, *cis*); *not located* (m, 1H; C*H*$_2$=CHPh); 4.12 (t, 10 Hz; 1H; CH$_2$=C*H*Ph); 4.67; 4.69; 4.99; 5.34; 5.36; *2 not located* (m, 1H, Cp). ^{13}C NMR (benzene-d_6): δ = -5.20 (Si*Me*$_2$); -6.02 (Si*Me*$_2$); 11.90 (*C*H$_2$=CHPh); 30.61 (CH$_2$=*C*HPh); 20.28 (*C*Me$_2$); 22.50 (CH*Me*$_2$); *not located* (*C*HMe$_2$); 87.25; 88.31; 91.15; 91.59; 93.95; 100.24; 104.60; 110.07, *2 not located* (Cp), 123.99 (C$_6$H$_5$, *meta*); *not located* (C$_6$H$_5$, *ortho*); *not located* (C$_6$H$_5$, *para*); *not located* (C$_6$H$_5$, *ipso*).

Me$_2$Si(η^5-C$_5$H$_4$)(η^5-C$_5$H$_2$-2,4-(CHMe$_2$)$_2$)Ta(η^2-CH$_2$CH$_2$)(H) (28). This compound was prepared in the similar manner to **25** employing 0.340 g (0.651 mmol) of **23** and 0.477 mL of a 3.0 M CH$_3$CH$_2$MgBr solution in diethyl ether. Extraction with petroleum ether afforded **28** as a yellow oil.

Major Isomer ^{1}H NMR (benzene-d_6): δ = -2.69 (s, 1H, Ta-*H*); 0.15 (s, 3H, Si*Me*$_2$); 0.29 (s, 3H, Si*Me*$_2$); 0.42 (m, 2H, C*H*$_2$=CH$_2$); 0.89 (m, 2H, CH$_2$=C*H*$_2$); 0.95 (d, 7 Hz, 3H, CH*Me*$_2$); 0.92 (d, 7 Hz, 3H, CH*Me*$_2$); 1.26 (d, 7 Hz, 3H, CH*Me*$_2$); 1.36 (d, 7 Hz, 3H, CH*Me*$_2$); 2.78 (sept, 7 Hz, 1H, C*H*Me$_2$); 2.47 (sept, 7 Hz, 1H, C*H*Me$_2$); 3.88, 4.45, 4.97, 5.02, 5.26, 5.41. ^{13}C NMR: (benzene-d_6): δ = -1.86 (Si*Me*$_2$); 1.36 (Si*Me*$_2$); 30.55 (*C*H$_2$=CH$_2$, *exo*); 8.80 (CH$_2$=*C*H$_2$, *endo*); 20.88 (*C*Me$_2$); 22.72 (*C*Me$_2$); 27.71 (*C*Me$_2$); 13.90 (*C*Me$_2$); 29.70 (*C*Me$_2$); 30.18 (*C*Me$_2$); 89.57, 92.60, 96.61, 102.03, 104.22, 123.89, 125.99, *3 not located* (Cp).

Minor Isomer ^{1}H NMR (benzene-d_6): δ = -2.78 (s, 1H, Ta-*H*); 0.17 (s, 3H, Si*Me*$_2$); 0.30 (s, 3H, Si*Me*$_2$); 0.25 (m, 2H, C*H*$_2$=CH$_2$); 0.76 (m, 2H, CH$_2$=C*H*$_2$); 0.97 (d, 7 Hz, 3H, CH*Me*$_2$); 1.30 (d, 7 Hz, 3H, CH*Me*$_2$); *2 not located* (CH*Me*$_2$); 2.04 (sept, 7 Hz,

1H, C*H*Me$_2$); 2.23 (sept, 7 Hz, 1H, C*H*Me$_2$); 4.26, 4.33, 4.78, 5.80, 5.10, 5.21. ^{13}C NMR: (benzene-*d*$_6$): δ = -4.63 (Si*Me*$_2$); 1.14 (Si*Me*$_2$); 30.61 (CH_2=CH_2, *exo*); 10.72 (CH_2=CH_2, endo); 11.31 (C*Me*$_2$); 16.52 (C*Me*$_2$); 18.62 (C*Me*$_2$); *not located* (C*Me*$_2$); 26.29 (C*Me*$_2$); *not located* (C*Me*$_2$); 91.12, 94.08, 95.16, 100.82, 100.91, 123.60, 125.73, *3 not located* (Cp).

$Me_2Si(\eta^5\text{-}C_5H_4)(\eta^5\text{-}C_5H_3\text{-}(CHMe_2)_2)Ta(\eta^2\text{-}CH_2CHCH_3)(H)$. An attempt to prepare this compound in a similar manner to **26** was employed with 0.320 g (0.613 mmol) of **23** and 0.700 mL of 2.0 M $CH_3CH_2CH_2MgBr$ solution in diethyl ether. Isolation and analysis of the yellow oil by ^{1}H NMR spectroscopy did not yield any tractible product.

$Me_2Si(\eta^5\text{-}C_5H_4)(\eta^5\text{-}C_5H_2\text{-}(CHMe_2)_2)Ta(\eta^2\text{-}CH_2CHPh)(H)$ (29). This compound was prepared in a similar manner to **25** employing 0.385 g (0.737 mmol) of **23** and 1.62 mL of 1.0 M $PhCH_2CH_2MgBr$ in THF yielding 0.145 g of **29** as a yellow solid. Anal. Cald. for $Ta_1Si_1C_{26}H_{35}$ C, 56.11%, H, 6.34%; Found C, 55.71%; H, 6.54%.

Major Isomer ^{1}H NMR (benzene-*d*$_6$): δ = (s, 1H, Ta-*H*); 0.172 (s, 3H, Si*Me*$_2$); 0.094 (s, 3H, Si*Me*$_2$); 0.940 (d, 6.5 Hz, 3H, CH*Me*$_2$); 1.06 (d, 6.5 Hz, 3H, CH*Me*$_2$); 1.08 (d, 6.5 Hz, 3H, CH*Me*$_2$); 1.54 (d, 6.5 Hz, 3H, CH*Me*$_2$); 2.61 (sept, 7 Hz, 1H, C*H*Me$_2$); 2.68 (sept, 1H, C*H*Me$_2$); *styrene resonances not located*; 4.46, 4.51, 4.75, 4.85, 4.99, 5.23 (m, 1H, Cp); 6.90 (t, 5 Hz, 1H, C_6H_5, *para*); 7.47 (d, 7 Hz, 2H, C_6H_5, *ortho*); 7.28 (m, 2H, C_6H_5, *meta*). ^{13}C NMR (benzene-*d*$_6$): δ = -3.82 (Si*Me*$_2$); -3.49 (Si*Me*$_2$);12.48 (CH_2=CHPh); 30.73 (CH_2=*C*HPh); 21.47 (CH*Me*$_2$); 22.79 (CH*Me*$_2$); 24.24 (CH*Me*$_2$); 27.28 (CH*Me*$_2$); 29.28 (CHMe$_2$); 29.64 (CHMe$_2$); 88.69, 92.12, 96.08, 104.54, 109.03, 111.11, 113.58, *3 not located* (Cp), 126.33 (C_6H_5, *para*); 136.96 (C_6H_5, *ortho*), 155.99 (C_6H_5, *meta*); *1 not located* (C_6H_5, *ipso*).

Minor Isomer ^{1}H NMR (benzene-*d*$_6$): δ = (s, 1H, Ta-*H*); -0.071 (s, 3H, Si*Me*$_2$); 0.257 (s, 3H, Si*Me*$_2$); 1.01 (d, 6.5 Hz, 3H, CH*Me*$_2$); 1.11 (d, 6.5 Hz, 3H, CH*Me*$_2$); 1.34 (d, 6.5 Hz, 3H, CH*Me*$_2$); 1.44 (d, 6.5 Hz, 3H, CH*Me*$_2$); 2.42 (sept, 7Hz, 1H, C*H*Me$_2$); 2.91(sept, 1H, C*H*Me$_2$); *styrene resonances not located*; 4.68, 4.82, 4.92, 5.07 5.17, 5.89 (m, 1H, Cp); 6.87 (t, 5 Hz, 1H, C_6H_5, *para*); 7.40 (d, 7 Hz, 2H, C_6H_5, *ortho*); 7.27 (m, 2H, C_6H_5, *meta*). ^{13}C NMR (benzene-*d*$_6$): δ = -1.94 (Si*Me*$_2$); -5.45 (Si*Me*$_2$); 7.70 (CH_2=CHPh); 34.05 (CH_2=*C*HPh); 18.37 (CH*Me*$_2$); 21.97 (CH*Me*$_2$);

25.78 ($CHMe_2$); 28.24 ($CHMe_2$); *not located* ($CHMe_2$); *not located* ($CHMe_2$); 86.32, 88.06, 92.94, 94.23, 103.48, 108.65, 112.78, *3 not located* (Cp), 125.52 (C_6H_5, *para*); 140.03 (C_6H_5, *ortho*), *2 not located.*

$Me_2Si(\eta^5\text{-}C_5H_4)(\eta^5\text{-}C_5H_3\text{-}3\text{-}CMe_3)Ta(\eta^2\text{-}CH_2{=}CHPh)(H)$ (30). Prepared in an analogous manner to **25** employing 0.500 g (0.935 mmol) of **24** and 2.10 mL (2.05 mmol) of 1.0 M $PhCH_2CH_2MgBr$ solution in THF. Cooling a concentrated petroleum ether solution affords 0.120 g (22.5%) of a yellow solid identified as **30**. ^1H NMR (benzene-d_6): δ = -1.602 (s, 1H, Ta-H); -0.0375 (s, 3H, $SiMe_3$); 0.0785 (s, 3H, $SiMe_3$); 1.41 (s, 9H, CMe_3); 0.928 (m, 1H, CH_2=CHPh); 1.54 (m,1H, CH_2=CHPh); 3.142 (t, 12.2 Hz, 1H, CH_2=CHPh); 3.33, 3.46, 4.06, 4.17, 5.27, 5.46, 5.60 (m, 1H, Cp). ^{13}C NMR (benzene-d_6): δ = -7.10 ($SiMe_2$); -4.15 ($SiMe_2$); 14.90 (CH_2=CHPh); 28.68 (CH_2=CHPh); 31.73 (CMe_3); 143.59 (CMe_3); 72.39, 73.32, 80.52, 84.60, 94.59, 96.27, 102.40, 105.11, *2 not located* (Cp); 109.73 (C_6H_5, *para*); 121.96 (C_6H_5, *ortho*), 154.63 (C_6H_5, *meta*); *1 not located* (C_6H_5, *ipso*).

$Me_2Si(\eta^5\text{-}C_5H_4)(\eta^5\text{-}C_5H_2\text{-}2,4\text{-}(CHMe_2)_2)TaMe_3$ (31). In the dry box, a 250 mL round bottom flask was charged with 1.01 g (3.55 mmol) of $Li_2[Me_2Si(\eta^5\text{-}C_5H_4)(\eta^5\text{-}C_5H_3\text{-}(CHMe_2)_2)]$. An addition funnel was charged with 1.00 g (3.55 mmol) of $TaCl_2Me_3$ and a 180 ° needle valve attached. On the vacuum line, approximately 100 mL of THF was added to the reaction flask forming a yellow solution. Similarly, the addition funnel was charged with approximately 20 mL of THF. The solution of ligand was added slowly to the tantalum over the course of 30 minutes at -80 °C. With addition, a brown solution forms. The reaction mixture was stirred overnight. The THF was removed *in vacuo* and replaced with petroleum ether. The reaction mixture was stirred for 30 minutes and then dried. The flask was then attached to a swivel frit assembly and the product extracted with Et_2O. The Et_2O was removed *in vacuo* leaving a yellow solid. Recrystallization from petroleum ether afforded 1.30 g (70.6%) of **31** as a yellow solid. ^1H NMR (dichloromethane-d_2): δ = -0.456 (s, 3H, Ta-*Me*); 0.403 (s, 3H, Ta-*Me*); 0.6675 (s, 3H, Ta-*Me*); 0.026 (s, 3H, $SiMe_2$); 0.097 (s, 3H, $SiMe_2$); 0.999 (d, 7 Hz, 3H, $CHMe_2$); 1.14 (d, 7 Hz, 3H, $CHMe_2$); 1.89 (d, 7 Hz, 3H, $CHMe_2$); 1.32 (d, 7 Hz, 3H, $CHMe_2$); 2.46 (sept, 6.5 Hz, 1H, CHMe$_2$); 2.84 (sept, 6.5 Hz, 1H, CHMe$_2$); 4.69, 4.91, 5.25, 5.30, 5.50, 5.86 (m, 1H, Cp). ^{13}C (dichloromethane-d_2): δ = -5.37 ($SiMe_2$); -0.019 ($SiMe_2$); 19.75 (Ta*Me*); 20.45 (Ta*Me*); 20.86 (Ta*Me*); 25.11, 25.95,

27.62, 28.87 (CH*Me*$_2$); 30.73, 31.56 (CHMe$_2$); 83.71, 88.16, 97.66, 106.37, 113.55, 117.60, 117.78, 121.46, 122.73, 127.64 (Cp). Anal. Cald. for $Ta_1Si_1C_{21}H_{35}$ C, 50.80%, H, 7.10%; Found C, 50.42%; H: 6.85%.

[Me$_2$Si(η^5-C$_5$H$_4$)(η^5-C$_5$H$_2$-2,4-(CHMe$_2$)$_2$)TaMe$_2$][BF$_4$] (32). In the dry box, a fine swivel frit assembly was charged with 0.203 g (0.392 mmol) of **31** and 0.130 g (0.392 mmol) of [Ph$_3$C][BF$_4$]. On the line, approximately 15 mL of CH_2Cl_2 was added by vacuum transfer. With addition, a yellow reaction mixture forms. The reaction was stirred at room temperature for 16 hours. The CH_2Cl_2 was removed *in vacuo* and replaced with Et_2O precipitating a yellow solid. The solid was collected by filtration and dried *in vacuo* yielding 0.150 g (65%) of **32**. ^{1}H NMR (dichloromethane-d_2): δ = 0.603 (s, 3H, Ta-*Me*); 0.661 (s, 3H, Ta-*Me*); 0.491 (s, 3H, Si*Me*$_2$); 0.724 (s, 3H, Si*Me*$_2$); 1.15 (d, 7Hz, 3H, CH*Me*$_2$); 1.28 (d, 7Hz, 3H, CH*Me*$_2$); 1.38 (d, 7 Hz, 3H, CH*Me*$_2$); 1.39 (d, 7 Hz, 3H, CH*Me*$_2$); 2.64 (sept, 6.9 Hz, 1H, C*H*Me$_2$); 2.69 (sept, 6.9 Hz, 1H, C*H*Me$_2$); 5.53, 5.72, 6.02, 7.02, 7.34, 7.54 (m, 1H, Cp). ^{13}C NMR (dichloromethane-d_2): δ = -3.13 (Si*Me*$_2$); -1.79 (Si*Me*$_2$); *2 not located* (Ta*Me*); 20.35, 21.72, 25.43, 29.38 (CH*Me*$_2$); 29.80, 31.85 (CHMe$_2$); 110.98, 113.81, 116.73, 120.09, 128.99, 143.96, 144.05, *3 not located* (Cp). Anal. Cald. for $Ta_1Si_1C_{20}H_{32}B_1F_4$ C, 42.27%, H, 5.68%; Found C, 41.91%; H: 5.48%.

Me$_2$Si(η^5-C$_5$H$_4$)(η^5-C$_5$H$_3$-(CHMe$_2$)$_2$)Ta(=CH$_2$)(CH$_3$) (33). In the dry box, a 25 mL round bottom flask was charged with 0.140 g (0.237 mmol) of **32** and 0.040 g (0.239 mmol) of LiCH(TMS)$_2$. The flask was attached to a fine swivel frit assembly. On the vacuum line, petroleum ether was added to the flask. With addition, a yellow slurry forms that turns brown/orange. The reaction was stirred for one hour and the white precipitate was removed by filtration. The petroleum ether was cooled to -80 °C precipitating a tan solid identified as **33**. This compound is both unstable in solution and the solid state and as a result only NMR spectroscopic data could be obtained. ^{1}H NMR (benzene-d_6): δ = 0.091 (s, 3H, Si*Me*$_2$); -0.198 (s, 3H, Si*Me*$_2$); 0.243 (s, 3H, Ta*Me*); 10.22 (d, 8 Hz, 1H, Ta*CH*$_2$); 10.30 (d, 8 Hz, 1H, Ta*CH*$_2$); 1.05 (d, 7 Hz, 3H, CH*Me*$_2$); 1.13 (d, 7 Hz, 3H, CH*Me*$_2$); 1.29 (d, 7 Hz, 3H, CH*Me*$_2$); 1.36 (d, 7 Hz, 3H, CH*Me*$_2$); 2.43 (sept, 7 Hz, 1H, C*H*Me$_2$); 3.31 (sept, 7 Hz, 1H, C*H*Me$_2$); 4.57, 4.68, 5.35, 5.73, 5.80, 6.01 (m, 1H, Cp).

$Me_2Si(\eta^5\text{-}C_5H_4)(\eta^5\text{-}C_5H_2\text{-}2,4\text{-}(CHMe_2)_2)Ta(\eta^2\text{-}CH_2CH_2)(CH_3)$ (34). This compound was prepared using an analogous procedure to **33** with the exception that the reaction was allowed to stir overnight. Removal of the petroleum ether afforded a tan solid identified as **34**. ^1H NMR (benzene-d_6): δ = -0.01 (s, 3H, Si*Me*$_2$); 0.32 (s, 3H, Si*Me*$_2$); 0.41 (s, 3H, Ta*Me*); 0.83 (m, 2H, *C*H_2=CH$_2$); 1.28 (m, 2H, CH$_2$=*C*H_2); 0.89 (d, 7 Hz, 3H, CH*Me*$_2$); 0.95 (d, 7 Hz, 3H, CH*Me*$_2$); 1.10 (d, 7 Hz, 3H, CH*Me*$_2$); 1.32 (d, 7 Hz, 3H, CH*Me*$_2$); 1.48 (sept, 7 Hz, 1H, C*H*Me$_2$); 2.72 (sept, 7 Hz, 1H, C*H*Me$_2$); 3.71, 4.42, 4.96, 5.30, 5.34, 5.48 (m, 1H, Cp).

$Me_2C(\eta^5\text{-}C_5H_4)(\eta^1\text{-Fluorenyl})TaMe_3$ (35). In the dry box, a 50 mL round bottomed flask was charged with 1.00 g (3.52 mmol) of $Li_2[Me_2C(C_5H_4)(Fluorenyl)]$ and 1.04 g (3.51 mmol) of $TaCl_2Me_3$. The reaction mixture was slowly warmed to room temperature and was stirred for 2.5 hours. The yellow solution was filtered from the brown precipitate and the precipitate was exhaustively washed with toluene. The toluene was removed *in vacuo* leaving 1.05 g (60.0%) of a golden solid identified as **35**. ^1H NMR (benzene-d_6): δ = 0.478 (s, 6H, Ta*Me*); 0.601 (s, 3H, Ta*Me*); 1.21 (s, 6H, C*Me*$_2$); 5.17 (s, 4H, Cp); 5.58 (s, 4H, Cp); 6.87 (d, 8 Hz, 2H, Flu); 7.13 (t, 5 Hz, 2H, Flu); 7.22 (t, 5 Hz, 2H, Flu); 7.87 (d, 8 Hz, 2H, Flu). ^{13}C NMR (benzene-d_6): δ = 29.35 (C*Me*$_2$); 35.89 (*C*Me$_2$); 53.84 (Ta*C*H_3, lateral); 85.15 (Ta*C*H_3 central); 100.69, 117.22, 120.7 (Cp); 125.01, 125.57, 125.78, 140.43, 144.61, *2 not located* (Flu). Anal. Cald for $Ta_1C_{24}H_{27}$ C, 58.07%, H, 5.48%; Found C, 57.49%; H: 5.56%.

$Ph_2C(\eta^5\text{-}C_5H_4)(\eta^1\text{-Fluorenyl})TaMe_3$ (36). This compound was prepared using an analogous procedure to **35** employing 1.40 g (3.42 mmol) of $Li_2[Ph_2C(C_5H_4)(Fluorenyl)]$ and 0.900 g (3.03 mmol) of $TaCl_2Me_3$. The reaction was stirred for 4 hours yielding 0.102 g (5.31%) of a yellow solid identified as **36**. ^1H NMR (benzene-d_6): δ = 0.317 (s, 6H, Ta*Me*); 0.497 (s, 3H, Ta*Me*); 5.40 (s, 4H, Cp); 5.58 (s, 4H, Cp); 6.07 (d, 8 Hz, 2H, Flu); 6.84 (t, 5 Hz, 2H, Flu); 6.92 (t, 5 Hz, 2H, Flu); 8.02 (d, 8 Hz, 2H, Flu); 6.35 (m, 1H, C*Ph*$_2$); 6.53 (m, 1H, C*Ph*$_2$); 7.02 (m, 1H, C*Ph*$_2$); 7.25 (m, 1H, C*Ph*$_2$); 7.73 (m, 1H, C*Ph*$_2$).

$Me_2C(\eta^5\text{-}C_5H_4)(Oct)TaMe_3$ (37). In the dry box, a round bottom flask was charged with 0.750 g (1.33 mmol) of $Li_2[Me_2C(C_5H_4)(Oct)]$. An addition funnel was charged with 0.395 g (1.33 mmol) of $TaCl_2Me_3$. On the vacuum line, 150 mL of THF was added to the flask and 25 mL of THF was added to the addition

funnel. The yellow tantalum solution was added to the ligand at -80 °C over the course of 30 minutes. The reaction was slowly warmed to room temperature and stirred for 16 hours. The THF was removed from the dark brown solution and replaced with petroleum ether. The petroleum ether was removed *in vacuo* leaving an oil. In the dry box, the oil was dissolved in 10 mL of petroleum ether and cooled to -30 °C. Over several days, a brown solid precipitates from the solution. The material was collected and dried *in vacuo* resulting in 0.123 g (12.1 %) of brown solid identified as **37**. ^{1}H NMR (benzene-d_6): δ = 0.528 (s, 6H, Ta*Me*); 0.645 (s, 3H, Ta*Me*); 1.36 (s, 12H, Oct), 1.38 (s, 12H, Oct), 1.40 (s, 6H, C*Me*$_2$); 1.66 (m, 4H, Oct); 5.33 (s, 2H, Cp); 5.57 (s, 2H, Cp); 6.99 (s, 2H, Flu); 8.14 (s, 2H, Flu). ^{13}C NMR (benzene-d_6): δ = 28.75 (C*Me*$_2$); 32.26, 32.55, 32.63, 32.97, 34.06, 34.83, 35.73 (Oct); 35.88 (Ta*Me*); 55.50 (Ta*Me*); 84.50, 100.21 (Cp), 116.53, 117.48, 123.86, 140.86, 141.14, 141.86, 142.24 (Flu).

Me$_2$C(η^5-C$_5$H$_4$)(η^1-Fluorenyl)TaMe$_2$F (38). In the dry box, a round bottom flask was charged with 0.500 g (1.00 mmol) of **35**, and a needle valve was attached. On the vacuum line, toluene was added at -80 °C. Against an Ar counterflow, 125 μL (1.00 mmol) of 54% wt. solution of HBF_4 in Et_2O was added at -80 °C. The reaction mixture was stirred for 10 minutes, and the volatiles were then removed *in vacuo* leaving 0.450 g (80%) of a red powder identified as **38**. ^{1}H NMR (THF-d_8): δ = 0.132 (d, 11 H, Ta*Me*); 1.49 (s, 6H, C*Me*$_2$); 6.06 (s, 4H, Cp); 6.45 (s, 4H, Cp); 7.15 (d, 8 Hz, 2H, Flu); 7.01 (t, 5 Hz, 2H, Flu); 7.18 (t, 5 Hz, 2H, Flu); 7.92 (d, 8 Hz, 2H, Flu). ^{13}C NMR (THF-d_8): δ = 28.35 (C*Me*$_2$); 34.63 (CMe$_2$); 46.21 (Ta*C*H$_3$) 100.34, 118.79, 120.72 (Cp); 125.41; 127.27; 129.42; 130.10; 131.89; 142.93; 143.01 (Flu). ^{19}F NMR (THF-d_8): δ = 36.40.

Me$_2$C(η^5-C$_5$H$_4$)(η^1-Fluorenyl)TaMe$_2$Cl (39). In the dry box, a round bottom flask was charged with 0.650 g (1.30 mmol) of **35** and 0.178 g (1.30 mmol) of $ZnCl_2$ and then was attached to a swivel frit assembly. On the vacuum line, CH_2Cl_2 added at -80 °C. The reaction mixture was stirred at room temperature and a deep red solid forms over time. The reaction mixture was stirred for two days, and the solvent was removed *in vacuo* and replaced with Et_2O. Red solid collected by filtration and dried *in vacuo* yielding 0.650 g (96%) of **39**. ^{1}H NMR (THF-d_8): δ = 0.56 (s, 6H, Ta*Me*); 1.26 (s, 6H, C*Me*$_2$); 6.16 (m, 2H, Cp); 6.52 (m, 2H, Cp); 6.98 (d, 8 Hz, 2H, Flu); 7.14 (m, 4H, Flu); 7.84 (d, 8 Hz, 2H, Flu). ^{13}C NMR (THF-d_8): δ = 28.96 (*Me*$_2$C); 52.76 (Ta*Me*); 102.05, 118.05, (Cp), 120.28,

124.82, 125.56, 126.67 (*benzo*, fluorenyl); 144.09, 145.81, *1 not located* (quaternary centers).

[(Me$_2$Si)$_2$(η^2-C$_5$H-3,5-(CHMe$_2$)$_2$)(η^5-C$_5$H$_2$-4-SiMe$_3$)]TaMe$_3$ (40). In the dry box, a swivel frit assembly was charged with 1.00 g (2.09 mmol) of K_2TMSThp and 0.600 g (2.02 mmol) of $TaCl_2Me_3$. On the vacuum line, approximately 15 mL of Et_2O was added at -80 °C. The reaction mixture was wrapped in foil, stirred and slowly warmed to room temperature. A yellow/orange solution and a white precipitate forms over time. After 2.5 hours, the reaction mixture was filtered and the white precipitate was washed with several portions of Et_2O. Slow cooling of yellow Et_2O solution results in formation of a golden solid. The solid was isolated by filtration and dried *in vacuo* yielding 0.400 g (30.2%) of **40**. ^{1}H NMR (benzene-*d*$_6$): δ = 0.685 (s, 6H, Si*Me*$_2$); 0.720 (s, 6H, Si*Me*$_2$); 0.140 (s, 9H, Si*Me*$_3$); 1.39 (s, 9H, Ta*Me*$_3$); 3.01 (sept, 2H, C*H*Me$_2$); 6.24 (s, 1H, Cp); 6.68 (s, 2H, Cp). Anal. Cald. for $Ta_1Si_3C_{26}H_{46}$ C, 50.06%, H, 7.43%; Found C, 49.82%; H, 7.25%.

[(Me$_2$Si)$_2$(η^2-C$_5$H-3,5-(CHMe$_2$)$_2$)(η^5-C$_5$H$_2$-4-SiMe$_3$)]TaMe$_2$Cl (41). In the dry box, 10.0 mg (0.016 mmol) of **40** was charged into a J. Young NMR tube and the sample dissolved in benzene-*d*$_6$ forming a yellow solution. On the vacuum line, the tube was degassed with three-freeze-pump-thaw cycles and 43 torr of anhydrous HCl was added via a 6.9 mL (0.016 mmol) calibrated gas volume at -196 °C. The tube was thawed and shaken and the reaction monitored by ^{1}H NMR spectroscopy. ^{1}H (benzene-*d*$_6$): δ = 0.15 (s, 9H, Si*Me*$_3$); 0.65 (s, 6H, Si*Me*$_2$); 0.75 (s, 6H, Si*Me*$_2$); 0.97 (d, 7 Hz, 3H, CH*Me*$_2$); 1.09 (d, 7Hz, 3H, CH*Me*$_2$); 2.95 (sept, 7 Hz, 1H, C*H*Me$_2$); 1.30 (s, 6H, Ta*Me*); 6.65 (s, 1H, Cp); 6.91 (s, 2H, Cp).

Kinetic Analysis of 6 with Ethylene. In the dry box, a flame sealable NMR tube was charged with 0.50 mL of 0.244 M stock solution of **6** in benzene-*d*$_6$. On the vacuum line, the desired amount of ethylene was added via a calibrated gas bulb at -196 °C. The solution was thawed and placed into a preheated NMR probe and approximately 10-15 ^{1}H NMR spectra were recorded over regular intervals during the course of the reaction, and the intensity of each peak was measured by integration versus an internal ferrocene standard. The rate of the reaction was then plotted, and the data were fitted using a least-squares analysis.

Structure Determinations for 27b, 29a, 31, 40. General Procedure: A suitable crystal was mounted on a glass fiber with Paratone-N oil. The data was collected on a Bruker Smart 1000 CCD diffractometer under a stream of N_2 gas at 98 K with the detector 5 cm (nominal) distance at Θ of -28 °. The initial cell for data reduction was calculated for just under 1000 reflections chosen throughout the data frames. For data processing with SAINT v.602, all defaults were used, except: box size optimization was enabled, periodic orientation matrix updating was disabled, the instrument error was set to zero, Laue class integration restraints were not used, the model profiles from all nine areas were blended and for the post-integration global least squares refinement, no constraints were applied.

27b. Six runs of data were collected with 20 second long, -0.20 ° wide ω-scans at three values of ϕ (0, 120, 240, 60, 180 and 300°). The data were corrected with SADABS v. 2.0 (beta) using a g-value of 0.0500 and a scale factor of 0.001 (minimum value). No decay correction was needed. The structure was solved using direct methods and the difference Fourier maps were used to locate all missing atoms, including hydrogens. Refinement of F^2 was against all reflections. A total of 4617 reflections were refined to R = 0.0837 (GOF = 1.584).

29a. Six runs of data were collected with 20 second long, -0.20 ° wide ω-scans at three values of ϕ (0, 120, 240, 60, 180 and 300°). The data were corrected with SADABS v. 2.0 (beta) using default parameters except that the scale factor esd was set to a minimum value of 0.001. No decay correction was needed. The structure was solved using direct methods and the difference Fourier maps were used to locate all missing atoms, including hydrogens. Refinement of F^2 was against all reflections. A total of 5074 reflections were refined to R = 0.0274 (GOF = 2.191).

30. Six runs of data were collected with 20 second long, -0.20 ° wide ω-scans at three values of ϕ (0, 120, 240, 60, 180 and 300°). The data were corrected with SADABS v. 2.0 (beta) using default parameters except that the scale factor esd was set to a minimum value of 0.001. No decay correction was needed. The structure was solved using direct methods and the difference Fourier maps were used to locate all missing atoms, including hydrogens. Refinement of F^2 was

against all reflections. A total of 4860 reflections were refined to R = 0.0462 (GOF = 1.291).

31. Three runs of data were collected with 30 second long, -0.25 ° wide ω-scans at three values of ϕ (0, 120, and 240°). The data were corrected with SADABS v. 2.0 (beta) using default parameters except that the scale factor esd was set to a minimum value of 0.001. No decay correction was needed. The structure was solved using direct methods and the difference Fourier maps were used to locate all missing atoms, including hydrogens. Refinement of F^2 was against all reflections. A total of 4126 reflections were refined to R = 0.0412 (GOF = 1.794).

40. Four runs of data were collected with 20 second long, -0.30 ° wide ω-scans at three values of ϕ (0, 120, 240 and 0°) under a dark sheet to protect the crystal from light. The data were corrected with SADABS v. 2.0 (beta) using a g-value of 0.0601 and a scale factor of 0.001 (minimum value). No decay correction was needed. The structure was solved using direct methods and the difference Fourier maps were used to locate all missing atoms, including hydrogens. Refinement of F^2 was against all reflections. A total of 3562 reflections were refined to R = 0.0592 (GOF = 7.042).

Structure Determinations for 35, 35a, 38. General Procedure: A suitable crystal was attached to a glass fiber and centered on an Enraf-Nonius CAD-4 diffractometer under an 85 K stream of N_2 gas. Unit cell parameters were obtained from the setting angles of 25 high-angle reflections. Three reference reflections were measured every 75 minutes to monitor crystal decay.

35. The structure was solved using direct methods and the difference Fourier maps were used to locate the missing atoms, including hydrogens. A total of 4350 data were refined to *R* = 0.0172 (GOF = 1.560).

35a. The structure was solved using direct methods and the difference Fourier maps were used to locate the missing atoms, including hydrogens. A total of 4439 data were refined to *R* = 0.0584 (GOF = 1.756).

38. The structure was solved using direct methods and the difference Fourier maps were used to locate the missing atoms, including hydrogens. A total of 4709 data were refined to $R = 0.0228$ (GOF = 1.360).

References.

1. For recent reviews see: a) Brintzinger, H.H.; Fischer, D.; Mülhaupt, R.; Reiger, B.; Waymouth, R.M. *Angew. Chem. Int. Ed. Engl.* **1995**, *34*, 1143. b) Bochmann, M. *J. Chem. Soc., Dalton Trans.* **1996**, 255.

2. a) Piers, W.E.; Bercaw, J.E. *J. Am. Chem. Soc.* **1990**, *112*, 9406. b) Krauledat, H.; Brintzinger, H.H. *Angew. Chem. Int. Ed. Engl.* **1990**, *102*, 1412. c) Grubbs, R.H.; Coates, G.W. *Acc. Chem. Res.* **1996**, *29*, 85.

3. Jordan, R.F. *Adv. Organomet. Chem.* **1991**, *32*, 325.

4. Guerra, G.; Cavallo, L.; Moscardi, G.; Vacetello, M.; Corradini, P. *J. Am. Chem. Soc.* **1994**, *116*, 2988.

5. Pino, P.; Cioni, P.; Wei, J. *J. Am. Chem. Soc.* **1987**, *109*, 6189.

6. Pino, P.; Galimberti, M. *J. Organomet. Chem.* **1989**, *370*, 1.

7. Gilchrist, J.H.; Bercaw, J.E. *J. Am. Chem. Soc.* **1996**, *118*, 12021.

8. Herzog, T.A.; Zubris, D.L.; Bercaw, J.E. *J. Am. Chem. Soc.* **1996**, *118*, 11988.

9 a) Mise, T.; Miya, S.; Yamazaki, H. *Chem. Lett.* **1989**, 1853. b) Zhong, A.H.; Bercaw, J.E. *unpublishded results*.

10. a) Doherty, N.M.; Bercaw, J.E. *J. Am. Chem. Soc.* **1985**, *107*, 2670. b) Burger, B.J.; Santarsiero, B.D.; Trimmer, M.S.; Bercaw, J.E. *J. Am. Chem. Soc.* **1988**, *110*, 3134.

11. a) Chernega, A.N.; Green, M.L.H.; Suárez, A.G. *Can. J. Chem.* **1995**, *73*, 1157. b) Bailey, N.J.; Cooper, J.A.; Gailus, H.; Green, M.L.H.; James, J.T.; Leech, M.A. *J. Chem. Soc. Dalton Trans.* **1997**, 3579. c) Bailey, N.J.; Green, M.L.H.; Leech, M.A.; Saunders, J.F.; Tidswell, H.M. *J. Organomet. Chem.* **1997**, *538*, 111. d) Conway, S.L; Doerrer, L.H.; Green, M.L.H.; Leech, M.A. *Organometallics* **2000**, *19, in press.*

12. Antinolo, A.; Martinez-Ripoll, M.; Mugnier, Y.; Otero, A.; Prashar, S.; Rodriguez, A.M. *Organometallics* **1996**, *15*, 3241.

13. a) Herrmann, W.A.; Baratta, W. *J. Organomet. Chem.* **1996**, *506*, 357. b) Herrmann, W.A.; Baratta, W.; Herdtweck, E. *Agnew. Chem. Int. Ed. Engl.* **1996**, *35*, 1951.

14. Shin, J.H.; Parkin, G. *Chem. Comm.* **1999**, *887*.

15. McGrady, N.D.; McDade, C.; Bercaw, J.E. in *Organometallic Compounds: Synthesis, Structure and Theory*; Shapiro, B.L., Ed.; Texas A&M University Press; College Station, TX, 1983; pp 46-85.

16. Tebbe, F.N.; Parshall, G.W. *J. Am. Chem. Soc.* **1981**, *93*, 3793.

17. Gibson, V.C.; Bercaw, J.E.; Bruton, W.J.; Sanner, R.D. *Organometallics* **1986**, *5*, 976.

18. The *endo* ethylene hydrogens are overlapping.

19. Wilson, R.D.; Koetzle, T.F.; Hart, D.W.; Kvick, A.; Tipton, D.L.; Bau, R. *J. Am. Chem. Soc.* **1977**, *99*, 1775.

20. Schrock, R.R.; Sharpe, P.R. *J. Am. Chem. Soc.* **1978**, *100*, 2389.

21. Zubris, D.L.; Bercaw, J.E. *unpublished results*.

22. This preparation is a modification of that reported for the preparation of $Me_2Si(C_5H_4)_2TaMe_3$. Cook, K.S.; Piers, W.E. *personal communication*.

23. An average tantalum-methyl bond distance is 2.217 Å. Orpen, A.G.; Brammer, L.; Allen, F.H.; Kennard, O.; Watson, D.G.; Taylor, R. *J. Chem. Soc. Dalton Trans.* **1989**, S1.

24. Ewen, J.A.; Jones, R.L; Razavi, A.; Ferrara, J.D. *J. Am. Chem. Soc.* **1988**, *110*, 6255.

25. Miller, S.A. *Ph.D. Thesis*, California Institute of Technology, 2000.

26. Rodriguez, G.; Graham, J.P.; Cotter, W.D.; Sperry, C.K.; Bazan, G.C.; Bursten, B.E. *J. Am. Chem. Soc.* **1998**, *120*, 12512.

27. Lucas, C.R.; Green, M.L.H.; Forder, R.A.; Prout, K. *J. Chem. Soc. Chem. Comm.* **1973**, 97.

28. Shapiro, P.J. *Coord. Chem. Rev.* **1999**, *189*, 1.

29. Burger, B.J.; Bercaw, J.E. In *Experimental Organometallic Chemistry*; Wayda, A.L.; Darensbourg, M.Y., Eds.; ACS Symposium Series 357; American Chemical Society: Washington, DC, 1987, Chapter 4.

30. Marvich, R.H.; Brintzinger, H.H. *J. Am. Chem. Soc.* **1971**, *93*, 2046.

31. Herzog, T.A. *Ph.D. Thesis* California Institute of Technology, **1997**.

Appendix A:

Select Kinetic Plots

1 with Isobutene (296 K)

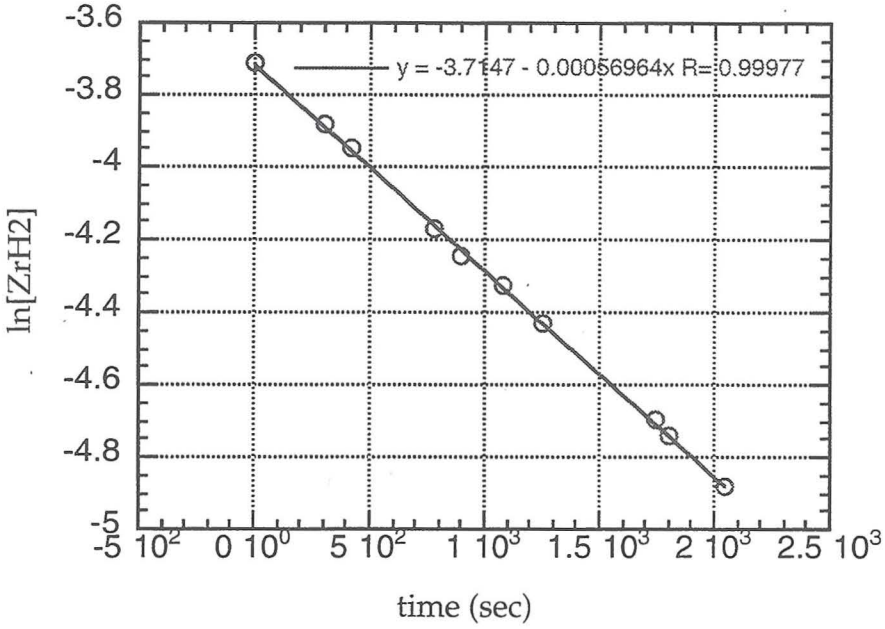

2 with c-2-butene (265 K)

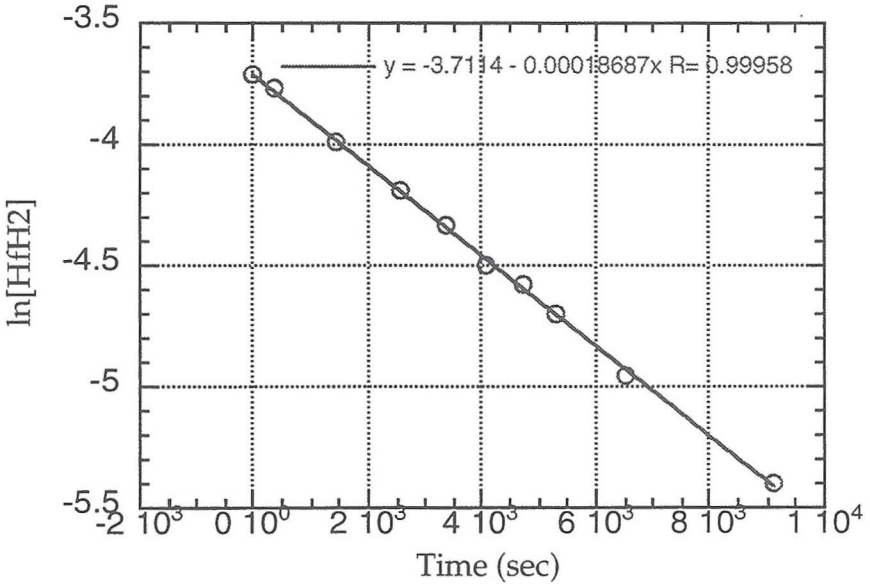

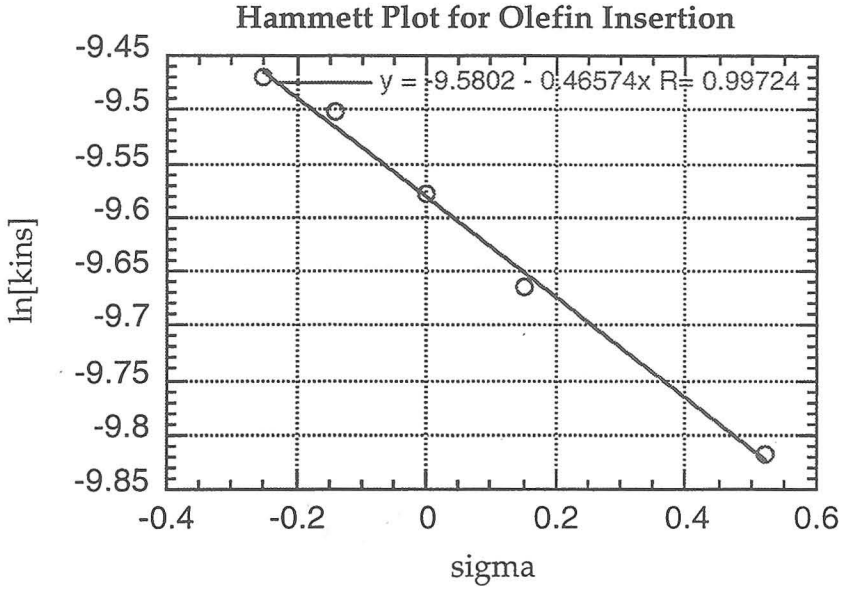
Hammett Plot for Olefin Insertion
y = -9.5802 - 0.46574x R= 0.99724
ln[kins]
-9.45
-9.5
-9.55
-9.6
-9.65
-9.7
-9.75
-9.8
-9.85
-0.4
-0.2
0
0.2
0.4
0.6
sigma

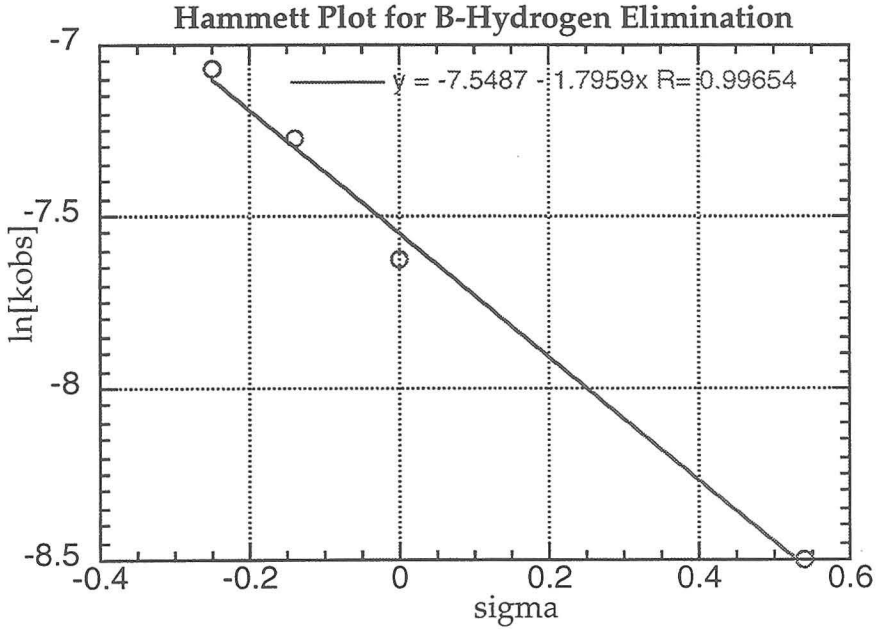
Hammett Plot for B-Hydrogen Elimination
y = -7.5487 - 1.7959x R= 0.99654
ln[kobs]
-7
-7.5
-8
-8.5
-0.4
-0.2
0
0.2
0.4
0.6
sigma

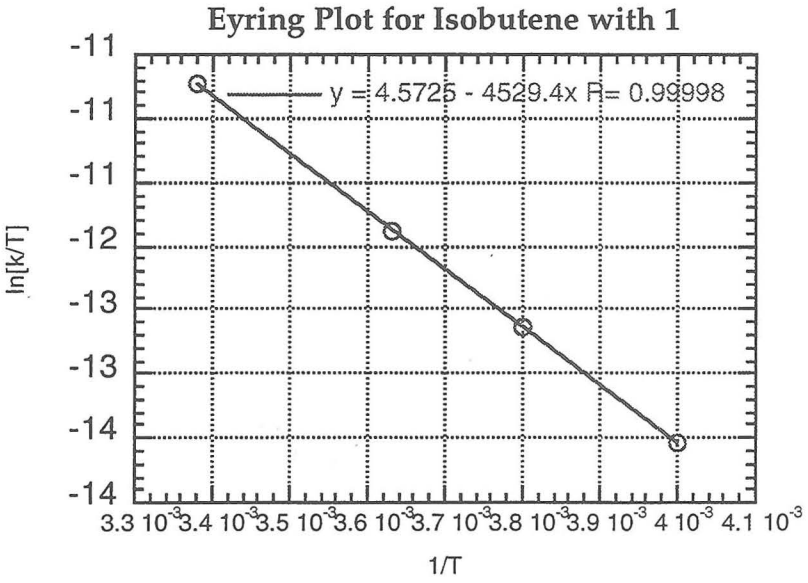
Eyring Plot for Isobutene with 1
y = 4.5725 - 4529.4x R= 0.99998
ln[k/T]
-11
-11
-11
-12
-13
-13
-14
-14
3.3 10-3 3.4 10-3 3.5 10-3 3.6 10-3 3.7 10-3 3.8 10-3 3.9 10-3 4 10-3 4.1 10-3
1/T

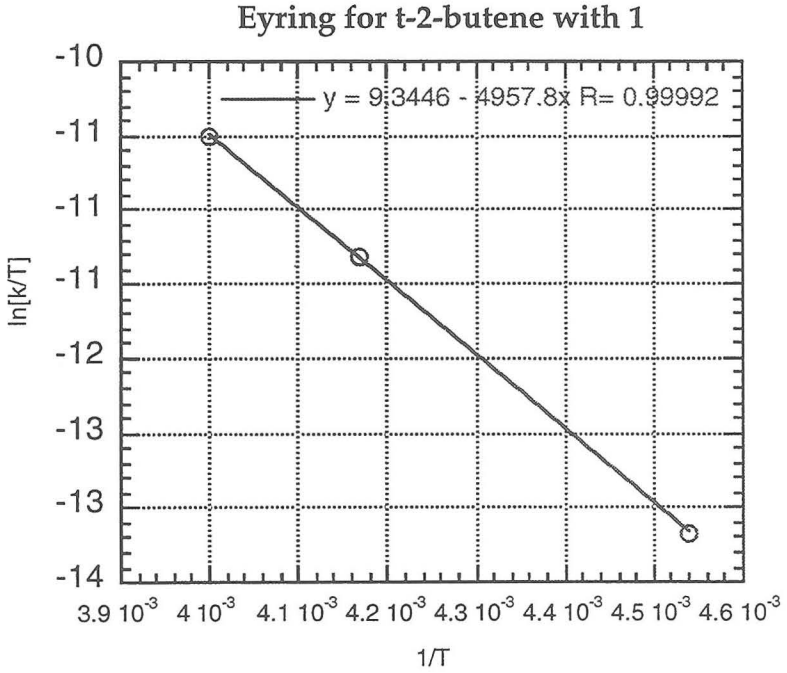
Eyring for t-2-butene with 1
y = 9.3446 - 4957.8x R= 0.99992
ln[k/T]
-10
-11
-11
-11
-12
-13
-13
-14
3.9 10-3 4 10-3 4.1 10-3 4.2 10-3 4.3 10-3 4.4 10-3 4.5 10-3 4.6 10-3
1/T

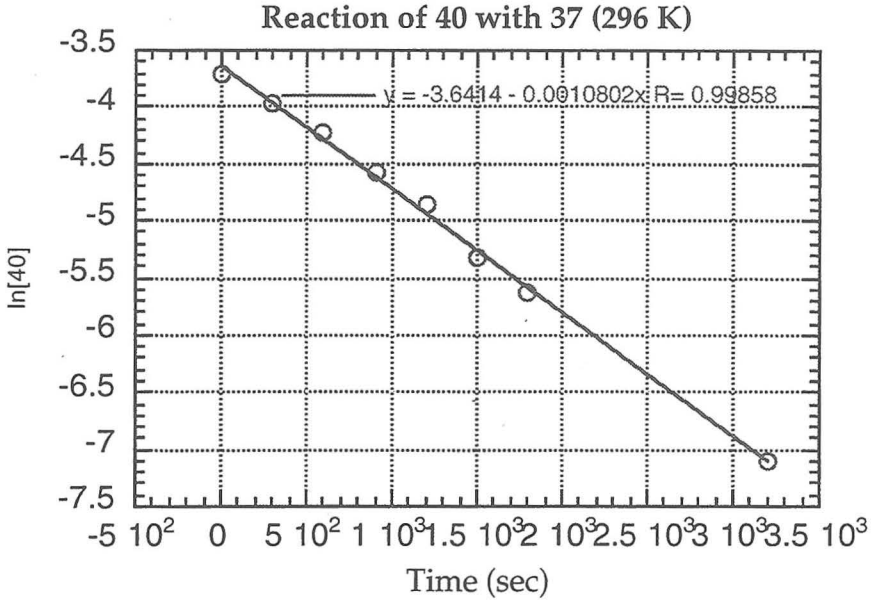
Reaction of 40 with 37 (296 K)
y = -3.6414 - 0.0010802x R= 0.99858
ln[40]
-3.5
-4
-4.5
-5
-5.5
-6
-6.5
-7
-7.5
-5 10^2 0 5 10^2 1 10^3 1.5 10^3 2 10^3 2.5 10^3 3 10^3 3.5 10^3
Time (sec)

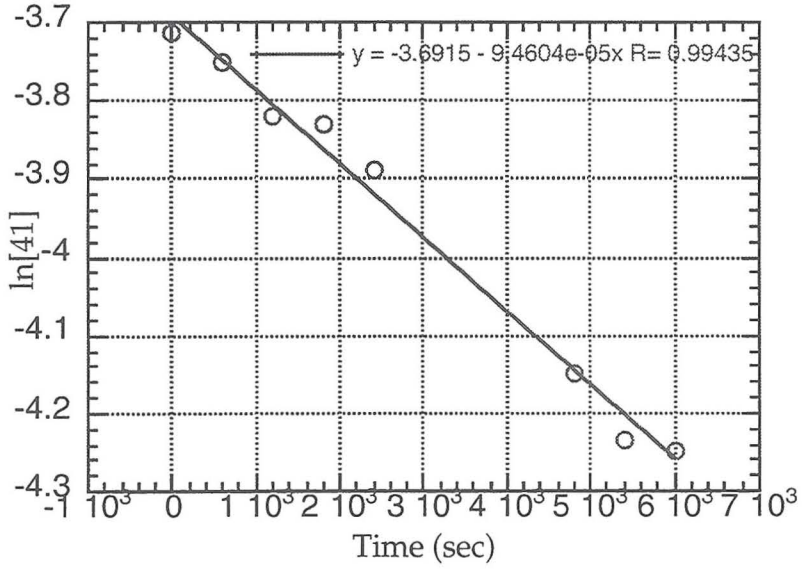
Reaction of 41 with 37 (270 K)
y = -3.6915 - 9.4604e-05x R= 0.99435
ln[41]
-3.7
-3.8
-3.9
-4
-4.1
-4.2
-4.3
-1 10^3 0 1 10^3 2 10^3 3 10^3 4 10^3 5 10^3 6 10^3 7 10^3
Time (sec)

Appendix B:

X-ray Crystallographic Data

Table 1. Crystal data and structure refinement for $Cp^*(\eta^5\text{-}C_5H_4\text{-}CMe_3)ZrCl_2$.

Empirical formula	$C_{18}H_{26}Cl_2Zr$	
Formula weight	404.51	
Crystallization Solvent	Toluene	
Crystal Habit	Block	
Crystal size	0.26 x 0.25 x 0.18 mm^3	
Crystal color	Colorless	
Data Collection		
Preliminary Photos		
Type of diffractometer	CAD-4	
Wavelength	0.71073 Å MoKa	
Data Collection Temperature	85 K	
Theta range for reflections used in lattice determination	15.5 to 21.7°	
Unit cell dimensions	a = 17.247(3) Å b = 6.5860(10) Å c = 15.549(2) Å	a= 90° b= 90° g = 90°
Volume	1766.2(5) $Å^3$	
Z	4	
Crystal system	Orthorhombic	
Space group	Cmcm	
Density (calculated)	1.521 Mg/m^3	
F(000)	832	
Theta range for data collection	2.36 to 29.97°	
Completeness to theta = 29.97°	99.8 %	
Index ranges	-24<=h<=24, 0<=k<=9, -21<=l<=21	
Data collection scan type	Omega scans	
Reflections collected	6261	
Independent reflections	1371 [R_{int}= 0.0103; GOF_{merge}=]	
Absorption coefficient	0.917 mm^{-1}	
Absorption correction	Psi scan	
Max. and min. transmission	0.96 and 1.04	
Number of standards	3 reflections measured every 75min.	
Variation of standards	-0.12%.	

Table 1 (cont.)

Structure solution and Refinement

Structure solution program	SHELXS-97 (Sheldrick, 1990)
Primary solution method	Direct methods
Secondary solution method	Direct methods
Hydrogen placement	Difference Fourier map
Structure refinement program	SHELXL-97 (Sheldrick, 1997)
Refinement method	Full matrix least-squares on F^2
Data / restraints / parameters	1371 / 0 / 80
Treatment of hydrogen atoms	Unrestrained
Goodness-of-fit on F^2	2.639
Final R indices [I>2s(I)]	R1 = 0.0203, wR2 = 0.0617
R indices (all data)	R1 = 0.0215, wR2 = 0.0620
Type of weighting scheme used	Sigma
Weighting scheme used	w=1/s^2^(Fo^2^)
Max shift/error	0.000
Average shift/error	0.000
Largest diff. peak and hole	0.508 and -0.369 e.Å^{-3}

Table 2. Atomic coordinates (x 10^4) and equivalent isotropic displacement parameters (Å^{2}x 10^3) for Cp*(η^5-C_5H_4-CMe_3)$ZrCl_2$. U(eq) is defined as the trace of the orthogonalized U^{ij} tensor.

	x	y	z	U_{eq}
Zr	0	578(1)	2500	6(1)
Cl	0	-1860(1)	3684(1)	12(1)
C(1)	883(1)	3548(3)	2500	10(1)
C(2)	1088(1)	2410(2)	3242(1)	9(1)
C(3)	1441(1)	576(2)	2956(1)	10(1)
C(4)	1018(1)	3082(3)	4162(1)	15(1)
C(5)	1830(1)	-979(3)	3509(1)	17(1)

Table 3. Bond lengths [Å] and angles [°] for $Cp^*(\eta^5\text{-}C_5H_4\text{-}CMe_3)ZrCl_2$.

Zr-Cent	2.2271(3)
Zr-Pln	2.2239(11)
Zr-Cl#1	2.4431(5)
Zr-Cl	2.4431(5)
Zr-C(1)	2.479(2)
Zr-C(1)#2	2.479(2)
Zr-C(2)	2.5118(14)
Zr-C(2)#2	2.5118(14)
Zr-C(2)#3	2.5118(14)
Zr-C(2)#1	2.5118(14)
Zr-C(3)#1	2.5834(15)
Zr-C(3)	2.5834(15)
Zr-C(3)#2	2.5834(15)
Zr-C(3)#3	2.5834(15)
C(1)-C(2)#1	1.4206(18)
C(1)-C(2)	1.4206(18)
C(1)-H(1)	0.95(3)
C(2)-C(3)	1.4236(19)
C(2)-C(4)	1.5013(19)
C(3)-C(3)#1	1.417(3)
C(3)-C(5)	1.496(2)
C(4)-H(4A)	0.95(2)
C(4)-H(4B)	0.91(2)
C(4)-H(4C)	0.99(2)
C(5)-H(5A)	0.95(3)
C(5)-H(5B)	0.95(3)
C(5)-H(5C)	0.92(3)
Cent-Zr-Cent	133.84(2)
Pln-Zr-Pln	127.46(6)
Cl#1-Zr-Cl	97.85(3)
Cl#1-Zr-C(1)	121.23(2)
Cl-Zr-C(1)	121.23(2)
Cl#1-Zr-C(1)#2	121.23(2)
Cl-Zr-C(1)#2	121.23(2)
C(1)-Zr-C(1)#2	75.79(9)
Cl#1-Zr-C(2)	131.45(3)
Cl-Zr-C(2)	88.25(3)
C(1)-Zr-C(2)	33.07(4)
C(1)#2-Zr-C(2)	94.57(5)
Cl#1-Zr-C(2)#2	88.25(3)
Cl-Zr-C(2)#2	131.45(3)
C(1)-Zr-C(2)#2	94.57(5)
C(1)#2-Zr-C(2)#2	33.07(4)
C(2)-Zr-C(2)#2	122.57(7)
Cl#1-Zr-C(2)#3	131.45(3)
Cl-Zr-C(2)#3	88.25(3)
C(1)-Zr-C(2)#3	94.57(5)
C(1)#2-Zr-C(2)#3	33.07(4)
C(2)-Zr-C(2)#3	96.68(6)
C(2)#2-Zr-C(2)#3	54.69(6)

Cl#1-Zr-C(2)#1	88.25(3)
Cl-Zr-C(2)#1	131.45(3)
C(1)-Zr-C(2)#1	33.07(4)
C(1)#2-Zr-C(2)#1	94.57(5)
C(2)-Zr-C(2)#1	54.69(6)
C(2)#2-Zr-C(2)#1	96.68(6)
C(2)#3-Zr-C(2)#1	122.57(7)
Cl#1-Zr-C(3)#1	78.05(3)
Cl-Zr-C(3)#1	101.92(3)
C(1)-Zr-C(3)#1	53.82(5)
C(1)#2-Zr-C(3)#1	126.23(5)
C(2)-Zr-C(3)#1	53.68(4)
C(2)#2-Zr-C(3)#1	126.35(5)
C(2)#3-Zr-C(3)#1	147.63(5)
C(2)#1-Zr-C(3)#1	32.41(4)
Cl#1-Zr-C(3)	101.92(3)
Cl-Zr-C(3)	78.05(3)
C(1)-Zr-C(3)	53.82(5)
C(1)#2-Zr-C(3)	126.23(5)
C(2)-Zr-C(3)	32.41(4)
C(2)#2-Zr-C(3)	147.63(5)
C(2)#3-Zr-C(3)	126.35(5)
C(2)#1-Zr-C(3)	53.68(4)
C(3)#1-Zr-C(3)	31.84(6)
Cl#1-Zr-C(3)#2	78.05(3)
Cl-Zr-C(3)#2	101.92(3)
C(1)-Zr-C(3)#2	126.23(5)
C(1)#2-Zr-C(3)#2	53.82(5)
C(2)-Zr-C(3)#2	147.63(5)
C(2)#2-Zr-C(3)#2	32.41(4)
C(2)#3-Zr-C(3)#2	53.68(4)
C(2)#1-Zr-C(3)#2	126.35(5)
C(3)#1-Zr-C(3)#2	148.16(6)
C(3)-Zr-C(3)#2	179.95(7)
Cl#1-Zr-C(3)#3	101.92(3)
Cl-Zr-C(3)#3	78.05(3)
C(1)-Zr-C(3)#3	126.23(5)
C(1)#2-Zr-C(3)#3	53.82(5)
C(2)-Zr-C(3)#3	126.35(5)
C(2)#2-Zr-C(3)#3	53.68(4)
C(2)#3-Zr-C(3)#3	32.41(4)
C(2)#1-Zr-C(3)#3	147.63(5)
C(3)#1-Zr-C(3)#3	179.95(7)
C(3)-Zr-C(3)#3	148.16(6)
C(3)#2-Zr-C(3)#3	31.84(6)
C(2)#1-C(1)-C(2)	108.62(17)
C(2)#1-C(1)-Zr	74.73(10)
C(2)-C(1)-Zr	74.73(10)
C(2)#1-C(1)-H(1)	125.66(10)
C(2)-C(1)-H(1)	125.66(10)
Zr-C(1)-H(1)	119.0(18)
C(1)-C(2)-C(3)	107.46(13)
C(1)-C(2)-C(4)	126.73(13)
C(3)-C(2)-C(4)	125.59(13)

C(1)-C(2)-Zr	72.21(9)
C(3)-C(2)-Zr	76.56(8)
C(4)-C(2)-Zr	121.28(9)
C(3)#1-C(3)-C(2)	108.22(8)
C(3)#1-C(3)-C(5)	125.06(9)
C(2)-C(3)-C(5)	126.35(13)
C(3)#1-C(3)-Zr	74.08(3)
C(2)-C(3)-Zr	71.03(8)
C(5)-C(3)-Zr	126.14(10)
C(2)-C(4)-H(4A)	111.3(13)
C(2)-C(4)-H(4B)	114.5(13)
H(4A)-C(4)-H(4B)	109.8(18)
C(2)-C(4)-H(4C)	111.0(12)
H(4A)-C(4)-H(4C)	103.8(17)
H(4B)-C(4)-H(4C)	105.7(16)
C(3)-C(5)-H(5A)	113.9(15)
C(3)-C(5)-H(5B)	111.3(15)
H(5A)-C(5)-H(5B)	105(2)
C(3)-C(5)-H(5C)	109.7(16)
H(5A)-C(5)-H(5C)	109(2)
H(5B)-C(5)-H(5C)	108(2)

Symmetry transformations used to generate equivalent atoms:
#1 x,y,-z+1/2 #2 -x,y,-z+1/2 #3 -x,y,z

Table 4. Crystal data and structure refinement for $Cp^*(iPr_2Cp)ZrCl_2$.

Empirical formula	$C_{21}H_{32}Cl_2Zr$	
Formula weight	446.59	
Crystallization Solvent	Toluene	
Crystal Habit	Rod	
Crystal size	0.37 x 0.29 x 0.15 mm^3	
Crystal color	Colorless	
Data Collection		
Preliminary Photos		
Type of diffractometer	CAD-4	
Wavelength	0.71073 Å MoK	
Data Collection Temperature	85 K	
Theta range for reflections used in lattice determination	14.4 to 15.2°	
Unit cell dimensions	a = 13.875(3) Å b = 16.059(5) Å c = 9.628(2) Å	a= 90° b= 90° g = 90°
Volume	2145.3(9) $Å^3$	
Z	4	
Crystal system	Orthorhombic	
Space group	Pnma	
Density (calculated)	1.383 Mg/m^3	
F(000)	928	
Theta range for data collection	2.5 to 27.5°	
Completeness to theta = 27.5°	100.0 %	
Index ranges	-18<=h<=18, 0<=k<=20, -12<=l<=12	
Data collection scan type	Omega scans	
Reflections collected	8633	
Independent reflections	2546 [R_{int}= 0.022; GOF_{merge}=]	
Absorption coefficient	0.762 mm^{-1}	
Absorption correction	None	
Number of standards	3 reflections measured every 75min.	
Variation of standards	Within counting statistics, zero%.	

Table 4 (cont.)

Structure solution and Refinement

Structure solution program	SHELXS-97 (Sheldrick, 1990)
Primary solution method	Patterson method
Secondary solution method	Difference Fourier map
Hydrogen placement	Difference Fourier map
Structure refinement program	SHELXL-97 (Sheldrick, 1997)
Refinement method	Full matrix least-squares on F^2
Data / restraints / parameters	2546 / 0 / 181
Treatment of hydrogen atoms	Unrestrained
Goodness-of-fit on F^2	1.834
Final R indices [I>2s(I)]	R1 = 0.0244, wR2 = 0.0548
R indices (all data)	R1 = 0.0290, wR2 = 0.0561
Type of weighting scheme used	Observed
Weighting scheme used	w=1/s^2^(Fo^2^)
Max shift/error	0.001
Average shift/error	0.000
Largest diff. peak and hole	0.666 and -0.409 e.$Å^{-3}$

Table 5. Atomic coordinates (x 10^4) and equivalent isotropic displacement parameters ($Å^2$x 10^3) for Cp*(iPr_2Cp)$ZrCl_2$. U(eq) is defined as the trace of the orthogonalized U^{ij} tensor.

	x	y	z	U(eq)
Zr	409(1)	2500	1917(1)	10(1)
Cl(1)	-715(1)	3659(1)	2245(1)	18(1)
C(1)	1628(2)	2500	-20(3)	34(1)
C(11)	2705(3)	2500	86(4)	99(3)
C(2)	1050(2)	3208(1)	-210(2)	28(1)
C(22)	1374(5)	4105(3)	-177(3)	88(2)
C(3)	117(1)	2935(1)	-599(2)	20(1)
C(33)	-703(3)	3472(2)	-1076(3)	54(1)
C(5)	1861(1)	2947(1)	3186(2)	13(1)
C(6)	1120(1)	3222(1)	4073(2)	13(1)
C(68)	1362(2)	4184(1)	6039(2)	27(1)
C(66)	939(1)	4096(1)	4575(2)	18(1)
C(67)	1348(2)	4763(1)	3622(2)	26(1)
C(7)	635(2)	2500	4559(2)	14(1)

Table 6. Bond lengths [Å] and angles [°] for $Cp^*(iPr_2Cp)ZrCl_2$.

Zr-Pln1	2.225(1)
Zr-Pln2	2.204(1)
Zr-Cent1	2.2262(5)
Zr-Cent2	2.2217(4)
Zr-Cl(1)#1	2.4478(6)
Zr-Cl(1)	2.4478(6)
Zr-C(5)	2.4632(16)
Zr-C(5)#1	2.4632(16)
Zr-C(2)#1	2.5059(18)
Zr-C(2)	2.5059(18)
Zr-C(1)	2.519(3)
Zr-C(3)#1	2.5537(17)
Zr-C(3)	2.5537(17)
Zr-C(7)	2.562(2)
Zr-C(6)	2.5737(16)
Zr-C(6)#1	2.5737(16)
C(1)-C(2)	1.404(3)
C(1)-C(2)#1	1.404(3)
C(1)-C(11)	1.498(4)
C(11)-H(11A)	0.97(4)
C(11)-H(11B)	0.75(3)
C(2)-C(3)	1.416(3)
C(2)-C(22)	1.508(4)
C(22)-H(22A)	0.74(5)
C(22)-H(22B)	0.98(4)
C(22)-H(22C)	0.96(3)
C(3)-C(3)#1	1.397(4)
C(3)-C(33)	1.500(3)
C(33)-H(33A)	0.95(3)
C(33)-H(33B)	0.92(3)
C(33)-H(33C)	0.99(3)
C(5)-C(6)	1.407(2)
C(5)-C(5)#1	1.434(3)
C(5)-H(5)	0.944(19)
C(6)-C(7)	1.420(2)
C(6)-C(66)	1.507(2)
C(68)-C(66)	1.533(3)
C(68)-H(68A)	1.02(2)
C(68)-H(68B)	0.94(2)
C(68)-H(68C)	1.00(2)
C(66)-C(67)	1.520(3)
C(66)-H(66)	0.95(2)
C(67)-H(67A)	1.00(2)
C(67)-H(67B)	0.94(2)
C(67)-H(67C)	0.96(2)
C(7)-C(6)#1	1.420(2)
C(7)-H(7)	0.96(3)
Pln1-Zr-Pln2	126.87(8)
Cent1-Zr-Cent2	131.49(2)
Cl(1)#1-Zr-Cl(1)	98.94(3)

Cl(1)#1-Zr-C(5)	132.73(4)
Cl(1)-Zr-C(5)	103.66(4)
Cl(1)#1-Zr-C(5)#1	103.66(4)
Cl(1)-Zr-C(5)#1	132.73(4)
C(5)-Zr-C(5)#1	33.84(8)
Cl(1)#1-Zr-C(2)#1	89.21(5)
Cl(1)-Zr-C(2)#1	132.55(4)
C(5)-Zr-C(2)#1	104.30(6)
C(5)#1-Zr-C(2)#1	89.01(6)
Cl(1)#1-Zr-C(2)	132.55(4)
Cl(1)-Zr-C(2)	89.22(5)
C(5)-Zr-C(2)	89.01(6)
C(5)#1-Zr-C(2)	104.30(6)
C(2)#1-Zr-C(2)	53.99(10)
Cl(1)#1-Zr-C(1)	121.55(3)
Cl(1)-Zr-C(1)	121.55(3)
C(5)-Zr-C(1)	79.49(7)
C(5)#1-Zr-C(1)	79.49(7)
C(2)#1-Zr-C(1)	32.45(6)
C(2)-Zr-C(1)	32.45(6)
Cl(1)#1-Zr-C(3)#1	79.24(4)
Cl(1)-Zr-C(3)#1	103.25(4)
C(5)-Zr-C(3)#1	132.81(6)
C(5)#1-Zr-C(3)#1	121.35(6)
C(2)#1-Zr-C(3)#1	32.50(6)
C(2)-Zr-C(3)#1	53.49(6)
C(1)-Zr-C(3)#1	53.39(7)
Cl(1)#1-Zr-C(3)	103.25(4)
Cl(1)-Zr-C(3)	79.24(4)
C(5)-Zr-C(3)	121.35(6)
C(5)#1-Zr-C(3)	132.81(6)
C(2)#1-Zr-C(3)	53.49(6)
C(2)-Zr-C(3)	32.50(6)
C(1)-Zr-C(3)	53.39(7)
C(3)#1-Zr-C(3)	31.76(8)
Cl(1)#1-Zr-C(7)	87.15(4)
Cl(1)-Zr-C(7)	87.15(4)
C(5)-Zr-C(7)	53.67(6)
C(5)#1-Zr-C(7)	53.67(6)
C(2)#1-Zr-C(7)	140.15(6)
C(2)-Zr-C(7)	140.15(6)
C(1)-Zr-C(7)	130.76(8)
C(3)#1-Zr-C(7)	163.94(4)
C(3)-Zr-C(7)	163.94(4)
Cl(1)#1-Zr-C(6)	118.87(4)
Cl(1)-Zr-C(6)	78.37(4)
C(5)-Zr-C(6)	32.35(5)
C(5)#1-Zr-C(6)	54.37(5)
C(2)#1-Zr-C(6)	136.65(6)
C(2)-Zr-C(6)	108.56(6)
C(1)-Zr-C(6)	109.84(6)
C(3)#1-Zr-C(6)	161.59(5)
C(3)-Zr-C(6)	134.62(5)
C(7)-Zr-C(6)	32.10(4)

Cl(1)#1-Zr-C(6)#1	78.37(4)
Cl(1)-Zr-C(6)#1	118.87(4)
C(5)-Zr-C(6)#1	54.37(5)
C(5)#1-Zr-C(6)#1	32.35(5)
C(2)#1-Zr-C(6)#1	108.56(6)
C(2)-Zr-C(6)#1	136.65(6)
C(1)-Zr-C(6)#1	109.84(6)
C(3)#1-Zr-C(6)#1	134.62(5)
C(3)-Zr-C(6)#1	161.59(5)
C(7)-Zr-C(6)#1	32.10(4)
C(6)-Zr-C(6)#1	53.53(7)
C(2)-C(1)-C(2)#1	108.2(2)
C(2)-C(1)-C(11)	125.40(12)
C(2)#1-C(1)-C(11)	125.40(12)
C(2)-C(1)-Zr	73.26(13)
C(2)#1-C(1)-Zr	73.26(13)
C(11)-C(1)-Zr	128.3(2)
C(1)-C(11)-H(11A)	107(2)
C(1)-C(11)-H(11B)	116(2)
H(11A)-C(11)-H(11B)	115(2)
C(1)-C(2)-C(3)	107.80(17)
C(1)-C(2)-C(22)	126.9(3)
C(3)-C(2)-C(22)	125.0(3)
C(1)-C(2)-Zr	74.29(13)
C(3)-C(2)-Zr	75.61(10)
C(22)-C(2)-Zr	121.48(17)
C(2)-C(22)-H(22A)	112(4)
C(2)-C(22)-H(22B)	110(2)
H(22A)-C(22)-H(22B)	119(4)
C(2)-C(22)-H(22C)	107.0(19)
H(22A)-C(22)-H(22C)	105(4)
H(22B)-C(22)-H(22C)	103(3)
C(3)#1-C(3)-C(2)	108.04(11)
C(3)#1-C(3)-C(33)	125.10(17)
C(2)-C(3)-C(33)	126.6(2)
C(3)#1-C(3)-Zr	74.12(4)
C(2)-C(3)-Zr	71.90(10)
C(33)-C(3)-Zr	124.60(14)
C(3)-C(33)-H(33A)	112(2)
C(3)-C(33)-H(33B)	112.9(18)
H(33A)-C(33)-H(33B)	98(3)
C(3)-C(33)-H(33C)	109.8(16)
H(33A)-C(33)-H(33C)	114(3)
H(33B)-C(33)-H(33C)	110(2)
C(6)-C(5)-C(5)#1	108.31(9)
C(6)-C(5)-Zr	78.15(9)
C(5)#1-C(5)-Zr	73.08(4)
C(6)-C(5)-H(5)	127.0(12)
C(5)#1-C(5)-H(5)	124.5(12)
Zr-C(5)-H(5)	118.8(12)
C(5)-C(6)-C(7)	106.86(15)
C(5)-C(6)-C(66)	127.52(15)
C(7)-C(6)-C(66)	125.20(15)
C(5)-C(6)-Zr	69.50(9)

C(7)-C(6)-Zr	73.50(11)
C(66)-C(6)-Zr	127.94(11)
C(66)-C(68)-H(68A)	110.2(12)
C(66)-C(68)-H(68B)	107.8(13)
H(68A)-C(68)-H(68B)	108.3(18)
C(66)-C(68)-H(68C)	110.5(13)
H(68A)-C(68)-H(68C)	110.9(17)
H(68B)-C(68)-H(68C)	109.0(19)
C(6)-C(66)-C(67)	113.62(15)
C(6)-C(66)-C(68)	108.47(14)
C(67)-C(66)-C(68)	110.34(16)
C(6)-C(66)-H(66)	108.5(12)
C(67)-C(66)-H(66)	108.7(12)
C(68)-C(66)-H(66)	107.0(12)
C(66)-C(67)-H(67A)	109.5(11)
C(66)-C(67)-H(67B)	111.9(13)
H(67A)-C(67)-H(67B)	107.3(17)
C(66)-C(67)-H(67C)	112.1(13)
H(67A)-C(67)-H(67C)	107.6(17)
H(67B)-C(67)-H(67C)	108.2(18)
C(6)#1-C(7)-C(6)	109.4(2)
C(6)#1-C(7)-Zr	74.40(11)
C(6)-C(7)-Zr	74.40(11)
C(6)#1-C(7)-H(7)	125.26(11)
C(6)-C(7)-H(7)	125.26(11)
Zr-C(7)-H(7)	119.7(18)

Symmetry transformations used to generate equivalent atoms:
#1 x,-y+1/2,z

Table 7. Crystal data and structure refinement for $(tBu_2Cp)_2ZrCl_2$.

Empirical formula	$C_{26}H_{42}Cl_2Zr$
Formula weight	516.72
Crystallization Solvent	Toluene
Crystal Habit	Blade
Crystal size	0.44 x 0.15 x 0.08 mm^3
Crystal color	Colorless

Data Collection

Preliminary Photos		
Type of diffractometer	CAD-4	
Wavelength	0.71073 Å MoKa	
Data Collection Temperature	85(2) K	
Theta range for reflections used in lattice determination	10.3 to 12.6°	
Unit cell dimensions	a = 21.110(19) Å b = 6.575(5) Å c = 19.132(9) Å	a= 90° b= 94.17(7)° g = 90°
Volume	2648(3) $Å^3$	
Z	4	
Crystal system	Monoclinic	
Space group	C2/c	
Density (calculated)	1.296 Mg/m^3	
F(000)	1088	
Theta range for data collection	1.9 to 25.0°	
Completeness to theta = 25.0°	99.7 %	
Index ranges	-24<=h<=24, 0<=k<=7, -22<=l<=22	
Data collection scan type	scans	
Reflections collected	5947	
Independent reflections	2330 [R_{int}= 0.026; GOF_{merge}=]	
Absorption coefficient	0.627 mm^{-1}	
Absorption correction	scan	
Max. and min. transmission	1.16 and 0.85	
Number of standards	3 reflections measured every 75 min.	
Variation of standards	-0.19%.	

Table 7 (cont.)

Structure solution and Refinement	
Structure solution program	SHELXS-97 (Sheldrick, 1990)
Primary solution method	Direct methods
Secondary solution method	Difference Fourier map
Hydrogen placement	Difference Fourier map
Structure refinement program	SHELXL-97 (Sheldrick, 1997)
Refinement method	Full matrix least-squares on F^2
Data / restraints / parameters	2330 / 0 / 216
Treatment of hydrogen atoms	Unrestrained
Goodness-of-fit on F^2	2.036
Final R indices [I>2s(I)]	R1 = 0.0358, wR2 = 0.0743
R indices (all data)	R1 = 0.0438, wR2 = 0.0756
Type of weighting scheme used	Sigma
Weighting scheme used	w=1/[^2^(Fo^2^)
Max shift/error	0.000
Average shift/error	0.000
Largest diff. peak and hole	1.154 and -1.461 e.$Å^{-3}$

Table 8. Atomic coordinates (x 10^4) and equivalent isotropic displacement parameters ($Å^2$x 10^3) for $(tBu_2Cp)_2ZrCl_2$. U(eq) is defined as the trace of the orthogonalized U^{ij} tensor.

	x	y	z	U_{eq}
Zr	0	-3313(1)	-2500	11(1)
Cl(1)	-261(1)	-5834(1)	-1633(1)	16(1)
C(1)	-731(2)	-381(5)	-2566(2)	15(1)
C(2)	-620(1)	-911(5)	-3269(2)	14(1)
C(3)	-944(1)	-2736(5)	-3436(2)	13(1)
C(4)	-1211(1)	-3397(5)	-2818(2)	15(1)
C(5)	-1106(1)	-1913(5)	-2289(2)	15(1)
C(11)	-1126(1)	-3539(5)	-4171(2)	16(1)
C(12)	-610(2)	-3144(6)	-4676(2)	20(1)
C(13)	-1722(2)	-2319(6)	-4423(2)	21(1)
C(14)	-1295(2)	-5792(5)	-4168(2)	22(1)
C(15)	-1446(1)	-1730(5)	-1611(2)	19(1)
C(16)	-1778(2)	-3693(6)	-1432(2)	26(1)
C(17)	-993(2)	-1069(6)	-998(2)	22(1)
C(18)	-1948(2)	-59(7)	-1751(2)	33(1)

Table 9. Bond lengths [Å] and angles [°] for $(tBu_2Cp)_2ZrCl_2$.

Zr-Pln(1)	2.231(3)
Zr-Pln(2)#1	2.231(3)
Zr-Cent(1)	2.238(3)
Zr-Cent(2)#1	2.238(3)
Zr-Cl(1)#1	2.4364(14)
Zr-Cl(1)	2.4364(14)
Zr-C(1)#1	2.467(3)
Zr-C(1)	2.467(3)
Zr-C(2)#1	2.468(3)
Zr-C(2)	2.468(3)
Zr-C(5)#1	2.568(3)
Zr-C(5)	2.568(3)
Zr-C(4)	2.585(4)
Zr-C(4)#1	2.585(4)
Zr-C(3)#1	2.609(4)
Zr-C(3)	2.609(4)
C(1)-C(5)	1.408(4)
C(1)-C(2)	1.425(4)
C(1)-H(1)	0.91(3)
C(2)-C(3)	1.406(4)
C(2)-H(2)	0.98(3)
C(3)-C(4)	1.415(4)
C(3)-C(11)	1.524(4)
C(4)-C(5)	1.412(4)
C(4)-H(4)	0.96(3)
C(5)-C(15)	1.531(4)
C(11)-C(14)	1.524(5)
C(11)-C(12)	1.530(4)
C(11)-C(13)	1.540(5)
C(12)-H(12A)	0.94(3)
C(12)-H(12B)	1.00(3)
C(12)-H(12C)	0.93(4)
C(13)-H(13A)	0.95(4)
C(13)-H(13B)	1.01(3)
C(13)-H(13C)	1.00(4)
C(14)-H(11A)	1.02(4)
C(14)-H(11B)	0.90(4)
C(14)-H(11C)	0.95(3)
C(15)-C(16)	1.520(5)
C(15)-C(17)	1.523(5)
C(15)-C(18)	1.537(5)
C(16)-H(16A)	0.96(4)
C(16)-H(16B)	1.00(4)
C(16)-H(16C)	0.99(4)
C(17)-H(17A)	0.98(4)
C(17)-H(17B)	1.02(3)
C(17)-H(17C)	0.88(4)
C(18)-H(18A)	1.04(4)
C(18)-H(18B)	0.96(4)
C(18)-H(18C)	0.97(4)

Pln(1)-Zr-Pln(2)#1	121.1(1)
Cent(1)-Zr-Cent(2)#1	129.7(1)
Cl(1)#1-Zr-Cl(1)	94.28(7)
Cl(1)#1-Zr-C(1)#1	113.26(9)
Cl(1)-Zr-C(1)#1	131.94(8)
Cl(1)#1-Zr-C(1)	131.94(8)
Cl(1)-Zr-C(1)	113.26(9)
C(1)#1-Zr-C(1)	77.19(17)
Cl(1)#1-Zr-C(2)#1	134.81(9)
Cl(1)-Zr-C(2)#1	99.55(9)
C(1)#1-Zr-C(2)#1	33.56(10)
C(1)-Zr-C(2)#1	80.38(12)
Cl(1)#1-Zr-C(2)	99.55(9)
Cl(1)-Zr-C(2)	134.81(9)
C(1)#1-Zr-C(2)	80.38(12)
C(1)-Zr-C(2)	33.56(10)
C(2)#1-Zr-C(2)	100.42(16)
Cl(1)#1-Zr-C(5)#1	83.33(9)
Cl(1)-Zr-C(5)#1	127.16(8)
C(1)#1-Zr-C(5)#1	32.39(10)
C(1)-Zr-C(5)#1	106.49(12)
C(2)#1-Zr-C(5)#1	54.23(10)
C(2)-Zr-C(5)#1	97.21(12)
Cl(1)#1-Zr-C(5)	127.16(8)
Cl(1)-Zr-C(5)	83.33(9)
C(1)#1-Zr-C(5)	106.49(12)
C(1)-Zr-C(5)	32.39(10)
C(2)#1-Zr-C(5)	97.21(12)
C(2)-Zr-C(5)	54.23(10)
C(5)#1-Zr-C(5)	137.97(15)
Cl(1)#1-Zr-C(4)	95.38(9)
Cl(1)-Zr-C(4)	82.95(9)
C(1)#1-Zr-C(4)	129.26(11)
C(1)-Zr-C(4)	53.17(11)
C(2)#1-Zr-C(4)	128.80(11)
C(2)-Zr-C(4)	53.18(11)
C(5)#1-Zr-C(4)	149.89(10)
C(5)-Zr-C(4)	31.81(10)
Cl(1)#1-Zr-C(4)#1	82.95(9)
Cl(1)-Zr-C(4)#1	95.38(9)
C(1)#1-Zr-C(4)#1	53.17(11)
C(1)-Zr-C(4)#1	129.26(11)
C(2)#1-Zr-C(4)#1	53.18(11)
C(2)-Zr-C(4)#1	128.80(11)
C(5)#1-Zr-C(4)#1	31.81(10)
C(5)-Zr-C(4)#1	149.89(10)
C(4)-Zr-C(4)#1	177.56(15)
Cl(1)#1-Zr-C(3)#1	111.57(8)
Cl(1)-Zr-C(3)#1	80.24(8)
C(1)#1-Zr-C(3)#1	53.66(10)
C(1)-Zr-C(3)#1	111.40(11)
C(2)#1-Zr-C(3)#1	32.01(10)
C(2)-Zr-C(3)#1	131.42(11)
C(5)#1-Zr-C(3)#1	53.01(10)

C(5)-Zr-C(3)#1	119.82(10)
C(4)-Zr-C(3)#1	149.06(10)
C(4)#1-Zr-C(3)#1	31.62(10)
Cl(1)#1-Zr-C(3)	80.24(8)
Cl(1)-Zr-C(3)	111.57(8)
C(1)#1-Zr-C(3)	111.40(11)
C(1)-Zr-C(3)	53.66(10)
C(2)#1-Zr-C(3)	131.42(11)
C(2)-Zr-C(3)	32.01(10)
C(5)#1-Zr-C(3)	119.82(10)
C(5)-Zr-C(3)	53.01(10)
C(4)-Zr-C(3)	31.62(10)
C(4)#1-Zr-C(3)	149.06(10)
C(3)#1-Zr-C(3)	163.25(14)
C(5)-C(1)-C(2)	108.4(3)
C(5)-C(1)-Zr	77.76(19)
C(2)-C(1)-Zr	73.26(18)
C(5)-C(1)-H(1)	127.8(19)
C(2)-C(1)-H(1)	123.7(19)
Zr-C(1)-H(1)	118.4(18)
C(3)-C(2)-C(1)	108.3(3)
C(3)-C(2)-Zr	79.52(18)
C(1)-C(2)-Zr	73.19(18)
C(3)-C(2)-H(2)	128.5(18)
C(1)-C(2)-H(2)	123.0(18)
Zr-C(2)-H(2)	117.7(17)
C(2)-C(3)-C(4)	106.7(3)
C(2)-C(3)-C(11)	126.3(3)
C(4)-C(3)-C(11)	125.1(3)
C(2)-C(3)-Zr	68.47(17)
C(4)-C(3)-Zr	73.28(18)
C(11)-C(3)-Zr	135.4(2)
C(5)-C(4)-C(3)	109.6(3)
C(5)-C(4)-Zr	73.43(18)
C(3)-C(4)-Zr	75.10(18)
C(5)-C(4)-H(4)	123.5(19)
C(3)-C(4)-H(4)	126.7(19)
Zr-C(4)-H(4)	121.7(18)
C(1)-C(5)-C(4)	106.7(3)
C(1)-C(5)-C(15)	125.0(3)
C(4)-C(5)-C(15)	127.0(3)
C(1)-C(5)-Zr	69.85(18)
C(4)-C(5)-Zr	74.76(18)
C(15)-C(5)-Zr	130.4(2)
C(3)-C(11)-C(14)	112.1(3)
C(3)-C(11)-C(12)	112.4(3)
C(14)-C(11)-C(12)	110.2(3)
C(3)-C(11)-C(13)	104.7(3)
C(14)-C(11)-C(13)	108.7(3)
C(12)-C(11)-C(13)	108.5(3)
C(11)-C(12)-H(12A)	114(2)
C(11)-C(12)-H(12B)	110.7(18)
H(12A)-C(12)-H(12B)	108(3)
C(11)-C(12)-H(12C)	107(2)

H(12A)-C(12)-H(12C)	107(3)
H(12B)-C(12)-H(12C)	109(3)
C(11)-C(13)-H(13A)	112(2)
C(11)-C(13)-H(13B)	113.2(19)
H(13A)-C(13)-H(13B)	108(3)
C(11)-C(13)-H(13C)	111.1(19)
H(13A)-C(13)-H(13C)	111(3)
H(13B)-C(13)-H(13C)	100(3)
C(11)-C(14)-H(11A)	113(2)
C(11)-C(14)-H(11B)	112(2)
H(11A)-C(14)-H(11B)	99(3)
C(11)-C(14)-H(11C)	110.4(19)
H(11A)-C(14)-H(11C)	117(3)
H(11B)-C(14)-H(11C)	104(3)
C(16)-C(15)-C(17)	110.1(3)
C(16)-C(15)-C(5)	112.1(3)
C(17)-C(15)-C(5)	111.6(3)
C(16)-C(15)-C(18)	108.8(3)
C(17)-C(15)-C(18)	108.4(3)
C(5)-C(15)-C(18)	105.7(3)
C(15)-C(16)-H(16A)	111(2)
C(15)-C(16)-H(16B)	114(2)
H(16A)-C(16)-H(16B)	110(3)
C(15)-C(16)-H(16C)	109(2)
H(16A)-C(16)-H(16C)	101(3)
H(16B)-C(16)-H(16C)	112(3)
C(15)-C(17)-H(17A)	116(2)
C(15)-C(17)-H(17B)	110.7(18)
H(17A)-C(17)-H(17B)	101(3)
C(15)-C(17)-H(17C)	107(2)
H(17A)-C(17)-H(17C)	108(3)
H(17B)-C(17)-H(17C)	114(3)
C(15)-C(18)-H(18A)	111(2)
C(15)-C(18)-H(18B)	113(2)
H(18A)-C(18)-H(18B)	107(3)
C(15)-C(18)-H(18C)	112(2)
H(18A)-C(18)-H(18C)	102(3)
H(18B)-C(18)-H(18C)	111(3)

Symmetry transformations used to generate equivalent atoms:
#1 -x,y,-z-1/2

Table 10. Crystal data and structure refinement for $Cp^*_2HfH_2$

Empirical formula	$C_{20}H_{32}Hf$
Formula weight	450.95
Crystallization Solvent	Petroleum ether
Crystal Habit	Fragment
Crystal size	0.38 x 0.15 x 0.08 mm^3
Crystal color	Colorless

Data Collection

Preliminary Photos		
Type of diffractometer	CAD-4	
Wavelength	0.71073 Å MoKa	
Data Collection Temperature	85 K	
Theta range for reflections used in lattice determination	10.6 to 11.3°	
Unit cell dimensions	a = 15.733(4) Å b = 15.366(4) Å c = 16.401(4) Å	a= 90° b= 109.38(2)° g = 90°
Volume	3740.3(16) $Å^3$	
Z	8	
Crystal system	Monoclinic	
Space group	p2(1)/c	
Density (calculated)	1.602 Mg/m^3	
F(000)	1792	
Theta range for data collection	1.9 to 25.0°	
Completeness to theta = 25.0°	84.9 %	
Index ranges	-18<=h<=17, -18<=k<=18, -19<=l<=19	
Data collection scan type	Omega scans	
Reflections collected	16022	
Independent reflections	6559 [R_{int}= 0.031; GOF_{merge}=]	
Absorption coefficient	5.572 mm^{-1}	
Absorption correction	Psi scan	
Max. and min. transmission	1.10 and 0.87	
Number of standards	3 reflections measured every 75min.	
Variation of standards	Within counting statistics, zero %.	

Structure solution and Refinement

Structure solution program	SHELXS-97 (Sheldrick, 1990)
Primary solution method	Direct methods
Secondary solution method	Difference Fourier map
Hydrogen placement	Geometric positions
Structure refinement program	SHELXL-97 (Sheldrick, 1997)
Refinement method	Full matrix least-squares on F^2

Data / restraints / parameters	5570 / 252 / 419
Treatment of hydrogen atoms	Restrained to Geometric positions
Goodness-of-fit on F^2	1.354
Final R indices [I>2s(I)]	R1 = 0.0418, wR2 = 0.0679
R indices (all data)	R1 = 0.0595, wR2 = 0.0715
Type of weighting scheme used	Sigma
Weighting scheme used	w=1/[^2^(Fo^2)
Max shift/error	0.286
Average shift/error	0.004
Largest diff. peak and hole	1.384 and -0.846 e.$Å^{-3}$

Table 11. Bond lengths [Å] and angles [°] for $Cp^*_2HfH_2$

HfA-Cent(1A)	2.192(3)
HfA-Cent(2A)	2.175(3)
HfA-Pln(1A)	2.192(3)
HfA-Pln(2A)	2.175(3)
HfA-C(9A)	2.493(7)
HfA-C(10A)	2.483(8)
HfA-C(3A)	2.479(7)
HfA-C(8A)	2.482(8)
HfA-C(2A)	2.515(8)
HfA-C(4A)	2.486(7)
HfA-C(6A)	2.490(7)
HfA-C(7A)	2.497(7)
HfA-C(1A)	2.516(7)
HfA-C(5A)	2.515(7)
C(1A)-C(2A)	1.418(11)
C(1A)-C(5A)	1.421(11)
C(1A)-C(11A)	1.506(10)
C(2A)-C(3A)	1.440(10)
C(2A)-C(12A)	1.476(11)
C(3A)-C(4A)	1.389(10)
C(3A)-C(13A)	1.519(10)
C(4A)-C(5A)	1.426(10)
C(4A)-C(14A)	1.495(10)
C(5A)-C(15A)	1.508(11)
C(11A)-H(11A)	0.9398
C(11A)-H(11B)	0.9398
C(11A)-H(11C)	0.9398
C(12A)-H(12A)	0.8775
C(12A)-H(12B)	0.8775
C(12A)-H(12C)	0.8775
C(13A)-H(13A)	0.9571
C(13A)-H(13B)	0.9571
C(13A)-H(13C)	0.9571
C(14A)-H(14A)	0.9379
C(14A)-H(14B)	0.9379
C(14A)-H(14C)	0.9379
C(15A)-H(15A)	0.9622
C(15A)-H(15B)	0.9622
C(15A)-H(15C)	0.9622
C(6A)-C(7A)	1.434(11)
C(6A)-C(10A)	1.426(11)
C(6A)-C(16A)	1.509(10)
C(7A)-C(8A)	1.411(10)
C(7A)-C(17A)	1.492(11)
C(8A)-C(9A)	1.403(11)
C(8A)-C(18A)	1.519(11)
C(9A)-C(10A)	1.435(11)
C(9A)-C(19A)	1.495(11)
C(10A)-C(20A)	1.505(11)
C(16A)-H(16A)	0.8652
C(16A)-H(16B)	0.8652

C(16A)-H(16C)	0.8652
C(17A)-H(17A)	0.9582
C(17A)-H(17B)	0.9582
C(17A)-H(17C)	0.9582
C(18A)-H(18A)	0.8480
C(18A)-H(18B)	0.8480
C(18A)-H(18C)	0.8480
C(19A)-H(19A)	0.9897
C(19A)-H(19B)	0.9897
C(19A)-H(19C)	0.9897
C(20A)-H(20A)	0.9523
C(20A)-H(20B)	0.9523
C(20A)-H(20C)	0.9523
HfB-Cent(1B)	2.175(3)
HfB-Cent(2B)	2.168(3)
HfB-Pln(1B)	2.175(3)
HfB-Pln(2B)	2.168(3)
HfB-C(9B)	2.481(7)
HfB-C(10B)	2.486(7)
HfB-C(4B)	2.500(7)
HfB-C(8B)	2.476(7)
HfB-C(3B)	2.491(7)
HfB-C(5B)	2.488(7)
HfB-C(2B)	2.486(7)
HfB-C(6B)	2.483(6)
HfB-C(1B)	2.489(7)
HfB-C(7B)	2.482(7)
C(1B)-C(2B)	1.421(9)
C(1B)-C(5B)	1.424(10)
C(1B)-C(11B)	1.490(10)
C(2B)-C(3B)	1.448(10)
C(2B)-C(12B)	1.509(9)
C(3B)-C(4B)	1.414(10)
C(3B)-C(13B)	1.496(10)
C(4B)-C(5B)	1.427(10)
C(4B)-C(14B)	1.474(10)
C(5B)-C(15B)	1.505(10)
C(11B)-H(11D)	0.9381
C(11B)-H(11E)	0.9381
C(11B)-H(11F)	0.9381
C(12B)-H(12D)	0.8323
C(12B)-H(12E)	0.8323
C(12B)-H(12F)	0.8323
C(13B)-H(13D)	0.9018
C(13B)-H(13E)	0.9018
C(13B)-H(13F)	0.9018
C(14B)-H(14D)	0.9711
C(14B)-H(14E)	0.9711
C(14B)-H(14F)	0.9711
C(15B)-H(15D)	0.8643
C(15B)-H(15E)	0.8643
C(15B)-H(15F)	0.8643
C(6B)-C(10B)	1.442(10)
C(6B)-C(7B)	1.398(10)

C(6B)-C(16B)	1.514(10)
C(7B)-C(8B)	1.412(10)
C(7B)-C(17B)	1.527(10)
C(8B)-C(9B)	1.425(11)
C(8B)-C(18B)	1.514(10)
C(9B)-C(10B)	1.421(10)
C(9B)-C(19B)	1.495(10)
C(10B)-C(20B)	1.502(10)
C(16B)-H(16D)	0.9272
C(16B)-H(16E)	0.9272
C(16B)-H(16F)	0.9272
C(17B)-H(17D)	0.9195
C(17B)-H(17E)	0.9195
C(17B)-H(17F)	0.9195
C(18B)-H(18D)	0.9950
C(18B)-H(18E)	0.9950
C(18B)-H(18F)	0.9950
C(19B)-H(19D)	0.8138
C(19B)-H(19E)	0.8138
C(19B)-H(19F)	0.8138
C(20B)-H(20D)	0.9535
C(20B)-H(20E)	0.9535
C(20B)-H(20F)	0.9535

Cent(1A)-HfA-Cent(2A)	144.1(2)
Pln(1A)-HfA-Pln(2A)	145.2(2)
C(9A)-HfA-C(10A)	33.5(3)
C(9A)-HfA-C(3A)	158.7(2)
C(10A)-HfA-C(3A)	162.4(2)
C(9A)-HfA-C(8A)	32.8(3)
C(10A)-HfA-C(8A)	54.2(2)
C(3A)-HfA-C(8A)	143.4(2)
C(9A)-HfA-C(2A)	153.7(3)
C(10A)-HfA-C(2A)	149.4(3)
C(3A)-HfA-C(2A)	33.5(2)
C(8A)-HfA-C(2A)	121.0(3)
C(9A)-HfA-C(4A)	151.5(2)
C(10A)-HfA-C(4A)	130.0(2)
C(3A)-HfA-C(4A)	32.5(2)
C(8A)-HfA-C(4A)	175.5(2)
C(2A)-HfA-C(4A)	54.6(2)
C(9A)-HfA-C(6A)	55.9(2)
C(10A)-HfA-C(6A)	33.3(2)
C(3A)-HfA-C(6A)	145.1(2)
C(8A)-HfA-C(6A)	54.8(2)
C(2A)-HfA-C(6A)	116.5(3)
C(4A)-HfA-C(6A)	127.1(2)
C(9A)-HfA-C(7A)	55.4(2)
C(10A)-HfA-C(7A)	54.9(3)
C(3A)-HfA-C(7A)	136.5(2)
C(8A)-HfA-C(7A)	32.9(2)
C(2A)-HfA-C(7A)	103.4(3)
C(4A)-HfA-C(7A)	145.9(2)
C(6A)-HfA-C(7A)	33.4(3)

C(9A)-HfA-C(1A)	145.1(2)
C(10A)-HfA-C(1A)	119.4(2)
C(3A)-HfA-C(1A)	54.9(2)
C(8A)-HfA-C(1A)	122.5(2)
C(2A)-HfA-C(1A)	32.7(2)
C(4A)-HfA-C(1A)	54.9(2)
C(6A)-HfA-C(1A)	90.2(2)
C(7A)-HfA-C(1A)	92.2(2)
C(9A)-HfA-C(5A)	144.3(3)
C(10A)-HfA-C(5A)	110.9(3)
C(3A)-HfA-C(5A)	54.3(2)
C(8A)-HfA-C(5A)	146.7(2)
C(2A)-HfA-C(5A)	54.2(3)
C(4A)-HfA-C(5A)	33.1(2)
C(6A)-HfA-C(5A)	95.7(2)
C(7A)-HfA-C(5A)	113.9(2)
C(1A)-HfA-C(5A)	32.8(2)
C(2A)-C(1A)-C(5A)	107.7(7)
C(2A)-C(1A)-C(11A)	125.7(7)
C(5A)-C(1A)-C(11A)	125.3(7)
C(2A)-C(1A)-HfA	73.6(4)
C(5A)-C(1A)-HfA	73.5(4)
C(11A)-C(1A)-HfA	128.9(5)
C(1A)-C(2A)-C(3A)	107.4(7)
C(1A)-C(2A)-C(12A)	126.4(7)
C(3A)-C(2A)-C(12A)	126.2(7)
C(1A)-C(2A)-HfA	73.7(4)
C(3A)-C(2A)-HfA	71.9(4)
C(12A)-C(2A)-HfA	120.7(5)
C(4A)-C(3A)-C(2A)	108.5(6)
C(4A)-C(3A)-C(13A)	126.6(7)
C(2A)-C(3A)-C(13A)	124.7(7)
C(4A)-C(3A)-HfA	74.0(4)
C(2A)-C(3A)-HfA	74.6(4)
C(13A)-C(3A)-HfA	121.3(5)
C(3A)-C(4A)-C(5A)	108.2(6)
C(3A)-C(4A)-C(14A)	127.4(7)
C(5A)-C(4A)-C(14A)	123.8(7)
C(3A)-C(4A)-HfA	73.5(4)
C(5A)-C(4A)-HfA	74.5(4)
C(14A)-C(4A)-HfA	125.1(5)
C(4A)-C(5A)-C(1A)	108.1(7)
C(4A)-C(5A)-C(15A)	124.4(7)
C(1A)-C(5A)-C(15A)	127.2(7)
C(4A)-C(5A)-HfA	72.3(4)
C(1A)-C(5A)-HfA	73.6(4)
C(15A)-C(5A)-HfA	124.4(5)
C(1A)-C(11A)-H(11A)	109.5
C(1A)-C(11A)-H(11B)	109.5
H(11A)-C(11A)-H(11B)	109.5
C(1A)-C(11A)-H(11C)	109.5
H(11A)-C(11A)-H(11C)	109.5
H(11B)-C(11A)-H(11C)	109.5
C(2A)-C(12A)-H(12A)	109.5

C(2A)-C(12A)-H(12B)	109.5
H(12A)-C(12A)-H(12B)	109.5
C(2A)-C(12A)-H(12C)	109.5
H(12A)-C(12A)-H(12C)	109.5
H(12B)-C(12A)-H(12C)	109.5
C(3A)-C(13A)-H(13A)	109.5
C(3A)-C(13A)-H(13B)	109.5
H(13A)-C(13A)-H(13B)	109.5
C(3A)-C(13A)-H(13C)	109.5
H(13A)-C(13A)-H(13C)	109.5
H(13B)-C(13A)-H(13C)	109.5
C(4A)-C(14A)-H(14A)	109.5
C(4A)-C(14A)-H(14B)	109.5
H(14A)-C(14A)-H(14B)	109.5
C(4A)-C(14A)-H(14C)	109.5
H(14A)-C(14A)-H(14C)	109.5
H(14B)-C(14A)-H(14C)	109.5
C(5A)-C(15A)-H(15A)	109.5
C(5A)-C(15A)-H(15B)	109.5
H(15A)-C(15A)-H(15B)	109.5
C(5A)-C(15A)-H(15C)	109.5
H(15A)-C(15A)-H(15C)	109.5
H(15B)-C(15A)-H(15C)	109.5
C(7A)-C(6A)-C(10A)	106.9(6)
C(7A)-C(6A)-C(16A)	128.0(7)
C(10A)-C(6A)-C(16A)	124.1(7)
C(7A)-C(6A)-HfA	73.5(4)
C(10A)-C(6A)-HfA	73.0(4)
C(16A)-C(6A)-HfA	127.8(5)
C(6A)-C(7A)-C(8A)	107.0(7)
C(6A)-C(7A)-C(17A)	126.9(7)
C(8A)-C(7A)-C(17A)	125.6(7)
C(6A)-C(7A)-HfA	73.0(4)
C(8A)-C(7A)-HfA	72.9(4)
C(17A)-C(7A)-HfA	126.1(5)
C(9A)-C(8A)-C(7A)	111.1(7)
C(9A)-C(8A)-C(18A)	126.2(7)
C(7A)-C(8A)-C(18A)	122.4(7)
C(9A)-C(8A)-HfA	74.1(4)
C(7A)-C(8A)-HfA	74.1(4)
C(18A)-C(8A)-HfA	123.9(5)
C(8A)-C(9A)-C(10A)	105.6(7)
C(8A)-C(9A)-C(19A)	127.8(7)
C(10A)-C(9A)-C(19A)	126.5(7)
C(8A)-C(9A)-HfA	73.2(4)
C(10A)-C(9A)-HfA	72.9(4)
C(19A)-C(9A)-HfA	121.0(5)
C(9A)-C(10A)-C(6A)	109.4(7)
C(9A)-C(10A)-C(20A)	127.4(7)
C(6A)-C(10A)-C(20A)	123.2(7)
C(9A)-C(10A)-HfA	73.6(4)
C(6A)-C(10A)-HfA	73.6(4)
C(20A)-C(10A)-HfA	120.3(5)
C(6A)-C(16A)-H(16A)	109.5

C(6A)-C(16A)-H(16B)	109.5
H(16A)-C(16A)-H(16B)	109.5
C(6A)-C(16A)-H(16C)	109.5
H(16A)-C(16A)-H(16C)	109.5
H(16B)-C(16A)-H(16C)	109.5
C(7A)-C(17A)-H(17A)	109.5
C(7A)-C(17A)-H(17B)	109.5
H(17A)-C(17A)-H(17B)	109.5
C(7A)-C(17A)-H(17C)	109.5
H(17A)-C(17A)-H(17C)	109.5
H(17B)-C(17A)-H(17C)	109.5
C(8A)-C(18A)-H(18A)	109.5
C(8A)-C(18A)-H(18B)	109.5
H(18A)-C(18A)-H(18B)	109.5
C(8A)-C(18A)-H(18C)	109.5
H(18A)-C(18A)-H(18C)	109.5
H(18B)-C(18A)-H(18C)	109.5
C(9A)-C(19A)-H(19A)	109.5
C(9A)-C(19A)-H(19B)	109.5
H(19A)-C(19A)-H(19B)	109.5
C(9A)-C(19A)-H(19C)	109.5
H(19A)-C(19A)-H(19C)	109.5
H(19B)-C(19A)-H(19C)	109.5
C(10A)-C(20A)-H(20A)	109.5
C(10A)-C(20A)-H(20B)	109.5
H(20A)-C(20A)-H(20B)	109.5
C(10A)-C(20A)-H(20C)	109.5
H(20A)-C(20A)-H(20C)	109.5
H(20B)-C(20A)-H(20C)	109.5
Cent(1B)-HfB-Cent(2B)	145.0(2)
Pln(1B)-HfB-Pln(2B)	145.9(2)
C(9B)-HfB-C(10B)	33.3(2)
C(9B)-HfB-C(4B)	156.2(2)
C(10B)-HfB-C(4B)	140.4(2)
C(9B)-HfB-C(8B)	33.4(3)
C(10B)-HfB-C(8B)	55.0(2)
C(4B)-HfB-C(8B)	164.5(2)
C(9B)-HfB-C(3B)	153.8(2)
C(10B)-HfB-C(3B)	172.6(2)
C(4B)-HfB-C(3B)	32.9(2)
C(8B)-HfB-C(3B)	131.7(2)
C(9B)-HfB-C(5B)	150.6(2)
C(10B)-HfB-C(5B)	117.8(2)
C(4B)-HfB-C(5B)	33.2(2)
C(8B)-HfB-C(5B)	153.0(3)
C(3B)-HfB-C(5B)	54.9(2)
C(9B)-HfB-C(2B)	147.2(2)
C(10B)-HfB-C(2B)	145.1(3)
C(4B)-HfB-C(2B)	55.2(2)
C(8B)-HfB-C(2B)	113.8(2)
C(3B)-HfB-C(2B)	33.8(2)
C(5B)-HfB-C(2B)	54.8(2)
C(9B)-HfB-C(6B)	55.5(2)
C(10B)-HfB-C(6B)	33.7(2)

C(4B)-HfB-C(6B)	136.7(2)
C(8B)-HfB-C(6B)	54.9(2)
C(3B)-HfB-C(6B)	144.4(2)
C(5B)-HfB-C(6B)	103.6(2)
C(2B)-HfB-C(6B)	111.4(2)
C(9B)-HfB-C(1B)	145.1(2)
C(10B)-HfB-C(1B)	119.4(2)
C(4B)-HfB-C(1B)	55.5(2)
C(8B)-HfB-C(1B)	122.8(3)
C(3B)-HfB-C(1B)	55.7(2)
C(5B)-HfB-C(1B)	33.3(2)
C(2B)-HfB-C(1B)	33.2(2)
C(6B)-HfB-C(1B)	90.4(2)
C(9B)-HfB-C(7B)	55.3(2)
C(10B)-HfB-C(7B)	55.0(2)
C(4B)-HfB-C(7B)	147.9(2)
C(8B)-HfB-C(7B)	33.1(2)
C(3B)-HfB-C(7B)	128.1(2)
C(5B)-HfB-C(7B)	120.0(3)
C(2B)-HfB-C(7B)	96.7(2)
C(6B)-HfB-C(7B)	32.7(2)
C(1B)-HfB-C(7B)	92.6(2)
C(2B)-C(1B)-C(5B)	107.2(6)
C(2B)-C(1B)-C(11B)	125.4(7)
C(5B)-C(1B)-C(11B)	125.9(6)
C(2B)-C(1B)-HfB	73.3(4)
C(5B)-C(1B)-HfB	73.3(4)
C(11B)-C(1B)-HfB	129.6(5)
C(3B)-C(2B)-C(1B)	108.3(6)
C(3B)-C(2B)-C(12B)	123.9(6)
C(1B)-C(2B)-C(12B)	127.6(7)
C(3B)-C(2B)-HfB	73.3(4)
C(1B)-C(2B)-HfB	73.5(4)
C(12B)-C(2B)-HfB	123.1(5)
C(4B)-C(3B)-C(2B)	107.7(6)
C(4B)-C(3B)-C(13B)	126.7(7)
C(2B)-C(3B)-C(13B)	125.2(6)
C(4B)-C(3B)-HfB	73.9(4)
C(2B)-C(3B)-HfB	72.9(4)
C(13B)-C(3B)-HfB	124.0(5)
C(3B)-C(4B)-C(5B)	107.8(6)
C(3B)-C(4B)-C(14B)	125.9(7)
C(5B)-C(4B)-C(14B)	126.3(7)
C(3B)-C(4B)-HfB	73.2(4)
C(5B)-C(4B)-HfB	72.9(4)
C(14B)-C(4B)-HfB	121.3(5)
C(4B)-C(5B)-C(1B)	109.1(6)
C(4B)-C(5B)-C(15B)	126.1(7)
C(1B)-C(5B)-C(15B)	124.7(7)
C(4B)-C(5B)-HfB	73.9(4)
C(1B)-C(5B)-HfB	73.4(4)
C(15B)-C(5B)-HfB	122.1(5)
C(1B)-C(11B)-H(11D)	109.5
C(1B)-C(11B)-H(11E)	109.5

H(11D)-C(11B)-H(11E)	109.5
C(1B)-C(11B)-H(11F)	109.5
H(11D)-C(11B)-H(11F)	109.5
H(11E)-C(11B)-H(11F)	109.5
C(2B)-C(12B)-H(12D)	109.5
C(2B)-C(12B)-H(12E)	109.5
H(12D)-C(12B)-H(12E)	109.5
C(2B)-C(12B)-H(12F)	109.5
H(12D)-C(12B)-H(12F)	109.5
H(12E)-C(12B)-H(12F)	109.5
C(3B)-C(13B)-H(13D)	109.5
C(3B)-C(13B)-H(13E)	109.5
H(13D)-C(13B)-H(13E)	109.5
C(3B)-C(13B)-H(13F)	109.5
H(13D)-C(13B)-H(13F)	109.5
H(13E)-C(13B)-H(13F)	109.5
C(4B)-C(14B)-H(14D)	109.5
C(4B)-C(14B)-H(14E)	109.5
H(14D)-C(14B)-H(14E)	109.5
C(4B)-C(14B)-H(14F)	109.5
H(14D)-C(14B)-H(14F)	109.5
H(14E)-C(14B)-H(14F)	109.5
C(5B)-C(15B)-H(15D)	109.5
C(5B)-C(15B)-H(15E)	109.5
H(15D)-C(15B)-H(15E)	109.5
C(5B)-C(15B)-H(15F)	109.5
H(15D)-C(15B)-H(15F)	109.5
H(15E)-C(15B)-H(15F)	109.5
C(10B)-C(6B)-C(7B)	107.7(6)
C(10B)-C(6B)-C(16B)	122.4(6)
C(7B)-C(6B)-C(16B)	129.1(7)
C(10B)-C(6B)-HfB	73.2(4)
C(7B)-C(6B)-HfB	73.6(4)
C(16B)-C(6B)-HfB	126.8(5)
C(8B)-C(7B)-C(6B)	108.8(6)
C(8B)-C(7B)-C(17B)	123.1(7)
C(6B)-C(7B)-C(17B)	127.1(7)
C(8B)-C(7B)-HfB	73.3(4)
C(6B)-C(7B)-HfB	73.7(4)
C(17B)-C(7B)-HfB	128.3(5)
C(9B)-C(8B)-C(7B)	108.4(6)
C(9B)-C(8B)-C(18B)	125.9(7)
C(7B)-C(8B)-C(18B)	125.4(7)
C(9B)-C(8B)-HfB	73.5(4)
C(7B)-C(8B)-HfB	73.7(4)
C(18B)-C(8B)-HfB	123.3(5)
C(8B)-C(9B)-C(10B)	107.3(6)
C(8B)-C(9B)-C(19B)	127.5(7)
C(10B)-C(9B)-C(19B)	125.2(7)
C(8B)-C(9B)-HfB	73.1(4)
C(10B)-C(9B)-HfB	73.5(4)
C(19B)-C(9B)-HfB	119.3(5)
C(9B)-C(10B)-C(6B)	107.7(6)
C(9B)-C(10B)-C(20B)	125.5(7)

C(6B)-C(10B)-C(20B)	126.6(6)
C(9B)-C(10B)-HfB	73.2(4)
C(6B)-C(10B)-HfB	73.0(4)
C(20B)-C(10B)-HfB	123.3(5)
C(6B)-C(16B)-H(16D)	109.5
C(6B)-C(16B)-H(16E)	109.5
H(16D)-C(16B)-H(16E)	109.5
C(6B)-C(16B)-H(16F)	109.5
H(16D)-C(16B)-H(16F)	109.5
H(16E)-C(16B)-H(16F)	109.5
C(7B)-C(17B)-H(17D)	109.5
C(7B)-C(17B)-H(17E)	109.5
H(17D)-C(17B)-H(17E)	109.5
C(7B)-C(17B)-H(17F)	109.5
H(17D)-C(17B)-H(17F)	109.5
H(17E)-C(17B)-H(17F)	109.5
C(8B)-C(18B)-H(18D)	109.5
C(8B)-C(18B)-H(18E)	109.5
H(18D)-C(18B)-H(18E)	109.5
C(8B)-C(18B)-H(18F)	109.5
H(18D)-C(18B)-H(18F)	109.5
H(18E)-C(18B)-H(18F)	109.5
C(9B)-C(19B)-H(19D)	109.5
C(9B)-C(19B)-H(19E)	109.5
H(19D)-C(19B)-H(19E)	109.5
C(9B)-C(19B)-H(19F)	109.5
H(19D)-C(19B)-H(19F)	109.5
H(19E)-C(19B)-H(19F)	109.5
C(10B)-C(20B)-H(20D)	109.5
C(10B)-C(20B)-H(20E)	109.5
H(20D)-C(20B)-H(20E)	109.5
C(10B)-C(20B)-H(20F)	109.5
H(20D)-C(20B)-H(20F)	109.5
H(20E)-C(20B)-H(20F)	109.5

Symmetry transformations used to generate equivalent atoms:

Table 12. Crystal data and structure refinement for *meso*-$DpZrMe_2$.

Empirical formula	$C_{22}H_{36}SiZr$
Formula weight	419.82
Crystallization Solvent	Petroleum ether
Crystal Habit	Chunk
Crystal size	0.296 x 0.185 x 0.074 mm^3
Crystal color	Pale yellow

Data Collection

Preliminary Photos		
Type of diffractometer	CAD-4	
Wavelength	0.71073 Å MoKa	
Data Collection Temperature	85 K	
Theta range for reflections used in lattice determination	11.5 to 12.2°	
Unit cell dimensions	a = 19.899(4) Å b = 16.667(6) Å c = 13.417(5) Å	a= 90° b= 94.16(2)° g = 90°
Volume	4438(2) $Å^3$	
Z	8	
Crystal system	Monoclinic	
Space group	P2(1)/c	
Density (calculated)	1.257 Mg/m^3	
F(000)	1776	
Theta range for data collection	1.60 to 24.97°	
Completeness to theta = 24.97°	81.2 %	
Index ranges	-22<=h<=22, -18<=k<=18, 0<=l<=14	
Data collection scan type	Omega scans	
Reflections collected	13928	
Independent reflections	6332 [R_{int}= 0.0318; GOF_{merge}=]	
Absorption coefficient	0.551 mm^{-1}	
Absorption correction	None	
Number of standards	3 reflections measured every 75min.	
Variation of standards	-0.75%.	

Table 12 (cont.)

Structure solution and Refinement

Structure solution program	SHELXS-97 (Sheldrick, 1990)
Primary solution method	Direct methods
Secondary solution method	Difference Fourier map
Hydrogen placement	Difference Fourier map
Structure refinement program	SHELXL-97 (Sheldrick, 1997)
Refinement method	Full matrix least-squares on F^2
Data / restraints / parameters	6332 / 0 / 721
Treatment of hydrogen atoms	Unrestrained
Goodness-of-fit on F^2	1.304
Final R indices [I>2s(I)]	R1 = 0.0342, wR2 = 0.0585
R indices (all data)	R1 = 0.0535, wR2 = 0.0634
Type of weighting scheme used	Sigma
Weighting scheme used	w=1/s^2^(Fo^2^)
Max shift/error	1.268
Average shift/error	0.002
Largest diff. peak and hole	0.427 and -0.378 e.$Å^{-3}$

Table 13. Bond lengths [Å] and angles [°] for *meso*-DpZrMe$_2$.

ZrA-Cent(1A)	2.2447(6)
ZrA-Cent(2A)	2.2459(7)
ZrA-Pln(1A)	2.235(2)
ZrA-Pln(2A)	2.241(2)
ZrA-C(22A)	2.275(4)
ZrA-C(21A)	2.273(4)
ZrA-C(6A)	2.470(3)
ZrA-C(1A)	2.476(3)
ZrA-C(2A)	2.469(3)
ZrA-C(7A)	2.467(3)
ZrA-C(5A)	2.543(3)
ZrA-C(10A)	2.552(3)
ZrA-C(3A)	2.582(3)
ZrA-C(8A)	2.601(3)
ZrA-C(4A)	2.657(3)
ZrA-C(9A)	2.685(3)
SiA-C(1A)	1.873(3)
SiA-C(19A)	1.849(4)
SiA-C(6A)	1.868(3)
SiA-C(20A)	1.851(4)
C(1A)-C(5A)	1.418(5)

C(1A)-C(2A)	1.430(5)
C(2A)-C(3A)	1.403(5)
C(2A)-H(2A)	0.92(3)
C(3A)-C(4A)	1.409(5)
C(3A)-H(3A)	0.89(3)
C(4A)-C(5A)	1.411(5)
C(4A)-C(11A)	1.522(5)
C(5A)-H(5A)	0.88(3)
C(6A)-C(10A)	1.429(4)
C(6A)-C(7A)	1.429(5)
C(7A)-C(8A)	1.397(5)
C(7A)-H(7A)	0.88(3)
C(8A)-C(9A)	1.409(5)
C(8A)-H(8A)	0.89(3)
C(9A)-C(10A)	1.414(4)
C(9A)-C(15A)	1.518(4)
C(10A)-H(10A)	0.87(3)
C(11A)-C(13A)	1.530(5)
C(11A)-C(14A)	1.537(5)
C(11A)-C(12A)	1.530(5)
C(12A)-H(12A)	1.01(3)
C(12A)-H(12A)	0.96(3)
C(12A)-H(12A)	0.97(3)
C(13A)-H(13A)	0.95(3)
C(13A)-H(13A)	0.99(4)
C(13A)-H(13A)	0.96(4)
C(14A)-H(14A)	0.94(3)
C(14A)-H(14A)	0.97(4)
C(14A)-H(14A)	1.00(4)
C(15A)-C(18A)	1.526(5)
C(15A)-C(16A)	1.538(5)
C(15A)-C(17A)	1.535(5)
C(16A)-H(16A)	0.98(3)
C(16A)-H(16A)	0.91(3)
C(16A)-H(16A)	0.92(4)
C(17A)-H(17A)	0.93(3)
C(17A)-H(17A)	0.94(3)
C(17A)-H(17A)	0.98(3)
C(18A)-H(18A)	0.97(3)
C(18A)-H(18A)	0.86(3)
C(18A)-H(18A)	0.97(3)
C(19A)-H(19A)	0.86(4)
C(19A)-H(19A)	0.95(4)
C(19A)-H(19A)	0.97(4)
C(20A)-H(20A)	0.92(3)
C(20A)-H(20A)	0.93(3)
C(20A)-H(20A)	0.93(4)
C(21A)-H(21A)	0.98(3)
C(21A)-H(21A)	0.94(4)
C(21A)-H(21A)	0.90(4)
C(22A)-H(22A)	0.94(4)
C(22A)-H(22A)	0.84(3)
C(22A)-H(22A)	0.90(4)
ZrB-Cent(1B)	2.2403(7)

ZrB-Cent(2B)	2.2513(5)
ZrB-Pln(1B)	2.242(2)
ZrB-Pln(2B)	2.231(2)
ZrB-C(21B)	2.264(4)
ZrB-C(22B)	2.273(4)
ZrB-C(6B)	2.472(3)
ZrB-C(7B)	2.461(3)
ZrB-C(1B)	2.484(3)
ZrB-C(2B)	2.487(3)
ZrB-C(5B)	2.533(3)
ZrB-C(10B)	2.537(3)
ZrB-C(8B)	2.579(3)
ZrB-C(3B)	2.596(4)
ZrB-C(4B)	2.663(3)
ZrB-C(9B)	2.654(3)
SiB-C(6B)	1.869(3)
SiB-C(20B)	1.850(4)
SiB-C(19B)	1.854(4)
SiB-C(1B)	1.874(3)
C(1B)-C(5B)	1.413(4)
C(1B)-C(2B)	1.433(5)
C(2B)-C(3B)	1.407(5)
C(2B)-H(2B)	0.89(3)
C(3B)-C(4B)	1.417(5)
C(3B)-H(3B)	0.91(3)
C(4B)-C(5B)	1.414(4)
C(4B)-C(11B)	1.517(4)
C(5B)-H(5B)	0.89(3)
C(6B)-C(10B)	1.414(5)
C(6B)-C(7B)	1.418(5)
C(7B)-C(8B)	1.401(5)
C(7B)-H(7B)	0.89(3)
C(8B)-C(9B)	1.416(5)
C(8B)-H(8B)	0.87(3)
C(9B)-C(10B)	1.408(5)
C(9B)-C(15B)	1.529(5)
C(10B)-H(10B)	0.83(3)
C(11B)-C(12B)	1.532(5)
C(11B)-C(14B)	1.524(5)
C(11B)-C(13B)	1.543(5)
C(13B)-H(13B)	0.98(3)
C(13B)-H(13B)	0.99(4)
C(13B)-H(13B)	0.91(4)
C(12B)-H(12B)	0.97(4)
C(12B)-H(12B)	1.00(4)
C(12B)-H(12B)	0.92(3)
C(14B)-H(14B)	0.92(3)
C(14B)-H(14B)	1.02(3)
C(14B)-H(14B)	0.88(4)
C(15B)-C(16B)	1.526(5)
C(15B)-C(18B)	1.530(5)
C(15B)-C(17B)	1.522(5)
C(16B)-H(16B)	1.00(4)
C(16B)-H(16B)	0.99(3)

C(16B)-H(16B)	0.90(3)
C(17B)-H(17B)	0.99(3)
C(17B)-H(17B)	0.89(4)
C(17B)-H(17B)	0.91(3)
C(18B)-H(18B)	0.88(4)
C(18B)-H(18B)	1.00(4)
C(18B)-H(18B)	1.03(3)
C(19B)-H(19B)	0.99(3)
C(19B)-H(19B)	0.96(4)
C(19B)-H(19B)	0.86(4)
C(20B)-H(20B)	0.99(3)
C(20B)-H(20B)	0.99(4)
C(20B)-H(20B)	0.95(4)
C(21B)-H(21B)	0.95(3)
C(21B)-H(21B)	0.97(4)
C(21B)-H(21B)	0.90(4)
C(22B)-H(22B)	0.91(4)
C(22B)-H(22B)	0.91(4)
C(22B)-H(22B)	0.91(4)

Cent(1A)-ZrA-Cent(2A)	126.86(2)
Pln(1A)-ZrA-Pln(2A)	116.34(13)
C(22A)-ZrA-C(21A)	99.63(15)
C(22A)-ZrA-C(6A)	112.85(14)
C(21A)-ZrA-C(6A)	131.49(13)
C(22A)-ZrA-C(1A)	112.48(12)
C(21A)-ZrA-C(1A)	130.30(12)
C(6A)-ZrA-C(1A)	68.83(11)
C(22A)-ZrA-C(2A)	135.22(13)
C(21A)-ZrA-C(2A)	97.40(13)
C(6A)-ZrA-C(2A)	84.40(11)
C(1A)-ZrA-C(2A)	33.61(11)
C(22A)-ZrA-C(7A)	134.84(14)
C(21A)-ZrA-C(7A)	98.25(14)
C(6A)-ZrA-C(7A)	33.64(11)
C(1A)-ZrA-C(7A)	85.38(11)
C(2A)-ZrA-C(7A)	82.28(12)
C(22A)-ZrA-C(5A)	83.40(12)
C(21A)-ZrA-C(5A)	126.32(13)
C(6A)-ZrA-C(5A)	93.46(11)
C(1A)-ZrA-C(5A)	32.77(10)
C(2A)-ZrA-C(5A)	53.52(12)
C(7A)-ZrA-C(5A)	117.17(11)
C(22A)-ZrA-C(10A)	83.38(13)
C(21A)-ZrA-C(10A)	128.46(13)
C(6A)-ZrA-C(10A)	33.01(10)
C(1A)-ZrA-C(10A)	93.21(10)
C(2A)-ZrA-C(10A)	116.33(11)
C(7A)-ZrA-C(10A)	53.44(12)
C(5A)-ZrA-C(10A)	105.19(11)
C(22A)-ZrA-C(3A)	113.25(13)
C(21A)-ZrA-C(3A)	78.90(13)
C(6A)-ZrA-C(3A)	116.34(11)
C(1A)-ZrA-C(3A)	54.24(11)

C(2A)-ZrA-C(3A)	32.14(11)
C(7A)-ZrA-C(3A)	110.73(11)
C(5A)-ZrA-C(3A)	52.20(11)
C(10A)-ZrA-C(3A)	146.75(11)
C(22A)-ZrA-C(8A)	112.55(13)
C(21A)-ZrA-C(8A)	80.93(13)
C(6A)-ZrA-C(8A)	54.12(11)
C(1A)-ZrA-C(8A)	116.93(11)
C(2A)-ZrA-C(8A)	110.87(12)
C(7A)-ZrA-C(8A)	31.85(11)
C(5A)-ZrA-C(8A)	147.06(11)
C(10A)-ZrA-C(8A)	51.90(11)
C(3A)-ZrA-C(8A)	132.24(11)
C(22A)-ZrA-C(4A)	84.50(12)
C(21A)-ZrA-C(4A)	95.10(13)
C(6A)-ZrA-C(4A)	122.05(10)
C(1A)-ZrA-C(4A)	53.80(10)
C(2A)-ZrA-C(4A)	52.86(11)
C(7A)-ZrA-C(4A)	134.49(11)
C(5A)-ZrA-C(4A)	31.39(10)
C(10A)-ZrA-C(4A)	136.13(10)
C(3A)-ZrA-C(4A)	31.15(10)
C(8A)-ZrA-C(4A)	162.88(11)
C(22A)-ZrA-C(9A)	84.19(13)
C(21A)-ZrA-C(9A)	97.45(12)
C(6A)-ZrA-C(9A)	53.79(10)
C(1A)-ZrA-C(9A)	121.84(10)
C(2A)-ZrA-C(9A)	133.91(11)
C(7A)-ZrA-C(9A)	52.49(11)
C(5A)-ZrA-C(9A)	135.89(11)
C(10A)-ZrA-C(9A)	31.20(10)
C(3A)-ZrA-C(9A)	162.50(11)
C(8A)-ZrA-C(9A)	30.88(11)
C(4A)-ZrA-C(9A)	164.33(10)
C(1A)-SiA-C(19A)	111.04(18)
C(1A)-SiA-C(6A)	96.68(14)
C(19A)-SiA-C(6A)	111.31(17)
C(1A)-SiA-C(20A)	112.41(16)
C(19A)-SiA-C(20A)	114.13(18)
C(6A)-SiA-C(20A)	109.97(16)
C(5A)-C(1A)-C(2A)	104.9(3)
C(5A)-C(1A)-SiA	129.0(2)
C(2A)-C(1A)-SiA	121.2(2)
C(5A)-C(1A)-ZrA	76.21(18)
C(2A)-C(1A)-ZrA	72.91(18)
SiA-C(1A)-ZrA	96.45(13)
C(3A)-C(2A)-C(1A)	109.1(3)
C(3A)-C(2A)-ZrA	78.4(2)
C(1A)-C(2A)-ZrA	73.48(18)
C(3A)-C(2A)-H(2A)	124.4(19)
C(1A)-C(2A)-H(2A)	126.5(19)
ZrA-C(2A)-H(2A)	115.2(18)
C(4A)-C(3A)-C(2A)	108.9(3)
C(4A)-C(3A)-ZrA	77.37(19)

C(2A)-C(3A)-ZrA	69.47(19)
C(4A)-C(3A)-H(3A)	127.1(19)
C(2A)-C(3A)-H(3A)	123.9(19)
ZrA-C(3A)-H(3A)	121.1(18)
C(3A)-C(4A)-C(5A)	106.2(3)
C(3A)-C(4A)-C(11A)	124.8(3)
C(5A)-C(4A)-C(11A)	128.1(3)
C(3A)-C(4A)-ZrA	71.48(18)
C(5A)-C(4A)-ZrA	69.84(18)
C(11A)-C(4A)-ZrA	131.9(2)
C(1A)-C(5A)-C(4A)	110.8(3)
C(1A)-C(5A)-ZrA	71.02(18)
C(4A)-C(5A)-ZrA	78.77(19)
C(1A)-C(5A)-H(5A)	125.2(19)
C(4A)-C(5A)-H(5A)	124(2)
ZrA-C(5A)-H(5A)	122.0(19)
C(10A)-C(6A)-C(7A)	104.4(3)
C(10A)-C(6A)-SiA	127.9(2)
C(7A)-C(6A)-SiA	123.3(2)
C(10A)-C(6A)-ZrA	76.68(18)
C(7A)-C(6A)-ZrA	73.09(19)
SiA-C(6A)-ZrA	96.80(13)
C(8A)-C(7A)-C(6A)	109.7(3)
C(8A)-C(7A)-ZrA	79.3(2)
C(6A)-C(7A)-ZrA	73.27(19)
C(8A)-C(7A)-H(7A)	125(2)
C(6A)-C(7A)-H(7A)	125(2)
ZrA-C(7A)-H(7A)	114(2)
C(7A)-C(8A)-C(9A)	109.2(3)
C(7A)-C(8A)-ZrA	68.8(2)
C(9A)-C(8A)-ZrA	77.9(2)
C(7A)-C(8A)-H(8A)	125(2)
C(9A)-C(8A)-H(8A)	126(2)
ZrA-C(8A)-H(8A)	123.3(19)
C(8A)-C(9A)-C(10A)	106.0(3)
C(8A)-C(9A)-C(15A)	124.8(3)
C(10A)-C(9A)-C(15A)	128.6(3)
C(8A)-C(9A)-ZrA	71.26(19)
C(10A)-C(9A)-ZrA	69.23(18)
C(15A)-C(9A)-ZrA	131.3(2)
C(9A)-C(10A)-C(6A)	110.7(3)
C(9A)-C(10A)-ZrA	79.57(19)
C(6A)-C(10A)-ZrA	70.31(18)
C(9A)-C(10A)-H(10A)	123(2)
C(6A)-C(10A)-H(10A)	126(2)
ZrA-C(10A)-H(10A)	115(2)
C(4A)-C(11A)-C(13A)	111.4(3)
C(4A)-C(11A)-C(14A)	106.8(3)
C(13A)-C(11A)-C(14A)	108.1(3)
C(4A)-C(11A)-C(12A)	112.2(3)
C(13A)-C(11A)-C(12A)	109.9(3)
C(14A)-C(11A)-C(12A)	108.3(3)
C(11A)-C(12A)-H(12A)	111.9(18)
C(11A)-C(12A)-H(12A)	109.7(18)

H(12A)-C(12A)-H(12A)	107(3)
C(11A)-C(12A)-H(12A)	109.3(18)
H(12A)-C(12A)-H(12A)	109(2)
H(12A)-C(12A)-H(12A)	110(2)
C(11A)-C(13A)-H(13A)	115(2)
C(11A)-C(13A)-H(13A)	111(2)
H(13A)-C(13A)-H(13A)	106(3)
C(11A)-C(13A)-H(13A)	112(2)
H(13A)-C(13A)-H(13A)	108(3)
H(13A)-C(13A)-H(13A)	105(3)
C(11A)-C(14A)-H(14A)	107.4(19)
C(11A)-C(14A)-H(14A)	114(2)
H(14A)-C(14A)-H(14A)	112(3)
C(11A)-C(14A)-H(14A)	109(2)
H(14A)-C(14A)-H(14A)	109(3)
H(14A)-C(14A)-H(14A)	105(3)
C(9A)-C(15A)-C(18A)	112.1(3)
C(9A)-C(15A)-C(16A)	107.5(3)
C(18A)-C(15A)-C(16A)	108.1(3)
C(9A)-C(15A)-C(17A)	111.5(3)
C(18A)-C(15A)-C(17A)	109.4(3)
C(16A)-C(15A)-C(17A)	108.1(3)
C(15A)-C(16A)-H(16A)	110.4(19)
C(15A)-C(16A)-H(16A)	112(2)
H(16A)-C(16A)-H(16A)	106(3)
C(15A)-C(16A)-H(16A)	107(2)
H(16A)-C(16A)-H(16A)	112(3)
H(16A)-C(16A)-H(16A)	110(3)
C(15A)-C(17A)-H(17A)	109.8(19)
C(15A)-C(17A)-H(17A)	108.8(19)
H(17A)-C(17A)-H(17A)	108(3)
C(15A)-C(17A)-H(17A)	112(2)
H(17A)-C(17A)-H(17A)	115(3)
H(17A)-C(17A)-H(17A)	104(3)
C(15A)-C(18A)-H(18A)	114.3(19)
C(15A)-C(18A)-H(18A)	112(2)
H(18A)-C(18A)-H(18A)	103(3)
C(15A)-C(18A)-H(18A)	110.5(18)
H(18A)-C(18A)-H(18A)	109(3)
H(18A)-C(18A)-H(18A)	108(3)
SiA-C(19A)-H(19A)	111(2)
SiA-C(19A)-H(19A)	113(2)
H(19A)-C(19A)-H(19A)	107(3)
SiA-C(19A)-H(19A)	114(2)
H(19A)-C(19A)-H(19A)	101(3)
H(19A)-C(19A)-H(19A)	110(3)
SiA-C(20A)-H(20A)	110(2)
SiA-C(20A)-H(20A)	113(2)
H(20A)-C(20A)-H(20A)	111(3)
SiA-C(20A)-H(20A)	111(2)
H(20A)-C(20A)-H(20A)	107(3)
H(20A)-C(20A)-H(20A)	105(3)
ZrA-C(21A)-H(21A)	112.3(18)
ZrA-C(21A)-H(21A)	111(2)

H(21A)-C(21A)-H(21A)	106(3)
ZrA-C(21A)-H(21A)	106(2)
H(21A)-C(21A)-H(21A)	110(3)
H(21A)-C(21A)-H(21A)	111(3)
ZrA-C(22A)-H(22A)	117(2)
ZrA-C(22A)-H(22A)	109(2)
H(22A)-C(22A)-H(22A)	108(3)
ZrA-C(22A)-H(22A)	111(2)
H(22A)-C(22A)-H(22A)	106(3)
H(22A)-C(22A)-H(22A)	107(3)
Cent(1B)-ZrB-Cent(2B)	126.66(2)
Pln(1B)-ZrB-Pln(2B)	116.34(14)
C(21B)-ZrB-C(22B)	97.20(16)
C(21B)-ZrB-C(6B)	129.31(13)
C(22B)-ZrB-C(6B)	116.24(13)
C(21B)-ZrB-C(7B)	96.21(14)
C(22B)-ZrB-C(7B)	135.79(13)
C(6B)-ZrB-C(7B)	33.40(11)
C(21B)-ZrB-C(1B)	131.00(14)
C(22B)-ZrB-C(1B)	115.07(14)
C(6B)-ZrB-C(1B)	68.41(10)
C(7B)-ZrB-C(1B)	85.71(11)
C(21B)-ZrB-C(2B)	97.81(15)
C(22B)-ZrB-C(2B)	135.25(14)
C(6B)-ZrB-C(2B)	84.65(11)
C(7B)-ZrB-C(2B)	83.73(11)
C(1B)-ZrB-C(2B)	33.50(11)
C(21B)-ZrB-C(5B)	129.14(14)
C(22B)-ZrB-C(5B)	85.01(14)
C(6B)-ZrB-C(5B)	92.55(11)
C(7B)-ZrB-C(5B)	117.10(11)
C(1B)-ZrB-C(5B)	32.70(10)
C(2B)-ZrB-C(5B)	53.35(12)
C(21B)-ZrB-C(10B)	128.18(14)
C(22B)-ZrB-C(10B)	85.88(13)
C(6B)-ZrB-C(10B)	32.77(11)
C(7B)-ZrB-C(10B)	53.40(12)
C(1B)-ZrB-C(10B)	91.65(11)
C(2B)-ZrB-C(10B)	115.82(11)
C(5B)-ZrB-C(10B)	102.68(11)
C(21B)-ZrB-C(8B)	79.32(14)
C(22B)-ZrB-C(8B)	111.18(13)
C(6B)-ZrB-C(8B)	54.20(11)
C(7B)-ZrB-C(8B)	32.16(11)
C(1B)-ZrB-C(8B)	117.42(11)
C(2B)-ZrB-C(8B)	112.93(11)
C(5B)-ZrB-C(8B)	146.57(11)
C(10B)-ZrB-C(8B)	52.28(12)
C(21B)-ZrB-C(3B)	80.69(14)
C(22B)-ZrB-C(3B)	111.33(13)
C(6B)-ZrB-C(3B)	116.43(11)
C(7B)-ZrB-C(3B)	112.34(11)
C(1B)-ZrB-C(3B)	54.23(11)
C(2B)-ZrB-C(3B)	32.05(10)

C(5B)-ZrB-C(3B)	52.28(11)
C(10B)-ZrB-C(3B)	145.53(11)
C(8B)-ZrB-C(3B)	134.73(11)
C(21B)-ZrB-C(4B)	98.00(13)
C(22B)-ZrB-C(4B)	83.53(13)
C(6B)-ZrB-C(4B)	121.45(10)
C(7B)-ZrB-C(4B)	135.57(11)
C(1B)-ZrB-C(4B)	53.80(10)
C(2B)-ZrB-C(4B)	52.74(11)
C(5B)-ZrB-C(4B)	31.46(10)
C(10B)-ZrB-C(4B)	133.57(11)
C(8B)-ZrB-C(4B)	165.23(11)
C(3B)-ZrB-C(4B)	31.23(10)
C(21B)-ZrB-C(9B)	97.28(14)
C(22B)-ZrB-C(9B)	83.64(13)
C(6B)-ZrB-C(9B)	53.81(10)
C(7B)-ZrB-C(9B)	52.92(11)
C(1B)-ZrB-C(9B)	120.99(10)
C(2B)-ZrB-C(9B)	135.30(10)
C(5B)-ZrB-C(9B)	133.23(11)
C(10B)-ZrB-C(9B)	31.36(10)
C(8B)-ZrB-C(9B)	31.36(11)
C(3B)-ZrB-C(9B)	165.02(11)
C(4B)-ZrB-C(9B)	161.13(10)
C(6B)-SiB-C(20B)	113.57(17)
C(6B)-SiB-C(19B)	110.63(18)
C(20B)-SiB-C(19B)	111.20(19)
C(6B)-SiB-C(1B)	96.22(14)
C(20B)-SiB-C(1B)	114.40(16)
C(19B)-SiB-C(1B)	109.95(17)
C(5B)-C(1B)-C(2B)	104.7(3)
C(5B)-C(1B)-SiB	130.9(3)
C(2B)-C(1B)-SiB	119.8(2)
C(5B)-C(1B)-ZrB	75.55(19)
C(2B)-C(1B)-ZrB	73.36(19)
SiB-C(1B)-ZrB	97.21(13)
C(3B)-C(2B)-C(1B)	109.4(3)
C(3B)-C(2B)-ZrB	78.3(2)
C(1B)-C(2B)-ZrB	73.14(19)
C(3B)-C(2B)-H(2B)	127(2)
C(1B)-C(2B)-H(2B)	123(2)
ZrB-C(2B)-H(2B)	119(2)
C(2B)-C(3B)-C(4B)	108.6(3)
C(2B)-C(3B)-ZrB	69.7(2)
C(4B)-C(3B)-ZrB	77.0(2)
C(2B)-C(3B)-H(3B)	126(2)
C(4B)-C(3B)-H(3B)	125.1(19)
ZrB-C(3B)-H(3B)	120.5(19)
C(5B)-C(4B)-C(3B)	105.9(3)
C(5B)-C(4B)-C(11B)	129.1(3)
C(3B)-C(4B)-C(11B)	123.9(3)
C(5B)-C(4B)-ZrB	69.18(18)
C(3B)-C(4B)-ZrB	71.78(19)
C(11B)-C(4B)-ZrB	132.5(2)

C(1B)-C(5B)-C(4B)	111.3(3)
C(1B)-C(5B)-ZrB	71.75(18)
C(4B)-C(5B)-ZrB	79.36(19)
C(1B)-C(5B)-H(5B)	125(2)
C(4B)-C(5B)-H(5B)	123(2)
ZrB-C(5B)-H(5B)	115(2)
C(10B)-C(6B)-C(7B)	105.0(3)
C(10B)-C(6B)-SiB	128.5(3)
C(7B)-C(6B)-SiB	122.2(2)
C(10B)-C(6B)-ZrB	76.11(19)
C(7B)-C(6B)-ZrB	72.84(18)
SiB-C(6B)-ZrB	97.74(13)
C(8B)-C(7B)-C(6B)	109.6(3)
C(8B)-C(7B)-ZrB	78.6(2)
C(6B)-C(7B)-ZrB	73.76(18)
C(8B)-C(7B)-H(7B)	127(2)
C(6B)-C(7B)-H(7B)	123(2)
ZrB-C(7B)-H(7B)	112.9(19)
C(7B)-C(8B)-C(9B)	108.5(3)
C(7B)-C(8B)-ZrB	69.25(19)
C(9B)-C(8B)-ZrB	77.2(2)
C(7B)-C(8B)-H(8B)	127(2)
C(9B)-C(8B)-H(8B)	125(2)
ZrB-C(8B)-H(8B)	118(2)
C(8B)-C(9B)-C(10B)	105.9(3)
C(8B)-C(9B)-C(15B)	124.7(3)
C(10B)-C(9B)-C(15B)	128.4(3)
C(8B)-C(9B)-ZrB	71.39(19)
C(10B)-C(9B)-ZrB	69.70(19)
C(15B)-C(9B)-ZrB	132.2(2)
C(6B)-C(10B)-C(9B)	111.0(3)
C(6B)-C(10B)-ZrB	71.11(19)
C(9B)-C(10B)-ZrB	78.9(2)
C(6B)-C(10B)-H(10B)	127(2)
C(9B)-C(10B)-H(10B)	122(2)
ZrB-C(10B)-H(10B)	117(2)
C(4B)-C(11B)-C(12B)	106.6(3)
C(4B)-C(11B)-C(14B)	112.2(3)
C(12B)-C(11B)-C(14B)	108.6(3)
C(4B)-C(11B)-C(13B)	112.3(3)
C(12B)-C(11B)-C(13B)	107.4(3)
C(14B)-C(11B)-C(13B)	109.5(3)
C(11B)-C(13B)-H(13B)	107.8(19)
C(11B)-C(13B)-H(13B)	109(2)
H(13B)-C(13B)-H(13B)	109(3)
C(11B)-C(13B)-H(13B)	109(2)
H(13B)-C(13B)-H(13B)	115(3)
H(13B)-C(13B)-H(13B)	107(3)
C(11B)-C(12B)-H(12B)	107(2)
C(11B)-C(12B)-H(12B)	111(2)
H(12B)-C(12B)-H(12B)	108(3)
C(11B)-C(12B)-H(12B)	110(2)
H(12B)-C(12B)-H(12B)	109(3)
H(12B)-C(12B)-H(12B)	112(3)

C(11B)-C(14B)-H(14B)	112(2)
C(11B)-C(14B)-H(14B)	109.4(18)
H(14B)-C(14B)-H(14B)	105(3)
C(11B)-C(14B)-H(14B)	114(2)
H(14B)-C(14B)-H(14B)	105(3)
H(14B)-C(14B)-H(14B)	111(3)
C(16B)-C(15B)-C(9B)	111.3(3)
C(16B)-C(15B)-C(18B)	108.9(3)
C(9B)-C(15B)-C(18B)	106.2(3)
C(16B)-C(15B)-C(17B)	110.5(3)
C(9B)-C(15B)-C(17B)	111.8(3)
C(18B)-C(15B)-C(17B)	108.0(3)
C(15B)-C(16B)-H(16B)	112(2)
C(15B)-C(16B)-H(16B)	113.4(18)
H(16B)-C(16B)-H(16B)	106(3)
C(15B)-C(16B)-H(16B)	110(2)
H(16B)-C(16B)-H(16B)	103(3)
H(16B)-C(16B)-H(16B)	112(3)
C(15B)-C(17B)-H(17B)	111.5(19)
C(15B)-C(17B)-H(17B)	108(2)
H(17B)-C(17B)-H(17B)	107(3)
C(15B)-C(17B)-H(17B)	110(2)
H(17B)-C(17B)-H(17B)	113(3)
H(17B)-C(17B)-H(17B)	106(3)
C(15B)-C(18B)-H(18B)	112(2)
C(15B)-C(18B)-H(18B)	113(2)
H(18B)-C(18B)-H(18B)	104(3)
C(15B)-C(18B)-H(18B)	113.5(19)
H(18B)-C(18B)-H(18B)	109(3)
H(18B)-C(18B)-H(18B)	104(3)
SiB-C(19B)-H(19B)	110(2)
SiB-C(19B)-H(19B)	115(2)
H(19B)-C(19B)-H(19B)	104(3)
SiB-C(19B)-H(19B)	112(2)
H(19B)-C(19B)-H(19B)	106(3)
H(19B)-C(19B)-H(19B)	109(3)
SiB-C(20B)-H(20B)	110.2(18)
SiB-C(20B)-H(20B)	112(2)
H(20B)-C(20B)-H(20B)	103(3)
SiB-C(20B)-H(20B)	115(2)
H(20B)-C(20B)-H(20B)	109(3)
H(20B)-C(20B)-H(20B)	108(3)
ZrB-C(21B)-H(21B)	107.4(19)
ZrB-C(21B)-H(21B)	113(2)
H(21B)-C(21B)-H(21B)	102(3)
ZrB-C(21B)-H(21B)	112(2)
H(21B)-C(21B)-H(21B)	108(3)
H(21B)-C(21B)-H(21B)	114(3)
ZrB-C(22B)-H(22B)	104(2)
ZrB-C(22B)-H(22B)	118(2)
H(22B)-C(22B)-H(22B)	103(3)
ZrB-C(22B)-H(22B)	113(2)
H(22B)-C(22B)-H(22B)	106(3)
H(22B)-C(22B)-H(22B)	112(3)

Symmetry transformations used to generate equivalent atoms:

Table 14. Crystal Data and Structure Analysis Details for *meso*-[$DpZrH_2$]$_2$.

Empirical formula	$C_{40}H_{62}Si_2Zr_2$
Formula weight	781.52
Crystallization solvent	toluene
Crystal habit	plate
Crystal size	0.08 x 0.07 x 0.04 mm
Crystal color	colorless

Data Collection

Preliminary photograph(s)	rotation	
Type of diffractometer	Bruker SMART 1000 ccd	
Wavelength	0.71073 Å MoKa	
Data collection temperature	98 K	
Theta range for 2846 reflections used in lattice determination	2.2 to 21.9°	
Unit cell dimensions	a = 10.0511(11) Å b = 14.2131(16) Å c = 15.3334(17) Å	a= 82.573(2)° b= 79.502(2)° g = 70.609(2)°
Volume	2026.1(4) $Å^3$	
Z	2	
Crystal system	triclinic	
Space group	P`1 (#2)	
Density (calculated)	1.281 g/cm^3	
F(000)	820	
Theta range for data collection	1.35 to 25.00°	
Completeness to theta = 25.00°	99.8 %	
Index ranges	-11 £ h £ 11, -16 £ k £ 16, -18 £ l £ 18	
Data collection scan type	w scans at 4 fixed f values	
Reflections collected	20564	
Independent reflections	7112 [R_{int}= 0.0851]	
Absorption coefficient	0.598 mm^{-1}	
Absorption correction	empirical	
Max. and min. transmission	1.00 and 0.93	
Number of standards	first scans recollected at end of runs	

Variation of standards	within counting statistics

Structure Solution and Refinement

Primary solution method	direct methods
Secondary solution method	difference map
Hydrogen placement	calculated
Refinement method	full-matrix least-squares on F^2
Data / restraints / parameters	7112 / 0 / 397
Treatment of hydrogen atoms	not refined; U_{iso}'s set at 120% U_{eq} of attached atom
Goodness-of-fit on F^2	1.734
Final R indices [I>2s(I), 4312 reflections]	R1 = 0.0610, wR2 = 0.1160
R indices (all data)	R1 = 0.1217, wR2 = 0.1273
Type of weighting scheme used	sigma
Weighting scheme used	$w=1/s^2(Fo^2)$
Max shift/error	0.010
Average shift/error	0.001
Largest diff. peak and hole	1.745 and -0.673 e.Å^{-3}

Programs Used

Cell refinement	Bruker SAINT v6.02
Data collection	Bruker SMART v5.054
Data reduction	Bruker SAINT v6.02
Absorption correction	SADABS V2.0 beta
Structure solution	SHELXS-97 (Sheldrick, 1990)
Structure refinement	SHELXL-97 (Sheldrick, 1997)

Special Refinement Details

A tiny, colorless irregular plate was mounted on a glass fiber with Paratone-N oil. Four runs of data were collected with 90 second long, –0.20∞ wide w-scans at four values of j (0, 120, 240 and 300∞) with the detector 5 cm (nominal) distant at a q of -28∞. The initial cell for data reduction was calculated from just under 1000 reflections chosen from throughout the data frames. For data processing with SAINT v6.02, all defaults were used, except: box size optimization was enabled, periodic orientation matrix updating was disabled, the instrument error was set to zero, no Laue class integration restraints were used, the model profiles from all nine areas were blended, and for the post-integration global least squares refinement, no

constraints were applied. The data were corrected with SADABS v. 2.0 (beta) using default parameters except that the scale factor esd was set to 0. No decay correction was needed.

No reflections were specifically omitted from the final processed dataset; the data were truncated at a 2q of 50∞, 4369 reflections were rejected, and there were 11 inconsistent equivalents. Refinement of F^2 was against all reflections. The weighted R-factor (*w*R) and goodness of fit (S) are based on F^2, conventional R-factors (R) are based on F, with F set to zero for negative F^2. The threshold expression of $F^2 > 2s(F^2)$ is used only for calculating R-factors(gt) etc. and is not relevant to the choice of reflections for refinement.

There are two dimers in the unit cell; each sits on a center of symmetry so that the asymmetric unit consists of two independent half-dimers. The bridging hydride atoms were not located in difference maps and so were excluded from the refinement. There are three peaks in the final difference map greater than |1| e◊Å^{-3} : 1.74 e◊Å^{-3} at 2.21 Å from H14A, 1.53 e◊Å^{-3} at (_,_,_) 1.75 Å from ZrA and 1.10 e◊Å^{-3} at 2.20 Å from H18D.

Table 15. Bond lengths [Å] and angles [°] for *meso*-[DpZrH2]2

ZrA-Cp1A	2.222
ZrA-Cp2A	2.215
ZrA···Pln1A	2.213(3)
ZrA···Pln2A	2.207(3)
ZrA-C1A	2.443(7)
ZrA-C6A	2.447(7)
ZrA-C7A	2.469(7)
ZrA-C2A	2.482(7)
ZrA-C5A	2.493(7)
ZrA-C10A	2.509(7)
ZrA-C8A	2.554(7)
ZrA-C3A	2.572(7)
ZrA-C9A	2.621(7)
ZrA-C4A	2.635(7)
ZrA-ZrA$^{(i)}$	3.4922(15)
SiA-C11A	1.816(8)
SiA-C6A	1.849(8)
SiA-C12A	1.849(7)
SiA-C1A	1.863(8)
C1A-C2A	1.403(10)
C1A-C5A	1.424(10)
C2A-C3A	1.420(10)
C2A-H2A	1.0000
C3A-C4A	1.408(9)
C3A-H3A	1.0000
C4A-C5A	1.414(10)
C4A-C13A	1.495(10)
C5A-H5A	1.0000
C6A-C7A	1.415(10)
C6A-C10A	1.447(10)
C7A-C8A	1.392(10)
C7A-H7A	1.0000
C8A-C9A	1.395(9)

C8A-H8A	1.0000
C9A-C10A	1.427(10)
C9A-C17A	1.509(10)
C10A-H10A	1.0000
C11A-H11A	0.9800
C11A-H11B	0.9800
C11A-H11C	0.9800
C12A-H12A	0.9800
C12A-H12B	0.9800
C12A-H12C	0.9800
C13A-C16A	1.522(10)
C13A-C15A	1.530(10)
C13A-C14A	1.535(11)
C14A-H14A	0.9800
C14A-H14B	0.9800
C14A-H14C	0.9800
C15A-H15A	0.9800
C15A-H15B	0.9800
C15A-H15C	0.9800
C16A-H16A	0.9800
C16A-H16B	0.9800
C16A-H16C	0.9800
C17A-C20A	1.520(10)
C17A-C18A	1.524(10)
C17A-C19A	1.546(10)
C18A-H18A	0.9800
C18A-H18B	0.9800
C18A-H18C	0.9800
C19A-H19A	0.9800
C19A-H19B	0.9800
C19A-H19C	0.9800
C20A-H20A	0.9800
C20A-H20B	0.9800
C20A-H20C	0.9800
ZrB-Cp1B	2.204
ZrB-Cp2B	2.229
ZrB···Pln1B	2.197(3)
ZrB···Pln2B	2.223(3)
ZrB-C1B	2.432(7)
ZrB-C5B	2.458(7)
ZrB-C6B	2.471(7)
ZrB-C7B	2.487(7)
ZrB-C2B	2.494(6)
ZrB-C10B	2.515(7)
ZrB-C3B	2.563(7)
ZrB-C8B	2.576(7)
ZrB-C4B	2.598(7)
ZrB-C9B	2.611(7)
ZrB-ZrB$^{(ii)}$	3.4498(15)
SiB-C11B	1.822(8)
SiB-C12B	1.839(8)
SiB-C1B	1.867(7)
SiB-C6B	1.867(7)
C1B-C2B	1.420(9)

C1B-C5B	1.421(9)
C2B-C3B	1.382(9)
C2B-H2B	1.0000
C3B-C4B	1.410(10)
C3B-H3B	1.0000
C4B-C5B	1.420(9)
C4B-C13B	1.495(9)
C5B-H5B	1.0000
C6B-C7B	1.409(9)
C6B-C10B	1.438(9)
C7B-C8B	1.412(9)
C7B-H7B	1.0000
C8B-C9B	1.410(9)
C8B-H8B	1.0000
C9B-C10B	1.405(9)
C9B-C17B	1.518(9)
C10B-H10B	1.0000
C11B-H11D	0.9800
C11B-H11E	0.9800
C11B-H11F	0.9800
C12B-H12D	0.9800
C12B-H12E	0.9800
C12B-H12F	0.9800
C13B-C16B	1.532(10)
C13B-C14B	1.545(10)
C13B-C15B	1.558(10)
C14B-H14D	0.9800
C14B-H14E	0.9800
C14B-H14F	0.9800
C15B-H15D	0.9800
C15B-H15E	0.9800
C15B-H15F	0.9800
C16B-H16D	0.9800
C16B-H16E	0.9800
C16B-H16F	0.9800
C17B-C20B	1.496(9)
C17B-C19B	1.519(10)
C17B-C18B	1.539(10)
C18B-H18D	0.9800
C18B-H18E	0.9800
C18B-H18F	0.9800
C19B-H19D	0.9800
C19B-H19E	0.9800
C19B-H19F	0.9800
C20B-H20D	0.9800
C20B-H20E	0.9800
C20B-H20F	0.9800
Cp1A-ZrA-Cp2A	125.1
Pln1A···Pln2A	62.4(3)
C11A-SiA-C6A	112.2(4)
C11A-SiA-C12A	115.2(4)
C6A-SiA-C12A	110.6(4)
C11A-SiA-C1A	109.9(4)
C6A-SiA-C1A	96.5(3)

C12A-SiA-C1A	110.9(4)
C2A-C1A-C5A	104.7(7)
C2A-C1A-SiA	128.1(6)
C5A-C1A-SiA	122.1(6)
C1A-C2A-C3A	109.6(7)
C1A-C2A-H2A	124.9
C3A-C2A-H2A	124.9
C4A-C3A-C2A	108.9(7)
C4A-C3A-H3A	125.3
C2A-C3A-H3A	125.3
C3A-C4A-C5A	105.2(7)
C3A-C4A-C13A	126.0(7)
C5A-C4A-C13A	128.2(7)
C4A-C5A-C1A	111.6(7)
C4A-C5A-H5A	123.9
C1A-C5A-H5A	123.9
C7A-C6A-C10A	103.9(7)
C7A-C6A-SiA	128.0(6)
C10A-C6A-SiA	122.9(6)
C8A-C7A-C6A	110.3(7)
C8A-C7A-H7A	124.5
C6A-C7A-H7A	124.5
C7A-C8A-C9A	109.8(7)
C7A-C8A-H8A	124.9
C9A-C8A-H8A	124.9
C8A-C9A-C10A	105.7(7)
C8A-C9A-C17A	127.3(7)
C10A-C9A-C17A	126.3(7)
C9A-C10A-C6A	110.2(7)
C9A-C10A-H10A	124.6
C6A-C10A-H10A	124.6
SiA-C11A-H11A	109.5
SiA-C11A-H11B	109.5
H11A-C11A-H11B	109.5
SiA-C11A-H11C	109.5
H11A-C11A-H11C	109.5
H11B-C11A-H11C	109.5
SiA-C12A-H12A	109.5
SiA-C12A-H12B	109.5
H12A-C12A-H12B	109.5
SiA-C12A-H12C	109.5
H12A-C12A-H12C	109.5
H12B-C12A-H12C	109.5
C4A-C13A-C16A	106.8(7)
C4A-C13A-C15A	112.9(6)
C16A-C13A-C15A	108.5(7)
C4A-C13A-C14A	111.4(6)
C16A-C13A-C14A	107.5(7)
C15A-C13A-C14A	109.6(7)
C13A-C14A-H14A	109.5
C13A-C14A-H14B	109.5
H14A-C14A-H14B	109.5
C13A-C14A-H14C	109.5
H14A-C14A-H14C	109.5

H14B-C14A-H14C	109.5
C13A-C15A-H15A	109.5
C13A-C15A-H15B	109.5
H15A-C15A-H15B	109.5
C13A-C15A-H15C	109.5
H15A-C15A-H15C	109.5
H15B-C15A-H15C	109.5
C13A-C16A-H16A	109.5
C13A-C16A-H16B	109.5
H16A-C16A-H16B	109.5
C13A-C16A-H16C	109.5
H16A-C16A-H16C	109.5
H16B-C16A-H16C	109.5
C9A-C17A-C20A	114.3(6)
C9A-C17A-C18A	110.6(6)
C20A-C17A-C18A	110.1(6)
C9A-C17A-C19A	106.1(6)
C20A-C17A-C19A	107.8(7)
C18A-C17A-C19A	107.7(6)
C17A-C18A-H18A	109.5
C17A-C18A-H18B	109.5
H18A-C18A-H18B	109.5
C17A-C18A-H18C	109.5
H18A-C18A-H18C	109.5
H18B-C18A-H18C	109.5
C17A-C19A-H19A	109.5
C17A-C19A-H19B	109.5
H19A-C19A-H19B	109.5
C17A-C19A-H19C	109.5
H19A-C19A-H19C	109.5
H19B-C19A-H19C	109.5
C17A-C20A-H20A	109.5
C17A-C20A-H20B	109.5
H20A-C20A-H20B	109.5
C17A-C20A-H20C	109.5
H20A-C20A-H20C	109.5
H20B-C20A-H20C	10
Cp1B-ZrB-Cp2B	124.6
Pln1B···Pln2B	62.8(3)
C11B-SiB-C12B	112.9(4)
C11B-SiB-C1B	111.1(3)
C12B-SiB-C1B	111.9(4)
C11B-SiB-C6B	113.9(4)
C12B-SiB-C6B	109.4(3)
C1B-SiB-C6B	96.5(3)
C2B-C1B-C5B	104.7(6)
C2B-C1B-SiB	129.0(5)
C5B-C1B-SiB	121.2(6)
C3B-C2B-C1B	109.8(7)
C3B-C2B-H2B	124.9
C1B-C2B-H2B	124.9
C2B-C3B-C4B	109.6(7)
C2B-C3B-H3B	125.0
C4B-C3B-H3B	125.0

C3B-C4B-C5B	105.3(7)
C3B-C4B-C13B	125.1(7)
C5B-C4B-C13B	129.1(7)
C4B-C5B-C1B	110.5(7)
C4B-C5B-H5B	124.3
C1B-C5B-H5B	124.3
C7B-C6B-C10B	104.6(6)
C7B-C6B-SiB	125.0(6)
C10B-C6B-SiB	124.2(5)
C6B-C7B-C8B	109.8(6)
C6B-C7B-H7B	124.7
C8B-C7B-H7B	124.7
C9B-C8B-C7B	108.7(6)
C9B-C8B-H8B	125.5
C7B-C8B-H8B	125.5
C10B-C9B-C8B	106.2(6)
C10B-C9B-C17B	127.5(7)
C8B-C9B-C17B	125.2(6)
C9B-C10B-C6B	110.8(7)
C9B-C10B-H10B	124.3
C6B-C10B-H10B	124.3
SiB-C11B-H11D	109.5
SiB-C11B-H11E	109.5
H11D-C11B-H11E	109.5
SiB-C11B-H11F	109.5
H11D-C11B-H11F	109.5
H11E-C11B-H11F	109.5
SiB-C12B-H12D	109.5
SiB-C12B-H12E	109.5
H12D-C12B-H12E	109.5
SiB-C12B-H12F	109.5
H12D-C12B-H12F	109.5
H12E-C12B-H12F	109.5
C4B-C13B-C16B	108.8(6)
C4B-C13B-C14B	113.3(6)
C16B-C13B-C14B	106.3(7)
C4B-C13B-C15B	111.5(6)
C16B-C13B-C15B	107.4(7)
C14B-C13B-C15B	109.2(6)
C13B-C14B-H14D	109.5
C13B-C14B-H14E	109.5
H14D-C14B-H14E	109.5
C13B-C14B-H14F	109.5
H14D-C14B-H14F	109.5
H14E-C14B-H14F	109.5
C13B-C15B-H15D	109.5
C13B-C15B-H15E	109.5
H15D-C15B-H15E	109.5
C13B-C15B-H15F	109.5
H15D-C15B-H15F	109.5
H15E-C15B-H15F	109.5
C13B-C16B-H16D	109.5
C13B-C16B-H16E	109.5
H16D-C16B-H16E	109.5

C13B-C16B-H16F	109.5
H16D-C16B-H16F	109.5
H16E-C16B-H16F	109.5
C20B-C17B-C9B	111.5(6)
C20B-C17B-C19B	109.1(7)
C9B-C17B-C19B	107.3(6)
C20B-C17B-C18B	108.9(6)
C9B-C17B-C18B	111.0(6)
C19B-C17B-C18B	109.0(7)
C17B-C18B-H18D	109.5
C17B-C18B-H18E	109.5
H18D-C18B-H18E	109.5
C17B-C18B-H18F	109.5
H18D-C18B-H18F	109.5
H18E-C18B-H18F	109.5
C17B-C19B-H19D	109.5
C17B-C19B-H19E	109.5
H19D-C19B-H19E	109.5
C17B-C19B-H19F	109.5
H19D-C19B-H19F	109.5
H19E-C19B-H19F	109.5
C17B-C20B-H20D	109.5
C17B-C20B-H20E	109.5
H20D-C20B-H20E	109.5
C17B-C20B-H20F	109.5
H20D-C20B-H20F	109.5
H20E-C20B-H20F	109.5

Symmetry transformations used to generate equivalent atoms:
(i) -x+1,-y+1,-z+1 (ii) -x+2,-y+2,-z

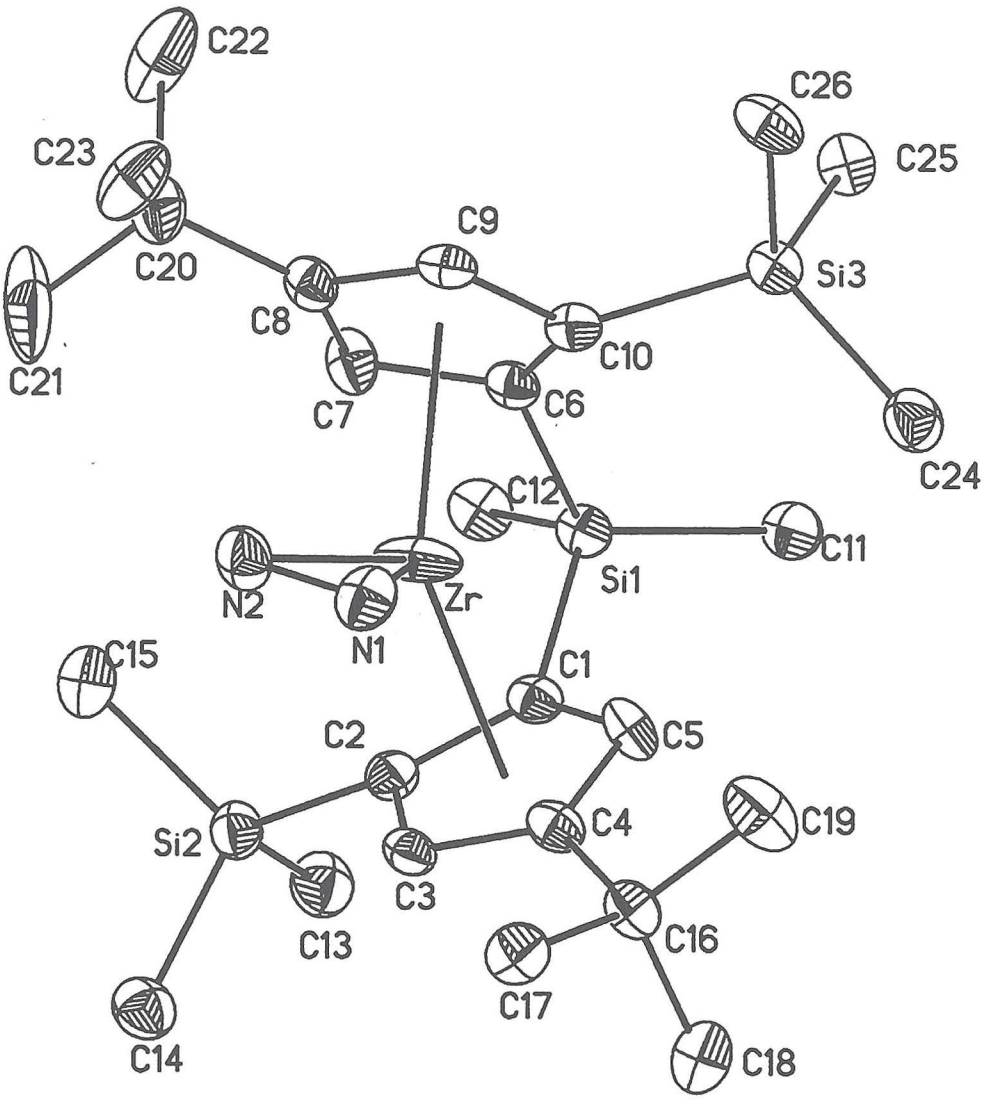

Labeled view of $BpZr(\mu_2\text{-}N_2)ZrBp$.

Table 16. Crystal Data and Structure Analysis Details for $BpZrN_2ZrBp$.

Empirical formula	$C_{59}H_{100}N_2Si_6Zr_2$
Formula weight	1188.39
Crystallization solvent	toluene
Crystal habit	wedge
Crystal size	0.33 x 0.26 x 0.19 mm
Crystal color	trichroic - pale yellow / rose / dark brown

Data Collection

Preliminary photograph(s)	rotation	
Type of diffractometer	Bruker SMART 1000 ccd	
Wavelength	0.71073 Å MoKa	
Data collection temperature	98 K	
Theta range for 7518 reflections used in lattice determination	2.2 to 28.4°	
Unit cell dimensions	a = 16.7641(9) Å b = 10.7439(6) Å c = 18.3696(10) Å	a= 90° b= 100.7580(10)° g = 90°
Volume	3250.4(3) $Å^3$	
Z	2	
Crystal system	monoclinic	
Space group	P 2/n (#13)	
Density (calculated)	1.214 g/cm^3	
F(000)	1264	
Theta range for data collection	1.51 to 28.73°	
Completeness to theta = 28.73°	92.3 %	
Index ranges	-21 £ h £ 22, -14 £ k £ 14, -24 £ l £ 23	
Data collection scan type	w scans at 3 fixed f values	
Reflections collected	31707	
Independent reflections	7795 [R_{int}= 0.0479]	
Absorption coefficient	0.466 mm^{-1}	
Absorption correction	empirical	
Max. and min. transmission	1.00 and 0.90	
Number of standards	first scans recollected at end of runs	
Variation of standards	within counting statistics	

Structure Solution and Refinement

Primary solution method	direct methods
Secondary solution method	difference map
Hydrogen placement	calculated
Refinement method	full-matrix least-squares on F^2
Data / restraints / parameters	7795 / 0 / 520
Treatment of hydrogen atoms	all parameters refined
Goodness-of-fit on F^2	2.286
Final R indices [I>2s(*i*), 6406 reflections]	R1 = 0.0458, wR2 = 0.0828
R indices (all data)	R1 = 0.0586, wR2 = 0.0853
Type of weighting scheme used	sigma
Weighting scheme used	$w=1/s^2(Fo^2)$
Max shift/error	0.024
Average shift/error	0.001
Largest diff. peak and hole	0.822 and -1.687 e.Å^{-3}

Programs Used

Cell refinement	Bruker SAINT v6.02
Data collection	Bruker SMART v5.054
Data reduction	Bruker SAINT v6.02
Absorption correction	SADABS V2.0 beta
Structure solution	SHELXS-97 (Sheldrick, 1990)
Structure refinement	SHELXL-97 (Sheldrick, 1997)

Special Refinement Details

A fragment of an incredibly trichroic (pale yellow / rose / dark brown) tabular crystal was mounted on a glass fiber with Paratone-N oil. Three runs of data were collected with 20 second long, –0.2° wide ω–scans at three values of φ (0, 120, and 240°) with the detector 5 cm (nominal) distant at a θ of -28°. The initial cell for data reduction was calculated from just under 1000 reflections chosen from throughout the data frames. For data processing with SAINT v6.02, all defaults were used, except: box size optimization was enabled, periodic orientation matrix updating was disabled, the instrument error was set to zero, no Laue class integration restraints were used, the model profiles from all nine areas were blended, and for the post-integration global least squares refinement, no constraints were applied. The data were corrected with SADABS v. 2.0 (beta) using default parameters except that the scale factor esd was set to 0.

No outlier reflections were omitted from the final processed dataset; 1000 reflections were rejected, there were 38 inconsistent equivalents and 4 systematic absence violations. Refinement of F^2 was against all reflections. The weighted R-factor (*w*R) and goodness of fit (S) are based on F^2, conventional R-factors (R) are based on F, with F set to zero for negative F^2. The threshold expression of $F^2 > 2\sigma(F^2)$ is used only for calculating R-factors(gt) etc. and is not relevant to the choice of reflections for refinement.

There is _ of the Zr complex in the asymmetric unit; the dimer lies on a two-fold axis which passes through both atoms of the bridging dinitrogen. There is also _ of a toluene in the asymmetric unit, which also lies on a twofold axis passing through the methyl carbon and bisecting the phenyl ring. All parameters were refined on all hydrogen atoms including the half hydrogen atoms of the solvent. The two peaks in the final difference map greater than |1| $e{\cdot}Å^{-3}$ are –1.69 $e{\cdot}Å^{-3}$ (0.91 Å from Zr) and –1.33 $e{\cdot}Å^{-3}$ (0.95 Å from Zr).

Table 17. Bond lengths [Å] and angles [°] for $BpZrN_2ZrBp$.

Zr-Cp1	2.242	Si2-C15	1.863(3)
Zr-Cp2	2.244	Si2-C13	1.866(3)
Zr···Pln1	2.238(1)	Si2-C14	1.868(3)
Zr···Pln2	2.237(1)	Si2-C2	1.882(2)
Zr···$Zr^{(i)}$	4.366	Si3-C26	1.868(2)
Zr-N2	2.2680(8)	Si3-C25	1.868(2)
Zr-N1	2.2717(8)	Si3-C24	1.869(3)
Zr-C6	2.485(2)	Si3-C10	1.882(2)
Zr-C1	2.500(2)	N1-N2	1.245(4)
Zr-C5	2.512(2)	N1-$Zr^{(i)}$	2.2717(8)
Zr-C10	2.513(2)	N2-$Zr^{(i)}$	2.2680(8)
Zr-C7	2.515(2)	C1-C5	1.417(3)
Zr-C2	2.526(2)	C1-C2	1.442(3)
Zr-C3	2.577(2)	C2-C3	1.435(3)
Zr-C9	2.585(2)	C3-C4	1.405(3)
Zr-C4	2.626(2)	C3-H3	0.98(2)
Zr-C8	2.647(2)	C4-C5	1.420(3)
Si1-C12	1.860(3)	C4-C16	1.518(3)
Si1-C11	1.863(3)	C5-H5	0.95(2)
Si1-C6	1.875(2)	C6-C7	1.422(3)
Si1-C1	1.875(2)	C6-C10	1.441(3)

C7-C8	1.420(3)		
C7-H7	0.91(2)	C27-C28$^{(ii)}$	1.369(3)
C8-C9	1.403(3)	C27-C28	1.369(3)
C8-C20	1.517(3)	C27-H27	0.97(3)
C9-C10	1.434(3)	C28-C29	1.377(4)
C9-H9	0.96(2)	C28-H28	0.91(3)
C11-H11A	0.95(3)	C29-C30	1.385(3)
C11-H11B	0.97(3)	C29-H29	0.90(2)
C11-H11C	0.91(3)	C30-C29$^{(ii)}$	1.385(3)
C12-H12A	0.99(2)	C30-C31	1.492(5)
C12-H12B	0.91(3)	C31-H31A	1.08(5)
C12-H12C	0.96(2)	C31-H31B	0.96(5)
C13-H13A	0.90(3)	C31-H31C	1.04(6)
C13-H13B	0.95(3)		
C13-H13C	0.94(3)	Cp1-Zr-Cp2	125.8
C14-H14A	0.99(3)	Cp1-Zr-N1	110.2
C14-H14B	0.94(3)	Cp1-Zr-N2	122.7
C14-H14C	0.99(3)	Cp2-Zr-N1	121.9
C15-H15A	0.94(3)	Cp2-Zr-N2	109.7
C15-H15B	0.94(3)	Pln1···Pln2	61.75(9)
C15-H15C	0.93(3)	N2-Zr-N1	31.83(9)
C16-C17	1.528(3)	N2-N1-Zr	73.92(7)
C16-C19	1.529(3)	N2-N1-Zr$^{(i)}$	73.92(7)
C16-C18	1.535(3)	Zr-N1-Zr$^{(i)}$	147.84(14)
C17-H17A	0.95(3)	N1-N2-Zr$^{(i)}$	74.25(7)
C17-H17B	0.96(2)	N1-N2-Zr	74.25(7)
C17-H17C	0.99(2)	Zr$^{(i)}$-N2-Zr	148.50(14)
C18-H18A	1.02(3)	C12-Si1-C11	107.84(12)
C18-H18B	0.93(3)	C12-Si1-C6	109.45(11)
C18-H18C	0.92(3)	C11-Si1-C6	117.07(11)
C19-H19A	0.88(3)	C12-Si1-C1	117.46(11)
C19-H19B	0.98(3)	C11-Si1-C1	109.93(11)
C19-H19C	0.97(3)	C6-Si1-C1	95.09(9)
C20-C21	1.514(4)	C15-Si2-C13	108.76(13)
C20-C23	1.521(3)	C15-Si2-C14	108.74(13)
C20-C22	1.531(4)	C13-Si2-C14	106.08(13)
C21-H21A	0.86(4)	C15-Si2-C2	116.09(12)
C21-H21B	0.96(3)	C13-Si2-C2	109.43(11)
C21-H21C	1.00(3)	C14-Si2-C2	107.27(11)
C22-H22A	0.94(3)	C26-Si3-C25	106.04(12)
C22-H22B	0.99(3)	C26-Si3-C24	107.48(13)
C22-H22C	0.96(4)	C25-Si3-C24	110.35(12)
C23-H23A	0.96(3)	C26-Si3-C10	107.99(11)
C23-H23B	0.92(3)	C25-Si3-C10	106.81(11)
C23-H23C	1.00(4)	C24-Si3-C10	117.58(11)
C24-H24A	0.97(3)	C5-C1-C2	106.75(19)
C24-H24B	0.92(2)	C5-C1-Si1	117.37(15)
C24-H24C	0.94(3)	C2-C1-Si1	131.44(17)
C25-H25A	0.93(3)	C3-C2-C1	106.02(19)
C25-H25B	0.98(3)	C3-C2-Si2	121.95(16)
C25-H25C	0.98(3)	C1-C2-Si2	129.11(17)
C26-H26A	0.93(3)	C4-C3-C2	110.91(19)
C26-H26B	0.92(3)	C4-C3-H3	124.8(12)
C26-H26C	0.99(3)	C2-C3-H3	124.1(12)

C3-C4-C5	105.42(19)	C4-C16-C18	106.34(19)
C3-C4-C16	128.13(19)	C17-C16-C18	108.6(2)
C5-C4-C16	125.4(2)	C19-C16-C18	108.8(2)
C1-C5-C4	110.83(19)	C16-C17-H17A	113.7(15)
C1-C5-H5	125.0(14)	C16-C17-H17B	107.7(13)
C4-C5-H5	124.1(14)	H17A-C17-H17B	110(2)
C7-C6-C10	106.58(19)	C16-C17-H17C	112.9(14)
C7-C6-Si1	116.90(15)	H17A-C17-H17C	107(2)
C10-C6-Si1	132.56(17)	H17B-C17-H17C	105.1(18)
C8-C7-C6	110.5(2)	C16-C18-H18A	112.5(14)
C8-C7-H7	125.5(15)	C16-C18-H18B	109.5(15)
C6-C7-H7	123.9(15)	H18A-C18-H18B	108(2)
C9-C8-C7	105.8(2)	C16-C18-H18C	115.9(16)
C9-C8-C20	128.3(2)	H18A-C18-H18C	103(2)
C7-C8-C20	124.8(2)	H18B-C18-H18C	108(2)
C8-C9-C10	110.6(2)	C16-C19-H19A	111.0(18)
C8-C9-H9	124.6(13)	C16-C19-H19B	113.2(15)
C10-C9-H9	124.4(13)	H19A-C19-H19B	106(2)
C9-C10-C6	106.40(19)	C16-C19-H19C	110.2(14)
C9-C10-Si3	121.54(16)	H19A-C19-H19C	108(2)
C6-C10-Si3	128.33(16)	H19B-C19-H19C	109(2)
Si1-C11-H11A	109.4(15)	C21-C20-C8	111.7(2)
Si1-C11-H11B	108.9(14)	C21-C20-C23	109.9(3)
H11A-C11-H11B	111(2)	C8-C20-C23	111.1(2)
Si1-C11-H11C	113.1(16)	C21-C20-C22	109.3(3)
H11A-C11-H11C	108(2)	C8-C20-C22	106.8(2)
H11B-C11-H11C	106(2)	C23-C20-C22	107.8(2)
Si1-C12-H12A	107.2(12)	C20-C21-H21A	112(3)
Si1-C12-H12B	114.5(18)	C20-C21-H21B	112(2)
H12A-C12-H12B	112(2)	H21A-C21-H21B	113(4)
Si1-C12-H12C	111.3(14)	C20-C21-H21C	109.2(17)
H12A-C12-H12C	108.1(19)	H21A-C21-H21C	110(3)
H12B-C12-H12C	103(2)	H21B-C21-H21C	100(3)
Si2-C13-H13A	105.7(18)	C20-C22-H22A	112.6(18)
Si2-C13-H13B	112.3(19)	C20-C22-H22B	110.3(16)
H13A-C13-H13B	105(2)	H22A-C22-H22B	110(2)
Si2-C13-H13C	114.4(16)	C20-C22-H22C	108(2)
H13A-C13-H13C	108(2)	H22A-C22-H22C	106(3)
H13B-C13-H13C	110(2)	H22B-C22-H22C	109(2)
Si2-C14-H14A	110.5(14)	C20-C23-H23A	108.4(17)
Si2-C14-H14B	111.1(15)	C20-C23-H23B	109.8(16)
H14A-C14-H14B	107(2)	H23A-C23-H23B	111(2)
Si2-C14-H14C	110.2(14)	C20-C23-H23C	114(2)
H14A-C14-H14C	109(2)	H23A-C23-H23C	110(3)
H14B-C14-H14C	110(2)	H23B-C23-H23C	104(3)
Si2-C15-H15A	108.6(16)	Si3-C24-H24A	110.1(14)
Si2-C15-H15B	113.3(17)	Si3-C24-H24B	108.2(14)
H15A-C15-H15B	108(2)	H24A-C24-H24B	108(2)
Si2-C15-H15C	111.6(18)	Si3-C24-H24C	111.3(16)
H15A-C15-H15C	107(2)	H24A-C24-H24C	106(2)
H15B-C15-H15C	108(2)	H24B-C24-H24C	113(2)
C4-C16-C17	111.4(2)	Si3-C25-H25A	109.4(17)
C4-C16-C19	111.99(19)	Si3-C25-H25B	110.5(14)
C17-C16-C19	109.6(2)	H25A-C25-H25B	108(2)

Si3-C25-H25C	111.9(14)
H25A-C25-H25C	112(2)
H25B-C25-H25C	105(2)
Si3-C26-H26A	111.4(15)
Si3-C26-H26B	113.0(17)
H26A-C26-H26B	111(2)
Si3-C26-H26C	112.0(15)
H26A-C26-H26C	104(2)
H26B-C26-H26C	105(2)
$C28^{(ii)}$-C27-C28	119.7(4)
C28-C27-H27	120.17(18)
C27-C28-C29	120.1(3)
C27-C28-H28	120.2(16)
C29-C28-H28	119.5(16)
C28-C29-C30	121.4(3)
C28-C29-H29	119.2(16)
C30-C29-H29	119.4(16)
$C29^{(ii)}$-C30-C29	117.3(3)
C29-C30-C31	121.33(16)
C30-C31-H31A	109(3)
C30-C31-H31B	106(3)
H31A-C31-H31B	108(3)
C30-C31-H31C	111(3)
H31A-C31-H31C	110(3)
H31B-C31-H31C	113(4)

Table 18. Crystal data and structure refinement for $[RpZr]_3(\mu_3\text{-}H)_2(\mu_2\text{-}H)_3$.

Empirical formula	$C_{42}H_{59}Si_6Zr_3$
Formula weight	1006.11
Crystallization Solvent	Benzene
Crystal Habit	Prism
Crystal size	0.52 x 0.26 x 0.10 mm^3
Crystal color	Dichroic, dark brown-green / colorless

Data Collection

Preliminary Photos		
Type of diffractometer	CAD-4	
Wavelength	0.71073 Å MoKa	
Data Collection Temperature	84 K	
Theta range for reflections used in lattice determination	15 to 17°	
Unit cell dimensions	a = 15.804(4) Å b = 15.804(4) Å c = 17.018(3) Å	a= 90° b= 90° g = 90°
Volume	4250.5(17) $Å^3$	
Z	4	
Crystal system	Tetragonal	
Space group	P4(3)2(1)2	
Density (calculated)	1.572 Mg/m^3	
F(000)	2060	
Theta range for data collection	1.5 to 25°	
Completeness to theta = 25°	100.0 %	
Index ranges	0<=h<=18, -18<=k<=18, 0<=l<=20	
Data collection scan type	scans	
Reflections collected	13292	
Independent reflections	3746 [R_{int}= 0.0206; GOF_{merge}=]	
Absorption coefficient	0.921 mm^{-1}	
Absorption correction	None	
Number of standards	3 reflections measured every 75min.	
Variation of standards	0, within experimental error%.	

Structure solution and Refinement

Structure solution program	SHELXS-97 (Sheldrick, 1990)
Primary solution method	direct
Secondary solution method	difmap
Hydrogen placement	difmap
Structure refinement program	SHELXL-97 (Sheldrick, 1997)
Refinement method	Full-matrix least-squares on F^2
Data / restraints / parameters	3746 / 0 / 349
Treatment of hydrogen atoms	all
Goodness-of-fit on F^2	1.627
Final R indices [I>2s(I)]	R1 = 0.0163, wR2 = 0.0403
R indices (all data)	R1 = 0.0168, wR2 = 0.0405
Type of weighting scheme used	calc
Weighting scheme used	calc w=1/^2^(Fo^2^)
Max shift/error	0.043
Average shift/error	0.002
Absolute structure parameter	0.00(2)
Largest diff. peak and hole	0.252 and -0.308 e.$Å^{-3}$

Table 19. Bond lengths [Å] and angles [°] for [RpZr]$_3$(μ_3-H)$_2$(μ_2-H)$_3$.

Zr1-Cp1C	2.2593
Zr1-Cp2C	2.2622
Zr1-Cp1P	2.2543(11)
Zr1-Cp2P	2.2591(11)
Zr1-Zr2	3.2687(9)
Zr1-Zr1#1	3.3443(9)
Zr1-H0	2.17(2)
Zr1-H1	1.93(2)
Zr1-H2	1.96(1)
H0-H0#1	1.85(4)
Zr1-C1	2.520(2)
Zr1-C2	2.504(2)
Zr1-C3	2.564(2)
Zr1-C4	2.635(2)
Zr1-C5	2.589(2)
Zr1-C6	2.521(2)
Zr1-C7	2.532(2)
Zr1-C8	2.578(2)
Zr1-C9	2.625(2)
Zr1-C10	2.570(2)
Zr2-Cp3C	2.2726
Zr2-Cp3P	2.2690(10)

Zr2-Zr1#1	3.2687(9)
Zr2-H0	2.04(2)
Zr2-H1	1.95(2)
Zr2-C15	2.525(2)
Zr2-C16	2.573(2)
Zr2-C17	2.634(2)
Zr2-C18	2.597(2)
Zr2-C19	2.537(2)
Si1-C11	1.862(2)
Si1-C12	1.869(2)
Si1-C6	1.871(2)
Si1-C1	1.882(2)
Si2-C14	1.858(2)
Si2-C13	1.868(2)
Si2-C2	1.871(2)
Si2-C7	1.879(2)
Si3-C21	1.862(2)
Si3-C20	1.865(2)
Si3-C15	1.873(2)
Si3-C19#1	1.877(2)
C1-C5	1.422(3)
C1-C2	1.447(3)
C2-C3	1.431(3)
C3-C4	1.410(3)
C3-H3	0.88(2)
C4-C5	1.402(3)
C4-H4	0.83(2)
C5-H5	0.97(2)
C6-C10	1.432(3)
C6-C7	1.444(3)
C7-C8	1.422(3)
C8-C9	1.412(3)
C8-H8	0.91(2)
C9-C10	1.404(3)
C9-H9	0.95(3)
C10-H10	0.95(2)
C11-H11A	0.86(2)
C11-H11B	0.94(3)
C11-H11C	0.91(3)
C12-H12A	0.92(3)
C12-H12B	0.83(3)
C12-H12C	0.85(3)
C13-H13A	0.93(3)
C13-H13B	1.00(3)
C13-H13C	0.85(3)
C14-H14A	0.88(3)
C14-H14B	0.88(3)
C14-H14C	0.92(3)
C15-C16	1.425(3)
C15-C19	1.443(3)
C16-C17	1.404(3)
C16-H16	0.94(2)
C17-C18	1.401(3)
C17-H17	0.89(2)

C18-C19	1.426(3)
C18-H18	0.90(2)
C19-Si3#1	1.877(2)
C20-H20A	0.88(3)
C20-H20B	0.90(3)
C20-H20C	0.92(3)
C21-H21A	0.87(3)
C21-H21B	0.95(3)
C21-H21C	1.00(3)

Cp1C-Zr1-Cp2C	116.630(17)
Cp1C-Zr1-Zr2	122.217(10)
Cp2C-Zr1-Zr2	113.452(9)
Cp1C-Zr1-Zr1#1	111.566(10)
Cp2C-Zr1-Zr1#1	121.781(13)
Zr2-Zr1-Zr1#1	59.232(4)
Cp1C-Zr1-H0	96.4(6)
Cp2C-Zr1-H0	146.8(6)
Zr2-Zr1-H0	37.6(6)
Zr1#1-Zr1-H0	38.8(6)
Cp1C-Zr1-H1	110.0(7)
Cp2C-Zr1-H1	100.3(6)
Zr2-Zr1-H1	32.8(6)
Zr1#1-Zr1-H1	91.9(6)
H0-Zr1-H1	63.0(8)
Cp1C-Zr1-H2	95.9(4)
Cp2C-Zr1-H2	111.7(3)
Zr2-Zr1-H2	90.8(7)
Zr1#1-Zr1-H2	31.6(7)
H0-Zr1-H2	64.9(8)
H1-Zr1-H2	123.5(9)
Cp1P-?-Cp2P	70.12(6)
Cp3C-Zr2-Zr1#1	114.354(8)
Cp3C-Zr2-Zr1	119.931(8)
Zr1#1-Zr2-Zr1	61.536(8)
Cp3C-Zr2-H0	148.8(6)
Zr1#1-Zr2-H0	39.6(7)
Zr1-Zr2-H0	40.5(7)
Cp3C-Zr2-H1	111.2(6)
Zr1#1-Zr2-H1	93.7(6)
Zr1-Zr2-H1	32.3(6)
H0-Zr2-H1	65.1(10)
Cp3P#1-?-Cp3P	70.46(6)
C11-Si1-C12	107.82(11)
C11-Si1-C6	108.87(10)
C12-Si1-C6	116.01(10)
C11-Si1-C1	112.66(10)
C12-Si1-C1	117.83(11)
C6-Si1-C1	92.95(9)
C14-Si2-C13	110.17(11)
C14-Si2-C2	111.37(11)
C13-Si2-C2	112.94(10)
C14-Si2-C7	110.60(10)
C13-Si2-C7	117.83(10)

C2-Si2-C7	92.91(9)
C21-Si3-C20	107.35(11)
C21-Si3-C15	111.48(10)
C20-Si3-C15	115.63(11)
C21-Si3-C19#1	109.93(11)
C20-Si3-C19#1	118.91(11)
C15-Si3-C19#1	93.04(9)
C5-C1-C2	106.76(18)
C5-C1-Si1	124.75(16)
C2-C1-Si1	123.07(15)
C3-C2-C1	106.87(18)
C3-C2-Si2	127.32(16)
C1-C2-Si2	121.29(15)
C4-C3-C2	108.91(19)
C4-C3-H3	129.4(14)
C2-C3-H3	121.7(14)
C5-C4-C3	107.82(19)
C5-C4-H4	126.2(17)
C3-C4-H4	125.9(17)
C4-C5-C1	109.64(19)
C4-C5-H5	127.0(12)
C1-C5-H5	123.4(12)
C10-C6-C7	107.25(18)
C10-C6-Si1	125.13(16)
C7-C6-Si1	122.37(15)
C8-C7-C6	106.81(18)
C8-C7-Si2	125.38(16)
C6-C7-Si2	122.19(15)
C9-C8-C7	109.14(19)
C9-C8-H8	127.4(14)
C7-C8-H8	123.5(14)
C10-C9-C8	108.14(19)
C10-C9-H9	127.9(15)
C8-C9-H9	123.9(15)
C9-C10-C6	108.64(18)
C9-C10-H10	122.7(14)
C6-C10-H10	128.7(14)
Si1-C11-H11A	111.7(15)
Si1-C11-H11B	109.0(17)
H11A-C11-H11B	100(2)
Si1-C11-H11C	110.0(17)
H11A-C11-H11C	117(2)
H11B-C11-H11C	108(2)
Si1-C12-H12A	110.8(18)
Si1-C12-H12B	113(2)
H12A-C12-H12B	107(3)
Si1-C12-H12C	111(2)
H12A-C12-H12C	108(3)
H12B-C12-H12C	106(3)
Si2-C13-H13A	112.0(18)
Si2-C13-H13B	109.9(15)
H13A-C13-H13B	104(2)
Si2-C13-H13C	111.1(17)
H13A-C13-H13C	114(2)

H13B-C13-H13C	106(2)
Si2-C14-H14A	110(2)
Si2-C14-H14B	109.4(17)
H14A-C14-H14B	104(2)
Si2-C14-H14C	114(2)
H14A-C14-H14C	118(3)
H14B-C14-H14C	101(2)
C16-C15-C19	107.2(2)
C16-C15-Si3	125.97(17)
C19-C15-Si3	121.67(17)
C17-C16-C15	108.9(2)
C17-C16-H16	125.6(14)
C15-C16-H16	125.6(14)
C18-C17-C16	108.08(18)
C18-C17-H17	125.6(12)
C16-C17-H17	126.3(12)
C17-C18-C19	109.3(2)
C17-C18-H18	125.6(14)
C19-C18-H18	125.0(14)
C18-C19-C15	106.5(2)
C18-C19-Si3#1	123.93(17)
C15-C19-Si3#1	124.05(17)
Si3-C20-H20A	108.7(17)
Si3-C20-H20B	114.4(19)
H20A-C20-H20B	108(3)
Si3-C20-H20C	108.7(17)
H20A-C20-H20C	99(2)
H20B-C20-H20C	117(3)
Si3-C21-H21A	112.9(19)
Si3-C21-H21B	109.3(16)
H21A-C21-H21B	111(2)
Si3-C21-H21C	109.7(15)
H21A-C21-H21C	108(2)
H21B-C21-H21C	106(2)

Symmetry transformations used to generate equivalent atoms:
#1 -y+1,-x+1,-z+1/2

Table 19. Crystal Data and Structure Refinement for $Cp_2Zr(CH_2CMe_3)(CH_3)$.

Empirical formula	$C_{16}H_{24}Zr$
Formula weight	307.57
Crystallization solvent	diethyl ether
Crystal habit	column
Crystal size	0.40 x 0.30 x 0.23 mm^3
Crystal color	yellow

Data Collection

Preliminary photograph(s)	rotation
Type of diffractometer	Bruker SMART 1000 ccd

Wavelength	0.71073 Å MoKa	
Data collection temperature	98 K	
Theta range for 6370 reflections used in lattice determination	2.5 to 28.6°	
Unit cell dimensions	a = 8.0303(3) Å b = 16.5205(7) Å c = 21.9315(9) Å	a= 90° b= 90° g = 90°
Volume	2909.5(2) $Å^3$	
Z	8	
Crystal system	orthorhombic	
Space group	Pbca	
Density (calculated)	1.404 g/cm^3	
F(000)	1280	
Theta range for data collection	1.86 to 28.77°	
Completeness to theta = 28.77°	95.5 %	
Index ranges	-10<=h<=10, -21<=k<=21, -29<=l<=28	
Data collection scan type	w scans at 3 fixed f values	
Reflections collected	27381	
Independent reflections	3612 [R_{int}= 0.0374]	
Absorption coefficient	0.734 mm^{-1}	
Absorption correction	SADABS v2.0 (beta)	
Max. and min. transmission	1.000 and 0.895	
Number of standards	first 90 scans recollected at end of runs	
Variation of standards	within counting statistics	

Structure Solution and Refinement

Structure solution program	SHELXS-97 (Sheldrick, 1990)
Primary solution method	direct methods
Secondary solution method	difference map
Hydrogen placement	calculated
Structure refinement program	SHELXL-97 (Sheldrick, 1997)
Refinement method	full-matrix least-squares on F^2
Data / restraints / parameters	3612 / 0 / 250
Treatment of hydrogen atoms	all parameters refined
Goodness-of-fit on F^2	2.581
Final R indices [I>2s(I), 3299 reflections]	R1 = 0.0219, wR2 = 0.0502
R indices (all data)	R1 = 0.0247, wR2 = 0.0508

Type of weighting scheme used	sigma
Weighting scheme used	$w=1/s^2(Fo^2)$
Max shift/error	0.065
Average shift/error	0.003
Largest diff. peak and hole	0.506 and -0.372 e.Å^{-3}

Special Refinement Details

A section was cut from a yellow column and mounted on a glass fiber with Paratone-N oil. Three runs of data were collected with 20 second long, –0.20° wide ω–scans at three values of φ (0, 120, and 240°) with the detector 5 cm (nominal) distant at a θ of -28°. The initial cell for data reduction was calculated from just under 1000 reflections chosen from throughout the data frames. For data processing with SAINT v6.02, all defaults were used, except: box size optimization was enabled, periodic orientation matrix updating was disabled, the instrument error was set to zero, no Laue class integration restraints were used, the model profiles from all nine areas were blended, and for the post-integration global least squares refinement, no constraints were applied. The data were corrected with SADABS v. 2.0 (beta) using default parameters except that the scale factor esd was set to 0. On the three .raw files the g value converged to 0.0428. No decay correction was needed.

There is one molecule in the asymmetric unit.

No reflections were specifically omitted from the final processed dataset; 2095 reflections were rejected, with 33 space group-absence violations and 32 inconsistent equivalents. Refinement of F^2 was against ALL reflections. The weighted R-factor (*w*R) and goodness of fit (S) are based on F^2, conventional R-factors (R) are based on F, with F set to zero for negative F^2. The threshold expression of $F^2 > 2\sigma(F^2)$ is used only for calculating R-factors(gt) etc. and is not relevant to the choice of reflections for refinement.

Table 20. Bond lengths [Å] and angles [°] for $Cp_2Zr(CH_2CMe_3)(CH_3)$.

Zr-Cp1	2.232
Zr-Cp2	2.234
Zr···Pln1	2.3209(6)
Zr···Pln2	2.2335(5)
Zr-C12	2.2719(12)
Zr-C11	2.2980(13)
Zr-C1	2.4990(13)
Zr-C5	2.5067(13)
Zr-C10	2.5184(13)
Zr-C9	2.5311(12)
Zr-C7	2.5391(13)
Zr-C8	2.5400(13)
Zr-C6	2.5400(13)
Zr-C2	2.5424(12)
Zr-C4	2.5507(13)
Zr-C3	2.5638(12)
C1-C2	1.4091(19)
C1-C5	1.413(2)

C1-H1	0.922(16)
C2-C3	1.399(2)
C2-H2	0.956(15)
C3-C4	1.4089(18)
C3-H3	0.895(16)
C4-C5	1.4035(19)
C4-H4	0.922(16)
C5-H5	0.945(16)
C6-C7	1.400(2)
C6-C10	1.411(2)
C6-H6	0.923(15)
C7-C8	1.4097(19)
C7-H7	0.951(15)
C8-C9	1.3999(19)
C8-H8	0.962(16)
C9-C10	1.409(2)
C9-H9	0.950(15)
C10-H10	0.942(15)
C11-H11A	0.933(16)
C11-H11B	0.940(16)
C11-H11C	0.912(17)
C12-C13	1.5418(17)
C12-H12A	0.989(14)
C12-H12B	0.964(14)
C13-C15	1.5280(18)
C13-C16	1.5285(18)
C13-C14	1.5354(18)
C14-H14A	0.960(15)
C14-H14B	0.961(16)
C14-H14C	0.911(17)
C15-H15A	0.931(16)
C15-H15B	0.960(14)
C15-H15C	0.979(15)
C16-H16A	1.053(15)
C16-H16B	0.951(15)
C16-H16C	0.939(15)

Cp1-Zr-Cp2	130.6
Cp1-Zr-C11	103.4
Cp1-Zr-C12	107.8
Pln1-Pln2	51.42(5)
C12-Zr-C11	94.99(5)
C12-Zr-C1	108.70(5)
C11-Zr-C1	130.53(5)
C12-Zr-C5	135.63(4)
C11-Zr-C5	102.33(5)
C1-Zr-C5	32.78(5)
C12-Zr-C10	135.08(4)
C11-Zr-C10	89.68(5)
C1-Zr-C10	101.45(5)
C5-Zr-C10	86.00(5)
C12-Zr-C9	105.67(5)
C11-Zr-C9	77.53(5)
C1-Zr-C9	131.79(5)

C5-Zr-C9	117.79(4)
C10-Zr-C9	32.41(5)
C12-Zr-C7	92.17(4)
C11-Zr-C7	130.35(4)
C1-Zr-C7	92.39(4)
C5-Zr-C7	106.12(5)
C10-Zr-C7	53.43(4)
C9-Zr-C7	53.32(4)
C12-Zr-C8	81.94(5)
C11-Zr-C8	100.75(5)
C1-Zr-C8	124.62(4)
C5-Zr-C8	132.66(4)
C10-Zr-C8	53.38(5)
C9-Zr-C8	32.05(4)
C7-Zr-C8	32.23(4)
C12-Zr-C6	123.99(4)
C11-Zr-C6	122.08(5)
C1-Zr-C6	79.28(4)
C5-Zr-C6	79.55(4)
C10-Zr-C6	32.40(5)
C9-Zr-C6	53.44(4)
C7-Zr-C6	32.01(4)
C8-Zr-C6	53.20(4)
C12-Zr-C2	82.05(4)
C11-Zr-C2	117.53(5)
C1-Zr-C2	32.45(4)
C5-Zr-C2	53.69(4)
C10-Zr-C2	133.85(5)
C9-Zr-C2	162.92(5)
C7-Zr-C2	112.11(4)
C8-Zr-C2	139.49(4)
C6-Zr-C2	109.56(4)
C12-Zr-C4	119.26(4)
C11-Zr-C4	76.95(5)
C1-Zr-C4	53.59(4)
C5-Zr-C4	32.21(4)
C10-Zr-C4	105.34(4)
C9-Zr-C4	129.56(4)
C7-Zr-C4	138.29(5)
C8-Zr-C4	158.72(4)
C6-Zr-C4	109.72(4)
C2-Zr-C4	53.07(4)
C12-Zr-C3	88.21(4)
C11-Zr-C3	86.00(5)
C1-Zr-C3	53.31(4)
C5-Zr-C3	53.29(4)
C10-Zr-C3	136.71(4)
C9-Zr-C3	159.18(5)
C7-Zr-C3	143.37(4)
C8-Zr-C3	168.47(5)
C6-Zr-C3	130.43(4)
C2-Zr-C3	31.79(4)
C4-Zr-C3	31.98(4)
C2-C1-C5	107.83(12)

C2-C1-Zr	75.47(8)
C5-C1-Zr	73.91(8)
C2-C1-H1	124.2(9)
C5-C1-H1	128.0(9)
Zr-C1-H1	117.9(9)
C3-C2-C1	108.03(12)
C3-C2-Zr	74.94(7)
C1-C2-Zr	72.08(7)
C3-C2-H2	126.3(10)
C1-C2-H2	125.6(10)
Zr-C2-H2	116.7(9)
C2-C3-C4	108.28(12)
C2-C3-Zr	73.26(7)
C4-C3-Zr	73.50(7)
C2-C3-H3	128.8(10)
C4-C3-H3	122.9(10)
Zr-C3-H3	116.7(10)
C5-C4-C3	107.95(12)
C5-C4-Zr	72.17(7)
C3-C4-Zr	74.52(7)
C5-C4-H4	126.3(9)
C3-C4-H4	125.8(9)
Zr-C4-H4	117.3(10)
C4-C5-C1	107.91(12)
C4-C5-Zr	75.62(7)
C1-C5-Zr	73.31(8)
C4-C5-H5	126.2(9)
C1-C5-H5	125.9(9)
Zr-C5-H5	117.0(9)
C7-C6-C10	107.92(12)
C7-C6-Zr	73.96(7)
C10-C6-Zr	72.96(8)
C7-C6-H6	127.3(9)
C10-C6-H6	124.7(9)
Zr-C6-H6	119.5(9)
C6-C7-C8	108.08(12)
C6-C7-Zr	74.03(8)
C8-C7-Zr	73.92(8)
C6-C7-H7	126.7(9)
C8-C7-H7	125.2(9)
Zr-C7-H7	119.9(9)
C9-C8-C7	108.14(12)
C9-C8-Zr	73.63(7)
C7-C8-Zr	73.85(7)
C9-C8-H8	126.8(9)
C7-C8-H8	125.0(9)
Zr-C8-H8	116.9(8)
C8-C9-C10	107.97(12)
C8-C9-Zr	74.33(7)
C10-C9-Zr	73.30(7)
C8-C9-H9	126.5(9)
C10-C9-H9	125.5(9)
Zr-C9-H9	118.4(9)
C9-C10-C6	107.88(12)

C9-C10-Zr	74.29(7)
C6-C10-Zr	74.64(7)
C9-C10-H10	124.5(9)
C6-C10-H10	127.5(9)
Zr-C10-H10	114.9(8)
Zr-C11-H11A	112.6(10)
Zr-C11-H11B	109.8(9)
H11A-C11-H11B	105.6(13)
Zr-C11-H11C	109.9(10)
H11A-C11-H11C	108.8(15)
H11B-C11-H11C	110.0(13)
C13-C12-Zr	141.94(9)
C13-C12-H12A	108.2(8)
Zr-C12-H12A	96.8(8)
C13-C12-H12B	109.2(8)
Zr-C12-H12B	91.6(8)
H12A-C12-H12B	103.7(11)
C15-C13-C16	108.62(11)
C15-C13-C14	108.62(10)
C16-C13-C14	107.61(11)
C15-C13-C12	110.72(10)
C16-C13-C12	111.48(10)
C14-C13-C12	109.69(11)
C13-C14-H14A	110.2(9)
C13-C14-H14B	112.1(9)
H14A-C14-H14B	110.8(12)
C13-C14-H14C	110.2(9)
H14A-C14-H14C	105.7(13)
H14B-C14-H14C	107.6(13)
C13-C15-H15A	112.7(10)
C13-C15-H15B	109.1(8)
H15A-C15-H15B	106.9(13)
C13-C15-H15C	110.2(9)
H15A-C15-H15C	111.3(12)
H15B-C15-H15C	106.3(12)
C13-C16-H16A	110.8(8)
C13-C16-H16B	111.5(9)
H16A-C16-H16B	107.2(12)
C13-C16-H16C	112.6(9)
H16A-C16-H16C	104.7(12)
H16B-C16-H16C	109.7(12)

Table 21. Crystal Data and Structure Analysis Details for iPrSpTa(η^2-$CH_2CHC_6H_5$)(H).

Empirical formula	$C_{23}H_{29}SiTa$
Formula weight	514.50
Crystallization solvent	petroleum ether
Crystal habit	needle
Crystal size	0.12 x 0.08 x 0.04 mm

Crystal color	yellow

Data Collection

Preliminary photograph(s)	rotation	
Type of diffractometer	Bruker SMART 1000 ccd	
Wavelength	0.71073 Å MoKa	
Data collection temperature	98 K	
Theta range for 6300 reflections used in lattice determination	2.8 to 24.6°	
Unit cell dimensions	a = 14.5277(9) Å b = 6.6809(4) Å c = 21.0147(12) Å	a= 90° b= 99.3310(10)° g = 90°
Volume	2012.7(2) $Å^3$	
Z	4	
Crystal system	monoclinic	
Space group	P2/n (#13)	
Density (calculated)	1.698 g/cm^3	
F(000)	1016	
Theta range for data collection	1.59 to 27.50°	
Completeness to theta = 27.50°	99.7 %	
Index ranges	-18 £ h £ 18, -8 £ k £ 8, -27 £ l £ 27	
Data collection scan type	w scans at 6 fixed f values	
Reflections collected	34421	
Independent reflections	4617 [R_{int}= 0.1013]	
Absorption coefficient	5.524 mm^{-1}	
Absorption correction	empirical	
Max. and min. transmission	1.00 and 0.79	
Number of standards	first scans recollected at end of runs	
Variation of standards	within counting statistics	

Structure Solution and Refinement

Primary solution method	direct methods
Secondary solution method	difference map
Hydrogen placement	calculated
Refinement method	full-matrix least-squares on F^2
Data / restraints / parameters	4617 / 0 / 226

Treatment of hydrogen atoms attached atom	not refined; U_{iso}'s set at 120% U_{eq} of the
Goodness-of-fit on F^2	1.584
Final R indices [I>2s(I), 3186 reflections]	R1 = 0.0420, wR2 = 0.0655
R indices (all data)	R1 = 0.0837, wR2 = 0.0719
Type of weighting scheme used	sigma
Weighting scheme used	$w=1/s^2(Fo^2)$
Max shift/error	0.024
Average shift/error	0.001
Largest diff. peak and hole	1.920 and -1.842 e.Å^{-3}

Programs Used

Cell refinement	Bruker SAINT v6.02
Data collection	Bruker SMART v5.054
Data reduction	Bruker SAINT v6.02
Absorption correction	SADABS V2.0 beta
Structure solution	SHELXS-97 (Sheldrick, 1990)
Structure refinement	SHELXL-97 (Sheldrick, 1997)

Special Refinement Details

A small fragment extracted from a yellow rosette was mounted on a glass fiber with Paratone-N oil. Six runs of data were collected with 20 second long, –0.20° wide ω–scans at six values of φ (0, 120, 240, 60, 180 and 300°) with the detector 5 cm (nominal) distant at a θ of -28°. The initial cell for data reduction was calculated from just under 1000 reflections chosen from throughout the data frames. There were a number of unindexed reflections, possibly indicating a twin. For data processing with SAINT v6.02, all defaults were used, except: box size optimization was enabled, periodic orientation matrix updating was disabled, the instrument error was set to zero, no Laue class integration restraints were used, the model profiles from all nine areas were blended, and for the post-integration global least squares refinement, no constraints were applied. The data were corrected with SADABS v. 2.0 (beta) using default parameters except that the scale factor esd was set to 0. No decay correction was needed.

There is one molecule in the asymmetric unit.

No reflections were specifically omitted from the final processed dataset; the dataset was truncated at a 2θ of 55°, 2289 reflections were rejected, with 2 space group-absence violations and 0 inconsistent equivalents. Refinement of F^2 was against all reflections. The weighted R-factor (*w*R) and goodness of fit (S) are based on F^2, conventional R-factors (R) are based on F, with F set to zero for negative F^2. The threshold expression of $F^2 > 2\sigma(F^2)$ is used only for calculating R-factors(gt) etc. and is not relevant to the choice of reflections for refinement.

There is one molecule in the asymmetric unit. The hydride atom was not located in a difference map and was excluded from the refinement. There are numerous large peaks in the final difference map; the first twenty are greater than |1| e·Å^{-3} with the two largest being 1.92 e·Å^{-3} (1.23 Å from H13) and –1.84 e·Å^{-3} (1.77 Å from H16).

Table 22. Bond lengths [Å] and angles [°] for iPrSpTa(η^2-$CH_2CHC_6H_5$)(H).

Ta-Cp1[a]	2.071	C13-C15	1.538(8)
Ta-Cp2[b]	2.066	C13-H13	1.0000
Ta-Cen[c]	2.173	C14-H14A	0.9800
Ta···Pln1[d]	2.068(3)	C14-H14B	0.9800
Ta···Pln2[e]	2.061(3)	C14-H14C	0.9800
Ta-C16	2.274(7)	C15-H15A	0.9800
Ta-C17	2.298(7)	C15-H15B	0.9800
Ta-C6	2.344(6)	C15-H15C	0.9800
Ta-C10	2.347(6)	C16-C17	1.420(9)
Ta-C5	2.352(6)	C16-H16A	0.9900
Ta-C2	2.354(6)	C16-H16B	0.9900
Ta-C7	2.359(6)	C17-C18	1.474(9)
Ta-C1	2.371(6)	C17-H17	1.0000
Ta-C9	2.436(6)	C18-C23	1.389(9)
Ta-C4	2.437(6)	C18-C19	1.412(9)
Ta-C3	2.449(6)	C19-C20	1.373(10)
Ta-C8	2.482(6)	C19-H19	0.9500
Si-C11	1.826(7)	C20-C21	1.373(11)
Si-C12	1.844(7)	C20-H20	0.9500
Si-C6	1.867(7)	C21-C22	1.383(11)
Si-C1	1.868(7)	C21-H21	0.9500
C1-C5	1.419(9)	C22-C23	1.383(9)
C1-C2	1.432(8)	C22-H22	0.9500
C2-C3	1.412(9)	C23-H23	0.9500
C2-H2	1.0000		
C3-C4	1.371(9)	Cp1-Ta-Cp2	132.8
C3-H3	1.0000	Cp1-Ta-C16	105.5
C4-C5	1.417(9)	Cp1-Ta-C17	112.3
C4-H4	1.0000	Cp2-Ta-C16	105.6
C5-H5	1.0000	Cp2-Ta-C17	113.9
C6-C10	1.417(8)	Cp1-Ta-Cen	109.9
C6-C7	1.433(8)	Cp2-Ta-Cen	110.8
C7-C8	1.422(8)	Pln1···Pln2	54.1(3)
C7-H7	1.0000	C16-Ta-C17	36.2(2)
C8-C9	1.404(9)	C11-Si-C12	113.2(3)
C8-C13	1.498(9)	C11-Si-C6	113.5(3)
C9-C10	1.434(8)	C12-Si-C6	110.8(3)
C9-H9	1.0000	C11-Si-C1	112.2(3)
C10-H10	1.0000	C12-Si-C1	112.2(3)
C11-H11A	0.9800	C6-Si-C1	93.5(3)
C11-H11B	0.9800	C5-C1-C2	104.5(6)
C11-H11C	0.9800	C5-C1-Si	126.6(5)
C12-H12A	0.9800	C2-C1-Si	121.8(5)
C12-H12B	0.9800	C3-C2-C1	110.0(6)
C12-H12C	0.9800	C3-C2-H2	124.7
C13-C14	1.515(8)	C1-C2-H2	124.7

C4-C3-C2	107.2(6)	C17-C16-Ta	72.8(4)
C4-C3-H3	126.3	C17-C16-H16A	116.3
C2-C3-H3	126.3	Ta-C16-H16A	116.3
C3-C4-C5	109.2(6)	C17-C16-H16B	116.3
C3-C4-H4	125.4	Ta-C16-H16B	116.3
C5-C4-H4	125.4	H16A-C16-H16B	113.3
C4-C5-C1	108.9(6)	C16-C17-C18	125.8(7)
C4-C5-H5	125.1	C16-C17-Ta	71.0(4)
C1-C5-H5	125.1	C18-C17-Ta	120.2(4)
C10-C6-C7	105.8(5)	C16-C17-H17	111.3
C10-C6-Si	126.4(5)	C18-C17-H17	111.3
C7-C6-Si	122.2(5)	Ta-C17-H17	111.3
C8-C7-C6	110.3(6)	C23-C18-C19	116.7(7)
C8-C7-H7	124.5	C23-C18-C17	122.9(7)
C6-C7-H7	124.5	C19-C18-C17	120.3(7)
C9-C8-C7	106.2(6)	C20-C19-C18	121.4(7)
C9-C8-C13	124.9(6)	C20-C19-H19	119.3
C7-C8-C13	128.7(6)	C18-C19-H19	119.3
C8-C9-C10	109.2(6)	C19-C20-C21	120.9(8)
C8-C9-H9	125.3	C19-C20-H20	119.6
C10-C9-H9	125.3	C21-C20-H20	119.6
C6-C10-C9	108.5(6)	C20-C21-C22	118.6(8)
C6-C10-H10	125.4	C20-C21-H21	120.7
C9-C10-H10	125.4	C22-C21-H21	120.7
Si-C11-H11A	109.5	C23-C22-C21	121.0(8)
Si-C11-H11B	109.5	C23-C22-H22	119.5
H11A-C11-H11B	109.5	C21-C22-H22	119.5
Si-C11-H11C	109.5	C22-C23-C18	121.2(8)
H11A-C11-H11C	109.5	C22-C23-H23	119.4
H11B-C11-H11C	109.5	C18-C23-H23	119.4
Si-C12-H12A	109.5		
Si-C12-H12B	109.5		
H12A-C12-H12B	109.5		
Si-C12-H12C	109.5		
H12A-C12-H12C	109.5		
H12B-C12-H12C	109.5		
C8-C13-C14	113.0(6)		
C8-C13-C15	109.3(5)		
C14-C13-C15	110.2(6)		
C8-C13-H13	108.1		
C14-C13-H13	108.1		
C15-C13-H13	108.1		
C13-C14-H14A	109.5		
C13-C14-H14B	109.5		
H14A-C14-H14B	109.5		
C13-C14-H14C	109.5		
H14A-C14-H14C	109.5		
H14B-C14-H14C	109.5		
C13-C15-H15A	109.5		
C13-C15-H15B	109.5		
H15A-C15-H15B	109.5		
C13-C15-H15C	109.5		
H15A-C15-H15C	109.5		
H15B-C15-H15C	109.5		

[a] Cp1 is the centroid of atoms C1, C2, C3, C4 and C5
[b] Cp2 is the centroid of atoms C6, C7, C8, C9 and C10
[c] Cen is the centroid of atoms C16 and C17
[d] Pln1 is the best plane through atoms C1, C2, C3, C4 and C5
[e] Pln2 is the best plane through atoms C6, C7, C8, C9 and C10

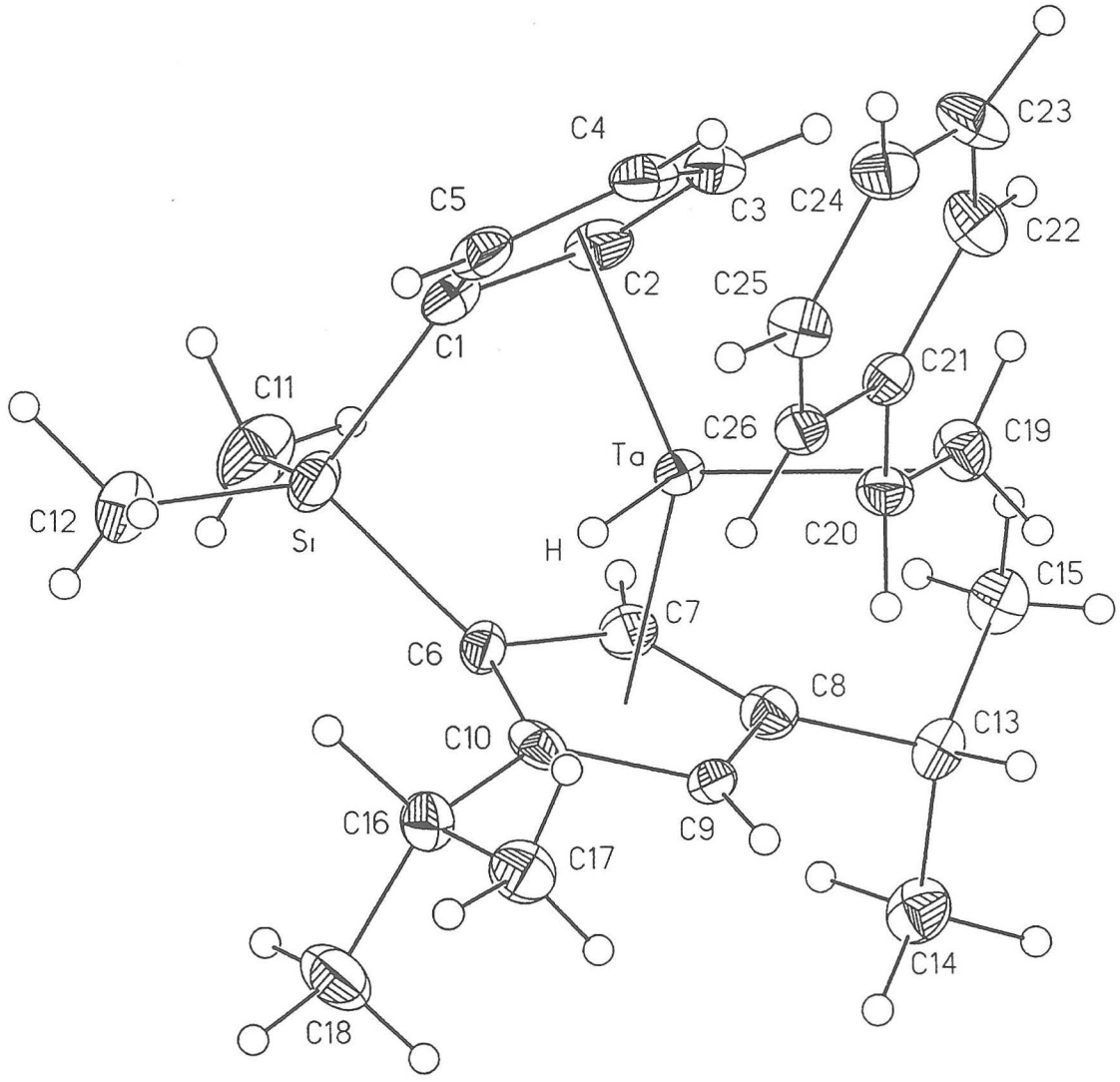

Labeled view of $iPr_2SpTa(\eta^2\text{-}CH_2CHC_6H_5)(H)$.

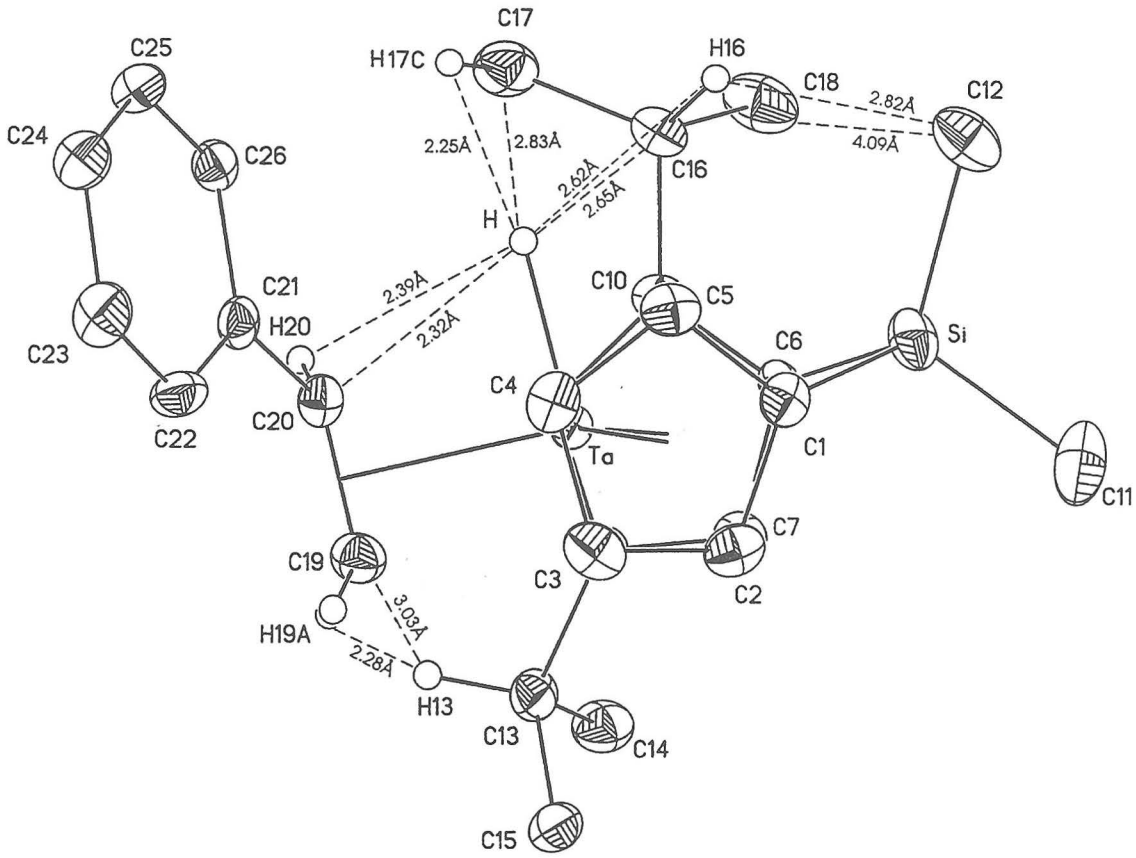

Top view of $iPr_2SpTa(\eta^2\text{-}CH_2CHC_6H_5)(H)$ with selected distances.

Table 23. Crystal data and structure refinement for $iPr_2SpTa(\eta^2\text{-}CH_2CHPh)(H)$.

Empirical formula	$C_{26}\ H_{35}\ Si\ Ta$
Formula weight	556.58
Crystallization Solvent	Petroleum ether
Crystal Habit	Thick blade
Crystal size	$0.33 \times 0.18 \times 0.14\ mm^3$
Crystal color	Yellow

Data Collection

Preliminary Photos		
Type of diffractometer	CCD area detector	
Wavelength	0.71073 Å MoKa	
Data Collection Temperature	95 K	
Theta range for 4398 reflections used in lattice determination	2.34 to 28.19°	
Unit cell dimensions	a = 9.2305(8) Å b = 10.1700(9) Å c = 12.9218(12) Å	a= 90.3360(10)° b= 104.1870(10)° g = 100.4140(10)°
Volume	1155.05(18) $Å^3$	
Z	2	
Crystal system	Triclinic	
Space group	P-1	
Density (calculated)	1.600 Mg/m^3	
F(000)	556	
Data collection program	Bruker SMART	
Theta range for data collection	2.04 to 28.23°	
Completeness to theta = 28.23°	88.8 %	
Index ranges	-11<=h<=12, -13<=k<=13, -17<=l<=16	
Data collection scan type	phi and omega scans	
Data reduction program	Bruker SAINT v6.2	
Reflections collected	10310	
Independent reflections	5071 [R_{int}= 0.0256; GOF_{merge}=]	
Absorption coefficient	4.819 mm^{-1}	
Absorption correction	SADABS	
Max. and min. transmission	1.000 and 0.688	
Number of standards	? reflections measured every ?min.	
Variation of standards	within counting statistics	

Structure solution and Refinement

Structure solution program	SHELXS-97 (Sheldrick, 1990)
Primary solution method	Patterson method
Secondary solution method	Difference Fourier map
Hydrogen placement	Difference Fourier map
Structure refinement program	SHELXL-97 (Sheldrick, 1997)
Refinement method	Full matrix least-squares on F^2
Data / restraints / parameters	5071 / 0 / 389
Treatment of hydrogen atoms	Unrestrained (see special details)
Goodness-of-fit on F^2	2.191
Final R indices [I>2s(I)]	R1 = 0.0259, wR2 = 0.0503
R indices (all data)	R1 = 0.0274, wR2 = 0.0504
Type of weighting scheme used	Sigma
Weighting scheme used	w=1/s^2^(Fo^2^)
Max shift/error	0.015
Average shift/error	0.002
Largest diff. peak and hole	2.328 and -1.763 e.$Å^{-3}$

Table 24. Bond lengths [Å] and angles [°] for $iPr_2SpTa(sty)(H)$.

Ta-C(19)	2.253(4)
Ta-C(20)	2.276(4)
Ta-C(6)	2.355(3)
Ta-C(7)	2.374(3)
Ta-C(1)	2.377(4)
Ta-C(2)	2.380(4)
Ta-C(5)	2.385(3)
Ta-C(10)	2.408(3)
Ta-C(4)	2.414(3)
Ta-C(3)	2.436(4)
Ta-C(9)	2.442(3)
Ta-C(8)	2.454(3)
Ta-H	1.7236
Si-C(11)	1.852(5)
Si-C(12)	1.858(5)
Si-C(1)	1.873(4)
Si-C(6)	1.875(4)
C(1)-C(5)	1.421(5)
C(1)-C(2)	1.435(5)
C(2)-C(3)	1.406(6)
C(2)-H(2)	0.96(4)
C(3)-C(4)	1.407(5)
C(3)-H(3)	0.90(5)
C(4)-C(5)	1.416(6)

C(4)-H(4)	0.98(3)
C(5)-H(5)	0.92(4)
C(6)-C(10)	1.436(5)
C(6)-C(7)	1.441(5)
C(7)-C(8)	1.396(5)
C(7)-H(7)	1.05(4)
C(8)-C(9)	1.422(5)
C(8)-C(13)	1.519(5)
C(9)-C(10)	1.415(5)
C(9)-H(9)	0.85(4)
C(10)-C(16)	1.513(5)
C(11)-H(11A)	0.76(5)
C(11)-H(11B)	1.06(4)
C(11)-H(11C)	0.99(6)
C(12)-H(12A)	1.15(4)
C(12)-H(12B)	0.87(5)
C(12)-H(12C)	0.79(6)
C(13)-C(15)	1.511(5)
C(13)-C(14)	1.533(5)
C(13)-H(13)	0.98(4)
C(14)-H(14A)	0.99(5)
C(14)-H(14B)	1.10(4)
C(14)-H(14C)	1.08(4)
C(15)-H(15A)	0.91(4)
C(15)-H(15B)	0.83(4)
C(15)-H(15C)	0.96(4)
C(16)-C(17)	1.520(6)
C(16)-C(18)	1.540(6)
C(16)-H(16)	1.07(3)
C(17)-H(17A)	0.93(4)
C(17)-H(17B)	1.02(4)
C(17)-H(17C)	0.96(4)
C(18)-H(18A)	0.99(5)
C(18)-H(18B)	1.06(5)
C(18)-H(18C)	0.95(4)
C(19)-C(20)	1.451(5)
C(19)-H(19A)	0.93(4)
C(19)-H(19B)	0.90(4)
C(20)-C(21)	1.478(5)
C(20)-H(20)	0.93(4)
C(21)-C(22)	1.389(5)
C(21)-C(26)	1.409(5)
C(22)-C(23)	1.400(5)
C(22)-H(22)	0.85(4)
C(23)-C(24)	1.379(5)
C(23)-H(23)	1.00(4)
C(24)-C(25)	1.386(5)
C(24)-H(24)	0.95(4)
C(25)-C(26)	1.387(5)
C(25)-H(25)	1.01(4)
C(26)-H(26)	0.94(4)

C(19)-Ta-C(20)	37.37(13)
C(19)-Ta-C(6)	139.59(13)

C(20)-Ta-C(6)	139.78(12)
C(19)-Ta-C(7)	108.78(13)
C(20)-Ta-C(7)	131.88(13)
C(6)-Ta-C(7)	35.49(12)
C(19)-Ta-C(1)	138.38(14)
C(20)-Ta-C(1)	143.05(12)
C(6)-Ta-C(1)	71.45(12)
C(7)-Ta-C(1)	84.71(12)
C(19)-Ta-C(2)	106.68(14)
C(20)-Ta-C(2)	131.84(13)
C(6)-Ta-C(2)	88.02(13)
C(7)-Ta-C(2)	80.33(13)
C(1)-Ta-C(2)	35.10(13)
C(19)-Ta-C(5)	123.66(14)
C(20)-Ta-C(5)	109.65(13)
C(6)-Ta-C(5)	96.09(12)
C(7)-Ta-C(5)	118.42(13)
C(1)-Ta-C(5)	34.72(12)
C(2)-Ta-C(5)	56.88(13)
C(19)-Ta-C(10)	121.69(14)
C(20)-Ta-C(10)	105.50(13)
C(6)-Ta-C(10)	35.08(12)
C(7)-Ta-C(10)	57.40(12)
C(1)-Ta-C(10)	99.00(13)
C(2)-Ta-C(10)	122.67(13)
C(5)-Ta-C(10)	109.22(13)
C(19)-Ta-C(4)	89.81(14)
C(20)-Ta-C(4)	86.26(13)
C(6)-Ta-C(4)	128.29(13)
C(7)-Ta-C(4)	136.72(13)
C(1)-Ta-C(4)	57.90(13)
C(2)-Ta-C(4)	56.68(13)
C(5)-Ta-C(4)	34.32(13)
C(10)-Ta-C(4)	141.81(13)
C(19)-Ta-C(3)	80.89(14)
C(20)-Ta-C(3)	98.27(13)
C(6)-Ta-C(3)	121.86(13)
C(7)-Ta-C(3)	109.39(13)
C(1)-Ta-C(3)	57.59(13)
C(2)-Ta-C(3)	33.92(14)
C(5)-Ta-C(3)	56.37(13)
C(10)-Ta-C(3)	155.65(14)
C(4)-Ta-C(3)	33.72(13)
C(19)-Ta-C(9)	89.00(13)
C(20)-Ta-C(9)	84.72(12)
C(6)-Ta-C(9)	57.22(12)
C(7)-Ta-C(9)	55.82(13)
C(1)-Ta-C(9)	128.57(12)
C(2)-Ta-C(9)	136.15(13)
C(5)-Ta-C(9)	142.65(13)
C(10)-Ta-C(9)	33.91(12)
C(4)-Ta-C(9)	166.62(12)
C(3)-Ta-C(9)	158.24(13)
C(19)-Ta-C(8)	81.67(13)

C(20)-Ta-C(8)	98.34(12)
C(6)-Ta-C(8)	57.94(12)
C(7)-Ta-C(8)	33.58(12)
C(1)-Ta-C(8)	118.25(12)
C(2)-Ta-C(8)	106.96(12)
C(5)-Ta-C(8)	151.67(13)
C(10)-Ta-C(8)	57.07(12)
C(4)-Ta-C(8)	158.54(12)
C(3)-Ta-C(8)	124.94(13)
C(9)-Ta-C(8)	33.76(11)
C(19)-Ta-H	106.5
C(20)-Ta-H	69.2
C(6)-Ta-H	90.2
C(7)-Ta-H	121.6
C(1)-Ta-H	98.0
C(2)-Ta-H	130.0
C(5)-Ta-H	73.7
C(10)-Ta-H	64.7
C(4)-Ta-H	87.3
C(3)-Ta-H	121.0
C(9)-Ta-H	80.3
C(8)-Ta-H	114.0
C(11)-Si-C(12)	112.0(3)
C(11)-Si-C(1)	110.1(2)
C(12)-Si-C(1)	111.9(2)
C(11)-Si-C(6)	110.76(19)
C(12)-Si-C(6)	115.93(19)
C(1)-Si-C(6)	95.00(16)
C(5)-C(1)-C(2)	105.3(3)
C(5)-C(1)-Si	124.6(3)
C(2)-C(1)-Si	123.0(3)
C(5)-C(1)-Ta	72.9(2)
C(2)-C(1)-Ta	72.6(2)
Si-C(1)-Ta	95.69(14)
C(3)-C(2)-C(1)	109.5(3)
C(3)-C(2)-Ta	75.2(2)
C(1)-C(2)-Ta	72.3(2)
C(3)-C(2)-H(2)	126(2)
C(1)-C(2)-H(2)	124(2)
Ta-C(2)-H(2)	123(2)
C(4)-C(3)-C(2)	108.0(4)
C(4)-C(3)-Ta	72.3(2)
C(2)-C(3)-Ta	70.9(2)
C(4)-C(3)-H(3)	131(3)
C(2)-C(3)-H(3)	121(3)
Ta-C(3)-H(3)	121(3)
C(3)-C(4)-C(5)	107.5(3)
C(3)-C(4)-Ta	74.0(2)
C(5)-C(4)-Ta	71.72(19)
C(3)-C(4)-H(4)	117.7(19)
C(5)-C(4)-H(4)	134.8(19)
Ta-C(4)-H(4)	119.7(19)
C(4)-C(5)-C(1)	109.7(3)
C(4)-C(5)-Ta	74.0(2)

C(1)-C(5)-Ta	72.35(19)
C(4)-C(5)-H(5)	128(2)
C(1)-C(5)-H(5)	122(2)
Ta-C(5)-H(5)	115(2)
C(10)-C(6)-C(7)	105.9(3)
C(10)-C(6)-Si	131.7(3)
C(7)-C(6)-Si	116.7(3)
C(10)-C(6)-Ta	74.50(19)
C(7)-C(6)-Ta	73.0(2)
Si-C(6)-Ta	96.39(14)
C(8)-C(7)-C(6)	110.4(3)
C(8)-C(7)-Ta	76.4(2)
C(6)-C(7)-Ta	71.54(19)
C(8)-C(7)-H(7)	128(2)
C(6)-C(7)-H(7)	122(2)
Ta-C(7)-H(7)	123(2)
C(7)-C(8)-C(9)	106.3(3)
C(7)-C(8)-C(13)	126.2(3)
C(9)-C(8)-C(13)	126.6(3)
C(7)-C(8)-Ta	70.06(19)
C(9)-C(8)-Ta	72.67(19)
C(13)-C(8)-Ta	130.7(2)
C(10)-C(9)-C(8)	110.0(3)
C(10)-C(9)-Ta	71.74(18)
C(8)-C(9)-Ta	73.6(2)
C(10)-C(9)-H(9)	119(3)
C(8)-C(9)-H(9)	131(3)
Ta-C(9)-H(9)	122(3)
C(9)-C(10)-C(6)	107.4(3)
C(9)-C(10)-C(16)	125.2(3)
C(6)-C(10)-C(16)	126.7(3)
C(9)-C(10)-Ta	74.36(19)
C(6)-C(10)-Ta	70.42(19)
C(16)-C(10)-Ta	128.3(2)
Si-C(11)-H(11A)	114(4)
Si-C(11)-H(11B)	119(2)
H(11A)-C(11)-H(11B)	105(4)
Si-C(11)-H(11C)	112(3)
H(11A)-C(11)-H(11C)	116(5)
H(11B)-C(11)-H(11C)	89(4)
Si-C(12)-H(12A)	109(2)
Si-C(12)-H(12B)	117(3)
H(12A)-C(12)-H(12B)	113(4)
Si-C(12)-H(12C)	111(4)
H(12A)-C(12)-H(12C)	92(5)
H(12B)-C(12)-H(12C)	112(5)
C(15)-C(13)-C(8)	112.4(3)
C(15)-C(13)-C(14)	110.9(3)
C(8)-C(13)-C(14)	108.1(3)
C(15)-C(13)-H(13)	108(2)
C(8)-C(13)-H(13)	106(2)
C(14)-C(13)-H(13)	111(2)
C(13)-C(14)-H(14A)	113(3)
C(13)-C(14)-H(14B)	112(2)

H(14A)-C(14)-H(14B)	112(3)
C(13)-C(14)-H(14C)	104(2)
H(14A)-C(14)-H(14C)	108(3)
H(14B)-C(14)-H(14C)	108(3)
C(13)-C(15)-H(15A)	110(2)
C(13)-C(15)-H(15B)	114(3)
H(15A)-C(15)-H(15B)	119(4)
C(13)-C(15)-H(15C)	109(2)
H(15A)-C(15)-H(15C)	105(3)
H(15B)-C(15)-H(15C)	99(4)
C(10)-C(16)-C(17)	114.0(3)
C(10)-C(16)-C(18)	107.9(3)
C(17)-C(16)-C(18)	110.7(4)
C(10)-C(16)-H(16)	107.4(18)
C(17)-C(16)-H(16)	112.1(18)
C(18)-C(16)-H(16)	104.1(18)
C(16)-C(17)-H(17A)	99(3)
C(16)-C(17)-H(17B)	115(2)
H(17A)-C(17)-H(17B)	118(3)
C(16)-C(17)-H(17C)	109(2)
H(17A)-C(17)-H(17C)	118(4)
H(17B)-C(17)-H(17C)	99(3)
C(16)-C(18)-H(18A)	111(3)
C(16)-C(18)-H(18B)	115(2)
H(18A)-C(18)-H(18B)	106(4)
C(16)-C(18)-H(18C)	103(2)
H(18A)-C(18)-H(18C)	120(4)
H(18B)-C(18)-H(18C)	103(3)
C(20)-C(19)-Ta	72.2(2)
C(20)-C(19)-H(19A)	116(2)
Ta-C(19)-H(19A)	122(2)
C(20)-C(19)-H(19B)	116(2)
Ta-C(19)-H(19B)	118(2)
H(19A)-C(19)-H(19B)	109(3)
C(19)-C(20)-C(21)	124.5(3)
C(19)-C(20)-Ta	70.5(2)
C(21)-C(20)-Ta	122.2(2)
C(19)-C(20)-H(20)	116(2)
C(21)-C(20)-H(20)	112(2)
Ta-C(20)-H(20)	104(2)
C(22)-C(21)-C(26)	116.7(3)
C(22)-C(21)-C(20)	123.9(3)
C(26)-C(21)-C(20)	119.3(3)
C(21)-C(22)-C(23)	121.5(4)
C(21)-C(22)-H(22)	116(3)
C(23)-C(22)-H(22)	123(3)
C(24)-C(23)-C(22)	120.8(4)
C(24)-C(23)-H(23)	123(2)
C(22)-C(23)-H(23)	116(2)
C(23)-C(24)-C(25)	118.6(3)
C(23)-C(24)-H(24)	124(2)
C(25)-C(24)-H(24)	118(2)
C(26)-C(25)-C(24)	120.7(3)
C(26)-C(25)-H(25)	122(2)

C(24)-C(25)-H(25)	117(2)
C(25)-C(26)-C(21)	121.5(3)
C(25)-C(26)-H(26)	122(2)
C(21)-C(26)-H(26)	117(2)

Symmetry transformations used to generate equivalent atoms:

Table 25. Crystal data and structure refinement for tBuSpTa(sty)(H).

Empirical formula	C_{24} H_{31} Si Ta
Formula weight	528.53
Crystallization Solvent	Petroleum ether
Crystal Habit	Stacked plates
Crystal size	0.26 x 0.15 x 0.03 mm^3
Crystal color	Yellow

Data Collection

Preliminary Photos		
Type of diffractometer	CCD area detector	
Wavelength	0.71073 Å MoKa	
Data Collection Temperature	93 K	
Theta range for 6528 reflections used in lattice determination	2.77 to 28.25°	
Unit cell dimensions	a = 10.2246(18) Å b = 10.5009(18) Å c = 11.1345(19) Å	a= 74.140(3)° b= 84.118(3)° g = 66.993(2)°
Volume	1058.5(3) $Å^3$	
Z	2	
Crystal system	Triclinic	
Space group	P-1	
Density (calculated)	1.658 Mg/m^3	
F(000)	524	
Data collection program	Bruker SMART	
Theta range for data collection	1.90 to 28.25°	
Completeness to theta = 28.25°	92.9 %	
Index ranges	-13<=h<=13, -13<=k<=13, -14<=l<=14	
Data collection scan type	phi and omega scans	
Data reduction program	Bruker SAINT v. 6.2	
Reflections collected	19961	
Independent reflections	4860 [R_{int}= 0.2215; GOF_{merge}=]	
Absorption coefficient	5.254 mm^{-1}	
Absorption correction	Analytical	
Max. and min. transmission	0.8571 and 0.2775	
Number of standards	? reflections measured every ?min.	
Variation of standards	?%.	

Structure solution and Refinement

Structure solution program	SHELXS-97 (Sheldrick, 1990)
Primary solution method	Patterson method
Secondary solution method	Difference Fourier map
Hydrogen placement	Calculated (see Special Details)
Structure refinement program	SHELXL-97 (Sheldrick, 1997)
Refinement method	Full matrix least-squares on F^2
Data / restraints / parameters	4860 / 0 / 257
Treatment of hydrogen atoms	Mixed (see Special Details)
Goodness-of-fit on F^2	1.291
Final R indices [I>2s(I), 4347 reflections]	R1 = 0.0469, wR2 = 0.1119
R indices (all data)	R1 = 0.0524, wR2 = 0.1141
Type of weighting scheme used	Sigma
Weighting scheme used	w=1/s^2^(Fo^2^)
Max shift/error	0.001
Average shift/error	0.000
Largest diff. peak and hole	3.625 and -3.292 e.$Å^{-3}$

Table 26. Bond lengths [Å] and angles [°] for tBuSpTa(sty)(H).

Ta-Cent(1)	2.068(5)
Ta-Cent(2)	2.084(5)
Ta-Pln(1)	2.081(3)
Ta-Pln(2)	2.062(3)
Ta-C(17)	2.267(9)
Ta-C(18)	2.307(7)
Ta-C(6)	2.334(5)
Ta-C(1)	2.359(6)
Ta-C(10)	2.358(5)
Ta-C(7)	2.367(7)
Ta-C(2)	2.381(8)
Ta-C(5)	2.375(7)
Ta-C(4)	2.419(7)
Ta-C(9)	2.449(6)
Ta-C(3)	2.466(6)
Ta-C(8)	2.476(7)
Ta-H	1.8669
Si-C(6)	1.858(7)
Si-C(11)	1.856(9)
Si-C(12)	1.850(8)
Si-C(1)	1.876(6)
C(1)-C(5)	1.409(12)
C(1)-C(2)	1.429(9)

C(2)-C(3)	1.401(10)
C(2)-H(2)	0.8711
C(3)-C(4)	1.387(12)
C(3)-H(3)	1.0994
C(4)-C(5)	1.380(8)
C(4)-H(4)	0.9300
C(5)-H(5)	0.9978
C(6)-C(10)	1.421(11)
C(6)-C(7)	1.433(10)
C(7)-C(8)	1.434(9)
C(7)-H(7)	1.0524
C(8)-C(9)	1.398(12)
C(8)-C(13)	1.510(9)
C(9)-C(10)	1.442(8)
C(9)-H(9)	0.7546
C(10)-H(10)	0.9396
C(11)-H(11A)	0.9312
C(11)-H(11B)	0.9312
C(11)-H(11C)	0.9312
C(12)-H(12A)	0.9587
C(12)-H(12B)	0.9587
C(12)-H(12C)	0.9587
C(13)-C(16)	1.528(9)
C(13)-C(14)	1.519(11)
C(13)-C(15)	1.538(10)
C(14)-H(14A)	1.0447
C(14)-H(14B)	1.0447
C(14)-H(14C)	1.0447
C(15)-H(15A)	0.9807
C(15)-H(15B)	0.9807
C(15)-H(15C)	0.9807
C(16)-H(16A)	0.7188
C(16)-H(16B)	0.7188
C(16)-H(16C)	0.7188
C(17)-C(18)	1.445(9)
C(17)-H(17A)	0.9739
C(17)-H(17B)	0.9739
C(18)-C(19)	1.483(7)
C(18)-H(18)	0.7398
C(19)-C(20)	1.384(12)
C(19)-C(24)	1.381(10)
C(20)-C(21)	1.398(8)
C(20)-H(20)	0.9300
C(21)-C(22)	1.377(12)
C(21)-H(21)	0.8784
C(22)-C(23)	1.361(13)
C(22)-H(22)	1.0306
C(23)-C(24)	1.380(8)
C(23)-H(23)	0.7862
C(24)-H(24)	0.8519

Cent(1)-Ta-Cent(2)	131.94(1)
Pln(1)-Ta-Pln(2)	125.2(3)
C(17)-Ta-C(18)	36.8(2)

C(17)-Ta-C(6)	113.8(2)
C(18)-Ta-C(6)	136.9(2)
C(17)-Ta-C(1)	114.8(3)
C(18)-Ta-C(1)	140.5(3)
C(6)-Ta-C(1)	70.7(2)
C(17)-Ta-C(10)	81.0(2)
C(18)-Ta-C(10)	102.3(2)
C(6)-Ta-C(10)	35.2(3)
C(1)-Ta-C(10)	95.5(2)
C(17)-Ta-C(7)	135.6(2)
C(18)-Ta-C(7)	131.9(2)
C(6)-Ta-C(7)	35.5(2)
C(1)-Ta-C(7)	87.4(2)
C(10)-Ta-C(7)	57.9(3)
C(17)-Ta-C(2)	135.4(3)
C(18)-Ta-C(2)	134.3(2)
C(6)-Ta-C(2)	88.6(2)
C(1)-Ta-C(2)	35.1(2)
C(10)-Ta-C(2)	122.2(2)
C(7)-Ta-C(2)	85.0(3)
C(17)-Ta-C(5)	82.3(3)
C(18)-Ta-C(5)	106.4(3)
C(6)-Ta-C(5)	94.1(2)
C(1)-Ta-C(5)	34.6(3)
C(10)-Ta-C(5)	102.7(2)
C(7)-Ta-C(5)	120.1(2)
C(2)-Ta-C(5)	57.0(3)
C(17)-Ta-C(4)	80.4(3)
C(18)-Ta-C(4)	86.5(3)
C(6)-Ta-C(4)	125.7(2)
C(1)-Ta-C(4)	56.6(2)
C(10)-Ta-C(4)	134.3(2)
C(7)-Ta-C(4)	140.0(3)
C(2)-Ta-C(4)	55.8(3)
C(5)-Ta-C(4)	33.45(19)
C(17)-Ta-C(9)	80.4(3)
C(18)-Ta-C(9)	82.1(2)
C(6)-Ta-C(9)	58.0(2)
C(1)-Ta-C(9)	127.74(19)
C(10)-Ta-C(9)	34.9(2)
C(7)-Ta-C(9)	56.5(3)
C(2)-Ta-C(9)	141.2(3)
C(5)-Ta-C(9)	136.2(2)
C(4)-Ta-C(9)	159.7(3)
C(17)-Ta-C(3)	109.7(3)
C(18)-Ta-C(3)	100.9(2)
C(6)-Ta-C(3)	121.8(2)
C(1)-Ta-C(3)	56.68(19)
C(10)-Ta-C(3)	152.2(2)
C(7)-Ta-C(3)	114.6(3)
C(2)-Ta-C(3)	33.5(2)
C(5)-Ta-C(3)	55.6(3)
C(4)-Ta-C(3)	33.0(3)
C(9)-Ta-C(3)	166.8(3)

C(17)-Ta-C(8)	110.2(3)
C(18)-Ta-C(8)	97.6(2)
C(6)-Ta-C(8)	58.0(2)
C(1)-Ta-C(8)	121.6(2)
C(10)-Ta-C(8)	57.0(2)
C(7)-Ta-C(8)	34.4(2)
C(2)-Ta-C(8)	114.3(3)
C(5)-Ta-C(8)	151.91(19)
C(4)-Ta-C(8)	167.0(3)
C(9)-Ta-C(8)	33.0(3)
C(3)-Ta-C(8)	134.1(3)
C(17)-Ta-H	112.4
C(18)-Ta-H	76.3
C(6)-Ta-H	125.4
C(1)-Ta-H	113.1
C(10)-Ta-H	136.5
C(7)-Ta-H	90.2
C(2)-Ta-H	78.1
C(5)-Ta-H	119.6
C(4)-Ta-H	89.2
C(9)-Ta-H	104.2
C(3)-Ta-H	64.5
C(8)-Ta-H	79.9
C(6)-Si-C(11)	110.0(4)
C(6)-Si-C(12)	113.3(4)
C(11)-Si-C(12)	113.1(4)
C(6)-Si-C(1)	93.2(3)
C(11)-Si-C(1)	113.6(3)
C(12)-Si-C(1)	112.1(3)
C(5)-C(1)-C(2)	106.2(5)
C(5)-C(1)-Si	124.3(5)
C(2)-C(1)-Si	123.6(6)
C(5)-C(1)-Ta	73.3(4)
C(2)-C(1)-Ta	73.3(4)
Si-C(1)-Ta	97.0(3)
C(3)-C(2)-C(1)	108.2(8)
C(3)-C(2)-Ta	76.6(5)
C(1)-C(2)-Ta	71.6(4)
C(3)-C(2)-H(2)	125.9
C(1)-C(2)-H(2)	125.9
Ta-C(2)-H(2)	117.8
C(4)-C(3)-C(2)	107.4(6)
C(4)-C(3)-Ta	71.6(4)
C(2)-C(3)-Ta	69.9(4)
C(4)-C(3)-H(3)	126.3
C(2)-C(3)-H(3)	126.3
Ta-C(3)-H(3)	123.8
C(3)-C(4)-C(5)	109.5(7)
C(3)-C(4)-Ta	75.4(4)
C(5)-C(4)-Ta	71.5(4)
C(3)-C(4)-H(4)	125.2
C(5)-C(4)-H(4)	125.2
Ta-C(4)-H(4)	119.5
C(1)-C(5)-C(4)	108.5(7)

C(1)-C(5)-Ta	72.1(4)
C(4)-C(5)-Ta	75.0(4)
C(1)-C(5)-H(5)	125.7
C(4)-C(5)-H(5)	125.7
Ta-C(5)-H(5)	119.0
C(10)-C(6)-C(7)	106.7(6)
C(10)-C(6)-Si	127.0(6)
C(7)-C(6)-Si	121.2(6)
C(10)-C(6)-Ta	73.3(3)
C(7)-C(6)-Ta	73.5(3)
Si-C(6)-Ta	98.4(3)
C(6)-C(7)-C(8)	109.1(7)
C(6)-C(7)-Ta	71.0(4)
C(8)-C(7)-Ta	77.0(4)
C(6)-C(7)-H(7)	125.5
C(8)-C(7)-H(7)	125.5
Ta-C(7)-H(7)	118.4
C(9)-C(8)-C(7)	107.3(6)
C(9)-C(8)-C(13)	127.0(7)
C(7)-C(8)-C(13)	124.5(8)
C(9)-C(8)-Ta	72.4(4)
C(7)-C(8)-Ta	68.7(4)
C(13)-C(8)-Ta	133.6(3)
C(8)-C(9)-C(10)	108.7(7)
C(8)-C(9)-Ta	74.6(4)
C(10)-C(9)-Ta	69.1(3)
C(8)-C(9)-H(9)	125.6
C(10)-C(9)-H(9)	125.6
Ta-C(9)-H(9)	122.3
C(6)-C(10)-C(9)	108.2(7)
C(6)-C(10)-Ta	71.4(3)
C(9)-C(10)-Ta	76.0(3)
C(6)-C(10)-H(10)	125.9
C(9)-C(10)-H(10)	125.9
Ta-C(10)-H(10)	118.5
Si-C(11)-H(11A)	109.5
Si-C(11)-H(11B)	109.5
H(11A)-C(11)-H(11B)	109.5
Si-C(11)-H(11C)	109.5
H(11A)-C(11)-H(11C)	109.5
H(11B)-C(11)-H(11C)	109.5
Si-C(12)-H(12A)	109.5
Si-C(12)-H(12B)	109.5
H(12A)-C(12)-H(12B)	109.5
Si-C(12)-H(12C)	109.5
H(12A)-C(12)-H(12C)	109.5
H(12B)-C(12)-H(12C)	109.5
C(8)-C(13)-C(16)	105.7(5)
C(8)-C(13)-C(14)	113.7(6)
C(16)-C(13)-C(14)	110.2(7)
C(8)-C(13)-C(15)	109.7(7)
C(16)-C(13)-C(15)	107.7(6)
C(14)-C(13)-C(15)	109.6(5)
C(13)-C(14)-H(14A)	109.5

C(13)-C(14)-H(14B)	109.5
H(14A)-C(14)-H(14B)	109.5
C(13)-C(14)-H(14C)	109.5
H(14A)-C(14)-H(14C)	109.5
H(14B)-C(14)-H(14C)	109.5
C(13)-C(15)-H(15A)	109.5
C(13)-C(15)-H(15B)	109.5
H(15A)-C(15)-H(15B)	109.5
C(13)-C(15)-H(15C)	109.5
H(15A)-C(15)-H(15C)	109.5
H(15B)-C(15)-H(15C)	109.5
C(13)-C(16)-H(16A)	109.5
C(13)-C(16)-H(16B)	109.5
H(16A)-C(16)-H(16B)	109.5
C(13)-C(16)-H(16C)	109.5
H(16A)-C(16)-H(16C)	109.5
H(16B)-C(16)-H(16C)	109.5
C(18)-C(17)-Ta	73.1(5)
C(18)-C(17)-H(17A)	116.2
Ta-C(17)-H(17A)	116.2
C(18)-C(17)-H(17B)	116.2
Ta-C(17)-H(17B)	116.2
H(17A)-C(17)-H(17B)	113.2
C(17)-C(18)-C(19)	126.9(7)
C(17)-C(18)-Ta	70.1(4)
C(19)-C(18)-Ta	120.8(5)
C(17)-C(18)-H(18)	116.5
C(19)-C(18)-H(18)	116.5
Ta-C(18)-H(18)	79.0
C(20)-C(19)-C(24)	117.2(6)
C(20)-C(19)-C(18)	123.2(7)
C(24)-C(19)-C(18)	119.4(7)
C(19)-C(20)-C(21)	121.8(7)
C(19)-C(20)-H(20)	119.1
C(21)-C(20)-H(20)	119.1
C(22)-C(21)-C(20)	119.0(8)
C(22)-C(21)-H(21)	120.5
C(20)-C(21)-H(21)	120.5
C(23)-C(22)-C(21)	119.7(6)
C(23)-C(22)-H(22)	120.1
C(21)-C(22)-H(22)	120.1
C(22)-C(23)-C(24)	120.9(8)
C(22)-C(23)-H(23)	119.5
C(24)-C(23)-H(23)	119.5
C(19)-C(24)-C(23)	121.2(8)
C(19)-C(24)-H(24)	119.4
C(23)-C(24)-H(24)	119.4

Symmetry transformations used to generate equivalent atoms:

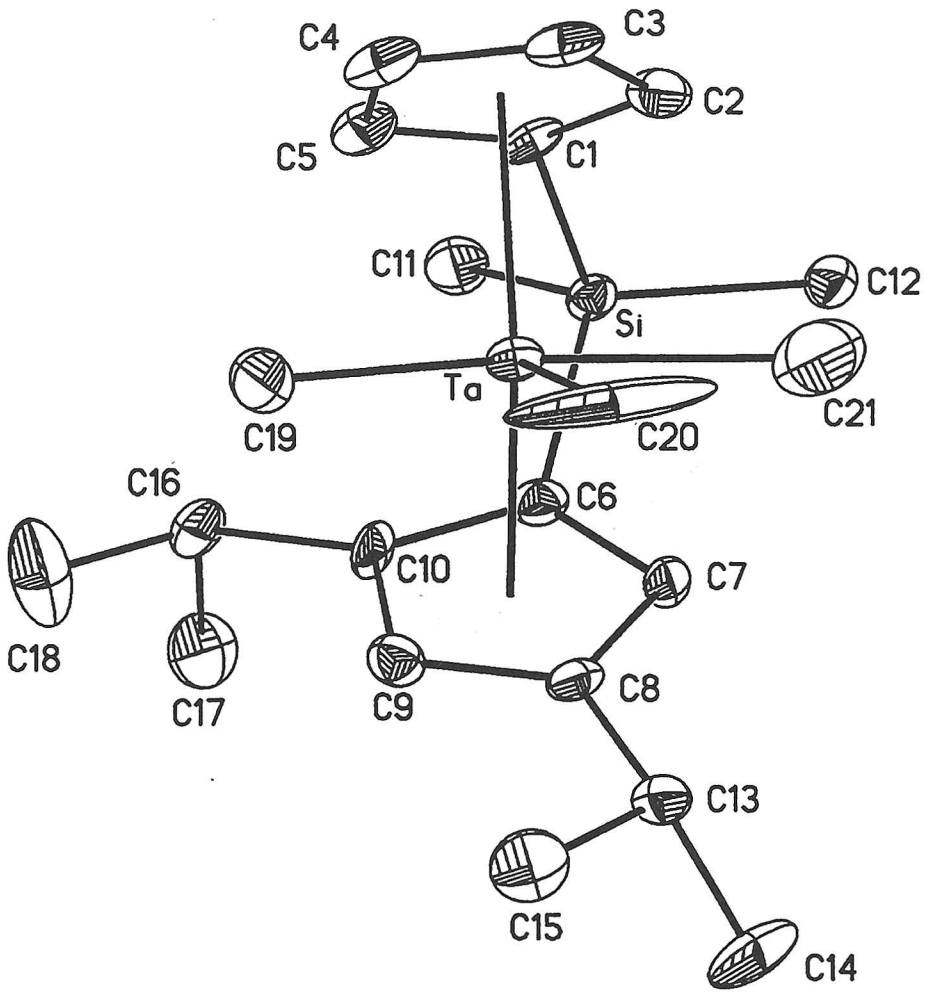

Labeled view of $iPr_2SpTaMe_3$.

Table 27. Crystal Data and Structure Analysis Details for $iPr_2SpTaMe_3$.

Empirical formula	$C_{21}H_{35}SiTa$
Formula weight	496.53
Crystallization solvent	ether
Crystal habit	rounded plate
Crystal size	0.22 x 0.22 x 0.07 mm
Crystal color	brown

Data Collection

Preliminary photograph(s)	rotation	
Type of diffractometer	Bruker SMART 1000 ccd	
Wavelength	0.71073 Å MoKa	
Data collection temperature	98 K	
Theta range for 1137 reflections used in lattice determination	2.7 to 8.2°	
Unit cell dimensions	a = 7.9023(14) Å b = 10.4850(19) Å c = 13.295(2) Å	a= 88.009(5)° b= 78.408(7)° g = 67.670(6)°
Volume	997.1(3) $Å^3$	
Z	2	
Crystal system	triclinic	
Space group	P $\bar{1}$ (#2)	
Density (calculated)	1.654 g/cm^3	
F(000)	496	
Theta range for data collection	2.10 to 28.70°	
Completeness to theta = 28.70°	80.1 %	
Index ranges	-10 £ h £ 10, -12 £ k £ 13, -17 £ l £ 17	
Data collection scan type	w scans at 3 fixed f values	
Reflections collected	7045	
Independent reflections	4126 [R_{int}= 0.0506]	
Absorption coefficient	5.571 mm^{-1}	
Absorption correction	empirical	
Max. and min. transmission	1.0 and 0.4	
Number of standards	first scans recollected at end of runs	
Variation of standards	within counting statistics	

Structure Solution and Refinement

Primary solution method	direct methods
Secondary solution method	difference map
Hydrogen placement	calculated
Refinement method	full-matrix least-squares on F^2
Data / restraints / parameters	4126 / 0 / 208
Treatment of hydrogen atoms	not refined
Goodness-of-fit on F^2	1.792
Final R indices [I>2s(I), 3825 reflections]	R1 = 0.0398, wR2 = 0.0800
R indices (all data)	R1 = 0.0417, wR2 = 0.0803
Type of weighting scheme used	sigma
Weighting scheme used	$w=1/s^2(Fo^2)$
Max shift/error	0.880
Average shift/error	0.061
Largest diff. peak and hole	3.491 and -1.534 e.Å^{-3}

Programs Used

Cell refinement	Bruker SAINT v6.02
Data collection	Bruker SMART v5.054
Data reduction	Bruker SAINT v6.02
Absorption correction	SADABS V2.0 beta
Structure solution	SHELXS-97 (Sheldrick, 1990)
Structure refinement	SHELXL-97 (Sheldrick, 1997)

Special Refinement Details

A small brown crystal which could not be satisfactorily indexed on a CAD-4 diffractometer was some time later transferred to the ccd on a glass fiber with Paratone-N oil. Three runs of data were collected with 30 second long, –0.25° wide ω–scans at three values of φ (0, 120, and 240°) with the detector 5 cm (nominal) distant at a θ of -28°. A short fourth run was not used. The initial cell for data reduction was calculated from just under 1000 reflections chosen from throughout the data frames; over a third were discarded as ill-fitting. For data processing with SAINT v6.02, all defaults were used, except: box size optimization was enabled, periodic orientation matrix updating was disabled, the instrument error was set to zero, no Laue class integration restraints were used, the model profiles from all nine areas were blended, and for the post-integration global least squares refinement, no constraints were applied. The data were corrected with SADABS v. 2.0 (beta) using default parameters except that the scale factor esd was set to 0.

One outlier reflection (0 –1 1) was omitted from the final processed dataset; there were 136 inconsistent equivalents. Refinement of F^2 was against all reflections. The weighted R-factor (wR) and goodness of fit (S) are based on F^2, conventional R-factors (R) are based on F, with F set

to zero for negative F^2. The threshold expression of $F^2 > 2\sigma(F^2)$ is used only for calculating R-factors(gt) etc. and is not relevant to the choice of reflections for refinement.

There is one molecule in the asymmetric unit. The structure is normal except for the elongated displacement ellipsoid of the central methyl carbon C20. No chemically reasonable disorder model could be found to account for this peculiarity. Some undetermined twinning is a possible explanation. There are numerous large excursions in the final difference map; all are near the Ta atom, except three in the vicinity of C20, the largest (1.58 e·Å^{-3}) is 0.46 Å distant.

Table 28. Bond lengths [Å] and angles [°] for iPr2SpTaMe3.

Ta-Cp1[a]	2.120	C12-H12B	0.9800
Ta-Cp2[b]	2.125	C12-H12C	0.9800
Ta···Pln1[c]	2.118(3)	C13-C14	1.521(9)
Ta···Pln2[d]	2.121(2)	C13-C15	1.530(9)
Ta-C20	2.288(7)	C13-H13	1.0000
Ta-C19	2.325(7)	C14-H14A	0.9800
Ta-C21	2.373(9)	C14-H14B	0.9800
Ta-C6	2.392(5)	C14-H14C	0.9800
Ta-C5	2.394(6)	C15-H15A	0.9800
Ta-C7	2.407(6)	C15-H15B	0.9800
Ta-C1	2.422(5)	C15-H15C	0.9800
Ta-C2	2.439(6)	C16-C18	1.489(10)
Ta-C10	2.440(5)	C16-C17	1.541(8)
Ta-C3	2.475(6)	C16-H16	1.0000
Ta-C8	2.480(5)	C17-H17A	0.9800
Ta-C4	2.480(6)	C17-H17B	0.9800
Si-C12	1.863(6)	C17-H17C	0.9800
Si-C11	1.875(5)	C18-H18A	0.9800
Si-C1	1.889(5)	C18-H18B	0.9800
Si-C6	1.904(6)	C18-H18C	0.9800
C1-C5	1.419(9)	C19-H19A	0.9800
C1-C2	1.434(8)	C19-H19B	0.9800
C2-C3	1.442(8)	C19-H19C	0.9800
C2-H2	1.0000	C20-H20A	0.9800
C3-C4	1.426(10)	C20-H20B	0.9800
C3-H3	1.0000	C20-H20C	0.9800
C4-C5	1.411(8)	C21-H21A	0.9800
C4-H4	1.0000	C21-H21B	0.9800
C5-H5	1.0000	C21-H21C	0.9800
C6-C10	1.406(8)		
C6-C7	1.436(8)	Cp1-Ta-Cp2	129.9
C7-C8	1.442(8)	Cp1-Ta-C19	100.9
C7-H7	1.0000	Cp1-Ta-C20	115.3
C8-C9	1.399(8)	Cp1-Ta-C21	95.7
C8-C13	1.526(7)	Cp2-Ta-C19	103.4
C9-C10	1.428(7)	Cp2-Ta-C20	113.1
C9-H9	1.0000	Cp2-Ta-C21	97.4
C10-C16	1.533(7)	Pln1···Pln2	54.9(2)
C11-H11A	0.9800	C20-Ta-C19	74.4(4)
C11-H11B	0.9800	C20-Ta-C21	60.2(5)
C11-H11C	0.9800	C19-Ta-C21	134.5(3)
C12-H12A	0.9800	C12-Si-C11	112.4(3)

C12-Si-C1	109.3(3)	C13-C14-H14B	109.5
C11-Si-C1	113.0(3)	H14A-C14-H14B	109.5
C12-Si-C6	111.3(3)	C13-C14-H14C	109.4
C11-Si-C6	115.4(3)	H14A-C14-H14C	109.5
C1-Si-C6	94.1(2)	H14B-C14-H14C	109.5
C5-C1-C2	107.8(5)	C13-C15-H15A	109.5
C5-C1-Si	124.9(4)	C13-C15-H15B	109.4
C2-C1-Si	120.1(4)	H15A-C15-H15B	109.5
C1-C2-C3	106.8(6)	C13-C15-H15C	109.5
C1-C2-H2	126.2	H15A-C15-H15C	109.5
C3-C2-H2	126.2	H15B-C15-H15C	109.5
C4-C3-C2	108.4(5)	C18-C16-C10	113.6(5)
C4-C3-H3	125.6	C18-C16-C17	109.6(6)
C2-C3-H3	125.7	C10-C16-C17	107.6(5)
C5-C4-C3	107.4(6)	C18-C16-H16	108.6
C5-C4-H4	126.2	C10-C16-H16	108.7
C3-C4-H4	126.2	C17-C16-H16	108.7
C4-C5-C1	109.3(5)	C16-C17-H17A	109.5
C4-C5-H5	124.9	C16-C17-H17B	109.5
C1-C5-H5	124.8	H17A-C17-H17B	109.5
C10-C6-C7	107.8(5)	C16-C17-H17C	109.4
C10-C6-Si	125.8(4)	H17A-C17-H17C	109.5
C7-C6-Si	121.1(4)	H17B-C17-H17C	109.5
C6-C7-C8	107.7(5)	C16-C18-H18A	109.5
C6-C7-H7	125.8	C16-C18-H18B	109.4
C8-C7-H7	125.8	H18A-C18-H18B	109.5
C9-C8-C7	107.3(5)	C16-C18-H18C	109.5
C9-C8-C13	127.4(5)	H18A-C18-H18C	109.5
C7-C8-C13	124.9(5)	H18B-C18-H18C	109.5
C8-C9-C10	109.1(5)	Ta-C19-H19A	109.5
C8-C9-H9	125.4	Ta-C19-H19B	109.5
C10-C9-H9	125.4	H19A-C19-H19B	109.5
C6-C10-C9	108.1(5)	Ta-C19-H19C	109.4
C6-C10-C16	126.1(5)	H19A-C19-H19C	109.5
C9-C10-C16	124.2(5)	H19B-C19-H19C	109.5
Si-C11-H11A	109.5	Ta-C20-H20A	109.5
Si-C11-H11B	109.5	Ta-C20-H20B	109.6
H11A-C11-H11B	109.5	H20A-C20-H20B	109.5
Si-C11-H11C	109.5	Ta-C20-H20C	109.4
H11A-C11-H11C	109.5	H20A-C20-H20C	109.5
H11B-C11-H11C	109.5	H20B-C20-H20C	109.5
Si-C12-H12A	109.4	Ta-C21-H21A	109.5
Si-C12-H12B	109.5	Ta-C21-H21B	109.5
H12A-C12-H12B	109.5	H21A-C21-H21B	109.5
Si-C12-H12C	109.5	Ta-C21-H21C	109.5
H12A-C12-H12C	109.5	H21A-C21-H21C	109.5
H12B-C12-H12C	109.5	H21B-C21-H21C	109.5
C14-C13-C8	110.2(5)		
C14-C13-C15	110.8(6)		
C8-C13-C15	111.3(5)		
C14-C13-H13	108.2		
C8-C13-H13	108.2		
C15-C13-H13	108.2		
C13-C14-H14A	109.5		

[a] Cp1 is the centroid of atoms C1, C2, C3, C4 and C5
[b] Pln1 is the best plane through atoms C1, C2, C3, C4 and C5
[c] Cp2 is the centroid of atoms C9, C10, C15, C16 and C21
[d] Pln2 is the best plane through atoms C9, C10, C15, C16 and C21

Table 29. Crystal Data and Structure Analysis Details for (Ewen)TaMe3.

Empirical formula	$C_{24}H_{27}Ta$	
Formula weight	496.41	
Crystallization solvent	dichloromethane	
Crystal habit	yellow	
Crystal size	0.33 x 0.33 x 0.26 mm	
Crystal color	irregular block	
Data Collection		
Preliminary photograph(s)	none	
Type of diffractometer	CAD-4	
Wavelength	0.71073 Å MoKa	
Data collection temperature	84 K	
Theta range for 25 reflections used in lattice determination	15 to 17°	
Unit cell dimensions	a = 8.717(2) Å b = 13.796(4) Å c = 15.763(4) Å	a= 90° b= 90° g = 90°
Volume	1895.7(9) $Å^3$	
Z	4	
Crystal system	orthorhombic	
Space group	$P2_12_12_1$ (#19)	
Density (calculated)	1.739 g/cm^3	
F(000)	976	
Theta range for data collection	1.5 to 27.5°	
Completeness to theta = 27.5°	99.9 %	
Index ranges	0 £ h £ 11, -17 £ k £ 17, -20 £ l £ 20	
Data collection device	CAD-4	
Data collection scan type	w-scan	
Reflections collected	12266	
Independent reflections	4350 [R_{int}= 0.0259; GOF_{merge}= 1.57]	
Absorption coefficient	5.801 mm^{-1}	

Absorption correction	y-scan
Max. and min. transmission	1.14 and 0.76
Number of standards	3 reflections measured every 75 min
Decay of standards	0.6%

Structure Solution and Refinement

Primary solution method	direct methods
Secondary solution method	difference map
Hydrogen placement	calculated
Refinement method	full-matrix least-squares on F^2
Data / restraints / parameters	4350 / 0 / 308
Treatment of hydrogen atoms attached atom	coordinates refined; U_{iso}'s fixed at 120% U_{eq} of
Goodness-of-fit on F^2	1.561
Final R indices [I>2s(I), 4292 reflections]	R1 = 0.0169, wR2 = 0.0406
R indices (all data)	R1 = 0.0172, wR2 = 0.0407
Type of weighting scheme used	sigma
Weighting scheme used	$w=1/s^2(Fo^2)$
Max shift/error	0.068
Average shift/error	0.002
Absolute structure parameter	-0.014(8)
Extinction coefficient	0.00076(9)
Largest diff. peak and hole	0.972 and -0.668 e.$Å^{-3}$

Programs Used

Cell refinement	CAD-4 Software (Enraf-Nonius, 1989)
Data collection	CAD-4 Software (Enraf-Nonius, 1989)
Data reduction	CRYM (Duchamp, 1964)
Structure solution	SHELXS-97 (Sheldrick, 1990)
Structure refinement	SHELXL-97 (Sheldrick, 1997)

Special Refinement Details

An irregular yellow block was carved from a yellow rosette and mounted on a glass fiber with Paratone-N oil. Data were collected with 1∞ w-scans. The individual measured backgrounds were replaced by a background function of 2q derived from weak reflections. The GOF_{merge} was 1.57 (4352 multiples) in point group 222; R_{merge} was 0.015 for 2993 duplicates with $F_o > 0$. Y-scan data were used for the absorption correction. There was minimal decay. Two outlier reflections (1 0 1, 0 1 1) were omitted from the refinement. A small extinction correction was included.

Weights w are calculated as $1/s^2(F_o^2)$; variances ($s^2(F_o^2)$) were derived from counting statistics plus an additional term, $(0.014I)^2$; variances of the merged data were obtained by propagation of error plus another additional term, $(0.014<I>)^2$. The refinement of F^2 is as always against all reflections. The weighted R-factor wR and goodness of fit S are based on F^2, conventional R-factors R are based on F, with F set to zero for negative F^2. The threshold expression of $F^2 > 2s(F^2)$ is used only for calculating R-factors(gt) etc. and is not relevant to the choice of reflections for refinement.

The asymmetric unit contains one Ta complex. $P2_12_12_1$ is a chiral, non-polar spacegroup. Although the molecule is not chiral; the structure is. The Flack parameter was not included in the full matrix least squares.

Table 30. Bond lengths [Å] and angles [°] for (Ewen)TaMe3.

Ta-Cp[a]	2.118	C7-H7B	0.97(5)
Ta···Pln[b]	2.114(2)	C7-H7C	0.94(4)
Ta-C23	2.188(4)	C8-H8A	0.98(4)
Ta-C22	2.194(4)	C8-H8B	0.97(4)
Ta-C24	2.210(3)	C8-H8C	0.92(5)
Ta-C9	2.294(3)	C9-C10	1.493(4)
Ta-C1	2.389(3)	C9-C21	1.502(4)
Ta-C5	2.390(3)	C10-C11	1.400(4)
Ta-C2	2.406(3)	C10-C15	1.417(4)
Ta-C4	2.484(4)	C11-C12	1.388(5)
Ta-C3	2.505(4)	C11-H11	0.91(4)
C1-C2	1.411(5)	C12-C13	1.385(5)
C1-C5	1.421(5)	C12-H12	0.83(4)
C1-C6	1.511(5)	C13-C14	1.395(5)
C2-C3	1.423(6)	C13-H13	0.93(4)
C2-H2	0.85(4)	C14-C15	1.395(5)
C3-C4	1.390(6)	C14-H14	0.92(4)
C3-H3	0.86(5)	C15-C16	1.448(4)
C4-C5	1.417(6)	C16-C17	1.393(4)
C4-H4	0.81(5)	C16-C21	1.417(5)
C5-H5	0.94(4)	C17-C18	1.396(5)
C6-C7	1.527(5)	C17-H17	1.00(4)
C6-C8	1.541(5)	C18-C19	1.394(5)
C6-C9	1.575(4)	C18-H18	0.96(4)
C7-H7A	0.91(4)	C19-C20	1.388(5)

C19-H19	0.76(4)
C20-C21	1.408(5)
C20-H20	0.97(4)
C22-H22A	1.07(4)
C22-H22B	0.92(5)
C22-H22C	1.10(4)
C23-H23A	0.87(5)
C23-H23B	1.07(4)
C23-H23C	0.98(4)
C24-H24A	0.99(4)
C24-H24B	0.88(4)
C24-H24C	1.02(4)
Cp-Ta-C9	90.7
Cp-Ta-C22	102.5
Cp-Ta-C23	101.6
Cp-Ta-C24	177.5
C23-Ta-C22	115.38(14)
C23-Ta-C24	78.58(14)
C22-Ta-C24	79.64(14)
C23-Ta-C9	117.93(13)
C22-Ta-C9	120.69(13)
C24-Ta-C9	87.01(12)
C2-C1-C5	105.9(3)
C2-C1-C6	125.2(3)
C5-C1-C6	124.2(3)
C1-C2-C3	109.3(3)
C1-C2-H2	130(3)
C3-C2-H2	121(3)
C4-C3-C2	107.6(4)
C4-C3-H3	123(3)
C2-C3-H3	129(3)
C3-C4-C5	108.1(4)
C3-C4-H4	119(3)
C5-C4-H4	133(3)
C4-C5-C1	109.0(3)
C4-C5-H5	128(3)
C1-C5-H5	123(3)
C1-C6-C7	111.5(3)
C1-C6-C8	111.8(3)
C7-C6-C8	106.2(3)
C1-C6-C9	98.7(3)
C7-C6-C9	114.6(3)
C8-C6-C9	114.1(3)
C6-C7-H7A	108(3)
C6-C7-H7B	112(3)
H7A-C7-H7B	104(4)
C6-C7-H7C	116(3)
H7A-C7-H7C	105(4)
H7B-C7-H7C	111(4)
C6-C8-H8A	107(3)
C6-C8-H8B	119(3)
H8A-C8-H8B	113(4)
C6-C8-H8C	107(3)
H8A-C8-H8C	106(4)
H8B-C8-H8C	103(4)
C10-C9-C21	102.9(3)
C10-C9-C6	120.0(3)
C21-C9-C6	120.4(3)
C10-C9-Ta	103.0(2)
C21-C9-Ta	107.1(2)
C6-C9-Ta	101.6(2)
C11-C10-C15	118.6(3)
C11-C10-C9	131.2(3)
C15-C10-C9	110.1(3)
C12-C11-C10	119.7(3)
C12-C11-H11	118(2)
C10-C11-H11	123(2)
C13-C12-C11	121.7(3)
C13-C12-H12	125(3)
C11-C12-H12	113(3)
C12-C13-C14	119.7(3)
C12-C13-H13	121(3)
C14-C13-H13	119(3)
C15-C14-C13	119.4(3)
C15-C14-H14	120(2)
C13-C14-H14	121(2)
C14-C15-C10	121.0(3)
C14-C15-C16	130.1(3)
C10-C15-C16	108.7(3)
C17-C16-C21	122.0(3)
C17-C16-C15	129.6(3)
C21-C16-C15	108.1(3)
C16-C17-C18	118.9(3)
C16-C17-H17	120(2)
C18-C17-H17	121(2)
C19-C18-C17	119.7(3)
C19-C18-H18	118(2)
C17-C18-H18	122(2)
C20-C19-C18	121.8(3)
C20-C19-H19	119(3)
C18-C19-H19	119(4)
C19-C20-C21	119.6(3)
C19-C20-H20	117(2)
C21-C20-H20	123(2)
C20-C21-C16	118.0(3)
C20-C21-C9	131.5(3)
C16-C21-C9	110.2(3)
Ta-C22-H22A	106(2)
Ta-C22-H22B	117(3)
H22A-C22-H22B	116(3)
Ta-C22-H22C	106(2)
H22A-C22-H22C	96(3)
H22B-C22-H22C	113(4)
Ta-C23-H23A	105(3)
Ta-C23-H23B	109(2)
H23A-C23-H23B	107(3)
Ta-C23-H23C	116(3)

H23A-C23-H23C	116(4)
H23B-C23-H23C	103(3)
Ta-C24-H24A	119(2)
Ta-C24-H24B	111(3)
H24A-C24-H24B	108(4)
Ta-C24-H24C	105(2)
H24A-C24-H24C	107(3)
H24B-C24-H24C	106(4)

[a] Cp is the centroid of atoms C1, C2, C3, C4 and C5
[b] Pln is the best plane through atoms C1, C2, C3, C4 and C5

Table 31. Crystal Data and Structure Analysis Details for Flyover.

Empirical formula	$C_{27}H_{36}Cl_2Ta_2$
Formula weight	793.36
Crystallization solvent	dichloromethane
Crystal habit	plate
Crystal size	0.33 x 0.26 x 0.04 mm
Crystal color	orange

Data Collection

Preliminary photograph(s)	none	
Type of diffractometer	CAD-4	
Wavelength	0.71073 Å MoKa	
Data collection temperature	84 K	
Theta range for 25 reflections used in lattice determination	11 to 14°	
Unit cell dimensions	a = 8.999(4) Å b = 11.960(3) Å c = 13.128(5) Å	a= 64.92(3)° b= 80.99(3)° g = 82.85(3)°
Volume	1261.3(8) $Å^3$	
Z	2	
Crystal system	triclinic	
Space group	P $\bar{1}$ (#2)	
Density (calculated)	2.089 g/cm^3	
F(000)	756	
Theta range for data collection	1.5 to 25°	
Completeness to theta = 25°	100.0 %	
Index ranges	-10 £ h £ 10, -12 £ k £ 14, -13 £ l £ 15	
Data collection device	CAD-4	
Data collection scan type	w-scan	
Reflections collected	10000	
Independent reflections	4439 [R_{int}= 0.0399; GOF_{merge}= 1.20]	
Absorption coefficient	8.894 mm^{-1}	
Absorption correction	y-scan	
Max. and min. transmission	1.33 and 0.30	

Number of standards	3 reflections measured every 75 min
Variation of standards	within counting statistics

Structure Solution and Refinement

Primary solution method	direct methods
Secondary solution method	difference map
Hydrogen placement	calculated
Refinement method	full-matrix least-squares on F^2
Data / restraints / parameters	4439 / 0 / 147
Treatment of hydrogen atoms	not refined
Goodness-of-fit on F^2	1.756
Final R indices [I>2s(I), 3627 reflections]	R1 = 0.0409, wR2 = 0.0744
R indices (all data)	R1 = 0.0584, wR2 = 0.0782
Type of weighting scheme used	sigma
Weighting scheme used	$w=1/s^2(Fo^2)$
Max shift/error	0.021
Average shift/error	0.001
Largest diff. peak and hole	1.942 and -2.234 e·Å^{-3}

Programs Used

Cell refinement	CAD-4 Software (Enraf-Nonius, 1989)
Data collection	CAD-4 Software (Enraf-Nonius, 1989)
Data reduction	CRYM (Duchamp, 1964)
Structure solution	SHELXS-97 (Sheldrick, 1990)
Structure refinement	SHELXL-97 (Sheldrick, 1997)

Special Refinement Details

This material is present as a small quantity of impurity in PJC17. Unwanted by its creator, a lonely orange triangular plate languished in Paratone-N on a glass slide during data collection for PJC17 and slowly turned colorless around the edges until it was finally mounted on a glass fiber with Paratone-N oil. Data were collected with 1.75∞ w-scans as the peaks were broad. The individual measured backgrounds were replaced by a background function of 2q derived from weak reflections. The GOF_{merge} was 1.20 (4439 multiples) in point group`1; R_{merge} was 0.031 for 3662 duplicates with $F_o > 0$. Y-scan data were used for the absorption correction. There was no decay. No outlier reflections were omitted from the refinement.

Weights w are calculated as $1/s^2(F_o^2)$; variances ($s^2(F_o^2)$) were derived from counting statistics plus an additional term, $(0.014I)^2$; variances of the merged data were obtained by

propagation of error plus another additional term, $(0.014<I>)^2$. The refinement of F^2 is as always against all reflections. The weighted R-factor wR and goodness of fit S are based on F^2, conventional R-factors R are based on F, with F set to zero for negative F^2. The threshold expression of $F^2 > 2s(F^2)$ is used only for calculating R-factors(gt) etc. and is not relevant to the choice of reflections for refinement.

This is not a high-quality structure. Only the Ta and Cl atoms were refined anisotropically; all other non-hydrogen atoms were refined isotropically and hydrogen atoms were placed at calculated positions with U_{iso}'s set at 120% of the U_{iso}'s of the attached atoms. There may be some confusion among the Cl's and several of the methyl groups; it is not possible to tell with this dataset. There are many large peaks in the final difference map; the four greater than |2| e◊Å^{-3} (-2.23, -2.11, -2.11 and –2.01) are all within 1.16Å of Ta1 or Ta2; 1.52 e◊Å^{-3} (1.26Å from C10) and –1.35 e◊Å^{-3} (1.19Å from H8C) are the largest positive and negative excursions not near a Ta or Cl atom.

Table 32. Bond lengths [Å] and angles [°] for Flyover.

Ta1-Cp1[a]	2.111	C7-H7A	0.9600
Ta1···Pln1[b]	2.109(4)	C7-H7B	0.9600
Ta1-C24	2.181(10)	C7-H7C	0.9600
Ta1-C23	2.207(9)	C8-H8A	0.9600
Ta1-C22	2.268(7)	C8-H8B	0.9600
Ta1-Cl1	2.355(2)	C8-H8C	0.9600
Ta1-C3	2.401(8)	C9-C21	1.458(11)
Ta1-C4	2.405(9)	C9-C10	1.466(11)
Ta1-C5	2.417(9)	C10-C11	1.419(11)
Ta1-C2	2.422(9)	C10-C15	1.422(11)
Ta1-C1	2.482(9)	C11-C12	1.355(12)
Ta2-Cp2[c]	2.164	C11-H11	0.9300
Ta2···Pln2[d]	2.156(4)	C12-C13	1.414(12)
Ta2-C26	2.168(11)	C12-H12	0.9300
Ta2-C27	2.189(8)	C13-C14	1.348(12)
Ta2-C25	2.190(9)	C13-H13	0.9300
Ta2-Cl2	2.358(2)	C14-C15	1.410(12)
Ta2-C9	2.377(8)	C14-H14	0.9300
Ta2-C10	2.475(8)	C15-C16	1.443(11)
Ta2-C21	2.476(9)	C16-C21	1.414(12)
Ta2-C16	2.546(9)	C16-C17	1.439(11)
Ta2-C15	2.555(8)	C17-C18	1.356(12)
C1-C5	1.405(12)	C17-H17	0.9300
C1-C2	1.420(11)	C18-C19	1.391(13)
C1-C6	1.522(11)	C18-H18	0.9300
C2-C3	1.381(12)	C19-C20	1.369(12)
C2-H2	0.9800	C19-H19	0.9300
C3-C4	1.412(12)	C20-C21	1.445(11)
C3-H3	0.9800	C20-H20	0.9300
C4-C5	1.408(12)	C22-H22A	0.9600
C4-H4	0.9800	C22-H22B	0.9600
C5-H5	0.9800	C22-H22C	0.9600
C6-C9	1.533(11)	C23-H23A	0.9600
C6-C7	1.534(11)	C23-H23B	0.9600
C6-C8	1.540(11)	C23-H23C	0.9600

C24-H24A	0.9600	C6-C7-H7A	109.5
C24-H24B	0.9600	C6-C7-H7B	109.5
C24-H24C	0.9600	H7A-C7-H7B	109.5
C25-H25A	0.9600	C6-C7-H7C	109.5
C25-H25B	0.9600	H7A-C7-H7C	109.5
C25-H25C	0.9600	H7B-C7-H7C	109.5
C26-H26A	0.9600	C6-C8-H8A	109.5
C26-H26B	0.9600	C6-C8-H8B	109.5
C26-H26C	0.9600	H8A-C8-H8B	109.5
C27-H27A	0.9600	C6-C8-H8C	109.5
C27-H27B	0.9600	H8A-C8-H8C	109.5
C27-H27C	0.9600	H8B-C8-H8C	109.5
		C21-C9-C10	104.7(7)
Cp1-Ta1-Cl1	119.6	C21-C9-C6	128.9(7)
Cp1-Ta1-C22	115.1	C10-C9-C6	122.0(6)
Cp1-Ta1-C23	106.0	C11-C10-C15	117.6(8)
Cp1-Ta1-C24	110.6	C11-C10-C9	132.8(8)
C24-Ta1-C23	76.7(4)	C15-C10-C9	109.6(7)
C24-Ta1-C22	132.1(3)	C12-C11-C10	119.5(8)
C23-Ta1-C22	77.8(3)	C12-C11-H11	120.3
C24-Ta1-Cl1	83.9(2)	C10-C11-H11	120.3
C23-Ta1-Cl1	134.3(2)	C11-C12-C13	122.0(8)
C22-Ta1-Cl1	85.91(18)	C11-C12-H12	119.0
Cp2-Ta2-Cl2	124.5	C13-C12-H12	119.0
Cp2-Ta2-C25	116.8	C14-C13-C12	120.6(9)
Cp2-Ta2-C26	103.2	C14-C13-H13	119.7
Cp2-Ta2-C27	111.6	C12-C13-H13	119.7
C26-Ta2-C27	78.0(4)	C13-C14-C15	118.7(8)
C26-Ta2-C25	79.4(4)	C13-C14-H14	120.6
C27-Ta2-C25	129.9(4)	C15-C14-H14	120.6
C26-Ta2-Cl2	132.1(3)	C14-C15-C10	121.6(7)
C27-Ta2-Cl2	80.2(3)	C14-C15-C16	130.8(8)
C25-Ta2-Cl2	83.0(2)	C10-C15-C16	107.4(7)
C5-C1-C2	106.3(7)	C21-C16-C17	123.2(8)
C5-C1-C6	126.9(7)	C21-C16-C15	108.3(7)
C2-C1-C6	126.3(8)	C17-C16-C15	128.4(8)
C3-C2-C1	107.8(8)	C18-C17-C16	116.3(9)
C3-C2-H2	125.7	C18-C17-H17	121.9
C1-C2-H2	125.7	C16-C17-H17	121.9
C2-C3-C4	110.3(8)	C17-C18-C19	122.1(8)
C2-C3-H3	124.7	C17-C18-H18	118.9
C4-C3-H3	124.7	C19-C18-H18	118.9
C5-C4-C3	105.1(8)	C20-C19-C18	123.1(9)
C5-C4-H4	127.0	C20-C19-H19	118.5
C3-C4-H4	127.0	C18-C19-H19	118.5
C1-C5-C4	110.3(8)	C19-C20-C21	118.2(9)
C1-C5-H5	124.6	C19-C20-H20	120.9
C4-C5-H5	124.6	C21-C20-H20	120.9
C1-C6-C9	110.5(6)	C16-C21-C20	117.0(7)
C1-C6-C7	109.4(7)	C16-C21-C9	109.7(7)
C9-C6-C7	112.3(7)	C20-C21-C9	133.1(8)
C1-C6-C8	108.9(7)	H22A-C22-H22B	109.5
C9-C6-C8	106.8(7)	H22A-C22-H22C	109.5
C7-C6-C8	108.9(6)	H22B-C22-H22C	109.5

H23A-C23-H23B	109.5
H23A-C23-H23C	109.5
H23B-C23-H23C	109.5
H24A-C24-H24B	109.5
H24A-C24-H24C	109.5
H24B-C24-H24C	109.5
H25A-C25-H25B	109.5
H25A-C25-H25C	109.5
H25B-C25-H25C	109.5
H26A-C26-H26B	109.5
H26A-C26-H26C	109.5
H26B-C26-H26C	109.5
H27A-C27-H27B	109.5
H27A-C27-H27C	109.5
H27B-C27-H27C	109.5

[a] Cp1 is the centroid of atoms C1, C2, C3, C4 and C5
[b] Pln1 is the best plane through atoms C1, C2, C3, C4 and C5
[c] Cp2 is the centroid of atoms C9, C10, C15, C16 and C21
[d] Pln2 is the best plane through atoms C9, C10, C15, C16 and C21

Table 33. Crystal Data and Structure Analysis Details for (Ewen)$TaMe_2F$.

Empirical formula	$C_{33.5}H_{36}FTa$ $[C_{23}H_{24}FTa \cdot 1\_C_7H_8]$
Formula weight	638.60 [500.39 · 1_ (92.14)]
Crystallization solvent	CH_2Cl_2/PE
Crystal habit	tabular fragment
Crystal size	0.30 x 0.30 x 0.22 mm
Crystal color	yellow

Data Collection

Preliminary photograph(s)	none	
Type of diffractometer	CAD-4	
Wavelength	0.71073 Å MoKa	
Data collection temperature	84 K	
Theta range for 25 reflections used in lattice determination	14 to 16°	
Unit cell dimensions	a = 13.505(3) Å b = 12.465(3) Å c = 16.034(4) Å	a= 90° b= 96.47(2)° g = 90°
Volume	2682.0(11) $Å^3$	
Z	4	
Crystal system	monoclinic	
Space group	$P2_1/n$ (#14)	
Density (calculated)	1.581 g/cm^3	
F(000)	1276	
Theta range for data collection	1.5 to 25°	
Completeness to theta = 25°	100.0 %	
Index ranges	-16 £ h £ 15, -14 £ k £ 14, 0 £ l £ 19	
Data collection device	CAD-4	
Data collection scan type	ω-scan	
Reflections collected	11341	

Independent reflections	4709 [R_{int}= 0.0203; GOF_{merge}= 1.05]
Absorption coefficient	4.125 mm^{-1}
Absorption correction	y-scan
Max. and min. transmission	1.06 and 0.85
Number of standards	3 reflections measured every 75 min
Variation of standards	within counting statistics

Structure Solution and Refinement

Primary solution method	direct methods
Secondary solution method	difference map
Hydrogen placement	calculated
Refinement method	full-matrix least-squares on F^2
Data / restraints / parameters	4709 / 0 / 448
Treatment of hydrogen atoms	coordinates refined; U_{iso}'s fixed at 120% U_{eq} of attached atom
Goodness-of-fit on F^2	1.363
Final R indices [I>2s(I), 4339 reflections]	R1 = 0.0193, wR2 = 0.0415
R indices (all data)	R1 = 0.0228, wR2 = 0.0425
Type of weighting scheme used	sigma
Weighting scheme used	$w=1/s^2(Fo^2)$
Max shift/error	0.061
Average shift/error	0.002
Largest diff. peak and hole	0.797 and -0.482 e.$Å^{-3}$

Programs Used

Cell refinement	CAD-4 Software (Enraf-Nonius, 1989)
Data collection	CAD-4 Software (Enraf-Nonius, 1989)
Data reduction	CRYM (Duchamp, 1964)
Structure solution	SHELXS-97 (Sheldrick, 1990)
Structure refinement	SHELXL-97 (Sheldrick, 1997)

Special Refinement Details

A pale yellow tabular fragment was mounted on a glass fiber with Paratone-N oil. Data were collected with 1.2∞ w-scans, as the peaks wereslightly broad. The individual measured backgrounds were replaced by a background function of 2q derived from weak reflections. The GOF_{merge} was 1.05 (4708 multiples) in point group 2/m; R_{merge} was 0.015 for 4195 duplicates with $F_o > 0$. Y-scan data were used for the absorption correction. There was no decay. No outlier reflections were omitted from the refinement.

Weights w are calculated as $1/s^2(F_o^2)$; variances ($s^2(F_o^2)$) were derived from counting statistics plus an additional term, $(0.014I)^2$; variances of the merged data were obtained by propagation of error plus another additional term, $(0.014<I>)^2$. The refinement of F^2 is as always against all reflections. The weighted R-factor wR and goodness of fit S are based on F^2, conventional R-factors R are based on F, with F set to zero for negative F^2. The threshold expression of $F^2 > 2s(F^2)$ is used only for calculating R-factors(gt) etc. and is not relevant to the choice of reflections for refinement.

The asymmetric unit contains one Ta complex and 1_ molecules of toluene. The toluene is disordered over a center of symmetry; the _ carbon atoms were refined anisotropically and the hydrogen atoms placed at calculated positions. All hydrogen atoms were given fixed U_{iso}'s.

Table 34. Bond lengths [Å] and angles [°] for (Ewen)TaMe2F.

Ta-Cp[a]	2.104	C8-H8C	0.91(4)
Ta···Pln[b]	2.100(2)	C9-C10	1.499(4)
Ta-F	1.9133(16)	C9-C21	1.505(4)
Ta-C23	2.173(3)	C10-C11	1.395(4)
Ta-C22	2.173(3)	C10-C15	1.406(4)
Ta-C9	2.290(3)	C11-C12	1.391(5)
Ta-C5	2.385(3)	C11-H11	0.95(3)
Ta-C1	2.385(3)	C12-C13	1.381(5)
Ta-C2	2.389(3)	C12-H12	1.01(4)
Ta-C4	2.476(3)	C13-C14	1.390(5)
Ta-C3	2.479(3)	C13-H13	0.88(4)
C1-C2	1.413(4)	C14-C15	1.391(4)
C1-C5	1.415(4)	C14-H14	0.96(3)
C1-C6	1.518(4)	C15-C16	1.453(4)
C2-C3	1.417(4)	C16-C17	1.395(4)
C2-H2	0.91(3)	C16-C21	1.415(4)
C3-C4	1.403(5)	C17-C18	1.381(5)
C3-H3	0.93(3)	C17-H17	0.83(3)
C4-C5	1.421(4)	C18-C19	1.376(5)
C4-H4	0.93(3)	C18-H18	0.89(3)
C5-H5	0.90(3)	C19-C20	1.392(4)
C6-C7	1.530(4)	C19-H19	0.94(3)
C6-C8	1.530(4)	C20-C21	1.405(4)
C6-C9	1.573(4)	C20-H20	0.96(3)
C7-H7A	0.85(4)	C22-H22A	0.92(4)
C7-H7B	0.93(3)	C22-H22B	0.81(4)
C7-H7C	0.96(3)	C22-H22C	1.00(4)
C8-H8A	0.98(4)	C23-H23A	1.01(3)
C8-H8B	0.95(3)	C23-H23B	0.88(4)

C23-H23C	0.98(3)
C24-C25	1.358(6)
C24-C29	1.416(5)
C24-H24	0.92(4)
C25-C26	1.406(6)
C25-H25	1.01(4)
C26-C27	1.364(6)
C26-H26	0.98(4)
C27-C28	1.394(5)
C27-H27	1.07(4)
C28-C29	1.372(5)
C28-H28	1.05(4)
C29-C30	1.490(5)
C30-H30A	1.08(4)
C30-H30B	1.00(4)
C30-H30C	1.03(4)
C31-C36	1.42(3)
C31-C32	1.48(3)
C31-H31	0.9300
C32-C33	1.20(2)
C32-H32	0.9300
C33-C34	1.32(3)
C33-H33	0.9300
C34-C35	1.43(4)
C34-H34	0.9300
C35-C36	1.48(2)
C35-H35	0.9300
C36-C37	1.476(18)
C37-H37A	0.9600
C37-H37B	0.9600
C37-H37C	0.9600
Cp-Ta-F	173.3
Cp-Ta-C9	90.2
Cp-Ta-C22	102.4
Cp-Ta-C23	102.9
F-Ta-C23	81.43(10)
F-Ta-C22	80.59(10)
C23-Ta-C22	110.96(14)
F-Ta-C9	83.10(9)
C23-Ta-C9	120.07(12)
C22-Ta-C9	122.86(12)
C2-C1-C5	106.7(3)
C2-C1-C6	124.3(3)
C5-C1-C6	124.3(3)
C1-C2-C3	108.8(3)
C1-C2-H2	126(2)
C3-C2-H2	125(2)
C4-C3-C2	108.1(3)
C4-C3-H3	125(2)
C2-C3-H3	127(2)
C3-C4-C5	107.5(3)
C3-C4-H4	125(2)
C5-C4-H4	127(2)
C1-C5-C4	108.9(3)
C1-C5-H5	127(2)
C4-C5-H5	124(2)
C1-C6-C7	111.2(2)
C1-C6-C8	111.9(2)
C7-C6-C8	106.8(3)
C1-C6-C9	97.6(2)
C7-C6-C9	115.0(2)
C8-C6-C9	114.3(2)
C6-C7-H7A	107(2)
C6-C7-H7B	110(2)
H7A-C7-H7B	105(3)
C6-C7-H7C	114.9(19)
H7A-C7-H7C	113(3)
H7B-C7-H7C	107(3)
C6-C8-H8A	112.4(19)
C6-C8-H8B	116.1(19)
H8A-C8-H8B	108(3)
C6-C8-H8C	106(2)
H8A-C8-H8C	107(3)
H8B-C8-H8C	108(3)
C10-C9-C21	103.1(2)
C10-C9-C6	120.0(2)
C21-C9-C6	119.7(2)
C10-C9-Ta	103.72(18)
C21-C9-Ta	106.00(17)
C6-C9-Ta	102.51(17)
C11-C10-C15	118.5(3)
C11-C10-C9	131.1(3)
C15-C10-C9	110.2(2)
C12-C11-C10	119.4(3)
C12-C11-H11	120(2)
C10-C11-H11	121(2)
C13-C12-C11	121.4(3)
C13-C12-H12	121(2)
C11-C12-H12	117(2)
C12-C13-C14	120.2(3)
C12-C13-H13	122(2)
C14-C13-H13	118(2)
C13-C14-C15	118.5(3)
C13-C14-H14	122(2)
C15-C14-H14	120(2)
C14-C15-C10	121.8(3)
C14-C15-C16	129.6(3)
C10-C15-C16	108.5(2)
C17-C16-C21	120.8(3)
C17-C16-C15	130.5(3)
C21-C16-C15	108.6(2)
C18-C17-C16	119.0(3)
C18-C17-H17	122(2)
C16-C17-H17	119(2)
C19-C18-C17	120.9(3)

C19-C18-H18	124(2)
C17-C18-H18	115(2)
C18-C19-C20	121.4(3)
C18-C19-H19	124(2)
C20-C19-H19	115(2)
C19-C20-C21	118.9(3)
C19-C20-H20	120.5(19)
C21-C20-H20	120.6(19)
C20-C21-C16	118.9(3)
C20-C21-C9	131.4(3)
C16-C21-C9	109.5(2)
Ta-C22-H22A	106(2)
Ta-C22-H22B	101(3)
H22A-C22-H22B	114(3)
Ta-C22-H22C	124.5(19)
H22A-C22-H22C	107(3)
H22B-C22-H22C	105(3)
Ta-C23-H23A	102.3(19)
Ta-C23-H23B	128(2)
H23A-C23-H23B	114(3)
Ta-C23-H23C	105.1(19)
H23A-C23-H23C	104(3)
H23B-C23-H23C	102(3)
C25-C24-C29	120.2(4)
C25-C24-H24	125(2)
C29-C24-H24	115(2)
C24-C25-C26	121.0(4)
C24-C25-H25	120(2)
C26-C25-H25	119(2)
C27-C26-C25	118.9(4)
C27-C26-H26	124(2)
C25-C26-H26	117(2)
C26-C27-C28	120.4(4)
C26-C27-H27	124(2)
C28-C27-H27	115(2)
C29-C28-C27	121.1(4)
C29-C28-H28	121(2)
C27-C28-H28	117(2)
C28-C29-C24	118.3(4)
C28-C29-C30	121.4(4)
C24-C29-C30	120.3(4)
C29-C30-H30A	111(2)
C29-C30-H30B	102(2)
H30A-C30-H30B	118(3)
C29-C30-H30C	110(2)
H30A-C30-H30C	112(3)
H30B-C30-H30C	103(3)
C36-C31-C32	103(2)
C36-C31-H31	128.6
C32-C31-H31	128.6
C33-C32-C31	134(2)
C33-C32-H32	112.8
C31-C32-H32	112.8
C32-C33-C34	124(3)
C32-C33-H33	118.2
C34-C33-H33	118.2
C33-C34-C35	117(2)
C33-C34-H34	121.7
C35-C34-H34	121.7
C34-C35-C36	116.3(14)
C34-C35-H35	121.8
C36-C35-H35	121.8
C31-C36-C37	106.5(15)
C31-C36-C35	126.2(13)
C37-C36-C35	127.2(17)
C36-C37-H37A	109.5
C36-C37-H37B	109.5
H37A-C37-H37B	109.5
C36-C37-H37C	109.5
H37A-C37-H37C	109.5
H37B-C37-H37C	109.5

[a] Cp is the centroid of atoms C1, C2, C3, C4 and C5
[b] Pln is the best plane through atoms C1, C2, C3, C4 and C5

Table 35. Crystal Data and Structure Analysis Details for TMSThpTaMe3.

Empirical formula	$C_{26}H_{47}Si_3Ta$
Formula weight	624.86
Crystallization solvent	Diethyl ether
Crystal habit	prism
Crystal size	0.31 x 0.26 x 0.23 mm
Crystal color	orange

Data Collection

Preliminary photograph(s)	rotation	
Type of diffractometer	Bruker SMART 1000 ccd	
Wavelength	0.71073 Å MoKa	
Data collection temperature	98 K	
Theta range for 7823 reflections used in lattice determination	2.4 to 28.5°	
Unit cell dimensions	a = 17.205(4) Å b = 16.270(3) Å c = 9.995(2) Å	a= 90° b= 90° g = 90°
Volume	2798.0(10) $Å^3$	
Z	4	
Crystal system	orthorhombic	
Space group	Pnma (#62)	
Density (calculated)	1.483 g/cm^3	
F(000)	1272	
Theta range for data collection	2.36 to 28.62°	
Completeness to theta = 28.62°	95.9 %	
Index ranges	-22 £ h £ 22, -21 £ k £ 21, -13 £ l £ 13	
Data collection scan type	w scans at 4 fixed f values	
Reflections collected	34549	
Independent reflections	3562 [R_{int}= 0.0385]	
Absorption coefficient	4.068 mm^{-1}	
Absorption correction	none	
Number of standards	first scans recollected at end of runs	
Variation of standards	within counting statistics	

Structure Solution and Refinement

Primary solution method	direct methods
Secondary solution method	difference map
Hydrogen placement	calculated
Refinement method	full-matrix least-squares on F^2
Data / restraints / parameters	3562 / 0 / 157
Treatment of hydrogen atoms	not refined; U_{iso}'s set at 120% U_{eq} of the attached atom
Goodness-of-fit on F^2	7.041
Final R indices [I>2s(I), 3358 reflections]	R1 = 0.0556, wR2 = 0.1222
R indices (all data)	R1 = 0.0592, wR2 = 0.1227
Type of weighting scheme used	sigma
Weighting scheme used	$w=1/s^2(Fo^2)$
Max shift/error	0.015
Average shift/error	0.001
Largest diff. peak and hole	11.952 and -6.111 e.Å^{-3}

Programs Used

Cell refinement	Bruker SAINT v6.02
Data collection	Bruker SMART v5.054
Data reduction	Bruker SAINT v6.02
Structure solution	SHELXS-97 (Sheldrick, 1990)
Structure refinement	SHELXL-97 (Sheldrick, 1997)

Special Refinement Details

Data for this material were previously collected on a CAD-4 diffractometer (PJC13); however the compound is light sensitive and there was a large decrease in the check reflections (>35%). For this dataset on the ccd, the terminated cap was cut from an orange prism and mounted on a glass fiber with Paratone-N oil. The ccd enclosure was covered in black plastic as a precaution. Four runs of data were collected with 20 second long, –0.3° wide ω–scans at three values of φ (0, 120, 240 and 0°) with the detector 5 cm (nominal) distant at a θ of -28°. The initial cell for data reduction was calculated from just under 1000 reflections chosen from throughout the data frames. For data processing with SAINT v6.02, all defaults were used, except: box size optimization was enabled, periodic orientation matrix updating was disabled, the instrument error was set to zero, no Laue class integration restraints were used, the model profiles from all nine areas were blended, and for the post-integration global least squares refinement, no constraints were applied. No SADABS manipulations were employed. No decay correction was needed.

No reflections were specifically omitted from the final processed dataset; 1783 reflections were rejected, with 84 space group-absence violations and 28 inconsistent equivalents. Refinement of F^2 was against all reflections. The weighted R-factor (wR) and goodness of fit (S) are based on F^2, conventional R-factors (R) are based on F, with F set to zero for negative F^2. The threshold expression of $F^2 > 2\sigma(F^2)$ is used only for calculating R-factors(gt) etc. and is not relevant to the choice of reflections for refinement.

The molecule lies on a mirror plane. The t-butyl group is disordered across this plane and modeled with two orientations (50:50 by symmetry). (Similar disorder occurs in at least one isostructural compound.) The goodness-of-fit is extraordinarily high and there are many extremely large peaks in the final difference map; the three greater than |2| e·Å^{-3} (11.95, -6.11 and -2.76) are all within 0.79 Å of the Ta atom. Nonetheless, this is a reasonable structure as evidenced by the R-indices, displacement ellipsoids and geometric parameters. This was a strongly diffracting crystal [3358 of 3562 reflections greater than 2σ(I)] and the sigmas are not correct, especially for the intense reflections.

Table 36. Bond lengths [Å] and angles [°] for TMSThpTaMe3

Ta-Cp	2.131	C9A-H9C	0.9800
Ta···Pln	2.126(3)	C9B-H9D	0.9800
Ta-Cen	2.378	C9B-H9E	0.9800
Ta-C14	2.203(6)	C9B-H9F	0.9800
Ta-C15	2.211(9)	C10-H10A	0.9800
Ta-C1	2.402(5)	C10-H10B	0.9800
Ta-C2	2.461(5)	C10-H10C	0.9800
Ta-C4	2.492(5)	C11-C12	1.526(8)
Ta-C3	2.538(8)	C11-C13	1.530(8)
Si1-C1	1.861(5)	C11-H11	1.0000
Si1-C8	1.864(7)	C12-H12A	0.9800
Si1-C7	1.872(6)	C12-H12B	0.9800
Si1-C4	1.874(6)	C12-H12C	0.9800
Si2-C9A	1.795(17)	C13-H13A	0.9800
Si2-C10	1.833(14)	C13-H13B	0.9800
Si2-C3	1.874(8)	C13-H13C	0.9800
Si2-C9B	1.915(15)	C14-H14A	0.9800
C1-C2	1.413(8)	C14-H14B	0.9800
C1-C1$^{(i)}$	1.459(10)	C14-H14C	0.9800
C2-C3	1.433(7)	C15-H15A	0.9613
C2-H2	0.9500	C15-H15B	0.9608
C4-C5	1.415(8)		
C4-C4$^{(i)}$	1.489(10)	Cp-Ta-C4	96.6
C5-C6	1.404(7)	Cp-Ta-C14	103.1
C5-C11	1.524(7)	Cp-Ta-C15	178.2
C6-H6	0.9500	Cp-Ta-Cen	96.9
C7-H7A	0.9800	Cen-Ta-C14	119.3
C7-H7B	0.9800	Cen-Ta-C15	85.0
C7-H7C	0.9800	C14$^{(i)}$-Ta-C14	110.9(4)
C8-H8A	0.9800	C14-Ta-C15	75.9(2)
C8-H8B	0.9800	C15-Ta-C4$^{(i)}$	85.2(3)
C8-H8C	0.9800	C14$^{(i)}$-Ta-C4	135.5(2)
C9A-H9A	0.9800	C14-Ta-C4	102.8(2)
C9A-H9B	0.9800	C15-Ta-C4	85.2(3)

C1-Si1-C8	107.9(3)	Si2-C9A-H9A	109.5
C1-Si1-C7	115.5(3)	Si2-C9A-H9B	109.5
C8-Si1-C7	106.8(4)	H9A-C9A-H9B	109.5
C1-Si1-C4	93.5(2)	Si2-C9A-H9C	109.5
C8-Si1-C4	116.1(3)	H9A-C9A-H9C	109.5
C7-Si1-C4	116.7(3)	H9B-C9A-H9C	109.5
C9A-Si2-C3	107.6(6)	Si2-C9B-H9D	109.5
C10-Si2-C3	113.4(5)	Si2-C9B-H9E	109.5
C3-Si2-C9B$^{(i)}$	106.8(5)	H9D-C9B-H9E	109.5
C9A$^{(i)}$-Si2-C10	109.9(11)	Si2-C9B-H9F	109.5
C10-Si2-C9B	105.3(8)	H9D-C9B-H9F	109.5
C9A$^{(i)}$-Si2-C9B	113.8(12)	H9E-C9B-H9F	109.5
C2-C1-C1$^{(i)}$	106.3(3)	Si2-C10-H10A	109.5
C2-C1-Si1	124.5(4)	Si2-C10-H10B	109.5
C1$^{(i)}$-C1-Si1	123.41(16)	H10A-C10-H10B	109.5
C1-C2-C3	112.0(5)	Si2-C10-H10C	109.5
C1-C2-H2	124.0	H10A-C10-H10C	109.5
C3-C2-H2	124.0	H10B-C10-H10C	109.5
C2$^{(i)}$-C3-C2	103.5(6)	C5-C11-C12	111.5(5)
C2$^{(i)}$-C3-Si2	128.1(3)	C5-C11-C13	112.7(5)
C2-C3-Si2	128.1(3)	C12-C11-C13	109.1(5)
C5-C4-C4$^{(i)}$	106.1(3)	C5-C11-H11	107.8
C5-C4-Si1	129.0(4)	C12-C11-H11	107.8
C4$^{(i)}$-C4-Si1	122.62(17)	C13-C11-H11	107.8
C5-C4-Ta	116.7(4)	C11-C12-H12A	109.5
C4$^{(i)}$-C4-Ta	72.62(12)	C11-C12-H12B	109.5
Si1-C4-Ta	93.0(2)	H12A-C12-H12B	109.5
C6-C5-C4	109.6(5)	C11-C12-H12C	109.5
C6-C5-C11	125.4(5)	H12A-C12-H12C	109.5
C4-C5-C11	125.0(5)	H12B-C12-H12C	109.5
C5$^{(i)}$-C6-C5	108.2(7)	C11-C13-H13A	109.5
C5$^{(i)}$-C6-H6	125.9	C11-C13-H13B	109.5
C5-C6-H6	125.9	H13A-C13-H13B	109.5
Si1-C7-H7A	109.5	C11-C13-H13C	109.5
Si1-C7-H7B	109.5	H13A-C13-H13C	109.5
H7A-C7-H7B	109.5	H13B-C13-H13C	109.5
Si1-C7-H7C	109.5	Ta-C14-H14A	109.5
H7A-C7-H7C	109.5	Ta-C14-H14B	109.5
H7B-C7-H7C	109.5	H14A-C14-H14B	109.5
Si1-C8-H8A	109.5	Ta-C14-H14C	109.5
Si1-C8-H8B	109.5	H14A-C14-H14C	109.5
H8A-C8-H8B	109.5	H14B-C14-H14C	109.5
Si1-C8-H8C	109.5	Ta-C15-H15A	109.8
H8A-C8-H8C	109.5	Ta-C15-H15B	109.3
H8B-C8-H8C	109.5	H15A-C15-H15B	109.5

Symmetry transformations used to generate equivalent atoms:
$^{(i)}$ x,-y+1/2,z